

VOLUME 79

AUGUST 14, 1975

NUMBER 17

JPCA x

THE JOURNAL OF

PHYSICAL

CHEMISTRY

PUBLISHED BIWEEKLY BY THE AMERICAN CHEMICAL SOCIETY

THE JOURNAL OF PHYSICAL CHEMISTRY

BRYCE CRAWFORD, Jr., *Editor*
STEPHEN PRAGER, *Associate Editor*
ROBERT W. CARR, Jr., **FREDERIC A. VAN-CATLEDGE**, *Assistant Editors*

EDITORIAL BOARD: C. A. ANGELL (1973-1977), F. C. ANSON (1974-1978), V. A. BLOOMFIELD (1974-1978), J. R. BOLTON (1971-1975), L. M. DORFMAN (1974-1978), H. L. FRIEDMAN (1975-1979), E. J. HART (1975-1979), W. J. KAUFMANN (1974-1978), R. L. KAY (1972-1976), D. W. McCLURE (1974-1978), R. M. NOYES (1973-1977), J. A. POPLE (1971-1975), B. S. RABINOVITCH (1971-1975), S. A. RICE (1969-1975), F. S. ROWLAND (1973-1977), R. L. SCOTT (1973-1977), A. SILBERBERG (1971-1975), J. B. STOTHERS (1974-1978), W. A. ZISMAN (1972-1976)

AMERICAN CHEMICAL SOCIETY, 1155 Sixteenth St., N. W., Washington, D. C. 20036

Books and Journals Division

D. H. MICHAEL BOWEN *Director*

CHARLES R. BERTSCH *Head, Editorial Processing Department*
BACIL GUILLEY *Head, Graphics and Production Department*
SELDON W. TERRANT *Head, Research and Development Department*

©Copyright, 1975, by the American Chemical Society. Published biweekly by the American Chemical Society at 20th and Northampton Sts., Easton, Pa. 18042. Second-class postage paid at Washington, D.C., and at additional mailing offices.

All manuscripts should be sent to *The Journal of Physical Chemistry*, Department of Chemistry, University of Minnesota, Minneapolis, Minn. 55455.

Additions and Corrections are published once yearly in the final issue. See Volume 78, Number 26 for the proper form.

Extensive or unusual alterations in an article after it has been set in type are made at the author's expense, and it is understood that by requesting such alterations the author agrees to defray the cost thereof.

The American Chemical Society and the Editor of *The Journal of Physical Chemistry* assume no responsibility for the statements and opinions advanced by contributors.

Correspondence regarding accepted copy, proofs, and reprints should be directed to Editorial Processing Department, American Chemical Society, 20th and Northampton Sts., Easton, Pa. 18042. Department Head: CHARLES R. BERTSCH. Associate Department Head: MARIANNE C. BROGAN, Assistant Editors: CELIA B. McFARLAND, JOSEPH E. YURVATI.

Advertising Office: Centcom, Ltd., 50 W. State St., Westport, Conn. 06880.

Business and Subscription Information

Send all new and renewal subscriptions *with payment to: Office of the Controller*, 1155 16th Street, N.W., Washington, D.C. 20036. Subscriptions should be renewed promptly to avoid a break in your series. All correspondence and telephone calls regarding

changes of address, claims for missing issues, subscription service, the status of records, and accounts should be directed to Manager, Membership and Subscription Services, American Chemical Society, P.O. Box 3337, Columbus, Ohio 43210. Telephone (614) 421-7230. For microfiche service, contact ACS Microfiche Service, 1155 16th St. N.W., Washington, D.C. 20036. Telephone (202) 872-4444.

On changes of address, include both old and new addresses with ZIP code numbers, accompanied by mailing label from a recent issue. Allow four weeks for change to become effective.

Claims for missing numbers will not be allowed (1) if loss was due to failure of notice of change in address to be received before the date specified, (2) if received more than sixty days from date of issue plus time normally required for postal delivery of journal and claim, or (3) if the reason for the claim is "issue missing from files."

Subscription rates (hard copy or microfiche) in 1975: \$20.00 for 1 year to ACS members; \$80.00 to nonmembers. Extra postage \$4.50 in Canada and PUAS, \$5.00 other foreign. Supplementary material (on microfiche only) available on subscription basis, 1975 rates: \$15.00 in U.S., \$19.00 in Canada and PUAS, \$20.00 elsewhere. All microfiche airmailed to non-U.S. addresses; air freight rates for hard-copy subscriptions available on request.

Single copies for current year: \$4.00. Rates for back issues from Volume 56 to date are available from the Special Issues Sales Department, 1155 Sixteenth St., N.W., Washington, D.C. 20036.

Subscriptions to this and the other ACS periodical publications are available on microfilm. For information on microfilm write Special Issues Sales Department at the address above.

THE JOURNAL OF
PHYSICAL CHEMISTRY

Volume 79, Number 17 August 14, 1975

JPCHAx 79(17) 1749-1890 (1975)

ISSN 0022-3654

Analytical Results for First-Order Kinetics in Flow Tube Reactors with Wall Reactions Paul J. Ogren	1749
Rates of Reaction of Hydrogen Atoms with Silane and Germane Kwang Yul Choo, Peter P. Gaspar,* and A. P. Wolf	1752
Reaction of Hydrogen Atoms with Thiirane T. Yokota, M. G. Ahmed, I. Safarik, O. P. Strausz,* and H. E. Gunning	1758
Rate Constants for the Reaction of OH Radicals with a Series of Aromatic Hydrocarbons D. A. Hansen, R. Atkinson, and J. N. Pitts, Jr.*	1763
Reaction of ·OH with Benzoic Acid. Isomer Distribution in the Radical Intermediates George W. Klein, Kishan Bhatia, V. Madhavan, and Robert H. Schuler*	1767
Polarographic and Optical Pulse Radiolysis Study of the Radicals Formed by OH Attack on Imidazole and Related Compounds in Aqueous Solutions K. M. Bansal and R. M. Sellers*	1775
Combination and Disproportionation of Allylic Radicals at Low Temperatures Ralph Klein* and Richard D. Kelley	1780
Thermodynamics of the Reaction of Ammonia and Sulfur Dioxide in the Presence of Water Vapor Ronald Landreth, Rosa G. de Pena, and Julian Heicklen*	1785
Electronic Excitation Transfer between the Same Kind of Excited Molecules in Rigid Solvents under High-Density Excitation with Lasers Nobuaki Nakashima, Yuji Kume, and Noboru Mataga*	1788
Structure, Energetics, and Dynamics of Small Water Clusters John C. Owicki, Lester L. Shipman, and Harold A. Scheraga*	1794
Influence of a First Hydrogen Bond on the Formation of a Second One by Alkyl- or Dialkylammonium Ions M. Cl. Haulait and P. L. Huyskens*	1812
Apparent and Partial Molar Polarizations in Solutions and the Halverstadt-Kumler and Hedestrand Equations William J. Taylor	1817
Calculation of the Elementary Graph of the Fourth Virial Coefficient of a Dilute Ionic Solution M. Dixon* and P. Hutchinson	1820
Expansion of the McDevit and Long Theory of Nonelectrolyte Activity Coefficients to a Consideration of Concentrated Aqueous Electrolyte Solutions R. F. Cross	1822
Voltammetry of Rhodium-1,10-Phenanthroline Complexes Gregory Kew, Kenneth Hanck, and Keith DeArmond*	1828
Oxygen Adducts of Cobalt(II)-Ethylenediamine Complexes in X- and Y-Type Zeolites R. F. Howe and J. H. Lunsford*	1836
Molecular Diffusion and Proton Exchange in Methanol Adsorbed by a Sodium and a Hydrogen Y Zeolite P. Salvador and J. J. Fripiat*	1842
Infrared Spectra of Matrix Isolated Disulfur Monoxide Isotopes Alfred G. Hopkins, Francis P. Daly, and Chris W. Brown*	1849

30.8.2519

Raman Spectroscopic Studies of Binary Systems. II. Effect of Temperature upon Molecular Association in the Ammonia-Hexadeuteriobenzene System	John H. Roberts* and Bertin de Bettignies	1852
Electron Spin Resonance Spectra of Certain Fluorohydride Radicals of Phosphorus, Arsenic, and Antimony	A. J. Colussi, J. R. Morton,* and K. F. Preston	1855
Electron Spin Resonance Study on the Structure of Radical Pairs in Irradiated Oriented Polyethylene	Takashi Fujimura* and Naoyuki Tamura	1859
Molecular Orbital Calculations on the Nitrogen Nuclear Spin-Spin Coupling Constants	Shinichi Nagata,* Tokio Yamabe, Kimihiko Hirao, and Kenichi Fukui	1863
Nuclear Magnetic Resonance Investigation of Cobalt(III) Outer-Sphere Complexes in Aqueous Solutions	K. L. Craighead, P. Jones, and R. G. Bryant*	1868
Crystal Structures of Hydrated and Dehydrated Divalent-Copper-Exchanged Faujasite	I. E. Maxwell* and J. J. de Boer	1874 ■
Polar Tensors and Effective Charges of Br ₂ CO	A. B. M. S. Bassi and Roy E. Bruns*	1880
Soret Coefficient of 1 N Lithium Iodide	Douglas R. Caldwell	1882
Pressure Dependence of Thermal and Fickian Diffusion in 0.1 N Sodium Chloride	Douglas F. Caldwell	1885
A Relationship between Hydroxyl Proton Chemical Shifts and Torsional Frequencies in Some Ortho-Substituted Phenol Derivatives	Ted Schaefer	1888

■ Supplementary material for this paper is available separately, in photocopy or microfiche form. Ordering information is given in the paper.

* In papers with more than one author, the asterisk indicates the name of the author to whom inquiries about the paper should be addressed.

AUTHOR INDEX

Ahmed, M. G., 1758	de Boer, J. J., 1874	Jones, P., 1868	Pitts, J. N., Jr., 1763
Atkinson, R., 1763	de Pena, R. G., 1785	Kelley, R. D., 1780	Preston, K. F., 1855
Bansal, K. M., 1775	Dixon, M., 1820	Kew, G., 1828	Roberts, J. H., 1852
Bassi, A. B. M. S., 1880	Fripiat, J. J., 1842	Klein, G. W., 1767	Safarik, I., 1758
Bhatia, K., 1757	Fujimura, T., 1859	Klein, R., 1780	Salvador, P., 1842
Brown, C. W., 1849	Fukui, K., 1863	Kume, Y., 1788	Schaefer, T., 1888
Bruns, R. E., 1880	Gaspar, P. P., 1752	Landreth, R., 1785	Scheraga, H. A., 1794
Bryant, R. G., 1868	Gunning, H. E., 1758	Lunsford, J. H., 1836	Schuler, R. H., 1767
Caldwell, D. R., 1882, 1885	Hanck, K., 1828	Madhavan, V., 1767	Sellers, R. M., 1775
Choo, K. Y., 1752	Hansen, D. A., 1763	Mataga, N., 1788	Shipman, L. L., 1794
Colussi, A. J., 1855	Haulait, M. Cl., 1812	Maxwell, I. E., 1874	Strausz, O. P., 1758
Craighead, K. L., 1868	Heicklen, J., 1785	Morton, J. R., 1855	Tamura, N., 1859
Cross, R. F., 1822	Hirao, K., 1863	Nagata, S., 1863	Taylor, W. J., 1817
Daly, F. P., 1849	Hopkins, A. G., 1849	Nakashima, N., 1788	Wolf, A. P., 1752
DeArmond, K., 1828	Howe, R. F., 1836	Ogren, P. J., 1749	Yamabe, T., 1863
de Bettignies, B., 1852	Hutchinson, P., 1820	Owicki, J. C., 1794	Yokota, T., 1758
	Huyskens, P. L., 1812		

THE JOURNAL OF PHYSICAL CHEMISTRY

Registered in U. S. Patent Office © Copyright, 1975, by the American Chemical Society

VOLUME 79, NUMBER 17 AUGUST 14, 1975

Analytical Results for First-Order Kinetics in Flow Tube Reactors with Wall Reactions

Paul J. Ogren

Department of Chemistry, Central College, Pella, Iowa 50219 (Received January 13, 1975)

An analysis of chemical reaction in a flow system is presented. The analysis is confined to cases of Poiseuille flow, with first-order gas-phase and wall reactions, and with negligible axial diffusion; these conditions permit exact solutions to be obtained. Particular attention is given to results for systems with nearly constant radial concentration, a condition of considerable experimental importance. A convenient method is outlined for correcting observed rate constants for the combined effects of wall reactions and small radial concentration gradients. Applications of the exact solutions agree well with the conclusions of previous workers.

Introduction

Flow tube reactors are commonly used for the study of fast gas-phase reactions. For simple interpretation, conditions are normally employed which give minimum viscous pressure drop, axial diffusion and wall reaction, and maximum radial diffusion. Such conditions, discussed in some detail by Kaufman,¹ allow the system to be treated as one with all fluid elements moving with the bulk velocity v with no radial concentration gradients. In this "ideal" case the concentration of a species disappearing by a first-order reaction is governed at any position z along the tube by the original concentration and the equation $dc/dz = -kc/v$, where k may include both bulk and wall reaction terms.

For many experimental systems, viscous pressure drop and axial diffusion can often be minimized; however, tube size and diffusion or pressure conditions chosen to give nearly uniform radial concentrations also increase the relative importance of wall reactions. In typical experimental studies, apparent rate constants are examined as a function of pressure to separate wall rate terms from bulk rate terms. At the increasingly higher pressures which increase the relative importance of bulk rate processes, however, appreciable radial concentration gradients may develop due to the decrease in molecular diffusion. In such circumstances, the main portion of the flowing gas, which is eventually studied at a downstream detection point, becomes increasingly "insulated" from the wall reaction and the observed rate may be less than the sum of wall and bulk reaction rates.

Some who have dealt fairly recently with the general problem of corrections to "ideal" flow behavior have suc-

cessfully used approximate analytical solutions to a restricted continuity equation to describe effects of viscous pressure drop, axial diffusion, and slip flow on observed axial decay constants.¹⁻³ The effect of wall reactions on radial concentration gradients has been evaluated approximately by Kaufman,¹ but the determination of nonideal effects of wall reactions and incomplete radial mixing on axial decay has thus far required numerical analysis.^{4,5} The primary contribution of the present work is to demonstrate that the restricted continuity equation used by others can be solved exactly for first-order reactions. These solutions are then used to examine nonideal effects of incomplete radial mixing and wall reactions on first-order rate processes in the absence of other complications. The analytical approach taken also provides some useful insight into the effects of initial and boundary conditions on apparent reaction parameters under fairly general flow conditions.

Theory and Discussion

General Development. The treatment here is restricted to Poiseuille flow; the development follows closely the notation of Poirier and Carr⁵ and is primarily aimed at evaluating wall effects on observed first-order kinetics in the absence of axial diffusion. The continuity equation for a flowing system at constant pressure and temperature with a small amount of component c undergoing experimental first-order reaction is

$$v_0 \left[1 - \left(\frac{r}{R_0} \right)^2 \right] \frac{\partial c}{\partial z} = D \left[\frac{1}{r} \frac{\partial}{\partial r} r \frac{\partial c}{\partial r} + \frac{\partial^2 c}{\partial z^2} \right] - kc \quad (1)$$

The general boundary conditions are $c = c_0(r)$ at $z = 0$; $c =$

0 at $z = \infty$; and $-D(\partial c/\partial r) = k_w c$ at $r = R$, the radius of the cylinder.⁹ We first assume that conditions making the axial gradient term negligible can be chosen.¹ Equation 1 may then be written in dimensionless form as

$$(1 - u^2) \frac{\partial \theta}{\partial \lambda} = \alpha \frac{1}{u} \frac{\partial}{\partial u} u \frac{\partial \theta}{\partial u} - \theta \quad (2)$$

where $\lambda = kz/v_0$, $\theta = c/c_0(0)$, $\theta = \theta_0(u)$ at $\lambda = 0$, $u = r/R$, $\alpha = D/kR^2$. Setting $\beta = k_w/kR$ the wall condition may be written as

$$\frac{\partial \theta}{\partial u} = -\frac{\beta}{\alpha} \theta \quad (3)$$

This restricted equation is separable;^{2,3} assuming $\theta(u, \lambda) = h(\lambda)f(u)$ one finds that:

$$\frac{1}{h} \frac{\partial h}{\partial \lambda} = -b \quad \text{or} \quad h = h_0 e^{-b\lambda} \quad (4)$$

and

$$\frac{\partial}{\partial u} u \frac{\partial f}{\partial u} = \frac{1-b}{\alpha} f u + \frac{b}{\alpha} f u^3 \quad (5)$$

where b is a positive number. Letting $d = 1/\alpha$, (5) is first solved by noting that the trial solution $e^{su^2}g(u)$ eliminates the u^3 term when $s = \frac{1}{2} \sqrt{b/\alpha}$. Equation 5 then may be reduced to an equation for g :

$$u g'' + (4su^2 + 1)g' + (4s + 4s^2 - d)u g = 0 \quad (6)$$

$g(u)$ may now be solved by the method of infinite series, assuming

$$g(u) = \sum_{n=0}^{\infty} a_n u^n$$

After some rearrangement and collection of coefficients of like powers of u , the following recursion formula is found:

$$a_n = -\frac{4(n-1)s + 4s^2 - d}{n^2} a_{n-2} \quad (7)$$

The ratio test shows this series to be convergent for $0 \leq u \leq 1$ for finite s and d . Only the even terms of the series satisfy (6), and thus $g(u)$ has been determined in principle except for the initial constant a_0 .¹⁰

Calling $g(u) = G(u)$ when $a_0 = 1$, we now have the exact solution to (2):

$$\theta(\lambda, u) = A_s e^{-b\lambda} e^{su^2} G(u) \quad (8)$$

and the general solution

$$\theta(\lambda, u) = \sum_{|s|} A_s e^{-b\lambda} e^{su^2} G(u) \quad (9)$$

where s values are chosen to meet the wall boundary condition (3) and the A_s are to be determined from initial conditions at $\lambda = 0$. The first few terms of $G(u)$ are given in

$$G(u) = 1 - \left[\frac{4s + 4s^2 - d}{4} \right] u^2 + \left[\frac{(12s + 4s^2 - d)(4s + 4s^2 - d)}{64} \right] u^4 - \dots \quad (10)$$

For suitably low values of s it is also possible to show that (10) becomes

$$G(u) = \frac{\sin \pi(\gamma/2 + 1/2)}{\pi} \int_0^{\infty} \frac{x^{-(\gamma/2 + 1/2)}}{1+x} e^{-25u^2/(1+x)} dx \quad (11)$$

where $\gamma = (4s^2 - d)/4s$. (This result can be verified by expansion of the exponential term in a $1/(1+x)$ power series, followed by integration of each term in the integrand using the Cauchy integral formula,⁶ and a term-by-term comparison with (10).) In practice, however, it was much easier to work with the series (10) than with (11).

Boundary Condition at the Wall. Writing $f(u) = e^{su^2}G(u)$, the boundary equation (3) may be written as:

$$2sG(1) + G'(1) + \frac{\beta}{\alpha} G(1) = 0 \quad (12)$$

This effectively becomes a condition on s , or, in turn, on b , as will now be shown. Further treatment is restricted to reasonably large values of α , a condition approaching the desired behavior mentioned in the beginning, except for wall reaction. The first few terms of $G'(u)$ are given in

$$G'(u) = - \left[\frac{4s + 4s^2 - d}{2} \right] u + \frac{[12s + 4s^2 - d][4s + 4s^2 - d]}{16} u^3 - \dots \quad (13)$$

When (10) and (13) are both evaluated at $u = 1$, (12) is seen to become essentially a power series in s (already shown to be convergent). Solution of (12) then amounts to finding the roots of (12) as a polynomial equation in s . Dealing first with a very simple case, suppose $\beta = 0$ and α is very large (e.g., 1000). s is of order $(1/\alpha)^{1/2}$ and d is of order $1/\alpha$. Keeping only the terms of lowest order in $1/\alpha$ and substituting (10) and (13) into (12), we have

$$-s \frac{d}{2} - s^2 + \frac{d}{2} = 0 \quad (14)$$

Keeping only the two lowest order terms, $s^2 = d/2 = b/4$ and thus $b = 2$. Putting this into eq 4 gives exactly the result expected for the "ideal" case discussed originally since the bulk velocity = $v_0/2$ for cylindrical laminar flow. An inclusion of nonzero β in the above treatment gives the ideal result

$$b = 2(1 + 2\beta) \quad \text{or} \quad k_{\text{exp}} = k + 2k_w/R \quad (15)$$

a result obtained earlier by Kaufman.¹

One may proceed beyond these initial results both analytically and numerically. Equation 12 may be written as

$$s^2 - \left(\frac{d}{2} + \frac{\beta}{\alpha} \right) + s \left(\frac{d}{2} + \frac{\beta}{\alpha} \right) - s^3 + \frac{5}{24} s^4 - \frac{d^2}{16} - \frac{\beta d}{4\alpha} + \frac{7}{24} s^2 d + \frac{\beta s^2}{4\alpha} + \dots = 0 \quad (16)$$

a result which includes explicitly all terms of order $1/\alpha$, $(1/\alpha)^{3/2}$, and $(1/\alpha)^2$. Equation 16 may be developed to give

$$b - b_0 - \sqrt{1/\alpha} \left[\frac{\sqrt{b}}{2} (b - b_0) \right] + \frac{1}{\alpha} \left[\frac{1}{96} (5b^2 - 24 - 96\beta + 28b + 24\beta b) \right] + \dots = 0 \quad (17)$$

where $b_0 = 2(1 + 2\beta)$, the "ideal" result. If the $1/\alpha$ term is dropped, one obtains

$$b = b_0 \quad (18)$$

and

$$b = 4\alpha \quad (19)^{11}$$

as the first two b roots satisfying (12). Keeping the $1/\alpha$ term and assuming a root near b_0 of the form

$$b = b_0 + p\left(\frac{1}{\alpha'}\right)^{1/2} + q\frac{1}{\alpha}$$

one can show that $p = 0$ and so (16) becomes

$$\frac{q}{\alpha} = -\frac{1}{96\alpha}(5b_0^2 - 24 - 96\beta + 28b_0 + 24\beta b_0) \quad (20)$$

keeping only terms in $1/\alpha$.

If $(b_0 - b)/b_0 = F$ is the relative fractional difference between b and the "ideal" b_0 value, then it can be shown that

$$F = \frac{\alpha}{b_0\alpha} = \frac{1}{96\alpha}\left(7b_0 + 16\beta + \frac{24}{b_0}\right) \quad (21)$$

which can be reexpressed as

$$\beta = 2.18F\alpha - 0.318 - \frac{0.545}{b_0} \quad (22)$$

Equation 22 may be interpreted as defining α and β values which produce a certain fractional error F in b relative to b_0 .

To obtain more accurate results corresponding to (22) one must deal with the obvious fact that each power of s appears an infinite number of times in the series forms (10) and (13). It was thus convenient to use an IBM 1130 computer to collect coefficients of s in eq 12 for a large number of terms in $G(u)$ and $G'(u)$. The roots of the resulting polynomial in s were then computed. Representative results of these calculations are shown in Table I.

It should be noted that the top three entries in Table I correspond to an F value of 0.001 for the lowest b root, illustrating the fact that the program was designed to find α and β values corresponding to a given F for comparison with (22). The slope of a β vs. α plot for the top three entries corresponds fairly well to (22) but the intercept at $\alpha = 0$ does not. This occurs because (17) converges rather slowly, especially at low α values, so that the approximations leading to (22) are somewhat inadequate.

Similar calculations are presented in a different manner in Figure 1, where β and α values corresponding to a fixed value of F are plotted for several F values. The plots shown are roughly linear and are approximated by the equation

$$\beta \approx 2.2F\alpha \quad (23)$$

As F increases, the slopes gradually increase from the 2.2 F value of (22).

Applications

Equation 23 may be used to evaluate F for experimental conditions and thus provide either a quantitative assurance that radial effects are negligible or a basis for correcting experimental axial decay values, b , for "nonideal" radial and wall effects. Making use of the relations given in (2), (23) may be arranged to yield

$$F \approx k_w R / 2.4D \quad (24)$$

Recent data of Howard and Evenson⁷ on the reaction of $\text{OH} + \text{NO} + \text{He} \rightarrow \text{HONO} + \text{He}$ may be used to illustrate the application of (24). Assuming an (NO) concentration of about 10×10^{13} molecules cm^{-3} , one can estimate $k_w \approx 0.4$ cm sec^{-1} ; with $D \approx 200$ $\text{cm}^2 \text{sec}^{-1}$ for OH in 4 Torr of He,⁵ and a flow tube radius of about 1 cm, $F \approx 0.001$, implying a negligible deviation from ideal flow behavior in this case. Furthermore, α is sufficiently large (ca. 200) that effects of higher s roots can be ignored (see below). For their study of $\text{CO} + \text{OH} \rightarrow \text{CO}_2 + \text{H}$ in 30 Torr of Ar, use of the same k_w

TABLE I:

$\beta = 0$	$\beta = 2$	$\beta = 4$
$\alpha = 21$	$\alpha = 836$	$\alpha = 1742$
$b_0 = 2$	$b_0 = 10$	$b_0 = 18$
$b = 1.998$	$b = 9.99$	$b = 17.982$
$= 541$	$= 21,500$	$= 44,700$
$\beta = 0$	$\beta = 1$	$\beta = 0$
$\alpha = .23$	$\alpha = 1.18$	$\alpha = .10$
$b_0 = 2$	$b_0 = 6$	$b_0 = 2$
$b = 1.84$	$b = 4.52$	$b = 1.69$
$= 7.9$	$= 36.6$	$= 4.25$

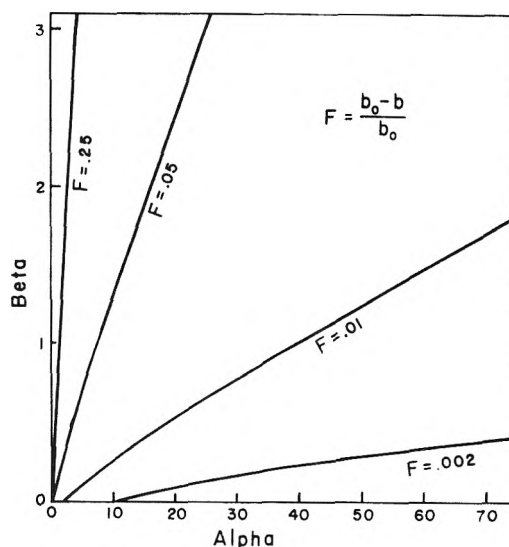


Figure 1. Deviations of b (and hence k_{exp}) from ideality as a function of α and β .

leads to $F \approx 0.03$. k_w was not measured, but a value larger than 0.4 cm sec^{-1} would be reasonable for this reaction and could account in part for the significant 60% drop in measured rate observed at high pressures.⁷

In cases where (24) implies a major correction, β and α may be used to determine a better correction from Figure 1. If $k_w = 0$, then (24) does not apply, but Figure 1 may again be used to estimate errors due solely to decreased radial diffusion.

Further Remarks

Table I shows that low α values give more than one reasonably low value of b , whereas high α values generally yield one low value $b \approx b_0$ and other much higher b values. Reference to (9) suggests that all these solutions should be combined in such a way as to meet the initial concentration conditions at $\lambda = 0$.¹² The point of greatest interest here is that the high b terms of (9) will quickly drop out as λ increases, leaving only the low b values, a phenomenon also discussed elsewhere.⁸ No special problems arise, then, if only one low b value is present, but if two distinct low values are present, further errors may be introduced. In practice, if $\alpha \geq 0.1$, one can assume that only the lowest b term will contribute to observed decay along most of the tube, and the corrections of Figure 1 can be safely applied.

As α decreases, the initial radial concentration profile at $\lambda = 0$ will have an increasing effect on the observed kinetics. If $\alpha = 0$, for example, eq 2 is easily solved: $\theta = \theta_0 \exp[-\lambda/(1 - u^2)]$, and decay constants for the cylindrical

shells will vary from 1 to ∞ . Although this suggests in general that initial conditions will have a great deal to do with the contributions of the various terms in (9), Poirier and Carr have shown for first-order reaction that choice of a constant initial radial concentration together with a technique which observes a cross section of the reaction tube minimizes such problems, even with very small α .⁵ Their numerical calculations for small α of $\log \theta$ vs. λ typically show some initial curvature followed by linear behavior over most of the λ range examined. The linear region suggests dominance by the lowest b root, and it is of some interest to note that the $\beta = 0$, $\alpha = 0.10$, $b = 1.69$ system of Table I is in excellent agreement with the final slopes calculated for these β and α parameters by Poirier and Carr.

The right side of (24) is very close to Kaufman's result for radial concentration gradients for slight deviations from "ideal" flow,¹ and (24) therefore clearly supports the usual assumption that a concentration gradient of 1% or less produces negligible effects on observed kinetics. Furthermore, it may be noted that the $\partial^2 c / \partial z^2$ term of (1) may be treated as a perturbation of the exact solutions of (2), leading to the result

$$b_{\text{corr}} = b \left(1 - \frac{b}{2} \frac{4Dk_{\text{gas}}}{v_0^2} \right) \quad (25)$$

The treatment and result correspond to those of Kaufman.¹ Equation 25 will not be valid for large b values, however, first because (25) is based on the assumption that $c(r)$ is nearly constant, and more importantly because $\partial^2 c / \partial z^2$ will not be small for very large b values.

Finally, if slip flow is included, the $1 - u^2$ term of (2) becomes $\epsilon - u^2$, where $\epsilon = 1 + 2.76 (\lambda_1 / PR)$.³ The subsequent

analyses are similar to those given here, with slight modification of the results for (10) and (13). Equation 15 becomes, for example, $k_{\text{exp}} = (1/\epsilon)(k + 2k_w/R)$, as expected for the ideal slip flow case. More refined calculations, such as those leading to Table I or Figure 1, must be done separately for each new ϵ value, however.

Acknowledgment. Much of the initial work on this problem was carried out in the Advanced Study Fellowship Program of the National Center for Atmospheric Research. Helpful discussions with Dr. Eric Allen and Dr. Geert Moortgat are gratefully acknowledged.

References and Notes

- (1) F. Kaufman in "Progress in Reaction Kinetics", G. Porter, Ed., Vol. 1, Pergamon Press, New York, N.Y., 1961, pp 11-13.
- (2) R. W. Huggins and J. H. Cahn, *J. Appl. Phys.*, **38**, 180 (1967).
- (3) R. C. Bolden, R. S. Hemsworth, M. J. Shaw, and N. D. Twiddy, *J. Phys. B, Atom. Mol. Phys.*, **3**, 45 (1970).
- (4) R. E. Walker, *Phys. Fluids*, **4**, 1211 (1961).
- (5) R. V. Poirier and R. W. Carr, Jr., *J. Phys. Chem.*, **75**, 1593 (1971).
- (6) R. V. Churchill, "Complex Variables and Applications", 2nd ed, McGraw-Hill, New York, N.Y., 1960, pp 168-171.
- (7) C. J. Howard and K. M. Evenson, *J. Chem. Phys.*, **61**, 1943 (1974).
- (8) E. E. Ferguson, F. C. Fehsenfeld, and A. L. Schmeltekopf, *Adv. At. Mol. Phys.*, **5**, 1 (1969).
- (9) k_w of this notation system is used throughout this paper and is equal to the k_w of Kaufman's paper¹ multiplied by $R/2$.
- (10) As $u \rightarrow 0$, $4su^2 + 1 \rightarrow 1$ and (6) becomes arbitrarily close to a Bessel equation. This implies that the second general solution will be a logarithmic function of u near $u = 0$. The singularity of this solution at $u = 0$ makes it of no physical interest.
- (11) Since α is assumed to be large here, this b value will also be large, and several terms which have been dropped will in fact be significant. Equation 19 is therefore only likely to be a crude approximation for this high b value (cf. Table I).
- (12) Although this can be done, it should be noted that a sufficiently high b value can make the $\partial^2 c / \partial z^2$ term of (1) important relative to the radial terms. As this would invalidate (2) and subsequent development, the higher b values may only be of qualitative interest.

Rates of Reaction of Hydrogen Atoms with Silane and Germane¹

Kwang Yul Choo, Peter P. Gaspar,* and A. P. Wolf

Departments of Chemistry, Brookhaven National Laboratory, Upton, New York 11973, and Washington University, Saint Louis, Missouri 63130 (Received March 5, 1973; Revised Manuscript Received May 2, 1975)

Publication costs assisted by the United States Energy Research and Development Administration

The rates of reaction of hydrogen atoms with silane, germane, and (for comparison) ethylene have been determined at 20 Torr in a discharge flow system. The apparent bimolecular rate constants are 8.5×10^{-12} , 4.3×10^{-10} , and 3.5×10^{-13} $\text{cm}^3 \text{ molecule}^{-1} \text{ sec}^{-1}$, respectively, which are substantially larger than previously reported values. Activation energies were calculated by the empirical methods of Johnston (BEBO) and Spirin and compared with the values estimated from the experimental rate constants. The experimentally estimated values are lower than those predicted by the BEBO method, suggesting that the activated complex for reaction of hydrogen atoms with silane and germane may differ from the simple linear model for hydrogen atom transfer.

Introduction

Reactions of hydrogen atoms with various hydrocarbons have been studied for many years.² However no direct ki-

netic study of reactions of atomic hydrogen with the methane analogs silane and germane has been published until recently.³

Recently reactions of hydrogen atoms,⁴ methyl radical,⁵ and trifluoromethyl radical⁶ with silicon and germanium hydrides and alkylsilanes have been reported. The results

* To whom correspondence should be addressed at Washington University.

indicate that compounds of silicon usually react more rapidly than their carbon analogs, principally due to the lower activation energy of the silicon reaction. Hot tritium reactions with silane and methylsilanes have also been studied.⁷ The Si-C bond was found to be more reactive than the C-C bond and Si-H more reactive than C-H. In 1966 Niki and Mains⁸ first suggested that the reaction rate of atomic hydrogen with silane might be greater than that of the reaction with ethylene. It was observed that added ethylene, which was known to be a good scavenger of atomic hydrogen in hydrocarbon reaction systems, affected neither the yield nor the isotopic ratio ($H_2:HD:D_2$) of molecular hydrogen produced in the mercury-photosensitized decomposition of SiH_4-SiD_4 mixtures.

We have studied the absolute rates of reaction of hydrogen atoms with silane, germane, and ethylene in order to shed new light on the reactivity of Si-H and Ge-H bonds and in order to assess the usefulness of ethylene as a radical scavenger in silane and germane. In order to assist in the interpretation of our results, estimates have been made of the activation energy for hydrogen abstraction, following the procedure used by Strausz, Gunning, and coworkers.^{3a,5b,6b}

Experimental Section

A schematic diagram of the flow discharge-atomic absorption system is shown in Figure 1.

The main flow line was made of 12-mm inner diameter glass tubing and the reaction zone (from D to the optical cell in Figure 1) was treated with orthophosphoric acid to reduce the wall recombination of atomic hydrogen. The pressures in the flow line and the substrate reservoir (S) were measured with Statham gauge transducers which were precalibrated with a fused-quartz absolute pressure gauge (Texas Instruments). The uncertainty in the pressure measurement is less than 1% in the range from 1 to 100 Torr. The helium flow rate in the main flow line was measured with a precalibrated ball-type flowmeter (Manostat Co.), while the substrate flow rate was calculated by monitoring the pressure drop in the substrate reservoir. Microwave discharges of 2450 MHz maintained with Evenson air-cooled microwave cavities⁹ were used for both the main flow line and the flow emission lamp. Since the concentration of hydrogen atoms generated in the flow line and the emission intensity of the lamp are dependent on the power input, pressure, and the input concentration of molecular hydrogen, these parameters were kept constant during each experiment. The discharge power input was measured with a bidirectional power meter (Ophos Ins.). Through inlets of minimum diameter (for the reduction of turbulence), substrates were injected along the axis of the flow tube to ensure complete mixing with the gas stream carrying the hydrogen atoms. The five inlet tubes were located 5 cm apart from each other, with the first inlet 35 cm and the last inlet 15 cm from the absorption cell.

Optical Parts. (i) *Emission Lamp.* A microwave discharge in hydrogen-doped helium was used as the Lyman α -line source. To reduce the self-reversal of the emission line, the concentration of hydrogen and the distance between the discharge and the LiF window were made as small as possible. The pressure in the lamp and the microwave power input were maintained at as low levels as possible to minimize Doppler and pressure broadening of the emission line. A similar microwave discharge flow lamp was used by Clyne and Cruse.¹⁰

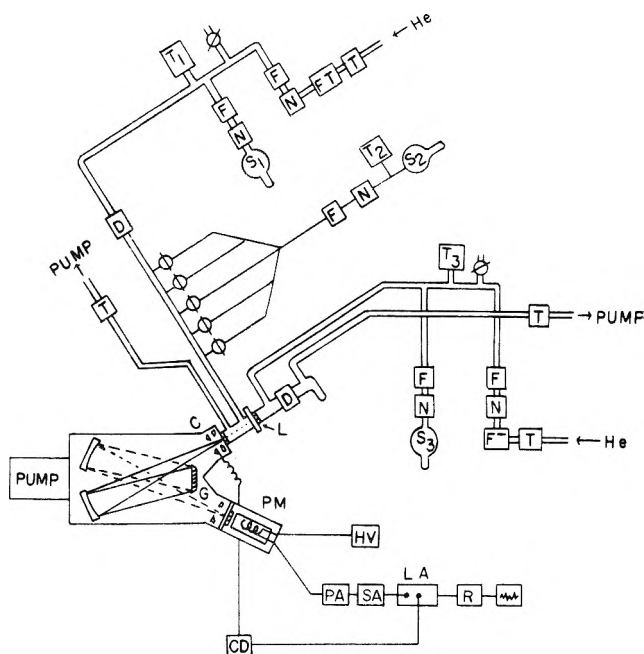


Figure 1. Discharge flow line: T, -196° trap; FT, filter; N, needle valve; F, flowmeter; S, substrate reservoir; T_1 , T_2 , T_3 , pressure transducers; D, microwave discharge; L, LiF window; C, chopper; PM, photomultiplier tube; CD, chopper driving unit; G, grating; HV, high-voltage supply; PA, preamplifier; SA, selective amplifier; LA, lock-in amplifier; R, recorder.

Self-reversal was considered negligible at the very low microwave input power and the low optical density of the lamp employed. The linearity of first-order decay plots ($\ln [H]$ vs. time) for hydrogen atoms in the presence of ethylene suggests that the Beer-Lambert law is obeyed under these conditions.¹¹

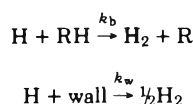
(ii) *Monochromator and Detector.* The Lyman α -emission line was isolated by a 0.3-m McPherson Model 213 monochromator with 60–120- μ entrance slit widths and a 1200-groove/mm grating with was coated with MgF_2 . The pressure inside the monochromator was always less than 10^{-6} Torr. At the exit slit a Model 650 McPherson photomultiplier detector (equipped with an EMI type 9514 photomultiplier tube) was attached with a vacuum-tight window which was coated with sodium salicylate. The photomultiplier output was preamplified and tuned to the frequency (100 Hz) of the electrical chopper (Bulova Co. Type L40C) which was positioned next to the entrance slit.

Materials. The source of compounds used and the nominal purities are as follows: hydrogen, Matheson Gas Products, 99.95%; silane, Matheson Gas Products, semiconductor grade; germane, Matheson Gas Products, 99.9%; ethylene, Phillips Petroleum Co., research grade 99.98%. The purity of these compounds was checked by gas chromatography (SiH_4 , GeH_4 , C_2H_4), infrared spectroscopy (SiH_4 , GeH_4), emission spectroscopy (H_2), and mass spectrometry (SiH_4 , GeH_4).

Kinetic Measurements. All absorption measurements were performed at less than 30% absorption to avoid deviations from the Beer-Lambert law. Linear velocity and the pressure in the line were maintained at rather high values to minimize the back-diffusion of hydrogen atoms and reaction substrates. This was necessary since the reaction rates were very fast. In a kinetic experiment, both microwave discharges were first turned on. Then, after selecting

the Lyman α -emission line by manually rotating the grating with the proper slit width set (usually between 60 and 120 μ) to give maximum signal intensity, the detector electronics were adjusted to give full scale on the recorder (I_0) for the unattenuated emission line. Hydrogen was then slowly added into the helium stream of the main flow line (the H_2 input concentration was less than 0.1% in the helium stream) until the transmitted light intensity (I) was reduced to about 70–80% of that of the original light intensity (i.e., $(I_0 - I)/I_0 \approx 20$ or 30%) by atomic absorption due to hydrogen atoms produced by the dissociation of H_2 . Next the desired capillary inlet was opened and the flow of substrate was slowly increased until a noticeable change in the atomic absorption was observed. This procedure was repeated for all the other capillary inlets and with various substrate concentrations in randomly chosen order. The substrate flow rate was determined by monitoring the pressure drop with exactly the same flow rate and pressure in the main flow line at the end of each kinetic experiment.

If we assume the flow is laminar and neglect diffusion of hydrogen atoms into helium,¹² the disappearance of the hydrogen atom can be written



so

$$-d[H]/dt = [H]\{k_b[RH] + k_w\} \quad (1)$$

Under the condition that $[RH]$ is almost constant during the reaction, eq 1 has the solution

$$\ln [H] - \ln [H]_{00} = -\{k_b[RH] + k_w\}t \quad (2)$$

where $[H]_{00}$ is the concentration of hydrogen atoms at substrate injection point, $t = x/V$, x is the distance between injection and the detection point, and V is the linear velocity of helium flow.

However, for an observation point at which $[H]$ is measured fixed with respect to the point at which hydrogen atoms are generated, the loss of hydrogen atoms due to wall reaction is independent of substrate concentration and we may write¹³

$$\ln [H] - \ln [H]_0 = -k_b[RH]t = -k_{\text{obsd}}t \quad (3)$$

where $[H]_0$ is the concentration of hydrogen atoms at detection point at zero substrate concentration. The relative concentration of atomic hydrogen can be obtained from the Beer-Lambert law

$$[H] = (1/k_a l) \ln (I_0/I) \quad (4)$$

where k_a is the absorption coefficient, l is the effective optical path length, I_0 is the intensity of the transmitted emission line without attenuation by atomic hydrogen, and I is the intensity of the transmitted line with atomic hydrogen in the optical path. Since k_a and l are constant under our experimental conditions, eq 3 and 4 indicate that a plot of $\ln \{ \ln (I_0/I) \}$ vs. t should give a straight line with slope k_{obsd} , and then k_b can be obtained from the slope of the k_{obsd} vs. $[RH]$ plot.

$$\ln \{ \ln (I_0/I) \} = \ln \{ \ln (I_0/I) \}_0 - k_{\text{obsd}}t \quad (5)$$

If the silyl or germyl radicals formed by hydrogen abstraction reacted principally by recombination with hydrogen atoms, as has been suggested for similar systems,^{4a}

TABLE I: Input Parameters for Calculation of Activation Energies

Parameter	Value	Ref
Bond dist, \AA		
Si-H	1.48	a
Ge-H	1.53	a
H-H	0.74	b
Bond energies (E), kcal/mol		
SiH ₃ -H	98.3	c
GeH ₃ -H	90.2	c
H-H	109.4	b
Bond energy index (p)		
Si-H	1.004	d
Ge-H	0.937	d
H-H	1.041	d
Force const $\times 10^5$, dyn/cm		
Si-H	2.9	a
Ge-H	2.6	a
H-H	5.7	e
Morse parameter (β)		
Si-H	1.414	f
Ge-H	1.46	f
Refractive index (P)		
H	1.02	g
Si	9.06	g
Ge	11.08	g
C	2.08	g
Fundamental str vib, cm^{-1}		
Si-H	2190	h
Ge-H	2110	h
H-H	4395	i

^a G. Thyagarajan, H. Herranz, and F. F. Cleveland, *J. Mol. Spectrosc.*, **7**, 154 (1961); E. B. Wilson, Jr., J. C. Decius, and P. C. Cross, "Molecular Vibrations", McGraw-Hill, New York, N.Y., 1955. ^b Reference 14. ^c Reference 22. ^d Calculated using the relationship $p = 0.26 \ln (E_{1S}/E_X)/(R_X - R_{1S})$ (see ref 14). E_X and R_X are the Lennard-Jones parameters for the noble gas equivalents of the Si-H (Ar-He) and Ge-H (Kr-He) bonds, and E_{1S} and R_{1S} are the bond energy and bond length, respectively. The subscript X refers to the noble gas equivalent and the subscript 1S to the Si-H and Ge-H bonds. ^e C. L. Kibby and R. E. Weston, Jr., *J. Chem. Phys.*, **49**, 4825 (1968). ^f Calculated using the relationship $\beta = 1.2177 \times 10^7 \omega_e (\mu/E_{3S})^{1/2}$ (see G. Herzberg, "Spectra of Diatomic Molecules", Van Nostrand-Reinhold, Princeton, N.J., 1950). ω_e is the fundamental vibrational stretching frequency for the Si-H or Ge-H bond, μ is the reduced mass of SiH₃-H or GeH₃-H, and E_{3S} is equivalent to E_{1S} of footnote d. ^g S. S. Batsanov, "Refractometry and Chemical Structure", translated by P. P. Sutton, Consultants Bureau, New York, N.Y., 1961. ^h K. Venkateswarlu and S. Sundaram, *J. Chem Phys.*, **23**, 2365 (1955), and ref 15. ⁱ T. Schimanonchi, *Natl. Stand. Ref. Data Ser., Natl. Bur. Stand.*, No. 6.

then the overall stoichiometry would be $2H + RH \rightarrow H_2 + RH$ and a stoichiometry correction would need to be applied to obtain k_b from k_{obsd} .

Calculation of Activation Energies

Calculations were carried out according to the bond energy bond order (BEBO) method of Johnston^{14,15} and the empirical method of Spirin.¹⁶ Input parameters for the calculations are given in Table I. Properties of activated complexes calculated by the BEBO method are given in Table

TABLE II: Properties of Activated Complexes Calculated by the BEBO Method

Property ^a	H ₃ Si···H···H	H ₃ Ge···H···H
n_1^\ddagger	0.75	0.88
n_2^\ddagger	0.25	0.12
$R_1^\ddagger, \text{Å}$	1.56	1.56
$R_2^\ddagger, \text{Å}$	1.10	1.29
$F_{11}^\ddagger \times 10^5, \text{dyn/cm}$	2.04	2.33
$F_{22}^\ddagger \times 10^5, \text{dyn/cm}$	-0.12	-0.26
$F_{12}^\ddagger \times 10^5, \text{dyn/cm}$	0.83	0.36
$F_\theta^\ddagger \times 10^{11}, \text{erg/radian}$	0.063	0.046
$\nu_s^\ddagger, \text{cm}^{-1}$	1369	1642
$\nu_b^\ddagger, \text{cm}^{-1}$	588	448
$\nu_i^\ddagger, \text{cm}^{-1}$	1303 <i>i</i>	904.2 <i>i</i>

^a Symbols defined in ref 14.**TABLE III: Calculated and Observed (Estimated from Experiment) Activation Energies for the Reaction H + RH → H₂ + R (R = CH₃, SiH₃, GeH₃)**

Reaction	$E_a(\text{BEBO}),^a$ kcal/mol	$E_a(\text{Spirin}),$ kcal/mol	Estd or determined by expt ^a
H + CH ₃ → H ₂ + CH ₃	11 ^b	12.8	11.8 ^d
H + SiH ₄ → H ₂ + SiH ₃	8.5 (98.3) 6.5 (94.3)	4.3 ^c 3.7	≤3.8 ^a
H + GeH ₄ → H ₂ + GeH ₃	5.2	2.7	≤1.5 ^a

^a Estimated from the experimentally determined rate constants at 300°K and assumed frequency factor $\log A = 14 + 1.4 = 15.4$ cm³ mol⁻¹ sec⁻¹. ^b Reference 14. ^c Niki and Mains⁸ have obtained 0.5 kcal/mol, but this value seems to have been estimated from thermochemically determined Si-H bond dissociation energy (= 78 kcal/mol). ^d Without including tunneling correction. Values in parentheses are the bond dissociation energies (Si-H) used in the calculation (including zero-point energy). ^e Reference 17a.

II, and activation energies, in Table III. Activation energies calculated with Spirin's equation, also given in Table III, agree well with the values estimated from experiment.

Results

Figure 2 shows the kinetic plots of $\ln [H]$ vs. t for two concentrations of SiH₄ and one of GeH₄. The linearity indicates that pseudo-first-order conditions prevailed under our experimental conditions. In GeH₄ + H reactions, however, $\ln [H]$ vs. t plots gave slight upward curvature at longer reaction times. The reaction of hydrogen atoms with germane is so rapid that only a very low concentration of germane is required for a rapid decrease in hydrogen atom concentration. At these low germane concentrations partial depletion of germane during reaction leads to a diminished rate of disappearance of hydrogen atoms. This deviation from first-order decay could be avoided if one used shorter reaction times and could detect very small changes in atomic hydrogen concentration. The practical constraint on the use of shorter reaction times is the maximum flow rate attainable by the available pumping speed. The minimum detectable concentration of hydrogen atoms is limited by the optical path length of the absorption cell and the

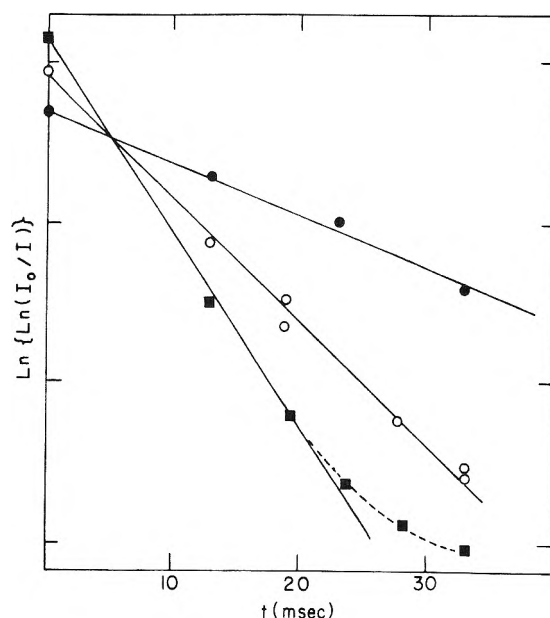


Figure 2. $\ln [H]$ vs. t (the slope is k_{obsd}) for GeH₄ and SiH₄: ●, [SiH₄] = 0.5×10^{13} molecules/cm³; ○, [SiH₄] = 1.0×10^{13} molecules/cm³; ■, [GeH₄] = 3.1×10^{11} molecules/cm³.

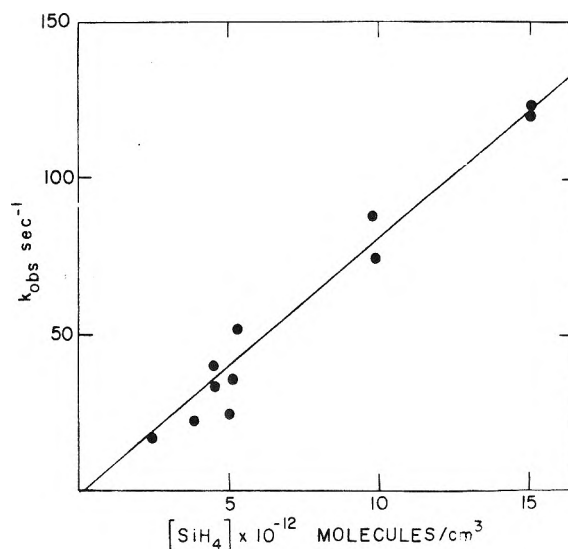


Figure 3. k_{obsd} vs. [SiH₄]; slope is $k_{\text{bim}}(\text{H} + \text{SiH}_4 \rightarrow)$.

stability of the light source and the detector circuitry. The hydrogen atom concentration is estimated to be 10^{11} – 10^{12} molecules/cm³ under the present experimental conditions. Sensitivity could be increased by multiple reflectance techniques. In the germane experiments the linear portion (first part) of the kinetic plot is utilized for rate measurements. As a consequence the error in the rate constant of the GeH₄ + H reaction may be slightly greater than that of the silane reaction. Figure 3 shows a plot k_{obsd} vs. [SiH₄], whose linearity indicates that the reaction is first order with respect to SiH₄. This linear dependence of the observed first-order rate constant for disappearance of hydrogen atoms on the silane concentration demonstrates that pseudo-first-order conditions prevail. Table IV includes the conditions for the rate measurement of the H + SiH₄ reaction as well as the rate constants.

The poisoning of the glass wall with orthophosphoric

TABLE IV: Data for the Measurement of $k_{\text{bim}}(\text{H} + \text{SiH}_4)$ at 300°K, 20 Torr, and 1010 cm/sec Linear Velocity^a

$10^{-12}[\text{SiH}_4]$, mole- cules/cm ³	k_{obsd} , ^b sec ⁻¹	$10^{-12}[\text{SiH}_4]$, mole- cules/cm ³	k_{obsd} , ^b sec ⁻¹
2.4	15.6 ± 4	5.2	61 ± 4
3.8	20.4 ± 4	9.7	88 ± 5, 74 ± 5
4.5	33 ± 4, 39 ± 4	15.0	120 ± 5, 122 ± 5
5.0	24 ± 4, 35 ± 4		

^a $k_{\text{bim}} = (8.5 \pm 0.7) \times 10^{-12} \text{ cm}^3 \text{ molecule}^{-1} \text{ sec}^{-1}$, with no stoichiometric correction applied. ^b These error limits are the standard deviations of the slope of the $\ln(I_0/I)$ vs. t plots. Since values of k_{obsd} for separate experiments differ by a greater amount, systematic errors obviously contribute to the total error which is ca. ±40%.

acid was essential since without wall coating only about 10–20% of the hydrogen atoms reached the absorption cell compared to the number which survived to that point when the wall was coated.

The experimentally determined rate constants along with reported values from the literature are shown in Table V. All the rate constants at 300°K taken from the literature were calculated from the most recently reported values of activation energies and frequency factors. To facilitate comparison of these results we measured the rate of reaction for the well-studied system $\text{H} + \text{C}_2\text{H}_4$ under the same conditions as $\text{H} + \text{SiH}_4$ and $\text{H} + \text{GeH}_4$.

Table III compares activation energies, estimated from the experimental rate constants by assuming a maximum frequency factor $\log A = 15.4 \text{ cm}^3 \text{ mol}^{-1} \text{ sec}^{-1}$,¹⁷ with values calculated by the BEBO and Spirin methods.

Discussion

The reaction rates of hydrogen atoms with silane and germane are both faster than that for $\text{H} + \text{CH}_4$ and even faster than the well-known hydrogen atom scavenging reaction $\text{H} + \text{C}_2\text{H}_4$ at room temperature. Although Niki and Mains⁸ have questioned the scavenging ability of ethylene for hydrogen atoms in silane, the failure to observe this scavenging effect has been interpreted as indicating the absence of hydrogen atoms in the reaction system. Obi et al. used ethylene scavenger to search for the possible formation of H atoms in the photolysis of CH_3SiD_3 .^{3b} The hydrogen isotopic product ratio (i.e., HD:H₂) was not altered by the presence of ethylene, a finding which was believed to preclude the formation of H atoms in the reaction pathway. These workers reported that the rate of addition of deuterium atoms to C_2D_4 is 5.5 times the rate of reaction with CH_3SiD_3 . In the thermal decomposition of $\text{GeH}_4 + \text{D}_2$ mixtures, Taylor and coworkers¹⁸ based their suggestion of $\text{GeH}_4 \rightarrow \text{GeH}_2 + \text{H}_2$ as the primary step upon the observation that no HD was found in the reaction product. This interpretation rests on the assumption that $\text{H} + \text{D}_2$ ($k = 0.2 \times 10^{-15} \text{ cm}^3 \text{ molecule}^{-1} \text{ sec}^{-1}$)¹⁹ is faster than $\text{H} + \text{GeH}_4$. Since $\text{H} + \text{GeH}_4$ is in fact much faster than $\text{H} + \text{D}_2$, D_2 could not give any HD even if the decomposition of germane did produce hydrogen atoms. Rousseau and Mains have suggested a very rapid reaction of hydrogen atoms (which they believed to be hot) with germane to explain the

TABLE V: Rate Constants of Hydrogen-Transfer Reactions of Group 4 Hydrides at 300°K

Reaction	Rate const, cm ³ molecule ⁻¹ sec ⁻¹	Ref
$\text{H} + \text{CH}_4 \rightarrow \text{H}_2 + \text{CH}_3$	3.2×10^{-18}	^a
$\text{H} + \text{SiH}_4 \rightarrow \text{H}_2 + \text{SiH}_3$	$(8.5 \pm 0.7) \times 10^{-12f}$	This work
$\text{H} + \text{GeH}_4 \rightarrow \text{H}_2 + \text{GeH}_3$	$(4.3 \pm 0.3) \times 10^{-10f}$	This work
$\text{CH}_3^* + \text{CH}_4 \rightarrow \text{CH}_4 + \text{CH}_3$	5.0×10^{-23}	^b
$\text{CH}_3^* + \text{SiH}_4 \rightarrow \text{CH}_4 + \text{SiH}_3$	9.0×10^{-18}	^c
$\text{CF}_3 + \text{SiH}_4 \rightarrow \text{CF}_3\text{H} + \text{SiH}_3$	1.1×10^{-16}	^d
$\text{H} + \text{C}_2\text{H}_4 \rightarrow \text{C}_2\text{H}_5^*$	$(3.5 \pm 0.1) \times 10^{-13f}$ (20 Torr)	This work
	$(5.26 \pm 0.13) \times 10^{-13}$ (20 Torr)	^e

^a References 17a and b. ^b F. S. Dainton, K. J. Ivin, and F. Wilkinson, *Trans. Faraday Soc.*, **55**, 929 (1959); G. A. Creak, F. S. Dainton, and K. J. Ivin, *ibid.*, **58**, 326 (1962). ^c Reference 5b. ^d Reference 6b. ^e M. J. Kurylo, N. C. Peterson, and W. Braun, *J. Chem. Phys.*, **53**, 2776 (1970). ^f The error limits are the standard deviations of the slope of the k_{obsd} vs. concentration plots. The estimated total errors are ±50%.

lack of scavenging of hydrogen atoms by propylene in the mercury-sensitized decomposition of germane.^{4a}

Recently Glasgow et al.^{3a} reported the relative rate constant $k(\text{D} + \text{C}_2\text{D}_4)/k(\text{D} + \text{SiH}_4) = 1.2$ in the photolysis of a C_2D_4 - SiH_4 mixture at -130° in the liquid phase. From our experimental values $k(\text{H} + \text{SiH}_4) = (8.5 \pm 0.7) \times 10^{-12} \text{ cm}^3 \text{ molecule}^{-1} \text{ sec}^{-1}$ and $k(\text{H} + \text{C}_2\text{H}_4) = 3.5 \pm 0.1 \times 10^{-13} \text{ cm}^3 \text{ molecule}^{-1} \text{ sec}^{-1}$ we obtain $k(\text{H} + \text{C}_2\text{H}_4)/k(\text{H} + \text{SiH}_4) = 0.04$ at 300°K and 20 Torr. Therefore, ethylene appears to be a very poor scavenger for hydrogen atoms in gaseous silane.

The experimentally determined rate constants for reactions of hydrogen atoms with silane and germane respectively are difficult to reconcile with the model for hydrogen atom transfer used to calculate the energy of activation by the BEBO method of Johnston.¹⁴ This semiempirical method usually gives energies of activation within 2 kcal/mol of experimental values.¹⁴ In the $\text{H} + \text{SiH}_4$ reaction the activation energy estimated from the experimental rate constant is 4.7 kcal/mol less (3.8 vs. 8.5) than that calculated by the BEBO method. The calculated value is however very sensitive to the SiH bond strength employed as an input parameter. A change in this parameter of 10% will change the calculated activation energy by more than 30%, since it also changes the ρ and β parameters. $D(\text{Si-H}) = 98.2 \text{ kcal/mol}$ (including zero-point energy) has given most satisfactory agreement between experimental E_a (7.0 and 6.0 kcal/mol) and calculated E_a (8.2 and 6.9 kcal/mol) for the reactions of methyl radicals with silane and disilane, respectively.^{5b}

This bond dissociation energy has been notoriously controversial.²⁰ The values of Steele and Stone,²¹ $D(\text{SiH}_3\text{-H}) = 94 \pm 3 \text{ kcal/mol}$, and Saalfeld and Svec,²² 95.2 kcal/mol, both obtained from electron-impact experiments, are gen-

erally accepted in place of the average bond dissociation energy, 76.8 kcal/mol.²³ We have used the electron-impact value,²² although this method often overestimates the bond dissociation energy. Even if the bond energy input parameter is reduced from 98.2 to 88.2 kcal/mol the BEBO calculation still gives an energy of activation (4.6 kcal/mol) 0.8 kcal/mol higher than estimated. The estimate uses the log of that Arrhenius preexponential factor for hydrogen abstraction from methane, *increased* by 10%. Therefore the activation energies estimated from experiment can be regarded as a maximum for the hydrogen atom transfer model. The assumed preexponential factor is near the upper limit for bimolecular reactions.²⁴

A recent modification of the BEBO calculation has predicted lower activation energies for hydrogen-transfer reactions than is normally obtained.²⁵

While it can be argued that the discrepancies between the BEBO activation energy and the values estimated from the H + SiH₄ and H + GeH₄ experiments are due to inaccuracies in the input parameters for the BEBO calculation, the differences may have another, more interesting origin.

The model used for the BEBO calculation is a linear activated complex H...H...R. Should the activated complex be nonlinear, or should a tunneling correction be significant, the discrepancies might be removed. In related systems, tunneling corrections as great as 2 kcal/mol have been calculated.¹⁴

A more interesting possibility is that the overall reaction H + MH₄ → H₂ + MH₃ involves an intermediate adduct MH₅.²⁶ This has been suggested recently by Glasgow, Olbrich, and Potzinger,^{3a} who have employed isotopic labeling experiments and quantum chemical calculations to explore for an intermediate adduct. The neutral radical SiH₅ was found to be at least 3.6 eV lower in energy than H + SiH₄. Therefore the addition of hydrogen atoms to silane and germane must be seriously considered as an explanation for the failure of a hydrogen atom transfer model to predict correctly the reaction rate for hydrogen atoms with silane and germane. The adduct radicals need not be stable, and the suggestion that SiH₅ is long-lived has been withdrawn.^{3e}

Further speculation about the activation energy for reactions of hydrogen atoms with silane and germane is pointless until the temperature dependence of the rate constant is determined experimentally. It should be noted that in contrast to the BEBO activation energies, the Spirin equation gives values in reasonable agreement with the estimates based on experiments.

The absolute rate constant determined in this work for the reaction of hydrogen atoms with silane is more than an order of magnitude greater than the value published by Obi, Sandhu, Gunning, and Strausz^{3a} ((8.5 ± 0.7) × 10⁻¹² vs. 1.9 × 10⁻¹³ cm³ molecule⁻¹ sec⁻¹)²⁷ for the reaction of deuterium atoms with silane. Recently a value of (3.0 ± 1.0) × 10⁻¹³ cm³ molecule⁻¹ sec⁻¹ has been reported for the rate constant for D + SiH₄.^{3e} A large isotope effect in H + SiH₄ vs. D + SiH₄ may contribute to the apparent discrepancy, and application of a stoichiometric correction would decrease our rate constant by 50%. A lower limit of 2.2 × 10⁻¹³ cm³ molecule⁻¹ sec⁻¹ has been reported for the rate constant for H + SiH₄.^{3c}

In summary, it has been found that the reactions of hydrogen atoms with silane and germane are very rapid, the rate constants being 1 and 3 orders of magnitude greater, respectively, than that for addition of hydrogen atoms to

ethylene. The activation energies calculated by the BEBO method are higher than the values estimated from experiment, the discrepancies giving rise to some questions about the applicability of a linear hydrogen atom transfer model for the activated complexes in these systems.

References and Notes

- (1) This work was carried out at the Brookhaven National Laboratory under the auspices of the U. S. Atomic Energy Commission. Partial support from special research support agreement AT(11-1)-1713 is gratefully acknowledged. This is technical Report No. COO-1713-37.
- (2) (a) A. F. Trotman-Dickenson and G. S. Milne, *Natl. Stand. Ref. Data Ser., Natl. Bur. Stand., No. 9* (1967); (b) B. A. Thrush, *Prog. React. Kinet.*, **3**, 63 (1965).
- (3) (a) During the preparation of this article the results of photochemical competition experiments giving the relative rate of reaction of hydrogen atoms with ethylene as 1.2 and 1.88 times that with silane have been published: L. C. Glasgow, G. Olbrich, and P. Potzinger, *Chem. Phys. Lett.*, **14**, 466 (1972); K. Obi, H. S. Sandhu, H. E. Gunning, and O. P. Strausz, *J. Phys. Chem.*, **76**, 3911 (1972). (b) A kinetic isotope effect in the reactions D + CH₃SiH₃ and D + CH₃SiD₃ has also been estimated in a photochemical experiment: K. Obi, A. Clement, H. E. Gunning, and O. P. Strausz, *J. Am. Chem. Soc.*, **91**, 1622 (1969). (c) G. K. Moortgat, Ph.D. Thesis, University of Detroit; *Diss. Abstr. Int. B*, **31**, 1879 (1970). (d) J. Hong, Ph.D. Thesis, University of Detroit, 1972. (e) D. Michelcic, P. Potzinger, and R. N. Schindler, *Ber. Bunsenges. Phys. Chem.*, **78**, 82 (1974). (f) P. Potzinger, L. C. Glasgow, and B. Reiman, *Z. Naturforsch., Teil A*, **29**, 493 (1974).
- (4) (a) Y. Rousseau and G. J. Mains, *J. Phys. Chem.*, **70**, 3158 (1966); (b) M. A. Contineanu, D. Michelcic, and R. N. Schindler, *Ber. Bunsenges. Phys. Chem.*, **75**, 426 (1971); (c) T. L. Pollock, H. S. Sandhu, A. Jodhan, and O. P. Strausz, *J. Am. Chem. Soc.*, **95**, 1017 (1973).
- (5) (a) E. R. Morris and J. C. J. Thynne, *J. Phys. Chem.*, **73**, 3294 (1969); (b) O. P. Strausz, E. Jakubowski, H. S. Sandhu, and H. E. Gunning, *J. Chem. Phys.*, **51**, 552 (1969).
- (6) (a) E. R. Morris and J. C. J. Thynne, *Trans. Faraday Soc.*, **66**, 183 (1970); (b) E. Jakubowski, H. S. Sandhu, H. E. Gunning, and O. P. Strausz, *J. Chem. Phys.*, **52**, 4242 (1970).
- (7) (a) G. Cetini, O. Gambino, M. Castiglioni, and P. Volpe, *J. Chem. Phys.*, **46**, 89 (1967); (b) S. H. Daniel and Y. N. Tang, *J. Phys. Chem.*, **73**, 4378 (1969); (c) J. Wilkin and R. Wolfgang, *ibid.*, **72**, 2631 (1968); (d) T. Tomimaga, A. Hosaka, and F. S. Rowland, *ibid.*, **73**, 465 (1969).
- (8) H. Niki and G. J. Mains, *J. Phys. Chem.*, **68**, 304 (1964).
- (9) F. C. Fehsenfeld, K. M. Evenson, and H. P. Broida, *Rev. Sci. Instrum.*, **36**, 294 (1965).
- (10) M. A. Clyne and H. W. Cruse, *Trans. Faraday Soc.*, **67**, 2869 (1973).
- (11) Strictly, the linearity of the ln [H] vs. time plots demonstrates the relationship $\log (I/I_0) = -\alpha([H])^\gamma$ where γ need not be unity; see R. J. Donovan, D. Husain, and L. J. Kirsch, *Trans. Faraday Soc.*, **66**, 2551 (1970).
- (12) If one considers diffusion, $k_{\text{obsd}}(\text{diff}) = k_{\text{obsd}}(1 + k_{\text{obsd}}D/V^2)$, where D is the diffusion coefficient of an H atom into He and V is linear velocity. At the pressure and linear flow rate employed in experiments, $k_{\text{obsd}}D/V^2 \ll 0.1$; see J. V. Michael and R. E. Weston, Jr., *J. Chem. Phys.*, **45**, 3632 (1966).
- (13) (a) A. A. Westenberg and N. de Haas, *J. Chem. Phys.*, **46**, 490 (1967); (b) M. A. Clyne and B. A. Thrush, *Proc. R. Soc. London, Ser. A*, **275**, 544 (1961).
- (14) H. S. Johnston, "Gas Phase Reaction Rate Theory", Ronald Press, New York, N.Y., 1965.
- (15) N. L. Arthur and J. A. McDonell, *J. Chem. Phys.*, **56**, 2100 (1973).
- (16) Yu. L. Spirin, *Russ. J. Phys. Chem. (Engl. Transl.)*, **36**, 636 (1962); *Zh. Fiz. Khim.*, **36**, 1202 (1962).
- (17) Since $\log A$ for the analogous reaction H + CH₄ is 14 cm³ mol⁻¹ sec⁻¹ (see (a) M. J. Kurylo and R. B. Timmons, *J. Chem. Phys.*, **50**, 5076 (1969); (b) R. W. Walker, *J. Chem. Soc. A*, 2391 (1968)) and the reactions CH₃ + SiH₄ and CF₃ + SiH₄ both have frequency factors similar to those of CH₃ + CH₄ and CF₃ + CH₄ (see ref 5 and 6), we assumed that the frequency factor for the reaction H + SiH₄ or H + GeH₄ is of the same magnitude as that for the H + CH₄ reaction (see also ref 14, p 221). Therefore we chose $\log A(\text{H} + \text{SiH}_4) = \log A(\text{H} + \text{CH}_4) \pm 10\% \leq 15.4 \text{ cm}^3 \text{ mol}^{-1} \text{ sec}^{-1}$.
- (18) P. J. Fensham, K. Tamaru, M. Boudart, and H. Taylor, *J. Phys. Chem.*, **59**, 806 (1955).
- (19) J. C. Polanyi, *J. Chem. Phys.*, **23**, 1505 (1955).
- (20) (a) J. H. Purnell and R. Walsh, *Proc. R. Soc. London, Ser. A*, **293**, 543 (1966); (b) M. A. Ring, M. J. Puentes, and H. E. O'Neal, *J. Am. Chem. Soc.*, **92**, 4845 (1970).
- (21) (a) W. C. Steele and F. G. A. Stone, *J. Am. Chem. Soc.*, **84**, 3599 (1962); (b) W. C. Steele, L. D. Nichols, and F. G. A. Stone, *ibid.*, **84**, 4441 (1962).
- (22) F. E. Saalfeld and H. J. Svec, *J. Phys. Chem.*, **70**, 1753 (1966).
- (23) S. R. Gunn and L. G. Freen, *J. Phys. Chem.*, **65**, 779 (1961).
- (24) S. W. Benson, "The Foundation of Chemical Kinetics", McGraw-Hill, New York, N.Y., 1960.
- (25) N. L. Arthur, K. F. Donchi, and J. A. McDonell, *J. Chem. Phys.*, **62**, 1585 (1975). (NOTE ADDED IN PROOF: This modification lowers the calculated

activation energy for hydrogen atom transfer from SiH₄ and GeH₄ to H by 3.2 and 3.1 kcal/mol, respectively, for Si-H and Ge-H bond energies of 98.3 and 90.2 kcal/mol, respectively. The generality of this new potential function remains however to be established.)

- (26) That hydrogen atoms may add to silane giving SiH₅ was suggested to P.P.G. by the late Professor Richard Wolfgang in 1970.

- (27) The relative rate of hydrogen abstraction from silane by deuterium atoms compared with the rate of addition of deuterium atoms to perdeuterioethylene obtained by Obi et al.^{3a} has been combined with our absolute value for addition of hydrogen atoms to ethylene for the purpose of comparing the absolute rate of hydrogen abstraction deduced by Obi et al. with our own.

Reaction of Hydrogen Atoms with Thiirane

T. Yokota, M. G. Ahmed, I. Safarik, O. P. Strausz,* and H. E. Gunning

Department of Chemistry and Hydrocarbon Research Center, University of Alberta, Edmonton, Alberta, Canada (Received December 3, 1974)

Publication costs assisted by the University of Alberta

Hydrogen atoms, produced from the mercury photosensitization of H₂, react with thiirane to yield ethylene and hydrogen sulfide as the only retrievable products with quantum yields of 2.46 and 0.40, respectively, at room temperature. The sole primary reaction occurring is sulfur atom abstraction, H + C₂H₄S → HS + C₂H₄ (1). The rate coefficient of reaction 1 was determined in competition with the reaction H + H₂S → H₂ + HS to have the value $k_1 = (5.7 \pm 0.7) \times 10^{13} \exp((-1944 \pm 175)/RT) \text{ cm}^3 \text{ mol}^{-1} \text{ sec}^{-1}$. It is shown that at room temperature 41% of the HS radicals undergo disproportionation, 2HS → H₂S + S(³P), while the rest are scavenged by mercury atoms, Hg + SH + M → ½(HgSH)₂ + M, and perhaps the S₂₋₇ and HS₃₋₇ radicals present in the system. The relative importance of disproportionation decreases with increasing temperature.

The desulfurization of thiiranes in the liquid phase by nucleophilic reagents such as tertiary phosphines,² tertiary phosphites,³ alkyl lithium, and aryl lithium⁴ has been reported. More recently studies on radical reactions in the gas phase with thiiranes also appeared. Desulfurization has been shown to occur upon attack by S(³P), S(¹D₂)⁵, carbon atoms,⁶ and excited triplet state thiiranes.⁷ In the case of the *tert*-butoxy radical + methylthiirane system,⁸ hydrogen abstraction was the only observable reaction.

The reactions of methyl radicals with thiirane, methylthiirane, and dimethylthiirane have been reported in recent studies from this laboratory.⁹ In all three cases there are two primary steps which occur parallel and in competition: hydrogen abstraction and sulfur abstraction. The latter is unique in that it is the first known example of a reaction wherein a divalent atom in a bridgehead position is abstracted by a monovalent radical. All desulfurization reactions feature a high degree of stereospecificity and probably occur in a single step, concerted process.

In order to ascertain whether the desulfurization reaction is common to other monovalent radicals the reaction of hydrogen atoms with thiirane was examined. The results are presented in this article.

Experimental Section

The apparatus, general vacuum, and analytical techniques were similar to those employed in previous studies.^{9,10}

Hydrogen atoms were produced by the mercury photosensitization of H₂. The light source was a low-pressure Hg resonance lamp equipped with a 253.7-nm interference filter and a collimating quartz lens. The cylindrical quartz reaction cell (5 × 10 cm) was enclosed in an aluminum

block furnace and connected to a circulatory system having a total volume of 510 cm³. Circulation was effected by a fan type, magnetically driven pump.

Pressures of thiirane and hydrogen sulfide were always very much smaller than that of hydrogen in order to avoid direct or Hg sensitized decomposition.

Light intensities, as in the previous study of the H + COS reaction,¹⁰ were determined by propane and nitrous oxide actinometry. The mean value of the absorbed intensity was about 0.03 μeinstein min⁻¹.

The reaction mixtures consisting of H₂ + C₂H₄S or H₂ + H₂S + C₂H₄S were equilibrated by circulation for 20 min prior to irradiation. After each experiment the cell window was thoroughly baked. At the conclusion of irradiation the excess hydrogen was pumped off through traps cooled with liquid nitrogen and solid nitrogen. Ethylene and hydrogen sulfide were distilled from the reaction mixture at -130°. In the runs with added hydrogen sulfide, ethylene was distilled at -161°. The yields of C₂H₄ and H₂S were determined by gas chromatography on a 6-ft silica gel column at 90° using He as carrier.

The upper limit of the reaction temperature, 150°, was determined by the thermal decomposition of thiirane.

Materials in general were the best grades available commercially. Hydrogen (Matheson, 99.999%) was used without purification. Hydrogen sulfide (Matheson) was purified by distillation at -130° and degassing at -196°. Thiirane (Aldrich, 99%) was distilled at -78° and degassed at -130°. It was stored in the dark at -78°.

Results and Discussion

The Hg(³P₁)(Hg*) photosensitization of hydrogen and thiirane mixtures leads to the formation of C₂H₄, H₂S, and

TABLE I: Quantum Yields for H₂S and C₂H₄ Formation as a Function of Exposure Time^c

Time, min	$I_a \times 10^8$ Einstein/min	$\phi(\text{C}_2\text{H}_4)$	$\phi(\text{H}_2\text{S})$
15	3.19	2.49	0.39
30	3.15	2.47	0.39
45	3.11	2.46	0.40
60	3.07	2.44	0.41
90	2.98	2.42	0.42

^a $P(\text{H}_2) = 500$ Torr, $P(\text{C}_2\text{H}_4\text{S}) = 5$ Torr, $T = 27^\circ$.

TABLE II: Rates of Formation of C₂H₄ and H₂S as a Function of Thiirane Pressure^a

$P(\text{C}_2\text{H}_4\text{S})$, Torr	Rates, $\times 10^8$ mole/min	
	C ₂ H ₄	H ₂ S
1.00	7.05	1.22
2.15	8.13	1.38
2.01	7.28	1.27
3.03	7.47	1.34
5.20	7.65	1.01
5.09	7.13	1.19
4.81	8.03	
5.32	7.60	1.30
7.22	7.82	1.27

^a $P(\text{H}_2) = 490 \pm 10$ Torr, $T = 27^\circ$, exposure time = 60 min.

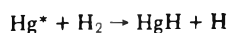
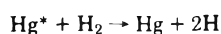
elemental sulfur which forms a solid deposit on the cell window. Ethanethiol, a possible product, was demonstrably absent.

First the quantum yields of C₂H₄ and H₂S were determined as a function of exposure time. In order to correct for the change in window transparency due to sulfur deposition during photolysis, light intensities were measured before and after each irradiation and the mean values were used to compute the quantum yields. The data compiled in Table I show that within experimental error, approximately $\pm 3\%$, the quantum yields determined this way are independent of the time of irradiation.

The effect of thiirane pressure on product yields was examined in a series of experiments by varying the pressure of thiirane between 1 and 7 Torr at a fixed hydrogen pressure of 490 Torr. The results are presented in Table II. Even at 1 Torr pressure the scavenging of hydrogen atoms appears to be complete and within the error limits of the experiments an increase in the pressure of thiirane has no significant effect on product yields.

The quantum yield data obtained at 96 and 152° are tabulated in Table III and the mean values for the three temperatures are given in Table IV.

Under the experimental conditions of the present study the excited mercury atoms are totally quenched by hydrogen



The quantum yield of HgH formation has been reported to be high,¹¹ 0.67, but the lifetime of HgH with respect to dissociation is short and overall kinetics would be indistinguishable from those of H atoms. Thus the system can be treated as a source of H atoms with $\phi(\text{H}) = 2.0$.¹²

TABLE III: Quantum Yields for C₂H₄ and H₂S Formation at 96 and 152°^a

$T, ^\circ\text{C}$	$P(\text{C}_2\text{H}_4\text{S})$, Torr	$\phi(\text{C}_2\text{H}_4)$	$\phi(\text{H}_2\text{S})$
96	5.4	2.38	0.39
96	5.4	2.29	0.38
96	5.0	2.33	0.36
96	4.9	2.38	0.41
96	5.0	2.55	0.39
152	5.5	2.25	0.16
152	5.2	2.22	0.16
152	5.1	2.27	0.21
152	5.1	2.19	0.22

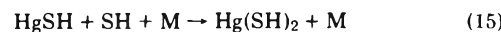
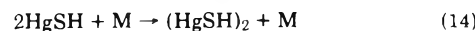
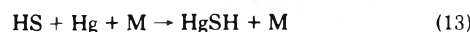
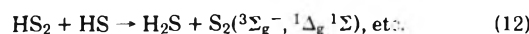
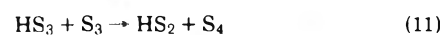
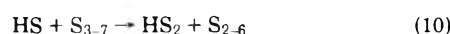
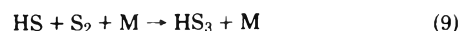
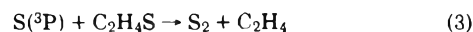
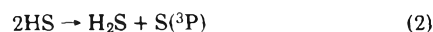
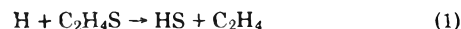
^a Exposure time 60 min.

TABLE IV: Mean Values of Quantum Yields for C₂H₄ and H₂S Formation as a Function of Temperature^a

Temp, °C	$\phi^0(\text{C}_2\text{H}_4)$	$\phi^0(\text{H}_2\text{S})$	$\phi^0(\text{C}_2\text{H}_4) - \phi^0(\text{H}_2\text{S})$
27	2.46 ± 0.03	0.40 ± 0.01	2.06
96	2.39 ± 0.07	0.39 ± 0.01	2.00
152	2.23 ± 0.03	0.19 ± 0.03	2.04

^a $P(\text{H}_2) = 490 \pm 10$ Torr, $P(\text{C}_2\text{H}_4\text{S}) = 5.2 \pm 0.2$ Torr. ϕ^0 's denote ϕ 's from H₂-C₂H₄S system.

The nature and yields of the observed products can be accounted for in terms of the following sequence of elementary steps:



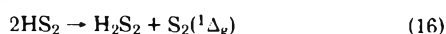
Scavenging of the H and S atoms by thiirane at the concentrations involved is complete. Consequently the yield of C₂H₄ from step 3 is equal to that of H₂S, and $\phi(\text{C}_2\text{H}_4)$ from reaction 1 should be equal to $\phi(\text{C}_2\text{H}_4) - \phi(\text{H}_2\text{S})$. The values for this quantity, given in the last column of Table IV, are equal to two, within experimental error, at the three temperatures studied and we are forced to conclude that the only primary mode of interaction between H atoms and thiirane is sulfur atom abstraction, step 1.

TABLE V: Rate of C₂H₄ Formation as a Function of P(H₂S)/P(C₂H₄S)^a

T, °C	P(H ₂), Torr	P(C ₂ H ₄ S), Torr	P(H ₂ S), Torr	P(H ₂ S)/P(C ₂ H ₄ S)	R _{C₂H₄} , 10 ⁻⁸ mol/min	φ(C ₂ H ₄)	γ
27	485	4.33	1.05	0.242	7.25	2.36	0.513
	474	3.02	1.02	0.300	7.37	2.40	0.503
	502	4.89	4.89	1.00	6.77	2.21	0.556
	487	3.00	3.02	1.00	6.42	2.09	0.595
	505	2.89	5.63	1.95	5.72	1.87	0.685
96	490	3.05	5.97	1.96	5.82	1.90	0.671
	488	3.07	0.998	0.325	7.23	2.36	0.508
	496	2.97	2.89	0.973	6.30	2.05	0.602
	458	3.02	3.07	1.02	6.67	2.17	0.562
	424	3.00	3.10	1.03	6.43	2.10	0.585
152	486	3.00	5.97	1.99	5.68	1.85	0.685
	441	2.77	5.91	2.13	5.77	1.88	0.671
	496	3.10	0.95	0.306	6.63	2.16	0.508
	498	2.94	0.97	0.330	6.38	2.08	0.529
	503	2.41	0.88	0.365	6.58	2.14	0.513
	497	3.43	3.00	0.875	6.20	2.02	0.546
	476	3.02	3.00	0.993	5.69	1.85	0.602
	499	3.00	3.20	1.07	5.98	1.95	0.568
	505	3.05	5.86	1.92	5.22	1.70	0.662
	504	3.02	5.99	1.98	5.28	1.72	0.654
	499	2.89	5.89	2.04	5.13	1.67	0.676

^a Exposure time, 60 mir.

With regard to reaction 2, a recent study of the photolysis of hydrogen sulfide established a quantum yield value of unity for hydrogen production¹³ suggesting that the only important mode of interaction between two sulfhydryl radicals is disproportionation into S + H₂S and that hydrogen or H₂S₂ are not produced in significant yields. The present results shed additional light on the fate of the HS radical the two plausible scavengers of which are the sulfur or sulfhydryl radicals and mercury atoms according to the scheme indicated by reactions 9–15. Mercurous sulfhydryde is a poorly characterized compound the synthesis of which has been reported^{14,15} in 1928 from the reaction of solid mercurous chloride with liquid hydrogen sulfide. In the interpretation of the present results cognizance must be taken of the data obtained in recent studies on the photolysis of hydrogen sulfide¹³ in the presence and absence of mercury. The mercury free photolysis gave a quantum yield value of unity for both hydrogen formation and hydrogen sulfide disappearance the latter determined from the yield of solid, elemental sulfur. In the presence of mercury vapor, however, while the yield of hydrogen remained unaffected, the yield of sulfur in the solid film which coated the cell wall increased by 19–29%. This yield increase in the sulfur content of the solid is attributed to the formation of (HgSH)₂ and perhaps Hg(SH)₂ via reactions 13–15. Therefore, we conclude that the principal scavengers of the sulfhydryl radical in the present system are the mercury atoms. If scavenging by the sulfur or sulfhydryl radicals occurs at all it must be via complexing with thiirane, C₂H₄S·SH, C₂H₄S·S_x, C₂H₄S·S_xH, since the pure hydrogen sulfide system where S_x radicals are also present, scavenging is inefficient. The presence of small concentrations of the HS₂ radical in flash photolyzed hydrogen sulfide and the production of S₂(¹Δ_g) in the self-disproportionation reactions of HS₂



and its cross disproportionation, step 12, have been demonstrated in previous flash spectroscopic studies.¹⁶ Also, the presence of small concentrations of H₂S₂ in flashed H₂S was detected earlier by kinetic mass spectrometric techniques.¹⁷ The detection of small concentrations of H₂S₂ and presumably of all higher polysulfides by conventional analytical techniques is exceedingly difficult and unreliable owing to their well-known tendency to undergo surface decomposition to yield H₂S and elemental sulfur.

It is interesting to note that the relative rates of scavenging and disproportionation of the HS radical are temperature dependent and scavenging becomes more important with increasing temperature. This may be due to a slight increase in the mercury vapor concentration at elevated temperatures.

Reaction 3 is very rapid, its rate coefficient being 1.7–2.7 × 10¹³ cm³ mol⁻¹ sec⁻¹.^{5,18}

In order to determine the rate coefficient of reaction 1, competitive studies were carried out with added H₂S, in which the ratio of H₂S to thiirane pressure was varied between 0.2 and 2 at a constant hydrogen pressure of 500 Torr. The ethylene yields obtained at 27, 96, and 152° are given in Table V.

Steady-state treatment of the competing reactions 1 and



leads to the following kinetic expression:

$$\gamma = [\phi(\text{C}_2\text{H}_4) - \phi^0(\text{H}_2\text{S})]^{-1} = 0.50 + \frac{k_{17} P(\text{H}_2\text{S})}{2k_1 P(\text{C}_2\text{H}_4\text{S})} \quad (\text{I})$$

As the yield of HS per hydrogen atom produced is unaffected by the H₂S to C₂H₄S ratios, the value of γ can be obtained from the measured yield of C₂H₄ and the H₂S yields φ⁰(H₂S), from the H₂-C₂H₄S system.

From the plots of γ vs. P(H₂S)/P(C₂H₄S), shown in Figure 1, it can be seen that eq I is obeyed and the slope and

intercept values obtained by least mean square treatment of the data are given in Table VI. Plotting the logarithm of k_1/k_{17} values against $1/T$, Figure 2, the activation energy difference and A factor ratio of reactions 17 and 1 are found to have the values: $E_1 - E_{17} = 235 \pm 115$ cal mol $^{-1}$ and 7.3 ± 1.2 , respectively. If Braun and coworkers'¹⁹ values of $E_{17} = 1709$ cal mol $^{-1}$ and $A_{17} = 7.78 \times 10^{12}$ cm 3 mol $^{-1}$ sec $^{-1}$ are accepted,²⁰ then for the Arrhenius parameters of reaction 1 we obtain

$$k_1 = (5.7 \pm 0.7) \times 10^{13} \exp\left(\frac{-1944 \pm 175}{RT}\right) \text{ cm}^3 \text{ mol}^{-1} \text{ sec}^{-1}$$

These values appear to be reasonable when compared to those of other, similar reactions, which are compiled in Table VII. The entropies of activation given in Table VII were obtained by the method of Benson.²¹ To calculate the entropy of the H...S Δ activated complex we start with the

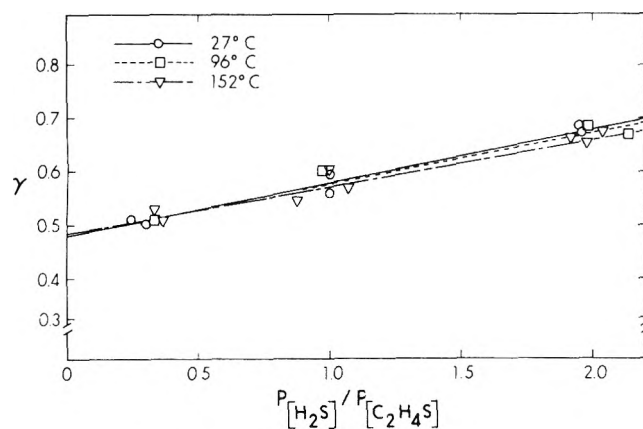


Figure 1. $\gamma = (\phi_{C_2H_4} - \phi_{H_2S}^0)^{-1}$ plot against $P_{[H_2S]}/P_{[C_2H_4S]}$.

TABLE VI: Slopes and Intercepts from γ vs. $P(H_2S)/P(C_2H_4S)$ Plots

$T, ^\circ\text{C}$	Slope, $k_{17}/2k_1$	Intercept
27	0.101 ± 0.006	0.478 ± 0.008
96	0.0942 ± 0.0082	0.485 ± 0.011
152	0.0899 ± 0.0051	0.485 ± 0.007

TABLE VII: Arrhenius Parameters and Entropies of Activation

Reaction	$A_f, \text{ cm}^3 \text{ mol}^{-1} \text{ sec}^{-1}$	$E_f, \text{ kcal mol}^{-1}$	$S_f^\ddagger, \text{ eu}$	Ref	$A_r, \text{ cm}^3 \text{ mol}^{-1} \text{ sec}^{-1}$	$E_r, \text{ kcal mol}^{-1}$	$\Delta S_r^\ddagger, \text{ eu}$
$\text{CH}_3 + \text{S} \xrightleftharpoons[k_r]{k_f} \text{CH}_3\text{S} + \text{C}_2\text{H}_4$	7.08×10^{10}	6.7	-24.6 (C_{2v})	10	8.65×10^9	18.5	-28.8
$\text{CH}_3 + \text{COS} \xrightleftharpoons[k_r]{k_f} \text{CH}_3\text{S} + \text{CO}$	3.80×10^{11}	11.35	-21.3	10	3.34×10^{10}	9.65	-26.1
$\text{CH}_3 + \text{H}_2\text{S} \xrightleftharpoons[k_r]{k_f} \text{CH}_3 + \text{HS}$	5.00×10^{10}	2.9	-25.3	25	3.94×10^{11}	16.0	-21.2
$\text{H} + \text{S} \xrightleftharpoons[k_r]{k_f} \text{HS} + \text{C}_2\text{H}_4$	5.66×10^{13}	1.9	-11.3 (C_{2v})	This work	2.78×10^{11}	26.8	-21.9
$\text{H} + \text{COS} \xrightleftharpoons[k_r]{k_f} \text{HS} + \text{CO}$	9.10×10^{12}	3.9	-15.0	11	3.17×10^{10}	15.3	-26.2
$\text{H} + \text{H}_2\text{S} \xrightleftharpoons[k_r]{k_f} \text{HS} + \text{H}_2$	7.77×10^{12}	1.7	-15.3	18	4.0×10^{12}	15.0	-16.6

S Δ molecule. If the C_{2v} symmetry is retained there will be a contribution of $R \ln 2$ from spin only, because the increase in the moments of inertia is negligible:

$$S^{\circ\dagger} = S^\circ(\text{S}\Delta) + 1.4 \text{ eu}$$

and the entropy of activation

$$\Delta S_p^\ddagger = S^\circ(\text{S}\Delta) + 1.4 - S^\circ(\text{S}\Delta) - S^\circ(\text{H}) = 1.4 - 27.4 = -26.0 \text{ eu}$$

or, by transformation to the standard state of 1 M

$$\Delta S_c^\ddagger = \Delta S_p^\ddagger - R\Delta n - (\Delta n)R \ln(RT) = -17.6 \text{ eu}$$

This value differs from the experimentally obtained entropy of activation by 6.3 eu. The difference can be assigned to the contribution from the degenerate bending modes of the new H...S bond corresponding to a vibrational frequency of 125 cm $^{-1}$ which seems to indicate a rather loose structure for the activated complex.

If the C_{2v} symmetry is lost in the activated complex, as is probably the case,⁹ another $R \ln 2$ term must be added to estimate the absolute $S^{\circ\dagger} = S^\circ(\text{S}\Delta) + 2.8$ eu, and the entropy of activation $\Delta S_p^\ddagger = 2.8 - 27.4 = -24.6$ eu or $\Delta S_c^\ddagger = -16.2$ eu. The difference from the experimental entropy of activation is now only 4.9 eu indicating somewhat stiffer H...S bending modes with frequencies of about 200 cm $^{-1}$.

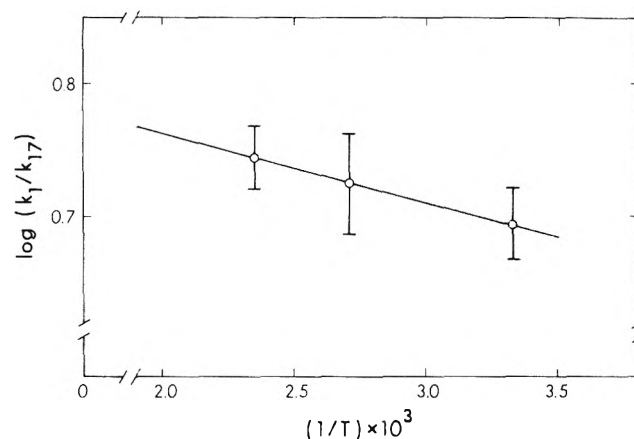
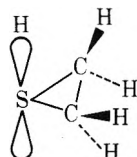


Figure 2. Arrhenius plot for S abstraction from ethylene episulfide by H atoms.

The Arrhenius parameters and activation entropies for the reverse of the reactions listed in Table VII were also calculated and are presented in the last three columns of Table VII.

As was noted before, all the known desulfurization reactions of thiiranes feature a high degree of stereospecificity from which it has been inferred that they proceed via single step, concerted reactions. The CH_3 and H reactions with thiiranes are further characterized by the complete absence of the addition products, the thio ether and thiol radicals, $\text{CH}_3\text{SCH}_2\text{CH}_2$ and HSCH_2CH_2 , respectively. It is likely that in the $\text{H} + \text{C}_2\text{H}_4\text{S}$ system the initial interaction involves the nonbonding $3p$ orbital of the S atom



leading to a symmetrical transition state. The potential energy of activation for a symmetrical pull of the sulfur using a modified form of the bond energy–bond order method,^{9,22} was found to be 4 kcal/mol if the sulfur atom is assumed to be transferred in its lowest lying ($^1\text{D}_2$) state or zero if the transfer is in the ($^3\text{P}_2$) ground state. In agreement with the earlier results on the $\text{CH}_3 + \text{COS}$ and $\text{CH}_3 + \text{S}$ systems⁹ the experimental value lies close to the arithmetic mean of the computed limits.

In conclusion it should be noted that the analogous deoxygenation reactions with oxirane have not been observed; hydrogen atoms,²³ CH_3 ,²⁴ and CF_3 ²⁵ radicals react with oxirane by hydrogen abstraction although energetically, oxygen abstraction would be more favorable. This difference between the chemical behavior of oxiranes and thiiranes has been interpreted⁹ as being due to the higher value of the activation energy for the deoxygenation of oxiranes as compared to desulfurization of thiiranes. The higher activation energy in turn is a consequence of the somewhat lower exothermicity, more stringent obedience of spin conservation in the reaction, and the higher value of the excitation energy of the $^1\text{D}_2$ state of the oxygen than sulfur atom.

Acknowledgments. The authors thank the National Research Council of Canada for financial support and Dr. E.M. Lown for helpful discussions.

References and Notes

- (1) Author to whom correspondences should be addressed.
- (2) B. Denney and M. J. Boskin, *J. Am. Chem. Soc.*, **82**, 4736 (1960); R. E. Davis, *J. Org. Chem.*, **23**, 1767 (1958).
- (3) R. D. Schuetz and R. L. Jakobs, *J. Org. Chem.*, **23**, 1799 (1958).
- (4) N. P. Neureiter and F. G. Bordwell, *J. Am. Chem. Soc.*, **81**, 578 (1958); F. G. Bordwell, H. M. Anderson, and B. Pitt, *ibid.*, **76**, 1082 (1954).
- (5) R. J. Donovan, D. Husain, R. W. Fair, O. P. Strausz, and H. E. Gunning, *Trans. Faraday Soc.*, **66**, 1635 (1970); O. P. Strausz, W. B. O'Callaghan, E. M. Lown, and H. E. Gunning, *J. Am. Chem. Soc.*, **93**, 559 (1971); J. Connor, A. Van Roodselaar, R. W. Fair, and O. P. Strausz, *J. Am. Chem. Soc.*, **93**, 560 (1971).
- (6) J. H. Plonka and P. S. Skell, *Chem. Commun.*, 1108 (1970); K. J. Klambunde and P. S. Skell, *J. Am. Chem. Soc.*, **93**, 3807 (1971).
- (7) E. M. Lown, H. S. Sandhu, H. E. Gunning, and O. P. Strausz, *J. Am. Chem. Soc.*, **90**, 7164 (1968).
- (8) E. Sabatino, Ph.D. Thesis, University of Connecticut, 1963.
- (9) E. Jakubowski, M. G. Ahmed, E. M. Lown, H. S. Sandhu, R. K. Gosavi, and O. P. Strausz, *J. Am. Chem. Soc.*, **94**, 4094 (1972).
- (10) S. Tsunashima, T. Yokota, I. Safarik, H. E. Gunning, and O. P. Strausz, *J. Phys. Chem.*, submitted for publication.
- (11) A. B. Callear and J. C. McGurk, *J. Chem. Soc., Faraday Trans. 2*, **68**, 289 (1972); A. B. Callear and P. M. Wood, *ibid.*, **68**, 302 (1972).
- (12) T. L. Pollock, E. J. Jakubowski, H. E. Gunning, and O. P. Strausz, *Can. J. Chem.*, **47**, 3474 (1969).
- (13) S. Tsunashima and O. P. Strausz, to be submitted for publication.
- (14) A. W. Ralston and J. A. Wilkinson, *J. Am. Chem. Soc.*, **50**, 258 (1928).
- (15) Gmelin's Handbuch der Anorganischen Chemie, Vol. 34, 8th ed, Verlag Chemie, Weinheim/Bengstr., Germany, 1968, p 954.
- (16) O. P. Strausz, R. J. Donovan, and M. de Sorigo, *Ber. Bunsenges. Phys. Chem.*, **72**, 253 (1968).
- (17) O. P. Strausz, S. C. Barton, and W. K. Duholke, to be submitted for publication.
- (18) R. B. Klemm and D. D. Davis, *Int. J. Chem. Kinet.*, **5**, 149 (1973); O. P. Strausz and A. van Roodselaar, unpublished results.
- (19) M. J. Kurylo, N. C. Peterson, and W. Braun, *J. Chem. Phys.*, **54**, 943 (1971).
- (20) Other rate constant measurements for reaction 14 include: B. de B. Darwent, R. L. Wadlinger, and M. J. Allard, *J. Phys. Chem.*, **71**, 2346 (1967); A. A. Westenberg and N. de Haas, *J. Chem. Phys.*, **40**, 707 (1969); D. Mihelcic and R. N. Schindler, *Ber. Bunsenges. Phys. Chem.*, **74**, 1280 (1970); H. Rommel and H. I. Schiff, *Int. J. Chem. Kinet.*, **4**, 547 (1972).
- (21) S. W. Benson, "Thermochemical Kinetics", Wiley, New York, N.Y., 1968.
- (22) S. W. Mayer, *J. Phys. Chem.*, **73**, 3941 (1969).
- (23) W. R. Trost, B. de B. Darwent, and E. W. Steacie, *J. Chem. Phys.*, **16**, 353 (1948).
- (24) R. Gomer and W. A. Noyes, Jr., *J. Am. Chem. Soc.*, **72**, 101 (1950); M. K. Phibbs and B. de B. Darwent, *Can. J. Res. Sect. B*, **28**, 395 (1950).
- (25) S. H. Jones and E. Whittle, *Can. J. Chem.*, **48**, 3601 (1970).
- (26) N. Imai and O. Toyama, *Bull. Chem. Soc. Jpn.*, **33**, 652 (1960).

Rate Constants for the Reaction of OH Radicals with a Series of Aromatic Hydrocarbons

D. A. Hansen, R. Atkinson, and J. N. Pitts, Jr.*

Chemistry Department and Statewide Air Pollution Research Center, University of California, Riverside, California 92502
(Received April 9, 1975)

Publication costs assisted by the University of California, Riverside

Absolute rate constants for the reaction of OH radicals with a series of aromatic hydrocarbons have been determined at room temperature using a flash photolysis-resonance fluorescence technique. The rate constants ($k_1 \times 10^{12} \text{ cm}^3 \text{ molecule}^{-1} \text{ sec}^{-1}$) obtained are as follows: benzene, 1.24 ± 0.12 ; toluene, 5.78 ± 0.58 ; *o*-xylene, 15.3 ± 1.5 ; *m*-xylene, 23.6 ± 2.4 ; *p*-xylene, 12.2 ± 1.2 ; 1,2,3-trimethylbenzene, 26.4 ± 2.6 ; 1,2,4-trimethylbenzene, 33.5 ± 3.4 ; 1,3,5-trimethylbenzene, 47.2 ± 4.8 . These absolute rate constants are in good agreement with those determined recently for benzene and toluene and with those derived for a series of aromatic hydrocarbons from a relative rate study in an environmental chamber.

Introduction

In recent years the OH radical has been shown to be an important and reactive species in a large variety of oxidation processes, including combustion reactions,¹ photochemical air pollution,^{2,3} and stratospheric chemistry,^{4,5} and has recently been detected in ambient air.⁶

While much work has been reported for the reactions of OH radicals with alkanes⁷⁻¹³ and alkenes,^{9-11,14-17} there are few data available for aromatic hydrocarbons.^{9,18,19} Recently the absolute rate constants for the reaction of OH radicals with benzene and toluene have been determined at 298°K over the pressure range 3–100 Torr of helium using a flash photolysis-resonance fluorescence technique.¹⁸ Rate constants for the reaction of OH radicals with a series of aromatic hydrocarbons have been calculated¹⁹ from the initial rates of disappearance of the aromatic hydrocarbons relative to that of *n*-butane in an environmental chamber at $304 \pm 1^\circ\text{K}$ and atmospheric pressure. Besides being of fundamental interest, absolute rate constants for the reaction of OH radicals with aromatic hydrocarbons are needed to model the chemistry occurring in polluted urban atmospheres,²⁰ particularly because of the increased use of aromatics in unleaded gasoline in the U.S.A.²¹ and the inherently high aromatic content of gasoline in Europe and Japan.²²

In this work the absolute rate constants for the reaction of OH radicals with a series of aromatic hydrocarbons have been determined using a flash photolysis-resonance fluorescence technique.

Experimental Section

The apparatus and techniques used have been described previously,²³ and hence only a brief summary will be given here. OH radicals were produced by the pulsed vacuum ultraviolet photolysis of H₂O at wavelengths longer than the LiF cutoff ($\geq 1050 \text{ \AA}$). OH radical concentrations were monitored as a function of time after the flash by resonance fluorescence using a cooled EMI 9659QA photomultiplier fitted with an interference filter transmitting the 3064-Å band of OH ($A^2\Sigma^+, v' = 0 \rightarrow X^2\Pi, v'' = 0$). The intersection of the detection system aperture and the resonance radiation beam defined a fluorescence viewing zone whose cross section was $\sim 2 \text{ cm}$ in diameter at the center of

the reaction vessel. This region was well separated from the reaction vessel walls, thus minimizing the contribution of wall losses to the observed OH radical decays.

The flash lamp was operated at discharge energies of 25–50 J per flash at repetition rates of one flash every 3 sec. Signals were obtained by photon counting with multichannel scaling. OH radical decay curves, such as that shown in Figure 1, were accumulated from 45 to 1620 flashes, depending on the signal strengths. OH half-lives ranged from 1.22 to 133 msec and the OH radical concentrations were followed over at least 3 half-lives. In all cases the flash duration was negligible in comparison to these OH radical half-lives.

All experiments were carried out under flow conditions so that the gas mixture in the reaction vessel was replenished every few flashes in order to avoid the accumulation of photolysis or reaction products. The partial pressure of H₂O in the reaction cell ranged from 0.01 to 0.03 Torr. The argon used had a purity level of $\geq 99.998\%$, according to the manufacturer, while gas chromatographic analysis showed the aromatic hydrocarbons to have the following impurities:²⁴ benzene, 0.5% toluene and $\leq 0.5\%$ xylene; toluene, 0.1% benzene and 0.05% *m*-xylene; *o*-xylene, $\leq 0.2\%$ impurity; *m*-xylene, 1.0% *p*-xylene and 0.4% ethylbenzene; *p*-xylene, 0.3% *m*-xylene; 1,2,3-trimethylbenzene, 0.2% of the 1,3,5 isomer and 2.2% of the 1,2,4 isomer; 1,2,4-trimethylbenzene, 1.0% of the 1,3,5-trimethylbenzene; 1,3,5-trimethylbenzene, 0.2% of the 1,2,4 isomer and 0.1% ethyltoluene. A known fraction of the total argon flow was saturated with the aromatic vapor at 255–293°K, depending on the aromatic hydrocarbon used. Aromatic hydrocarbon partial pressures in this fraction of the argon flow were determined by their ultraviolet absorption using a 9.0-cm path length cell and a Cary 15 spectrophotometer. The absorption cell was calibrated using known pressures of the aromatic hydrocarbons as measured by an MKS Baratron capacitance manometer. All flows were monitored by calibrated flowmeters and the gases were premixed before entering the reaction vessel.

Results

The reaction of OH radicals with a series of aromatic hydrocarbons was studied at room temperature with argon as

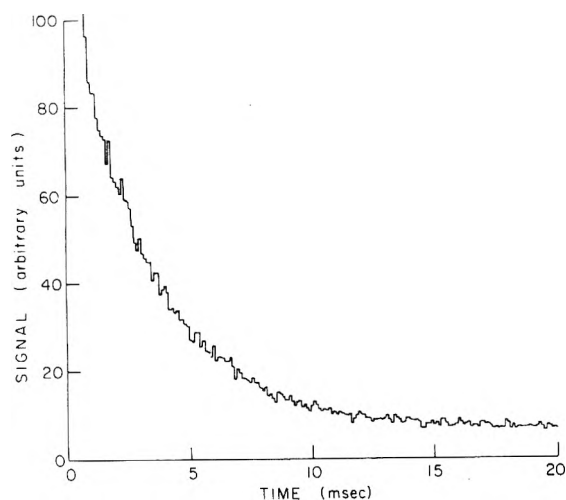
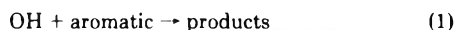


Figure 1. Time dependence of the OH resonance fluorescence signal intensity accumulated from 377 flashes of an H₂O (0.010 Torr)-toluene (0.00145 Torr)-argon (99.7 Torr) mixture with a multichannel scaler channel width of 100 μ sec and a flash energy of 50 J per flash.

the diluent gas. Under the experimental conditions used, the decay of the OH radical concentration, [OH], is given by the integrated rate expression

$$[\text{OH}]_0/[\text{OH}] = S_0/S = \exp[(k_0 + k_1[\text{aromatic}])(t - t_0)] \quad (1)$$

where [OH]₀ and [OH] are the concentrations of OH at times t_0 and t , respectively, S_0 and S are the corresponding resonance fluorescence intensities, k_0 is the first-order rate constant for removal of OH in the absence of added reactant (primarily attributed to diffusion out of the viewing zone and to reaction with impurities), and k_1 is the rate constant for the reaction



In all experiments exponential decays of the resonance fluorescence signal were observed and the measured decay rate, defined as $R = (t - t_0)^{-1} \ln(S_0/S)$, was found to depend linearly on the concentration of added reactants. The decay rates obtained from OH radical decay curves such as shown in Figure 1 typically had error limits of ± 2 -3%. Equation 1 was thus obeyed and rate constants k_1 were accordingly derived from the slopes of plots of the decay rate R against the reactant concentration. In the absence of added reactant, the OH radical decay rates, $R = k_0$, ranged from 5.2 to 10.3 sec^{-1} and were similar to those reported previously²³ from this laboratory.

Figures 2-4 show plots of the OH radical decay rate against the aromatic hydrocarbon concentration for the aromatic hydrocarbons studied at a total pressure of ~ 100 Torr, while Table I gives the rate constants k_1 obtained from such plots. For benzene and toluene, total pressures were varied over the ranges 50-600 and 100-620 Torr, respectively. Within the experimental errors, no dependence of the rate constants k_1 on total pressure was observed over these pressure ranges, and hence rate constants k_1 for the other aromatic hydrocarbons were determined at ~ 100 Torr total pressure only. In all cases, a variation of a factor of 2 in the flash energy (from 25 to 50 J per flash) produced no change in the rate constant within the experimental errors, indicating that secondary reactions were negligible under these conditions.

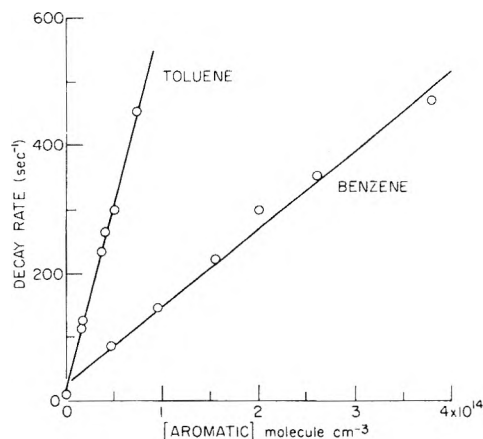


Figure 2. Plots of OH decay rate against aromatic concentration for benzene and toluene; total pressure ~ 100 Torr of argon.

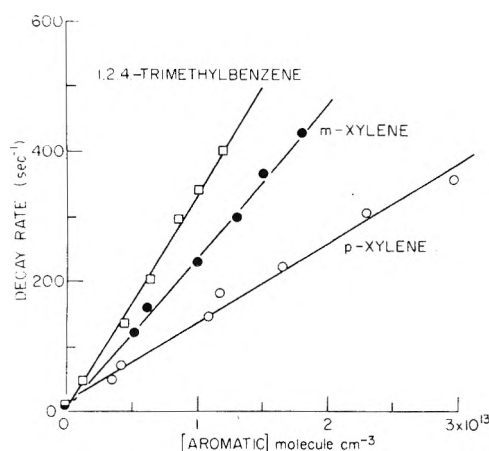


Figure 3. Plots of OH decay rate against aromatic concentration for *m*-xylene, *p*-xylene, and 1,2,4-trimethylbenzene; total pressure ~ 100 Torr of argon.

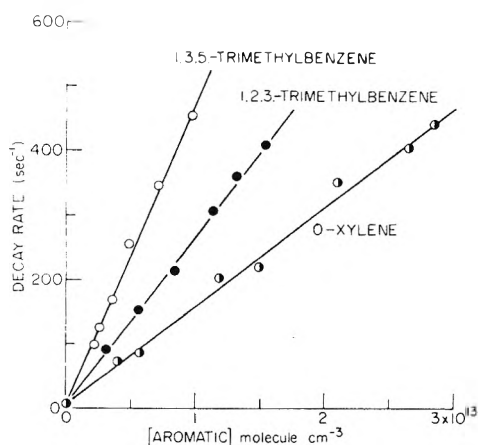


Figure 4. Plots of OH decay rate against aromatic concentration for *o*-xylene, 1,2,3-trimethylbenzene, and 1,3,5-trimethylbenzene; total pressure ~ 100 Torr of argon.

Discussion

The initial OH radical concentration after the photolysis flash can be estimated from the flash energies and H₂O concentrations used and from previous work^{13,25} to be $\sim 10^{11}$ molecules cm^{-3} . From these initial OH radical concentrations and the aromatic hydrocarbon concentrations

TABLE I: Rate Constants k_1 for the Reaction of OH Radicals with a Series of Aromatic Hydrocarbons

Aromatic hydrocarbon	Temp, °C	Total pressure, Torr	k_1 , cm ³ molecule ⁻¹ sec ⁻¹	
			<i>a</i>	<i>b</i>
Benzene	24.8 ± 0.5	50.4 ± 0.4	(1.28 ± 0.04) × 10 ⁻¹²	
	24.3 ± 0.4	100.0 ± 0.2	(1.22 ± 0.06) × 10 ⁻¹²	(1.24 ± 0.12) × 10 ⁻¹²
	24.5 ± 0.5	199.9 ± 0.6	(1.20 ± 0.06) × 10 ⁻¹²	
	24.6 ± 0.3	600.0 ± 0.4	(1.24 ± 0.11) × 10 ⁻¹²	
Toluene	25.0 ± 0.5	99.7 ± 0.3	(5.90 ± 0.16) × 10 ⁻¹²	
	24.6 ± 0.2	249.7 ± 0.6	(5.69 ± 0.27) × 10 ⁻¹²	(5.78 ± 0.58) × 10 ⁻¹²
	24.7 ± 0.5	618.6 ± 0.5	(5.75 ± 0.16) × 10 ⁻¹²	
<i>o</i> -Xylene	24.8 ± 0.2	101.3 ± 0.2		(1.53 ± 0.15) × 10 ⁻¹¹
<i>m</i> -Xylene	24.1 ± 0.5	99.9 ± 0.3		(2.36 ± 0.24) × 10 ⁻¹¹
<i>p</i> -Xylene	24.1 ± 0.6	99.6 ± 0.3		(1.22 ± 0.12) × 10 ⁻¹¹
1,2,3-Trimethylbenzene	23.9 ± 0.4	99.9 ± 0.3		(2.64 ± 0.26) × 10 ⁻¹¹
1,2,4-Trimethylbenzene	23.7 ± 0.6	100.3 ± 0.3		(3.35 ± 0.34) × 10 ⁻¹¹
1,3,5-Trimethylbenzene	23.9 ± 0.3	100.4 ± 0.3		(4.72 ± 0.48) × 10 ⁻¹¹

^a Error limits are the least-squares standard deviations of plots such as those shown in Figures 2-4. ^b Error limits shown are the estimated overall error limits which include the least-squares standard deviations as well as estimated accuracy limits of other parameters such as total pressure and aromatic concentrations.

TABLE II: Comparison of Room Temperature Rate Constants, k_1 , for the Reaction of OH Radicals with Aromatic Hydrocarbons from the Present Work with Literature Values and with the Room Temperature Rate Constants for the Reaction of O(³P) Atoms with Aromatic Hydrocarbons

Aromatic hydrocarbon	OH radical $k_1 \times 10^{12}$, cm ³ molecule ⁻¹ sec ⁻¹				O(³ P) atom $k \times 10^{13}$, cm ³ mole- cule ⁻¹ sec ⁻¹
	This work ^a	Ref 19 ^b	Ref 18 ^c	Ref 9 ^d	
Benzene	1.24 ± 0.12	≤3.8	1.59 ± 0.12		0.24 ± 0.033
Toluene	5.78 ± 0.58	4.2 ± 1.5	6.11 ± 0.40		0.75 ± 0.075
<i>o</i> -Xylene	15.3 ± 1.5	12.8 ± 3.8		} 18.7	1.74 ± 0.18
<i>m</i> -Xylene	23.6 ± 2.4	23.2 ± 1.7			3.52 ± 0.35
<i>p</i> -Xylene	12.2 ± 1.2	12.3 ± 2.5			1.81 ± 0.18
1,2,3-Trimethylbenzene	26.4 ± 2.6	23 ± 5			11.5 ± 1.2
1,2,4-Trimethylbenzene	33.5 ± 3.4	33 ± 5			10.0 ± 1.0
1,3,5-Trimethylbenzene	47.2 ± 4.8	51.5 ± 6.5			27.9 ± 3.3

^a Total pressure ≥ 50 Torr (Ar). ^b Total pressure 1 atm of air; rates relative to OH + *n*-butane placed on an absolute basis using the rate constant for OH + *n*-butane as 3.0 × 10⁻¹² cm³ molecule⁻¹ sec⁻¹.^{8-10,12} ^c Total pressure 100 Torr (He). ^d Total pressure ~1 Torr (He) mixture of isomers.

used it can be estimated that errors in the measured rate constants due to the reaction of OH radicals with reaction products would be typically <5-10%, using an assumed rate constant of 10⁻¹⁰ cm³ molecule⁻¹ sec⁻¹ for the reaction of OH radicals with all reaction products. This conclusion is substantiated by the good linearity of the plots shown in Figures 2-4 for variations of factors of 3-9 in the aromatic hydrocarbon concentrations. Similarly, the reaction of OH radicals with reactant impurities can be calculated to cause errors in the measured rate constants of ≤5%.

Table I shows that the rate constants k_1 for benzene and toluene are, within experimental error, independent of the total pressure of argon over the ranges 50-600 Torr for benzene and 100-620 Torr for toluene. This is in agreement with the recent data of Davis and coworkers,¹⁸ who observed a pressure dependence of k_1 for benzene and toluene in the range 3-100 Torr of helium but concluded from Lindemann plots that the rate constants measured at 100 Torr were essentially the high-pressure limiting values.

Table II gives a comparison of the present rate constants k_1 with the available literature values. It can be seen that the present rate constants k_1 are in good agreement with the absolute rate data of Davis and coworkers¹⁸ (also obtained using a flash photolysis-resonance fluorescence technique) and in excellent agreement with the rate constants derived from the relative rate study of Doyle et al.¹⁹ The latter workers monitored the rates of disappearance of a series of aromatic hydrocarbons and *n*-butane in the early stages of an irradiated NO_x-hydrocarbon-air mixture in an environmental chamber and assumed that this hydrocarbon loss was due to reaction with OH radicals. The relative rate constants were placed on an absolute basis using a rate constant for the reaction of OH with *n*-butane of 3.0 × 10⁻¹² cm³ molecule⁻¹ sec⁻¹ derived from the literature.^{8-10,12} It thus appears that this relative rate technique using an environmental chamber may be used to determine reliable OH radical rate constants for a variety of other reactants. The present values of k_1 for the xylenes deter-

mined at ~ 100 Torr total pressure of argon are also consistent with that determined by Morris and Niki⁹ for a mixture of isomers using a discharge flow technique at ~ 1 Torr total pressure of helium.

Table II also gives the rate constants for the reaction of $O(^3P)$ atoms with the aromatic hydrocarbons determined using a modulation phase-shift technique.²⁴ It can be seen that the OH radical rate constants show the same trend with degree and position of alkylation as for $O(^3P)$ atom reactions demonstrating the electrophilic character of the OH radical. This suggests¹⁹ that in the reaction of OH radicals with aromatic hydrocarbons, the major reaction path is that of addition to the aromatic ring, in agreement with the conclusions reached by Davis and coworkers¹⁸ from the pressure dependence of the rate constants for benzene and toluene over the range 3–100 Torr of helium. The mechanism and products for the reaction of OH radicals with aromatic hydrocarbons are presently unknown, but it may be speculated that the aromatic ring undergoes substantial cleavage following addition of the OH radical with subsequent production of a variety of long-chain organics. This would be similar to the reaction of $O(^3P)$ atoms^{26–29} and O_3 ^{30,31} with aromatic hydrocarbons where a large amount of ring cleavage is observed to occur. However, OH radicals are much more reactive than $O(^3P)$ atoms toward these aromatic hydrocarbons and hence, as previously discussed,^{18,19} the more reactive aromatic hydrocarbons should contribute significantly to the formation of photochemical air pollutants.

Acknowledgment. The authors are grateful to Drs. A. C. Lloyd and J. L. Sprung for helpful discussions and gratefully acknowledge the financial support of NSF Grant GP-38053X.

References and Notes

- (1) R. R. Baker, R. R. Baldwin, and R. W. Walker, *Symp. (Int.) Combust., Proc.*, **13**, 291 (1971).
- (2) J. Heicklen, K. Westberg, and N. Cohen, Report No. 115-69, Center for Air Environmental Studies, 1969.
- (3) D. H. Stedman, E. D. Morris, Jr., E. E. Daby, H. Niki, and B. Weinstock, paper presented at the 160th National Meeting of the American Chemical Society, Chicago, Ill., Sept 14–18, 1970.
- (4) D. D. Davis, *Can. J. Chem.*, **52**, 1405 (1974).
- (5) M. B. McElroy, S. C. Wofsy, J. E. Penner, and J. C. McConnell, *J. Atmos. Sci.*, **31**, 287 (1974).
- (6) C. C. Wang and L. I. Davis, Jr., *Phys. Rev. Lett.*, **32**, 349 (1974).
- (7) N. R. Greiner, *J. Chem. Phys.*, **46**, 2795, 3389 (1967).
- (8) N. R. Greiner, *J. Chem. Phys.*, **53**, 1070 (1970).
- (9) E. D. Morris, Jr., and H. Niki, *J. Phys. Chem.*, **75**, 3640 (1971).
- (10) R. A. Gorse and D. H. Volman, *J. Photochem.*, **1**, 1 (1972); **3**, 115 (1974).
- (11) J. N. Bradley, W. Hack, K. Hoyermann, and H. Gg. Wagner, *J. Chem. Soc., Faraday Trans. 1*, **69**, 1889 (1973).
- (12) F. Stuhl, *Z. Naturforsch., Teil A*, **28**, 1383 (1974).
- (13) D. D. Davis, S. Fischer, and R. Schiff, *J. Chem. Phys.*, **61**, 2213 (1974).
- (14) N. R. Greiner, *J. Chem. Phys.*, **53**, 1284 (1970).
- (15) E. D. Morris, Jr., D. H. Stedman, and H. Niki, *J. Am. Chem. Soc.*, **93**, 3570 (1971).
- (16) I. W. M. Smith and R. Zellner, *J. Chem. Soc., Faraday Trans. 2*, **69**, 1617 (1973).
- (17) F. Stuhl, *Ber. Bunsenges. Phys. Chem.*, **77**, 674 (1973).
- (18) D. D. Davis, W. Bollinger, and S. Fischer, *J. Phys. Chem.*, **79**, 293 (1975).
- (19) G. J. Doyle, A. C. Lloyd, K. R. Darnall, A. M. Winer, and J. N. Pitts, Jr., *Environ. Sci. Technol.*, **9**, 237 (1975).
- (20) M. C. Dodge, Report EPA-R4-73-010, Environmental Protection Agency, Washington, D. C., 1973.
- (21) J. M. Heuss, G. J. Nebel, and B. A. D'Alleva, *Environ. Sci. Technol.*, **8**, 641 (1974).
- (22) J. Kondo and H. Akimoto, *Adv. Environ. Sci. Technol.*, in press.
- (23) R. Atkinson, D. A. Hansen, and J. N. Pitts, Jr., *J. Chem. Phys.*, **62**, 3284 (1975).
- (24) R. Atkinson and J. N. Pitts, Jr., *J. Phys. Chem.*, **78**, 1780 (1974).
- (25) F. Stuhl and H. Niki, *J. Chem. Phys.*, **57**, 3671 (1972).
- (26) G. Boocock and R. J. Cvetanovic, *Can. J. Chem.*, **39**, 2436 (1961).
- (27) G. R. H. Jones and R. J. Cvetanovic, *Can. J. Chem.*, **39**, 2444 (1961).
- (28) R. A. Bonanno, P. Kim, J. H. Lee, and R. B. Timmons, *J. Chem. Phys.*, **57**, 1377 (1972).
- (29) J. S. Gaffney, R. Atkinson, and J. N. Pitts, Jr., to be submitted for publication.
- (30) K. Nojima, K. Fukaya, S. Fukai, and S. Kanno, *Chemosphere*, **5**, 247 (1974).
- (31) C. T. Pate, R. Atkinson, and J. N. Pitts, Jr., to be submitted for publication.

Reaction of ·OH with Benzoic Acid. Isomer Distribution in the Radical Intermediates¹

George W. Klein, Kishan Bhatia, V. Madhavan, and Robert H. Schuler*

Radiation Research Laboratories and Department of Chemistry, Mellon Institute of Science, Carnegie-Mellon University, Pittsburgh, Pennsylvania 15213 (Received February 28, 1975)

Publication costs assisted by the U.S. Energy Research and Development Administration and Carnegie-Mellon University

Products of the reaction of radiation-produced OH radicals with benzoic acid under conditions where the intermediate hydroxycyclohexadienyl radicals are quantitatively oxidized to hydroxybenzoic acids have been examined by liquid chromatographic methods. In N₂O-saturated 1 mM benzoic acid solutions containing 0.5 mM ferricyanide as the radical oxidant the initial radiation chemical yields of *o*-, *m*-, and *p*-hydroxybenzoic acids are 1.7, 2.3, and 1.2, respectively. Decarboxylation contributes an additional phenol yield of 0.4 to give a total product yield of 5.6 which accounts for essentially all of the OH radicals produced in this system. Material balance considerations show that no major product is unaccounted for. Reaction at the various ortho, meta, and para positions is very nearly statistical ($k(\text{ortho}):k(\text{meta}):k(\text{para}) = 0.7:0.9:1$ per position). ESR experiments show a similar ratio of radical concentrations at steady state so that there can be little selectivity in the second-order radical combination processes. Because of the high reactivities of the phenolic products toward OH radicals, secondary reactions become important at very low conversions (a 10% reduction in yield occurs at a conversion of only 5%). The initially produced hydroxybenzoic acids are, however, not consumed to any important extent in the secondary processes so that the resultant phenoxyl radicals must, in this mixed-radical system, be reduced back to the original products rather than being oxidized further. A detailed model is described which allows one to use numerical integration methods to take the competitive effects of the secondary processes into account and to describe the course of the reaction quite well up to conversions of ~25%. The present study serves to illustrate the application of spectrophotometric and radiotracer approaches in liquid chromatographic investigations of the radiation chemistry of dilute aqueous solutions.

The reaction of OH radicals with benzoic acid has been examined in numerous pulse radiolysis,² ESR,^{3,4} and radiation chemical studies⁵⁻⁷ which show quite conclusively that the principal reaction is addition to the ring to form carboxylated hydroxycyclohexadienyl radicals. At question are the quantitative aspects of this addition, particularly with respect to possible interferences from secondary reactions, and the relative importance for OH attack at each of the ring positions. From observations during steady-state ESR studies Eiben and Fessenden³ have concluded that to a first approximation addition at the meta and para positions of the benzoate anion occurs statistically with addition at the ortho position being only ~50% as great. In a brief report on radiation chemical studies in acidic solutions in which ferricyanide was used to oxidize the intermediate carboxylated hydroxycyclohexadienyl radicals to the corresponding phenols, Volkert and Schulte-Frohlinde⁵ found that at high ferricyanide concentrations the three isomers were produced very nearly statistically. However they also reported a complicated dependence on ferricyanide concentration which indicates that secondary processes are important. Mathews and Sangster⁶ have examined the radiolysis of solutions of carboxyl-labeled benzoic acid and have found yields of 0.5-1 for hydroxyl-induced decarboxylation which occurs at least partially via postirradiation effects. We have reexamined the products resulting from the addition of radiation-produced OH radicals to benzoate anion taking advantage of recent developments in liquid chromatography⁸ to study the dose dependences in some detail. It is found that, as for hydroxycyclohexadienyl radical itself,⁹ the intermediate radicals produced in this system are quantitatively oxidized by ferricyanide. Material balance considerations show that even though secondary

reactions become important at low conversions, the initially produced hydroxybenzoic acids are, for the most part, not oxidized further. Detailed kinetic treatment allows one to extract the initial yields from the data even though it is clear that the observed yields are significantly affected by the secondary processes. One is, of course, interested in the relative yields of the initial products so that one can describe the relative frequency for attack of OH at each of the ring positions. Because these studies on a relatively simple system have been used to explore the potentialities and limitations of spectrophotometric and radiochemical detection methods in the application of high-pressure liquid chromatography to aqueous radiation chemistry, the experimental approaches are described here in some detail.

Experimental Section

Materials and Irradiations. Water was triply distilled, including distillation from basic permanganate and acid dichromate solutions. Solutions containing the desired concentrations of benzoic acid and potassium ferricyanide were purged of oxygen and saturated with N₂O by bubbling in the irradiation cell for 20-30 min. All solutions were buffered at pH 7 with 2 mM phosphate buffer.

For the ¹⁴C tracer experiments both carboxyl- and ring-labeled benzoic acid were measured (New England Nuclear Co.; specific activities respectively of 18 and 3.3 Ci/mol). Blank chromatographic experiments showed that the carboxyl-labeled material was free of any detectable radiochemical impurity. The ring-labeled sample had a small amount of impurity that eluted with *m*-hydroxybenzoic acid and had to be corrected for in the actual experiments. In order to conserve the total amount of activity these samples were diluted with inactive material to give specific ac-

tivities of ~ 2 Ci/mol. The solute concentrations (mostly 0.7 or 1.0 mM) were determined from the known content of active material (measured chromatographically) and inactive material (measured by weight) and the radiochemical sensitivities determined in terms of these concentrations. Usually 1.6 ml of the sample was irradiated so that the individual experiments required $\sim 3 \mu\text{Ci}$ of activity. At low solute concentrations the sensitivity can be improved somewhat by using samples of higher specific activities. At higher concentrations ($>10^{-3} M$) a limitation is usually imposed by the total amount of activity one is willing to consign to an experiment which, for practical purposes, means dilution with inactive material.

Irradiations were carried out in ^{60}Co sources at absorbed dose rates of 6.4×10^{17} or $4.5 \times 10^{16} \text{ eV g}^{-1} \text{ min}^{-1}$ as determined by Fricke dosimetry. Doses ranged from 10^{17} to $3 \times 10^{18} \text{ eV/g}$.

Chromatographic Separation. The characteristics of the high-pressure liquid chromatograph used in these laboratories for the analysis of irradiated aqueous solutions have been previously described.^{8,10} Chromatographic resolution of benzoic acid and the three hydroxybenzoic acids is possible¹¹ but only with considerable difficulty and only under conditions where the peaks are broadened and the sensitivity suffers. In particular it is difficult to separate *m*-hydroxybenzoic acid from both benzoic acid and its para isomer and this problem is accentuated by the fact that the meta isomer has relatively low absorption in the accessible uv region. In the present study a different separation system was used to examine each of the products. All employed either a 1- or 2-m column (2.2-mm i.d.) of "ZIPAX" strong anion-exchange resin (Du Pont No. 820960005). *p*-Hydroxybenzoic acid was eluted in front of the benzoic acid and separated from all other components using 20 mM acetic acid-acetate buffer at pH 4.2 containing 0.5 mM perchlorate (system A) as the eluent (the meta isomer is eluted with the benzoic acid). The *m*- and *p*-hydroxybenzoic acids were eluted together after the benzoic acid peak using 20 mM borate buffer at pH 9.2 containing 10 mM nitrate (system B) (phenol is eluted with the benzoic acid). Separation of the meta isomer from the other components could be obtained by using 0.1 M sodium acetate at pH 7.2 (system C) as the eluent. The separation is, however, poor and the chromatographic peak considerably wider than in the other analyses so the sensitivity is reduced accordingly. With all three systems the ortho isomer (salicylic acid) was retained on the column for a long period but could be eluted rapidly and in a reasonably narrow peak by adding a high concentration of perchlorate or nitrate. In the spectrophotometric studies this component was eluted using 20 mM acetate-2.5 mM perchlorate at pH 4.2 (system D). In the radiochemical experiments, after the other isomers had been eluted, 14 mM perchlorate was added to system A or 80 mM nitrate was added to system B. Flow rates of 1 ml/min were used in the optical studies and 0.2 ml/min in the radiochemical studies.

It was found that the column characteristics changed as the experiments progressed because of the accumulation of relatively large amounts of ferricyanide on the column. After the source of this difficulty was recognized it was found that the columns could be regenerated by eluting the ferricyanide with 0.5 M nitrate at pH 3.

Spectrophotometric Detection. In the present study the 254-nm fixed-wavelength detector used in previous investigations^{8,9} has been replaced with a Varian 635m spectro-

photometer equipped with 8- μl cells (10-mm path length). This detector has a somewhat lower signal-to-noise ratio than the previously used fixed-wavelength detector (with a time constant of 1 sec the short-term noise level corresponded to an absorbance of $\sim 10^{-4}$; see Figure 1) but permits selection of an optimum analytical wavelength and allows one optically to resolve overlapping components that have significantly different absorption spectra.^{12,13} In the present study one is fortunate in that the meta isomer absorbs in the region of 300 nm where its para isomer and benzoic acid have no significant absorption. *p*-Hydroxybenzoic acid was analyzed at 250 nm using eluting system A and the ortho isomer at 300 nm using system D. As is illustrated in Figure 1 using system C the meta isomer is best examined at 285 nm where the sensitivity is optimum and, because of the combined chromatographic and optical resolution, there is essentially no interference from the benzoic acid or the para isomer. The advantages available in the spectrophotometric approach over one using a mercury resonance line detector (254 nm) are very apparent in Figure 1. The meta isomer can also be examined at 300 nm using system A where this component is eluted along with the benzoic acid but can be examined because the latter does not absorb significantly at concentrations of $10^{-3} M$ or less. System B cannot be used because the basic form of the para isomer absorbs significantly at the high pH of the eluent. Phenol was examined at 270 nm.

The sensitivity of the apparatus for each of these components was calibrated with known samples (50 μM) containing also benzoic acid, ferricyanide, and buffer at the concentrations of the experiment. The presence of 2 mM ferricyanide in the sample has a small effect on the peak shapes and resultant sensitivities so it is important that calibrations be done with samples similar to those produced by the irradiations. At the very low concentration in these references samples the hydroxybenzoic acids are slowly oxidized so that freshly prepared solutions are required. With the above systems the analytical sensitivity (in units of absorbance at the chromatographic peak) was 0.0022/ μM for *p*-hydroxybenzoic acid, 0.0001/ μM for the meta isomer, 0.0002/ μM for the ortho isomer, 0.0005/ μM for phenol, and 0.00006/ μM for benzoic acid. Sample injection was via a 0.18-ml loop, as previously described.⁸ In general peak height reproducibility was quite good (of the order of a few percent) so that the overall analytical reliability is largely limited by problems of calibration in the detector noise level.

Radiochemical Experiments. Radiotracer experiments possess the obvious advantage that the sensitivities of all labeled products are known a priori in terms of the sensitivity of the starting material. After passing through an auxiliary optical detector the column effluent was monitored with a 1-ml flow-through scintillation cell packed with cerium-activated lithium glass scintillator beads (Packard Instrument Co.). Counting was with a Packard "Tri-Carb" coincidence scintillation spectrometer. Although the large sample volume (~ 0.4 ml) of this cell limited the overall chromatographic resolution, such a large volume was necessary in order to achieve reasonable counting rates. Little mixing occurred with the cell since the peaks were broadened only by the cell volume and no spurious "tailing" occurred. A relatively low flow rate was used (0.2 ml/min) so that the residence time of the sample within the counter volume was ~ 2 min. Preliminary experiments with anthracene as the scintillator showed it to be unsuitable

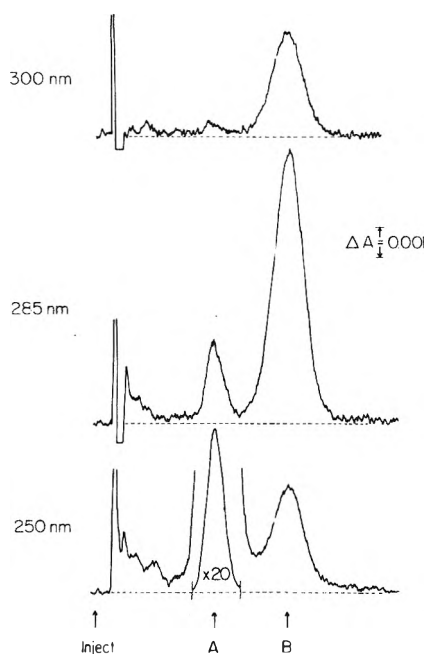


Figure 1. Chromatograms of 1 mM benzoic acid solution containing 0.5 mM ferricyanide irradiated to a dose of 3.2×10^{18} eV/g as detected at 250, 285, and 300 nm. Elution is done with 0.1 M acetate at pH 7.2. Benzoic acid (800 μM) and *p*-hydroxybenzoic acid (41 μM) are eluted at A. *m*-Hydroxybenzoic acid (69 μM) is eluted at B (elution time 13 min).

because of background increases resulting from retention of active material on the anthracene. Use of glass scintillator beads avoids memory effects almost completely (the counting level recovers to within 50 cpm of normal 10 min after passage of a benzoic acid peak of 100,000 cpm). Occasionally small increases in the background level did occur but it was found that the counting cell could be cleaned rapidly by flushing it with a detergent solution.

In order to improve the counting rates, the volume of the loop injector was increased to 0.38 ml but this increase had little effect on the peak widths. With the glass scintillator ^{14}C counting efficiency was only $\sim 10\%$ and the background rather high (>200 cpm). These values impose a fundamental detectability limit of $\sim 10^{-9}$ Ci for chromatographic peaks that have a reasonable width (~ 2 ml or 5 times the sample volume). Using a specific activity of 20 Ci/mol a practical detectability limit of $\sim 10^{-7}$ M can be readily attained in this type of experiment. By collecting samples and counting them internally in a scintillation solution this limit can be extended by about 2 orders of magnitude provided the components can be adequately resolved chromatographically. In the present experiments the specific activities used were an order of magnitude lower than above and the sensitivities reduced accordingly. The concentration of each of the products was determined by comparing the activity under a chromatographic peak with that in the benzoic acid peak of an unirradiated sample of known concentration and, in general, should be accurate to of the order of a few percent with a detectability limit of about 1 μM . Maximum counting rates were $<100,000$ cpm so that coincidence losses were less than a few percent (coincidence losses were measured to be 10% at 500,000 cpm). For the on-line measurements the total count will vary inversely with the flow rate so that it is important to maintain constant flow rates, particularly where differences are to be ex-

amined. In any one experiment the flow was set and not disturbed during the course of the experiment (including the examination of the reference solution). For the experiments where material balance was examined in detail the complete benzoic acid peaks of the initial and irradiated samples were collected, the total samples weighed, and aliquots counted internally in a liquid scintillator ("Hand-fluor"; Mallinckrodt Chemical Works). Total activities measured in this way do not involve any consideration of flow and in any one set of experiments were reproducible to $\sim 1\%$ so that the yield for consumption of benzoic acid can be determined to $\sim 5\%$ in the region of 25% conversion.

Pulse Radiolysis and ESR Experiments. Pulse radiolytic determinations of the rate for reaction of OH with *m*-hydroxybenzoic acid and for the oxidation of the intermediate hydroxycyclohexadienyl radicals by ferricyanide were carried out using the computer-controlled pulse radiolysis apparatus described by Patterson and Lillie.¹⁴ ESR studies of the relative steady-state concentrations for each of the intermediate radicals were carried out by the in situ radiolysis-ESR methods described by Eiben and Fessenden.³

Results

As expected the principal products produced in the presence of ferricyanide are the hydroxybenzoic acids. This aspect is illustrated very well by the radiochromatograms of Figure 2. Since the sensitivity for each of the *tagged* products is identical with that of the starting material, in these chromatograms one can see directly the importance of each group of products and be virtually certain that no others are produced in any appreciable yield. In the absence of ferricyanide the yields of the hydroxybenzoic acids are low and a melange of additional unidentified products is produced as is illustrated in Figure 3.

It is seen in Figure 2b that, in addition to the hydroxybenzoic acids, a significant fraction of the product activity ($\sim 10\%$) from the carboxyl-labeled benzoic acid is eluted with little or no retention (peak A). This activity represents, to a large extent, bicarbonate produced by decarboxylation. With ring-labeled material this peak (cf. Figure 2a) is very much smaller ($\sim 2\%$) and, since any CO_2 will be unlabeled, must be attributed to organic products (e.g., hydroquinone) which are very likely produced in secondary reactions. Using eluting system A the yield of phenol from the ring-labeled material accounts for only 7% of the activity. One also sees a small peak (peak D from Figure 1a) just in front of the salicylic acid which amounts to 2–3% of the product and must contain both a ring and a carboxyl group since it is observed with both types of label. Presumably this product is produced in secondary reactions but because of the low yield cannot be followed in any detail. Increasing the nitrate or perchlorate concentration in the eluent does not wash any additional activity off the column so that one can be quite sure that compounds of greater retention volumes are not produced to any significant extent.

Material Balance. The uniform detection sensitivity for each of the products makes these radiochemical experiments ideal for considerations of material balance. In general it was found that within experimental error the total activity in the product chromatogram was equal to the activity in the benzoic acid peak in a parallel chromatogram of the starting sample so that no important component is being missed. Data for two experiments with carboxyl-labeled material taken at a dose sufficient to consume $\sim 25\%$ of the benzoic acid are given in Table I. The loss in activity

TABLE I: Illustrative Radiochemical Experiments and Material Balance^a

	Expt A ^b		Expt B	
	Activity ^c	Concn. μM	Activity ^c	Concn. μM
Collected samples				
Initial soln	1,092,782	720	1,159,996	720
Irradiated soln	823,508	543	845,524	525
Benzoic acid consumed		177 (24.6%)		195 (27.1%)
On line counting				
Initial soln	412,720 ^d	720	452,585 ^c	720
Irradiated soln	307,336	536	340,028	541
Benzoic acid consumed	(105,384)	184 (25.5%)	(112,457)	179 (24.9%)
Peak A	11,673	21	13,732	22
<i>m</i> - + <i>p</i> -Hydroxybenzoic acid	62,470	109	65,840	105
<i>o</i> -Hydroxybenzoic acid	32,008	56	33,385	53
Peak D	1,685	3	2,032	3
Total products	107,836	189 (26.2%)	114,989	183 (25.4%)

^a Duplicate samples containing 0.72 mM carboxyl-labeled benzoic acid, 2 mM phosphate buffer, and 2 mM ferricyanide as oxidant. Irradiations were at a dose of 3.2×10^{18} eV/g. Elution was with a nitrate-borate system. A priori calculation based on integration of eq 7 with $G(\text{OH}) = 5.6$ indicates that consumption of benzoic acid should be 199 mM or 27.6% at this dose. ^b Experiment illustrated in Figure 2b and c. ^c For collected samples the total activities (in cpm) were determined from measurements in a liquid scintillator on 500- μl aliquots of the collected samples (volume ~ 5 ml as determined by weight). On-line activities represent the integrated count (corrected for background) obtained for a sample residence time of ~ 2 min and will be inversely dependent on the flow rate. Slight differences in activities reflect day to day variations in counting efficiencies and flow rates. ^d Relative specific activities calculated from these values were used in determining the concentrations in the subsequent data.

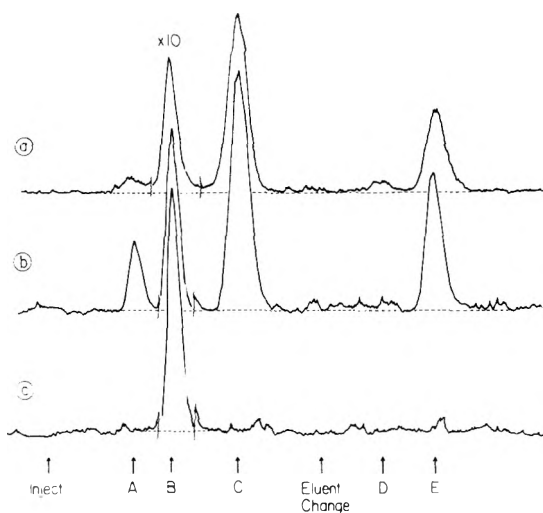


Figure 2. Radiochromatograms of (a) 0.64 mM ring-labeled benzoic acid solution and (b) 0.72 mM carboxyl-labeled benzoic acid solution containing 2 mM ferricyanide and saturated with N_2O . Both were irradiated to a dose of 3.2×10^{18} eV/g; part (c) is the blank for (b). Eluent was initially 20 mM borate-10 mM nitrate at pH 9.2; nitrate is increased to 80 mM at the point marked for eluent change. A is the point at which unretained components will pass through the detector (HCO_3^- , hydroquinone). Peak B is benzoic acid (and phenol) sensitivity decreased by a factor of 10; note that this peak is 25% smaller in (b) than in (c). Peak C is unresolved *m*- and *p*-hydroxybenzoic acid and peak E the *o*-hydroxybenzoic acid. Peak D is very likely a dihydroxybenzoic acid produced in a secondary reaction. Increasing the nitrate to 0.5 M showed very little additional activity so that there can be no significant products with greater retention volumes. Entire chromatogram takes ~ 160 min.

in the benzoic acid fraction is essentially completely accounted for by the activities observed in the three major product peaks. These data show very clearly that even though the product hydroxybenzoic acids must be attacked

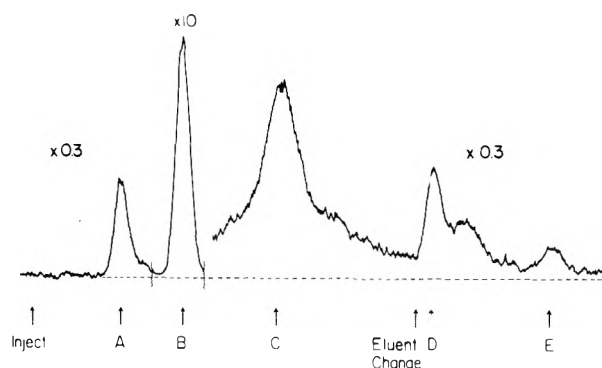


Figure 3. Radiochromatogram of 1.28 mM ring-labeled benzoic acid irradiated to a dose of 1.9×10^{18} eV/g; no ferricyanide present. Peaks A, B, C, and E are as in Figure 2. D is a false peak that arises because of a pile up of activity after the eluent change. Note that peaks C and E are considerably smaller than in Figure 2 and account for only about one-third of the total activity eluted after the benzoic acid. Peak A contains $\sim 10\%$ of the product activity and is much larger than observed for the ring-labeled material in the presence of ferricyanide (see Figure 2a).

to a significant extent at the conversion levels involved in these experiments these products are not, for the most part, oxidized further to carboxyl-labeled secondary products (which would presumably fall elsewhere in the chromatogram). Small amounts of additional products are, indeed, formed ($\sim 5\%$) but they account for only a small fraction of the secondary reactions that must be occurring.

Dependence of Yield on Dose. The dose dependence for each of the components measured in the radiochemical experiments is illustrated by the solid symbols in Figure 4. It is seen that the yields fall off considerably at doses sufficient to convert a significant fraction of the benzoic acid to product and that in the region of 25% conversion the total yield is only 3.5. The ratio of the yields of *o*- and *p*-hydroxybenzoic acids from the relative activities in their respec-

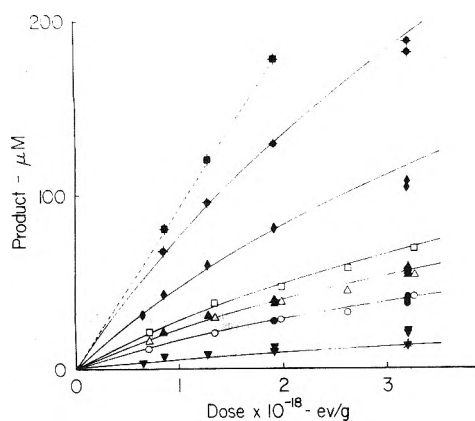


Figure 4. Dose dependence of the product yields from 0.7–1 mM benzoic acid solutions (N_2O saturated containing 2.0 mM ferricyanide): closed symbols from radiochemical experiments; open symbols from experiments with spectrophotometric detection; \blacklozenge , from total product activity (\blacksquare , corrected by factor indicated by numerical integration of eq 7; see text); \blacklozenge , from activity in peak C of Figure 2 (sum of *m*- and *p*-hydroxybenzoic acids); \blacktriangle , \blacktriangle , *o*-hydroxybenzoic acid; \bullet , \circ , *p*-hydroxybenzoic acid; \square , *m*-hydroxybenzoic acid; \blacktriangledown , CO_2 fraction; \blacktriangledown , phenol. Solid curves are calculated by integration of eq 7 and 8 as described in the text (dotted curve by integration of eq 10).

tive peaks using eluting system A is identical for both the ring- and carboxyl-labeled samples ($G(\text{ortho})/G(\text{para}) = 1.4 \pm 0.1$). The ratio of the sum of the yields for the meta and para isomers to that of the ortho isomer (as measured with eluting system B) is within experimental error independent of dose and equal to 2.05 ± 0.10 . The *m*-hydroxybenzoic acid was not sufficiently well resolved to allow independent measurements of its yield in the radiochemical experiments. Subtracting the yield of the para isomer as determined with eluting system A from that of the combined peaks determined with eluting system B one obtains a ratio for $G(\text{meta})$ to $G(\text{para})$ of 1.9 ± 0.1 .

Spectrophotometric Detection. The production of each of the hydroxybenzoic acids was examined in chromatographic experiments with spectrophotometric detection but only in the case of the para isomer was the sensitivity high enough to make it possible to examine the yields at doses significantly lower than those used in the radiochemical experiments. These results, included as the open symbols in Figure 4, show that the production curves for the ortho and para isomers are similar to those found in the radiochemical studies. The ratios of yields do not observably change with dose. The yields of the meta isomer are slightly lower than those indicated by the differences mentioned above. From these spectrophotometric studies the averages of the ratios measured at each dose for $G(\text{ortho}):G(\text{meta}):G(\text{para})$ are 1.35:1.75:1.

Dependence on Ferricyanide Concentration. Yields of the para isomer were examined at lower doses and at lower ferricyanide concentrations. These data, given in Figure 5, show that the yields are not dependent on ferricyanide concentration over the range of 0.2–2 mM, as was also found in the case for hydroxylation of benzene.⁹ There clearly is no concentration dependence of the magnitude reported by Volkert and Schulte-Frohlinde⁷ although it should be pointed out that their study was carried out at pH 4 where the chemistry may be somewhat different. In the absence of ferricyanide the yield of *p*-hydroxybenzoic acid at low dose, as detected optically, is about one-fourth of that indicated in Figure 5. It is not clear what fraction of this yield

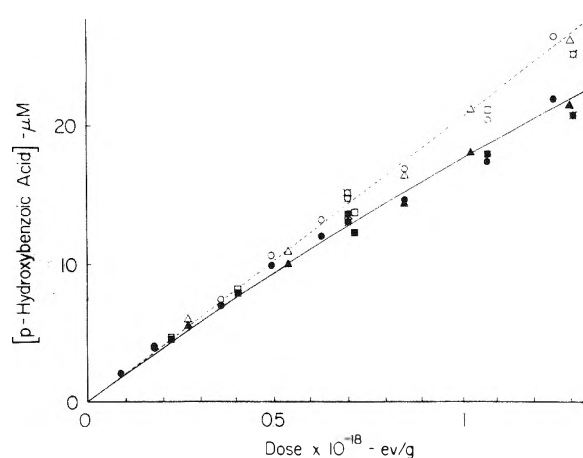


Figure 5. Dose dependence of the yield of *p*-hydroxybenzoic acid from 1 mM benzoic acid solutions (N_2O saturated): solid symbols are the experimental data; open symbols are corrected by the factors indicated by numerical integration of eq 8; \bullet , \blacksquare , samples containing 2.0 mM ferricyanide; \blacktriangle , containing 0.5 mM ferricyanide; \blacksquare , containing 0.2 mM ferricyanide. The yields for the 2.0 mM solution have been corrected by a factor of 5.8/5.6 to take into account the slightly lower OH yield expected at this concentration. Dose rate was $4.5 \times 10^{16} \text{ eV g}^{-1} \text{ min}^{-1}$ except for the flagged circles where it was $6.4 \times 10^{17} \text{ eV g}^{-1} \text{ min}^{-1}$.

results from disproportionation of the intermediate radicals or how large a contribution is made by spurious oxidation processes.

Rate Information. In order to treat the competitive secondary reactions properly one needs a complete set of rate constants for reaction of OH with benzoic acid and with the reaction products. The rate constants for reaction of OH with benzoic acid, phenol, *o*-hydroxybenzoate anion, and *p*-hydroxybenzoate anion have been reported as 6.0×10^9 , 1.4×10^{10} , 1.2×10^{10} , and $9 \times 10^9 \text{ M}^{-1} \text{ sec}^{-1}$, respectively.^{2,15,16} During the present study we have measured the rate constant for reaction of OH with *m*-hydroxybenzoic acid at pH 7 to be $(7.8 \pm 0.4) \times 10^9 \text{ M}^{-1} \text{ sec}^{-1}$ from observations on the rate of buildup of the intermediate hydroxycyclohexadienyl radicals.

The oxidation of the intermediate hydroxycyclohexadienyl radicals by ferricyanide was examined by following the absorption of the radicals at 355 nm where they have an extinction coefficient of $\sim 2000 \text{ M}^{-1} \text{ cm}^{-1}$ and there is a window in the ferricyanide spectrum (extinction coefficient of $360 \text{ M}^{-1} \text{ cm}^{-1}$). Experiments were carried out at radical concentrations of $\sim 1 \mu\text{M}$ where the median lifetimes were observed to be $\sim 1 \text{ msec}$. In the initial experiments using a 2-cm absorption cell it was shown that in the presence of 0.5 mM ferricyanide the hydroxycyclohexadienyl absorption decayed by $<10\%$ over a period of 200 μsec which sets an upper limit of $2 \times 10^6 \text{ M}^{-1} \text{ sec}^{-1}$ on the rate constant. Using a 0.5-cm absorption cell and signal-averaging methods (100 experiments) we were able to examine the reaction at 11.5 mM ferricyanide even though the transmission of the sample was only $\sim 1\%$. A decay period of 130 μsec was observed. Making a 10% correction for the second-order decay of the radicals a rate constant of $4 \times 10^5 \text{ M}^{-1} \text{ sec}^{-1}$ is obtained for the oxidation reaction in this solution. The rate constant in the millimolar solutions, which is expected to be a factor of ~ 2 – 3 less because of the lower ionic strength, can reasonably be given as $(2 \pm 1) \times 10^5 \text{ M}^{-1} \text{ sec}^{-1}$. The reaction cannot be much slower since the ferricyanide is effective as an oxidant at $2 \times 10^{-4} \text{ M}$ at a dose rate where, in the absence of the ferricyanide, the median

radical lifetime is ~ 0.1 sec. With a rate constant of $2 \times 10^5 M^{-1} \text{ sec}^{-1}$ for the oxidation the reaction period is 0.02 sec and the radicals are not permitted to build up to a concentration where second-order recombination plays a significant role. At dose rates only somewhat higher than those used here complications from second-order reactions between radicals should set in and one can expect a dependence of the yields on the ferricyanide concentration. It is clear that in studies with chemically produced OH radicals, e.g., in the hydroxylation of aromatic systems using Fenton's reagent, ferricyanide will not be effective as a radical oxidant unless one is careful to maintain the radical production rate less than $\sim 10^{-3} M/\text{sec}$.

ESR Experiments. Eiben and Fessenden³ have given an ESR spectrum observed during the irradiation of benzoic acid solutions which shows that at steady state all of the isomeric carboxyl-substituted hydroxycyclohexadienyl radicals are present at comparable concentrations. They have commented that the observed relative intensities indicate that the meta and para adducts are produced at similar rates (per position available) and the ortho adduct is produced at about half the rate. We have repeated their experiment to examine in slightly greater detail the region 20 G above the spectral center where lines from each of the three radicals appear adjacent to each other. This study was carried out at pH 13 where the splitting by the OH proton is eliminated by exchange but the radical identity is maintained. Modulation conditions were adjusted so that slight differences in line width would not affect the relative intensities. The spectrum given in Figure 6 shows that the steady-state concentrations of radicals produced by OH addition at the ortho, meta, and para positions are in the ratios 1.4:1.8:1. Since essentially identical relative production rates are indicated by the present product studies, it is clear that there is very little selectivity in the second-order processes that control the steady state in the ESR experiments. It is perhaps a little surprising that the hydroxycyclohexadienyl radicals carboxylated at the 1 or 3 positions are not observed in somewhat higher relative intensities (since in more highly carboxylated cyclohexadienyl radicals substitution at the positions of high spin density does tend to interfere with the recombination processes⁴) but apparently the effects of a single substitution are not sufficient to produce an observable difference.

Kinetic Analysis and Initial Yields

The initial yield of hydroxy radicals expected for an N_2O -saturated solution 1 mM in benzoic acid and 2 mM in ferricyanide is 5.6.¹⁷ The total product yield of ~ 4.7 observed at a dose of 10^{18} eV/g is reasonably in accord with this value but it is quite clear from the pronounced curvature of the data of Figure 4 that secondary processes are coming into play at even lower doses. This strong dependence of yield on dose is expected since, as indicated above, the rate constants for reaction of OH with the products are all somewhat greater than for reaction with benzoic acid. Proceeding iteratively one can estimate appropriate corrections to the data from preliminary calculations based on integration of the kinetic expressions that describe the competitive effects of the buildup of product, apply these corrections to the experimental data to determine the initial yields, and then refine the calculations to obtain more accurate values. In practice for solutions ~ 1 mM in benzoic acid and doses less than $\sim 10^{18}$ eV/g the corrections are small ($< 20\%$) and insensitive to the kinetic details so that

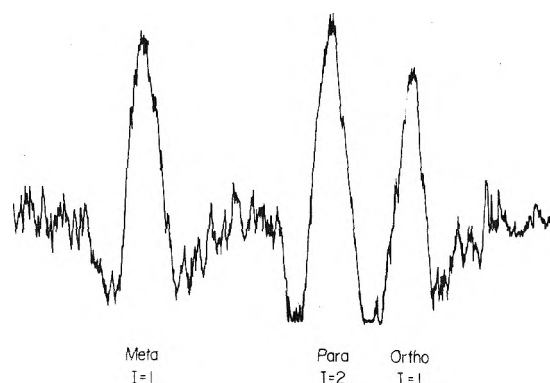
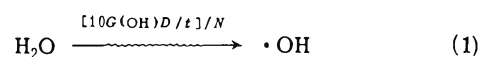


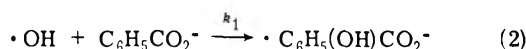
Figure 6. ESR spectrum observed during the irradiation of a 1 mM benzoic acid solution at pH 13 in the region of ~ 20 G above the spectral center. The three lines represent unit intensity lines of the radical produced by OH addition at the meta and ortho positions and a doubly intense line of the isomer produced by addition at the para position (see Figure 7 in ref 3). If addition occurs statistically, all three lines should be equally intense. The relative intensities are estimated to be 0.7, 0.9, and 1 for the ortho, meta, and para adducts.

only one iteration is necessary. The calculated corrections depend on the relative values of the rate constants involved but it is believed that these are known sufficiently well that the possible errors cannot be more than a few percent (a 20% uncertainty in the relative rate constants introduces an uncertainty of only 3% in the correction at a dose of 2×10^{18} eV/g).

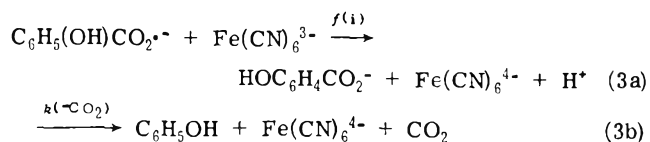
The reaction of prime interest is, of course, that of the OH radicals produced from the water



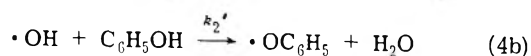
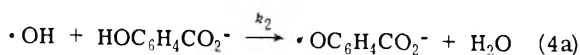
with the benzoic acid



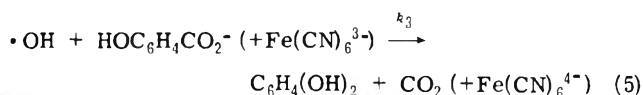
where the production rate of OH radicals ($10G(OH)D/tN$) is given by OH yield ($G(OH)$ in radicals/100 eV) and the dose rate D/t in $eV g^{-1} \text{ sec}^{-1}$ (N is Avogadro's number). The stoichiometry involved in the subsequent oxidation of the hydroxycyclohexadienyl radicals can be represented by



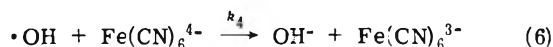
The hydroxybenzoic acids and phenol produced in reaction 3 will, as they build up, compete more and more for the OH radicals. It is known that in the presence of millimolar phosphate buffer the initial adduct of OH to phenol eliminates water with a period $\sim 25 \mu\text{sec}$ to form phenoxyl radical¹⁵ so that phenoxyl and the carboxyl-substituted phenoxyl radicals are expected to be the important intermediate produced in the secondary processes



Some decarboxylation is also expected and should be accompanied by reduction of ferricyanide



but the fractional contribution of this reaction, $\sim k_3/k_2$, is expected to be small (<10%). Phenoxy radicals are strong oxidizing agents so that it seems likely that they will either oxidize the intermediate hydroxycyclohexadienyl radicals or the ferrocyanide and, as a result, be converted back to the hydroxybenzoic acids. The initial products will, therefore, not be destroyed by the secondary reactions (as is indicated experimentally by the almost complete absence of more highly oxidized products (see Figure 2)). It is known that OH radicals react very rapidly with ferrocyanide



($k_4 = 1.1 \times 10^{10} \text{ M}^{-1} \text{ sec}^{-1}$)²¹ so that this product will also cause appreciable interference with reaction 2. The carboxylated cyclohexadienyl radicals produced from H atoms are expected to be oxidized to benzoic acid and should not directly affect reaction 2 nor contribute to the organic products.²²

According to the above, the differential equation which describes the consumption of benzoic acid as a function of dose (D) is

$$-\frac{d[\text{S}]}{dD} = \frac{10G(\text{OH})}{N} \frac{1}{1 + \frac{k_2([\text{S}]_0 - [\text{S}])}{k_1[\text{S}]} + \frac{k_4[\text{Fe}(\text{CN})_6^{4-}]}{k_1[\text{S}]}} \quad (7)$$

where $[\text{S}]_0$ and $[\text{S}]$ are the initial and instantaneous benzoic acid concentrations, k_2 is the average rate constant applicable to the reaction of OH with the organic products, and k_4 is the rate constant for reaction of OH with ferrocyanide. Peroxide will also build up in this system but its reaction with OH is so slow ($\sim 10^7 \text{ M}^{-1} \text{ sec}^{-1}$)²³ that no significant removal of OH will occur at small conversions of the benzoic acid. The production of the individual hydroxybenzoic acids (P_i) should be given quite well by

$$\frac{d[\text{P}_i]}{dD} = -\frac{d[\text{S}]}{dD} \left(f(i) - \frac{k_3[\text{P}_i]}{k_1[\text{S}]} \right) \approx -\frac{d[\text{S}]}{dD} f(i) \left(1 - \frac{k_3 \sum[\text{P}_i]}{k_2[\text{S}]} \right) \quad (8)$$

where $f(i)$ is the fractional yield for production of a particular isomer. The second term in eq 8 corrects for any decarboxylation that occurs and presumably is small so that one does not expect any large change in the isomer distribution with increased dose. For phenol $f(i)$ is replaced in eq 8 by $f(-\text{CO}_2)$ and the second term will, of course, be absent. Calculation of the dose dependence of the ferricyanide concentration requires correction for the reoxidation of the ferrocyanide by reaction 6 and for the additional reduction of ferricyanide that accompanies the secondary decarboxylation reactions. Ferrocyanide will also be produced by the oxidation of the H atom adducts.

$$\frac{d[\text{Fe}(\text{CN})_6^{4-}]}{dD} = \left(-\frac{d[\text{S}]}{dD} \right) \left(1 - \frac{k_4[\text{Fe}(\text{CN})_6^{4-}]}{k_1[\text{S}]} - \left(1 - 2\frac{k_3 \sum[\text{P}_i]}{k_2[\text{S}]} \right) \right) + \frac{10G(\text{H})}{N} \quad (9)$$

The production of CO_2 should be given by

$$\frac{d[\text{CO}_2]}{dD} = -\frac{d[\text{S}]}{dD} \left(\frac{1}{1 + \frac{k_3}{k_2}} \right) \frac{k_3}{k_2} \left(1 + \frac{k_2 \sum[\text{P}_i]}{k_1[\text{S}]} \right) \quad (10)$$

Numerical integration of the above set of differential equations was carried out on a Hewlett-Packard 9830 calculator with the average value of k_2/k_1 (appropriately weighted according to the relative yield of products) taken as 1.65, k_3/k_1 as 2.9, and k_3/k_2 as 0.07. These calculations show that for doses up to $\sim 10^{18} \text{ eV/g}$ the principal complications result from removal of OH radicals by reaction with the organic products and with ferrocyanide. Decarboxylation of the hydroxybenzoic acids reduces the yield of these products slightly in the region of $3 \times 10^{18} \text{ eV/g}$ and contributes somewhat to the CO_2 production (compare the dotted line and lowest solid curve in Figure 4). At still higher doses the second-order reactions between phenoxy radicals can be expected to lead to partial consumption of the products²⁴ but more detailed knowledge of the steady-state concentrations of each of the intermediates is required to take these reactions into account quantitatively.

If the radiochemical measurements for total product formation from the carboxyl-labeled material are corrected for the expected loss in the secondary processes, then, as indicated by the dashed curve in Figure 4, one finds a linear increase with dose up to $\sim 2 \times 10^{18} \text{ eV/g}$. A slight ($\sim 5\%$) decrease is observed in the region $\sim 3 \times 10^{18} \text{ eV/g}$ which can be attributed to reactions not adequately accounted for by the above equations. The initial yield for production of products (and consumption of benzoic acid) from the three points at the lowest doses is 5.7 in excellent agreement with the expected yield of 5.6.¹⁷ Turning the calculation around, if we assume an OH yield of 5.6, then the dose dependence for the consumption of benzoic acid (the integral of eq 7) is given by the uppermost solid line of Figure 4. Within a possible error of $\sim 5\%$ (from dosimetry, analysis and interpretation) it is seen that all of the OH radicals are accounted for. In the radiochemical measurements the initial product distribution is broken down to 62% for the sum of the *m*- and *p*-hydroxybenzoic acids and 30% for the *o*-hydroxybenzoic acid. The curves in Figure 4 for these components are calculated from eq 8 using these fractions. The contribution of the para isomer, as measured radiochemically, is 21% leaving 42% of the activity to be assigned to the meta isomer. Unfortunately this latter product could not be sufficiently well resolved from the other components to make an accurate radiochemical measurement practical. From the overall fit of the curves to the data ratios of 1.43:1.95:1 for *G*(ortho):*G*(meta):*G*(para) are indicated by the radiochemical measurements. Measurements of phenol production from the ring-labeled material show it represents $\sim 7\%$ of the total expected product. Because of possible contributions from secondary processes the production of CO_2 from the carboxyl-labeled material is more difficult to interpret but an initial fractional yield of decarboxylation in the range of 7–10% is indicated.

The spectrophotometric measurements of the production of the *o*-, *m*-, and *p*-hydroxybenzoic acids reported in Figure 4 can be fitted quite well by integration of eq 8 with fractional contributions of 30, 37, and 21%. The fractional yields of the ortho and para isomers are in good agreement with those measured radiochemically. The fractional yield of the meta isomer (37%) is somewhat lower than indicated

by the difference noted above in the radiochemical experiments (41%).

The higher analytical sensitivity in the spectrophotometric determination of *p*-hydroxybenzoic acid allows measurements at doses in the range of 10^{17} – 10^{18} eV/g where the corrections are less than 20% and can be made very accurately. The experimental data in Figure 5 (solid symbols) have been approximately corrected (open symbols) to give a linearized plot with a slope corresponding to an initial yield of 1.22 for the formation of *p*-hydroxybenzoic acid. At these doses the only important complication is the loss of OH radicals in reactions 4 and 6 so that interpretive difficulties are at a minimum and the uncertainty in the initial yield can reasonably be estimated as ± 0.05 . This initial yield (1.22) is, in fact, 21.0% of the expected OH yield of 5.8^{17} in agreement with the fractional production determined in the radiochemical experiments at higher doses.

The individual initial yield of the *o*-hydroxybenzoic acid, as indicated by the above yield for the para isomer and the ratios determined in the spectrophotometric and radiochemical experiments, is $1.7 (\pm 0.1)$. The spectrophotometric measurements give an initial yield of 2.2 for the meta isomer while the radiochemical measurements indicate a slightly higher value of 2.4 so that this yield can be reasonably given as 2.3 ± 0.2 . In the initial stages, the three isomeric hydroxybenzoic acids, therefore, account for a total yield of 5.2 ± 0.3 or $90 \pm 5\%$ of the OH reactions. Decarboxylation accounts for a yield of 0.4 ± 0.1 ($7 \pm 2\%$) or most of the remainder. It, of course, does not seem likely that in the absence of complications other reaction paths will be open to the OH radicals. It is indeed comforting that essentially all of the expected radical intermediates can be converted to well-defined products.

Summary

In summary these studies show that at low production rates ($<10^{-6}$ M/sec) the hydroxycyclohexadienyl radicals produced in the reaction of OH radicals with benzoic acid are quantitatively oxidized to phenolic products with ferricyanide at concentrations as low as 2×10^{-4} M. The measured oxidation rate is low (2×10^5 M⁻¹ sec⁻¹) so that complications can be expected at low ferricyanide concentrations and high radical production rates. The individual initial yields of the *o*-, *m*-, and *p*-hydroxybenzoic acids produced in N₂O-saturated solutions are 1.7, 2.3, and 1.2 with decarboxylation contributing an additional yield of 0.4. Secondary reactions involving attack of OH on the products are clearly very important, even at low conversions, but these secondary reactions do not lead to further oxidation of the products. Finally, the ratios of the product

yields are very similar to the ratios of the precursor radicals observed at steady state so that there can be little selectivity in the second-order reactions removing these radicals in the latter instance.

Acknowledgment. The authors wish to thank Dr. P. Neta for valuable discussions on the rate constants for reaction of intermediates with the various materials present in the systems studied here.

References and Notes

- (1) Supported in part by the U.S. Energy Research and Development Administration.
- (2) P. Neta and L. M. Dorfman, *Adv. Chem. Ser.*, **No. 81**, 222 (1968).
- (3) K. Eiben and R. W. Fessenden, *J. Phys. Chem.*, **75**, 1186 (1971).
- (4) K. Eiben and R. H. Schuler, *J. Chem. Phys.*, **62**, 3093 (1975).
- (5) I. Loeff and A. J. Swallow, *J. Phys. Chem.*, **68**, 2470 (1964).
- (6) R. W. Mathews and D. F. Sangster, *J. Phys. Chem.*, **69**, 1938 (1965).
- (7) O. Volkert and D. Schulte-Frohlinde, *Tetrahedron Lett.*, **17**, 2151 (1968). See this paper for reference to other earlier studies.
- (8) See K. Bhatia and R. H. Schuler, *J. Phys. Chem.*, **77**, 1356 (1973), for an illustrative example of the application of high-pressure liquid chromatography to studies of the radiation chemistry of aqueous systems.
- (9) K. Bhatia and R. H. Schuler, *J. Phys. Chem.*, **78**, 2335 (1974).
- (10) K. Bhatia, *Anal. Chem.*, **45**, 1344 (1973). In the spectrophotometric studies reported here the pump has been replaced with a Waters Associates Model 6000 digitally controlled chromatographic pump.
- (11) U. Kramer and K. Bhatia, *J. Chromatogr.*, **89**, 348 (1974).
- (12) This technique has recently been used in a recent study of the radiation-induced oxidation of nitrobenzenes: K. Bhatia, *J. Phys. Chem.*, **79**, 1032 (1975).
- (13) Extinction coefficients of benzoic acid and the *o*-, *m*-, and *p*-hydroxybenzoic acids are (at pH 7) 920, 500, 1000, and $12,000$ M⁻¹ cm⁻¹ at 250 nm and <1 , 3700, 900, and <10 M⁻¹ cm⁻¹ at 300 nm. The extinction coefficient of *m*-hydroxybenzoic acid is 2200 M⁻¹ cm⁻¹ at 285 nm. Phenol was detected at 270 nm where its extinction coefficient is 1500 M⁻¹ cm⁻¹.
- (14) L. K. Patterson and J. Lilie, *Int. J. Radiat. Phys. Chem.*, **6**, 129 (1974).
- (15) E. J. Land and M. Ebert, *Trans. Faraday Soc.*, **63**, 1181 (1967).
- (16) C. B. Amphlett, G. E. Adams, and B. D. Michael, *Adv. Chem. Ser.*, **No. 81**, 231 (1968).
- (17) From the reported rate constants¹⁸⁻²⁰ it is estimated that for solutes containing 1 mM benzoic acid and 0.5 and 2.0 mM ferricyanide, 5 and 14% of the hydrated electrons, respectively, do not react with the N₂O. The OH yields will, therefore, be 0.2 and 0.4 unit lower than the yield of 6.0 expected for N₂O-saturated water.
- (18) J. P. Keene, *Radiat. Res.*, **22**, 1 (1964).
- (19) M. Anbar and E. J. Hart, *J. Phys. Chem.*, **69**, 973 (1965).
- (20) S. Gordon, E. J. Hart, M. S. Matheson, J. Rabani, and J. K. Thomas, *J. Am. Chem. Soc.*, **85**, 1375 (1963).
- (21) J. Rabani and M. S. Matheson, *J. Am. Chem. Soc.*, **86**, 3175 (1964).
- (22) The studies of C. L. Brett and V. Gold, *J. Chem. Soc., Perkin Trans. 2*, 1437 (1973), with tritium atoms make it clear that the hydrogen atom adducts of aromatics can be readily oxidized back to the starting materials.
- (23) H. A. Schwarz, *J. Phys. Chem.*, **66**, 255 (1962).
- (24) During the course of these studies it has been shown that N₂O-saturated *p*-hydroxybenzoic acid, when irradiated by itself in the presence of ferricyanide, is consumed with a $G \approx 3$. The products have not, as yet, been identified. In the present instance reducing entities produced by the reaction of OH with benzoic acid dominate the products up to 25% conversion so that it is reasonable that phenoxy radicals will be reduced back to the hydroxybenzoic acids at low conversions. At high conversions, however, phenoxy radicals will dominate the intermediates and loss of product can be expected.

Polarographic and Optical Pulse Radiolysis Study of the Radicals Formed by OH Attack on Imidazole and Related Compounds in Aqueous Solutions

K. M. Bansal¹ and R. M. Sellers*²

Hahn-Meitner-Institut für Kernforschung Berlin GmbH, Bereich Strahlenchemie, 1 Berlin 39, West Germany (Received December 6, 1974)

Publication costs assisted by Hahn-Meitner-Institut für Kernforschung Berlin GmbH

Polarographic and optical pulse radiolysis studies of the radicals formed by OH attack on imidazole, 1-methylimidazole, 2-methylimidazole, and histidine have been performed. The absorption spectra of the radicals are characterized by peaks at 300 ± 15 and 390 ± 10 nm. The pK_a values of the radicals, measured from the pH dependence of the spectra, are ca. 1–2 units below those of the corresponding parent compound. At high pH's (>11) a first-order, pH-dependent decay was observed with imidazole, 2-methylimidazole, and histidine, and is attributed to a water elimination reaction. The principal features of the polarograms are (i) a flat cathodic wave at potentials more negative than 0 V for the protonated radicals and (ii) for the unprotonated radicals a steep anodic wave extending up to ca. -0.5 V followed by a flatter cathodic wave. The polarographic data at high pH's (>11) are consistent with the rearrangement reaction observed in the optical experiments.

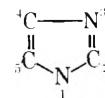
The imidazole ring is an important functional group in many biochemicals. It is widely distributed in nature as part of the histidine residue, and as such is an important constituent, for instance, of the active center of enzymes such as ribonuclease.³ It also occurs, fused to aromatic rings, in compounds such as the purines and benzimidazoles, while metronidazole (1- β -hydroxyethyl-2-methyl-5-nitroimidazole), because of its low toxicity, has found some application as a radiosensitizer of anoxic cells.⁴ Much interest in radiation chemistry and biology has focussed on inactivation studies of biochemicals, and radiation effects on tissue, and it is clearly relevant to these to find out how the primary radiation produced radicals in water, e_{aq}^- , OH, and H, react with the individual constituents of these macromolecules. Much work has been done on this, although compounds containing the imidazole ring have received little attention. We report here a study using polarographic and optical pulse radiolysis techniques on the radicals formed by OH attack on imidazole, 1-methylimidazole, 2-methylimidazole, and histidine which indicate (i) that they have absorption maxima at 300 ± 15 and 390 ± 10 nm, (ii) that the pK_a 's of the radicals are ca. 1–2 pH units less than those of the corresponding parent compounds, and (iii) that in alkaline solutions (pH >11) a water elimination reaction occurs. Some preliminary results with imidazole have been reported elsewhere.⁵

Experimental Section

Apparatus. Optical pulse radiolysis experiments were carried out using 0.5–5.0- μ sec pulses of 1.6-MeV electrons from a Van de Graaff accelerator. The optical system consisted of a 450-W xenon lamp, a 1.5-cm path length cell, a Zeiss MQ4 III prism monochromator, and an EMI 9558 QB photomultiplier. Other details were as described elsewhere.^{6–8} Dosimetry was performed using aerated 10^{-2} M CNS⁻, taking $G((CNS)_2^-) = 2.8$ and $\epsilon_{475}((CNS)_2^-)$ as 7600 $M^{-1} \text{ cm}^{-1}$.

The polarographic pulse radiolysis experiments were performed using 20-nsec pulses of 12-MeV electrons from a linear accelerator. The polarographic circuit consisted of a hanging mercury drop electrode (surface area 0.02 cm^2),

the solution containing 0.35 M Na_2SO_4 as the supporting electrolyte, a mercury pool 8 mm from the drop as the second electrode, the potential supply, and a working resistance of 20 ohms. All potentials were measured vs. the saturated calomel electrode (SCE). Other details have been described elsewhere.^{9,10}



Materials. Imidazole (Fluka), 2-methylimidazole (Sigma), and histidine (Merck) were used as received. 1-Methylimidazole (Fluka) was purified by distillation under reduced pressure. Other chemicals were of AR grade and were used without further purification. The pH of the solutions was adjusted by addition of NaOH or HClO_4 . All experiments were performed at $20 \pm 2^\circ$.

Results and Discussion

Optical Measurements. Spectra and pK_a Determinations. The spectra of the radicals produced by OH attack on imidazole and its derivatives were measured by the pulse radiolysis of N_2O -saturated solutions containing 10^{-3} M of the imidazoles. Under these conditions >95% of the hydrated electrons react with the N_2O to give OH radicals, and these react with the imidazoles with $\tau_{1/2} < 1 \mu\text{sec}$. In each case the spectra of the radicals formed have absorption maxima near 300 and 390 nm (Figure 1, Table I), and there is evidence for a further band at ≤ 240 nm. With increasing pH the 300-nm peak becomes more strongly absorbing and that at 390 nm less strong (with the exception of 2-methylimidazole). From the effect of pH on these absorptions, titration curves could be measured (Figure 1) and from the midpoints of which the pK_a values listed in Table II were found. For 1-methyl- and 2-methylimidazole the oscillograms showed a small spike immediately after the pulse at pH's a little above the pK_a of the parent and a rapid build-up at pH's a little below. This behavior is due to the presence at the end of the pulse of a nonequilibrium mixture of protonated and unprotonated radicals. Approximate values for the pK_a 's could be obtained by making

TABLE I: Decay Rates and Spectral Data

Compound	pH	λ_{\max}^a , nm	$G\epsilon_{\max}^b$	Rate constant	
				$10^{-5} 2k/\epsilon^c$	λ , nm ^d
Imidazole	3.3	290	8,600	2.1	300
	3.3	380	7,300	2.5	390
	9.9	300	15,100	4.8	300
	9.9	380	6,000	5.5	390
1-Methylimidazole	3.1	305	14,500	0.9	305
	3.1	400	9,100	2.2	400
	10.8	315	21,600	<i>e</i>	320
	10.8	390	5,800	<i>e</i>	400
2-Methylimidazole	3.0	285	10,800	2.7	280
	3.0	370	7,700	2.5	370
	10.8	290	18,800	<i>e</i>	290
	10.8	380	8,600	<i>e</i>	380
Histidine	3.05	290	14,400	1.6	300
	3.05	400	9,100	<i>f</i>	410
	7.4	300	20,200	1.0	300
	7.4	380	6,900	3.0	400
	10.45	300	18,900	<i>e</i>	300
	10.45	385	6,500	<i>e</i>	400

^a ± 5 nm. ^b $\pm 10\%$. ^c $\pm 10\%$, units cm sec^{-1} . ^d Wavelength at which decay monitored. ^e First- and second-order components. ^f Approximately first-order decay with $k = \text{ca. } 1.4 \times 10^3 \text{ sec}^{-1}$.

TABLE II: pK_a Values

Compound	Parent pK_a^a	Radical	
		λ , nm ^b	pK_a
Imidazole	7.1 (>NH^+)	300	5.3 ± 0.2
	14.4 (>NH)	390	ca. 6
1-Methylimidazole	7.06 (>NH^+)	320	5.8 ± 0.2^c
		400	ca. 6.5
2-Methylimidazole	ca. 7.5 ^d (>NH^+)	300	6.0 ± 0.2^c
Histidine	2.0 ($\text{—CO}_2\text{H}$)	260	3.6 ± 0.2 ; 8.8 ± 0.3
	6.1 (>NH^+)	310	4.35 ± 0.2 ; 9.4 ± 0.2
	9.2 (—NH_3^+)	410	5.0 ± 0.2

^a Taken from ref 11. Dissociating group (in parentheses) refers to parent only. ^b Wavelength at which pK_a of radical measured. ^c Measured in the presence of $2 \times 10^{-3} \text{ M}$ phosphate buffer. ^d Estimated by pH titration.

measurements 10 μsec after the pulse and gave $\text{pK}_a = 6.2$ (1-methylimidazole at 320 nm) and $\text{pK}_a = 6.5$ (2-methylimidazole at 300 nm). The experiments were repeated in solutions containing $2 \times 10^{-3} \text{ M}$ phosphate buffer, the presence of which ensures complete equilibration during the pulse and gave values for the pK_a 's ca. 0.5 units lower (see Table II). These difficulties were not encountered with imidazole or histidine.

The pK_a values < 7 are attributed to deprotonation of the nitrogen at position 3 in the ring. It will be noted that

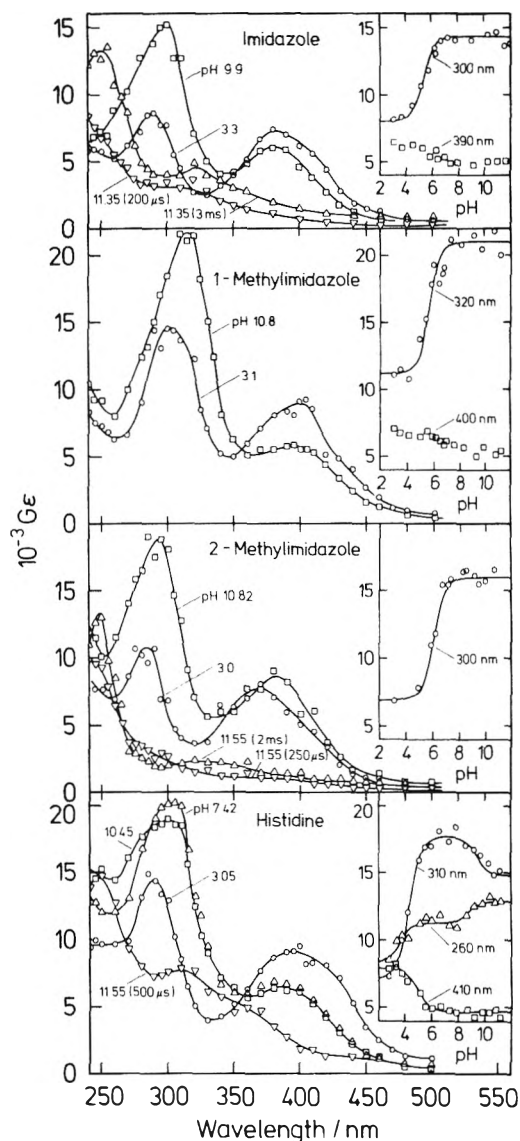


Figure 1. Spectra of the radicals produced by OH attack on imidazole, 1-methylimidazole, 2-methylimidazole, and histidine at various pH's obtained by the pulse radiolysis of N_2O saturated solutions of 10^{-3} M imidazole etc. Dose 0.3–1.0 krad/pulse. Measurements made at the end of the pulse unless otherwise stated. Insets show the effect of pH on $G\epsilon$ at various wavelengths. Solid lines are calculated using the pK_a values listed in Table II.

these are all ca. 1–2 pH units below those of the corresponding equilibria for the parent compounds under similar conditions. The two pK_a values > 7 measured for histidine may be due to deprotonation of the radical side chain amine group or to a change in the site of OH attack on deprotonation of the parent side chain amine group.

The hydroxyl radical may react with imidazole by addition at positions 2 and 5 to give an allylic type radical and at position 4 to give a radical where the unpaired electron is β to the OH group and α to the >NH group. Of the two further possibilities addition of OH at position 3 is probably not a significant reaction pathway when N_3 is protonated, but may occur when it is unprotonated (addition of OH to the N in pyridine, for instance, has been suggested¹² to occur, although the evidence is not compelling), and comparison with other compounds¹³ suggests that abstraction of an H atom from position 1 is negligible. With the methyl-substituted derivatives there is also the possibility

of H abstraction from the methyl group and with histidine from the side chain. In view of the complexities it is not possible to assign particular structures to the absorptions and pK_a values measured. With histidine the pK_a 's measured at 260, 310, and 410 nm differ significantly from one another (Table II), and we conclude that at least three different radicals are formed in this case. For imidazole and 1-methylimidazole the uncertainty of the pK_a values measured at 390 and 400 nm, respectively, is too great to permit any definite statement about the number of radicals formed in either case. The marked similarity of the absorption spectra from all four compounds studied is, however, to be noted. Samuni and Neta¹⁴ have unequivocally shown, using the in situ ESR radiolysis technique, that OH + imidazole gives rise, at least in part, to the 5-hydroxyimidazolyl radical.

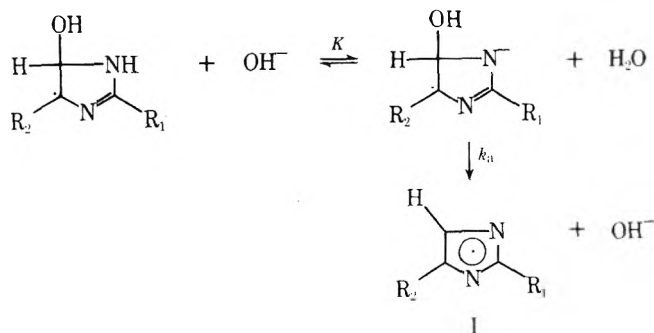
It has also been found that there is 84% electron transfer from the OH adducts of imidazole to menaquinone (pH 6.9),¹⁵ 88% from the histidine radicals to menaquinone (pH 6.9),¹⁵ and 93% from the histidine radicals to 1,4-benzoquinone (pH 7.7).¹⁶ The ca. 10% of the radicals which do not react in the histidine case can probably be identified with attack at the side chain. For imidazole it is expected that all the possible radicals would transfer to menaquinone. One possible explanation why 16% do not is that another reaction pathway, e.g., addition of the OH adducts to the quinones, might be important.

Optical Measurements. Kinetics. At pH <10 the first half-life for the decay of the radicals was inversely dependent on dose. The rate constants ($2k/\epsilon$) shown in Table I were measured from plots of reciprocal optical density vs. time, which were linear over ca. two half-lives; at longer times some deviation from linearity was observed. These results are consistent with radical-radical reactions.

At higher pH's the decay of the radicals became first order (with the exception of 1-methylimidazole), and an absorption rising toward shorter wavelengths remained after this first-order decay was complete. Rate constants for this decay were determined from plots of $\ln(D_t - D_\infty)$ vs. time, where D_∞ is the optical density of the absorption remaining after the decay was complete. Some difficulty was experienced with the histidine radical due to the concomitant decay of this second absorption at 300 nm (but not at 390 nm; apparently the long-lived absorption is due to two different species). Values of k_{obsd} were determined at various pH's and are shown in Table III. Plots of k_{obsd}^{-1} vs. $[\text{OH}^-]^{-1}$ give a straight line with an intercept (Figure 2), and indicate a rate law of the following form:

$$k_{\text{obsd}}^{-1} = a[\text{OH}^-]^{-1} + b \quad (1)$$

We ascribe this decay to a base-catalyzed water elimination reaction (taking the example of the 5-hydroxy adduct):



where the process labeled k_a is rate determining. In sup-

TABLE III: Kinetic Data for Rearrangement Reaction

Compound	pH	$10^{-4}k_{\text{obsd}}, \text{sec}^{-1}^a$	
Imidazole		300 nm	390 nm
	11.15	<i>b</i>	2.0
	11.35	<i>b</i>	2.6
	11.58	3.2	4.0
	11.75	4.5	6.2
	12.00	7.0	7.9
	12.20	9.4	11.5
	12.38	13.5	17
2-Methylimidazole		290 nm	380 nm
	11.22	1.1	1.3
	11.40	1.5	1.7
	11.62	2.5	2.6
	11.85	3.35	3.8
	12.07	5.3	5.6
	12.32	8.1	8.1
Histidine		390 nm	
	11.55	1.3	
	11.78	1.6	
	12.05	3.6	
	12.27	3.9	

^a $\pm 10\%$. Solutions contained $10^{-3} M$ of the imidazole and were saturated with N_2O . Dose ca. 500 rad/s/pulse.

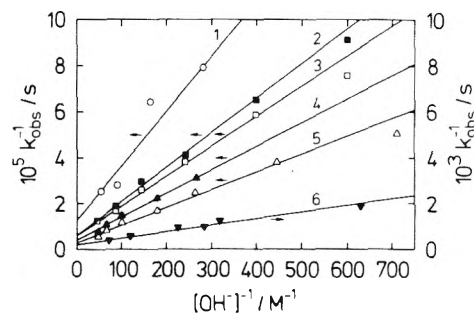


Figure 2. Plot of k_{obsd}^{-1} vs. $[\text{OH}^-]^{-1}$ for histidine at 390 nm (line 1), 2-methylimidazole at 290 (2) and 380 nm (3), and imidazole at 300 (4), 390 (5), and 260 nm (6).

port of this are the following observations: (i) the polarographic experiments described below, (ii) Samuni and Neta's¹⁴ experiments using the in situ ESR radiolysis technique indicate that at pH >11 the reaction of OH with imidazole and 2-methylimidazole yields radicals such as I, where the unpaired electron is delocalized over the whole imidazolyl ring. (iii) No first-order decay was observed with 1-methylimidazole. In this case there is no ionizable hydrogen atom attached to N_1 and a rearrangement reaction is not possible.

It seems unlikely that the deprotonation equilibrium involves the hydroxyl group rather than the $>\text{NH}$ group since the rate-determining step would then involve either O^{2-} or OH^- elimination (e.g., via a cyclic four-centered transition state), both of which are likely to have large activation energies. There is evidence from in situ ESR radiolysis experiments¹⁴ that the hydroxyl group of the 2-hydroxyimidazolyl-4,5-dicarboxylate radical ionizes with $pK_a = 12$. It is noteworthy, however, that this radical undergoes no detectable water elimination reaction.¹⁴

The proposed mechanism predicts a rate expression of the form¹⁷

$$\frac{-d[R]}{dt} = \frac{k_a K [OH^-]}{1 + K [OH^-]} [R] = k_{\text{obsd}} [R] \quad (2)$$

where $[R]$ is the total reactant radical concentration, assuming that radical-radical reactions are negligible and that $[OH^-]$ remains constant. Therefore

$$k_{\text{obsd}}^{-1} = k_a^{-1} + (k_a K [OH^-])^{-1} \quad (3)$$

which is of the same form as that found experimentally. Values of k_a and K calculated from the experimental data are shown in Table IV. For convenience the values of pK_1 , the acid dissociation constant of the $>NH$ group are also shown. This is related to K by $K = 10^{14} K_1$. For imidazole and its 2-methyl derivative the rate constants for the decays of the 300- and 390-nm absorptions are very similar.

In the imidazole solutions at $pH > 11$ an increase in absorption was noted in the region 240–300 nm after the 300- and 390-nm peaks had decayed away (see Figure 1). This buildup was approximately first order and pH dependent. Plots of $\ln(D_\infty - D_t)$ vs. time showed some curvature, although the half-life was essentially independent of dose. Rate constants for the reaction were therefore estimated from the initial rate of the reaction (Table V). A plot of k_{obsd}^{-1} vs. $[OH^-]^{-1}$ is linear (Figure 2), and we believe that these results indicate a further yield of radical I produced by water elimination from another OH-imidazole adduct. Clearly the spectrum at 200 μsec after the pulse (Figure 1, pH 11.35) must represent the sum of the absorptions of I formed by the decay of the 300 nm/390 nm peaks and this other OH adduct. If it is assumed that the latter absorbs little at ca. 250 nm, then the yields of I formed by the rapid and slow reactions are approximately equal.

A somewhat similar situation was found with 2-methylimidazole (Figure 1, pH 11.55). Here however the buildup was only observed at wavelengths ≤ 260 nm, and no reliable estimate of the rate constants could be made. It seems that in this case the yield of radical I formed by the slow reaction is considerably less than that from the rapid one. No buildup was observed in the histidine case, although the absorption at 500 μsec (Figure 1, pH 11.55) does seem to be due to two species as noted above.

No evidence was obtained in any of these experiments at $pH > 11$ for an uncatalyzed pathway for the elimination of water from the OH-imidazolyl ring adducts. Unfortunately the range of pH's over which the reaction could be studied was limited, at the lower end by competition with radical-radical reactions, and at the upper end because of complications due to the formation of O^- ($pK(OH) = 11.9^{18}$). The uncatalyzed pathway may, nevertheless, be significant under low dose rate conditions (e.g., γ radiolysis), and we estimate an upper limit of $k \leq 10^3 \text{ sec}^{-1}$ for this reaction (in competition with the rapid, base-catalyzed reaction) for imidazole, 2-methylimidazole, and histidine.

The approximately first-order decay noted with histidine at pH 3.05 and 410 nm (Table I) is presumably due to an acid-catalyzed pathway for the elimination reaction. It was not possible to study this reaction at lower pH's because of complications arising from the increase in the yield of hydrogen atoms under these conditions. No evidence for the acid-catalyzed pathway was found with the other compounds studied.

Polarographic Measurements. The polarograms of the radicals produced by OH attack on imidazole and its 1-

TABLE IV: Rate Constants for Rearrangement Reaction

Compound	λ , nm	$10^{-4} k_a$, ^a sec^{-1}	K , ^b M^{-1}	pK_1
Imidazole	260	0.5	80	12.1
	300	25	40	12.4
	390	36	40	12.4
2-Methylimidazole	290	17	40	12.4
	380	17	50	12.3
Histidine	390	7.7	55	12.3

^a $\pm 15\%$. ^b $\pm 25\%$.

TABLE V: Kinetic Data for Buildup in Imidazole Solutions^a

$10^3 [\text{Imid}]$, M	pH	$10^{-3} k_{\text{obsd}}$, ^b sec^{-1}
0.5	11.50	0.8 ^c
1.0	11.55	1.0 ^c
2.0	11.65	1.1 ^c
1.0	11.20	0.6 ^c
1.0	11.92	1.9 ^c
1.0	12.15	2.7

^a All solutions saturated with N_2O . Dose ca. 500 rads/pulse. ^b $\pm 15\%$. Measured at 260 nm. ^c Estimated from the initial rate.

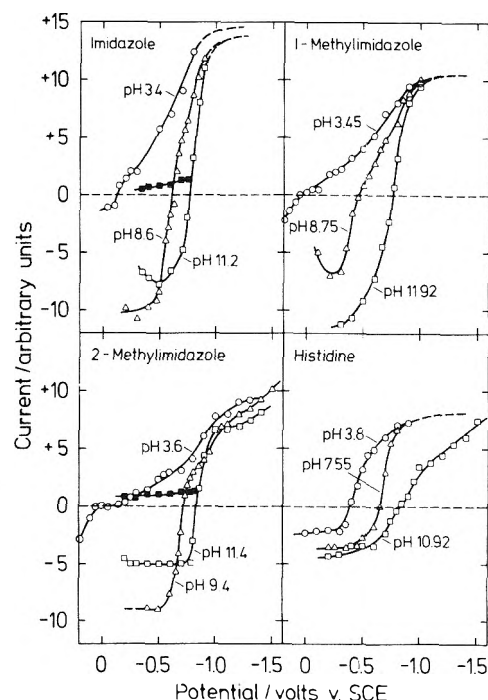


Figure 3. Polarograms of radicals produced by OH attack on imidazole, 1-methylimidazole, 2-methylimidazole, and histidine at various pH's. Measured in N_2O -saturated solutions containing $10^{-3} M$ imidazole etc. + $0.35 M Na_2SO_4$. Open symbols measured 20 μsec after the pulse, solid symbols 100 (imidazole) and 70 μsec (2-methylimidazole) after the pulse.

methyl and 2-methyl derivatives show a flat cathodic wave at pH's 3–4, where the radicals are protonated (see above) and a weak anodic wave at potentials more positive than 0 V (Figure 3). While these polarograms give no information on the relative yields of the radicals formed, the ease of reduction is consistent with the formation of any of the possi-

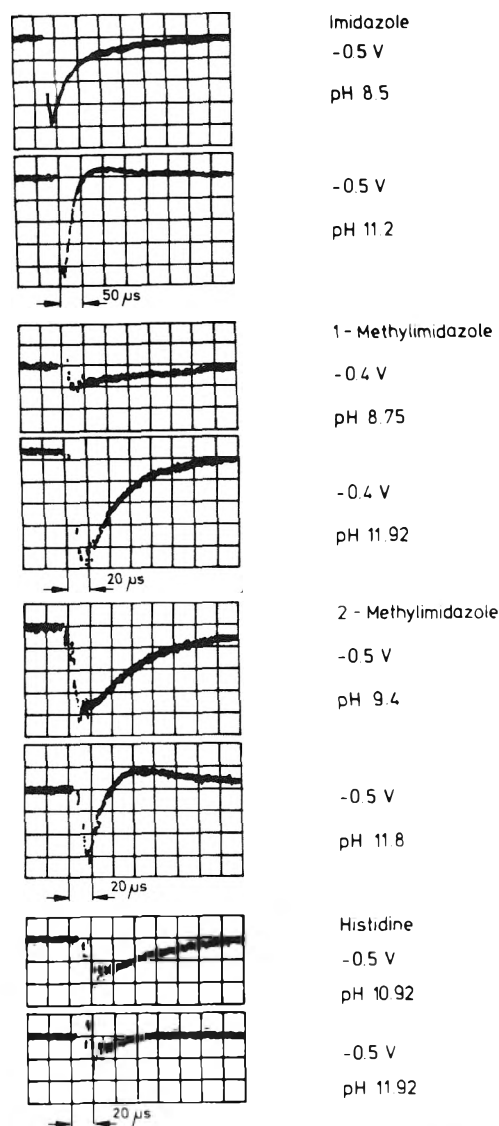
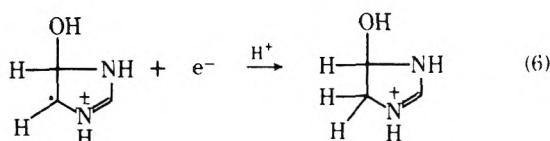
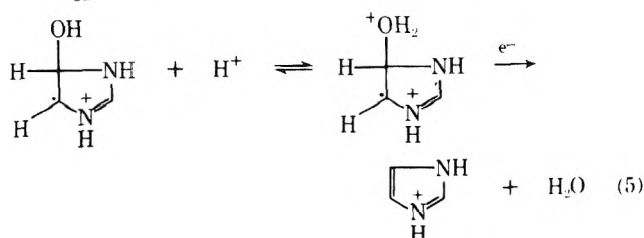
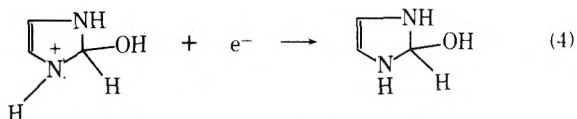


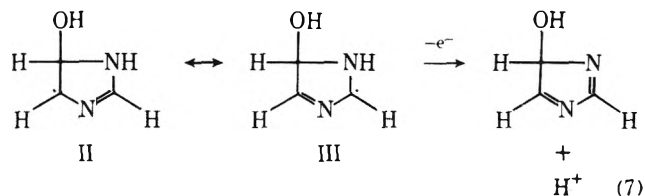
Figure 4. Effect of alkali on polarographic current vs. time curves. Measured in N_2O -saturated solutions containing 10^{-3} M imidazole etc. + 0.35 M Na_2SO_4 .

ble OH adducts. For the 2-hydroxy adduct the cathodic reaction is particularly favorable because of the positive charge on N_3 (4). With the 4- and 5-hydroxy adducts the



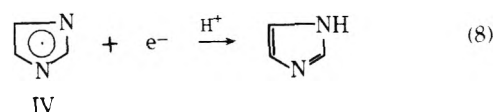
unpaired electron is β to the hydroxyl group so that the reduction probably involves elimination of OH^- and may be catalyzed by H^+ as has been suggested^{19,20} to occur with other β -alcohol radicals (5). The reduction of the 5-hydroxy adduct may also be favorable because of the proximity of the $>\text{N}^+-\text{H}$ group (6). With histidine the oxidation wave, extends to -0.4 V.

In alkaline solutions (pH 7–10) where the radicals are unprotonated a steep anodic wave extending up to ca. -0.5 V, immediately followed by a somewhat flatter cathodic wave, was found (Figure 3). These polarograms correspond to the case of competitive oxidation and reduction of the radicals where the rates of the oxidation and reduction are comparable over a narrow potential range.^{20,21} The ease of oxidation is attributed to canonical contributions such as that of form III to structure II (7) (similar reactions can be



written for the other adducts). A mechanism of this type has been proposed for the electrode oxidation of the OH adducts of furan and pyrrole.²⁰

At higher pH's (>11) the oscillograms for imidazole and 2-methylimidazole showed, at potentials of ca. -0.5 V, an oxidation at times shortly after the pulse, and reduction at longer times (see Figure 4; for comparison typical oscillograms at the same potentials but at less alkaline pH's are shown). With histidine the oxidation current falls rapidly to zero, but no reduction signal was observed, and with 1-methylimidazole the oscillograms were similar to those at lower pH's. These changes of oxidation to reduction are due to the transformation of one radical to another with different electrochemical properties and have been observed in a number of other systems.^{5,22} No reliable kinetic data for these processes can be obtained from the polarographic measurements, but the timescale of the changes are of the same magnitude as the first-order reactions observed optically (see Table III). The latter has been interpreted in terms of a base-catalyzed water elimination reaction and the polarographic data are in accord with this. Radical IV produced in the rearrangement reaction is expected to be easily reduced (8) as was found (Figure 3).



Acknowledgment. We thank Professor A. Henglein for many helpful discussions.

References and Notes

- (1) Radiation Research Laboratories, Center for Special Studies and Department of Chemistry, Mellon Institute of Science, Carnegie-Mellon University, Pittsburgh, Pa. 15213.
- (2) Address correspondence to this author at the Materials Division, Central Electricity Generating Board, Berkeley Nuclear Laboratories, Berkeley, Gloucestershire GL13 9PB, England.
- (3) A. M. Crestfield, W. H. Stein, and S. Moore, *J. Biol. Chem.*, **238**, 2413, 2421 (1963).
- (4) (a) J. L. Foster and R. L. Willson, *Brit. J. Radiol.*, **46**, 234 (1973); (b) A.

- C. Begg, P. W. Sheldon, and J. L. Foster, *ibid.*, **47**, 399 (1974); (c) J. C. Asquith, J. L. Foster, R. L. Willson, R. Ings, and J. A. McFadzean, *ibid.*, **47**, 474 (1974).
- (5) K. M. Bansal and R. M. Sellers in "Fast Processes in Radiation Chemistry and Biology", G. E. Adams, E. M. Fielden, and B. D. Michael, Ed., Wiley, London, 1975, p. 259.
- (6) A. Henglein, *Allg. Prakt. Chem.*, **17**, 295 (1966).
- (7) G. Beck, Dissertation, T.U. Berlin, 1968.
- (8) A. Henglein, W. Schnabel, and J. Wendenburg, "Einführung in die Strahlenchemie", Verlag Chemie, Weinheim, W. Germany, 1969.
- (9) M. Grätzel, A. Henglein, J. Lilie, and M. Scheffler, *Ber. Bunsenges. Phys. Chem.*, **76**, 67 (1972).
- (10) M. Grätzel and A. Henglein, *Ber. Bunsenges. Phys. Chem.*, **77**, 2 (1973).
- (11) (a) *Chem. Soc. Spec. Publ.*, No. 17 (1964); (b) *ibid.*, No. 25 (1971).
- (12) B. Cercek and M. Ebert, *Trans Faraday Soc.*, **63**, 1687 (1967).
- (13) E.g., (a) E. Hayon, T. Ibata, N. N. Lichtin, and M. Simic, *J. Am. Chem. Soc.*, **92**, 3898 (1970); **93**, 5388 (1971); (b) M. Simic, P. Neta, and E. Hayon, *ibid.*, **92**, 4763 (1970); (c) E. Hayon and M. Simic, *ibid.*, **93**, 6781 (1971).
- (14) A. Samuni and P. Neta, *J. Phys. Chem.*, **77**, 1629 (1973).
- (15) P. S. Rao and E. Hayon, *Biochim. Biophys. Acta*, **292**, 516 (1973).
- (16) M. Simic and E. Hayon, *Biochem. Biophys. Res. Commun.*, **50**, 364 (1973).
- (17) R. P. Bell, "The Proton in Chemistry", Methuen, London, 1959, p. 133.
- (18) J. Rabani and M. S. Matheson, *J. Phys. Chem.*, **70**, 761 (1966).
- (19) K. M. Bansal, A. Henglein, E. Janata, and R. M. Sellers, *Ber. Bunsenges. Phys. Chem.*, **77**, 1139 (1973).
- (20) K. M. Bansal, A. Henglein, and R. M. Sellers, *Ber. Bunsenges. Phys. Chem.*, **78**, 569 (1974).
- (21) K. M. Bansal and A. Henglein, *J. Phys. Chem.*, **78**, 160 (1974).
- (22) K. M. Bansal, M. Grätzel, A. Henglein, and E. Janata, *J. Phys. Chem.*, **77**, 13 (1973).

Combination and Disproportionation of Allylic Radicals at Low Temperatures

Ralph Klein* and Richard D. Kelley

Physical Chemistry Division, National Bureau of Standards, Washington, D.C. 20234 (Received November 1, 1974; Revised Manuscript Received May 12, 1975)

Publication costs assisted by the National Bureau of Standards

The disproportionation-combination ratio for several allylic type radicals has been measured in the condensed phase at 90 K. Pairs of allylic radicals react exclusively by combination, with no disproportionation found within the limits of the analytical technique. Cross combination and disproportionation occurs between an allylic radical and an alkyl radical. In the cross disproportionation, the allylic radical acts exclusively as a hydrogen donor. This effect is attributed to the delocalization of the free spin, the hydrogen acceptor function being completely inhibited. Because of this, two allylic type radicals (or any radicals in which the density of the free spin is sufficiently delocalized) can only combine. The contribution of the resonant components of the allylic radicals to the combination products is found to be greatly dependent on steric effects.

Introduction

Reactions at low temperatures in a condensed phase are relatively simple because high activation energy paths are eliminated, while enthalpy developed in the reaction processes is efficiently dissipated. Advantage was taken of low temperature techniques to observe a series of alkyl radical cross disproportionation reactions.¹ In an extension of that work we consider here allylic radicals to determine the effect of the resonance structure on their combination and disproportionation reactions and contrast them with non-resonant radicals in this regard.

A convenient method for preparation of radicals is the hydrogen atom addition to an appropriate olefin.² The condensed olefin, either with or without a diluent such as propane, is present as a layer on the bottom of a flask immersed in a refrigerant such as liquid oxygen. Hydrogen atoms are produced by thermally dissociating molecular hydrogen on a heated tungsten filament. The atoms bombard the condensed layer and react with the olefin by addition to form radicals. These diffuse away from the surface, where they are formed, and undergo radical-radical reactions.³

To prepare allylic radicals, conjugated dienes are used. Thus, H atom addition to 1,3-butadiene gives the methylal-

lyl radical. Higher homologs may possess isomers of the cis and trans variety. These are useful for assessing rotation in the allylic radical by way of the diene-radical-product path. A substantial activation energy barrier for rotation exists, one estimate being 70 kJ/mol.⁴ Sustman and Trill,⁵ using a flow system and ESR spectroscopy, found a value of 34-42 kJ/mol for an allyl radical containing CN and isobutyl groups. Doering and Beasley⁶ gave 75 kJ/mol for the cis-trans isomerization of some hexatrienes via the allylic radical. Rotation of allylic radicals, as evidenced by a cis-trans isomerization, would not be expected to be observed in the low-temperature region. The preparation of the allylic radicals at low temperatures, as noted, is through hydrogen atom addition to a diene. The exothermicity of the process is approximately 209 kJ/mol and consideration must be given to the question of whether or not configuration is retained. We give here the results of several observations that are pertinent.

A further purpose of this paper is to determine some of the disproportionation-combination characteristics of allylic radicals, particularly in the low temperature region. Nelsen and Bartlett⁷ first pointed out the striking difference between cumyl radicals and *tert*-butyl radicals in their disproportionation-combination reactions. Cumyl radicals combine to an extent of 94% at 20° whereas *tert*-

butyl radicals combine to an extent of only 20%. Nelsen and Bartlett suggested that the anomalous behavior with regard to the low disproportionation rate may be associated with the benzylic delocalization of the free electron. They also noted, however, that a lowering of the combination rate might have also been expected on this basis and no prediction could have been made. Engel and Bishop⁸ reported that for the methylallyl radical, there was less than 2% disproportionation relative to combination. James and Kambanis⁹ found that the ratio of combination to disproportionation for the radical pair allyl and cyclohexadienyl is 91 to 9, confirming the propensity of allyl type radicals to favor combination. Al-Sader and Crawford¹⁰ showed that in the interaction of allyl radicals, 1,5-hexadiene is produced with only a trace of propene. Again, the major, if not exclusive, process is combination.

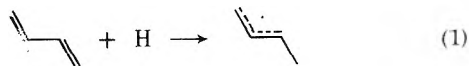
Previous work has shown that there is a temperature effect in the disproportionation-combination ratio¹⁵ for alkyl radicals,³ lower temperatures favoring disproportionation. For *sec*-propyl radicals, for example, $k_d/k_c = 0.6$ at 300 K and $k_d/k_c = 5.5$ at 90 K. Disproportionation for the allylic radicals would, by analogy, be enhanced at low temperatures, and it might be expected that disproportionation would be observed.

Experimental Section

Experimental details of the low-temperature technique have been published previously.¹ Following the reaction, the film is warmed and transferred to the inlet of a gas chromatograph. Analysis of the entire film, typically 0.5×10^{-3} mol, was accomplished by chromatographically separating the mixture into three fractions: (1) diluent; (2) reactant and disproportionation products; and (3) radical dimer products. A squalane column was used for the initial separation. A 10 m, 20%, 3,3'-oxydipropionitrile (saturated with AgNO_3) column was used at 25° for the analysis of the second fraction, while a 4-m version of this column was used at 35° for the third fraction. Standard samples were used wherever possible to verify that these procedures yield accurate quantitative results.

Results

Allylic-Allylic Radical Reactions. H atom addition to 1,3-butadiene at a concentration of 0.3% in propane at 90 K yields the methylallyl radical



It will be shown that the alternate reaction



is negligible. If both disproportionation and combination reactions of these radicals occur, C_4 and C_8 compounds would be produced. A precise indication of the amount of disproportionation is available through the C_4 analysis. Disproportionation of methylallyl would necessarily yield 1-butene or 2-butene. Neither of these compounds was detected in the reaction products following the H-atom addition to 1,3-butadiene. The product analysis from a typical experiment is given in Table I. The distribution of the C_8 diene products (given in Table V) indicates that the only radical present in this system is methylallyl and therefore that reaction 2 is not significant. Consideration of the absence of four carbon products and the equivalence of C_8 diene with the depleted reactant requires us to conclude

TABLE I: Product Analysis from Methylallyl + Methylallyl at 90 K

Product	mol $\times 10^9$
$n\text{-C}_4\text{H}_{10}$	< 1
1-C ₄ H ₈	
2-C ₄ H ₈	
1,2-C ₄ H ₆	< 1
$\Delta(1,3\text{-C}_4\text{H}_6)^a$	160 \pm 5%
C_8H_{14}	156

^a $\Delta(1,3\text{-C}_4\text{H}_6)$ is the 1,3-butadiene depleted by reaction with H atoms. The quantity indicated represents approximately 10% conversion.

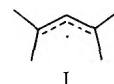
that greater than 99% of the reaction of methylallyl with methylallyl at 90 K is by way of combination.

In another example, the radical 1,3-dimethylallyl



was prepared by the H atom addition to *cis*-1,3-pentadiene diluted to 0.3% with propane at 90 K. Disproportionation of these radicals would yield 1- and 2-pentenes. These compounds were not detected in the products within the limits of the chromatographic technique. The quantity of C_{10} diene observed indicates that the C_{10} dimer to pentene ratio exceeds 100.






The disproportionation-combination reactions of alkyl radicals show steric effects for branched chain radicals markedly favoring disproportionation. The k_d/k_c ratio for isobutyl at 90 K is approximately 500. Whether the effect of branching is applicable to allylic radicals was determined with



Not only is this radical branched, but there are seven "donor" hydrogens associated with each of the "free spin" carbons. These characteristics should be especially favorable to disproportionation. The preparation of I was by H atom addition to 2,4-dimethyl-1,3-pentadiene in a 0.1% solution in propane at 90 K. The reactions of the allylic radicals were followed by the formation of the C_{14} dimers and the diminution of the parent olefin. More than 99% of the reaction is combination. Table II summarizes the disproportionation-combination data for these allylic radicals. Included are related data for radicals derived from unconjugated dienes and a C_5 olefin. The 4-penten-2-yl radical and the 2-pentyl radical were generated at 90 K in propane films by the H atom addition to 1,4-pentadiene and 1-pentene, respectively.¹ The disproportionation to combination ratio for 4-penten-2-yl is given by the product ratio, $1\text{-C}_5\text{H}_{10}/\text{C}_{10}\text{H}_{18}$ while that of 2-pentyl is given by $n\text{-C}_5\text{H}_{12}/\text{C}_{10}\text{H}_{22}$. In both cases, these product ratios were found to be constant, within 5%, for a series of six runs with each radical. The difference between the allylic and these nonallylic radicals is striking. Clearly, a generalization may be deduced, that allylic-allylic radical reactions are exclusively combination, and that disproportionation does not occur.

Allylic-Alkyl Radical Reactions. The question arises as to whether or not the absence of disproportionation is characteristic of allylic radical reactions in general or only in those reactions where both radicals are allylic. The results

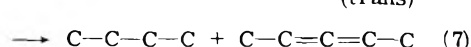
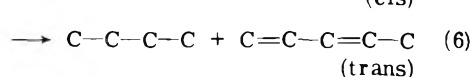
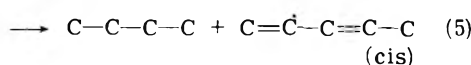
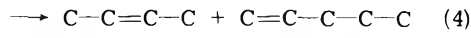
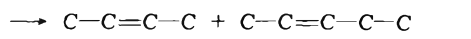
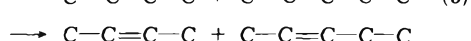
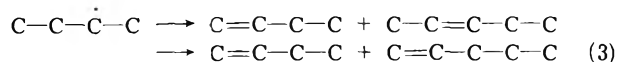
TABLE II: Autodisproportionation-Combination Ratios at 90 K for Several Allylic and Alkyl Radicals^a

Radical	k_d/k_c
	<0.01
	<0.01
	<0.01
	7.6
	6.4

^a The radicals are produced by the H atom addition to an appropriate olefin or diolefin highly diluted in propane. See text for experimental details of these measurements.

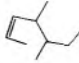
of James and Troughton¹¹ show that disproportionation for an allylic radical occurs provided it reacts with an alkyl radical. The reaction between allyl and ethyl at 410 K showed 85% combination, and 15% disproportionation. 73% of the disproportionation involved allyl as the H atom acceptor and 27% as the donor radical. These experiments were done in the temperature range 137–175°. The preparation of ethyl and allyl radicals involved photolysis of a mixture of diethyl ketone and diallyl at 3130 Å. Conclusions with regard to disproportionation between ethyl and allyl depend on the assumption that propylene and allene arise exclusively from disproportionation of ethyl and allyl. The complexity of the generating system would dictate caution in this regard, however.

We have investigated the alkyl-allyl type radical-radical reaction of 2-butyl with 1,3-dimethylallyl. The reactions were at 90 K and the radicals were generated by exposure to gas phase atomic hydrogen of a condensed phase consisting of *cis*-1,3-pentadiene, *cis*-2-butene, and propane in a ratio of 10:1:3000. Hydrogen atom addition generates 1,3-dimethylallyl and 2-butyl. These react via biradical encounters. The 1,3-pentadiene is in considerable excess of the *cis*-2-butene so there will be an excess of 1,3-dimethylallyl over 2-butyl. Auto 2-butyl reactions are hence minimized. The experimental results are shown in Table III. Several significant conclusions may be drawn. The absence of 3,4-dimethylhexane shows that 2-butyl-2-butyl reactions are negligible. Thus, essentially all 2-butyl radicals react by cross disproportionating or cross combining with the dominant radical, 1,3-dimethylallyl. The cross disproportionation reactions possible are



Previously it was noted that when 2-butene was formed from 2-butyl in reactions at 90 K where 2-butyl acted as a

TABLE III: Products from the Reaction of  and  at 90 K^a

Product	Relative yield
<i>n</i> -C ₄ H ₁₀	25
1-C ₄ H ₈	<0.5
<i>l</i> -2-C ₄ H ₈	<0.5
<i>l</i> -1,3-C ₅ H ₈	<0.1
2,3-C ₅ H ₈	<0.1
3,4-Dimethylhexane	<0.1
	25
C ₁₀ diene	4,000

^a Film composition C₃H₈:*cis*-1,3-C₅H₈:*cis*-2-C₄H₈ = 3000:10:1.

TABLE IV: Product Analysis from 1,3-Dimethylallyl + 2-Methyl-2-butyl at 90 K

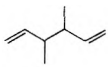
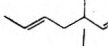
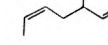
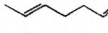
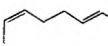

Product	Relative yield
2-Methylbutane	1.0
2-Methyl-1-butene	<0.01
<i>n</i> -Pentane	<0.02
1-Pentene	
2-Pentene	
C ₁₀ H ₂₀	1.7
C ₁₀ H ₁₈	250

hydrogen donor, the 2-butene was 98% *trans*.³ The advantage of using *cis*-2-butene as the 2-butyl source is that products are distinguishable from reactants. For the reaction between 1,3-dimethylallyl and 2-butyl, the ratio *n*-C₄H₁₀/(1-C₄H₈ + *trans*-2-C₄H₈) is greater than 25. The ratio *n*-butane/4,5-dimethyl-2-heptene, a measure of k_{da}/k_c where the k 's refer to the cross radical process, is equal to 1 ± 0.2 . Where butene is formed in the cross disproportionation, equal amounts of 2-pentene (reactions 3 and 4) must be produced. The ratio of *n*-butane/2-pentene = 100. The small amount of C₄ monoolefin products found were extraneous to the cross disproportionation reaction and probably arose from a small amount of 2-butyl + 2-butyl reaction.

In a similar manner we investigated the cross-disproportionation of 2-methyl-2-butyl with 1,3-dimethylallyl (in great excess). The reaction products from one run are indicated in Table IV. The reaction produced 2-methylbutane (from the reaction analogous to (5)). However, 2-methyl-1-butene, 2-pentene, and 1-pentene (from reactions analogous to (3) and (4)) were not detected. Thus, the 1,3-dimethylallyl radical reacts by cross disproportionation in the same way with both of these alkyl radicals. The outstanding feature, and the point to be emphasized, is that in the cross disproportionation reaction of the allylic radical, the radical acts only as a hydrogen donor. Because allylic type radicals cannot function as hydrogen acceptors, in allylic-allylic radical reactions only combination is possible.

Rotation about a C—C bond in an allylic radical moiety presents a 40 to 80 kJ/mol activation barrier. Rotation at low temperatures, for example 90 K, would not be expected. However, in a sequential reaction series, where the initial preparative step is highly exothermic, uncertainty exists as to the retention of configuration. Information in this

TABLE V: Combination Products of Methylallyl Radicals at 90 K

Product	% total dimer		
	90 K ^a	398 K ^b	
	Meso	8.4 ± 0.15	} 17.2
	Rac	7.5 ± 0.16	
	Trans	43.5 ± 0.53	} 47.1
	Cis	<0.1	
	Trans, trans	40.5 ± 0.63	} 35.8
	Cis, trans	0.22 ± 0.03	
	Cis, cis	<0.1	

^a Source of the methylallyl radicals is the H atom addition to 1,3-C₄H₆ (0.3% in propane at 90 K). The uncertainty is one σ for 14 determinations in which the conversion was varied by more than 10-fold. The gc analysis was accomplished with a 4-m 20% 3,3'-oxydipropionitrile (saturated with AgNO₃) column. ^b R. J. Crawford, J. Hamelin, and B. Strehle, *J. Am. Chem. Soc.*, 93, 3810 (1971).

regard can be obtained from the data in Table III in which the products of the H atom addition to *cis*-1,3-pentadiene (in large excess) and *cis*-2-butene are given. In the cross disproportionation of 1,3-dimethylallyl with 2-butyl, 1,3-dimethylallyl acts exclusively as the hydrogen donor, and the 1,3-pentadiene is re-formed. Rotation in the allylic radical would result in the formation of *trans*-1,3-pentadiene. In the experiments where the 1,3-dimethylallyl radical was in excess, butane formation indicated that a cross disproportionation reaction had occurred, but no trace of *trans*-1,3-pentadiene was found. The sensitivity of the analysis was such that 1 part of *trans*-1,3-pentadiene out of 250 parts of *n*-butane would have been detected. Clearly, the exothermic heat of H atom addition to the 1 position of *cis*-1,3-pentadiene is dissipated to the condensed phase sufficiently rapidly that the energy equivalent to the rotation barrier is not accumulated at the 3 position.

The cross combination of 2-propyl with the methylallyl radical is interesting because there is a secondary as well as a primary carbon in the methylallyl radical capable of combination with the free spin carbon of the 2-propyl radical:

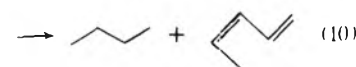
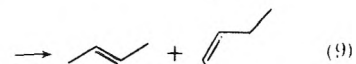
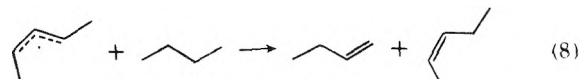


The radicals were prepared by exposing an equimolar mixture of propene and 1,3-butadiene in propane (olefin concentration 1%) at 90 K to H atoms in the gas phase. The reaction products, 3,4-dimethyl-1-pentene and 5-methyl-2-hexene (B + 2-propyl), were measured in several runs in which the conversion of the reactants varied considerably. The ratio 5-methyl-2-hexene to 3,4-dimethyl-1-pentene was found to be 4 and constant for conversions up to 10%. Favoring of B in the cross combination with *sec*-propyl over that of A by a factor of 4 may be explained on the basis of steric hindrance. Engel and Bishop⁸ considered an analogous problem involving the autocombination of unsymmetrical allylic radicals. They noted that neither relative spin densities nor product stabilities were determining factors for the combination distribution. Steric effects seemed to be the most likely explanation for their results on the combination of 1,1-dimethylallyl radicals. With the tertiary carbon of the 1,1-dimethylallyl radical designated as the H (head) end and the terminal allylic carbon as the T (tail) end, Engel and Bishop found the distribution of di-

mers to be HH-16, HT-30, and TT-54. The TT dimer, showing the least steric hindrance for the approach of the two carbon atoms to be bonded, is highly favored.

Discussion

The unusual features of reactions of allylic radicals is that, in the reaction of an allylic radical pair, combination is essentially quantitative. Disproportionation can occur between an allylic radical and alkyl radical, but the former functions only as a hydrogen donor. The fact that the allylic radical is not a hydrogen acceptor implies that an allylic-allylic radical interaction can only be of the combination type. James and Suart,¹⁴ in studies of disproportionation reactions of the cyclohexadienyl radical and methyl, ethyl, 2-propyl, and isobutyl radicals, noted that the cyclohexadienyl radical did not accept a hydrogen atom. The explanation proposed by them was based on energetic grounds. If the cyclohexadienyl radical acted as a hydrogen acceptor, in which case cyclohexadiene either in the 1,3 or 1,4 configuration is formed, a considerable fraction of the stabilization energy of 104 kJ/mol would be lost compared to the



situation where cyclohexadienyl is the hydrogen donor and benzene results. Since, as we have shown, allylic radicals also react in this manner, i.e., they function exclusively as the donor radical in cross disproportionation reactions with alkyl radicals, the resonance energy suggestion is not convincing. The enthalpy change in the cross-disproportionation reactions 8–10 of the 1,3-dimethylallyl and the 2-butyl radicals are (ΔH_8)_{298K} = -230 kJ/mol; (ΔH_9)_{298K} = -243 kJ/mol, (ΔH_{10})_{298K} = -251 kJ/mol.¹⁶ Our observation is that reaction 10 predominates while reactions 8 and 9 occur, if at all, to a negligible extent. It is unlikely that the course of these highly exothermic reactions would be deter-

mined by differences of a few percent in the total enthalpy change. In fact, the autodisproportionation reaction of the 2-butyl radical producing 1-C₄H₈ and *n*-C₄H₁₀ [$\Delta H_{298K} = -229$ kJ/mol] is favored over that producing *t*-2-C₄H₁₀ [$\Delta H_{298K} = -280$ kJ/mol]. If the overall exothermicity were controlling, the opposite result would be found.

Disproportionation of two alkyl radicals is characterized by a near zero activation energy and hence is mechanistically unrelated to hydrogen abstraction reactions where a 25 to 40 kJ/mol activation energy is usual. The "head to tail" transition complex has been widely accepted as a basis for consideration of the disproportionation reaction. The transfer of hydrogen in a disproportionation reaction is concerted. The p electron of the free radical carbon interacts with the C-H σ bond, the acceptor radical changing from sp² to sp³ hybridization. The donor radical simultaneously develops the π bond characteristic of the olefin. Allylic radicals, as we have shown, do not disproportionate with other allylic radicals, and when disproportionating with alkyl radicals, function exclusively as hydrogen donors. Their activity as hydrogen acceptors is absent. It is suggested that this characteristic is attributable to the electron delocalization in the allylic radical. The free electron has a probability of 1/2 of being associated with an end carbon of the allylic radical grouping. This contrasts with a probability of 1 for the appropriate alkyl radical carbon. The smaller effective charge density on the carbon available as a potential acceptor in allylic type radicals inhibits the interaction with the σ C-H bond of the counter radical so that allylic type radicals (or resonance type radicals in general where the free electron density is reduced) no longer function as H atom acceptors in disproportionation. The donor effectiveness of the allylic radical is unaffected by these considerations.

Table VI shows the disproportionation-combination ratio of 2-butyl with dimethylallyl and of 2-methyl-2-butyl with dimethylallyl, though they differ by a factor of 2, are nevertheless both considerably lower than that of alkyl-alkyl radical ratios. The lowest k_d/k_c ratio found for alkyl radicals under cryogenic conditions is that of 2-propyl-2-propyl with a value of 5.5. The value for 2-butyl + 2-butyl is 9.5 and for 2-methyl-2-butyl + 2-methyl-2-butyl is 1500. The cross reactions of allylic radicals with alkyl radicals favor combination relative to alkyl with alkyl reactions. This is true even considering the absence of H atom transfer to the allylic radical which would account for only a factor of about 2. The notably low value of the k_d/k_c ratio for cross allylic-alkyl radical reactions could be accounted for by assuming that the H atom transfer to the alkyl radical is inhibited. The rationale for such an assumption is not evident. It is more likely that the combination reaction is favored with respect to H atom transfer to the alkyl radical because the delocalization of the free electron in the allylic radical furnishes two reactive centers for combination.

Data for the k_d/k_c ratio for several pertinent radical pairs may be seen in Table II. The absence of disproportionation between allylic radicals, and the favoring of combination in cross reactions between allylic and alkyl radicals, has been noted. The autodisproportionation-combination of 4-pentene-2-yl, with $k_d/k_c = 7.6$, shows clearly that the presence of a simple olefinic bond in the radical has no effect on the k_d/k_c ratio, the value of 7.6 being "normal" for alkyl radicals. The values of 9.5, 35, and 1500 for

TABLE VI: Disproportionation-Combination Ratios^a

Reaction	k_d/k_c
	1.7 ± 0.2
	1.0 ± 0.2

^a In the condensed phase at 90 K. The k_d/k_c values are derived from the data given on Tables III and IV.

the pairs (2-butyl, 2-butyl), (2-butyl, 2-methyl-2-butyl), and (2-methyl-2-butyl, 2-methyl-2-butyl) show clearly that there is no simple relationship among the k_d/k_c ratios (for example, that the cross reaction ratio is the geometric mean between the two autoreaction ratios). In the three pairs (dimethylallyl, dimethylallyl), (dimethylallyl, 2-butyl), and (2-butyl, 2-butyl), the k_d/k_c ratios are ~0, 1, and 9.5, respectively.

Summary

Allylic radicals are found to react in a remarkably different manner than alkyl radicals. Low temperature reactions of pairs of allylic radicals occur by combination, with no disproportionation observed. In contrast, alkyl radicals react predominantly by disproportionation. However, cross disproportionation as well as combination with alkyl radicals can occur. In the cross disproportionation between an allyl and an alkyl radical, the allylic radical acts exclusively as a hydrogen donor. This effect is attributed to the inhibition of the hydrogen acceptor function by the delocalization of the free spin. Because of this, two allylic type radicals (or any radicals in which the density of the free spin is sufficiently delocalized) can only combine. The contribution of the resonant components of the allylic radicals to the combination products is greatly dependent on steric effects.

References and Notes

- (1) R. D. Kelley and R. Klein, *J. Phys. Chem.*, **78**, 1586 (1974).
- (2) R. Klein and M. D. Scheer, *J. Phys. Chem.*, **62**, 1011 (1958).
- (3) R. Klein, M. D. Scheer, and R. D. Kelley, *J. Phys. Chem.*, **68**, 598 (1964).
- (4) D. M. Golden, *Int. J. Chem. Kinet.*, **1**, 127 (1969).
- (5) R. Sustman and H. Trill, *J. Am. Chem. Soc.*, **96**, 4343 (1974).
- (6) W. von E. Doering and G. H. Beasley, *Tetrahedron*, **29**, 2231 (1973).
- (7) S. F. Nelson and P. D. Bartlett, *J. Am. Chem. Soc.*, **88**, 137 (1966).
- (8) P. S. Engel and D. J. Bishop, *J. Am. Chem. Soc.*, **94**, 2148 (1972).
- (9) D. G. L. James and S. M. Kambanis, *Trans. Faraday Soc.*, **66**, 2081 (1969).
- (10) B. H. Al-Sader and R. J. Crawford, *Can. J. Chem.*, **48**, 2745 (1970).
- (11) D. G. L. James and G. E. Troughton, *Trans. Faraday Soc.*, **62**, 145 (1966).
- (12) R. J. Crawford, J. Hamelin, and B. Strehlke, *J. Am. Chem. Soc.*, **93**, 3810 (1971).
- (13) J. C. Aston, G. Szasy, H. W. Wooley, and F. G. Brickwedde, *J. Chem. Phys.*, **14**, 67 (1946).
- (14) D. G. L. James and R. D. Suart, *Trans. Faraday Soc.*, **64**, 2735 (1968).
- (15) The ratio k_d/k_c is defined as the ratio of the sum of the rate constants of the possible disproportionation reactions to that of the possible combination reactions.
- (16) Although ΔH_{90K} will differ from ΔH_{298K} , the latter values nevertheless give a valid indication of the relative ordering for the three reactions.

Thermodynamics of the Reaction of Ammonia and Sulfur Dioxide in the Presence of Water Vapor¹

Ronald Landreth, Rosa G. de Pena, and Julian Heicklen*

Departments of Chemistry and Meteorology and Center for Air Environment Studies, The Pennsylvania State University, University Park, Pennsylvania 16802 (Received August 22, 1974; Revised Manuscript Received May 27, 1975)

Publication costs assisted by the Environmental Protection Agency

The reaction of NH_3 , SO_2 , and H_2O vapor to produce particulate matter was examined at 14, 24, 35, and 44°. At the three highest temperatures a white solid is produced consisting of two NH_3 molecules, one SO_2 molecule, and one H_2O molecule. Infrared studies have shown the solid to be $(\text{NH}_4)_2\text{SO}_3$. Thus the reaction is $2\text{NH}_3(\text{g}) + \text{SO}_2(\text{g}) + \text{H}_2\text{O}(\text{g}) \rightleftharpoons (\text{NH}_4)_2\text{SO}_3(\text{s})$. The enthalpy and entropy of the reaction are -53 kcal/mol and -113 cal/(mol deg), respectively. There is about $\pm 20\%$ uncertainty in both values, so that the data are consistent with the enthalpy of -60.9 kcal/mol for the normal solid form of $(\text{NH}_4)_2\text{SO}_3$. At 14°, there is less H_2O in the solid, and presumably some $(\text{NH}_4)_2\text{S}_2\text{O}_5$ is produced.

Introduction

Due to the presence of ammonium sulfate in the atmosphere and the strong desire to determine how it is formed,² the reaction of ammonia, sulfur dioxide, and water vapor is of importance. The reaction of SO_2 and NH_3 under anhydrous conditions has been reported previously.^{2a,3,4} The history of the water reaction is closely related to that of the anhydrous reaction and was reviewed by Scott et al.^{2a} Friend et al.⁵ could not produce particles in a similar experiment but their gas pressures were much smaller than used in the other investigations.

Neither the chemical structures nor the thermodynamics of the adducts are precisely known. McLaren et al.⁴ have reported a ΔH of reaction of -34 kcal/mol for the reaction of SO_2 and NH_3 in wet nitrogen and -45 kcal/mol in O_2 . No temperature ranges for the experiments were stated. Scargill⁶ identified two products from the NH_3 - SO_2 - H_2O reaction as $(\text{NH}_4)_2\text{SO}_3$ and $(\text{NH}_4)_2\text{S}_2\text{O}_5$ using chemical analysis and infrared spectroscopy. The dissociation constants of both compounds were measured by a transpiration method from 273 to 298°K. The values found for ΔS and ΔH for the two sublimations were 152.2 cal/(mol deg) and 64.8 kcal/mol, respectively, for $(\text{NH}_4)_2\text{SO}_3$ and 191.7 cal/(mol deg) and 81.0 kcal/mol, respectively, for $(\text{NH}_4)_2\text{S}_2\text{O}_5$.

In this paper, we have examined the reactions from 14 to 44° between SO_2 , NH_3 , and H_2O vapor in N_2 . The stoichiometry and thermodynamic functions are reported.

Experimental Section

The reaction was carried out in a 2.9-l. cylindrical cell 149 cm long and 5 cm in diameter. The cell was capped at each end by a quartz window. Along the length of the interior of the cell was a narrow tube with holes every 10 cm through which the gases entered to allow thorough mixing. Temperature regulation was made with a constant-temperature water bath surrounding the cell.

During the experiments SO_2 absorption at 3340 Å was monitored photometrically. The 3340-Å radiation was from

a Hanovia Utility 30620 Hg lamp which had been passed through a Jarrell-Ash 82-410 monochromator set at 3340 Å. The light beam was split and half of it passed through the reaction vessel to a RCA 935 phototube; the other half impinged directly on a second RCA 935 phototube. When the reaction vessel was empty, the signals from the two beams were balanced by a Wheatstone bridge. Thus with SO_2 in the cell the difference in beam signals was a direct measure of the SO_2 pressure.

The SO_2 and NH_3 gases were from the Matheson Co. and the N_2 gas was from Phillip and Sons Inc. Before use, the N_2 was passed through a trap packed with glass wool at -196° to remove water and impurities. Both SO_2 and NH_3 were twice purified by distillation from -98 to -196° . Sometimes further distillation was performed from -98 to -130° . Distilled water was used after being degassed at various temperatures from -10 to -196° . The gases were handled in a mercury and grease-free vacuum line containing Teflon stopcocks with Viton "O" rings. The vacuum line could be evacuated to less than 1×10^{-4} Torr.

The gases were introduced into the cell and the experiments performed as follows. Water was the first gas introduced and was allowed to stand for 5 min to obtain a constant-pressure reading. A known prepared mixture of SO_2 , NH_3 , and N_2 (the pressures of SO_2 and NH_3 were below the point at which they react in the absence of H_2O ³) was added in increments to the water in the cell. All gas pressures were read on a calibrated National Research Corp. 820 alphanon vacuum gauge.

After each incremental addition of the SO_2 - NH_3 - N_2 mixture, the SO_2 absorption increased and then remained constant if particles were not produced. Ultimately the reactant pressures became sufficiently high so that particles were produced and the SO_2 absorption decreased slowly over a period of a few minutes after the sharp increase accompanying the incremental addition. This peak was taken as the nucleation pressure. Then the contents of the cell were expanded by 4.5% into a small evacuated volume connected by a stopcock to the reaction vessel. If the particles sublimed to restore the SO_2 pressure, then the expansion was repeated until the SO_2 pressure could not be restored. At this point all of the solid had just sublimed, and the NH_3 and H_2O pressures could be computed from their

* To whom correspondence should be addressed at the Department of Chemistry, The Pennsylvania State University.

initial pressures and the expansion factor. These pressures were taken as the equilibrium vapor pressures.

When N_2 was used as a diluent, the ratio of its pressure to that of SO_2 varied from 77 to 292 and to that of NH_3 from 81 to 146. Reactions without nitrogen were done in a similar manner as above except that water was not necessarily added first. The order of addition of the reactants did not affect the results.

Results

When SO_2 , NH_3 , and H_2O gases were mixed, a white solid was produced instantly if the gas pressures were sufficiently high. The reaction was reversible and when the gas pressures were reduced, the solid sublimed back to its gaseous reactants. When N_2 was used as a diluent there was a slight delay and a noticeable slowing of the reaction.

Gas pressures could be measured to within 7–10% accuracy. To be sure that the reaction was not affected by the monitoring light, runs were done with the light off using it only to make a measurement. The results were the same as with continuous monitoring.

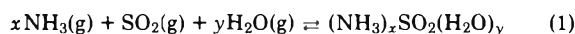
The pressures of SO_2 and H_2O in equilibrium with the solid at 24° are shown graphically in log-log plots in Figure 1 for three mixture ratios of $[SO_2]/[NH_3]$. The plots are linear, and as the ratio is lowered, the lines lie successively lower. The results in N_2 are the same as without it. All the plots of SO_2 pressure vs. H_2O pressures are linear and can be fitted with a line of slope $-1/3$.

The equilibrium pressures of SO_2 and H_2O at 14, 24, 35, and 44° are shown graphically in log-log plots in Figure 2 for a 1:1 ratio of $[SO_2]/[NH_3]$. As the temperature is lowered, so are the points on the plot. At the three higher temperatures, the points can be fitted to a line of slope $-1/3$. However, at 14° the plot cannot be fitted to a line of slope $-1/3$ but is best fitted by a line of slope $-1/6$.

The supersaturation ratio needed for particle nucleation (i.e., the absorbance of SO_2 needed to form particles divided by the absorbance of SO_2 at equilibrium) was obtained in each experiment. A plot of this ratio vs. H_2O pressure in any series showed considerable scatter. For some of the series there was no trend in the data. For other series, there may have been a slight downward trend as the H_2O vapor pressure was raised. However the scatter was sufficiently large so that this trend may not have been meaningful. The average values for the six series of runs are tabulated in Table I. There is considerable scatter, but no obvious trend in the data. The average value for the six series is 1.50 ± 0.10 .

Discussion

The heterogeneous equilibrium under study is



The equilibrium expression is

$$K = 1/[NH_3]^x [SO_2] [H_2O]^y \quad (2)$$

where K is the equilibrium constant at a given temperature. Equation 2 can be rearranged to give

$$\log [SO_2] = -x \log [NH_3] - y \log [H_2O] - \log K \quad (3)$$

If $[H_2O]$ is held constant, a log-log plot of $[SO_2]$ vs. $[NH_3]$ will give a plot of slope $-x$. Such a plot is shown in Figure 3 for $[H_2O] = 1$ Torr. The $[SO_2]$ values were taken from Figure 1, and $[NH_3]$ was computed from the known value of

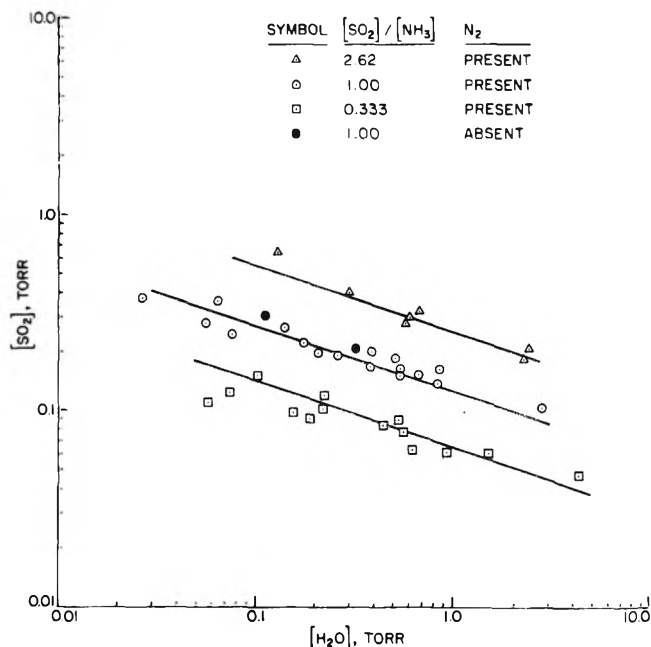


Figure 1. log-log plots of the vapor pressures of SO_2 vs. the final H_2O pressure in equilibrium with the solid at 2.62:1, 1:1, and 1:3 mixtures of SO_2 and NH_3 at 24° .

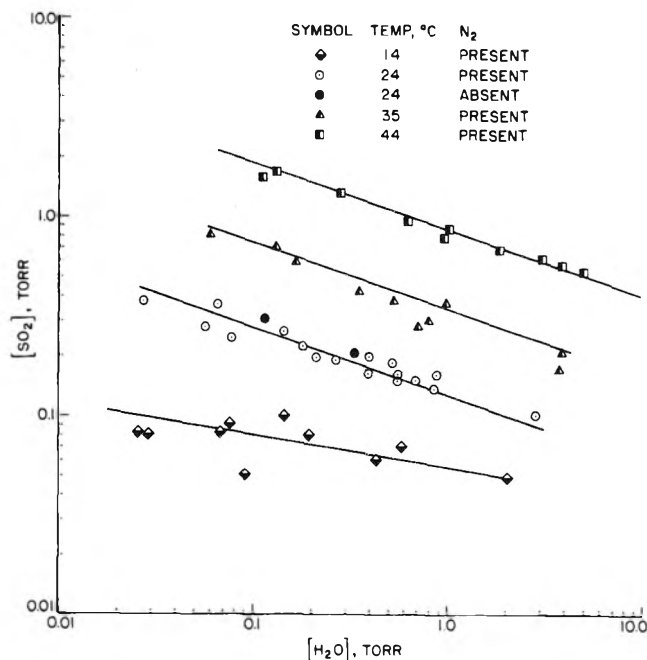


Figure 2. log-log plots of the vapor pressures of SO_2 vs. the final H_2O pressure in equilibrium with the solid at 14, 24, 35, and 44° . A 1:1 ratio of $[SO_2]$ to $[NH_3]$ was used in all reactions.

the $[SO_2]/[NH_3]$ ratio. The plot is linear with a slope of -2 ; thus $x = 2$.

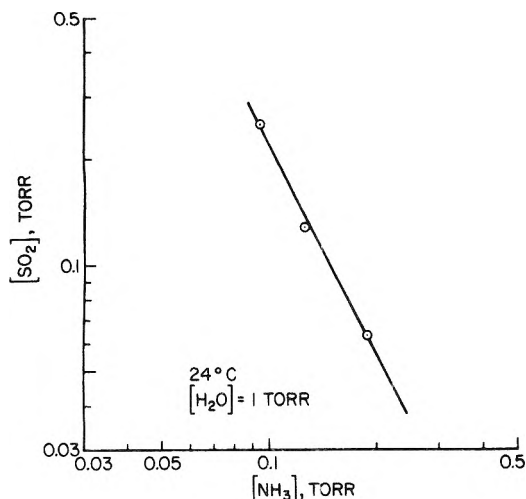
Now if we consider those series of runs with $[SO_2]/[NH_3] = 1.00$, then eq 2 can be rearranged to

$$\log [SO_2] = \frac{-\log K - y \log [H_2O]}{1 + x} \quad (4)$$

The log-log plots of $[SO_2]$ vs. $[H_2O]$ shown in Figure 2 have slopes $-1/3$ at 24, 35, and 44° and $-1/6$ at 14° . Thus $y = 1$ at

TABLE I: Average Values of the Supersaturation Ratios Needed for Nucleation

$[\text{SO}_2]/[\text{NH}_3]$	Temp, °C	Supersatn ratio
1.00	14	1.51
2.62	24	1.39
1.00	24	1.62
0.33	24	1.63
1.00	35	1.33
1.00	44	1.54
		Av 1.50 ± 0.10

**Figure 3.** log-log plot of $[\text{SO}_2]$ vs. $[\text{NH}_3]$ in equilibrium with 1 Torr of H_2O and the solid at 24° .

the three highest temperatures and $1/2$ at the lowest temperature.

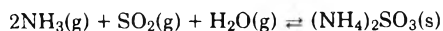
The formula of the solid at 24° and above is $(\text{NH}_3)_2\text{SO}_2 \cdot \text{H}_2\text{O}$. From the intercepts of the plots in Figure 2, the equilibrium constants can be evaluated, and they are listed in Table II.

The equilibrium constants in Table II are plotted on the van't Hoff plot, Figure 4, since

$$\ln K(\text{atm}^{-4}) = \Delta S/R - \Delta H/RT \quad (5)$$

A straight line can be drawn reasonably through the points. The slope gives $\Delta H = -53$ kcal/mol and the intercept gives $\Delta S = -113$ cal/(mol deg), both with an uncertainty of about $\pm 20\%$. Our value of ΔH is considerably lower than the value of -34 kcal/mol reported by McLaren et al.,⁴ and our thermodynamic functions are somewhat higher than those of Scargill.⁶ Also shown in Figure 4 is the plot based on Scargill's thermodynamic functions. It can be seen that, in spite of the differences in thermodynamic functions, which are quite inaccurate because of the small temperature ranges involved, the equilibrium constants from the two studies are in excellent agreement.

Infrared measurements in our laboratory have shown that the solid $(\text{NH}_3)_2\text{SO}_2 \cdot \text{H}_2\text{O}$ is $(\text{NH}_4)_2\text{SO}_3$.⁷ The enthalpy of formation of this compound is known to be -211.6 kcal/mol.⁸ For the gases the enthalpies of formation, ΔH°_{298} (kcal/mol), are:⁹ NH_3 , -10.970 ; H_2O , -57.798 ; SO_2 , -70.947 . Thus the enthalpy for the reaction

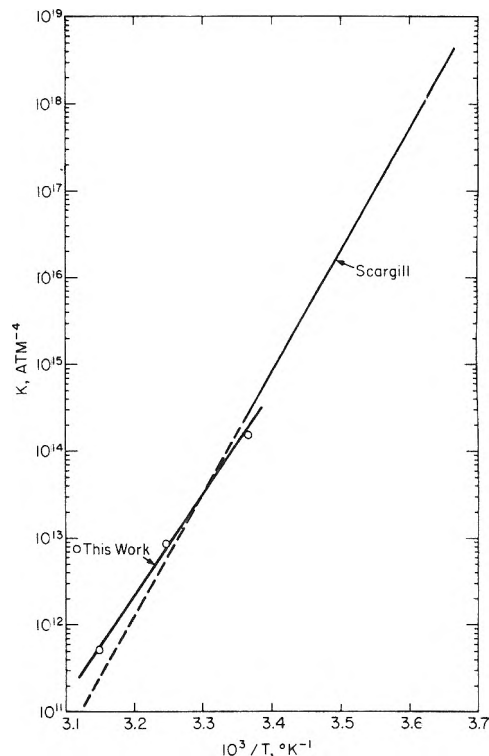
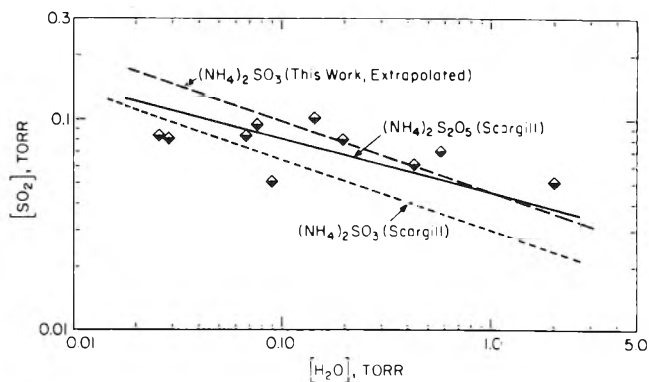


is -60.9 kcal/mol, a value intermediate to those found here

TABLE II: Equilibrium Constants for the Reaction $2\text{NH}_3(\text{g}) + \text{SO}_2(\text{g}) + \text{H}_2\text{O}(\text{g}) \rightleftharpoons (\text{NH}_3)_2\text{SO}_2 \cdot \text{H}_2\text{O}(\text{s})^a$

Temp, °C	K, Torr^{-4}	$10^{-12} K, \text{atm}^{-4}$
24 ± 1	460	154
35 ± 1	25.5	8.51
44 ± 1	1.54	0.51

^a $\ln K(\text{atm}^{-4}) = \Delta S/R - \Delta H/RT$; $\Delta S = -113$ cal/(mol deg); $\Delta H = -53$ kcal/mol.

**Figure 4.** Semilog plot of the equilibrium constant K vs. the reciprocal temperature for the reaction $2\text{NH}_3(\text{g}) + \text{SO}_2(\text{g}) + \text{H}_2\text{O}(\text{g}) \rightleftharpoons (\text{NH}_3)_2\text{SO}_2 \cdot \text{H}_2\text{O}(\text{s})$.**Figure 5.** Comparison of 14° data for a 1:1 mixture of SO_2 and NH_3 with the equilibrium vapor pressure curves expected for $(\text{NH}_4)_2\text{SO}_3$ and $(\text{NH}_4)_2\text{S}_2\text{O}_5$ from Scargill⁶ and for $(\text{NH}_4)_2\text{SO}_3$ extrapolated from the higher temperature data of this study.

and those found by Scargill,⁶ but within the uncertainty limits of both measurements.

The formula for the solid at 14° is not established. The data are replotted in Figure 5 along with the expected lines

for $(\text{NH}_4)_2\text{SO}_3$ and $(\text{NH}_4)_2\text{S}_2\text{O}_5$ from Scargill's results and the extrapolated plot from our higher temperature data for $(\text{NH}_4)_2\text{SO}_3$. The solid formed should correspond to that with the lowest equilibrium vapor pressure. The data, though badly scattered, can conform to either our extrapolated plot for $(\text{NH}_4)_2\text{SO}_3$ or Scargill's plot for $(\text{NH}_4)_2\text{S}_2\text{O}_5$. Probably both compounds are present and this may account for the scatter. Scargill's plot for $(\text{NH}_4)_2\text{SO}_3$ appears to lie too low to be consistent with the data.

Acknowledgment. The authors wish to thank Drs. K. Olszyna and L. Stockburger for their assistance. This work

was supported by the Environmental Protection Agency through Grant No. 800874, for which we are grateful.

References and Notes

- (1) CAES Report No. 369-74.
- (2) (a) W. D. Scott, D. Lamb, and D. Duffy, *J. Atmos. Sci.*, **26**, 727 (1969); (b) C. S. Kaing, D. Stauffer, and V. A. Mohnen, *Nature (London), Phys. Sci.*, **244**, 53 (1973).
- (3) R. Landreth, R. G. de Pena, and J. Heicklen, *J. Phys. Chem.*, **78**, 1378 (1974).
- (4) E. McLaren, A. J. Yench, J. M. Kushnir, and V. K. Mohnen, *Tellus*, **26**, 1 (1974).
- (5) J. P. Friend, R. Leifer, and M. Trichon, *J. Atmos. Sci.*, **30**, 465 (1973).
- (6) D. Scargill, *J. Chem. Soc. A*, 2461 (1971).
- (7) I. C. Hisatsune and J. Heicklen, unpublished results, 1974.
- (8) *Nat. Bur. Stand. (U.S.), Tech. Note*, No. 270-3 (1968).
- (9) "JANAF Thermochemical Tables", Dow Chemical Co., Midland, Mich., 1966.

Electronic Excitation Transfer between the Same Kind of Excited Molecules in Rigid Solvents under High-Density Excitation with Lasers

Nobuaki Nakashima, Yuji Kume, and Noboru Mataga*

*Department of Chemistry, Faculty of Engineering Science, Osaka University, Toyonaka, Osaka, Japan
(Received November 1, 1974; Revised Manuscript Received June 3, 1975)*

By means of high-density excitation with a Q-switched ruby laser, the electronic excitation transfer between excited pyrenes in the fluorescent state ($S_1 + S_1 \rightarrow S_0 + S_n$) and that between excited perdeuterio-phenanthrenes in the phosphorescent state ($T_1 + T_1 \rightarrow S_0 + T_n$) in rigid solvents at 77°K have been observed by directly measuring the luminescence decay curves. Comparing the theoretical decay functions derived in the present work with the experimental ones, it has been proved that the excitation transfers in these systems are due to Förster's dipole-dipole coupling mechanism.

Introduction

Bimolecular quenching of fluorescence due to the interaction between excited aromatic molecules was first found by Tolstoi and Abramov¹ as well as by Bergman et al.² It has been confirmed by many other investigations³⁻⁶ following the above ones that this phenomenon is occurring in general under high-density excitation.

This bimolecular quenching seems to consist of the following two processes: (1) mutual approach of excited molecules to a distance where they can interact with each other; (2) an actual quenching process due to the interaction between the excited molecules. However, in many cases, including the excited molecules in solution and excitons in crystals, the actual quenching process is masked by the rapid "bimolecular collision". The bimolecular collision process has been confirmed for many cases, and its rate constant has been determined. Such a study has proved to be a powerful mean especially for the investigation on the diffusion of excitons in crystals.⁴

As for the mechanisms of the actual quenching process, Abramov¹ has insisted that the overlapping between the $S_n \leftarrow S_1$ absorption and $S_1 \rightarrow S_0$ fluorescence bands is essential for the quenching process to occur. Babenco et al.⁵ as well as Kobayashi and Nagakura⁶ have also insisted that

the quenching occurs owing to the electronic excitation transfer between the excited states due to the Förster mechanism.⁷ However, there has been no direct experimental proof for that so far as we know.

In order to elucidate the mechanism of this bimolecular interaction, we have derived decay functions of excited states for the systems fixed in rigid solvents assuming the excitation transfer between excited states due to Förster's very weak interaction mechanism of the dipole-dipole coupling⁷ and have compared them with observed decay curves of excited molecules fixed in rigid organic solvents at 77°K under high-density excitation with a Q-switched ruby laser. We have proved that the mechanism of the bimolecular quenching in these excited molecules is Förster's dipole-dipole coupling.

Experimental Procedure

The second harmonic of a Q-switched ruby laser was used for exciting the rigid solution. The ruby laser system was the same one as used before.^{8,9} Its maximum output at 3472 Å was 2×10^{17} photons/pulse and the pulse width was ca. 15 nsec. Fluorescence decay curves were observed by using a Nalumi R21 monochromator, an RCA 1P28 photomultiplier, and a Tektronix 585A oscilloscope. The re-

sponse time of the detecting system was ca. 5 nsec. For the measurement of phosphorescence decay curves, an HTV R213 photomultiplier with an amplifier was used and the decay curves were recorded on a X-Y recorder. The response time of this system was ca. 0.25 sec. The exciting light pulse was focused on the surface of the sample cell which is made of two glass tubes whose optical thickness was ca. 0.1 mm, so that only the fluorescent light from the part of the cell under high-density excitation was monitored. As it will be described later in detail, we have confirmed that if one uses a cell with optical thickness larger than 0.1 mm, the effects of the fluorescence reabsorption due to the $S_n \leftarrow S_1$ or $T_n \leftarrow T_1$ transitions are not negligibly small.

Pyrene was chromatographed on activated alumina using *n*-hexane for elution. Chromatographed pyrene was sublimated under vacuum. Nakara's 1,12-benzperylene containing 0.02% perylene and Merck's perdeuteriophenanthrene containing ca. 2.5% anthracene were used without further purification. Since the fluorescence decay time of perylene is much shorter than that of 1,12-benzperylene and also the phosphorescence decay of anthracene is very much faster than that of perdeuteriophenanthrene, the existence of these impurities does not affect the results of the luminescence decay function measurements to be described. Methylcyclohexane (Wako, Spectrograde), dibutyl ether (Merck, Spectrograde), methanol (Wako, analytical grade reagent), and ethanol (Wako, analytical grade reagent) were used without further purification. Decaline was Wako analytical grade reagent and distilled under reduced pressure before use. All sample solutions were deaerated by freeze-pump-thaw cycles.

Results and Discussion

a. Luminescence Decay Functions in the Presence of Excitation Transfer between Excited Molecules. The decay function of the excited molecules fixed in a rigid solvent in the presence of excitation transfer of the type $D(S_1) + A(S_0) \rightarrow D(S_0) + A(S_1)$ or $D(T_1) + A(S_0) \rightarrow D(S_0) + A(S_1)$, due to the dipole-dipole interaction, is given by eq 1^{7,10} assuming that D is excited at $t = 0$ by a light flash with duration much shorter than the decay time of the excited state.

$$\overline{P}(t) = \exp\left(-\frac{t}{\tau_0} - 2\xi\left(\frac{t}{\tau_0}\right)^{1/2}\right) \quad (1)$$

Here τ_0 is the lifetime of excited D in the absence of the energy acceptor A, ξ is a function of the acceptor concentration, i.e., $\xi = C_A/C_A^0$, $C_A^0 = 4.77 \times 10^{-10} n^2/(K^2\phi_D\Omega)^{1/2}$ mol/l. and $\Omega = \int_0^\infty [f_D(\bar{\nu})\epsilon_A(\bar{\nu})/\bar{\nu}^4] d\bar{\nu}$. K^2 is the average value of the square of orientation factor between transition dipoles of energy donor and acceptor, respectively.¹⁰ When molecules are fixed but in a random orientation state, the value 0.475 is usually used. n is the refractive index of solvent, ϕ_D is the fluorescence quantum yield of D, and Ω is the so-called overlap integral between the donor fluorescence spectra and acceptor absorption spectra.

On the other hand, for the excitation transfer of the type $S_1 + S_1 \rightarrow S_0 + S_n$ or $T_1 + T_1 \rightarrow S_0 + T_n$, between the same kind of molecules fixed in the rigid solvent, we can derive easily the decay function of eq 2, where we must take into consideration the fact that the energy acceptors are also decaying in the same way as the energy donors. Namely, the decay function may be written as

$$\overline{P}(t) = \exp\left(-\frac{t}{\tau_0} - N_0 \prod_{k=1}^{N_0} \exp\left[-\left(\frac{R_0}{R_k}\right)^6 \frac{t}{\tau_0}\right]\right) \quad (2)$$

where $N_0 \overline{P}(t)$ is the number of the excited molecules at the delay time t from the exciting pulse, R_k is the distance between excited molecules, and R_0 is the critical transfer distance where the rate of the excitation transfer becomes the same as the rate of the decay of the excited state. Taking average of $P(t)$ over the statistical distribution of molecules in a way similar to that for the derivation of eq 1,⁷ one obtains

$$\overline{P}(t) = \exp\left[-\frac{t}{\tau_0} - 2\xi \overline{P}(t) \left(\frac{t}{\tau_0}\right)^{1/2}\right] \quad (3)$$

In the above derivation, it is assumed that the molecules excited to the S_n state return very rapidly to the S_1 state. This assumption seems to be quite reasonable since the relaxation time of $S_n \rightarrow S_1$ internal conversion may certainly be much smaller compared to the decay times we are measuring in this work. Throughout this paper, we are assuming that the molecules excited to S_n or T_n by the excitation transfer or fluorescence reabsorption return very rapidly to S_1 or T_1 , respectively. The validity of this assumption may be demonstrated in section b by analyzing the observed results with equations derived under this assumption. Another possible type of excitation transfer due to the dipole-dipole interaction between the excited molecules of the same kind may be $S_1 + T_1 \rightarrow S_0 + T_n$. In this case, the decay function of the S_1 state can be obtained by the procedure similar to that for the derivation of eq 3.

$$\overline{P}(t) = \exp\left[-\frac{t}{\tau_0} - 2\xi(t) \left(\frac{t}{\tau_0}\right)^{1/2}\right] \quad (4)$$

$$\xi(t) = \frac{C_A \phi_{ST}}{C_A^0 \tau_0} \int_0^t \overline{P}(t') \exp\left(\frac{t' - t}{\tau_p}\right) dt'$$

Here ϕ_{ST} is the quantum yield of the T_1 state formation, τ_p is the decay time of the T_1 state, and it is assumed that the T_1 state is formed from the relaxed S_1 state (fluorescent state). The $S_1 \rightarrow T_1$ excitation transfer between the same kind of molecules has been confirmed in the case of crystals under steady excitation.^{5,11}

In the case of the rapid diffusion of excited molecules in solution or rapid diffusion of excitons in crystals, the $S_1 \rightarrow S_1$ or $T_1 \rightarrow T_1$ excitation transfer becomes a diffusion-controlled bimolecular process. The decay function in this case may be given by

$$1/\overline{P}(t) = (1 + C_A \tau_0 \gamma) \exp(t/\tau_0) - C_A \tau_0 \gamma \quad (5)$$

where γ is the rate constant of the bimolecular process.¹⁻⁶ The decay function seems to be rather complicated when the thermal diffusion is possible but is not so rapid as in the above case, i.e., when the rate of diffusion is comparable with that of excitation transfer. In the case of the $S_1 \rightarrow S_0$ transfer ($D(S_1) + A(S_0) \rightarrow D(S_0) + A(S_1)$) due to the Förster mechanism, an appropriate decay function can be derived even for such a complicated case, and it can reproduce the experimental observation satisfactorily.¹² In the case of the excitation transfer between excited molecules, we can derive also such a decay function. However, it seems to be rather difficult to get a clear-cut conclusion by comparing such a complicated formula with experimental observations for the intermediate case.

b. Luminescence Decay Functions in the Presence of Reabsorption Effects. Actually, we are observing the luminescence decay curve instead of the decay function itself.

Therefore, we need the luminescence intensity to be proportional to the decay function $\bar{P}(t)$. However, it may be possible in the actual systems that the emitted luminescence is reabsorbed by the excited molecule: leading to the loss of proportionality between the observed luminescence intensity and $\bar{P}(t)$.^{8,13} Thus, it is necessary to investigate the effect of reabsorption on the observed luminescence decay curves for our present purpose.

When the fluorescent light is partly reabsorbed by the ground-state molecules ($S_1 \leftarrow S_0$ absorption), the decay curve of the fluorescence measured at a wavelength where the reabsorption can be neglected is experimentally confirmed to be written approximately as

$$q(t) \propto \exp \left[\left(-\frac{1}{\tau_0} - C_1 \right) t \right] \quad (6)$$

where C_1 is a constant independent of t . This equation represents the fact that the apparent decay time becomes longer owing to the reabsorption of fluorescence by the $S_1 \leftarrow S_0$ transition. When the fluorescence is reabsorbed by S_1 molecules ($S_n \leftarrow S_1$ absorption), its decay curve measured at the wavelength where the absorption is considerable may be given by⁸

$$q(t) \propto 1 - 10^{C_2 \exp(-t/\tau_0)} \quad (7)$$

where C_2 is a constant independent of t .⁸ It can be shown that the apparent fluorescence decay time becomes longer due to the reabsorption effect according to eq 7. In the case of the reabsorption of phosphorescence by the T_1 state molecules, the phosphorescence decay curve may be given by the same type of equation as (7) except that τ_0 is replaced by τ_p .

When the fluorescence is reabsorbed by the T_1 molecules ($T_n \leftarrow T_1$ absorption), the fluorescence decay curve may be given by eq 8, where C_3 is a constant independent of t .

$$q(t) \propto [1 - 10^{C_3 [1 - \exp(t/\tau_0)]}] \left[\exp\left(\frac{t}{\tau_0}\right) - 1 \right]^{-1} \quad (8)$$

Here it is assumed that the T_1 state is formed from the relaxed S_1 state (fluorescent state) and that the lifetime of the T_1 state is much longer than that of the S_1 state. Equation 8 can be derived easily by the procedure similar to that for the derivation of eq 7. In contrast to the case of eq 7, one can show that the apparent fluorescence decay time becomes shorter due to the reabsorption by the $T_n \leftarrow T_1$ transition.

Not only in the above cases of the fluorescence reabsorption but also in the presence of the induced emission from the S_1 state, $q(t)$ does not agree with $\bar{P}(t)$ and the apparent fluorescence decay time becomes shorter.¹⁴ However, since there has been no report about the induced emission from the S_1 state of pyrene as well as the T_1 state of perdeuterio-phenanthrene and, moreover, since there should be no induced emission when the quenching due to the energy transfer between excited molecules is dominant,⁹ we do not take into consideration the effect of the induced emission on the fluorescence decay curve.

c. Characteristics of Calculated Decay Curves. Some examples of decay curves of eq 1, 3–5, 7, and 8 for appropriate values of parameters are indicated in Figures 1 and 2, where $1/q(t)$ or $1/\bar{P}(t)$ is plotted against $\exp(t/\tau_0)$. One can see evidently from these plots that we get a curve which is convex upward in the case of the $S_1 \rightarrow S_0$ or the $T_1 \rightarrow T_1$ excitation transfer (eq 3), which can be distinguished from others. Contrary to this, in the case of the $S_1 \rightarrow T_1$ excita-

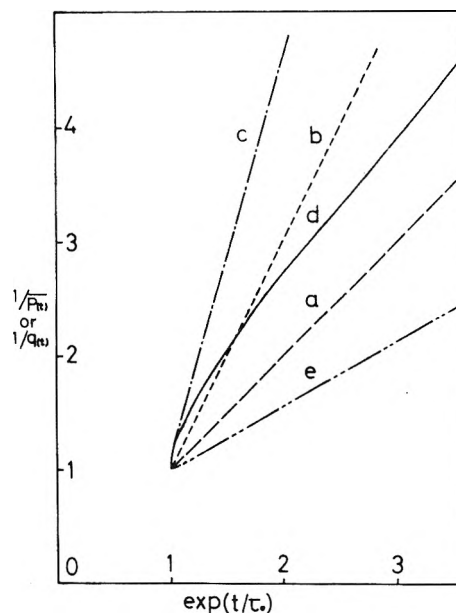


Figure 1. Plots of calculated $1/\bar{P}(t)$ and $1/q(t)$ against $\exp(t/\tau_0)$ for various cases: (a) single-exponential decay in the absence of excitation transfer and fluorescence reabsorption; (b) diffusion-controlled bimolecular quenching (eq 5, $C_A \tau_0 \gamma = 1$); (c) $S_1 \rightarrow S_0$ excitation transfer (eq 1, $\xi = 1/2$); (d) $S_1 \rightarrow S_1$ excitation transfer (eq 3, $\xi = 1/2$); (e) reabsorption of fluorescence by $S_n \leftarrow S_1$ absorption (eq 7, $C_2 = -0.5$).

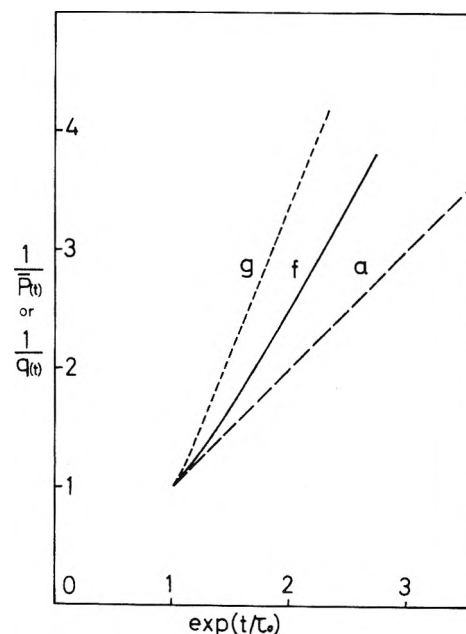


Figure 2. Continuation of Figure 1: (f) $S_1 \rightarrow T_1$ excitation transfer (eq 4, $C_A \phi_{ST}/C_A^0 = 1/4$, $\tau_p \gg \tau_0$); (g) reabsorption of fluorescence by $T_n \leftarrow T_1$ absorption (eq 8, $C_3 = -1.0$).

tion transfer (eq 4), we have a curve that is convex downward. This case also seems to be distinguished from others. However, the plots of other cases including eq 1, 5, and 8, where the fluorescence lifetime is shortened by energy transfer or reabsorption effect, all give straight lines or curves very close to line, so that these three cases cannot be distinguished by this sort of plot but another kind of analysis is necessary. Moreover, when $S_1 \rightarrow S_1$ and $S_1 \rightarrow T_1$ transfers are occurring at the same time, for example, the

plot of $1/\overline{P}(t)$ or $1/q(t)$ vs. $\exp(t/\tau_0)$ may give a straight line or a curve very close to the line. Accordingly, when one obtains a straight line in this sort of plot for the system in rigid solvent, it is rather difficult to get any definite conclusion about the mechanisms of interactions in the excited state.

d. Results of Measurements of Excitation Transfer between Excited Molecules. The possible existence of $T_1 \rightarrow T_1$ excitation transfer due to the dipole-dipole interaction was already demonstrated in the case of perdeuteriophenanthrene in solid solution by measuring the dependence of the phosphorescence yield upon the triplet concentration.¹⁵ Therefore, we have examined first whether the phosphorescence decay curve of perdeuteriophenanthrene under high-density excitation in a rigid solvent can be reproduced by eq 3.

For the measurement of $T_1 \rightarrow T_1$ excitation transfer, perdeuteriophenanthrene was dissolved in a methylcyclohexane-decaline 1:1 mixture. The phosphorescence decay curve of 10^{-4} M solution at 77°K under low-density excitation was a single-exponential type and the decay time was ca. 12.1 sec. The phosphorescence decay curve of the 10^{-1} M solution under high-density excitation is not exponential. The plot of the reciprocal of phosphorescence intensity against $\exp(t/\tau_0)$ is quite similar to the theoretical curve of eq 3, as one can see from Figure 3.

For the measurement of the $S_1 \rightarrow S_1$ excitation transfer we have examined the pyrene-toluene system as well as the pyrene-dibutyl ether (DBE) system. Under low-density excitation with reduced intensity of laser light, both of these systems showed single exponential decay. In the case of 10^{-4} M solution at 77°K, the fluorescence decay time was determined as follows: $\tau_0 = 346 \pm 19$ nsec in toluene and $\tau_0 = 456 \pm 17$ nsec in DBE. The fluorescence decay times of 10^{-1} M solutions in toluene and DBE under low-density excitation were the same as those of 10^{-4} M solutions, respectively. Therefore, the fluorescence reabsorption effect by the ground-state molecules (eq 6) can be neglected in the case of the pyrene solutions.

Fluorescence decay curves of 10^{-1} M solutions under high-density excitation are not exponential. As it is indicated in Figures 4 and 5, the plot of the reciprocal of fluorescence intensity against $\exp(t/\tau_0)$ shows the characteristics of eq 3. In the case of Figure 4, however, the discrepancy between the experimental values and predicted ones with eq 3 becomes larger at later stages of the decay. Possible explanations for this result will be given later.

e. Analysis of Experimental Results. 1. Elimination of Reabsorption Effects. We have actually confirmed that eq 7 and 8 can reproduce very well the observed reabsorption effects in the case of 1,12-benzperylene as shown in Figure 6. Fluorescence decay curves were measured at 77°K with the sample cell which was made of a 4-mm i.d. quartz tube. They were single-exponential types ($\tau_0 \approx 160$ nsec) at all wavelengths under low-density excitation. Even under high-density excitation, they were single-exponential types at 407 nm where $S_n \leftarrow S_1$ and $T_n \leftarrow T_1$ absorption intensities were relatively weak. However, the fluorescence observed at the peak of the $S_n \leftarrow S_1$ absorption spectrum (420 nm)¹⁶ and at the peak of the $T_n \leftarrow T_1$ absorption spectrum (455 nm)¹⁶ under high-density excitation exhibited characteristic decay curves in agreement with those calculated by eq 7 and 8, respectively. Thus, the reabsorption effect is directly demonstrated when the optical thickness is not very small. However, as we have pointed out already, the reab-

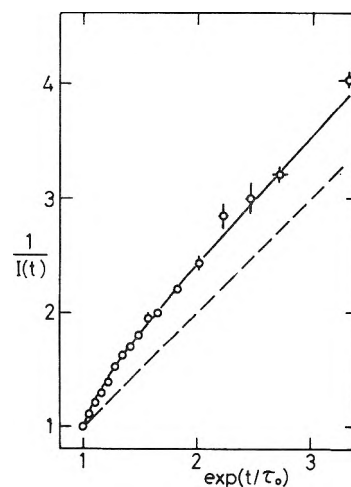


Figure 3. Plot of the reciprocal of observed phosphorescence intensity, $1/I(t)$, against $\exp(t/\tau_0)$ for the perdeuteriophenanthrene-methylcyclohexane-decaline system under high-density excitation: \bigcirc , experimental values obtained by averaging several observations; the horizontal and vertical lines indicate the magnitudes of the standard deviations due to τ_0 and $1/I(t)$, respectively; —, theoretical curve (eq 3, $\xi = 0.28$) showing the best fit to the observed values; - - -, single-exponential curve.

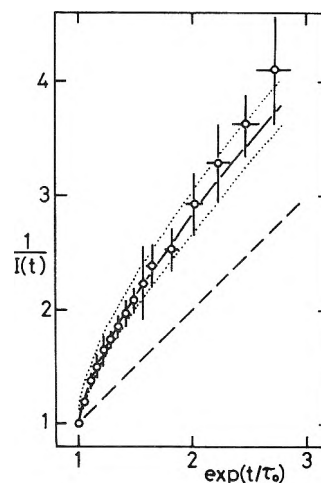


Figure 4. Plot of the reciprocal of observed fluorescence intensity, $1/I(t)$, against $\exp(t/\tau_0)$ for the pyrene-toluene system under high-density excitation: \bigcirc ; experimental values obtained by averaging several observations; the meanings of horizontal and vertical lines are the same as those in Figure 3, respectively. Theoretical curves (eq 3): —, $\xi = 0.6$; ·····, $\xi = 0.75$ (upper one) and $\xi = 0.45$ (lower one). The curve with $\xi = 0.6$ shows the best fit to the experimental values; - - - single exponential curve.

sorption effect becomes negligibly small if we use a cell with an optical thickness of 0.1 mm. We have used the 0.1-mm cell for the measurement of excitation transfer throughout the present work. One should note here that the decay functions of eq 7 and 8 should depend on the wavelength where the fluorescence is observed, while those of eq 1, 3, 4, and 5 should not show such a wavelength dependence. Thus, it has been confirmed that one can eliminate the reabsorption effects by employing the 0.1-mm cell.

2. $T_1 \rightarrow T_1$ Excitation Transfer. Since the phosphorescence spectrum of perdeuteriophenanthrene overlaps strongly with its $T_n \leftarrow T_1$ absorption spectrum, the probability of the $T_1 \rightarrow T_1$ excitation transfer by the Förster

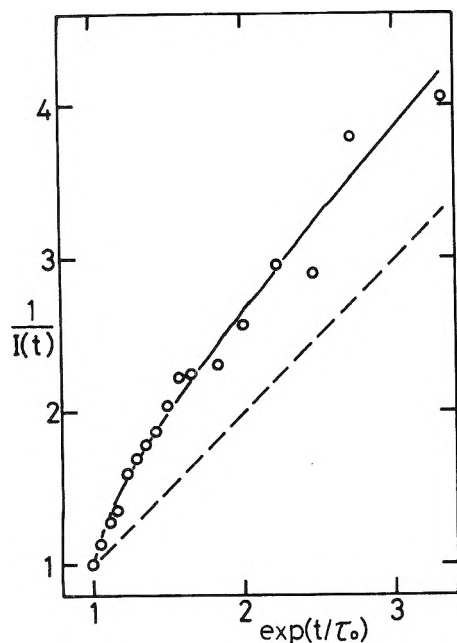


Figure 5. Plot of the reciprocal of observed fluorescence intensity, $1/I(t)$, against $\exp(t/\tau_0)$ for the pyrene-DBE system under high-density excitation: O, experimental values; the possible errors seem to be as large as those in Figure 4; —, theoretical curve (eq 3, $\xi = 0.45$) showing the best fit to the observed values; ---, single-exponential curve.

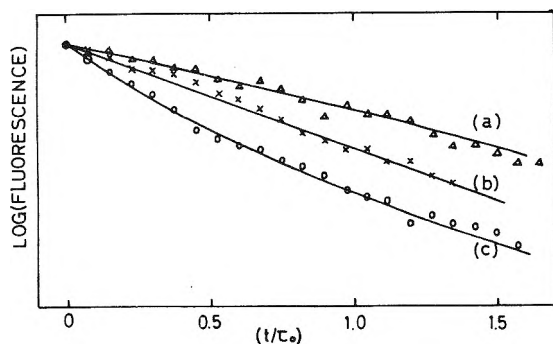


Figure 6. Wavelength dependence of reabsorption effects in the case of 1,12-benzperylene, $7 \times 10^{-3} M$ in a mixed solvent of toluene-ether-ethanol (2:2:1 by volume), at 77°K. Observed fluorescence decay curves: Δ , at 420 nm; \times , at 407 nm; \circ , at 455 nm. Calculated decay curves (—): (a) eq 7; (b) single-exponential curve; (c) eq 8. The experimental values in this figure contain possible errors as large as those in Figure 4.

mechanism seems to be fairly large.¹⁵ According to the estimation by Kellogg,¹⁵ the value of Ω between the phosphorescence and the $T_n \leftarrow T_1$ absorption spectra is 2.2×10^{-12} and C_A^0 is $1.7 \times 10^{-3} M$.

In the present work, we have confirmed the $T_1 \rightarrow T_1$ excitation transfer due to dipole-dipole interaction by directly measuring the phosphorescence decay curves under high-density excitation. As indicated in Figure 3, the agreement between the experimental values and the theoretical decay curve calculated with $\xi = 0.28$ is quite satisfactory, which is a direct proof that the $T_1 \rightarrow T_1$ excitation transfer occurs by the Förster's dipole-dipole coupling mechanism.

3. $S_1 \rightarrow S_1$ Excitation Transfer. Fluorescence spectra and $S_n \leftarrow S_1$ and $T_n \leftarrow T_1$ absorption spectra of pyrene are shown in Figure 7. The experimental values of the longer

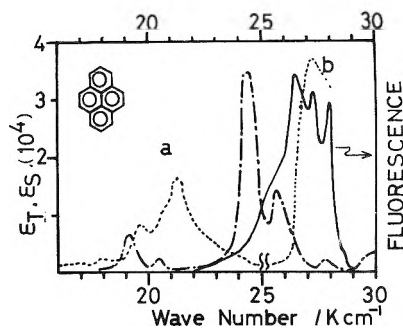


Figure 7. Fluorescence, $S_n \leftarrow S_1$ absorption (ϵ_s), and $T_n \leftarrow T_1$ absorption (ϵ_T) spectra of pyrene: —, fluorescence spectra; ·····, $S_n \leftarrow S_1$ absorption spectra (a) measured by Post et al.¹⁷ and (b) measured by Nakato et al.;¹⁸ - · - ·, $T_n \leftarrow T_1$ absorption spectra.²⁰

wavelength band in the $S_n \leftarrow S_1$ spectra were taken from the measurement by Post et al.¹⁷ (ϵ (at 470 nm) $\approx 1.6 \times 10^4 \pm 10\%$) and the experimental values of the shorter wavelength band were taken from the measurement by Nakato et al.¹⁸ The extinction coefficient of the shorter wavelength band was adjusted so as to agree with the result of Post et al. at its long-wavelength edge. There is another experimental measurement of the extinction coefficient of the longer wavelength band by Müller et al.¹⁹ According to their result, ϵ (at 450 nm) is $\approx 3.6 \times 10^3 \pm 30\%$. The $T_n \leftarrow T_1$ absorption spectra were taken from the measurement by Heinzelmann et al.²⁰ With these spectra, we can evaluate the critical transfer distance R_0 and the critical concentration C_A^0 , as indicated in Table I. There are no experimental values of the fluorescence quantum yield ϕ_D of pyrene in toluene as well as in DBE at 77°K which are necessary for the evaluations of Table I. However, ϕ_D in ethanol at 77°K is obtained to be 0.91,²¹ and 0.8–0.95 in PMMA.^{22,23} In view of these experimental values, we have assumed the value 0.9 for our systems.

In Table I, not only the R_0 and C_A^0 values for $S_1 \rightarrow S_1$ and $S_1 \rightarrow T_1$ transfers but also those for the $S_1 \rightarrow S_0$ transfer as well as the transfer from pyrene S_1 to perylene S_0 ²² are shown for the purpose of comparison. One can see that the $S_1 \rightarrow S_0$ transfer between pyrenes can occur rather difficultly just as one can surmise it easily from the fact that the $S_1 \leftarrow S_0$ absorption intensity of pyrene is very small. However, the $S_1 \rightarrow S_1$ transfer can occur much more easily than the $S_1 \rightarrow S_0$ transfer. The critical distance of $S_1 \rightarrow S_1$ transfer is rather close to that of pyrene(S_1) \rightarrow perylene(S_0) transfer. We can see also that the values of Ω and R_0 for the $S_1 \rightarrow T_1$ transfer between pyrenes are as large as those of the $S_1 \rightarrow S_1$ transfer, respectively. However, since the fluorescence yield of pyrene at 77°K is ca. 0.9, the concentration of triplet pyrene molecules acting as energy acceptors is quite small. Moreover, when the $S_1 \rightarrow S_1$ transfer is occurring, the yield of the triplet molecules will be further decreased. Thus, the effect of the $S_1 \rightarrow T_1$ transfer on the observed fluorescence decay curves may be negligibly small. Actually, the experimental result plotted in Figure 5 shows clearly that the $S_1 \rightarrow S_1$ transfer is predominating. The result in Figure 4, however, does not satisfy eq 3 at the later stages of the decay. Presumably, the quantum yield of the triplet-state formation, ϕ_{ST} , in toluene might be larger than that in DBE, since the fluorescence lifetime in toluene is shorter than that in DBE. The $S_1 \rightarrow T_1$ energy transfer to the accumulated triplets might be occurring at the later stages of the decay in toluene. Nevertheless, the plot at the

TABLE I: Values of Parameters Relevant to the Excitation Transfers from the S_1 State of Pyrene due to Förster's Mechanism

Acceptor	Ω	$R_0, \text{\AA}$	$10^2 C_A^0, M$
Perylene (S_0) ^{Ia}	3.4×10^{-14}	37	0.87
Pyrene (S_0) ^{II}	$< 2 \times 10^{-17}$	< 10	> 32
Pyrene (S_1) ^{II}	$(0.9, 4.0) \times 10^{-14}$ ^{III}	$30, 40$ ^{III}	$1.5, 0.7$ ^{III}
Pyrene (T_1) ^{II}	3.4×10^{-14}	39	0.77

^a The following values were used for calculation of R_0 : (I) in PMMA at 77°K, $K^2 = 0.475$, $\phi_D = 0.95$, $n = 1.5$; (II) in DEE at 77°K, $K^2 = 0.475$, $\phi_D = 0.90$, $n = 1.4$; (III) two different values are due to the use of the different values¹⁷⁻¹⁹ of extinction coefficient of the longer wavelength band in the $S_n \leftarrow S_1$ spectra.

early stage of the decay clearly shows the curve characteristic of eq 3, which seems to be an evidence that $S_1 \rightarrow S_1$ transfer is predominating.

Since the samples are subjected to high-density excitation, one might argue that there occurs the local heating of the solution due to the radiationless degradation leading to the shortening of the decay time. However, according to our estimation, the extent of the temperature raising by such a mechanism is smaller than 3–4°. Accordingly, it may not affect the fluorescence decay time in the rigid solvent at 77°K.²³ One might argue also that the sample solution may be partly destroyed by some nonlinear photochemical reaction, and excitation transfer from the S_1 state pyrene to the ground-state reaction product may bring about the shortening of the fluorescence decay time. However, if this is the case, the plots in Figures 4 and 5 must be straight lines as indicated in Figure 1 for the $S_1 \rightarrow S_0$ transfer. Thus, in both toluene and DBE solutions at 77°K, the $S_1 \rightarrow S_1$ transfer by the Förster mechanism occurs predominantly between excited pyrenes.

References and Notes

- (1) N. A. Tolstoi and A. P. Abramov, *Sov. Phys.—Solid State (Engl. Transl.)*, **9**, 255 (1967); **9**, 1516 (1968).
- (2) A. Bergman, M. Levine, and J. Jortner, *Phys. Rev. Lett.*, **10**, 593 (1967).
- (3) C. R. Goldschmidt, Y. Tomkiewicz, and I. B. Beriman, *Chem. Phys. Lett.*, **2**, 520 (1968); H. Masuhara and N. Mataga, *ibid.*, **7**, 417 (1970).
- (4) A. Inoue, K. Yoshihara, and S. Nagakura, *Bull. Chem. Soc. Jpn.*, **45**, 1973 (1972).
- (5) S. D. Babenko, V. A. Benderskii, V. I. Gol'danskii, A. G. Lavrushko, and V. P. Tyehinskii, *Chem. Phys. Lett.*, **8**, 598 (1971); *Phys. Status Solidi B*, **45**, 91 (1971).
- (6) T. Kobayashi and S. Nagakura, *Mol. Phys.*, **23**, 1211 (1972); **24**, 695 (1972).
- (7) Th. Förster, *Ann. Phys. (Leipzig)*, **2**, 55 (1948); *Z. Naturforsch.*, **4a**, 321 (1949).
- (8) H. Masuhara and N. Mataga, *Chem. Phys. Lett.*, **6**, 608 (1970); *Bull. Chem. Soc. Jpn.*, **45**, 43 (1972).
- (9) N. Nakashima, N. Mataga, C. Yamanaka, R. Ide, and S. Misumi, *Chem. Phys. Lett.*, **18**, 386 (1973).
- (10) R. G. Bennett, *J. Chem. Phys.*, **41**, 3037 (1964); R. G. Bennett and R. E. Kellogg, *Prog. React. Kinet.*, **4**, 215 (1967).
- (11) V. Ern, J. L. Saint-Clair, M. Schott, and G. Delacote, *Chem. Phys. Lett.*, **10**, 287 (1971); J. Fourny, M. Schott, and G. Delacote, *ibid.*, **20**, 559 (1973).
- (12) M. Tomura, E. Ishiguro, and N. Mataga, *J. Phys. Soc. Jpn.*, **22**, 1117 (1967); **25**, 1439 (1968); M. Yokota and O. Tanimoto, *ibid.*, **22**, 779 (1967); N. Mataga and T. Kubota, "Molecular Interactions and Electronic Spectra", Marcel-Dekker, New York, N.Y., 1970.
- (13) G. Porter and M. R. Topp, *Proc. R. Soc. London, Ser. A*, **315**, 168 (1970).
- (14) H. Lessing, E. Lippert, and W. Rapp, *Chem. Phys. Lett.*, **7**, 247 (1970).
- (15) R. E. Kellogg, *J. Chem. Phys.*, **41**, 3046 (1964).
- (16) D. Lavaleffer, C. J. Werkhoven, D. Bebelaar, J. Langelaar, and J. D. W. Van Voorst, *Chem. Phys. Lett.*, **9**, 230 (1971).
- (17) M. F. M. Post, J. Langelaar, and J. D. W. Van Voorst, *Chem. Phys. Lett.*, **10**, 468 (1971).
- (18) Y. Nakato, N. Yamamoto, and H. Tsubomura, *Chem. Phys. Lett.*, **2**, 57 (1968).
- (19) A. Müller and U. Sommer, *Ber. Bunsenges. Phys. Chem.*, **73**, 819 (1969).
- (20) W. Heinzelmann and H. Labhart, *Chem. Phys. Lett.*, **4**, 20 (1969).
- (21) J. Langelaar, R. P. H. Rettschnick, and G. J. Hoijtink, *J. Chem. Phys.*, **54**, 1 (1971).
- (22) N. Mataga, H. Obashi, and T. Okada, *Chem. Phys. Lett.*, **1**, 133 (1967); *J. Phys. Chem.*, **73**, 370 (1969).
- (23) J. L. Kropp, W. R. Dawson, and M. W. Windsor, *J. Phys. Chem.*, **73**, 1747 (1969).

Structure, Energetics, and Dynamics of Small Water Clusters^{1,2}

John C. Owicki,^{3a} Lester L. Shipman,^{3b} and Harold A. Scheraga*

Department of Chemistry, Cornell University, Ithaca, New York 14853 (Received March 24, 1975)

The empirical potential using electrons and nuclei (EPEN) has been applied to a study of water clusters containing from two to five molecules. Cluster structures corresponding to potential energy minima have been characterized structurally and energetically. Among dimers and trimers, the *only* minimum-energy structures (on the six- and twelve-dimensional potential energy surfaces, respectively) that have been found are the trans near-linear dimer (TNLD) and the cyclic trimer. The cyclic dimer and open trimer are *not* potential-energy minima. In contrast, many local minimum-energy tetramers and pentamers exist. The most stable of these are cage-like structures which owe their low potential energy to the formation of a large number of *highly strained* hydrogen bonds. No open tetramer or pentamer structures have been found which are minima on their 18- and 24-dimensional respective potential energy surfaces. For the dimer and trimer, transition states for the interconversion between superimposable or enantiomeric minimum-energy structures are discussed along with their effects on the dynamics of these systems. An approximate statistical mechanical calculation of the thermodynamics of water cluster association equilibria in the gas phase is presented and analyzed. Selected water clusters obtained with other published empirical potentials are analyzed; also, the implications of the EPEN results for the structures of bulk liquid water, water surfaces, and droplet nuclei are discussed.

I. Introduction

Liquid water continues to be the subject of intense research effort because of its importance in biological, chemical, and physical systems as well as its great theoretical importance as an example of a liquid with strong noncentral intermolecular forces.

In a previous paper,⁴ we studied the structure, energetics, and dynamics of the water dimer by using the Shipman-Scheraga (SS) empirical effective pair potential for water.⁵ Our ultimate interests in this laboratory are not, however, in water per se, but in the hydration of biologically important macromolecules. Thus, it is appropriate to our goals to use an empirical potential for water interactions which is compatible with similar potentials for other molecules. In this way, knowledge of the pure liquid at the molecular level can be applied readily to the study of aqueous solutions. During attempts to derive a family of compatible pair potentials in this laboratory, it was found that the overlap repulsion model chosen for the SS potential did not generalize easily to intramolecular (conformational) potentials for other molecules in which it was necessary to reproduce energy barriers for internal rotations about single bonds. However, an extension of the approach used to derive the SS potential, viz., the empirical potential using electrons and nuclei (EPEN), has been developed recently and does meet the compatibility criterion.⁶ In this paper we have applied EPEN to the study of water clusters containing from two to five molecules. In addition to the ultimate applicability of these results to the problem of hydration in aqueous solutions, they are also relevant to studies of nucleation in aerosols and to other atmospheric problems.

Several pair potentials for water have been published recently.^{5,7-12} We have generated and compared the minimum-energy dimers and trimers predicted by these potentials to determine how much of a consensus has been reached regarding the structures of small water clusters and to give a preliminary evaluation of the relative usefulness of the various potentials.

II. Brief Description of EPEN

EPEN⁶ may be thought of in terms of the localized molecular orbital theory view of the water molecule. Its electrostatic component consists of point charges representing the nuclei, lone pair electrons, and bonding electron pairs of the molecule as depicted in Figure 1. An attractive R^{-6} term acts between oxygen nuclei, and exponential repulsions act between electron pairs. The complete potential of interaction for N water molecules is, thus

$$U = \sum_{i < j}^N \left\{ \sum_{k=1}^7 \sum_{l=1}^7 332.0719 \frac{z_k z_l}{r_{kl}} + \sum_{m=1}^4 \sum_{n=1}^4 A \exp(-Br_{mn}) - CR_{ij}^{-6} \right\} \quad (1)$$

where U is the potential energy in kilocalories/mole; R_{ij} is the $O_i \cdots O_j$ distance in Å units; r_{kl} is the distance in Å units between point charges k on molecule i and l on molecule j ; r_{mn} is the distance in Å units between electron pairs m on molecule i and n on molecule j ; z_k and z_l are the point charges in atomic units; A , B , and C are parameters for the $\exp 6$ part of the potential. The experimental infrared and microwave monomer geometry¹³ is used. Values for point-charge coordinates and parameters⁶ are presented in Table I. It should be noted that the zero of potential energy corresponds to infinite separation of all molecules. Since each molecule is treated as a rigid body, no intramolecular degrees of freedom are considered.

III. Procedures

Minima on the EPEN energy hypersurface of aggregates of water molecules were located with the aid of computerized function minimization algorithms, and the resulting minimum-energy structures were characterized.

Starting points for the minimizations were selected by constructing hydrogen-bonded molecular models and by considering the results of other theoretical studies.^{4,14-16} The choice of starting points also was influenced by the

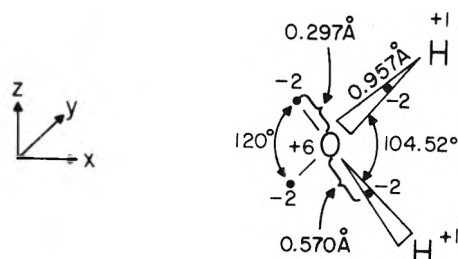


Figure 1. Positions of point charges for water EPEN. Charges are given in atomic units (see ref 6).

TABLE I: Parameters⁶ and Coordinates of EPEN

Electrostatic component	Coordinates, Å			Charge
	x	y	z	
O nucleus	0.000000	0.000000	0.000000	+6e
H nucleus	0.585850	0.756900	0.000000	+1e
H nucleus	0.585850	-0.756900	0.000000	+1e
Bonding pair	0.348938	0.450850	0.000000	-2e
Bonding pair	0.348938	-0.450850	0.000000	-2e
Lone pair	-0.148239	0.000000	0.256750	-2e
Lone pair	-0.148239	0.000000	-0.256750	-2e
Exponential and R^{-6} components:	$A = 2.798 \times 10^3$ kcal/mol $B = 3.35$ (Å) ⁻¹ $C = 3.299 \times 10^3$ (kcal/mol) (Å) ⁶			

findings of the present study as we progressed from the analysis of smaller to larger clusters.

Specifically, seven types of starting points were chosen for the dimer, corresponding to the trans near-linear dimer (TNLD) and dimer transition states reported in ref 4. The trimer starting points were about ten composites of EPEN TNLD minima (see section IV) and of TNLD minima and dimer transition states (see section VIII). Several cyclic trimer starting points also were investigated. The 20 tetramer starting conformations included open- and branched-chain composites of EPEN TNLD minima as well as structures similar to the four-, five-, and six-hydrogen-bonded tetramers discussed in section VI. Finally, the 20 pentamer starting points were generated using EPEN TNLD minima, cyclic structures, and by the addition of one H₂O molecule to the EPEN pyramid tetramer minimum (see section VI).

In the case of the dimer, about 100 additional starting points in six-dimensional space were generated randomly from the set of all relative intermolecular configurations with O...O distances ($R_{O...O}$) between 2.0 and 4.0 Å using the RANDU subprogram from the IBM Scientific Subroutine Package. A grid search or a random generation of starting points for the larger clusters would require an excessive amount of computer time. For example, for a water pentamer (24 degrees of freedom), using all combinations of only two values of each coordinate requires over 10⁷ starting points. Although we have no mathematical guarantee, we feel that our searches have been thorough enough so that we have found *all* the EPEN minima corresponding to

dimers and trimers. We probably have found a majority of the tetramer minima but only a minority of the pentamer minima.

Two minimization algorithms have been used. The first, developed by Powell¹⁷ and modified by Zangwill,¹⁸ was used to get close to a local energy minimum. Since its convergence near the minimum was fairly slow for the tetramers and pentamers, a second algorithm, a multidimensional numerical Newton-Raphson¹⁹ iterative method, was used to refine the results. All cartesian atomic coordinates of minimum-energy structures so obtained are precise to within 10⁻⁴ Å.

Each minimum-energy structure was characterized with respect to atomic coordinates (listed in Appendix A), O...O distances ($R_{O...O}$), hydrogen-bond nonlinearity (δ) as defined in Figure 2, and potential energy (U). For the trimer, the inclinations of the O-H bonds of the non-hydrogen-bonded hydrogens from the plane of the oxygen ring also were calculated. An intermolecular vibrational normal mode analysis (in the harmonic approximation) was performed to obtain normal-mode vibrational frequencies (ω_i), intermolecular vibrational zero point energies (ZPE), and internal energies at absolute zero temperature [$E_{int}(T = 0^\circ\text{K}) = U + \text{ZPE}$]. Because of the low concentrations of water clusters observed in water vapor, the experimental difficulty of studying these structures is great. The dimer and trimer are probably the most experimentally accessible species (see section VIII). Therefore, for comparison with existing²⁰ and possible future microwave and infrared spectroscopic studies, we have presented the following additional information for the dimer and trimer EPEN minimum-energy structures: the principal moments of inertia (I_a, I_b, I_c), the dipole moment resolved in the principal axis coordinate system (μ_a, μ_b, μ_c), and the squared moduli of the dipole moment derivatives with respect to the normal mode motions ($|\partial\mu/\partial Q_i|^2$, which are proportional to the integrated infrared absorptivities). The dipole moment was calculated using the recently determined experimental permanent monomer dipole moment of 1.847 D²¹ and an atom-atom induced dipole moment model.²² Most calculations were carried out for both H₂O and D₂O. The two isotopic species were assumed to interact according to the same isotope-independent potential (which is valid under the Born-Oppenheimer approximation); hence the only differences which arise are in properties which are sensitive to the mass differences in the inertia tensor and vibrational analysis.

We considered a hydrogen bond to be formed in a given molecular configuration if $R_{O...O} < 3.2$ Å and $\delta < 90^\circ$ simultaneously. All definitions of hydrogen bonding are arbitrary to some extent; ours allowed an intuitively satisfactory classification of the minimum-energy configurations that we obtained.

A statistical mechanical analysis of the thermodynamics of the equilibrium $n\text{H}_2\text{O} \rightleftharpoons (\text{H}_2\text{O})_n$ was performed for $n = 2$ to 5. The standard Gibbs free energy change (ΔG_n°), enthalpy change (ΔH_n°), and entropy change (ΔS_n°) were calculated for temperatures from 100 to 700°K. The clusters were assumed to be ideal gases with classical translational partition functions. Classical overall rotational partition functions with a quantum correction²³ were used. Intermolecular vibrations within the clusters were assumed to be harmonic in accordance with our normal mode analysis. Intramolecular vibrations were not considered, since the water molecule is a rigid body in the EPEN approxima-

tion.²⁴ The partition functions and thermodynamic expressions are derived in Appendix B.

By using the Newton-Raphson technique to search for points of zero potential energy gradient rather than minima, we easily located saddle points on the six-dimensional dimer and twelve-dimensional trimer potential energy surfaces. These structures, which represent transition states for the interconversions between minimum-energy structures (see section VIII), were characterized in much the same way as were the minimum-energy structures.

Calculations performed with the empirical potentials described below were similar to those carried out with the EPEN, though they generally were limited to dimers and trimers.

(1) *Shipman-Scheraga (SS) Potential*.⁵ The coulombic component of the SS potential has seven point charges placed similarly to those in the EPEN. An exponential repulsion and an R^{-6} attraction act between H_2O molecular centers of mass. The parameters of the potential were set during the derivation of the potential to achieve the best fit to a variety of gas-phase and crystal data.

(2) *Analytical Fit to Hartree-Fock (AFHF) Potential*.^{7,8} This potential has three electrostatic point charges: two (positive) are placed on hydrogen nuclei, with the third (negative) on the molecular C_2 axis. Exponential repulsions act between pairs of atoms. Since the potential was derived to fit the Hartree-Fock water dimer potential energy surface (without correlation effects), there is no R^{-6} dispersion term. The second parameterization⁸ of the AFHF potential was used in our calculations.

(3) *Ben-Naim-Stillinger (BNS) Potential*.^{9,10} Two positive (hydrogen nuclei) and two negative (lone pairs) point charges are placed at the vertices of a regular tetrahedron. A polynomial "switching function" reduces the coulombic potential for small O...O distances. A Lennard-Jones 12-6 potential acts between oxygen nuclei centered in the point charge tetrahedron. The BNS potential was derived to fit water vapor second virial coefficient data classically. The revised version¹⁰ used here is equal to the original⁹ BNS potential multiplied by 1.06, a change introduced¹⁰ to strengthen the potential slightly. The positions of energy minima are the same for the two versions, but energies obtained with the revised potential are equal to 1.06 times the energies for the same configurations calculated with the original potential. Intermolecular vibrational energy levels and frequencies are likewise multiplied by $(1.06)^{1/2}$.

(4) *ST2 Potential*.¹¹ This potential is very similar to the BNS potential, the most important difference being that the lone-pair point charges are moved closer^{25a} to the oxygen nucleus, reducing the excessively high librational frequencies calculated with the BNS potential.^{25,26}

(5) *Weissmann-Blum (WB) Potential*.¹² The coulombic component of this potential is similar to those of the SS and EPEN potentials except that the lone-pair and bonding-electron point charge positions were adjusted to fit the CNDO/2 electron distribution for H_2O . An exponential repulsive term acting between oxygen nuclei was adjusted so that the trans linear dimer equilibrium $R_{O...O}$ was 2.76 Å as in ice I_h .

IV. EPEN Dimer

Only one minimum-energy dimer was found on the six-dimensional EPEN potential energy surface. This structure, which is pictured in Figure 2, has a symmetry plane (and belongs to the point group C_s) and a single hydrogen

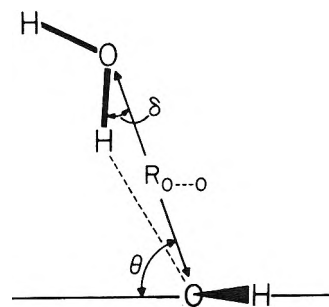


Figure 2. Structure of TNLD.

bond. The hydrogen bond is nearly linear, and the remaining hydrogens are trans to each other across it. We have termed this structure the trans near-linear dimer (TNLD), the same name given to the very similar dimer found in our previous study⁴ with the SS potential. The TNLD is characterized further in Tables II and III. Figure 3 depicts the intermolecular vibrational normal mode motions approximately, and Figure 4 is a graphical presentation of the integrated infrared absorptivity data from Table III. Figure 5 shows the dependence of U on $R_{O...O}$ for configurations like the TNLD.

Dyke and Muentzer,²⁰ using molecular beam microwave spectroscopy, have published an experimental structure for the dimer (see Table II) with which the EPEN TNLD is in substantial agreement. The deviations of the calculated angular variables θ and δ (as defined in Figure 2) from experiment are less than experimental error. The theoretical value of $R_{O...O}$ is about 3% smaller than the experimental value. Part of this discrepancy may arise from the fact that the theoretical value refers to the structure at the potential-energy minimum while the experimental one is a quantum-mechanical average on the structure in its vibrational ground state. Our calculations agree with the experimental²⁰ finding that the water dimer is very close to being an accidental symmetric top (for the theoretical H_2O TNLD, $I_c/I_b = 1.0009$). Alternatively, the asymmetry parameter²⁷ $\kappa = -0.99994$, indicating that the EPEN TNLD is an almost perfect prolate top ($\kappa = -1$).

The 10% disagreement between the calculated and experimental²⁰ values of μ_a arises more from approximations in the dipole-moment model²² that we have used than from structural disagreements between the calculated and experimental TNLD's. This can be seen clearly if we use the experimental TNLD structure from Table II to calculate μ_a , obtaining 2.37 D. This is very close to the value calculated for the EPEN TNLD (2.35 D), but it is about 9% below the experimentally determined value (2.601 D). The major approximation in the dipole-moment model²² is the assumption that the induced dipole moment is produced by charges and scalar, first-order, bulk polarizabilities centered on the atomic nuclei.

It should be noted that we have used a value of the static polarizability, α , which includes only the electronic polarizability of water ($\alpha = 1.444 \times 10^{-24} \text{ cm}^3$).²⁵ Nir et al.²⁹ have found that, for water, there are important contributions to α from intra- and intermolecular motions. These effects, which previously have been neglected, respectively contribute an additional 0.16×10^{-24} and $2.34 \times 10^{-24} \text{ cm}^3$ to α , for a total of $3.95 \times 10^{-24} \text{ cm}^3$. In our calculations of the dipole moments of minimum-energy water clusters in the absence of external fields, it might be valid to include the

TABLE III: TNLID Intermolecular Vibrational Normal Mode Frequencies and Integrated Infrared Absorptivities

Sym- metry	Approximate characterization ^a	EPEN ^b		SS ^b		AFHF ^b		ST2 ^b		BNS ^b		WB ^b													
		ω_i^c	$ \partial\mu/\partial Q_i ^{2d}$	ω_i^c	$ \partial\mu/\partial Q_i ^{2d}$	ω_i^c	$ \partial\mu/\partial Q_i ^{2d}$	ω_i^c	$ \partial\mu/\partial Q_i ^{2d}$	ω_i^c	$ \partial\mu/\partial Q_i ^{2d}$	ω_i^c	$ \partial\mu/\partial Q_i ^{2d}$												
1 A ₁ '	Out of plane H-bond shear	593	425	2.41	1.35	681	487	2.03	1.17	537	366	3.13	1.73	653	471	2.79	2.30	775	559	2.12	1.15	688	514	2.61	1.47
2 A ₁ '	In plane H- bond shear	496	374	2.02	1.30	451	332	0.63	0.22	319	237	1.96	1.10	640	489	3.88	1.54	881	669	4.19	2.46	576	415	2.40	1.24
3 A ₁ '	In plane H- bond bend	189	134	5.54	2.69	106	77	6.50	2.47	116	87	4.32	2.49	275	192	3.59	0.71	316	227	3.41	1.74	287	213	5.37	3.11
4 A ₁ '	H-bond stretch	168	162	0.35	0.39	183	175	1.44	1.09	161	150	0.76	0.32	213	206	0.02	1.13	185	176	0.03	0.02	366	350	0.36	0.07
5 A ₁ '	Out of plane H-bond bend	161	116	0.03	0.05	63	45	0.53	0.28	127	92	0.68	0.21	269	195	0.02	0.03	337	244	0.15	0.13	215	152	0.17	0.09
6 A ₁ '	H-bond torsion	98	71	3.59	1.91	173	82	3.46	1.86	105	76	2.24	1.33	126	91	3.06	1.63	116	83	3.42	1.83	93	67	3.42	1.75

^aThe intermolecular normal-mode vibrations are pictured approximately in Figure 3.
^bSee Section III for an explanation of the nomenclature for the potentials. For each quantity calculated, the first column refers to (H₂O)₂, the second to (D₂O)₂.
^cIntermolecular.

TABLE II: Characterization of Theoretical and Experimental Dimers^a

Potential ^b	$U^{c,d}$	ZPE ^{e,g}	$E_{\text{int}} (T = 0^\circ\text{K})^{c,f}$		$R_{\text{O}\cdots\text{O}}^g$	θ^h	δ^h	I_a^i	I_b^i	I_c^i	$ \mu ^j$	μ_a^k	μ_b^k	μ_c^k												
			E_{int}	E_{int}																						
EPEN	-5.44	2.44	1.83	-3.00	-3.61	2.88	61.9	2.8	2.38	4.51	76.76	87.25	76.83	87.36	2.35	2.35	2.34	-0.01	0.00	0.00	-0.07					
SS	-5.76	2.28	1.71	-3.48	-4.05	2.85	79.9	8.7	2.48	4.70	74.41	83.98	74.59	84.06	1.73	1.72	1.73	0.18	0.11	0.00	0.00					
AFHF	-4.58	1.95	1.47	-2.63	-3.11	3.00	38.0	2.4	2.15	4.11	84.26	96.39	84.43	96.92	2.89	2.86	2.85	0.00	0.00	0.45	0.53					
ST2	-6.84	3.11	2.35	-3.73	-4.49	2.85	51.8	-1.1	2.52	4.80	75.97	86.78	76.14	87.34	2.72	2.71	2.71	0.00	0.00	-0.16	-0.26					
BNS	-6.89	3.73	2.80	-3.16	-4.09	2.76	54.7	0.0	2.53	4.82	71.27	81.49	71.42	82.04	2.63	2.63	2.62	0.00	0.00	-0.12	-0.32					
WB	-5.06	3.18	2.45	-1.88	-2.61	2.75	48.0	0.9	2.26	4.32	70.93	81.20	71.14	81.84	2.66	2.65	2.64	0.00	0.00	-0.25	-0.34					
Ab initio ⁷	-4.60					3.00	30	0																		
Experiment ²⁰						2.98 ± 0.04	60 ± 10	0 ± 10			H ₂ O: 82.11 ¹ D ₂ O: 93.18 ¹				2.601 ± 0.005	2.603 ± 0.008										

^aAll dimers listed possess the C_s symmetry of the EPEN TNLID of Figure 2 and differ from that dimer only in detail. Where two columns occur for a particular quantity, the first refers to (H₂O)₂ and the second to (D₂O)₂.
^bSee Section III for an explanation of the nomenclature for the potentials.
^cUnits are kcal/mol of dimer.
^dPotential energy at minimum on six-dimensional dimer potential-energy surface.
^eIntermolecular vibrational zero-point energy.
^fInternal energy at absolute zero temperature.
^g $E_{\text{int}} = U + \text{ZPE}$.
^hOxygen-oxygen distance in Å.
ⁱSee Figure 1 for a definition of these angles. Units are degrees.
^jPrincipal moments of inertia, in amu Å². The a principal axis of the inertia tensor coincides approximately with the O...O internuclear line. The b axis is perpendicular to the TNLID mirror plane, and the c axis is in the mirror plane perpendicular to the a and b axes. In the EPEN D₂O TNLID and in the SS H₂O and D₂O TNLIDs, the b and c axes are interchanged relative to the above description. This happens because we follow the spectroscopic convention of labeling the principal axes so that $I_a < I_b < I_c$. The TNLIDs are almost accidental symmetric tops ($I_b \sim I_c$), so that small variations in structure or isotopic substitution can interchange the formal roles of the b and c axes.
^kDipole moment in Debyes.
^lDipole moment along principal inertial axis, in Debyes.
^mAn average value $2b_l/(I_b + I_c)$ from ref 20 for the $K = 2, j = 2 \rightarrow j = 3$ transition.

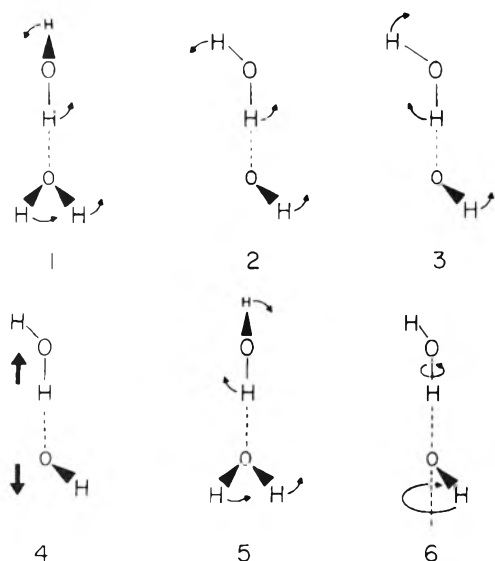


Figure 3. Intermolecular normal-mode vibrations of the TNLD. Modes numbered as in Table III.

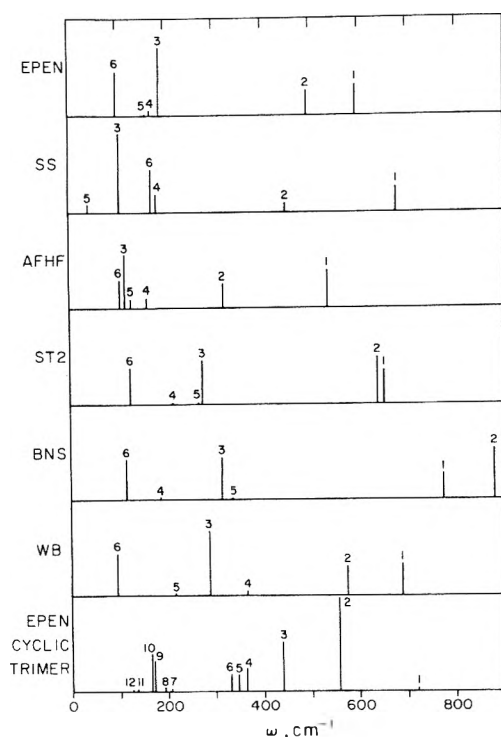


Figure 4. Approximate integrated infrared spectra for the H₂O TNLD's produced with various potentials and for the EPEN H₂O cyclic trimer. The positions of absorption lines are determined by an intermolecular vibrational normal-mode analysis. The line heights are proportional to the calculated integrated absorptivities of the modes. This is a plot of data in Table III, and the normal modes are numbered as in Table III.

small intramolecular increment to α , but the large intermolecular contribution should *not* be included. This exclusion follows from the fact that EPEN already explicitly takes into account the effects of σ^2 interactions of the molecular charge distributions on relative molecular orientations. Indeed, a calculation of μ_a for the experimental geometry

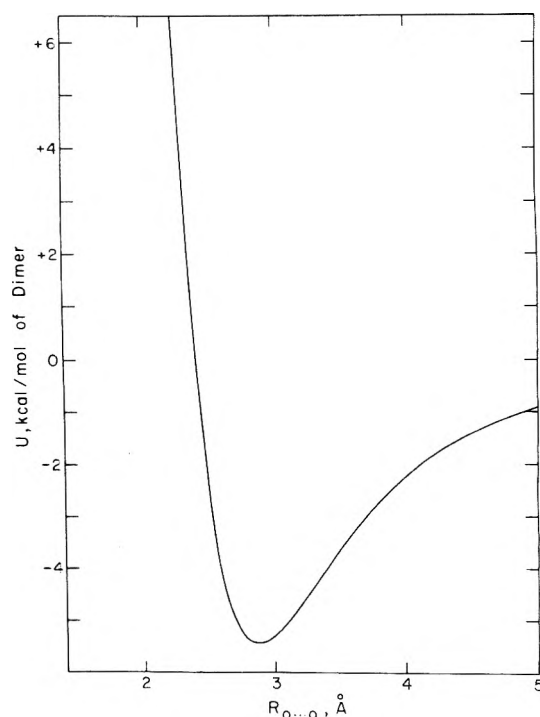


Figure 5. Variation of U with $R_{O...O}$ for the EPEN TNLD. For each value of $R_{O...O}$, θ and δ are varied to minimize U , with C_s symmetry maintained.

TNLD using the full Nir et al. α gives a result 16% above that of experiment.

The above analysis leads to three conclusions. First, the dipole moments that we have calculated using the atom-atom induced-dipole-moment model²² should not be expected to agree precisely with experimentally determined values (i.e., to closer than about 10%). Second, a similar statement is true about the integrated infrared absorptivities, which we have calculated using the same dipole-moment model. Third, *within the model*, the dipole moments of the experimental and EPEN TNLD structures agree very closely.

The EPEN results also can be compared with those of extended basis set ab initio calculations. The most recent ab initio water dimer study (and one of the best yet with respect to the quality of the basis set) is that of Popkie et al.⁷ This is the same calculation used in deriving the AFHF potential.

The accuracy of the ab initio results, which are given in Table II, must be viewed in the light of two factors. First, because of the time-consuming nature of the computer calculations, a complete minimization (in six dimensions) was not performed. For example, the hydrogen bond was constrained to be linear. Second, θ was reported only to the nearest 10°. Popkie et al.⁷ noted that, because of the flatness of the potential energy vs. θ curve, greater precision was beyond the limits of accuracy of their basis set. This flatness can be seen in Figure 4 of ref 7 or, for EPEN, in Figure 6 of this paper. In spite of these limitations, the ab initio dimer structure in Table II should be fairly close to the minimum on the six-dimensional Hartree-Fock potential energy surface.

The ab initio dimer potential energy (U) is algebraically greater than that for the EPEN TNLD. This is understandable, because the ab initio result does not include sta-

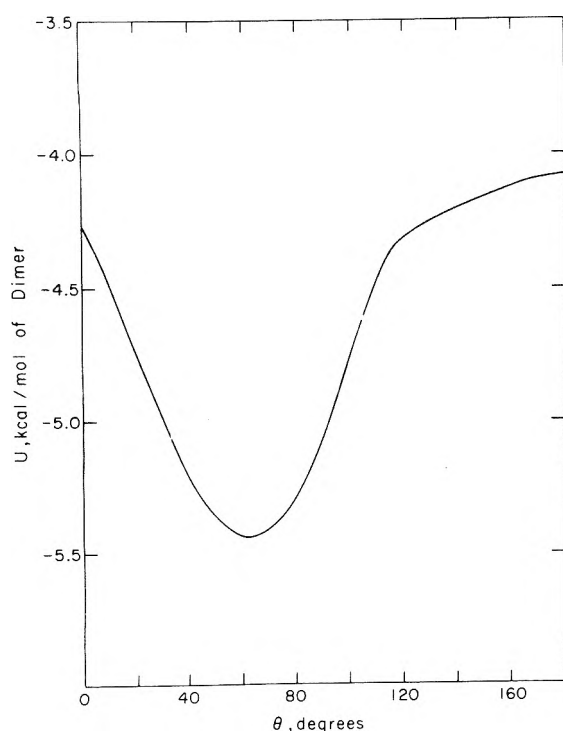


Figure 6. Variation of U with θ for the EPEN TNLD. For each value of θ , $R_{O\cdots O}$ and δ are varied to minimize U , with C_s symmetry maintained.

bilizing correlation effects (estimated conservatively by Popkie et al.⁷ at 0.3–0.5 kcal/mol of dimer). The 4% disagreement in $R_{O\cdots O}$ between EPEN and ab initio also would be reduced by the inclusion of correlation effects, which would tend to contract the hydrogen bond. The biggest discrepancy between the results of the two techniques is in the calculated values of θ . The small dependence of the potential energy on θ near the minimum makes the equilibrium value of θ difficult to predict, and, in any event, such disagreements are of comparatively small energetic consequence.

There exist few direct experimental measurements or ab initio calculations of the water dimer intermolecular vibration normal mode frequencies or absorptivities with which to compare the EPEN results from Table III and Figure 4. Dyke and Muentner³⁰ have obtained a preliminary value of about 145 cm^{-1} for both the H_2O and D_2O hydrogen-bond stretching vibrational frequencies. The EPEN results for normal mode 4 (168 cm^{-1} for H_2O , 162 cm^{-1} for D_2O) are in good agreement with experiment considering the approximations made to deduce the frequencies from experimental data and the fact that mode 4 is not a completely pure hydrogen-bond stretch.

We note three additional vibrational results here.

(1) The vibrations are strongly quantum mechanical.³¹ The lowest normal mode frequency for the EPEN H_2O TNLD corresponds to a thermal excitation temperature of 141°K, the highest to 853°K. The equivalent values for D_2O are 102 and 611°K. Thus, the two highest modes of both H_2O and D_2O are virtually unexcited at room temperature. Because of the quantum-mechanical nature of the vibrations, the use of classical statistical mechanics to compute the virial coefficient, or of classical mechanics in molecular-dynamics studies of water, may possibly introduce errors or artifacts.

(2) Analysis of the normal mode eigenvectors reveals that there is little coupling between motions of the centers of mass of the individual water molecules and rotations (librations) about their centers of mass. This results in a relatively pure hydrogen-bond stretch mode (mode 4 in Table III) and five modes which are essentially hydrogen-bond bending motions of various types. The hydrogen-bond stretch mode, being primarily translational, is predicted to be only weakly infrared active (see Table III). Charge transfer between molecules, which is predicted by ab initio studies,⁷ would increase the integrated absorptivity^{32,33} over our calculated value.

(3) Although Figure 4 does not take into account such effects as line width broadening, anharmonicity, and vibrational overtones, it should be a rough representation of the integrated infrared spectrum of the dimer in the intermolecular vibrational region. The EPEN results suggest that the greatest intermolecular dimer infrared absorption should occur in the region of 100–200 cm^{-1} for H_2O and 50–150 cm^{-1} for D_2O .

V. EPEN Trimer

Ab initio calculations^{14,15} have been performed to determine the relative stability of open and cyclic water trimers (as in Figure 7). These studies have been inconclusive because of the prohibitive computational expense of performing a complete minimization on the twelve-dimensional trimer potential energy surface. Empirical potentials, much less expensive to evaluate, greatly reduce this problem. Indeed, Kistenmacher et al.⁸ recently have published a fully minimized cyclic trimer structure obtained with the AFHF potential. They concluded that configurations similar to the open trimer were of higher potential energy than the cyclic trimer, though they did not perform a minimization in all twelve degrees of freedom for the open structure to prove this conclusively.

Calculations with EPEN have shown that there is *only one* stable trimer on the twelve-dimensional potential-energy surface. That structure is the cyclic trimer pictured in Figure 7b and characterized in Table IV. We have found no minimum corresponding to an open structure such as in Figure 7a, nor are there minima for the analogous open structures in which the middle molecule accepts or donates two hydrogens in the hydrogen bonds formed with the end molecules. It is not surprising that the open trimer in Figure 7a is not at a potential-energy minimum, since cyclization involves the completion of a hydrogen bond that already is weakly formed between the end molecules.

These results, together with those of Kistenmacher et al.,⁸ provide the strongest evidence to date that the cyclic structure is the only important water trimer. They also suggest that, at least in small systems, compact (cyclic) configurations with a large number of bent hydrogen bonds are more stable than open configurations with fewer but less-strained hydrogen bonds. This is borne out by our results for water tetramers and pentamers in sections VI and VII.

There are no published experimentally determined water trimer or larger cluster structures. However, Dyke and Muentner³⁴ have obtained evidence that trimers and higher water clusters are only very slightly polar or are nonpolar, which is more consistent with cyclic than with open structures.

The EPEN cyclic trimer intermolecular vibrational normal-mode frequencies (Table V and Figure 4) span ap-

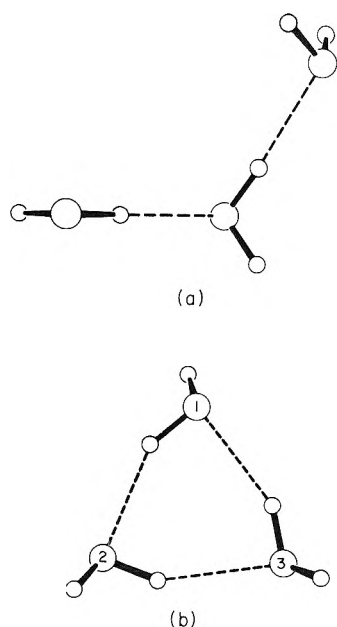


Figure 7. (a) Hypothetical open trimer, (b) EPEN cyclic trimer.

TABLE IV: Characteristics of EPEN Cyclic Trimer^a

Quantity	H ₂ O	D ₂ O
U	-14.81	-14.81
ZPE	5.36	4.06
$E_{int}(T = 0^\circ K)$	-9.45	-10.75
I_a	77.94	89.31
I_b	79.44	90.81
I_c	153.90	173.68
$ \mu $	1.10	1.10
μ_a	0.06	0.06
μ_b	0.12	0.16
μ_c	-1.08	-1.08
$R_{O_1 \dots O_2} = 2.89$	$\delta(O_1-H \dots O_2) = 28^b$	$\alpha(1) = 60^c$
$R_{O_2 \dots O_3} = 2.91$	$\delta(O_2-H \dots O_3) = 30$	$\alpha(2) = 57$
$R_{O_3 \dots O_1} = 2.89$	$\delta(O_3-H \dots O_1) = 27$	$\alpha(3) = 57$

^a Quantities defined as in Table II and molecules numbered as in Figure 7b. ^b Deviation of hydrogen bond from linearity, in degrees. ^c Inclination of non-hydrogen-bonded hydrogen from plane of ring, measured in degrees as the dihedral angle between the H₂O or D₂O molecular plane and the plane of the O-O-O ring.

proximately the same range as those for the EPEN TNLD. The trimer frequencies are, on the average, somewhat higher than are those of the dimer, even though the trimer hydrogen bonds individually are weaker. This probably reflects the greater orientational constraint to librations imposed by a cyclic structure with two hydrogen bonds per molecule rather than one, as in the dimer. That is, if only one O-H is hydrogen bonded, the molecule can rotate about that O-H axis without breaking the hydrogen bond. However, if the molecule participates in two or more hydrogen bonds, rotation about any axis must break at least one hydrogen bond.

The cyclic trimer has no symmetry, and the translational and librational modes of the constituent molecules are highly coupled in the normal modes. The normal modes

TABLE V: EPEN Cyclic Trimer Intermolecular Normal-Mode Vibrational Frequencies and Integrated Infrared Absorptivities^a

Mode ^b	(H ₂ O) ₃		(D ₂ O) ₃	
	ω_i	$ \partial\mu/\partial Q_i ^2$	ω_i	$ \partial\mu/\partial Q_i ^2$
1	720	0.26	519	0.16
2	556	7.80	409	4.44
3	438	4.12	321	2.34
4	362	1.91	268	1.08
5	345	1.36	256	0.40
6	331	1.38	248	0.70
7	207	0.22	191	0.03
8	192	0.28	149	0.39
9	170	2.45	135	1.50
10	164	3.08	127	0.93
11	135	0.02	111	0.08
12	131	0.07	110	0.65

^a Quantities defined as in Table III. ^b Modes numbered in order of decreasing frequency. Unlike in Table III, no correspondence between like-numbered H₂O and D₂O normal-mode eigenvectors is implied here.

therefore cannot be described as concisely as those of the TNLD. We note, however, that the modes which are predominantly librations tend to be higher in frequency than those which are predominantly hindered translations.

VI. EPEN Tetramers

Ab initio potential energy minimization studies of water tetramers^{14,15} have, of necessity, consisted of incomplete energy minimizations carried out on structures of high symmetry, in which all intermolecular degrees of freedom were not allowed to vary independently. The potential energies of open tetramers (analogous to the open trimer in Figure 7a) have been calculated but without energy minimization.^{14,15} The primary conclusion drawn from those studies is that cyclic structures probably are more stable than open structures. Kistenmacher et al.⁸ using the AFHF potential and more complete energy minimizations have reached the same conclusion.

Our energy minimizations on the 18-dimensional EPEN water tetramer potential energy surface confirm this conclusion. Furthermore, they extend it as follows. (1) There probably are no minimum-energy open tetramers on the complete potential energy surface. (2) There are at least nine unique tetramer minima (not counting enantiomers). (3) These minima consist of cyclic tetramers (with four hydrogen bonds connecting the four molecules into a ring) as well as more complex structures having five or six hydrogen bonds. Three representative tetramers (the pyramid, S₄ symmetry cyclic, and asymmetric cyclic tetramers) are pictured in Figure 8 and characterized in Table VI. The potential energy of the pyramid is lowest, that of the S₄ cyclic is next, and the asymmetric cyclic lies in the middle of the range of energies of the nine tetramer minima.

There are several ways to form cyclic tetramers. For example, there can be zero, one, or two water molecules which donate two hydrogens to the hydrogen-bond ring system. The S₄ cyclic tetramer and asymmetric cyclic tetramers belong to the first and second of these classes, respectively.

The pyramid tetramer, the global minimum-energy structure, has the most highly strained (nonlinear) hydro-

TABLE VI: Characteristics of EPEN Tetramers^a

Structure	U	ZPE	$E_{\text{int}}(T = 0^\circ\text{K})$	$R_{\text{O}_i \cdots \text{O}_j}$				$\delta(\text{O}_i - \text{H} \cdots \text{O}_j)$						
				j	$i = 1$	2	3		i	j				
Pyramid tetramer	-25.11	H ₂ O: 7.93 D ₂ O: 6.05	-17.18 -19.06	2	2.85			1	2	26				
				3	2.87	2.97		2	3	63				
				4	3.00	2.89	2.90	2	4	38				
								3	1	38				
								4	1	58				
S ₄ cyclic tetramer	-24.65	H ₂ O: 8.84 D ₂ O: 6.72	-15.80 -17.93	2	2.83			1	4	11				
				3	4.00	2.83		2	1	11				
				4	2.83	4.00	2.83	3	2	11				
								4	3	11				
												4	2	16
Asymmetric cyclic tetramer	-21.12	H ₂ O: 7.98 D ₂ O: 6.04	-13.14 -15.08	2	2.90			1	2	12				
				3	2.88	4.04		1	3	13				
				4	4.09	2.87	2.85	3	4	10				
												4	2	16

^a Quantities defined as in Tables II and IV. Molecules numbered as in Figure 8.

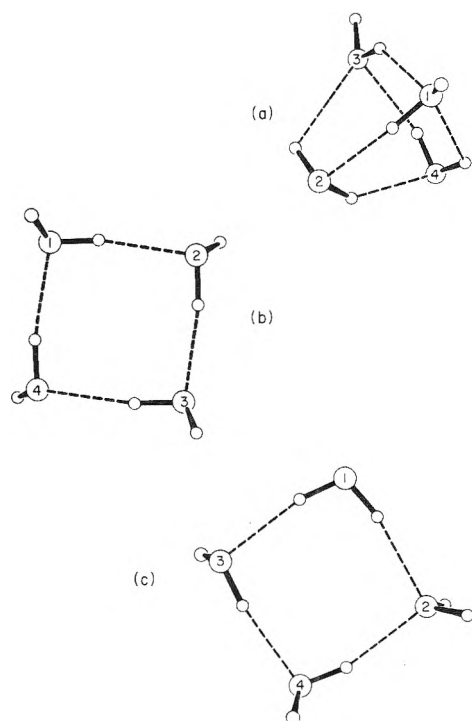


Figure 8. EPEN minimum-energy water tetramers: (a) pyramid, (b) S₄ cyclic, (c) asymmetric cyclic.

gen bonds of any cluster that we have studied. It is the most extreme example in which the stability of individual hydrogen bonds is sacrificed to maximize the number of hydrogen bonds (six in this case). The pyramid tetramer also may be viewed as a cyclic tetramer whose ring is highly puckered to accommodate two ring-bridging hydrogen bonds. Indeed, the O \cdots O distances in Table VI show that the hydrogen bonds (O₂-H \cdots O₃) and (O₄-H \cdots O₁) are distinctly longer (weaker) than the remaining four, in accordance with the puckered ring interpretation. EPEN tetramers with five hydrogen bonds can be thought of as puckered-ring systems with single bridging hydrogen bonds.

One tetramer displays the only exception to conventional

(O-H \cdots O) hydrogen bonding that we yet have obtained with the EPEN. This structure ($U = -21.43$ kcal/mol of tetramer) is essentially a cyclic trimer which has one hydrogen simultaneously involved in hydrogen bonds in the ring and to a fourth water molecule outside of the ring.

The nine EPEN tetramers span a fairly narrow range of potential energies (from -19.92 to -25.11 kcal/mol of tetramer). There is a tendency for a direct relationship to exist between the sizes of the vibrational frequencies of these clusters and the depths of their potential-energy wells; i.e., the energetically less favorable tetramers generally have a higher entropy. This suggests that several forms may be present in comparable quantities in water vapor, as opposed to the single forms of the dimer and trimer. This hypothesis is investigated further in section IX.

VII. EPEN Pentamers

Eight local minimum-energy structures have been found on the 24-dimensional EPEN pentamer potential-energy surface, again not considering enantiomers. Since our search of this extensive surface was far from thorough, it is possible that we have not located the global energy minimum, and it is certain that we have not found all of the local minima. Representative EPEN pentamers are presented in Figure 9 and Table VII.

The minimum-energy pentamers found here are of three types: (1) irregular cage structures with seven hydrogen bonds connected similarly to those of the pentamer in Figure 9a (the lowest potential-energy pentamer that we discovered); (2) six hydrogen-bonded cage structures similar to Figure 9a but without the hydrogen bond between molecules 4 and 5 (analogous to tricyclo[1.1.1]pentane); and (3) the C₂ symmetry structure in Figure 9b, which is the analog of spiro-pentane.

We have looked for but have *not* found potential-energy minima corresponding to the following: (1) open pentamers (extensions of the open trimer); (2) simple cyclic pentamers (analog of the cyclic tetramers); and (3) branched pentamers with four hydrogen bonds formed between a central molecule and four peripheral molecules in configurations reminiscent of the ice lattices ("star" pentamer). One branched pentamer starting point for an energy minimization led to the C₂ pentamer by formation of two hydrogen

TABLE VII: Characteristics of EPEN Pentamers^a

Structure	U	ZPE	$E_{\text{int}} (T = 0^\circ\text{K})$	$R_{O_i \cdots O_j}$				i	j	$\delta(O_i - H \cdots O_j)$	
				j	$i = 1$	2	3				4
Cage pentamer	-35.51	H ₂ O: 11.26 D ₂ O: 8.61	-24.25 -26.91	2	2.81				1	2	13
				3	3.62	2.81			2	3	16
				4	2.88	4.09	2.87		3	4	28
				5	2.85	4.09	2.89	2.97	3	5	41
									4	1	37
C_2 pentamer	-29.41	H ₂ O: 10.06 D ₂ O: 7.66	-19.35 -21.74	2	2.90				1	3	27
				3	2.87	2.91			1	5	27
				4	2.90	5.66	5.32		2	1	27
				5	2.87	5.32	5.03	2.91	3	2	32
									4	1	27
					5	4	32				

^a Quantities defined as in Tables II and IV. Molecules numbered as in Figure 9.

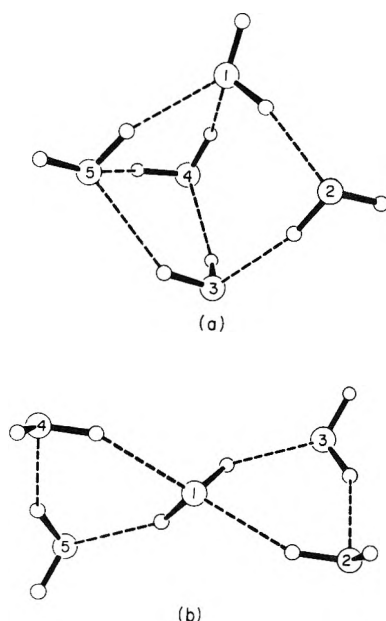


Figure 9. EPEN minimum-energy water pentamers: (a) cage, (b) C_2 .

bonds between peripheral molecules. In other words, these particular structures are *not* minima on the 24-dimensional EPEN potential-energy surface.

The pentamers that we studied are even closer together in potential energy than are the tetramers. The C_2 structure is the least stable ($U = -29.41$ kcal/mol of pentamer), and the other seven minima all fall between -34.90 and -35.51 kcal/mol. The pentamer hydrogen bonds are generally less strained than are those of the pyramid tetramer.

VIII. Transition States

As discussed in ref 4 and Appendix B, there are eight minima on the six-dimensional water dimer EPEN surface, corresponding to superimposable TNLD's. This multiplicity is related to the C_{2v} symmetry of the water molecule and physically corresponds to the eight ways of producing a hydrogen bond between two molecules with artificially labeled hydrogen nuclei and lone-pair electrons. Similarly,

there exist 96 isoenergetic cyclic trimer minima (of the type shown in Figure 7b) on the twelve-dimensional water trimer EPEN surface. Since the cyclic trimer is chiral, it occurs in 48 enantiomeric pairs. We now proceed to a discussion of the transition states and barriers to the interconversions among these structures.

Dimers. The five types of EPEN trimer transition states found here are pictured in Figure 10. They are the cyclic dimer (CD), planar linear dimer (PLD), perpendicular plane bifurcated dimer (PePBD), parallel plane bifurcated dimer (PaPBD), and perpendicular plane opposed dimer (PePOD).

The positive PePOD potential energy ($U = +0.06$ kcal/mol) represents a high barrier to dimer interconversion and implies that the water dimer classically would dissociate ($U = 0.00$ kcal/mol) rather than pass through this transition state. We therefore have dropped the PePOD from further consideration. We likewise have eliminated the PaPBD because it is an energetically high-lying ($U = -3.13$ kcal/mol) transition state connecting other transition states and should not be important for dimer interconversions.

The CD, PLD, and PePBD are characterized in Table VIII with respect to $R_{O \cdots O}$, their energetics, and their normal mode vibrational frequencies for both H₂O and D₂O. We have reported fewer than six frequencies because one normal mode (two in the PLD and PePBD) is a transition coordinate rather than a bound vibrational mode. In other words, it is a coordinate for which the transition state is a point of unstable equilibrium on the six-dimensional potential energy surface. The most important result presented in Table VIII is that the barriers to the interconversions of dimers are small. At 0°K, as indicated by E_{int} , the barriers are at most a few tenths of a kilocalorie/mole; the PLD barrier for H₂O (but not D₂O) is essentially zero. Moreover, since the transition-state normal-mode vibrational frequencies tend to be lower than those for the TNLD, the interconversion barriers should decrease with increasing temperature. In fact, a statistical-mechanical analysis (as in section IX, but treating the transition motions as monomer rotations instead of translations) of the "equilibrium" TNLD \rightleftharpoons PLD suggests that the PLD should predominate over the TNLD at temperatures above 0°K. Though such a treatment is at best of dubious validity, it illustrates clearly the importance of considering the

TABLE VIII: Characterization of EPEN Dimer Transition States^a

Properties	Cyclic dimer		Planar linear dimer		Perpendicular plane bifurcated dimer	
$R_{O...O}$	2.91		3.00		2.90	
U	-4.48		-4.13		-4.08	
ZPE	1.65	1.25	1.13	0.87	1.37	1.05
$E_{int}(T = 0^\circ\text{K})$	-2.83	-3.23	-3.00	-3.26	-2.71	-3.03
$E_{int}(T = 0^\circ\text{K}) - E_{int}(T = 0^\circ\text{K})$ of TNLD	0.17	0.38	0.00	0.35	0.29	0.58
ω_1	438	312	288	208	306	234
ω_2	300	221	275	200	302	220
ω_3	185	160	146	139	208	147
ω_4	148	121	81	59	140	133
ω_5	83	60				

^a Quantities defined as in Tables II and III.

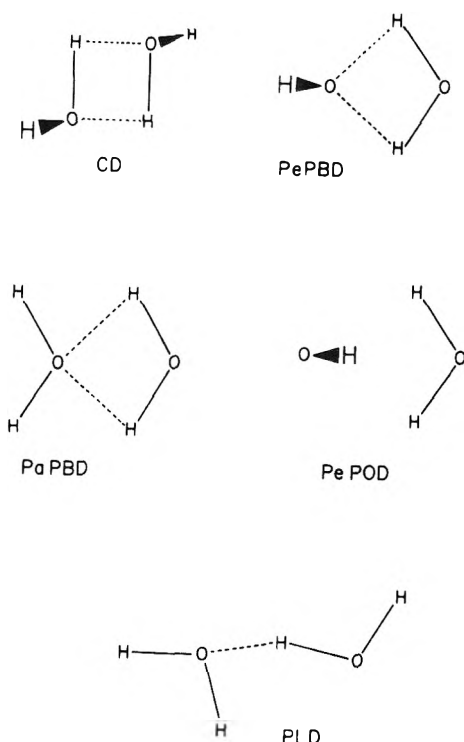


Figure 10. EPEN water dimer transition states. For an explanation of the nomenclature, see section VIII. For those molecules for which only a single hydrogen is shown, a second hydrogen lies directly behind the one shown, and its position is determined by reflecting the pictured hydrogen through the plane of the paper.

curvature of the potential energy surface as well as the depths of its minima.

Though it is contrary to intuition to have a transition state more stable than a minimum-energy structure of lower potential energy, this actually is quite acceptable physically if the dimer is viewed as a quantum system having a higher probability density in a region of very low curvature of the potential than it has in a region of slightly lower potential energy but of higher curvature. In fact, however, the PLD structure is incompatible with the experimental observation²⁰ that the *b* and *c* principal moments of inertia of the water dimer cannot differ from each other by more than a few tenths of a percent (for the PLD, the difference as computed from the coordinates in Appen-

dix A is 2.2%). We must conclude that either the EPEN or our harmonic analysis produces transition states whose potential energies or calculated potential energy surface curvatures are slightly too low relative to those of the TNLD.

Since interconversion involves primarily hydrogen motions, the combination of the low mass and low transition-state barriers makes it likely that there is substantial quantum mechanical tunneling between potential-energy wells. At high temperatures (certainly in the supercritical region) there should be significant population of excited vibrational states lying above the barriers. Viewed classically, the dimer then interconverts freely among the eight potential energy minima. From a quantum-mechanical point of view, these effects increase the symmetry of the dimer so that the dimer can be classified under the permutation-inversion group³⁵ isomorphic to the D_{4h} point group³⁶ rather than under the C_s point group to which the rigid nontunneling model of the TNLD belongs.

As discussed in Appendix B, the presence of the many isoenergetic minima does not in itself affect the entropy of the cluster. However, the additional fact, that the barriers to interconversion are low, should lead to an entropic increase and an enthalpic stabilization because of a decrease in the spacing of excited vibrational levels.

The conclusions that we have reached about the water dimer transition states are in general agreement with those from our earlier SS potential water dimer study,⁴ and we direct the reader there for a fuller discussion of the interconversion process. Dyke and Muentzer²⁰ have found evidence of tunneling and large-amplitude proton motions in the water dimer, and our conclusion that interconversion is rapid is in accord with their observations.

Trimers. The energetically most stable transition state for the interconversions of cyclic trimers that we have found is that pictured in Figure 11 and characterized in Table IX. While the cyclic trimer has its three non-hydrogen-bonded hydrogens arranged one on one side of the oxygen ring and two on the other, the transition state has one on each side with the third approximately in the plane of the ring. It thus represents a transition state for the interconversion of enantiomers by the flipping of a non-hydrogen-bonded hydrogen from one side of the oxygen ring to the other.

Reference to Table IX shows that the potential energy of the transition state is 0.62 kcal/mol higher than that of the cyclic trimer minimum. However, if one includes the effects of vibrational zero-point energy, the energy difference

TABLE IX: Characterization of the Cyclic Trimer Transition State^a

	U	ZPE	$E_{\text{int}} (T = 0^\circ\text{K})$	Normal-mode frequencies					
H ₂ O	-14.19	4.70	-9.49	668	558	450	328	292	214
				193	184	144	137	115	
D ₂ O	-14.19	3.56	-10.63	484	408	331	240	216	187
				158	139	125	113	91	
	$R_{\text{O}_1 \cdots \text{O}_2} = 2.87$		$\delta(\text{O}_1\text{-H}\cdots\text{O}_2) = 23$			$\alpha(1) = 62$			
	$R_{\text{O}_2 \cdots \text{O}_3} = 2.97$		$\delta(\text{O}_2\text{-H}\cdots\text{O}_3) = 25$			$\alpha(2) = 65$			
	$R_{\text{O}_3 \cdots \text{O}_1} = 2.89$		$\delta(\text{O}_3\text{-H}\cdots\text{O}_1) = 44$			$\alpha(3) = 6$			

^a Quantities defined as in Tables II, III, and IV. Molecules numbered as in Figure 11.

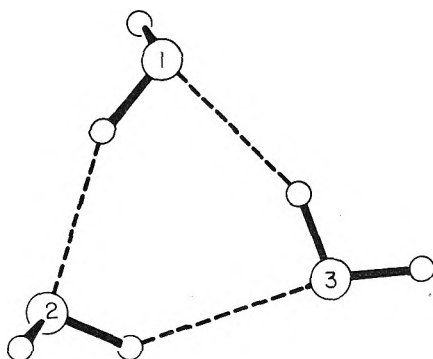


Figure 11. EPEN cyclic trimer transition state.

($E_{\text{int}}, T = 0^\circ\text{K}$) drops to 0.12 kcal/mol for D₂O. For H₂O, the internal energy at 0°K corresponding to the transition state actually is computed to be 0.04 kcal/mol lower than that of the cyclic trimer minimum. Since discriminations of energy as small as this are beyond the accuracy of our model, it would be rash to assert that what we have termed the cyclic trimer transition state really is the most stable form of the trimer at 0°K. One can conclude that the trimer exists in a cyclic form but that the time-averaged positions of the nuclei, particularly those hydrogens not involved in hydrogen bonds, are somewhat in doubt. That is, there are large-amplitude motions even at 0°K. As in the case of the dimer, tunneling between the cyclic trimer minima probably is important on a rotational time scale.

As noted above, the entropy of the trimer is increased by the presence of low-energy barriers for the interconversions between minima. Therefore, it is of interest to note (by examination of molecular models) that not all 96 minima on the twelve-dimensional EPEN trimer potential-energy surface are interconnected by the transition states described above. The minima can be divided into 16 groups of six each in which only members of a group can be interconverted by a succession of such low-energy paths. Passage between groups requires the interchange of hydrogens on one of the water molecules (i.e., a net 180° rotation about the molecular C₂ axis) or the interchange of water molecules and, therefore, the rupture and re-formation of a hydrogen bond. The barrier to this process should be at least several kilocalories/mole of trimer; thus it should occur much more slowly than the interconversion of enantiomers.

Although we have not analyzed transition states for larger clusters, it seems likely that interconversion barriers will be higher for the more rigid, highly coordinated structures than for the dimer and trimer.

IX. Vapor-Phase Association Equilibria

With the EPEN theoretical results so far presented, we are in a position to carry out an approximate statistical-mechanical calculation of the thermodynamics of the gas-phase water cluster association equilibria



where (H₂O)_n is any of the seven water clusters that we have described. Other statistical-mechanical treatments of the dimer equilibrium have been reported by Bolander et al.³⁷ and by Braun and Leidecker.³² Our statistical-mechanical model is of rigid-rotor clusters which execute small-amplitude harmonic vibrations about the EPEN minima. The straightforward derivation of the standard free energy, enthalpy, and entropy changes (ΔG_n° , ΔH_n° , and ΔS_n°) for reaction 2 with this model is given in Appendix B.

It should be noted that reaction 2 pertains to a single type of *n*-mer structure (e.g., the pyramid tetramer) rather than to all varieties of *n*-mer (e.g., pyramid tetramer, S₄ cyclic tetramer, etc.). If all varieties were included, the computed entropy change probably (but not necessarily) would be larger, and the computed enthalpy change would be a Boltzmann-weighted mean of the enthalpy changes of the various *n*-mer structures.

The calculated values for these thermodynamic functions in the temperature range 100–700°K for all H₂O and D₂O clusters treated in this study are presented in Table X. The H₂O data are plotted in Figures 12–14. The general features of these results are similar to those of most association equilibria. ΔH_n° is negative, reflecting the potential-energetic stability of the cluster, and ΔS_n° is also negative, primarily reflecting the conversion of free translational and rotational degrees of freedom in the monomers to relatively restricted vibrational modes in the cluster. The temperature dependence of ΔH_n° and ΔS_n° can be explained generally in terms of the population of the excited vibrational states with increasing temperature.

From Figure 12 it is apparent that, in the temperature range studied, and at normal pressures, water vapor is composed primarily of monomers. From calculations of equilibrium concentrations using ΔG_n° and K_n , dimers are present in much smaller amounts, and higher clusters represent only a minute fraction of the total. It might seem that the equilibrium concentration of small clusters relative to monomers should be high at low temperatures ($\Delta G_n^\circ < 0$), but this is illusory because of the low equilibrium water vapor pressure there ($P \ll 1$ atm), which favors dissociation; i.e., the vapor pressure is much lower than the standard-state value of 1 atm, to which ΔG_n° applies.

Any analysis of tetramer contributions to water vapor

TABLE X: Water Cluster Association Equilibrium Thermodynamic Functions

Cluster	Species	ΔG_i° ^a			$-\Delta H_i^\circ$ ^a			$-\Delta S_i^\circ$ ^b		
		T = 100°K	400°K	700°K	100°K	400°K	700°K	100°K	400°K	700°K
EPEN TNLD	H ₂ O	-1.53	4.65	10.31	3.57	3.28	2.32	20.4	19.8	18.1
	D ₂ O	-1.89	4.52	10.23	4.09	3.53	2.47	22.0	20.1	18.2
EPEN cyclic trimer	H ₂ O	-5.82	9.29	23.48	10.71	10.37	8.50	48.9	49.2	45.7
	D ₂ O	-6.61	9.00	23.31	11.87	10.92	8.83	52.6	49.8	45.9
EPEN pyramid tetramer	H ₂ O	-11.05	13.54	36.74	19.05	18.49	15.67	79.9	80.1	74.9
	D ₂ O	-12.21	13.11	36.48	20.75	19.29	16.15	85.4	81.0	75.2
EPEN S ₄ cyclic tetramer	H ₂ O	-9.90	14.13	37.05	17.61	17.45	14.84	77.1	78.9	74.1
	D ₂ O	-11.31	13.56	36.71	19.58	18.49	15.49	82.7	80.1	74.6
EPEN asymmetric cyclic tetramer	H ₂ O	-7.43	15.19	36.49	14.79	14.29	11.54	73.6	73.7	68.6
	D ₂ O	-8.67	14.71	36.20	16.55	15.18	12.09	78.8	74.7	69.0
EPEN cage pentamer	H ₂ O	-15.73	18.09	50.29	26.66	26.24	22.64	109.3	110.8	104.2
	D ₂ O	-17.46	17.42	49.88	29.12	27.49	23.41	116.6	112.3	104.7
EPEN C ₂ penta-mer	H ₂ O	-11.07	20.75	50.63	21.51	20.57	16.80	104.4	103.3	96.3
	D ₂ O	-12.58	20.17	50.28	23.69	21.64	17.46	111.1	104.5	96.8
Exptl dimer ^c	H ₂ O		3.41	8.78		3.75	3.75		17.9	17.9
Exptl trimer ^c	H ₂ O		6.93	17.34		6.95	6.95		34.7	34.7
Exptl tetramer ^c	H ₂ O		9.49	24.79		10.91	10.91		51.0	51.0

^a Units: kcal/mol of cluster. ^b Units: cal/deg/mol of cluster. ^c ΔH_i° and ΔS_i° assumed constant throughout experimental temperature range of 150–450°.³⁸

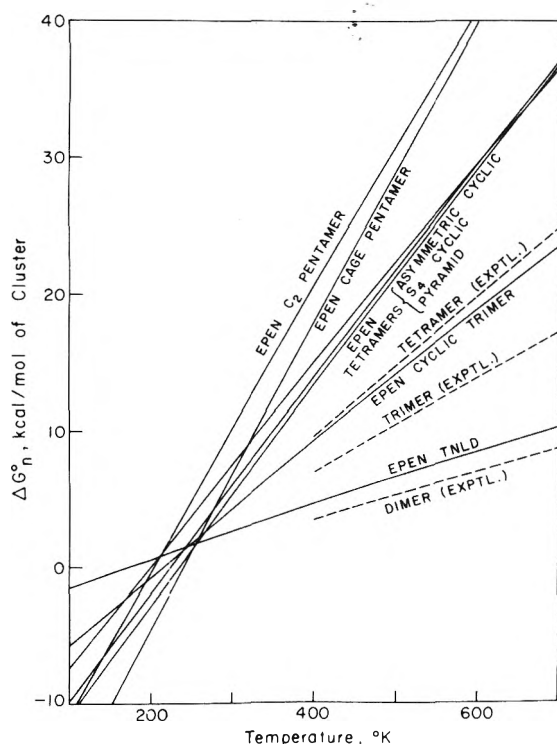


Figure 12. Plot of standard free energy change ΔG_n° (per mole of *n*mer) vs. temperature for gas-phase EPEN water cluster association equilibria. Dashed lines are experimental results from ref 38.

should take into account the fact that many different tetramer structures are present. The same is true for pentamers and, presumably, for higher structures.

For $T = 373^\circ\text{K}$, $P = 1$ atm, we have used our results to calculate the equilibrium mole fractions of H₂O found in the various types of EPEN clusters reported in this paper. We have found the following distribution: monomer, 0.991;

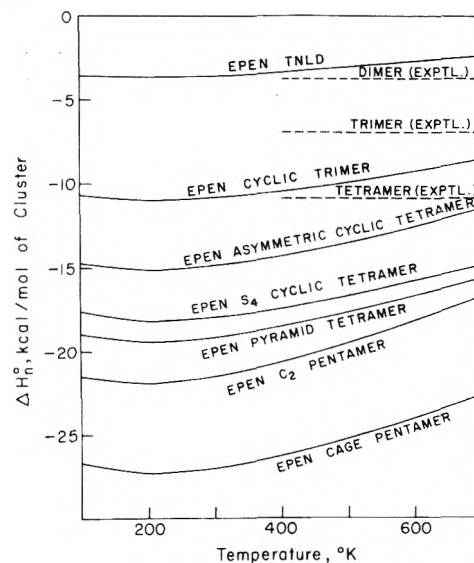


Figure 13. Plot of standard enthalpy change ΔH_n° (per mole of *n*mer) vs. temperature for gas-phase EPEN water cluster association equilibria. Dashed lines are experimental results from ref 38.

TNLD, 9×10^{-3} ; cyclic trimer, 6×10^{-5} ; tetramers (each type), $\sim 10^{-7}$ to 10^{-6} ; pentamers (each type), $\sim 10^{-10}$ to 10^{-8} .

Three experimental techniques have been employed to elucidate the thermodynamics of water clusters (usually the dimer) in water vapor. They are (1) the analysis of *PVT* data for nonideality,^{38,39} (2) the study of the pressure dependence of the speed of sound in water vapor,⁴⁰ (3) the study of the temperature dependence of water vapor absorptions in the far infrared ($7\text{--}30\text{ cm}^{-1}$),⁴¹ which have been attributed to $\Delta K = 1$ dimer rotational transitions.⁴²

Results have varied widely. For example, experimental estimates of ΔH_2° range from -3.75 kcal/mol ³⁹ to -12

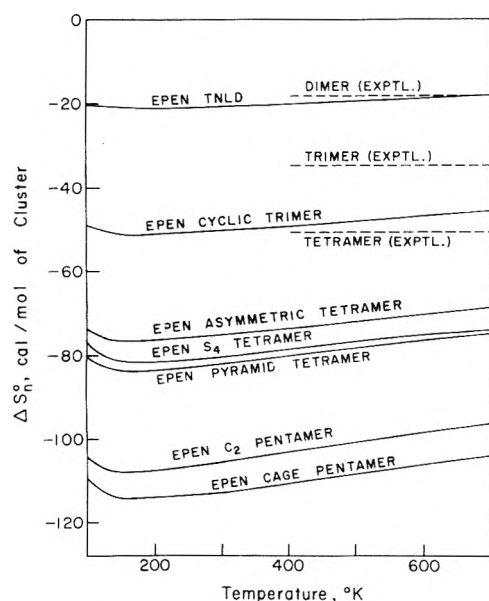


Figure 14. Plot of standard entropy change ΔS_n^0 (per mole of n mer) vs. temperature for gas-phase EPEN water cluster association equilibria. Dashed lines are experimental results from ref 38.

kcal/mol.⁴⁰ The most complete and, probably, the most accurate study is that of Kell and McLaurin,³⁸ in which water vapor virial coefficient data are analyzed by assuming that nonideality results from water cluster association equilibria. These results for the dimer, trimer, and tetramer are presented in Table X and Figures 12–14.⁴³ In analyzing their accuracy, one must consider both experimental error in the virial coefficient determination and approximations in the theoretical model which translates virial coefficient data into association equilibrium constants. The most important of these approximations probably is the use of a somewhat arbitrary temperature-independent hard-sphere excluded volume to describe the effects of intermolecular interactions which are not productive of clusters. Taking these uncertainties into account, we estimate the uncertainty in the experimental ΔG_2^0 at less than 1 kcal/mol. That in ΔG_3^0 may be as great as 2 kcal/mol, and that in ΔG_4^0 should be somewhat higher. Also, it should be noted that the experimental quantities refer to tetramers as a group, and thus technically are not directly comparable to the calculations for any one of our single tetramer equilibria.

We turn now to a comparison of our EPEN theoretical results with the experimental results. The agreement is good considering the accuracy of the experimentally derived data and the fact that our theoretical calculations have made no use of experimental data on water clusters. Our values of ΔG_n^0 are somewhat too positive, while ΔH_n^0 and ΔS_n^0 (except for the TNLD) are significantly too negative. These deviations may be caused by approximations either in EPEN itself and/or in our statistical-mechanical analysis. In making this comparison, it should be recalled that reaction 2 applies to a single n mer species, while the experimental results are for a mixture of n mers for a given n . This is not important for $n = 2$ and 3, since we believe that the TNLD and cyclic trimer are the only dimer and trimer minima. For $n > 3$, however, many different types of n mers should be present. Since we have not found and characterized all of these, our results are difficult to compare with experiment.

One important cause of the deviations of our results from experiment is our use of a rigid-rotor, harmonic-oscillator model in a system where anharmonicity and quantum-mechanical tunneling between potential-energy minima probably are important. The neglect of anharmonicity in this model leads to an overprediction of the separation of vibrational energy levels, which is consistent with the observed discrepancies between calculated and experimental thermodynamic properties. Bolander et al.³⁷ tried to overcome this limitation, partially, for the dimer by assuming free rotation about the hydrogen bond. While, in our case, this procedure might improve the agreement between calculations and experimental data somewhat, it is neither readily applicable to cyclic clusters nor (according to our calculations) physically valid. In section VIII, we discussed the energetically most feasible dimer interconversions or large-amplitude internal motions. Rather than hydrogen-bond torsions, they are complicated combinations of monomer rotations and translations which are difficult to treat except in the classical limit, and our calculations suggest that the system is far from classical.

Kell et al.⁴⁴ have determined the D_2O vapor virial coefficients as functions of temperature. Using an analysis similar to that in ref 38, they calculated that, near 600°K, $\Delta\Delta H_2^0 \equiv \Delta H_2^0_{H_2O} - \Delta H_2^0_{D_2O} = 0.02$ kcal/mol and $\Delta\Delta S_2^0 \equiv \Delta S_2^0_{H_2O} - \Delta S_2^0_{D_2O} = -0.03$ cal/mol deg. Our EPEN-calculated values (at 600°K) are somewhat larger: 0.17 kcal/mol and +0.14 cal/mol deg, respectively.

In this paper, as in ref 32 and 37, the standard approximations of quantum mechanics (e.g., the separation of internal variables and the harmonic-oscillator assumption) have been employed. It should be emphasized that these provide only a very crude representation of the real system, which is extraordinarily complex and difficult to treat accurately.

X. Comparison of Water Pair Potentials

Tables II and III and Figure 4 present the results of our dimer calculations with the water pair potentials listed in section III. The purpose of the following discussion is a comparison of these results with experimental water dimer data and a discussion of the areas of consensus about the water dimer structure and energetics.

Reference to Table II shows that the AFHF value of $R_{O...O}$ is correct within experimental error;^{45,46} those predicted by the EPEN, SS, and ST2 potentials are somewhat too small, and the BNS and WB values are much too small. The latter two are approximately the same $R_{O...O}$ that is found for ice I_h ,⁴⁷ which is not characteristic of the dimer. The agreements between theoretical and experimental values of I_b and I_c parallel those for $R_{O...O}$, since the quantities are related closely. The dimers formed with all of the potentials conform to the experimental finding that the dimer is almost an accidental symmetric top.

The values of θ predicted by the EPEN, ST2, and BNS potentials are correct within experimental error. The WB result is marginal, and the SS and AFHF predictions are definitely wrong. All of the potentials correctly predict that the hydrogen bond is linear to within 10°.

The theoretical results for μ_a in Table II reflect both the dimer structure computed with each potential and our dipole-moment model. As was discussed in section IV, all of our calculated TNLD dipole moments are about 10% too low. Therefore, the seemingly excellent agreement of the BNS and WB μ_a 's with experiment is due largely to a can-

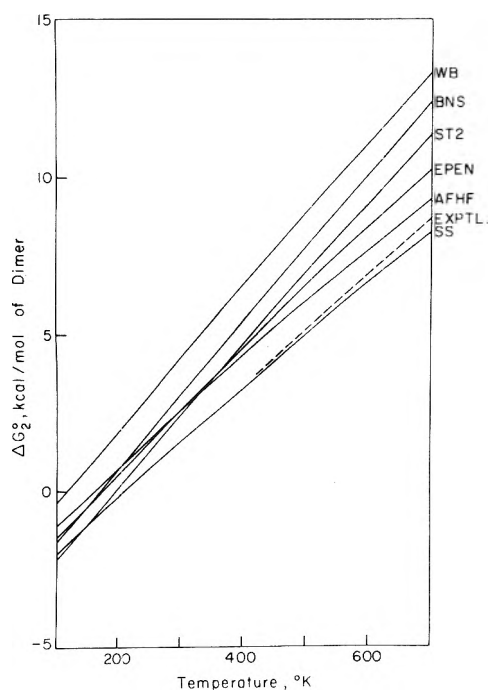


Figure 15. Plot of standard free energy change ΔG_2° (per mole of dimer) vs. temperature for gas-phase water dimerization equilibria calculated with various pair potentials. Dashed line is experimental results from ref 38.

cellation of structural and dipole-moment model errors. Within the dipole-moment model used,²² the EPEN TNLD gives the best agreement with the experimental value.

All of the potentials produce hydrogen-bond stretching frequencies (ω_4 , Table III) which are above the experimental estimate of 145 cm^{-1} . The AFHF potential and EPEN results are closest. The ST2 value is poor, and that predicted by the WB potential is in serious disagreement with experiment.

For each of the potentials, ΔG_2° was calculated (by the method in Appendix B) and compared with experimental values;³⁸ this information is plotted in Figure 15. The SS potential results appear to fit available experimental data best, followed by the AFHF, EPEN, ST2, BNS, and WB potentials in that order. As noted in section IX, an exact treatment of the internal cluster degrees of freedom would decrease the calculated ΔG_2° 's. Since the SS results are the only ones to fall below the experimental results, such a correction would lower the agreement between them while improving the agreements between the predictions of the other potentials and experiment.

In summary, none of the potentials studied here fits all of the available water dimer experimental data. The best overall agreement is found for the EPEN, AFHF, and ST2 potentials. The water EPEN has the considerable advantage of compatibility with EPEN's for other types of molecules,⁶ facilitating the analysis of mixed molecular systems such as solutions.

We now turn to the areas of agreement between the water cluster results obtained using the different potentials. All predict a stable dimer structure which has C_s symmetry and whose non-hydrogen-bonded hydrogens are trans across a nearly (but not precisely) linear hydrogen bond. We have not carried out exhaustive searches of the dimer configuration spaces for potentials other than the SS and EPEN, but in those two cases the TNLD has been

found to be almost certainly the only minimum-energy structure.

Kistenmacher et al.⁸ reported tentatively that a structure resembling the EPEN cyclic dimer transition state (see Figure 10) is a minimum-energy configuration on the six-dimensional AFHF potential-energy surface. In fact, the cyclic dimer was shown⁸ to be at a minimum only on a five-dimensional surface (restricted to $Z = -3.3\text{ au}$; see Figure 1 of ref 8). We have performed a full six-dimensional energy minimization with the AFHF potential, and we have found that the AFHF cyclic dimer is a transition state rather than a true minimum-energy structure. If the Z coordinate is allowed to vary, the cyclic dimer is transformed smoothly into the TNLD without encountering an energy barrier. Thus, the AFHF results agree with our EPEN and SS findings.

The dimer intermolecular vibrational normal-mode eigenvectors produced with the various potentials are quite similar, over and above similarities caused by group-theoretical considerations. For example, in all cases there exist fairly well-defined hydrogen-bond stretch and torsional normal modes. Although there is some disagreement about the frequencies of the normal modes, there is a general agreement that those of modes 1 and 2 are highest and, in H_2O , are separated from the frequencies of the other modes by a distinct gap (see Figure 4).

Computerized energy minimizations using reasonable hydrogen-bonded structures as starting points suggest that the potentials all predict that the energetically most stable trimer is cyclic. Only the BNS⁴⁸ and WB potentials predict a local minimum-energy open trimer (as in Figure 7a); these are of higher potential energy than the corresponding cyclic trimers. The BNS results are not very significant evidence for the existence of an open trimer, since the BNS potential has been superseded by the more accurate ST2 potential, which does not predict a stable open trimer. The WB result is also questionable, since the WB potential generally gives very poor agreement with dimer experimental data.

Our EPEN calculations have indicated that the deepest potential-energy minima for tetramers and pentamers (and, probably, for larger clusters as well) correspond to cage-like structures with highly strained hydrogen bonds. In order to test whether this is a real effect or merely an artifact of EPEN, we have performed a short calculation on the AFHF pentamer system. We have found a minimum-energy AFHF pentamer with hydrogen-bond connectivity identical with that of the EPEN cage pentamer in Figure 9. Moreover, the intermolecular potential energy of this AFHF cluster (-25.82 kcal/mol) is comparable to the energies of the most stable AFHF pentamers found by Kistenmacher et al.⁸ Hence, it appears that the EPEN minima which we have reported here also may be among the lowest-energy minima on the corresponding AFHF potential-energy surfaces. This strengthens the case for the physical validity of our conclusions drawn with the EPEN.

XI. Summary and Conclusions

In this paper, we have applied the empirical potential using electrons and nuclei (EPEN) to a study of the structure, energetics, and dynamics of gas-phase water clusters containing from two to five molecules. We have found that, on the EPEN potential-energy surfaces, there exist a unique minimum-energy dimer (the trans near-linear dimer or TNLD) and trimer (which is cyclic). There are,

however, many local minimum-energy tetramers and pentamers. The presence of multiple minima of comparable energies probably is true for larger clusters as well, and is of great entropic importance to the formation of such structures.⁴⁹

The calculated intermolecular potential energy per mole of water monomers in our clusters ($-U/n$ in Figure 16) is far below the value for an infinite cluster, represented by the experimental lattice energy of ice I_h.⁵⁰ This happens because, in ice (as opposed to smaller clusters), complete hydrogen bonding, energetically stable hydrogen bonding geometries, and favorable non-nearest-neighbor interactions are allowed simultaneously. A major conclusion of this study is that hydrogen bonding in smaller water clusters often is significantly distorted from the tetrahedral linear hydrogen bonds found in ice.

Nor are our results characteristic of bulk liquid water, which may have *local* C_{2v} symmetry.⁵¹ Using a cluster model, Lentz et al.^{25b} have shown that there are strong, orientationally dependent interactions between clusters in liquid water. We would expect these interactions to stabilize more regular, tetrahedrally coordinated structures than those which we have obtained for the gas phase.

Instead, our findings are more applicable at surfaces or at interfaces between an aqueous phase and another without hydrogen-bonding capability. This is related closely to the question of solvent structural changes due to hydrophobic interactions. The EPEN formalism now is being used in our laboratory to investigate this subject.

Our results also have important implications for atmospheric processes such as the water-vapor association equilibrium and water droplet nucleation. Dae et al.⁵² have developed a molecular theory of homogeneous nucleation in water based on a statistical-mechanical analysis of clathrate-like water clusters. We suggest that, in view of the present results, it would be profitable to explore a model in which there are many compact, irregular structures for a given cluster size. These should be more characteristic of the true water prenucleation clusters than the clathrate forms.

We have confirmed and extended our earlier study of water cluster transition states⁴ in which we predicted low barriers for interconversions among potential-energy minima and attendant quantum-mechanical tunneling.

An approximate statistical-mechanical treatment of the gas-phase water association equilibrium has been carried out with results which are in moderate agreement with experimental data.

Finally, we have analyzed the water dimer and trimer structures produced by a variety of water pair potentials. Among these, the EPEN, AFHF,^{7,8} and ST2¹¹ potentials generally give the best results in comparison to experiment. All of the potentials predict essentially the same type of minimum-energy dimer, and they are unanimous in their prediction that the lowest minimum-energy trimer is cyclic.

Acknowledgments. We wish to thank Drs. John S. Muentner and Benjamin A. Widom for helpful discussions of this work.

Appendix A

This Appendix lists the cartesian coordinates (in Å) of the oxygen and hydrogen atoms of the water molecules in the EPEN water clusters described in the text of this

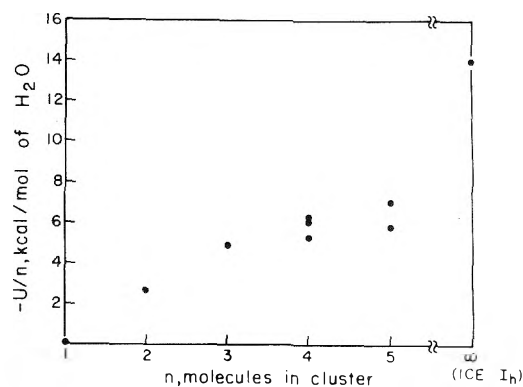


Figure 16. Intermolecular potential energy per water molecule ($-U/n$) for EPEN clusters plotted vs. number of molecules (n) per cluster. At the right is the limit for infinite n (the experimental ice I_h lattice energy⁵⁰).

paper. In each cluster, one molecule has the following coordinates:

Atom	X	Y	Z
O	0.0000	0.0000	0.0000
H	0.5859	0.7569	0.0000
H	0.5859	-0.7569	0.0000

The coordinates of the additional molecules in the various clusters are listed in Table XI.

Appendix B

Water vapor is assumed to be a mixture of water monomers and clusters whose partial pressures are governed by relations such as



$$K_n = P_n/P_1^n \quad (\text{B2})$$

where P_1 and P_n are the partial pressures of the monomer and n mer, respectively, and K_n is the pressure equilibrium constant for the reaction. It should be noted that $(\text{H}_2\text{O})_n$ pertains to a single n mer structure rather than to all varieties of n mers. Thus, for example, we will have separate equilibria for the *pyramid tetramer* and *S₄ cyclic tetramer*.

For a water n mer, each point on the $(6n - 6)$ -dimensional potential-energy surface is a member of a set of $n!(2^n)$ points corresponding to superimposable structures. These may be viewed as the $n!$ permutations of the n water molecules, multiplied by the 2^n permutations of the hydrogen nuclei generated by 180° rotations of the individual molecules about their C₂ symmetry axes. In cases where a molecular symmetry axis is also a symmetry element of the cluster, some of these points in the cluster configurational space are degenerate. For example, there are only four distinct PePBD points on the six-dimensional dimer potential-energy surface instead of eight [= 2!(2²)]. Finally, if a configuration is *chiral*, there exists an additional set of $n!(2^n)$ enantiomeric configurations. In this case, there are a total of $n!(2^{n+1})$ isoenergetic configurations in two enantiomeric classes, each formed of $n!(2^n)$ superimposable structures.

It might seem that the existence of all these minima would lead to a great entropic contribution, but such is not the case. In statistical-mechanical theory, configurations

TABLE XI:

Cluster	Atom	Coordinates			Cluster	Atom	Coordinates		
		X	Y	Z			X	Y	Z
TNLD	O	-1.3582	-0.0000	2.5388	Cage pentamer	O	1.3890	2.4393	-0.1214
	H	-0.9484	-0.0000	1.6739		H	0.5633	2.9175	-0.1971
	H	-2.2984	-0.0000	2.3590		H	1.8148	2.8160	0.6486
Cyclic trimer	O	-0.9133	1.3245	2.4000	O	-1.2489	3.3942	-0.2215	
	H	-0.8172	0.6634	1.7145	H	-1.5951	2.9479	-0.9943	
	H	-1.8087	1.6471	2.2986	H	-1.6142	2.9102	0.5190	
	O	1.2666	2.4683	0.8821	O	-2.2141	1.2225	1.3850	
	H	0.5710	2.3609	1.5308	H	-1.4441	0.6589	1.3097	
	H	2.0720	2.5067	1.3979	H	-2.7960	0.9289	0.6841	
Pyramid tetramer	O	0.9960	2.6613	0.1749	O	-2.1527	1.0110	-1.5749	
	H	0.6119	2.9116	1.0151	H	-1.3507	0.5464	-1.3358	
	H	0.3319	2.8978	-0.4726	H	-2.3798	0.6686	-2.4394	
	O	-1.4456	1.8533	1.6556	C ₂ pentamer	O	-0.6344	1.1938	2.5635
	H	-2.0377	1.6890	2.3895		H	-0.5935	0.5731	1.8360
	H	-1.0673	0.9970	1.4559		H	-1.5511	1.4675	2.5942
	O	-1.5092	2.2932	-1.2091		O	1.3832	2.3768	0.8251
	H	-1.8834	2.2544	-0.3290		H	0.8373	2.2617	1.6030
H	-1.3152	1.3818	-1.4278	H		1.1679	3.2541	0.5085	
O	0.2282	2.9513	2.6969	O		-0.6344	-1.1938	-2.5635	
H	0.6901	2.8652	3.5308	H		-1.5511	-1.4675	-2.5942	
S ₄ cyclic tetramer	H	-0.3780	2.2107	2.6807	H	-0.5935	-0.5731	-1.8360	
	O	-1.3385	0.6079	2.4210	O	1.3832	-2.3768	-0.8251	
	H	-0.9294	0.2909	1.6157	H	1.1679	-3.2541	-0.5085	
	H	-2.2613	0.7206	2.1931	H	0.8373	-2.2617	-1.6030	
	O	1.6536	2.2734	0.3452	CD transition state	O	0.3515	2.2096	1.8615
	H	1.2649	2.5740	1.1666		H	-0.2344	1.4527	1.8615
	H	1.5286	3.0037	-0.2608		H	-0.2344	2.9665	1.8615
	Asymmetric cyclic tetramer	O	2.0523	2.0431	-0.1368	PePBD transition state	O	-2.8958	0.0000
H		2.0079	2.7649	0.4902	H		-2.3099	0.0000	0.7569
H		2.0040	2.4663	-0.9939	H		-2.3099	0.0000	-0.7569
O		2.0716	-1.9940	-0.1446	PLD transition state	O	-2.8799	-0.8439	0.0000
H		2.8151	-1.3925	-0.1851		H	-3.4407	-0.0683	0.0000
H		2.0767	-2.4394	-0.9918		H	-1.9884	-0.4955	0.0000
O		4.0863	0.0181	-0.1623	Cyclic trimer transition state	O	-0.9442	0.7945	2.5946
H		3.5352	0.7982	-0.0998		H	-0.8119	0.3450	1.7599
H	4.5726	0.0012	0.6619	H		-1.8183	1.1782	2.5245	
				O		1.3367	2.1922	1.4989	
				H		0.6383	1.8945	2.0819	
				H	1.8260	2.8310	2.0173		

corresponding to the interchange of identical particles (here, water molecules or hydrogen nuclei) cannot be counted twice in the partition function. For a given type of cluster, then, we may develop the partition function in one of two equivalent ways. Either we may consider all $n!(2^n)$ superimposable structures and then divide the partition function by $n!(2^n)$ to correct for overcounting, or we may treat only one of the configurations and not divide by $n!(2^n)$. In this paper we have used the latter procedure. In the case of a chiral structure, this produces a partition function for only one member of the enantiomeric pair. Since we have chosen to treat both members together in the development below, we have added a multiplicative factor ($q_{i,s}$) to the partition function to account for the effects of chirality.

We now present a derivation of the statistical thermodynamics of reaction B1 based upon our EPEN results and

making use of standard statistical-mechanics theory.⁵³ Although reaction B1 refers to H₂O, our results will apply equally well to D₂O.

Choosing a standard state of 1 atm pressure (P°) for each component, we obtain the standard Gibbs free energy change for reaction B1 as

$$\Delta G_n^\circ \equiv G_n^\circ - nG_1^\circ = -RT \ln K_n \quad (\text{B3})$$

Expression B3 can be related to the cluster molecular partition function q_i ($i = 1, n$) under the assumption of ideal-gas behavior between clusters by

$$G_i^\circ = -RT \ln \left(q_i \frac{kT}{P_i^\circ V} \right) \quad (i = 1, n) \quad (\text{B4})$$

We assume that q_i is expressible as a product of independent partition functions from translational ($q_{i,t}$), rotational

($q_{i,r}$), and vibrational ($q_{i,v}$) degrees of freedom, as well as terms involving the depth of the intermolecular potential-energy minimum ($q_{i,p}$) and the existence of enantiomorphic forms of the structure ($q_{i,s}$):

$$q_i = q_{i,t}q_{i,r}q_{i,v}q_{i,p}q_{i,s} \quad (\text{B5})$$

$q_{i,t}$ is the classical translational partition function

$$q_{i,t} = \frac{V}{\Lambda_i^3}, \quad \Lambda_i = \left(\frac{h^2}{2\pi m_i kT} \right)^{1/2} \quad (\text{B6})$$

where Λ_i is the thermal wavelength of species i and m_i is the corresponding mass.

$q_{i,r}$ is the classical rigid-rotor partition function multiplied by the Stripp-Kirkwood quantum correction:²³

$$q_{i,r} = (q_{i,r})_{\text{class}} \left\{ 1 + \frac{1}{2\pi T} \left[2(\theta_{r,a} + \theta_{r,b} + \theta_{r,c}) - \frac{\theta_{r,a}\theta_{r,b}}{\theta_{r,c}} - \frac{\theta_{r,b}\theta_{r,c}}{\theta_{r,a}} - \frac{\theta_{r,c}\theta_{r,a}}{\theta_{r,b}} \right] \right\} \quad (\text{B7})$$

where

$$(q_{i,r})_{\text{class}} = \frac{\pi^{1/2}}{\sigma_i} \left(\frac{T^3}{\theta_{r,a}\theta_{r,b}\theta_{r,c}} \right)^{1/2}$$

and

$$\theta_{r,j} = \frac{h^2}{8\pi^2 k I_j} = \frac{24.26 \text{ amu } \text{\AA}^2 \text{ deg}}{I_j} \quad j = a, b, c$$

$\theta_{r,j}$ is the rotational excitation temperature for rotation about the j principal inertial axis with inertial moment I_j ($j = a, b, c$). σ_i is the rotational symmetry number.

The classical rotational partition function is valid where $\theta_r/T \ll 1$. We have used the quantum correction²³ to improve the low-temperature accuracy, primarily because of the high rotational excitation temperatures of the monomer ($\theta_{r,a} = 39^\circ\text{K}$). The quantum correction is $\sim 4\%$ of $(q_{i,r})_{\text{class}}$ for the monomer at 100°K , and it is insignificant for $n \geq 2$ at or above this temperature. In the calculations, we have used cluster principal inertial moments obtained for the EPEN structures; the monomer principal moments have been given by Benedict et al.¹³

$q_{i,v}$ is obtained by assuming that the cluster executes small-amplitude harmonic vibrations about the potential-energy minimum. The vibrational partition function is then a product of harmonic-oscillator partition functions for the various intermolecular normal-mode vibrations.

$$q_{i,v} = \prod_j \frac{e^{-\theta_{v,j}/2T}}{1 - e^{-\theta_{v,j}/T}} \quad (\text{B8})$$

where

$$\theta_{v,j} = \frac{hc}{k} \omega_j = 1.439 \omega_j \text{ cm deg} \\ j = 1, 2, \dots, (6i - 6)$$

$\theta_{v,j}$ is the vibrational excitation temperature for the j th normal mode, which has a vibrational frequency of ω_j , in wave numbers. This vibrational model is of questionable validity, as is discussed in sections VIII and IX of this paper.

We have neglected intramolecular vibrations under the assumption that they are not affected significantly in the association reaction. This introduces a small error, but it is a necessary assumption within the EPEN rigid-monomer theoretical framework.

$q_{i,p}$ is introduced to compensate for the fact that, in $q_{i,v}$,

energy levels are measured with reference to the bottom of the intermolecular potential energy well rather than with respect to isolated, noninteracting molecules:

$$q_{i,p} = e^{-U_i/RT} \quad (\text{B9})$$

Here U_i is the EPEN intermolecular potential energy of interaction as reported in the text of this paper for the various water clusters.

$q_{i,s}$ is an entropic factor having the value 1 unless species i exists as a pair of enantiomers (is chiral), in which case $q_{i,s} = 2$. Of the clusters presented in this paper, all except the monomer, TNLD, and C_2 pentamer are chiral.

It should be noted that $q_{1,v} = q_{1,p} = 1$ for the monomer.

Once ΔG_n° is known as a function of temperature, the standard enthalpy change ΔH_n° and entropy change ΔS_n° can be obtained analytically or numerically from relations such as

$$\Delta S_n^\circ = - \left. \frac{\partial \Delta G_n^\circ}{\partial T} \right|_p; \quad \Delta H_n^\circ = \Delta G_n^\circ + T \Delta S_n^\circ \quad (\text{B10})$$

NOTE ADDED IN PROOF: In a recent study of correlation effects in hydrogen-bonding systems, Diercksen et al.⁵⁴ have found that the inclusion of configurational interaction (CI) in ab initio SCF calculations on the water dimer reduces the minimum-energy value of $R_{O\dots O}$ from 3.00 \AA , as obtained without CI, to 2.92 \AA . This is about 0.06 \AA lower than the experimental (quantum-mechanical average) value²⁰ of 2.98 \AA . As noted in section IV, differences between such average and minimum-energy quantities are to be expected and may be due to anharmonicity in the effective hydrogen-bond stretching potential. This decrease in the calculated value of $R_{O\dots O}$ reduces the difference between the calculated values of $R_{O\dots O}$ for the EPEN and ab initio minimum-energy water dimers to 1.4%. Diercksen et al. also found $\theta = 42.4^\circ$ and $U = -6.05$ kcal/mol for the SCF-CI dimer; δ was constrained to be zero.

In another recent paper, Curtiss and Pople⁵⁵ have performed a theoretical (ab initio SCF) intra- and intermolecular vibrational normal-mode analysis on the water dimer using a 4-31G basis set. They obtained the following H_2O intermolecular normal-mode vibrational frequencies (with the approximately corresponding mode numbers from Table III of this paper): 536 cm^{-1} (1), 452 cm^{-1} (2), 204 cm^{-1} (4), 185 cm^{-1} (3), 118 cm^{-1} (5, 6), 81 cm^{-1} (5, 6). These results agree with those of the better empirical potentials in Table III in several respects. In particular, there are two high-frequency librations and a fairly well-defined hydrogen-bond stretch, and the remaining modes have frequencies below 300 cm^{-1} . The authors reported that, with an improved basis set (6-31G*, which gave a much more accurate structural and energetic description of the dimer), the hydrogen-bond stretching normal mode dropped to about 170 cm^{-1} . Similar variations might be expected for the other frequencies.

References and Notes

- (1) This work was supported by research grants from the National Institute of General Medical Sciences of the National Institutes of Health, U.S. Public Health Service (GM-14312), and from the National Science Foundation (BMS71-00872 A04).
- (2) Part of this work was presented before the Division of Physical Chemistry at the 169th National Meeting of the American Chemical Society, Philadelphia, Pa., April, 1975, Abstracts, Phys. 137.
- (3) (a) NSF Predoctoral Fellow, 1968-1969 and 1972-1974; NIH Trainee, 1974-1975. (b) NIH Postdoctoral Fellow, 1972-1974.
- (4) L. L. Shipman, J. C. Owicki, and H. A. Scheraga, *J. Phys. Chem.*, **78**, 2055 (1974).
- (5) L. L. Shipman and H. A. Scheraga, *J. Phys. Chem.*, **78**, 909 (1974).

- (6) (a) L. L. Shipman, A. W. Burgess, and H. A. Scheraga, *Proc. Nat. Acad. Sci. U.S.A.*, **72**, 543 (1975); (b) A. W. Burgess, L. L. Shipman, and H. A. Scheraga, *ibid.*, **72**, 854 (1975).
- (7) H. Popkie, H. Kistenmacher, and E. Clementi, *J. Chem. Phys.*, **59**, 1325 (1973).
- (8) H. Kistenmacher, G. C. Lie, H. Popkie, and E. Clementi, *J. Chem. Phys.*, **61**, 546 (1974).
- (9) A. Ben-Naim and F. H. Stillinger, Jr., in "Structure and Transport Processes in Water and Aqueous Solutions", R. A. Horne, Ed., Wiley, New York, N.Y., 1972, p 295.
- (10) A. Rahman and F. H. Stillinger, Jr., *J. Chem. Phys.*, **55**, 3336 (1971).
- (11) F. H. Stillinger, Jr., and A. Rahman, *J. Chem. Phys.*, **60**, 1545 (1974).
- (12) M. Weismann and L. Blum, *Trans. Faraday Soc.*, **64**, 2605 (1968).
- (13) W. S. Benedict, N. Gailar, and E. F. Flyer, *J. Chem. Phys.*, **24**, 1139 (1956).
- (14) B. R. Lentz and H. A. Scheraga, *J. Chem. Phys.*, **58**, 5296 (1973); **61**, 3493 (1974).
- (15) J. Del Bene and J. A. Pople, *J. Chem. Phys.*, **52**, 4858 (1970).
- (16) D. Hankins, J. W. Moskowitz, and F. H. Stillinger, Jr., *J. Chem. Phys.*, **53**, 4544 (1970).
- (17) M. J. D. Powell, *Comput. J.*, **7**, 155 (1964).
- (18) W. I. Zangwill, *Comput. J.*, **10**, 293 (1967).
- (19) J. Raphson, "Analysis Equationum Universalis", 1690, cited by T. Cajori in "A History of Mathematics", McMillan, New York, N.Y., 1919, p 203.
- (20) T. R. Dyke and J. S. Muentner, *J. Chem. Phys.*, **60**, 2929 (1974).
- (21) S. A. Clough, Y. Beers, G. P. Klein, and S. Rothman, *J. Chem. Phys.*, **59**, 2254 (1973).
- (22) L. L. Shipman and H. A. Scheraga, *J. Phys. Chem.*, **79**, 380 (1975).
- (23) K. F. Stripp and J. G. Kirkwood, *J. Chem. Phys.*, **19**, 1131 (1951).
- (24) For a discussion of the approximations made in the derivation of EPEN, see ref 6.
- (25) (a) B. R. Lentz, A. T. Hagler, and H. A. Scheraga, *J. Phys. Chem.*, **78**, 1844 (1974); (b) *ibid.*, **78**, 1531 (1974).
- (26) O. Weres and S. A. Rice, *J. Am. Chem. Soc.*, **94**, 8983 (1972).
- (27) κ is defined as $(2I_b^{-1} - I_a^{-1} - I_c^{-1})/(I_b^{-1} - I_c^{-1})$. See, e.g., J. C. Davis, Jr., "Advanced Physical Chemistry", Ronald Press, New York, N.Y., 1965, p 324.
- (28) J. B. Hasted in "Water, a Comprehensive Treatise", Vol. 1, F. Franks, Ed., Plenum Press, New York, N.Y., 1972, p 257.
- (29) S. Nir, S. Adams, and R. Rein, *J. Chem. Phys.*, **59**, 3341 (1973).
- (30) J. S. Muentner, private communication. These were calculated in the harmonic approximation from spectroscopic determinations of D_J , the centrifugal distortion constant. The water dimer was taken to be a pair of point molecules to evaluate the hydrogen-bond stretching force constant.
- (31) This fact has been noted before. See, e.g., ref 4 and 5.
- (32) C. Braun and H. Leidecker, *J. Chem. Phys.*, **61**, 3104 (1974).
- (33) K. Morokuma and J. R. Winick, *J. Chem. Phys.*, **52**, 1301 (1970).
- (34) T. R. Dyke and J. S. Muentner, *J. Chem. Phys.*, **57**, 5011 (1972).
- (35) H. C. Longuet-Higgins, *Mol. Phys.*, **8**, 445 (1963).
- (36) This analysis has been carried out by Dyke and Muentner in ref 20 to analyze the tunneling splitting of the dimer rotational energy levels.
- (37) R. W. Bolander, J. L. Kassner, Jr., and J. T. Zung, *J. Chem. Phys.*, **50**, 4402 (1969).
- (38) G. S. Kell and G. E. McLaurin, *J. Chem. Phys.*, **51**, 4345 (1969).
- (39) G. S. Kell, G. E. McLaurin, and E. Whalley, *J. Chem. Phys.*, **48**, 3805 (1968).
- (40) G. E. Ashwell, P. A. Eggert, R. Emery, and H. A. Gebbie, *Nature (London)*, **247**, 196 (1974).
- (41) H. A. Gebbie, W. J. Burroughs, J. Chamberlain, J. E. Harries, and R. G. Jones, *Nature (London)*, **221**, 143 (1969).
- (42) A. A. Viktorova and S. A. Zhevakin, *Sov. Phys. Dokl. (Engl. Trans.)*, **11**, 1059 (1967).
- (43) In comparing thermodynamic quantities in this paper to those in ref 38, it should be noted that ours refer to the equilibrium $n(\text{H}_2\text{O}) \rightleftharpoons (\text{H}_2\text{O})_n$ while those in ref 38 refer to the sequential polymerization equilibria $(\text{H}_2\text{O})_{n-1} + \text{H}_2\text{O} \rightleftharpoons (\text{H}_2\text{O})_n$. The experimental data in Table X and Figures 12-14 have been transformed to refer to our equilibria.
- (44) G. S. Kell, G. E. McLaurin, and E. Whalley, *J. Chem. Phys.*, **49**, 2834 (1968).
- (45) Kistenmacher et al.⁴⁶ have added a term to the AFHF potential to account for electron correlation effects. With this modification, $R_{O...O}$ decreases slightly to 2.97 Å. The changes in the dimer structure are small, and U becomes only 0.26 kcal/mol more negative (by our calculation).
- (46) H. Kistenmacher, H. Popkie, E. Clementi, and R. O. Watts, IBM Research Report No. RJ 1335, San Jose, Calif., Jan 20, 1974. See also F. F. Abraham, *J. Chem. Phys.*, **61**, 1221 (1974).
- (47) D. Eisenberg and W. Kauzmann, "The Structure and Properties of Water", Oxford University Press, New York, N.Y., 1969, p 71.
- (48) This structure also has been found by Lentz et al.^{25a}
- (49) This has been noted previously by Kistenmacher et al.⁸
- (50) E. Whalley in "Physics and Chemistry of Ice", E. Whalley, S. Jones, and J. W. Gold, Ed., Royal Society of Canada, 1973, p 73.
- (51) G. E. Walrafen in "Water, a Comprehensive Treatise", Vol. 1, F. Franks, Ed., Plenum Press, New York, N.Y., 1972, p 170.
- (52) M. Daele, L. H. Lund, P. L. M. Plummer, J. L. Kassner, Jr., and B. N. Hale, *J. Colloid Interface Sci.*, **39**, 65 (1972).
- (53) T. L. Hill, "An Introduction to Statistical Thermodynamics", Addison-Wesley, Reading, Mass., 1960.
- (54) G. H. Diercksen, W. P. Kraemer, and B. O. Roos, *Theor. Chim. Acta*, **36**, 249 (1975).
- (55) L. A. Curtiss and J. A. Pople, *J. Mol. Spectrosc.*, **55**, 1 (1975).

Influence of a First Hydrogen Bond on the Formation of a Second One by Alkyl- or Dialkylammonium Ions

M. Cl. Haulait and P. L. Huyskens*

Laboratorium voor Fysicochemie en Stralingschemie, Universiteit te Leuven, Celestijnenlaan 200-F, 3030 Heverlee, Belgium
(Received March 10, 1975)

Publication costs assisted by KUL and F.C.F.O (Belgium)

From conductimetric measurements, the dissociation constants K_d of dialkyl- and monoalkylammonium picrates and dialkylammonium perchlorates, bromides, and chlorides in nitrobenzene were determined in the presence of various amounts of basic ligands such as pyridine and aliphatic amines. From these data, it was possible to show that the solvation of the ion pairs is effective and to estimate the values of k_1^+ and k_2^+ , the equilibrium constants for the successive additions of ligand molecules to the cation, and of K_1 , the addition constant for the ion pair. It appears that $k_1^+ > K_1 > k_2^+$. A first hydrogen bond between the cation and a ligand molecule decreases thus more the proton donor ability of the second N-H link than the first hydrogen bond between the cation and the anion. This can be explained by a greater stretching of the first N-H link in the former case. This stretching is related to the difference between the two minima of the curve of the potential energy of the proton of the first bond. This stretching is the greatest in the case of a symmetrical hydrogen bond as in $R_2HNNH^+ \cdots NHR_2$ and is less important in the ion pairs considered here. The perturbation of the proton donor ability of the second N-H link by the formation of a first hydrogen bond seems thus to depend more on covalent than on electrostatic effects.

Introduction

Positive ions with N-H links are able to form hydrogen bonded complexes with basic molecules such as pyridine or aliphatic amines.

Witschonke and Kraus¹ and Gilkerson^{2,3} ascribed the large increase of the conductivity of solutions of mono-, di-, and trialkylammonium salts when basic ligands are added to the solutions to the formation of such hydrogen bonds, whereas in the case of the tetraalkylammonium salts these substances practically do not affect the conductivity.

The occurrence of these hydrogen bonds has been directly demonstrated by vibrational spectroscopy⁴ and furthermore NMR measurements performed by Clements and Wood⁵ showed that in the case of the pyridine the lone pair of electrons of the nitrogen atom and not the π system acts as proton acceptor.

In the case of monoalkyl- and dialkylammonium salts, the formation of higher complexes must be considered.

As a matter of fact, a cation, such as RNH_3^+ , which bears several sites can bind several ligand molecules L. In the presence of the ligand L, the solution can in principle contain, besides uncomplexed cations RNH_3^+ , complexes ions of the types RNH_3^+L , $RNH_3^+L_2$, and $RNH_3^+L_3$. The formation of such complexed ions of higher stoichiometry was considered by several authors.⁶⁻⁸

At the same time, however, solvation of the parent ion pair $RNH_3^+X^-$ can then occur and the possibility of formation of the neutral complexes $RNH_3^+X^-L$ and $RNH_3^+X^-L_2$ must be considered.

The solvation of these different species has an effect upon the conductivity of the solutions. The formation of a hydrogen bond between the cation and the ligand increases the number of types of conducting species but reduces their mobility as a consequence of the increase of their size. On the other hand, the solvation of the ion pair tends to strengthen the stability of the nondissociated and thus nonconducting species and disfavors the conductivity.

Our experimental approach is based upon the determination of the dependence of the electric conductivity of the solutions of the ionophore $RNH_3^+X^-$ on the concentration of free ligand. From these data, it was possible not only to show that the solvation of the ion pairs by the ligand is effective but also to estimate the values of the various equilibrium constants.

The ionophores were diethylammonium perchlorate ($Et_2NH_2ClO_4$), diethylammonium picrate (Et_2NH_2Pi), diethylammonium bromide (Et_2NH_2Br), diethylammonium chloride (Et_2NH_2Cl), dibutylammonium picrate (Bu_2NH_2Pi), and butylammonium picrate ($BuNH_3Pi$).

The ligands were 3,4-dimethylpyridine (3,4-lutidine), dibutylamine (Bu_2NH), and butylamine ($BuNH_2$).

It was important to choose a solvent which should not be too competitive with the ligands in their interaction with the acidic sites of the cations and the ion pairs. Among the solvents generally used for a conductimetric study, we have selected nitrobenzene (NB), a dipolar aprotic solvent ($D = 34.82$).

All experiments were performed at $25 \pm 0.1^\circ$.

Experimental Section

A. Materials. Nitrobenzene was a Fluka puriss product and was distilled from activated alumina under reduced pressure. The specific conductance was then 5×10^{-9} ohm⁻¹ cm⁻¹.

Butylamine, dibutylamine, and 3,4-dimethylpyridine were Fluka products and were distilled under reduced pressure just prior to use.

The specific conductance of solvent containing basic ligands (for instance, 3×10^{-8} ohm⁻¹ cm⁻¹ for a 0.2 M solution of 3,4-dimethylpyridine in nitrobenzene) was above that of pure solvent but was always less than 1% of the measured conductance of the most dilute salt solutions. In each case, the specific conductance of the solvent was sub-

tracted from that of the salt solution to obtain the specific conductance due to the salt.

The partially substituted ammonium picrates were prepared by interaction of picric acid with the corresponding amine in methanol. Butylammonium picrate was recrystallized from methanol. Dibutylammonium picrate and diethylammonium picrate were recrystallized from ether at the temperature of Dry Ice. Triethylammonium picrate was recrystallized from a benzene-methanol mixture.

Diethylammonium perchlorate was obtained from 70% perchloric acid and diethylamine in ethanol. The salt was recrystallized from ethanol at the temperature of Dry Ice.

Diethylammonium bromide was prepared by neutralization of an aqueous solution of hydrobromic acid with diethylamine. The solution was evaporated and the salt was recrystallized from a dichloroethane-methanol mixture.

Diethylammonium chloride was an Eastman Kodak product recrystallized from a dichloroethane-methanol mixture.

B. Measurements. Electrical conductances were measured with a Wayne Kerr universal bridge B 221 having a frequency of 1592 Hz. The conductance cells were of the Philips type with parallel platinum electrodes.

In these conditions, the equivalent conductances, Λ , were measured with a precision of about 1%.

The dielectric constants were determined with a W.T.W. DM01 dipolemeter.

Method

In a previous work, Macau, Lamberts, and Huyskens⁹ have proposed a general relation between the specific conductivity of the solutions and the concentration of free ligand, which is a generalization of the equation proposed by Gilkerson.^{2,10,11}

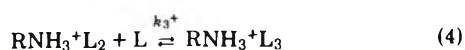
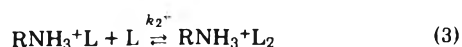
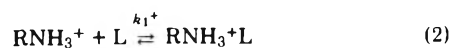
The overall dissociation constant, K_d , of the ionophore is defined as

$$K_d \equiv ([\text{ions}]^2 f_{\pm}^2) / [\text{ion pairs}] \quad (1)$$

where [ions] is the total concentration of the various positive ions and [ion pairs] is the total concentration of the nondissociated ionophores.

In the absence of ligands, the dissociation constant will be noted K_d^0 .

Let us consider the more general case of a monoalkyl cation with three acidic sites. In the presence of a basic ligand which is not able to bind the anions to any appreciable extent, the equilibria which are to be considered are the following: (a) for the ions



(b) for the ion pairs



Under these circumstances the ratio $R \equiv K_d/K_d^0$ must obey the following relation:

TABLE I: Equivalent Conductance of the Solutions as a Function of the Formal Concentration C of the Salt $\text{Et}_2\text{NH}_2\text{Pi}$ in the Presence of 0.1 Mol of 3,4-Lutidine in Nitrobenzene

$C, 10^{-4} M$	$\Lambda, \text{ohm}^{-1} \text{cm}^2 \text{mol}^{-1}$	$C, 10^{-4} M$	$\Lambda, \text{ohm}^{-1} \text{cm}^2 \text{mol}^{-1}$
0.000	30.00	4.544	19.55
	(calcd)		
0.738	25.79	5.845	18.35
1.092	24.90	7.550	17.12
1.545	23.88	8.475	16.59

$$R \equiv \frac{K_d}{K_d^0} = (1 + k_1^+L + k_1^+k_2^+L^2 + k_1^+k_2^+k_3^+L^3) / (1 + K_1L + K_1K_2L^2) \quad (7)$$

where k_1^+ , k_2^+ , and k_3^+ are the equilibrium constants for the successive additions of ligand molecules L to the cation and K_1 and K_2 are the addition constants for the ion pair, the latter always possessing one site less than the corresponding cation.

A similar relation has been previously used for the study of the solvation of the anions by an acidic ligand.¹²

The dissociation constant K_d^* in a given medium can be computed from the conductivity data using the method of Fuoss and Kraus:¹³

$$F(z)/\Lambda = 1/\Lambda_0 + \Delta C f_{\pm}^2 / \Lambda_0^2 K_d^* F(z) \quad (8)$$

where $F(z)$ is the Fuoss function¹⁴ and f_{\pm}^2 is calculated from the Debye-Hückel theory. C is the formal concentration of the ionophore.

It is necessary to know the value of Λ_0 to calculate K_d^* from the slope of $F(z)/\Lambda$ plotted vs. $C\Lambda f_{\pm}^2/F(z)$.

In the case of dibutyl-, diethyl-, and monobutylammonium picrates and of diethylammonium perchlorate, the value of the limiting molar conductivity Λ_0 which appears in eq 8 can be easily computed by the extrapolation of the Λ vs. $C^{1/2}$ curves. At the lowest concentrations used in this study, the dissociation of the salts is indeed strong enough to allow an accurate extrapolation. An example is given in Table I. The obtained values of Λ_0 vary however with the concentration L of the added ligand, owing to the effect of the solvation on the mean mobility of the conducting species.

In the case of diethylammonium bromide and of diethylammonium chloride, the dissociation constants become too low to allow the foregoing extrapolation. Here the value of Λ_0 was estimated on the basis of the Kohlrausch's equation:

$$\Lambda_0 = \lambda_0^+ + \lambda_0^- \quad (9)$$

using for λ_0^+ the value computed from Λ_0 for the picrate at the same ligand concentration (λ_0^- for the picrate ion in nitrobenzene was taken as $16 \text{ ohm}^{-1} \text{cm}^2 \text{mol}^{-1}$). The λ_0^- values of Br^- and Cl^- were taken from the literature: $\lambda_0^- (\text{Br}^-) = 21.60 \text{ ohm}^{-1} \text{cm}^2 \text{mol}^{-1}$ and $\lambda_0^- (\text{Cl}^-) = 22.20 \text{ ohm}^{-1} \text{cm}^2 \text{mol}^{-1}$.

In order to compare the values of R at different ligand concentrations, it is very important that the K_d values refer to a medium having the same dielectric constant. The dielectric constant D of the solutions were therefore determined and all the K_d values were reduced to the reference

value of the dielectric constant of pure nitrobenzene ($D = 34.82$) using the equation

$$\log K_d = \log K_d^* + B(1/D^* - 1/34.82) \quad (10)$$

The value of the factor B was computed from measurements of K_d^* for solutions of Et_3NHPi in mixtures of benzene and nitrobenzene having a known dielectric constant. This value, namely 56, was taken as being approximately the same for the other systems.

Results and Discussion

The values of K_d and R for the various salts studied in the nitrobenzene–ligand solvent systems are listed in Table II.

R is plotted vs. the formal concentration of ligand L in Figures 1 and 2. These graphs show in all cases a downward curvature. This negative curvature is clearly demonstrated in the last column of Table II by the variation of the $(R - 1)/L$ ratio with the concentration of the ligand L .

This allows us to conclude that the solvation of the ion pair by the ligand occurs to a nonnegligible extent. Since all the higher terms appearing in the numerator of eq 7 are positive, only the terms of the denominator which correspond to the solvated ion pairs can bring about a decrease of the slope of the R vs. L curve.

The relative importance of the solvation constants are given by the computation of the first and the second derivatives of expression 7 at the origin:

$$R_0' = k_1^+ - K_1 \quad (11)$$

$$R_0'' = 2\{k_1^-(k_2^+ - K_1) + K_1(K_1 - K_2)\} \quad (12)$$

The fact that the R vs. L curves show a positive slope demonstrates that the first complexation of the ion is stronger than that of the ion pair ($k_1^+ > K_1$). The decrease of the slope with increasing L shows that the constant K_1 for the solvation of the ion pair is greater than the constant k_2^+ corresponding to the addition of a second ligand molecule to the free cation (while the difference $K_1 - K_2$ must be positive).

The existence of this second solvation of the free cation (k_2^+) can be made evident by the variation of the quantity $(R - 1)/L$ vs. R according to

$$(R - 1)/L = k_1^+ - RK_1 + k_1^+k_2^+L \quad (13)$$

This variation is not linear and the last term of this expression may not be neglected (Figure 3).

From the graphs of Figures 1 and 2, it is possible to estimate which values of k_1^+ , k_2^+ and K_1 , in the expression

$$R = (1 + k_1^+L + k_1^+k_2^+L^2)/(1 + K_1L) \quad (14)$$

will be in best agreement with our experimental values. It is not necessary to take the constants k_3^+ and K_2 into account for the systems including diethylammonium and dibutylammonium ions with only two sites on the free cation and one site on the ion pair. For monobutylammonium picrate, these constants are supposed to be negligible.

The values of the constants k_1^+ , k_2^+ , and K_1 are listed in Table III for the systems studied in nitrobenzene.

As expected, the values of k_1^+ and k_2^+ for the solvation of a given cation are independent of the nature of the anion and remain constant within the limits of the experimental errors.

The solvation constant of the ion pair, K_1 , is systematically smaller than k_1^+ . The solvation of the ion pair implies

TABLE II: Conductance Parameters in Nitrobenzene at 25°

$L, 10^{-2} M$	$\Lambda_0,$ ohm $^{-1}$ cm 2 mol $^{-1}$	K_d, M	R	$(R - 1)/L, M^{-1}$
(a) Cation BuNH_3^+ ; Anion Picrate; Ligand BuNH_2				
0.00	32.90	1.52×10^{-4}	1.00	
0.25	32.80	2.36×10^{-4}	1.56	224
0.50	32.80	3.05×10^{-4}	2.01	202
1.00	32.60	4.21×10^{-4}	2.77	177
2.00	32.20	5.92×10^{-4}	3.89	145
3.00	32.00	7.41×10^{-4}	4.87	129
5.00	31.60	9.33×10^{-4}	6.14	103
7.00	31.30	11.65×10^{-4}	7.66	95
8.00	31.20	12.40×10^{-4}	8.16	89.5
10.00	31.10	14.40×10^{-4}	9.48	84.8
15.00	30.80	18.82×10^{-4}	12.38	75.9
20.00	30.60	23.27×10^{-4}	15.31	71.5
(b) Cation Bu_2NH_2^+ ; Anion Picrate; Ligand Bu_2NH				
0.00	30.40	1.56×10^{-4}	1.00	
1.00	30.30	1.77×10^{-4}	1.13	13
2.10	30.20	1.92×10^{-4}	1.23	11
3.94	30.00	2.25×10^{-4}	1.44	11.2
6.00	29.80	2.55×10^{-4}	1.63	10.5
8.00	29.60	2.78×10^{-4}	1.78	9.8
9.60	29.50	2.97×10^{-4}	1.90	9.4
(c) Cation Et_2NH_2^+ ; Anion Perchlorate; Ligand 3,4-Lutidine				
0.00	40.55	2.17×10^{-3}	1.00	
2.00	37.05	3.46×10^{-3}	1.60	30.0
4.00	36.05	4.54×10^{-3}	2.09	27.2
5.97	35.65	5.51×10^{-3}	2.54	25.7
7.95	35.35	6.10×10^{-3}	2.81	22.8
10.00	35.15	6.64×10^{-3}	3.06	20.6
15.00	34.75	8.20×10^{-3}	3.78	18.5
20.00	34.35	9.90×10^{-3}	4.56	17.8
(d) Cation Et_2NH_2^+ ; Anion Picrate; Ligand 3,4-Lutidine				
0.00	35.40	1.65×10^{-4}	1.00	
2.00	31.90	2.96×10^{-4}	1.79	39.5
6.04	30.50	4.83×10^{-4}	2.93	31.9
10.00	30.00	6.34×10^{-4}	3.84	28.4
15.00	29.60	8.18×10^{-4}	4.96	26.4
19.80	29.20	9.77×10^{-4}	5.92	24.8
(e) Cation Et_2NH_2^+ ; Anion Bromide; Ligand 3,4-Lutidine				
0.00	41.00	6.90×10^{-6}	1.00	
2.00	37.50	13.52×10^{-6}	1.96	48.0
4.00	36.50	18.89×10^{-6}	2.74	43.5
6.00	36.10	23.52×10^{-6}	3.41	39.8
8.08	35.80	28.23×10^{-6}	4.09	38.2
10.10	35.60	32.14×10^{-6}	4.66	36.2
15.10	35.20	43.17×10^{-6}	6.26	34.8
20.10	34.80	56.65×10^{-6}	8.21	35.0
(f) Cation Et_2NH_2^+ ; Anion Chloride; Ligand 3,4-Lutidine				
0.00	41.60	3.80×10^{-7}	1.00	
2.00	38.10	9.03×10^{-7}	2.38	69.0
4.00	37.10	12.44×10^{-7}	3.27	56.7
6.00	36.70	17.44×10^{-7}	4.59	59.6
10.00	36.20	24.85×10^{-7}	6.54	55.4
15.10	35.80	36.96×10^{-7}	9.73	57.9
22.00	35.20	53.24×10^{-7}	14.01	58.6

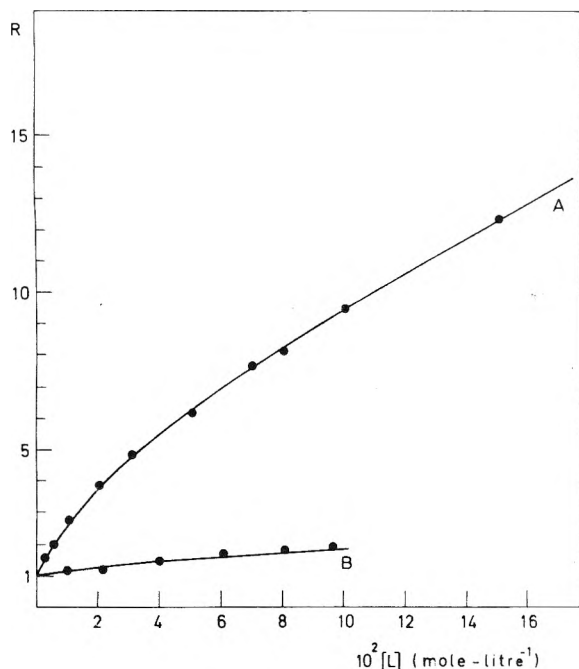


Figure 1. Graph of $R = K_d/K_d^0$ vs. concentration of added ligand: (A) BuNH_3^+Pi with BuNH_2 in nitrobenzene; (B) $\text{Bu}_2\text{NH}_2^+\text{Pi}$ with Bu_2NH in nitrobenzene.

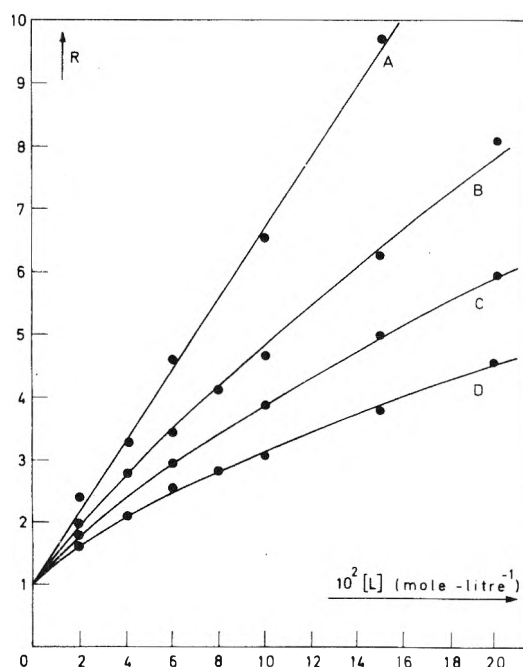


Figure 2. Graph of R vs. concentration of added 3,4-lutidine for (A) $\text{Et}_2\text{NH}_2^+\text{Cl}^-$, (B) $\text{Et}_2\text{NH}_2^+\text{Br}^-$, (C) $\text{Et}_2\text{NH}_2^+\text{Pi}^-$, and (D) $\text{Et}_2\text{NH}_2^+\text{ClO}_4^-$ in nitrobenzene.

the formation of a hydrogen bond between the second N-H link of the cation and the ligand molecule, the first N-H link of the cation being included in the cation-anion hydrogen bond. It can be observed in Table III that as the bond between the anion and the cation becomes stronger ($\text{Et}_2\text{NH}_2^+\text{Cl}^- > \text{Et}_2\text{NH}_2^+\text{Br}^- > \text{Et}_2\text{NH}_2^+\text{Pi}^- > \text{Et}_2\text{NH}_2^+\text{ClO}_4^-$), the ratio K_1/k_1^+ becomes smaller.

This leads to the conclusion that the hydrogen bond between the anion and the cation clearly disfavors the pro-

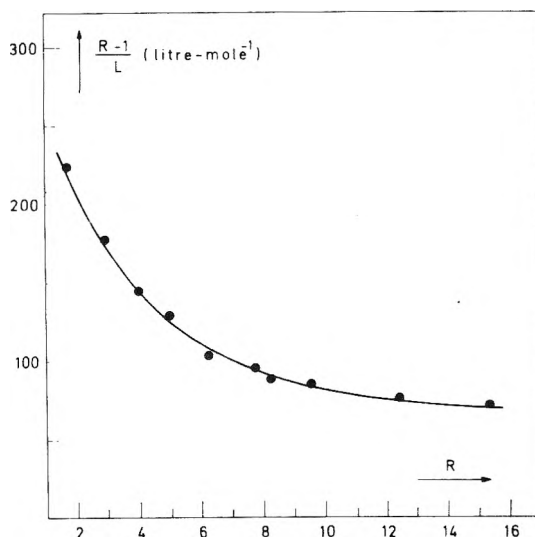


Figure 3. Graph of $(R-1)/L$ vs. R for BuNH_3^+Pi in the presence of BuNH_2 in nitrobenzene.

TABLE III: Complexation Constants (M^{-1}) in Nitrobenzene

Cation	Anion	Ligand	k_1^+	k_2^+	K_1
BuNH_3^+	Picrate	BuNH_2	279 ± 10	10 ± 1	50 ± 2
Bu_2NH_2^+	Picrate	Bu_2NH	16.5 ± 0.5	0.5	4 ± 0.2
Et_2NH_2^+	Perchlorate	3,4-Lutidine	60 ± 2	5.1 ± 0.6	22.7 ± 2
Et_2NH_2^+	Picrate	3,4-Lutidine	61 ± 2	5 ± 0.5	16.5 ± 2
Et_2NH_2^+	Bromide	3,4-Lutidine	61 ± 2	5 ± 0.5	11 ± 1
Et_2NH_2^+	Chloride	3,4-Lutidine	62 ± 2	5.2 ± 0.6	5.5 ± 0.7

ton donor properties of the second N-H group of the cation.

However, it appears that if the first anion-cation hydrogen bond decreases the acidity of the other N-H groups, this effect is even more important when the first hydrogen bond is a cation-pyridine or a cation-amine bond. In this case, the reduction of the constant k_2^+ as compared with k_1^+ is still stronger.

These results appear at a first sight as rather unexpected. Indeed, the presence of a negative ion near the cation in the ion pair must have an unfavorable effect upon the attraction between the cation and the dipole of the ligand molecule (Figure 4a). Such an effect must be smaller when the first entity bound to the cation is no more an ion but only a polar entity (Figure 4b).

On the other hand, the first hydrogen bond is much stronger in the cation-anion bond than in the cation-ligand bond.

From these two facts, it could a priori be assumed that the perturbations brought about in the acidic character of the second N-H link of the cation should be more important when the first N-H link is bound to an anion.

Our results prove that this supposition is not correct. The opposite effect was indeed observed.

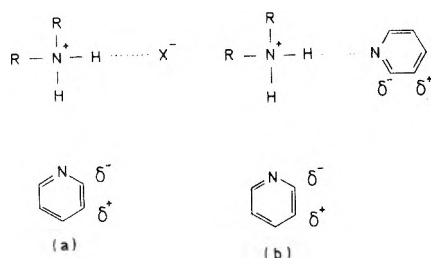


Figure 4. Interaction between a ligand molecule and the second N-H link of the cation: (a) the first N-H link is bound to an anion; (b) the first N-H link is bound to a ligand molecule.

This can be explained by the inherent properties of the first hydrogen bonds formed by the cation. All these hydrogen bonds increase the N-H distance with respect to the N-H distance in the free cation. It can be estimated, in first approximation, that a greater N-H distance in the first group induces a greater charge density around the nitrogen atom and thus induces a greater perturbation in the acidic character of the other N-H groups.

In recent works Wood et al. have studied the vibrational spectra of complex hydrogen bonded cations of the type $(B_1HB_2)^+$ where B_1 and B_2 may be identical or different monofunctional bases. For the homoconjugated complex $Me_3NH^+ \cdots NMe_3$, these authors find a ν_s band with a single broad maximum at 2100 cm^{-1} .¹⁵ For the heteroconjugated complex $Me_3NH^+ \cdots NC_5H_5$ the ν_s band appears at significantly higher wave numbers with maxima at 2650 and 2450 cm^{-1} .¹⁶ We can thus conclude that the N-H distance is greater in the homoconjugated bond. A similar observation is made by Wood in the case of the complex ions of triethylenediamine where for the complex $TEDH^+ \cdots TED$ the ν_s lies at 2200 cm^{-1} whereas for the hydrogen bond between $TEDH^+$ and another cation, the maximum of ν_s appears at 2500 cm^{-1} .¹⁷ In the cation $(B_1HB_2)^+$ the N-H distance depends thus on the difference of the pK values of the bases B_1 and B_2 and is maximal in the case of the homoconjugation.

As we consider the distance N-H in the first hydrogen bond between the cations RNH_3^+ or $R_2NH_2^+$ and the basic ligands, this distance will be greater in the case of homoconjugation. The perturbation of the acidic character of a second N-H group will thus be the greatest in this case.

Effectively the constant k_2^+ is more reduced as compared with k_1^+ in the complexation of the cation with the another aliphatic amine than with the pyridine.

If sufficient long time scales are considered, the potential

energy curves of the proton show two minima the vertical distance of which depends on the difference in pK_a between the donor and the acceptor. The distance N-H in this first hydrogen bond and the perturbation brought about in the other sites, is thus related to the vertical difference between the two minima of the potential energy curve of the proton.

Thus it can be considered that, although the anion-cation hydrogen bond in the ion pair is very strong, the vertical difference between the two potential minima of the proton is important. As a consequence, the distance N-H is smaller as compared with the distance N-H in the cation-amine hydrogen bond and the perturbation of the acidity of the second N-H group is also more reduced.

This is confirmed if we consider the four last-mentioned systems of Table III including the same cation $Et_2NH_2^+$ but different anions. The distance between the two minima of the potential energy curve of the proton increases with the acidity of the conjugated acid of the anion. This will thus be more important in the case of the perchlorate than in the case of the chloride and the reduction of K_1 compared to k_1^+ , due to the hydrogen bond formed by the cation with the anion, will increase according to the sequence: $ClO_4^- < Pi^- < Br^- < Cl^-$.

The effect of the first hydrogen bond upon the formation of a second one depends thus more on covalent than on electrostatic effects.

Acknowledgment. The authors wish to express their thanks to Professor J. L. Wood for his interesting suggestions.

References and Notes

- (1) C. R. Witschonke and C. A. Kraus, *J. Am. Chem. Soc.*, **69**, 2472 (1947).
- (2) E. K. Ralph, III, and W. R. Gilkerson, *J. Am. Chem. Soc.*, **86**, 4783 (1964).
- (3) H. W. Aitken and W. R. Gilkerson, *J. Am. Chem. Soc.*, **95**, 8551 (1973).
- (4) R. Clements, F. N. Masri, and J. L. Wood, *Chem. Commun.*, 1530 (1971).
- (5) R. Clements and J. L. Wood, *J. Mol. Struct.*, **17**, 265 (1973).
- (6) M. L. Junker and W. R. Gilkerson, *J. Am. Chem. Soc.*, **97**, 493 (1975).
- (7) Z. Pawlak, *Rocz. Chem. Ann. Soc. Chim. Polon.*, **47**, 347 (1973).
- (8) D. J. Pirson and P. L. Huyskens, *J. Solution Chem.*, **3**, 515 (1974).
- (9) J. Macau, L. Lamberts, and P. Huyskens, *Bull. Soc. Chim. Fr.*, 2387 (1971).
- (10) W. R. Gilkerson and J. B. Ezell, *J. Am. Chem. Soc.*, **89**, 808 (1967).
- (11) H. B. Flora, II, and W. R. Gilkerson, *J. Am. Chem. Soc.*, **92**, 3273 (1970).
- (12) D. J. Pirson and P. L. Huyskens, *J. Solution Chem.*, **3**, 503 (1974).
- (13) R. M. Fuoss and C. A. Kraus, *J. Am. Chem. Soc.*, **55**, 476, 2387 (1933).
- (14) R. M. Fuoss and F. Accascina, "Electrolytic Conductance", Interscience, New York, N.Y., 1959.
- (15) F. N. Masri and J. L. Wood, *J. Mol. Struct.*, **14**, 217 (1972).
- (16) F. N. Masri and J. L. Wood, *J. Mol. Struct.*, **14**, 201 (1972).
- (17) R. L. Dean and J. L. Wood, *J. Mol. Struct.*, **26**, 237 (1975).

Apparent and Partial Molar Polarizations in Solutions and the Halverstadt-Kumler and Hedestrand Equations

William J. Taylor

Department of Chemistry, Ohio State University, Columbus, Ohio 43210 (Received February 18, 1975)

Publication costs assisted by the Ohio State University

Hedestrand and Halverstadt and Kumler have developed methods for the extrapolation of the molar polarization of a dilute solution of a polar molecule in a nonpolar solvent, to obtain the *apparent* molar polarization of the *solute* at infinite dilution, $P_{2\infty}$. The precise significance of these extrapolated values has, however, remained unclear; thus, one recognized authority in the field has claimed that they are in error when the molar polarization of the *solvent* varies with concentration. This question is reexamined from the viewpoint of *partial* molar polarizations, and it is demonstrated that the preceding methods of extrapolation yield the partial molar polarization of the solute at infinite dilution, \bar{P}_2° , a quantity which has an unambiguous theoretical interpretation. The calculation of the dipole moment of the solute molecule from \bar{P}_2° is also discussed.

Introduction

In the determination of dipole moments from measurements of dielectric constants of dilute solutions of polar molecules in nonpolar solvents it is customary to use Debye's equation¹⁻³

$$\bar{P} = \left(\frac{\epsilon - 1}{\epsilon + 2} \right) \bar{V} = N_1 \bar{P}_1 + N_2 \bar{P}_2 \quad (1)$$

Here ϵ is the dielectric constant of the solution, and N_1 and N_2 are the mole fractions of solvent and solute, respectively. The molar polarization and molar volume of the solution are denoted by \bar{P} and \bar{V} , respectively,⁴ while \bar{P}_1 and \bar{P}_2 denote the molar polarizations of solvent and solute in the solution, which are not rigorously defined in the standard discussions. For dilute solutions it is usual to set \bar{P}_1 equal to \bar{P}_1° , the molar polarization of pure solvent (at the same temperature), and then to solve eq 1 for \bar{P}_2

$$\bar{P}_{2a} = (\bar{P} - N_1 \bar{P}_1^\circ) / N_2 = \bar{P}_2^\circ + [(\bar{P} - \bar{P}_1^\circ) / N_2] \quad (2)$$

This is generally regarded as simply a useful approximation; however, in the present discussion we wish to emphasize that \bar{P}_{2a} as given by eq 2 is a *well-defined* quantity, the *apparent molar polarization* of the solute at mole fraction N_2 , in the sense in which "apparent" is used in the thermodynamics of binary solutions.⁵ In general, \bar{P}_{2a} is a function of N_2 , and may vary markedly with N_2 over the range $N_2 = 0$ to $N_2 = 1$;⁶ the two most obvious causes of this are polarization of the solvent in the neighborhood of a solute molecule by the dipole field of the latter (the so-called *solvent effect*⁷), and the dipole-dipole (and other) interactions between solute molecules which may affect their orientation polarization (especially). The effects of solute-solute interaction can be eliminated by making measurements at several values of N_2 in the low-concentration range and extrapolating to $N_2 = 0$ to obtain \bar{P}_{2a}° .⁸ However, a *direct* extrapolation of \bar{P}_{2a} vs. N_2 is inaccurate, because of the marked increase in the *relative* errors of measured values of \bar{P}_{2a} as $N_2 \rightarrow 0$. Extrapolation procedures which appear to overcome this difficulty have been given by Hedestrand,⁹ and by Halverstadt and Kumler,^{10,11} and are widely used. On the other hand, Smith^{12,13} has claimed that *all*

procedures for the extrapolation of \bar{P}_{2a} to $N_2 = 0$ which are based on eq 2 give incorrect results to the degree that \bar{P}_1 varies with N_2 , and to the author's knowledge no refutation of Smith's proof of this has appeared heretofore in the literature.

In the present article the significance of extrapolated values of \bar{P}_{2a} is reconsidered from the viewpoint of the theory of *partial molar properties*. It was suggested many years ago by Orr and Butler¹⁴ that the proper measure of the contribution of an individual species to the polarization of a solution is the partial molar polarization, \bar{P}_i , of this species in the given solution. These authors proposed the application of the *graphical method of intercepts* for the calculation of \bar{P}_1 and \bar{P}_2 in a binary solution, but did not develop analytical expressions for these quantities. The method of intercepts was applied in this context by Goss,¹⁵ but so far as the writer has been able to determine there has been no further application of the concept of partial molar properties in connection with polarization of solutions; the term is not even mentioned in the standard monographs in this field,^{2,3,16-18} and Smith^{12,13} has stated that the concept is not meaningful when applied to the polarization of solutions.

In the next section we formulate the essential equations for the partial molar polarizations of solvent and solute, and the relation of the latter to the *apparent* molar polarization, \bar{P}_{2a} , of the solute defined by eq 2. Following this we consider the extrapolation of \bar{P}_{2a} to $N_2 = 0$, and show that (in the absence of experimental error) the methods of Hedestrand, and of Halverstadt and Kumler, yield the true partial molar polarization of the solute at infinite dilution, or \bar{P}_2° , regardless of the extent to which \bar{P}_1 varies with N_2 . We also point out the source of the errors in Smith's criticisms of the preceding extrapolation methods, and of the method of intercepts. Finally, we discuss the solvent effect, and the calculation of the dipole moment from \bar{P}_2° .

Partial Molar and Apparent Polarizations

Let P and V represent the *total* polarization and volume, respectively, of a solution containing n_1 moles of species 1, and n_2 moles of species 2; although it will be convenient in the present context to refer to these two species as the sol-

vent and solute, respectively, all the equations in the present section are valid *formally* over the entire range $N_2 = 0$ to $N_2 = 1$, given the assumed functional dependence of the polarization, P , on ϵ and V .¹⁹ The partial molar polarizations, $\bar{P}_1 = (\partial P/\partial n_1)_{n_2}$ and $\bar{P}_2 = (\partial P/\partial n_2)_{n_1}$, are calculated by partial differentiation of the equation²⁰

$$P = \left(\frac{\epsilon - 1}{\epsilon + 2} \right) V \quad (3)$$

It will be convenient to regard the dielectric constant, ϵ , as a function of $N_2 = n_2/(n_1 + n_2)$, and to denote $d\epsilon/dN_2$ by $\alpha = \alpha(N_2)$. Also required are the relations $(\partial N_2/\partial n_1)_{n_2} = -N_2/(n_1 + n_2)$ and $(\partial N_2/\partial n_2)_{n_1} = N_1/(n_1 + n_2)$. We obtain in this way

$$\bar{P}_1 = \left(\frac{\epsilon - 1}{\epsilon + 2} \right) \bar{V}_1 - \frac{3\alpha}{(\epsilon + 2)^2} N_2 \bar{V} \quad (4a)$$

$$\bar{P}_2 = \left(\frac{\epsilon - 1}{\epsilon + 2} \right) \bar{V}_2 + \frac{3\alpha}{(\epsilon + 2)^2} N_1 \bar{V} \quad (4b)$$

where \bar{V}_1 and \bar{V}_2 are partial molar volumes, and $\bar{V} = V/(n_1 + n_2)$ is the molar volume of the solution.

It follows from the definition of \bar{P}_1 and \bar{P}_2 that $dP = \bar{P}_1 dn_1 + \bar{P}_2 dn_2$, and by integration of this equation at a fixed mole ratio, $n_2/n_1 = \text{constant}$, that $P = n_1 \bar{P}_1 + n_2 \bar{P}_2$.²¹ Equations 4a and 4b are seen to be consistent with the last equation, or the alternative form $\bar{P} = N_1 \bar{P}_1 + N_2 \bar{P}_2$; thus, the use of partial molar polarizations eliminates the need for the usual assumption, implicit in eq 1, that the polarizations of the two species are additive.

On taking the differential of the relation $P = n_1 \bar{P}_1 + n_2 \bar{P}_2$, and comparing with $dP = \bar{P}_1 dn_1 + \bar{P}_2 dn_2$, one obtains $n_1 d\bar{P}_1 + n_2 d\bar{P}_2 = 0$, which is the analog of the Gibbs–Duhem equation for partial molar polarizations; it will be convenient for subsequent use to rewrite this in the form

$$N_1(d\bar{P}_1/dN_2) + N_2(d\bar{P}_2/dN_2) = 0 \quad (5)$$

The method of intercepts suggested by Orr and Butler¹⁴ for the determination of \bar{P}_1 and \bar{P}_2 for general values of N_2 is based on the equations

$$\bar{P}_1 = \bar{P} - N_2(d\bar{P}/dN_2) \quad (6a)$$

$$\bar{P}_2 = \bar{P} + (1 - N_2)(d\bar{P}/dN_2) \quad (6b)$$

These relations are derived by eliminating first \bar{P}_2 , and then \bar{P}_1 , from $\bar{P} = N_1 \bar{P}_1 + N_2 \bar{P}_2$ and the equation obtained from it by differentiation (with the use also of eq 5), i.e., $d\bar{P}/dN_2 = \bar{P}_2 - \bar{P}_1$. The claim of Smith²² that the intercept method yields erroneous results for \bar{P}_1 and \bar{P}_2 is not valid, because he overlooked the identity represented by eq 5; the existence of this important relation is a further persuasive argument for the use of partial molar polarizations.

Alternatively, \bar{P}_2 may be calculated from values of \bar{P}_{2a} , as defined by eq 2. On multiplying eq 2 by n_2 and rearranging one obtains $P = (n_1 + n_2)\bar{P} = n_1 \bar{P}_1 + n_2 \bar{P}_{2a}$; partial differentiation with respect to n_2 , and use of the equation preceding eq 4a, then yields

$$\bar{P}_2 = \bar{P}_{2a} + N_2(1 - N_2)(d\bar{P}_{2a}/dN_2) \quad (7)$$

Limit of Infinite Dilution

As $N_2 \rightarrow 0$, \bar{V}_1 and \bar{V} approach \bar{V}_1° , the molar volume of pure solvent, while \bar{V}_2 approaches \bar{V}_2° , the partial molar volume of solute in its standard state.⁸ Hence, in the limit eq 4a yields $\bar{P}_1 = \bar{P}_1^\circ$, the molar polarization of pure sol-

vent. On the other hand, the partial molar polarization of solute in its standard state at $N_2 = 0$, as obtained from eq 4b is

$$\bar{P}_2^\circ = \left(\frac{\epsilon_1^\circ - 1}{\epsilon_1^\circ + 2} \right) \bar{V}_2^\circ + \frac{3\alpha^\circ}{(\epsilon_1^\circ + 2)^2} \bar{V}_1^\circ \quad (8)$$

Here ϵ_1° is the dielectric constant of pure solvent, and α° is the limiting value of $d\epsilon/dN_2$ at $N_2 = 0$. The two terms on the right-hand side of eq 8 represent the contributions to \bar{P}_2° of changes in *volume* and *dielectric constant*, respectively, when 1 mol of solute is added to an indefinitely large quantity of solvent.

We show next that \bar{P}_{2a} approaches \bar{P}_2° as $N_2 \rightarrow 0$. Substitution of $\bar{P} = \bar{P}_1 + N_2(\bar{P}_2 - \bar{P}_1)$ in eq 2 yields

$$\bar{P}_{2a} = \bar{P}_2 + \left(\frac{1 - N_2}{N_2} \right) (\bar{P}_1 - \bar{P}_1^\circ) \quad (9)$$

In the limit $N_2 = 0$, eq 9 becomes

$$\bar{P}_{2a}^\circ = \bar{P}_2^\circ + (d\bar{P}_1/dN_2)^\circ \quad (10)$$

which is equivalent to the result obtained by a different argument by Smith.²³ However, in view of eq 5, $(d\bar{P}_1/dN_2)^\circ = 0$, and therefore (contrary to the assertion of Smith)

$$\bar{P}_{2a}^\circ = \bar{P}_2^\circ \quad (11)$$

this result may also be obtained from eq 7.²⁴

Since the methods of Hedstrand,⁹ and of Halverstadt and Kumler,¹⁰ are based on the extrapolation of \bar{P}_{2a} to $N_2 = 0$, they must yield \bar{P}_2° if the extrapolation is carried out correctly. We now show explicitly that their equations for \bar{P}_{2a}° are equivalent to eq 8 for \bar{P}_2° . Both procedures involve the extrapolation of dielectric constant, ϵ , for the solution to obtain the value ϵ_1° for pure solvent.²⁵ In addition, Halverstadt and Kumler extrapolate the *specific volume*, $\nu = \bar{V}/(M_1 N_1 + M_2 N_2)$ to $N_2 = 0$ (the molecular weights of solvent and solute are denoted by M_1 and M_2 , respectively), and their result is expressed in terms of the value of $d\nu/dN_2$ for $N_2 = 0$. Differentiation of the relation $\bar{V} = N_1 \bar{V}_1 + N_2 \bar{V}_2$ with respect to N_2 , and use of the Gibbs–Duhem type equation (or analog of eq 5 for partial molar volumes), yields $d\bar{V}/dN_2 = \bar{V}_2 - \bar{V}_1$. Substitution of this result in $d\nu/dN_2$, and passage to the limit $N_2 = 0$, then yields $(d\nu/dN_2)^\circ = (\bar{V}_2^\circ - M_2 \nu_1^\circ)/M_1$, where $\nu_1^\circ = \bar{V}_1^\circ/M_1$ is the specific volume of pure solvent; rearrangement of this result gives

$$\bar{V}_2^\circ = M_2 \nu_1^\circ + M_1 (d\nu/dN_2)^\circ \quad (12)$$

Halverstadt and Kumler's equation¹⁰ for \bar{P}_{2a}° is identical (except for notation) with the result obtained by substitution of eq 12 for \bar{V}_2° in eq 8. Substitution of $\rho = 1/\nu$, and $\rho_1^\circ = 1/\nu_1^\circ$, in the preceding derivation, where ρ and ρ_1° are the *densities* of solution and pure solvent, respectively, has the effect of replacing eq 12 by

$$\bar{V}_2^\circ = [M_2 \rho_1^\circ - M_1 (d\rho/dN_2)^\circ]/(\rho_1^\circ)^2 \quad (13)$$

Hedstrand's equation⁹ for \bar{P}_{2a}° is obtained by substitution of eq 13 for \bar{V}_2° in eq 8. This confirms that both extrapolation procedures yield a value for \bar{P}_{2a}° which is equal to \bar{P}_2° , in accord with eq 11, and removes any ambiguity regarding the interpretation of such extrapolated values of the apparent molar polarization.²⁶

Solvent Effect and Calculation of Dipole Moment

By definition \bar{P}_2° is the change in the polarization of an

indefinitely large quantity of pure solvent when 1 mol of solute is added to it (at constant temperature and pressure). Under these conditions, as remarked in the Introduction, dipole-dipole (and other) interactions between solute molecules are absent. Any remaining difference between the polarization of the molecules in solution and in the gas phase (at the same temperature and zero density) is then due solely to the interactions between *separated* solute molecules and surrounding solvent molecules. This *solvent effect*⁷ may be expressed as the difference between the *apparent* dipole moment of a solute molecule in the infinitely dilute solution, or μ_s° , and the *true* permanent dipole moment of an isolated solute molecule, μ_g , as obtained from measurements on the gas phase. We make the usual assumption that this difference represents the mean vector sum of the moments induced in the solvent molecules by the dipole field of a typical solute molecule. We assume, further, that the symmetry of the molecule and its environment is sufficiently great so that this induced moment is colinear with the permanent moment of the solute molecule, so that we need consider only the scalar value, μ_i , of the induced moment; then

$$\mu_s^\circ = \mu_g + \mu_i \quad (14)$$

The value of μ_i is susceptible to approximate theoretical estimation on the basis of certain plausible models for the solute molecule and surrounding solvent.²⁷ Since the dipole field at each point in space is proportional to μ_g , the induced moment is given by an expression of the form

$$\mu_i = A\mu_g \quad (15)$$

where A is a factor which depends on the shape of the molecule, the location and orientation of the point dipole in the molecule, and the polarizability and number density of solvent molecules. For the present discussion we do not need to be concerned with the detailed dependence of A on these factors; we merely remark that Higasi²⁸ has shown that if the dipole is at the center of an ellipsoid of revolution, and directed along the symmetry axis, A is *negative* for *prolate* ellipsoids, *positive* for *oblate* ellipsoids, and zero for *spherical* molecules. Combination of eq 14 and 15 yields²⁹

$$\mu_g = (1 + A)^{-1}\mu_s^\circ \quad (16)$$

On the assumption that the moments, μ_i , induced in the solvent by the fields of the solute dipoles follow the rotation of the latter, the total *orientation* polarization of an infinitely dilute solution of 1 mol of polar solute in a nonpolar solvent is given by Debye's formula, $(4\pi N/3)(\mu^2/3kT)$, with μ set equal to μ_s° of eq 14 (here N is Avogadro's number, k is Boltzmann's constant, and T is the absolute temperature). However this orientation polarization is also equal to $\bar{P}_2^\circ - \bar{P}_{2d}$, where \bar{P}_{2d} is the *distortion* (or *deformation*) polarization for 1 mol of solute (equal to the sum of the *electronic* and *atomic* polarizations), which may be estimated from the *molar refraction* of the pure solute.^{30,31} It follows that

$$\mu_s^\circ = [(9kT/4\pi N)(\bar{P}_2^\circ - \bar{P}_{2d})]^{1/2} \quad (17)$$

Finally, μ_g is obtained from eq 16 and 17, provided an estimate of A is available.³²

Discussion

The continuing importance that chemists and chemical physicists attach to molecular dipole moments is indicated

by the fact that the comprehensive tabulation by McClellan³³ lists values for over 11,000 compounds published in the period 1962-1971, compared with 6500 for the preceding four decades. Molecular dipole moments are frequently useful in deciding between alternative structures or conformers, in estimating bond or group moments, and as a check on calculated molecular wave functions. McClellan lists more than 60 experimental methods for the determination of dipole moments. Although many of these are of minor importance, some (e.g., molecular beam, electron resonance, and microwave methods) are capable of considerably greater accuracy than is obtainable from measurements of dielectric constants of dilute solutions of polar molecules, and have the important advantage of yielding values for individual vibronic states. Nevertheless, an inspection of McClellan's tables shows that the great majority of reported dipole moments (especially for molecules which cannot be studied in the gas phase) are still obtained from measurements of dielectric constants of dilute solutions. The values given in McClellan's tables for the latter method are values of μ_s° calculated from eq 17; i.e., no corrections for the solvent effect are included. The analysis given in the present article does not require any change in these values, since we have merely shown that the extrapolated solute polarization commonly denoted by $P_{2\infty}$ is equal to the partial molar polarization of solute at infinite dilution, \bar{P}_2° . However, it is felt that this clarifies the theoretical significance of the extrapolated values, since \bar{P}_2° is rigorously defined.

Finally, we remark that the analysis in the present article is easily adapted to use of *mass* (or *weight*) fractions as concentration variables, in place of the *mole* fractions adopted here. The use of mass fractions was advocated by Sugden,³⁴ and is preferred by many workers in the field. To convert to a mass basis, set $M_1 = M_2 = 1$ (unit mass); then n_1 and n_2 become the masses, and N_1 and N_2 the mass fractions of solvent and solute, respectively. All molar, apparent molar, and partial molar quantities are replaced by corresponding *specific* quantities; for example, \bar{P}_2° of eq 8 becomes the partial specific polarization of solute in its standard state of infinite dilution.

References and Notes

- (1) P. Debye, "Polar Molecules", Chemical Catalog Company, New York, N.Y., 1929, p 45.
- (2) C. P. Smyth, "Dielectric Behavior and Structure", McGraw-Hill, New York, N.Y., 1955, p 18.
- (3) J. W. Smith, "Electric Dipole Moments", Butterworths, London, 1955, p 52.
- (4) The molar polarization is frequently denoted by $[P]$; however, for consistency we denote all molar quantities with a *tilde* (except the *partial* molar quantities to be introduced subsequently, which are denoted by the conventional bar).
- (5) G. N. Lewis and M. Randall, "Thermodynamics and the Free Energy of Chemical Substances", McGraw-Hill, New York, N.Y., 1923, p 35.
- (6) See ref 1, Figures 14 and 15, where (as is usual) P_{2a} is denoted by P_2 .
- (7) See ref 2, p 40, for a definition of "solvent effect".
- (8) The extrapolated value at infinite dilution is commonly denoted by $P_{2\infty}$ or ${}^\infty P_2$; since the spirit of the present discussion is that of the thermodynamic treatment of *dilute* solutions (and we will not be concerned with the pure solute), we define the *standard state* of the solute to be that of *infinite dilution* and distinguish quantities associated with it by the conventional superscript $^\circ$.
- (9) G. Hedestrand, *Z. Phys. Chem. B*, **2**, 428 (1929), eq 8.
- (10) I. F. Halverstadt and W. D. Kumler, *J. Am. Chem. Soc.*, **64**, 2988 (1942), eq 5.
- (11) Halverstadt and Kumler¹⁰ do not give a derivation of their equation; for a derivation of this equation, as well as a more explicit derivation of the Hedestrand equation,⁹ see ref 3, pp 54-55.
- (12) J. W. Smith, *Sci. Prog.*, **36**, 483 (1948).
- (13) J. W. Smith, *Trans. Faraday Soc.*, **48**, 802 (1952).
- (14) W. J. C. Orr and J. A. V. Butler, *Nature (London)*, **130**, 930 (1932).

- (15) F. R. Goss, *J. Chem. Soc.* 19⁵ (1937); 752 (1940).
- (16) H. Fröhlich, "Theory of Dielectrics", 2nd ed, Oxford University Press, London, 1958.
- (17) N. E. Hill, W. E. Vaughan, A. F. Price, and M. Davies, "Dielectric Properties and Molecular Behaviour", Van Nostrand-Reinhold, London, 1969.
- (18) C. J. F. Bottcher, "Theory of Electric Polarization", 2nd ed, Elsevier, Amsterdam, 1973 (material in Chapter 9 of the 1952 edition which is relevant to the present discussion is omitted in the second edition).
- (19) For concentrated solutions of polar solvents the Clausius-Mosotti expression for the "cavity" field acting on a polar solute molecule is inaccurate and Debye's equation must be modified (ref 2, pp 19-39; ref 3, pp 145-159).
- (20) All derivatives in the present article refer to conditions of constant temperature and pressure; since the quantity conventionally referred to as the *molar polarization* is in fact $4\pi/3$ times the *molar polarizability*, it is not necessary to specify constant electric field strength (in the absence of saturation effects).
- (21) This result depends, of course, on the fact that partial molar properties are *intensive*; alternatively, it may be regarded as an application of Euler's theorem to the function P , which is *homogeneous* and of *first degree* in the mole numbers n_1 and n_2 .
- (22) See ref 13, eq 6.1 and following two equations.
- (23) See ref 13, eq 5.2.
- (24) The result $(d\bar{P}_1/dN_2)_{N_2=0} = 0$ follows from eq 5 only if $(d\bar{P}_2/dN_2)_{N_2=0}$ is finite. Lewis and Randall (ref 5, pp 44, 45) have pointed out that there are *two types* of partial molar properties, \bar{G}_i : those like partial molar volume and enthalpy for which $(\partial\bar{G}_i/\partial N)_{N_2=0}$ is *finite* and those like partial molar entropy and free energy (or chemical potential) for which the magnitude of this derivative *approaches infinity* as $N_1 \rightarrow 0$. It is clear from eq 4 and the known behavior of ϵ that partial molar polarizations behave in this respect in essentially the same way as partial molar volumes and are thus of the *first* type. Similar considerations apply to the derivation of eq 11 from eq 7.
- (25) See ref 10 for a discussion of the advantages of using an extrapolated value for ϵ_1^0 , rather than a value measured for a sample of pure solvent.
- (26) The analysis leading to eq 12 and 13 for \bar{V}_2^0 (which appear to be new) makes it clear that the *volumetric* aspects of Halverstadt and Kumler's and Hedestrand's procedures represent *particular* methods for obtaining the partial molar volume of the solute at infinite dilution, \bar{V}_2^0 . One advantage of eq 8 for \bar{P}_2^0 , relative to the equations of these authors, is that \bar{V}_2^0 may also be determined by other procedures (see, for example, ref 5, pp 36-40).
- (27) For reviews of methods for calculation of the inductive solvent effect see ref 2, pp 39-51, and ref 3, pp 133-143. The most useful and widely used formulas are probably those due to Higasi²⁸ (eq 6.16 of ref 3 contains misprints; see eq 18 of Higasi's paper or eq 18.28, p 44 of ref 2).
- (28) K. Higasi, *Sci. Pap. Inst. Phys. Chem. Res. (Jpn.)*, **28**, 284 (1936).
- (29) For typical observed values of the ratio μ_s^0/μ_g , see ref 2, Table 18.1, or ref 3, Table 12.
- (30) Reference 2, Chapter 14.
- (31) R. J. W. Le Fèvre, "Dipole Moments", 2nd ed, Methuen, London, 1948, pp 10-13.
- (32) It might be asked why μ_g cannot be computed *directly* from an equation similar to eq 17 but with $\bar{P}_2^0 - P_{2g}$ replaced by $\bar{P}_2^0 - P_1 - P_{2g}$, where $P_1 = (4\pi N/3)(\mu_i^2/3kT)$ is the polarization of the solvent induced by 1 mol of solute molecules, at infinite dilution. However, this procedure would be inconsistent with the additivity of dipole moments implied by eq 14.
- (33) A. L. McClellan, "Tables of Experimental Dipole Moments", Vol. 1, W. H. Freeman, San Francisco, Calif., 1963; Vol. 2, Raha Enterprises, El Cerrito, Calif., 1974.
- (34) S. Sugden, *Trans. Faraday Soc.*, **30**, 720 (1934).

Calculation of the Elementary Graph of the Fourth Virial Coefficient of a Dilute Ionic Solution

M. Dixon*

CECAM, Bâtiment 506, Orsay, France

and P. Hutchinson

Theoretical Physics Division, Atomic Energy Research Establishment, Harwell, Oxfordshire, United Kingdom

(Received January 23, 1975)

From the Mayer function $f(r_{ij}) = \exp(-r_{ij})/r_{ij}$ the elementary graph, \boxtimes , is calculated by numerical quadrature in Fourier transform space. The value $\boxtimes = 43.091$ is obtained.

Friedman and Krishnan¹ have studied the models for the mixing of ionic solutions within the McMillan-Mayer² theory. They have calculated the excess free energy and the enthalpy mixing coefficients, g_1' and h_1' , from the cluster expansions using an approximate fourth virial coefficient and from the hypernetted chain approximation which assumes a zero value for all elementary graphs. For the charge types studied experimentally³ (BaCl₂-NaCl and Na₂SO₄-NaCl) the coefficients g_1' and h_1' depend on the third and the fourth virial coefficients even in the limiting law region. The cluster theory calculation of the limiting law behavior of g_1' and h_1' is reasonably consistent with the HNC calculations for higher concentrations but the calculated h_1' function agrees neither in sign nor in magnitude with the experimental data. These contradictions might be

*To whom correspondence should be addressed at the Department of Physics, The University, Reading, U.K.

resolved if the contribution from the elementary graph to the fourth virial coefficient was significantly larger than the approximate value.

The Mayer function corresponding to a dilute electrolyte in the McMillan-Mayer theory is $f(r_{ij}) = \exp(-r_{ij})/r_{ij}$ which is infinite at $r_{ij} = 0$; we take the Debye length as unity. Although the elementary graph is finite, it cannot be evaluated analytically, and the singularity at the origin, although integrable, makes the direct evaluation intractable. However, the Fourier transform of $f(r_{ij})$ yields a function which decays slowly and is everywhere finite, i.e.

$$\hat{f}(k) = \int f(r)e^{ikr} dr = 4\pi/(1+k^2) = x \text{-----} x \quad (1)$$

and

$$f(r) = (1/2\pi)^3 \int \hat{f}(k)e^{-ikr} dk = x \text{-----} x \quad (2)$$

with

$$\hat{\delta}(k) = 1 \quad \delta(r) = (1/2\pi)^3 \int e^{-ikr} dk \quad (3)$$

Then

$$\begin{array}{c}
 \begin{array}{ccc}
 & \diagup & \\
 x & & x \\
 & \diagdown & \\
 1 & & 2 \\
 & \diagup & \\
 & 4 &
 \end{array}
 = E_1(r_{12})
 \end{array}$$

$$= \int dr_3 \int dr_4 f(r_{13})f(r_{14})f(r_{23})f(r_{24})f(r_{34}) \quad (4a)$$

$$\begin{aligned}
 &= (1/2\pi)^{15} \int dr_3 \int dr_4 \int \int \int \int \prod_{c=1}^5 [dk_c \hat{f}(k_c)] \times \\
 &\exp\{-i[k_1(r_3 - r_1) + k_2(r_1 - r_4) + k_3(r_2 - r_3) + \\
 &\quad k_4(r_4 - r_2) + k_5(r_4 - r_3)]\} \quad (4b)
 \end{aligned}$$

$$\begin{aligned}
 &= (1/2\pi)^{15} \int \int \int \int \int \prod_{i=1}^5 dk_i \hat{f}(k_i) \delta(k_1 - k_3 - \\
 &\quad k_5) \delta(-k_2 + k_4 + k_5) \exp\{-i(-k_1 r_1 + k_2 r_1 + \\
 &\quad k_3 r_2 - k_4 r_2)\} \quad (4c)
 \end{aligned}$$

Thus

$$\hat{E}_1(k) = \int E_1(r_{12}) e^{ikr_{12}} dr_{12} \quad (5a)$$

$$\begin{aligned}
 &= (1/2\pi)^6 \int \int \int \int \int \prod_{i=1}^5 dk_i \hat{f}(k_i) \delta(k_3 - k_4 + \\
 &\quad k_2) \delta(k_4 + k_5 - k_2) \delta(k_1 - k_3 - k_5) \quad (5k)
 \end{aligned}$$

$$\begin{array}{ccc}
 & \begin{array}{c} \diagup \\ \diagdown \end{array} & \\
 (1/2\pi)^6 & \begin{array}{c} \diagup \\ \diagdown \end{array} & \\
 & \begin{array}{c} \diagdown \\ \diagup \end{array} &
 \end{array} \quad (5c)$$

and

$$\begin{array}{ccc}
 \begin{array}{c} \diagup \\ \diagdown \end{array} & = (1/2\pi)^6 \begin{array}{c} \diagup \\ \diagdown \end{array} & = \int \int \int dr_2 dr_3 dr_4 \times \\
 & & f(r_{12})f(r_{13})f(r_{14})f(r_{23})f(r_{24})f(r_{34}) \quad (6)
 \end{array}$$

Dixon and Hutchinson⁴ used both these relationships to check the accuracy of these calculations for potentials of the form r^{-m} where $4 \leq m \leq 25$ and found extremely good agreement for the independent paths of calculation. In the calculations performed here the topological relationship permits the calculation of \boxtimes . Following Henderson and Oden⁵ we can perform the angular integrations using the orthogonality relationships of associated Legendre polynomials and reduce the nine-dimensional integral to a three-dimensional one, i.e.

$$\begin{array}{ccc}
 \begin{array}{c} \diagup \\ \diagdown \end{array} & = 64\pi^3 \sum_{l=0}^{\infty} \int \int \int k_1^{2l} \hat{f}(k_1) k_2^{2l} \hat{f}(k_2) k_3^{2l} \hat{f}(k_3) \times \\
 & A_l(k_1, k_2) A_l(k_1, k_3) A_l(k_2, k_3) dk_1 dk_2 dk_3 \quad (7)
 \end{array}$$

where

$$A_l(k_i, k_j) = [(2l + 1)/2] \int_0^\pi P_l(\cos \theta_{ij}) (\sin \theta_{ij}) f(k_{ij}) d\theta_{ij} \quad (8)$$

The Fourier transforms were carried out using the fast Fourier transform algorithm with removal of the aliased peaks using 1024 mesh points. The interpolations were carried out using cubic splines and the numerical quadrature followed Simpson's rules with the function values tabulated at the necessary points and the accuracy on the integrals for $A_l(k_i, k_j)$ of 10^{-5} .

Although $\hat{f}(k)$ decays slowly and in fact appears in the integrand as

$$\left(\frac{k_1^2}{1 + k_1^2} \right) \left(\frac{k_2^2}{1 + k_2^2} \right) \left(\frac{k_3^2}{1 + k_3^2} \right) (4\pi)^3$$

TABLE I^a

k_{max}	NPT	R_{max}	\boxtimes	\boxminus
50.26	128	8.0	43.107	
47.12	150	10.0	43.048	
40.2	128	10.0	43.023	
39.27	150	12.0	43.010	
33.5	128	12.0	42.970	
62.83	200	10.0	43.073	
33.5	160	15.0	42.969	
59.95	229	12.0	43.063	55.144
50.27	192	12.0	43.048	

^a k_{max} is cut off in reciprocal space. R_{max} defined as in the step length in reciprocal space = π/R_{max} . NPT is number of quadrature points.

where the numerators arise from the remaining integration over spatial variables, the function $\hat{E}_1(k)$ decays through more than four decades in the spatial range used.

The results of these calculations are given in Table I. It is clear from the calculations that a conflict is arising between the need to pack many points in the region of maximum variation of $\hat{f}(k)$ which occurs at small k and the need to take a satisfactory account of the slowly decaying tail. Haga⁶ has made an estimate of the value of this graph of 51.164 which seems to be in fair agreement with the values obtained here. The values of the graph calculated with the same $k_{max} = 33.5$ appeared to be independent of whether a step length of $\pi/12$ or $\pi/15$ was used. This suggested that the step length of $\pi/12$ was sufficient to represent the function at low k so that step length was used in the later calculations. Extrapolation against $(1/k_{max})^m$ yields a limiting value of 43.091 for $m = 2.5$ but it was too time consuming to perform the calculation with more than 229 quadrature points. In order to provide a check of the calculation, we used the relationship

$$\begin{array}{ccc}
 \begin{array}{c} \diagup \\ \diagdown \end{array} & = 4\pi \int r^2 x \begin{array}{c} \diagup \\ \diagdown \end{array} x dr = 4\pi \int r^2 E_1(r) dr \quad (9a)
 \end{array}$$

$$= 4\pi \int r^2 dr \left(\frac{1}{2\pi} \right)^3 \int \hat{E}_1(k) e^{-ikr} dk \quad (9b)$$

This way both \boxtimes and \boxminus were calculated from the same graph. However \boxminus can be obtained accurately by an independent path and has a value of 55.122⁷ in comparison with the present calculation which yields 55.144. Consequently it may be assumed that $\boxtimes = 43.091$ is a good estimate of the graph. However this value does not produce sufficient change in either g_i or h_i predicted by Friedman and Krishnan to make them compatible with the experimental results.⁷

Acknowledgments. It is a pleasure to thank Professor H. L. Friedman for suggesting this project and for discussions during its implementation. We are grateful to the SRC for financial support and to CECAM for facilities.

References and Notes

- (1) H. L. Friedman and C. V. Krishnan, *J. Phys. Chem.*, **78**, 1927 (1974).
- (2) W. G. McMillan and J. E. Mayer, *J. Chem. Phys.*, **13**, 276 (1945).
- (3) R. R. Cassel and R. H. Wood, *J. Phys. Chem.*, **78**, 1924 (1974).
- (4) M. Dixon and P. Hutchinson, unpublished work.
- (5) D. Henderson and L. Oden, *Mol. Phys.*, **10**, 405 (1965); J. A. Barker and J. J. Monaghan, *J. Chem. Phys.*, **36**, 2564 (1962).
- (6) E. Haga, *J. Phys. Soc. Jpn.*, **8**, 714 (1953).
- (7) H. L. Friedman, private communication.

Expansion of the McDevit and Long Theory of Nonelectrolyte Activity Coefficients to a Consideration of Concentrated Aqueous Electrolyte Solutions

R. F. Cross*

University of Melbourne, Parkville, Victoria, Australia, 3052 and The Swinburne College of Technology, Hawthorn, Victoria, Australia, 3122
(Received November 25, 1974; Revised Manuscript Received May 19, 1975)

The McDevit and Long theory of nonelectrolyte activity coefficients in aqueous salt solutions has previously been developed only in its limiting form. In this paper the theory is expanded to a consideration of concentrated aqueous electrolyte solutions and is applied to the solutions of several nonpolar nonelectrolytes for which experimental data exist in the literature and for which a comparison can also be made with calculations based upon the statistical mechanical description of hard-sphere fluids. The alternate approaches are found to have similar success in prediction.

Introduction

The addition of a salt to a solution of a nonelectrolyte brings about a change in the activity coefficient of the nonelectrolyte and hence a change in its solubility. A knowledge and understanding of nonelectrolyte activity coefficients is therefore fundamental to any study of salt effects upon chemical or electrochemical processes. Bockris and Reddy¹ have pointed out the importance of both salting out (increase in nonelectrolyte activity coefficient and decrease in solubility) in many established processes in the chemical industry and Tiepel and Gubbins² have referred to the problem of the salting out of oxidant and fuels in the development of new electrochemical power sources. The magnitudes of activity coefficients of nonelectrolytes in salt solutions are therefore of very great interest on both practical and theoretical grounds.

In this paper the McDevit and Long theory of nonelectrolyte activity coefficients in aqueous salt solutions (previously only presented for determinations in limiting small concentrations of electrolyte) is expanded so that it may be applied to solutions of concentrated electrolyte solutions. Some calculations are done on systems containing nonpolar nonelectrolytes and the results compared with experiment and with calculations based upon the statistical mechanics of hard-sphere fluids.

Early attempts to calculate activity coefficients were based upon electrostatics (Debye and McAulay,³ Debye⁴) and generally failed to account for the high specificity of activity coefficients, both with respect to the nonelectrolyte and the salt. Subsequent developments of electrostatic theories were largely extensions or reformulations of the earlier theories. The exceptions being the work of Bockris, Bowler-Reed, and Kitchener,⁵ and of Conway, Desnoyers, and Smith.⁶ The former development⁵ was significant in that the role of specific interactions was first recognized. Nonelectrolyte activity coefficients were described as a balance between electrostatic salting out and salting in due to dispersion force interactions between the salt and the nonelectrolyte. Consequently the theory was able to predict the common form of salting in which previous electrostatic theories had failed to do. However, the order of magnitude of calculated activity coefficients was not correct. In contrast to previous electrostatic treatments, Conway, Des-

noyers, and Smith⁶ retained the later terms in the series expansion of the exponential energy term of the Debye theory. In addition, they allowed for the effect of ionic hydration upon the dielectric decrement. As the authors point out, previous electrostatic theories had enjoyed success that was perhaps unwarranted in view of the compensatory effects of neglect of hydration and of consideration of only the initial term of the series expansion. Unfortunately, this meant that the sounder theoretical treatment of Conway et al. was to yield little improvement in the prediction of nonelectrolyte activity coefficients in salt solutions.

In 1952, McDevit and Long⁷ published their theory, which was a correlation between the nonelectrolyte activity coefficient and the limiting values of bulk properties of the nonelectrolyte and of the salt solution at infinite dilution. Hence it was only possible to calculate the limiting values of the activity coefficient. However, the theory was able to predict (i) the wide spread of salt effects observed, (ii) the low salting out of Li^+ and H^+ and the correct cation and anion sequences (except in some cases where the effects of some salts are very similar) and, (iii) salting in where it was observed. For very small nonelectrolyte molecules (O_2 , H_2) the calculated salt effect was generally of the correct magnitude. However, for larger molecules the calculated salt effect was two to three times too large.^{7,9-12} Many criticisms of the theory have been based upon this discrepancy, a discrepancy which can be accounted for by a correction factor allowing for the nonzero distance of closest approach of ion and nonelectrolyte in solution.⁷ Other criticisms of the McDevit and Long approach have been to the usage of the somewhat nebulous intrinsic volume of the salt (the molar volume of the liquid salt at solution temperature) and to the inability of the theory (as presented) to calculate salt effects as a function of electrolyte concentration. This latter shortcoming is rectified below. In addition, Altshuller and Everson¹¹ have questioned the form of the McDevit and Long correction factor. However, with the exception of their activity coefficient data in solutions of iodide salts, the validity of which has been questioned in other places,¹³ their data on ethyl acetate support the form of the correction factor proposed by McDevit and Long. As well, Masterton and others^{14,15} have brought forward experimental data that seem difficult to correlate with the McDevit and Long theory. The significance of these results is uncertain as the subsidiary thermodynamic data necessary for a quantitative test are not available.

* Address correspondence to this author at The Swinburne College of Technology, Hawthorn, Victoria, Australia, 3122.

The most recent approach to the calculation of nonelectrolyte activity coefficients in salt solutions is based upon the exact formulation of the statistical mechanics of hard-sphere fluids,^{16a,b} in which particles obey a pairwise additive potential. As developed^{16c-f} (largely) by Pierotti and applied by Shoor and Gubbins,¹⁷ the solubility of a nonpolar gas in a fluid is calculated by the "scaled particle theory" (SPTh) from the summation of the Gibb's free energy terms associated with the change of the phase of the solute, the creation of a cavity in fluid (g^h) and the solute-solvent interactions (g^s), water dipole-solute induced-dipole, and all dispersion interactions being considered in g^s .

g^h is determined directly from the hard-sphere statistical mechanics. This raises three difficulties. (i) The assumption that all particles in solution have a "hard core" or, in other words, that the placement of a particle in a cavity of a given size in the solution does not alter the nature of the cavity. Apart from the problem posed in the selection of the correct hard-sphere diameters (to which the theory is understandably sensitive), there is the question of whether the particle placed in the created cavity can impose specific orientational restrictions upon neighboring particles in solution. In view of the highly polar nature of water and our current picture of solute-solvent interactions,¹⁸ the answer to this question must be yes.¹⁹ (ii) A related difficulty arises from the assumption that particles obey a pairwise additive potential. This seems most unlikely in aqueous solutions.²⁰ (iii) The approximation of a uniform distribution of particles in solution is likely to break down for large nonpolar solutes or bulky ions and also for polar solutes. In addition, (iv) the approximation is made that $g^s = e^s$ (the internal energy contribution to g^s). According to Pierotti this is reasonable, but Shoor and Gubbins have pointed out that while the pv^s term may safely be discarded at normal pressures, the approximation that $Ts^s \ll e^s$ is also likely to become less reasonable as the size of solute particles increase.

Shoor and Gubbins have found very good agreement between experiment and theory for several nonpolar gases in concentrated KOH solutions, while other SPTh calculations^{21,22} upon nonpolar solutes in aqueous solutions containing small ion salts have been less successful. In each study, agreement between experiment and theory can be seen to noticeably deteriorate with the increasing size of the solute or ion. Also as expected, the choice of the "correct" or appropriate ancillary data is a recurrent problem in these and similar calculations.^{2,17,21-23}

A further development based upon the statistical mechanics of hard-sphere fluids has been presented by Tjebel and Gubbins.^{24,2} The equations developed in this "perturbation theory" are similar to those of the SPTh but are free from approximation iv of the Pierotti approach since a Taylor series expansion is made about the Helmholtz free energy of a fluid mixture of hard spheres. Also, a temperature-dependent expression is used for the hard-sphere diameters of the particles. Calculated values of activity coefficients of nonpolar solutes are generally in good agreement with experiment and are slightly better than SPTh estimates, although subject to similar limitations with respect to the size and polarity of solutes.

Theory

McDevit and Long's expression for the activity coefficient of a nonelectrolyte in a salt solution at limiting, small concentrations of both nonelectrolyte and salt are based

upon a Taylor's expansion of the Helmholtz free energy of the solution around $V_0 = n_w V_w + n_s V_s$. V_w is the molar volume of water and V_s the molar volume of pure liquid salt at the temperature of the solution. The Helmholtz free energy after mixing the liquid salt and water is

$$A(V_0 + \Delta V^m) = A(V_0) + \left(\frac{dA}{dV}\right)_{T, V=V_0} \Delta V^m + \frac{1}{2} \left(\frac{d^2 A}{dV^2}\right)_{T, V=V_0} (\Delta V^m)^2 + \frac{1}{3!} \frac{d^3 A}{dV^3} (\Delta V^m)^3 + \dots$$

$\Delta V^m = n_s(\phi_s - V_s)$ and is the volume change upon mixing, ϕ_s being the apparent molar volume of the salt. McDevit and Long then introduce the identity $(dA/dV)_T = -p$ and the isothermal compressibility $(\beta = -(1/V)(dV/dp)_T)$, thus obtaining an expression in p , $1/\beta V$ and differentials of $1/\beta V$ with respect to V . An expression, analogous to the one thus obtained, but allowing for the introduction of an additional volume of nonelectrolyte (V_n) is then differentiated with respect to V_n at constant T and p . In the case of vanishingly small amounts of the nonelectrolyte, since $(dG/dV)_{T,p} = (dA/dV)_{T,p} + p$, the resultant expression is

$$\lim_{V_n \rightarrow 0} \left(\frac{dG}{dV_n}\right)_{T,p} = -\frac{1}{\beta V} \Delta V^m + \left[\frac{d}{dV} \left(\frac{1}{\beta V}\right)\right]_T \frac{(\Delta V^m)^2}{2} + \left[\frac{d^2}{dV^2} \left(\frac{1}{\beta V}\right)\right]_T \frac{(\Delta V^m)^3}{6} + \left[\frac{d^3}{dV^3} \left(\frac{1}{\beta V}\right)\right]_T \frac{(\Delta V^m)^4}{24} + \dots \quad (1)$$

The first derivative of $1/\beta V$ with respect to V may be expressed in terms of c_s as follows:

$$\frac{d}{dV} \left(\frac{1}{\beta V}\right)_T = \frac{1}{\beta} \left[\frac{d}{dV} \left(\frac{1}{V}\right)\right]_T + \frac{1}{V} \left[\frac{d}{dc_s} \left(\frac{1}{\beta}\right)\right]_T \frac{dc_s}{dV}$$

As $dc_s/dV = -c_s/V$

$$\frac{d}{dV} \left(\frac{1}{\beta V}\right)_T = -\frac{1}{V^2} \left\{ \frac{1}{\beta} + c_s \left[\frac{d}{dc_s} \left(\frac{1}{\beta}\right)\right]_T \right\} \quad (2)$$

Similarly

$$\frac{d^2}{dV^2} \left(\frac{1}{\beta V}\right)_T = \frac{1}{V^3} \left\{ \frac{2}{\beta} + 4c_s \left[\frac{d}{dc_s} \left(\frac{1}{\beta}\right)\right]_T + c_s^2 \left[\frac{d^2}{dc_s^2} \left(\frac{1}{\beta}\right)\right]_T \right\} \quad (3)$$

If we assume, as Long and McDevit did, that a neutral nonelectrolyte occupies the same molar volume when infinitely dilute in a salt solution (V_n^∞) as when both the nonelectrolyte and salt are infinitely dilute ($V_n^{\infty,\infty}$), $V_n = n_n V_n^\infty = n_n V_n^{\infty,\infty}$. This assumption is not correct, but reference to Table II (for example) shows that the error introduced in this approximation is only of the order of a few percent. The left hand side of eq 1 may then be written as

$$\lim_{V_n \rightarrow 0} \left\{ \frac{1}{V_n^{\infty,\infty}} \left(\frac{dG}{dn_n}\right)_{T,p} \right\} = \lim_{n_n \rightarrow 0} \left\{ \frac{2.303RT}{V_n^{\infty,\infty}} (\log f_n) \right\}$$

where f_n is the mole fraction activity coefficient of the nonelectrolyte. We may compensate for the approximation mentioned above by writing the left hand side of eq 1 as

$$\lim_{n_n \rightarrow 0} \left\{ \frac{2.303RT}{V_n^\infty} (\log f_n) \right\}$$

Using this expression in eq 1, combining eq 1-3, replacing ΔV^m with $n_s(\phi_s - V_s)$, and rearranging

$$\lim_{n_a \rightarrow 0} [\log f_a] = \frac{V_a^\infty c_s (V_s - \phi_s)}{2.303 RT} \left\{ \frac{1}{\beta} - \frac{c_s}{2} \left[\frac{1}{\beta} + c_s \frac{d}{dc_s} \left(\frac{1}{\beta} \right) \right] (V_s - \phi_s) - \frac{c_s^2}{6} \left[\frac{2}{\beta} + 4c_s \frac{d}{dc_s} \left(\frac{1}{\beta} \right) + c_s^2 \frac{d^2}{dc_s^2} \left(\frac{1}{\beta} \right) \right] (V_s - \phi_s)^2 - \dots \right\} \quad (4)$$

Gibson²⁵ has expressed the isothermal compressibility (β) of a salt solution at any externally applied pressure (P) and 25° in terms of the internal pressure of that solution (P_e). Where x_1 and x_2 are the weight fractions of water and salt respectively, ρ is the density of the solution, and v_s is the specific volume of the solid salt, the relationship is

$$\beta = \rho \left\{ \frac{0.13337x_1}{296.2 + P_e + P} - x_2 \frac{dv_s}{dP} \right\}$$

The pressures are expressed in $M N m^{-2}$. As dv_s/dP is negligibly small.²⁶

$$\frac{1}{\beta} = \frac{296.2 + P_e + P}{0.13337x_1\rho} \quad (5)$$

and from Gibson^{25,26}

$$P = Lc_1c_s \quad (6)$$

where L is a constant. Also

$$x_1 = c_1M_1/\rho \quad (7)$$

where M_1 is the molecular weight of water.

$$c_1 = \frac{10^3\rho - c_sM_s}{M_1} \quad (8)$$

and according to Root,²⁷ the density of certain aqueous salt solutions may be expressed as

$$\rho = \rho_0 + k_1c_s + k_2c_s^{3/2} \quad (9)$$

where k_1 and k_2 are constants and ρ_0 is the density of water. From eq 5-9, at atmospheric pressure

$$\frac{1}{\beta} = 7.50 \left[\frac{0.2963}{\rho_0 + k_1 - 10^{-3}M_s)c_s + c_s^{3/2}} + \frac{Lc_s}{M_1} \right] \quad (10)$$

$$\frac{d}{dc_s} \left(\frac{1}{\beta} \right) = 7.50 \left[- \frac{0.2963(k_1 + \frac{3}{2}k_2c_s^{1/2})}{(\rho_0 + k_1c_s + k_2c_s^{3/2})^2} + \frac{L}{M_1} \right] \quad (11)$$

$k_4 = k_1 - 10^{-3}M_s$, where M_s is the molecular weight of the salt.

$$\frac{d^2}{dc_s^2} \left(\frac{1}{\beta} \right) = \frac{2.222}{(\rho_0 + k_1c_s + k_2c_s^{3/2})^2} \times \left[\frac{2(k_1 + \frac{3}{2}k_2c_s^{1/2})}{\rho_0 + k_1c_s + k_2c_s^{3/2}} - \frac{3k_2}{4c_s^{1/2}} \right] \quad (12)$$

Values of $1/\beta$, $(d/dc_s)(1/\beta)$, and $(d^2/dc_s^2)(1/\beta)$ calculated from eq 10-12 are given in Table I for solutions of NaCl at several concentrations. A plot of $(\rho - \rho_0)/c_s$ vs. $c_s^{1/2}$ is linear, giving $k_1 = 5.75 \times 10^{-2}$ and $k_2 = -2.60 \times 10^{-3}$. From Gibson,²⁵ $L = 0.567 \text{ bar } M^{-2}$ for NaCl solutions. Even for quite large values of c_s , the terms involving the derivatives of $1/\beta$ in eq 4 will be negligible with respect to those involving $1/\beta$, thus yielding the final expression:

TABLE I: Relative Magnitudes of Terms Involving the Isothermal Compressibility (β)

c_{NaCl} , mol dm ⁻³	$1/\beta$, 10 ³ J ⁻¹ dm ³	(d/dc_s) (1/ β), 10 ³ J ⁻¹ dm ⁶ mol ⁻¹	(d^2/dc_s^2) (1/ β), 10 ³ J ⁻¹ dm ⁹ mol ⁻²
1	2440	0.244	0.00443
2	2700	0.247	0.00327
3	2990	0.250	0.00283
4	3290	0.253	0.00261
5	3560	0.255	0.00250

$$\lim_{n_a \rightarrow 0} [\log f_a] = \frac{V_a^\infty c_s (V_s - \phi_s)}{2.303 RT \beta} \times \left[1 - \frac{c_s}{2} (V_s - \phi_s) - \frac{c_s^2}{3} (V_s - \phi_s)^2 - \dots \right] \quad (13)$$

If \bar{r} is the radius of the average ion present in solution and r_n is the van der Waals radius of the nonelectrolyte, correcting eq 13 for the distance of closest approach of ion and nonelectrolyte wil. yield:

$$\lim_{n_a \rightarrow 0} [\log f_a] = \frac{V_a^\infty c_s (V_s - \phi_s)}{2.303 RT \beta} \times \left[1 - \frac{c_s}{2} (V_s - \phi_s) - \frac{c_s^2}{3} (V_s - \phi_s)^2 - \dots \right] \frac{\bar{r}}{\bar{r} + r_n} \quad (14)$$

As the various parameters in eq 5-9 are of similar magnitude for the other alkali halides and for the alkali hydroxides, eq 13 and 14 will also hold true in these cases.

Results

The systems chosen with which to test the above equations have been restricted to those for which comparison may be made with both measured values of the activity coefficients and estimates made according to the calculations based upon hard-sphere fluid statistical mechanics. A further limitation arises due to the ancillary thermodynamic data required.

In the McDevit and Long(McDL) approach, the most troublesome parameter is the intrinsic volume, V_s . Values vary appreciably, according to the method of estimation, and the $(V_s - \phi_s)$ term is typically only 10 to 25% of the magnitude of its component terms so that a 10% variation in V_s may well lead to a 100% variation in $\log f_n$. Hence considerable care is necessary in choosing values of V_s . Figure 1 shows several sets of V_s data for a range of salts. The scale on the abscissa was arranged by plotting the data of Scott (●)²⁸ vs. itself and then labeling these positions on the abscissa with the salt concerned. Certainly the nature of this plot will vary according to the set of V_s values chosen to set up this scale, but for the salts considered in this paper there is no significant variation. Scott's data were chosen in view of the fairly complete range of alkali halide salts contained, the absence of extreme V_s values, and the inclusion of V_s values for CsCl that are derived the true structure of the solid salt, as well as from the hypothetical rock salt structure. V_s from Lunden²⁹ in the case of NaClO₄ and NaNO₃ and from McDevit and Long⁷ in the case of KOH (assuming additivity of ionic contributions) have also been plotted against themselves. Choosing the data estimated by Scott (□)²⁸ using a different method,

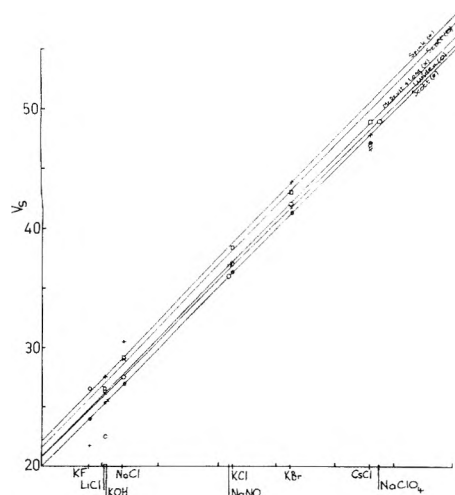


Figure 1. Plots of the intrinsic volumes (V_s) of electrolytes (see text) according to several sources: ●, Scott (ref 28); ×, McDevit and Long (ref 7); □, Scott (ref 28); ○, Lunden (ref 29); +, Spink (ref 30).

$V_s(\text{NaCl}) = 29.1 \text{ cm}^3 \text{ mol}^{-1}$. For KOH, the difference between the lines of best fit representing the Scott (□) and the McDevit and Long (×) values ($0.8 \text{ cm}^3 \text{ mol}^{-1}$) is added to the value obtained from McDevit and Long to give $V_s(\text{KOH}) = 26.3 \text{ cm}^3 \text{ mol}^{-1}$. Isothermal compressibility data for NaCl solutions were taken from Gibson²⁵ and for KOH solutions adiabatic compressibility data³¹ were converted according to ref 31, using density data from ref 32 and heat capacity measurements from ref 33. Apparent molar volumes were taken from ref 34 and 35 for NaCl and from ref 32 for KOH. As the nonelectrolyte molar volume term appearing in eq 13 and 14 was obtained as a value at infinite dilution of salt of virtue of a simplification, the more correct values which have been determined at finite concentrations of salt (V_n) have been used where possible. V_n values are given in Table II.

For the nonelectrolytes, the distance of closest approach, r_n , has been taken as the van der Waal's radius, where possible.⁴⁰ (H_2 , 1.2 Å; O_2 , 1.4 Å; C_6H_6 , 1.85 Å.) In the absence of an equivalent value for SF_6 , the radius corresponding to V_n (3.28 Å) has been used. Radii of the average ion present in solution, \bar{r} , are shown in Table III. (a) For the bare ions, crystallographic data have been taken from Shoor and Gubbins paper¹⁷ for KOH and from Desnoyers and Jolicoeur⁴¹ for NaCl (Goldschmidt radii). (b) Radii of the average hydrated ion, \bar{r}_h , have been calculated from individual radii of hydrated ions as determined from density measurements.⁶ These radii are the smaller of the two sets quoted by Conway, Desnoyers, and Smith,⁶ and correspond roughly to the number of waters of hydration described by Bockris and Saluja as the solvation number.⁴² The exception is ^-OH for which no value is given. In this case \bar{r}_h has been taken from Nightingale.⁴³

Table IV shows the relative magnitudes of the first three terms in the series in eq 13 and 14, for NaCl solutions. The relative orders of magnitude are the same for KOH solutions and other common salts. Clearly there is no point in considering the third and higher members of the series.

Figures 2–5 show the results of calculations of $\log f_n$ according to eq 14 using the radii of (a) the bare ions and (b) the hydrated ions. Experimental data are shown for comparison. So too are calculations based upon the statistical mechanics of hard-sphere fluids.

TABLE II: Nonelectrolyte Molar Volumes in Salt Solutions

Nonelectrolyte	Salt	c_s , mol dm ³	V_n , cm ³ mol ⁻¹	Ref
H_2	KOH	2.0	24.1	24
		5.0	22.4	24
O_2	KOH	2.0	29.0	24
		5.0	28.0	24
SF_6			89	36
C_6H_6			89.4	7 ^a

^a From the density of the pure liquid at 25°.

TABLE III: Radii of Average Ions Present in Solution

Electrolyte	Radius of average ion, Å	
	(a) unhydrated	(b) hydrated
NaCl	1.51	2.43
KOH	1.57	2.72

TABLE IV: Relative Magnitudes of Series Terms in Eq 13 and 14 for NaCl Solutions

Term	c_{NaCl}				
	1	2	3	4	5
1	1	1	1	1	1
$(c_s/2)(V_s - \phi_s)$	0.005	0.010	0.013	0.017	0.019
$(c_s^2/3)(V_s - \phi_s)^2$					0.001

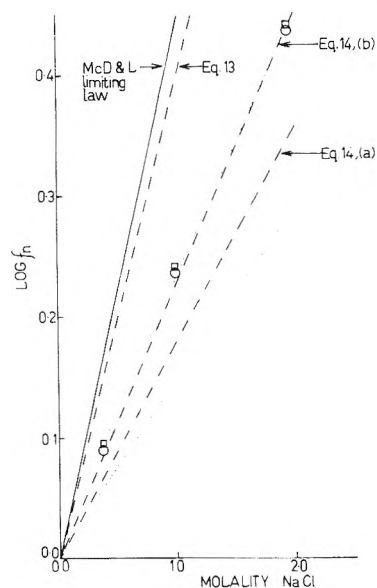


Figure 2. Plots of the logarithm of the rational activity coefficient (f_n) of benzene vs. the molality of NaCl, at 25°; □ (ref 7) and ○ (ref 23), experiment; ·····, alternate calculations SPT; ---, expanded McDevit and Long theory (see text); —, McDevit and Long limiting law (ref 7).

Discussion

Figure 2 concerns the salting out of benzene by NaCl solutions. Of the nonelectrolytes examined by Shoor and

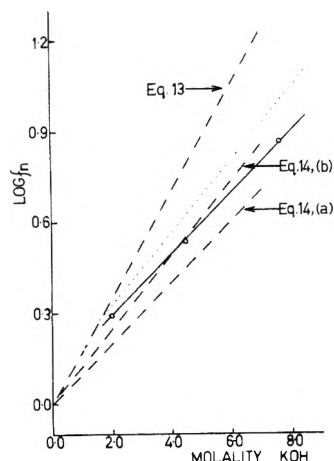


Figure 3. Plots of the logarithm of the rational activity coefficient (f_n) of hydrogen vs. molality of KOH, at 25°C: —○—, experiment (ref 17); SPTH (ref 17); ---, expanded McDevit and Long theory (see text).

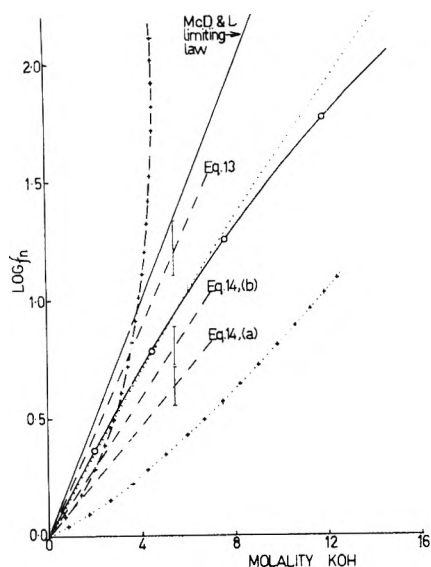


Figure 4. Plots of the logarithm of the rational activity coefficient (f_n) of oxygen vs. molality of KOH, at 25°C: —○—, experiment (ref 17); SPTH (ref 17); +-+, theory of Conway, Desnoyers, and Smith (ref 2); +...+, theory of Debye and McAulay (ref 2); ---, expanded McDevit and Long theory (see text); —, McDevit and Long limiting law (ref 7).

Gubbins¹⁷ in KOH solutions, H₂, O₂, and SF₆ were chosen in view of the accurate V_n data available (Figures 3–5).

In Figures 2 and 4 (the benzene–NaCl and O₂–KOH, respectively) the plot corresponding to McDL limiting expression⁷ for the salting constant (k_s) is shown. For these systems, the difference between the limiting expression and eq 13 is not as great as may be expected in either case as the increases in c_s and the series terms and the decrease in β largely offset the decrease in $(V_s - \phi_s)$. The sensitivity of the theory to the value of ϕ_s is shown in Figure 4 by the bars on the McDevit and Long plots. In this example, where strong salting out occurs, and $(V_s - \phi_s)$ is consequently large, a variation of only 1 cm³ mol⁻¹ (4%) in the value of V_s (26.3 cm³ mol⁻¹) still gives rise to the 11% change seen in log f_n . Nonetheless, for an uncorrected estimate of k_s giving rise to log f_n values about the same as those due to the Debye and McAulay theory, Tjepel and

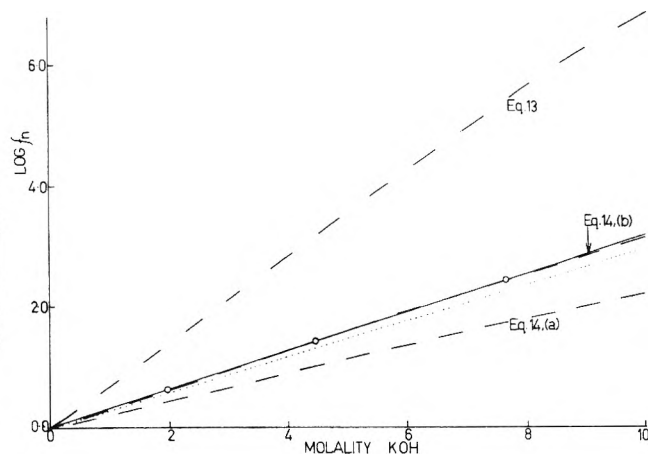


Figure 5. Plots of the logarithm of the rational activity coefficient (f_n) of SF₆ vs. molality of KOH, at 25°C: —○—, experiment (ref 17); theory of Tjepel and Gubbins (ref 2); --- expanded McDevit and Long theory (see text).

Gubbins² would have needed to use $V_s \approx 12$ cm³ mol⁻¹ for KOH. Such a value seems most unreasonable in view of the data available in the literature: 21.7 cm³ mol⁻¹,⁴⁴ 24.2 cm³ mol⁻¹ (15°),²⁸ and 25.5 cm³ mol⁻¹.⁷

Estimates of the salt effect of KOH on O₂ calculated by Tjepel and Gubbins² according to electrostatic theories (of Debye and McAulay and of Conway, Desnoyers, and Smith) have also been included in Figure 4. Clearly the electrostatic theories are least accurate in prediction, the Debye and McAulay approach being least accurate at all salt concentrations while the theory of Conway, Desnoyers, and Smith breaks down completely at moderately high salt concentrations.

As with estimates of k_s for small nonelectrolytes in solutions of salts from which strong salting out occurs,⁸ Figures 2–5 tend to indicate that there is no marked difference between the salt effects calculated for small and large nonelectrolytes according to the McDevit and Long approach.

It is obvious that estimates of log f_n using eq 13 are consistently too high for the systems examined, as is commonly the experience in applications of the McDL limiting expression for k_s . Equation 14, (a) used in conjunction with the radii of the unhydrated ions (crystallographic radii) lead to consistently low estimates whereas (b) the use of hydrated radii to define the distance of closest approach to ions give use to values of log f_n that are intermediate in magnitude and are generally in good quantitative agreement with experiment. Indeed, in the case of the H₂–KOH system agreement with experiment is far better than the SPTH estimate although for O₂–KOH the reverse is true. For C₆H₆–NaCl and SF₆–KOH, SPTH and eq 14, (b) give almost identical and good estimates. (The SPTH calculation for SF₆–KOH¹⁷ is not shown in Figure 5 but is virtually identical with eq 14 (b). Tjepel and Gubbins calculation according to their “perturbation theory”² is shown in Figure 5 and is less successful in this case.) Generally, it appears that the expanded McDL approach may give rise to good estimates of the activity coefficients of nonpolar nonelectrolytes in salt solutions, when corrected using the radii of hydrated ions⁵⁰ and the van der Waal’s radius of the nonelectrolyte to define the distance of closest approach.

Salting in systems have also been examined by Tjepel and Gubbins,² but without success. k_s is generally found to become less negative with increasing size of the alkane and sometimes also with increasing size of the tetraalkylammo-

nium ion present in solution; the opposite of that observed experimentally. In fact, the theory predicts salting out for *n*-butane in solutions of (*n*-C₄H₁₀)₄NBr. The system examined most closely was methane in (CH₃)₄NBr solutions. Tiepel and Gubbins have calculated a value of *k_s* according to the McDL limiting expression which is an order of magnitude larger than observed experimentally. Even allowing for a larger than usual uncertainty in *V_s* for this salt, literature ϕ_s ,^{46,47} *V_n*,²⁴ and β ⁴⁸ data for this system at the finite salt concentrations considered indicate that their estimate is probably too small. Whatever assumptions are made with respect to distances of closest approach, eq 13 and 14 seems incapable of dealing with this system. However, this particular system appears to be atypical inasmuch as other McDL applications to salting in^{7,10} yield *k_s* only 2–3 times too large, and consistently so. Taking $r((\text{CH}_3)_4\text{N}^+) = 2.70 \text{ \AA}$ ⁴⁹ and $r(\text{Br}^-) = 2.23 \text{ \AA}$ ⁶ gives $\bar{r}((\text{CH}_3)_4\text{NBr}) = 2.49 \text{ \AA}$. With the van der Waal's radius for benzene = 1.85 \AA ,⁴⁰ $\bar{r}/(\bar{r} + r_n) = 0.573$ and the experimental value of *k_s* for this system (approximately one-half *k_s* calculated by the McDL limiting expression) is well within the range of the corrected McDL approach. For benzene in solutions of the larger quaternary ammonium salts, the discrepancy is about 3 and the larger cations would lead to larger correction factors not smaller as required. Nevertheless, with the large uncertainty in *V_s* for these systems and the differences in experimental salting constants^{7,10} the McDL approach seems still to be reasonable. In addition, the radii of quaternary ammonium cations referred to in ref 41 give rise to molar volumes that seem to be more compatible with effective volumes occupied than with distances of closest approach. Setting $r((\text{CH}_3)_4\text{N}^+) = 2.70 \text{ \AA}$, the volume occupied by this ion is 85 cm³ (g ion)⁻¹ according to eq 11 of ref 49. *V_s* for the same ion is 73 cm³ (g ion)⁻¹ as calculated from eq 6 of ref 41. The intrinsic volume (*V_s*) takes in some of the free space between the ion and the solvent molecules. This indicates that distances of closest approach to the bulky R₄N⁺ ions may be less than the radii indicated in ref 41 and the correction factors subsequently smaller as required.

It may be concluded that, for nonpolar nonelectrolytes in solutions of small ions, the McDL approach and the SPTh (and related calculations) appear to be similarly accurate in predicting the nonelectrolyte activity coefficients. In solutions of large ion salts the McDL approach seems superior at this time. Of the SPTh, and particularly the more recent developments based upon the statistical mechanics of hard-sphere fluids, it must be said that this more fundamental approach has considerable appeal, especially in view of the success of the theories in some systems and the ability of the theory to calculate actual solubilities and a wide range of other thermodynamic properties. However, in the systems where it has been less successful and for systems involving polar molecules, the assumptions upon which the theories have operated until now are likely to be invalid. In these cases, the theories may require modification to the point of complexity at which their usefulness may be largely lost. Meanwhile, the McDL approach may prove to be a useful tool. This approach has considerable appeal for two reasons. First, the treatment requires no assumptions about the molecular distribution of particles in solution or the precise mathematical description of interactions between particles. It is based upon observable thermodynamic bulk properties. Hence it is likely that this approach may be equally successful for polar nonelectrolytes.

This will be the subject of a later communication. Secondly, the final equations of the expanded McDL approach are such that once a single nonelectrolyte-salt solution system has been considered, application to further nonelectrolytes in solutions of the same salt requires only knowledge of the molar volumes of the nonelectrolytes (and van der Waals radii for nonpolar nonelectrolytes). The major difficulty of the McDevit and Long approach lies in the assignment of values of the intrinsic volume.

Acknowledgment. The author wishes to thank Dr. E.H. Bode and The Swinburne College of Technology for the grant of partial release during which time some of this work was carried out.

References and Notes

- (1) J. O'M. Bockris and A. K. N. Reddy, "Modern Electrochemistry", Vol. 1, Plenum Press, New York, N.Y., 1970, p 164.
- (2) E. W. Tiepel and K. E. Gubbins, *Ind. Eng. Chem., Fundam.*, **12**, 18 (1973).
- (3) P. Debye and J. McAulay, *Phys. Z.*, **26**, 22 (1925).
- (4) P. Debye, *Z. Phys. Chem.*, **130**, 56 (1927).
- (5) J. O'M. Bockris, J. Bowler-Reed, and J. A. Kitchener, *Trans. Faraday Soc.*, **47**, 184 (1951).
- (6) B. E. Conway, J. E. Desnoyers, and A. C. Smith, *Phil. Trans. R. Soc., London, Ser. A*, **256** (1074), 389 (1964).
- (7) W. F. McDevit and F. A. Long, *J. Am. Chem. Soc.*, **74**, 1773 (1952).
- (8) F. A. Long and W. F. McDevit, *Chem. Rev.*, **51**, 119 (1952).
- (9) J. L. Lui and T. C. Huang, *Sci. Sinica*, **10**, 700 (1961).
- (10) N. C. Deno and C. H. Spink, *J. Phys. Chem.*, **67**, 1347 (1963).
- (11) A. P. Altshuller and H. E. Everson, *J. Am. Chem. Soc.*, **75**, 4823 (1953).
- (12) W. L. Masterton and T. P. Lee, *J. Phys. Chem.*, **74**, 1776 (1970).
- (13) S. Glasstone and A. Pound, *J. Chem. Soc.*, **127**, 2660 (1925).
- (14) W. L. Masterton and R. N. Schwartz, *J. Phys. Chem.*, **69**, 1546 (1965).
- (15) W. L. Masterton, T. P. Lee, and R. L. Boyington, *J. Phys. Chem.*, **73**, 2761 (1969).
- (16) (a) H. Reiss, H. L. Frish, and J. L. Lebowitz, *J. Chem. Phys.*, **31**, 369 (1959); (b) H. Reiss, H. L. Frish, E. Helfand and J. L. Lebowitz, *ibid.*, **32**, 119 (1960); (c) R. A. Pierotti, *J. Phys. Chem.*, **67**, 1840 (1963); (d) S. W. Mayer, *J. Chem. Phys.*, **38**, 1805 (1963); (e) R. A. Pierotti, *J. Phys. Chem.*, **69**, 281 (1965); (f) J. L. Lebowitz, E. Helfand, and E. Praestgaard, *J. Chem. Phys.*, **43**, 774 (1965).
- (17) S. K. Shoor and K. E. Gubbins, *J. Phys. Chem.*, **73**, 498 (1969).
- (18) See, for example, H. S. Frank and M. W. Evans, *J. Chem. Phys.*, **13**, 507 (1945).
- (19) F. H. Stillinger, *J. Solution Chem.*, **2**, 141 (1973).
- (20) H. S. Frank, *Z. Phys. Chem. (Leipzig)*, **228**, 364 (1965).
- (21) M. Lucas, *Bull. Soc. Chim. Fr.*, 2994 (1969).
- (22) W. L. Masterton and T. P. Lee, *J. Phys. Chem.*, **74**, 1776 (1970).
- (23) Y. L. Tien, M. Y. Schrier, and E. E. Schrier, *J. Phys. Chem.*, **78**, 165 (1974).
- (24) E. W. Tiepel and K. E. Gubbins, *J. Phys. Chem.*, **76**, 3044 (1972).
- (25) R. E. Gibson, *J. Am. Chem. Soc.*, **57**, 284 (1935).
- (26) R. E. Gibson, *J. Am. Chem. Soc.*, **56**, 4 (1934).
- (27) W. C. Root, *J. Am. Chem. Soc.*, **55**, 850 (1933).
- (28) A. F. Scott, *J. Phys. Chem.*, **35**, 3379 (1931).
- (29) B. Lunden, *Z. Phys. Chem. (Leipzig)*, **192**, 345 (1943).
- (30) C. H. Spink, Ph.D. Thesis, Pennsylvania State University, 1962.
- (31) D. S. Allam and W. H. Lee, *J. Chem. Soc. A*, 5 (1966).
- (32) G. Akerlof and P. Bender, *J. Am. Chem. Soc.*, **63**, 1085 (1941).
- (33) L. V. Puhkov, T. A. Baranova, and M. E. Lapidus, *J. Appl. Chem. USSR*, **43**, 463 (1970).
- (34) W. Geffcken, *Z. Phys. Chem. A*, **155**, 1 (1931).
- (35) F. Vaslow, *J. Phys. Chem.*, **70**, 2286 (1966).
- (36) Reference 37 gives a value of 101 cm³ for the partial molar volume (\bar{V}) of SF₆ in cyclohexane at 25°. However, \bar{V} for nonpolar solutes is usually less in water than in hydrocarbon solvents.³⁸ An alternate value of $\bar{V}(\text{SF}_6) = 77.7 \text{ cm}^3 \text{ mol}^{-1}$ may be obtained from the density of pure liquid SF₆ at -50.5°. As a larger volume would be occupied by SF₆ at 25° an averaged value of the two (89 cm³ mol⁻¹) has been taken.
- (37) R. G. Linford and J. H. Hildebrand, *Trans. Faraday Soc.*, **65**, 1470 (1969).
- (38) R. Battino and H. L. Clever, *Chem. Rev.*, **66**, 395 (1966).
- (39) "Handbook of Chemistry and Physics", 51st ed, The Chemical Rubber Co., Cleveland, Ohio, 1970–1971.
- (40) F. A. Cotton and G. Wilkinson, "Advanced Inorganic Chemistry", 1st ed, Interscience, New York, N.Y., 1962, p 104.
- (41) J. E. Desnoyers and C. Jolicoeur in "Modern Aspects of Electrochemistry", Vol. 5, J. O'M. Bockris and B. E. Conway, Ed., Plenum Press, New York, N.Y., 1969.
- (42) J. O'M. Bockris and P. P. S. Saluja, *J. Phys. Chem.*, **76**, 2140 (1972).
- (43) E. R. Nightingale, *J. Phys. Chem.*, **63**, 138 (1959).
- (44) J. Pavoda, *J. Chem. Phys.*, **40**, 691 (1964).
- (45) J. O'M. Bockris and P. P. S. Saluja, *J. Electrochem. Soc.*, **119**, 106C (1972).

- (46) Y. W. Wen and S. Saito, *J. Phys. Chem.*, **68**, 2639 (1964).
 (47) H. E. Wirth, *J. Phys. Chem.*, **71**, 2922 (1967).
 (48) S. Schiavo, B. Scrosati, and A. Tommasini, *Ric. Sci.*, **37**, 219 (1967).
 (49) W. L. Masterton, D. Eolocofsky, and T. P. Lee, *J. Phys. Chem.*, **75**, 2809 (1971).
 (50) The question of "What is the radius of an ion in solution?" is a vexed one; and not only because of the difficulty of precise definition and the uncertainty of the exact meaning of any value calculated from experimental data, or otherwise. There is also the problem of selecting the

value that is most appropriate for a particular application. In the present context, the distance of closest approach of a nonpolar nonelectrolyte to an ion seems best defined in terms of the size of an ion plus the very small number of tightly bound water molecules which could be described as "having lost their own degrees of translation freedom and have those of the ion".⁴⁵ Bockris and Saluja^{42,45} define this number of water molecules of the solvation number of an ion. A set of radii of hydrated ions approximately corresponding to this extent of hydration have been used.

Voltammetry of Rhodium-1,10-Phenanthroline Complexes

Gregory Kew, Kenneth Hanck, and Keith DeArmond*

Department of Chemistry, North Carolina State University, Raleigh, North Carolina 27607 (Received February 5, 1975)

Cyclic voltammetry data have been obtained for the tris- and bis(1,10-phenanthroline) (phen) complexes of rhodium(III) in acetonitrile. The basic reaction sequence involves four one-electron transfers and is analogous to that reported earlier for rhodium(III)-2,2'-bipyridyl (bpy) complexes. The first two-electron transfers are followed by chemical reactions; the rate of these reactions is considerably slower than in the bpy complexes. The third and fourth reduction steps occur through both a soluble and an adsorbed pathway. Addition of an electron to either $[\text{Rh}(\text{bpy})_2(\text{phen})]^{3+}$ or $[\text{Rh}(\text{bpy})(\text{phen})_2]^{3+}$ appears preferentially to involve the phen ligand. The role of delocalization in the electrochemistry of rhodium(III)- and ruthenium(II)-diimine complexes is also discussed.

Introduction

Electrochemical reduction of $[\text{Rh}(\text{bpy})_3]^{3+}$ occurs by an ECEC mechanism in which two successive one-electron transfers appear under a single peak at voltammetric scan rates below approximately 1–2 V/sec. Higher scan rates result in separation of the two reduction processes due to differences in kinetic influence of the reactions following each one-electron reduction.¹ The reduction of $[\text{Rh}(\text{bpy})_3]^{3+}$ in acetonitrile (AN) is thus unique since the $(\text{bpy})_3$ complexes of a number of other first and second transition series metals in acetonitrile undergo relatively straightforward successive one-electron transfers through the first three to five reduction steps.² (More complex behavior is found in aqueous solution³ and at very negative potentials in nonaqueous solvents.⁴)

Luminescence data for tris(bidentate)rhodium(III) complexes of both 2,2'-bipyridine and 1,10-phenanthroline imply relative independence of each bidentate ligand from others present.⁵ Voltammetric measurements on the tris-, bis-, and mono(bipyridine)rhodium(III) complexes seem consistent with such an interpretation.¹ Determination of the reduction mechanisms of $[\text{Rh}(\text{phen})_3]^{3+}$, $[\text{Rh}(\text{phen})_2(\text{bpy})]^{3+}$, and $[\text{Rh}(\text{bpy})_2(\text{phen})]^{3+}$ can furnish answers to the following questions. (a) What is the nature of the primary reductant orbital for these complexes? (b) Is the reduction mechanism determined for $[\text{Rh}(\text{bpy})_3]^{3+}$ a prototype for rhodium(III)-tris(diimine) complexes in acetonitrile?

Experimental Section

Materials. The acetonitrile (Fisher reagent grade and Eastman Spectro Grade) and tetraethylammonium per-

chlorate (TEAP) used as a base electrolyte (Eastman White Label) were further purified and dried by methods reported previously.¹ The complexes were synthesized using $\text{RhCl}_3 \cdot 3\text{H}_2\text{O}$ (Engelhard Industries), 2,2'-bipyridine (Aldrich Chemical Co.), and 1,10-phenanthroline (Aldrich Chemical Co.). All three were used as received. Preparation and chemical and spectral analysis of all Rh(III) complexes used in this study have been described elsewhere.^{5,6} Complexes containing Rh in lower valence states were obtained by methods paralleling those used for the analogous complexes involving bpy.⁷

Techniques. The apparatus employed was identical with that reported in a preceding study with the exception that a Princeton Applied Research (PAR) Model 173 Potentiostat/Galvanostat, employing positive feedback iR compensation, was used instead of a PAR Model 174 Polarographic Analyzer.¹ All potentials reported are vs. an aqueous saturated calomel electrode (SCE) connected to the electrochemical cell by a large-diameter agar-4% KCl salt bridge immersed in AN. Liquid-junction potentials were not determined. Voltammetric peaks were reproduced within ± 10 mV. All complexes were dissolved in AN which also contained TEAP as a base electrolyte (0.10 M in TEAP).

Several phenomena involving adsorption and precipitation of reduced species on the surface of the platinum test electrode were noted in the cyclic voltammetry of phen-containing Rh(III) complexes. For consistent observation of these phenomena extreme care must be taken to exclude oxygen. The electrochemical cell was enclosed in a well-flushed, dry glove bag; the test solution was deaerated for a minimum of 60 min with 99.995% pure nitrogen which had been passed through a Radox oxygen-removal catalyst and an AN scrubbing tower.

The platinum working electrode must be reproducibly cleaned and conditioned prior to each scan if reproducible voltammograms are to be obtained. Two conditioning procedures were used. The first will be designated procedure A and the second procedure B. In procedure A the Pt working electrode was immersed in concentrated nitric acid at room temperature for 1–2 min and then rinsed in deionized water for a similar period. After removal from water and drying, the electrode was immersed in a blank solution of AN-0.10 M TEAP for 1–2 min. The solvent was allowed to evaporate from the electrode upon removal from the blank solution. The electrode was then installed in the electrochemical cell and conditioned by applying a potential of -0.4 V vs. SCE for 15–30 sec until the cathodic current had decayed to a constant value. The potential was removed, the test solution stirred vigorously and allowed to become quiescent, the initial potential applied to the cell, and the recorded scan started a few seconds later. Procedure B is the same as A except prior to removing the potential of -0.4 V, several (10–15) cyclic scans of the test solution were performed at a scan rate of ca. 30 V/sec. Procedure A yields a Pt surface which reproducibly exhibits adsorption phenomena. Procedure B yields a Pt electrode whose surface activity has been greatly reduced by the adsorption-desorption which occurs during the conditioning scans.

Results and Discussion

Redox couples observed for the complex ions are designated by Roman numerals I–IV, increasing toward more negative potentials. For some complexes certain numerals are omitted from the series to emphasize better and to designate uniformly electron transfers thought to involve identical species. In other instances waves which appear to arise from overlap of waves due to two distinct processes are designated by a sum of roman numerals, e.g., I + II.

Voltammetry of Rh^{III} -phen Complexes. Cyclic voltammograms of $[Rh(phen)_3]^{3+}$ are seen in Figures 1–3. The relationship between various waves may be seen by altering the time at which potential scan was reversed while holding scan rate constant (Figure 1). Figure 2 illustrates all waves due to nonadsorbed species in the same potential range as in Figure 1. Figure 3a shows the effect of varying scan rate when the potential range covered is similar to that in Figure 1b. Figure 3b–f illustrates the effect of varying scan rate over a constant potential range. Data from Figures 1–3 are found in Table I.

The cyclic voltammograms for $[Rh(phen)_2Cl_2]^+$ shown in Figures 4–6 are exactly analogous to those for the tris species in Figures 1–3, respectively. Comparisons and discussion are found below and corresponding data are found in Table II.

A redox couple appearing at $E_{1/2} = +0.9$ V vs. aqueous SCE for $[Rh(phen)_2Cl_2]^+$ has not been examined in detail as part of the present study since the tris species do not undergo a parallel electron transfer. Some data are presented in Table II where this process is designated "0" rather than where the series of couples designated by roman numerals.

An aqueous suspension of $[Rh(phen)_2Cl_2]ClO_4$ was treated with $NaBH_4$ yielding a black solid which was isolated and dried. The solid was redissolved in AN-0.10 M TEAP and a cyclic voltammogram obtained (Figure 7a). Figure 7b was obtained from an AN solution initially containing $[Rh(phen)_2Cl_2]^+$ to which a small quantity of solid $NaBH_4$ was added. (See Table III.)

To ascertain the role of mono(phenanthroline) com-

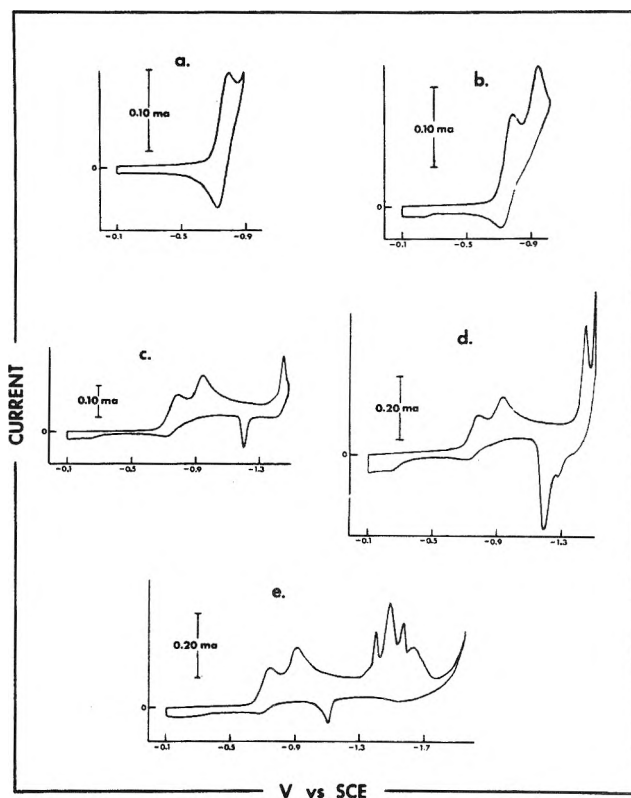


Figure 1. Cyclic voltammograms of $[Rh(phen)_3]^{3+}$, 5.90×10^{-4} M; $v = 0.10$ V/sec; electrode conditioning A.

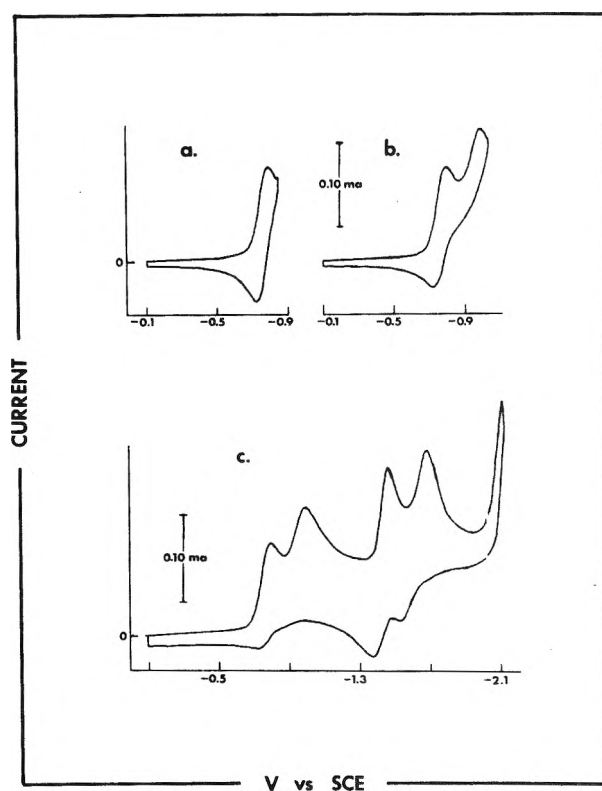


Figure 2. Cyclic voltammograms of $[Rh(phen)_3]^{3+}$, 4.90×10^{-4} M; $v = 0.10$ V/sec; electrode conditioning B.

plexes in the electron-transfer sequence of the bis- and tris(phenanthroline) complexes, $(phenH)[Rh(phen)Cl_4]$ was synthesized by literature methods.^{6b} Synthesis, purifica-

TABLE I: Examples of Variation in E_p with Change in v for $[\text{Rh}(\text{phen})_3]^{3+}$ ^{a, b}

v	$(E_{pc})_I$	$(E_{pa})_I$	$(E_{pc})_{II}$	$(E_{pc})_{III-P}$	$(E_{pa})_{III-R}$	$(E_{pc})_{III}$	$(E_{pa})_{III}$	$(E_{pc})_{IV-R}$	$(E_{pc})_{IV}$	$(E_{pa})_{IV}$
0.100	0.791	0.727	0.963	A. $5.90 \times 10^{-4} M$ (Figure 1e) ^c				1.573	1.635	
0.100	0.787	0.710	0.930	B. $4.50 \times 10^{-4} M$ (Figure 2c) ^c			1.452	1.373	1.670	1.540
0.147	0.780	0.720	0.966	C. $5.90 \times 10^{-4} M$ (Figure 3b-f) ^d				1.581	1.633	1.581
0.987	0.788	0.724	0.999	1.465	1.116	1.553?		1.553?	1.649	1.602
9.39	0.797	0.711	1.030		1.255	1.507			1.679	1.597
31.6	0.799	0.699	1.062	1.228	1.214	1.538			1.688	1.574
89.2	0.826	0.697	1.108	1.297	1.234	1.598			1.698	1.548

^a Results for complex in 0.10 M TEAP-AN solutions at a Pt electrode. ^b v in V/sec; E_p in -V vs. aqueous SCE. ^c Data obtained with PAR 174 potentiostat; no positive iR compensation. ^d Data obtained with PAR 173 potentiostat; positive iR compensation.

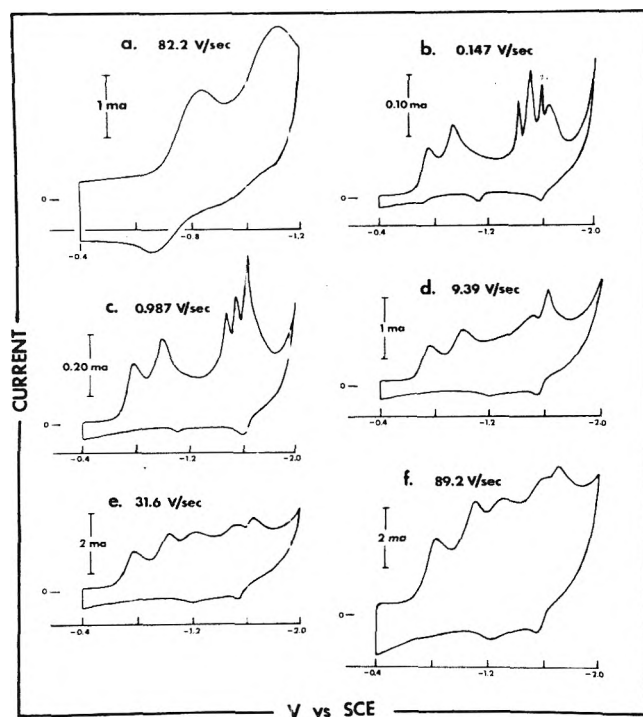


Figure 3. Cyclic voltammograms of $[\text{Rh}(\text{phen})_3]^{3+}$ as a function of voltage sweep rate, $5.90 \times 10^{-4} M$; electrode conditioning A.

tion, and voltammetry of this complex in polar solvents were hampered by the facile ligand-exchange reaction resulting in the bis species $[\text{Rh}(\text{phen})_2\text{Cl}_2]^+$. Indeed, under the experimental conditions of this study, the voltammeters of AN solutions to which the solid mono(phenanthroline) compound was added were essentially identical with those of the $[\text{Rh}(\text{phen})_2\text{Cl}_2]^+$ species, therefore it was concluded that the mono(phenanthroline) species did not contribute to the voltammograms of the other phen complexes.

Electron-Transfer Sequence for $E > -1.1$ V. $[E_{pa} - E_{pc}]_I = 64$ mV (at $v = 0.10$ V/sec) for $[\text{Rh}(\text{phen})_3]^{3+}$ (Figure 1a), so it appears that redox couple I is electrochemically reversible but is followed by a slow chemical reaction. The presence of a following reaction is shown by a marked decrease in $(i_{pa})_I$ with increasing elapsed time before potential scan reversal (e.g., Figure 1e). Since the main structural difference between $[\text{Rh}(\text{phen})_3]^{3+}$ and $[\text{Rh}(\text{phen})_2\text{Cl}_2]^+$ is the additional phen ligand of the tris

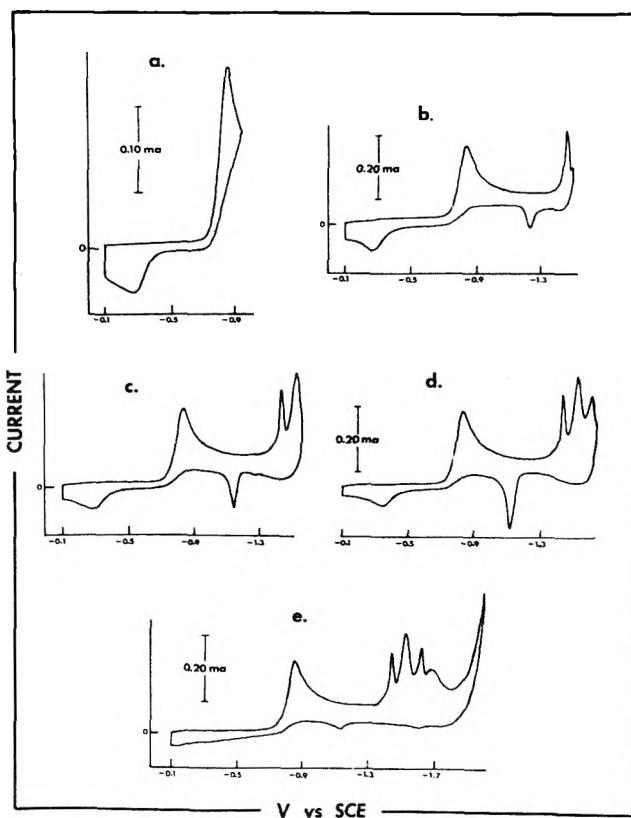


Figure 4. Cyclic voltammograms of $[\text{Rh}(\text{phen})_2\text{Cl}_2]^+$, saturated solution; $v = 0.10$ V/sec; electrode conditioning A.

compound and since voltammograms of the bis and tris complexes differ only by lack of a discrete redox couple of $E_{1/2} = -0.75$ V in the bis case, the chemical reaction following reduction I is probably substitution of one or more solvent molecules for a phen ligand. The rate constant of the following reaction was found to be $0.12 \pm 0.04 \text{ sec}^{-1}$ using a method⁸ based on variation of (i_{pc}/i_{pa}) with sweep rate.

$[E_{(p/2)c} - E_{pc}]_{II} = 58$ mV (at $v = 0.10$ V/sec) for $[\text{Rh}(\text{phen})_3]^{3+}$; no corresponding oxidation wave is detectable at scan rates up to 200 V/sec. Redox couple II therefore appears to involve one electron and to be followed by a very fast chemical reaction. No oxidation wave may be observed corresponding to the least negative reduction for

TABLE II: Examples of Variation in E_p with Change in v for $[\text{Rh}(\text{phen})_2\text{Cl}_2]^+$ ^{a, b}

v	$(E_{pc})_0$	$(E_{pa})_0$	$(E_{pc})_{I+II}$	$(E_{pc})_{III-P}$	$(E_{pa})_{III-R}$	$(E_{pc})_{III}$	$(E_{pa})_{III}$	$(E_{pc})_{IV-R}$	$(E_{pc})_{IV}$	$(E_{pa})_{IV}$
A. Figure 4e ^c										
0.100			0.822	1.422	1.115	1.503		1.600	1.658	1.59
B. Figure 5b ^c										
0.100			0.855			1.453	1.380		1.670	1.532
C. Figures 6b-f ^d										
0.147	+0.851	+0.971	0.825	1.428	1.123	1.515		1.612	1.670	1.605
0.989	+0.821	+1.008	0.874	1.451	1.224	1.513		? — 1.635 — ?		1.590
9.39	+0.777	+1.049	0.924		1.247	1.574			1.673	1.584
31.6	+0.707	+1.077	0.952	1.286	1.249	1.557			1.689	1.563
89.2	+0.677	+1.176	1.008	1.344	1.214	1.618			1.743	1.525

^a Results for saturated solutions of $[\text{Rh}(\text{phen})_2\text{Cl}_2]^+$ in 0.10 M TEAP-AN at a Pt electrode. ^b v in V/sec; E_p in -V vs. aqueous SCE, unless sign given. ^c Data obtained with PAR 174 potentiostat; no positive iR compensation. ^d Data obtained with PAR 173 potentiostat; positive iR compensation.

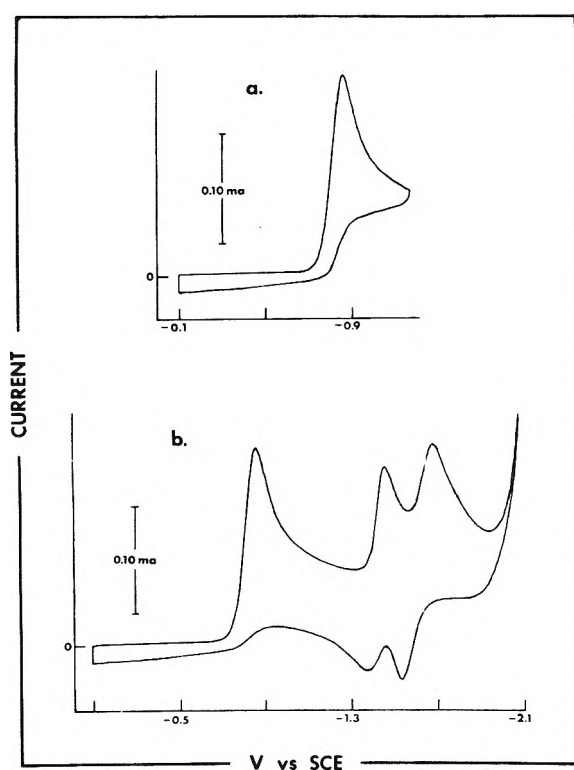


Figure 5. Cyclic voltammograms of $[\text{Rh}(\text{phen})_2\text{Cl}_2]^+$, saturated solution; $v = 0.10$ V/sec; electrode conditioning B.

$[\text{Rh}(\text{phen})_2\text{Cl}_2]^+$ up to 200 V/sec. Overall, the charge transfers and following reaction for both $[\text{Rh}(\text{phen})_3]^{3+}$ and $[\text{Rh}(\text{phen})_2\text{Cl}_2]^+$ starting materials at $E > -1.1$ V seem to involve reduction to a nominally Rh(I) species and ligand exchange at two coordination sites. Thereafter, the species predicted to exist for both is $[\text{Rh}(\text{phen})_2]^+$. Comparison of Figures 2, 5, and 7 tends to support the prediction.

The height and slope of the least negative reduction wave for $[\text{Rh}(\text{phen})_2\text{Cl}_2]^+$ are consistent with an ECEC process as observed for $[\text{Rh}(\text{bpy})_2\text{Cl}_2]^+$ and explained in detail earlier.¹ The peak potential of this wave will therefore be referred to as $(E_{pc})_{I+II}$, the subscript I + II indicating that two distinct electron transfers (each followed by a chemical reaction involving monodentate ligand loss) are actually involved.

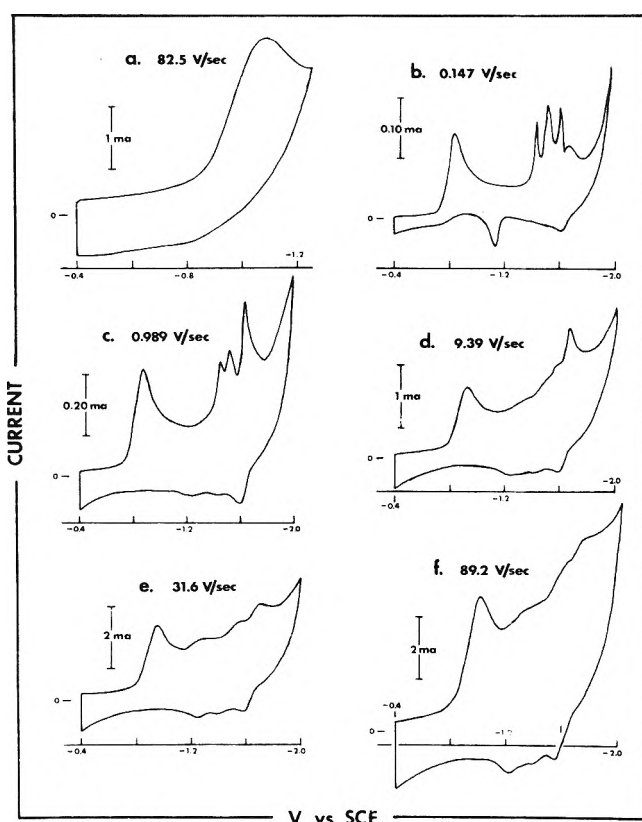


Figure 6. Cyclic voltammograms of $[\text{Rh}(\text{phen})_2\text{Cl}_2]^+$ as a function of voltage sweep rate, saturated solution; electrode conditioning A.

Thus it appears that the fundamental electron transfers and following chemical reactions of the Rh-phen complexes for the region positive of -1.1 V, during a single cyclic scan, exactly parallel those set forth earlier for the Rh-bpy analogs.

Shown in Figure 8 are multiple-cyclic voltammograms for the starting materials $[\text{Rh}(\text{phen})_3]^{3+}$, $[\text{Rh}(\text{phen})_2\text{Cl}_2]^+$, and $[\text{Rh}(\text{bpy})_2(\text{phen})]^{3+}$. The working electrode surface used in obtaining these voltammograms was freshly cleaned and conditioned at -0.4 V just before the first scan by procedure A described earlier. Waves appearing during most of the first cycle have been discussed in preceding sections. However, a small anodic wave appearing at ap-

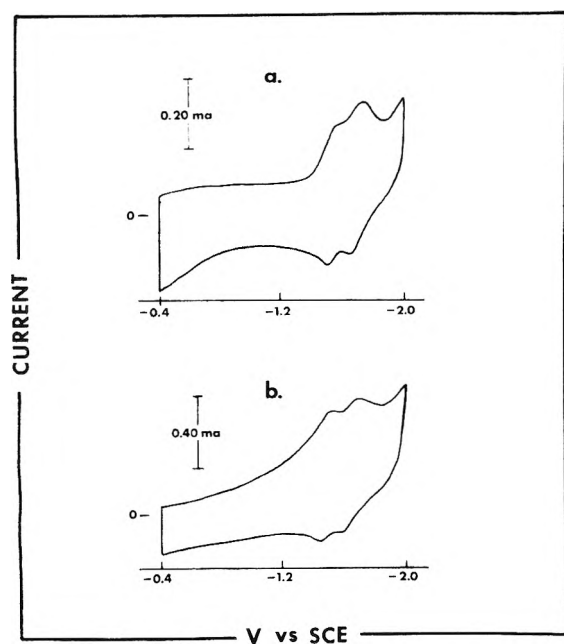


Figure 7. Cyclic voltammograms of $[\text{Rh}(\text{phen})_2]^+$; $\nu = 9.35$ V/sec; electrode conditioning B.

TABLE III: Peak Potentials for Solutions Containing Reduced $[\text{Rh}(\text{phen})_2\text{Cl}_2]^+$ ^a

ν	$(E_{pc})_{\text{III-P}}$	$(E_{pc})_{\text{III}}$	$(E_{pc})_{\text{IV}}$	$(E_{pa})_{\text{IV}}$
A. Figure 7a				
9.35	1.45	1.53	1.70	1.59
B. Figure 7b				
9.35	1.44	1.53	1.70	1.60

^a ν in V/sec; E_p in -V vs. aqueous SCE.

proximately -0.3 V on the first scan has not. This wave does not appear unless an appreciable amount of reduction II has occurred (compare Figure 1a and b). The wave is of very low magnitude unless potential scan is reversed soon after exceeding $(E_{pc})_{\text{II}}$. On the second and succeeding scans the anodic wave at approximately -0.3 V is found to have a corresponding reduction wave. As the amount of material undergoing these electron transfers increases with successive scans, the anodic and cathodic waves can be further resolved to the extent that two anodic and two cathodic waves may be distinguished. These waves are not well resolved but seem to be "normal" redox couples involving dissolved species rather than the characteristic, symmetrical "spikes" seen at 0.10 V/sec for charge transfers involving adsorbed species.⁹

Because the anodic wave at approximately -0.3 V appears only if reduction II and the fast following chemical reaction have occurred, some waves positive of -0.6 V probably arise from charge transfer to $[\text{Rh}(\text{phen})_2]^+$ or $[\text{Rh}(\text{phen})(\text{bpy})]^+$. It is possible that the two redox couples arise from successive one-electron transfers to the species above. However, further study will be necessary to confirm this or to clarify what other species are involved.

Electron-Transfer Sequence for $E < -1.1$ V. The ECEC mechanism demonstrated previously for $[\text{Rh}(\text{bpy})_3]^{3+}$ and $[\text{Rh}(\text{bpy})_2\text{Cl}_2]^+$ complexes leads to identical electroactive species for both materials in the region from -1.1 to -2.0

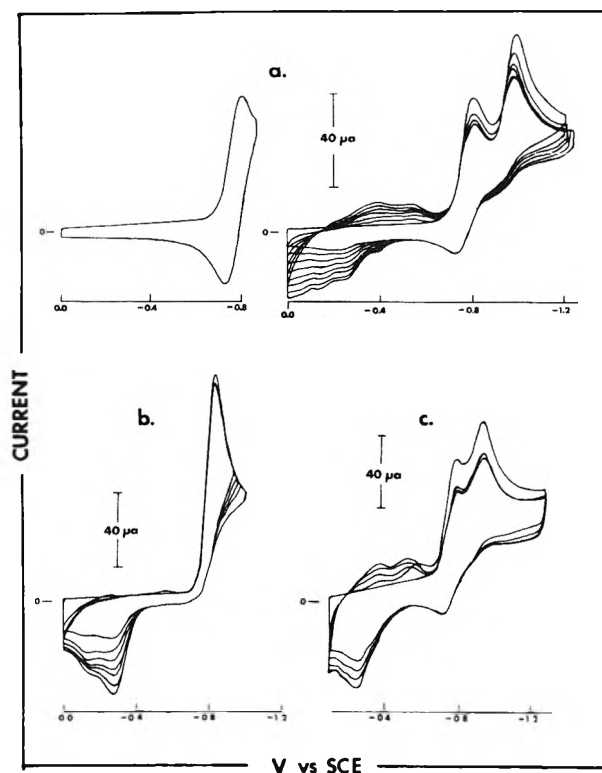


Figure 8. Multiple-cyclic voltammograms at $\nu = 0.10$ V/sec: (a) $[\text{Rh}(\text{phen})_3]^{3+}$, 3.63×10^{-4} M; (b) $[\text{Rh}(\text{phen})_2\text{Cl}_2]^+$, $\sim 5 \times 10^{-4}$ M; (c) $[\text{Rh}(\text{bpy})_2(\text{phen})]^{3+}$, 5.47×10^{-4} M.

V. Examination and comparison of Figures 1–6 reveals a similar correspondence in the number, peak potential, and potential variation with scan rate for waves of the starting materials $[\text{Rh}(\text{phen})_3]^{3+}$ and $[\text{Rh}(\text{phen})_2\text{Cl}_2]^+$. If the cathode is "precoated" by a number of fast cyclic scans, electrode conditioning B, the voltammograms obtained from either $[\text{Rh}(\text{phen})_3]^{3+}$ or $[\text{Rh}(\text{phen})_2\text{Cl}_2]^+$ in the range from -1.1 to -2.0 V closely resemble those found for $[\text{Rh}(\text{phen})_2]^+$ on a similar electrode surface (Figure 7).

The additional waves present in voltammograms of phen-containing complexes for $E < -1.1$ V, using a freshly cleaned electrode, were difficult to reproduce exactly but were always seen when electrode conditioning A was used. A detailed study of these waves was not carried out. Although several models were examined we shall discuss only the reaction scheme which best fits the experimental data.

The peak at -1.41 V (Table IC) is symmetrical and shifts in a positive direction as sweep rate increases. This peak is designated $(E_{pc})_{\text{III-P}}$ because it involves the transfer of the third electron; the P subscript indicates that the product of the reduction is adsorbed.

The peak at -1.49 V, $(E_{pc})_{\text{III}}$, is seen when either electrode-conditioning procedure is used; narrower half-widths are observed at slow sweep rates than at faster ones. Controlled-potential electrolysis of $[\text{Rh}(\text{phen})_3]^{3+}$ at -1.5 V produced large quantities of a black, paramagnetic solid. Electron spin resonance studies of this material are under way and will be reported later; it is clear, however, that the product of the reduction is of limited solubility in acetonitrile.

The species $[\text{Rh}(\text{phen})_2]^0$ is produced as a soluble entity until the solvent near the electrode has become saturated; $[\text{Rh}(\text{phen})_2]^0$ then precipitates onto the electrode. The quantity of $[\text{Rh}(\text{phen})_2]^0$ deposited will depend on several

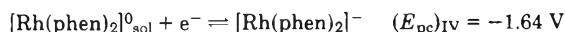
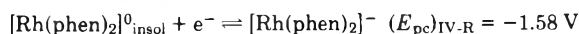
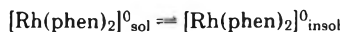
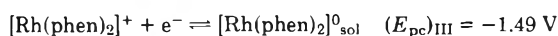
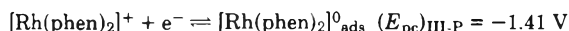
factors including the rate of nucleation, magnitude of the solubility product, and the rate at which $[\text{Rh}(\text{phen})_2]^0$ diffuses into the bulk of solution.

The spike at -1.58 V, $(E_{\text{pc}})_{\text{IV-R}}$, is observed only at slow sweep rates. Its potential is too positive to involve an adsorbed Rh(0) species. We have interpreted this peak to be the further reduction of the insoluble fraction of $[\text{Rh}(\text{phen})_2]^0$ produced at ~ -1.5 V. At sweep rates greater than ~ 1 V/sec an insignificant amount of $[\text{Rh}(\text{phen})_2]^0$ precipitates onto the electrode; consequently the peak at -1.58 V disappears.

The peak at -1.64 V, $(E_{\text{pc}})_{\text{IV}}$, is seen when either electrode conditioning is used; it results from the reduction of soluble $[\text{Rh}(\text{phen})_2]^0$ to $[\text{Rh}(\text{phen})_2]^-$.

Further reduction of adsorbed $[\text{Rh}(\text{phen})_2]^0$ is not observed prior to the reduction of the supporting electrolyte. The strength of the interaction between $[\text{Rh}(\text{phen})_2]^0$ and the Pt electrode suggests the presence of a chemical bond between the electrode and the complex. The ease of reduction to $[\text{Rh}(\text{phen})_2]^-$ is $[\text{Rh}(\text{phen})_2]_{\text{insol}}^0 > [\text{Rh}(\text{phen})_2]_{\text{sol}}^0 \gg [\text{Rh}(\text{phen})_2]_{\text{ads}}^0$.

A reaction sequence summarizing the behavior of $[\text{Rh}(\text{phen})_2]^+$ is shown as follows (abbreviations: sol, soluble; insol, insoluble; ads, adsorbed).



For both $[\text{Rh}(\text{phen})_3]^{3+}$ and $[\text{Rh}(\text{phen})_2\text{Cl}_2]^+$, the corresponding series of oxidations are less clearly resolved than the reductions in this region. The peaks at -1.58 and -0.72 V are seen when either electrode conditioning is used and result from the oxidation of $[\text{Rh}(\text{phen})_2]^-$ to $[\text{Rh}(\text{phen})_2]^0$ and the oxidation of a Rh(II) species (probably $[\text{Rh}(\text{phen})_2(\text{AN})_2]^{2+}$) to a Rh(III) species (probably $[\text{Rh}(\text{phen})_2(\text{AN})_2]^{3+}$). The sharp oxidation peak observed at -1.11 V (Figures 1-4) has a shape and sweep rate dependence consistent with the oxidation of $[\text{Rh}(\text{phen})_2]_{\text{ads}}^0$ to $[\text{Rh}(\text{phen})_2]^+$; the fact that the "desorption" of $[\text{Rh}(\text{phen})_2]_{\text{ads}}^0$ occurs nearly 0.5 V positive of the "adsorption" peak attests to the strength of the Pt- $[\text{Rh}(\text{phen})_2]^0$ interaction.

Voltammetry of Mixed-Ligand Complexes. Two modes of behavior seem possible for the mixed-ligand tris complexes. First, the presence of a relatively independent phen ligand in a tris complex containing both bpy and phen could lead to preferential electron transfer to phen only, at an electrode potential characteristic of $[\text{Rh}(\text{phen})_3]^{3+}$. A second possibility is that a combination of factors such as ionic charge and geometry might give reduction peak potentials showing a gradual shift from those of $[\text{Rh}(\text{bpy})_3]^{3+}$ to those of $[\text{Rh}(\text{phen})_3]^{3+}$ with increase in the ratio of phen to bpy. Peak overlaps might produce a similar result. Further, a triply charged ion in a high dielectric constant solvent such as AN should carry along a substantial "solvation sphere" tending to moderate the influence of disparate ligands.

Cyclic voltammograms of the ions $[\text{Rh}(\text{phen})_2(\text{bpy})]^{3+}$, $[\text{Rh}(\text{bpy})_2(\text{phen})]^{3+}$ and $[\text{Rh}(\text{bpy})_3]^{3+}$ are seen in Figure 9. Both the tris(bipyridine)- and tris(phenanthroline)rhodium(III) complexes undergo essentially the same reduction

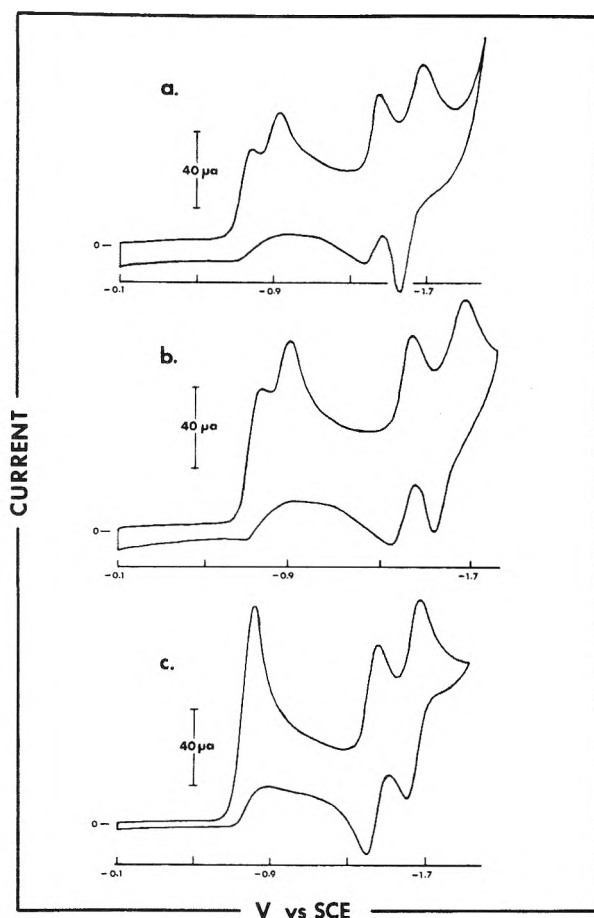


Figure 9. Cyclic voltammograms at $v = 0.10$ V/sec: (a) $[\text{Rh}(\text{phen})_2(\text{bpy})]^{3+}$, 4.53×10^{-4} M; (b) $[\text{Rh}(\text{bpy})_2(\text{phen})]^{3+}$, 5.47×10^{-4} M; (c) $[\text{Rh}(\text{bpy})_3]^{3+}$, 6.27×10^{-4} M; electrode conditioning B.

sequence on a cyclic voltammetry time scale so the overall resemblance of voltammograms for $[\text{Rh}(\text{phen})_2(\text{bpy})]^{3+}$ is not surprising. $(E_{\text{pc}})_{\text{I}}$ and $(E_{\text{pc}})_{\text{II}}$ prove to be largely independent of the ratio of phen to bpy. That is, so long as one or more phen ligands are present, $(E_{\text{pc}})_{\text{I}}$ and $(E_{\text{pc}})_{\text{II}}$ values are essentially identical with those of $[\text{Rh}(\text{phen})_3]^{3+}$. Data illustrating this point have been collected in Table IV. Thus the amount of interaction of each 1,10-phenanthroline ligand with other ligands containing large ring systems seems to be small.

Recall that only phen-containing complexes exhibit strong adsorption-type phenomena, though adsorption processes are not directly known to affect reduction waves I and II. The rate of ionic rotation in the vicinity of the platinum electrode surface is expected to be high relative to diffusion rate of the ions to the electrode. Consequently the ions are easily able to assume an orientation placing any phen ligands present closest to the electrode before charge transfer occurs. A "driving force" for this could be lowered system free energy when ions are weakly adsorbed on the platinum surface. A less negative potential is required for reduction of phen-containing complexes, but in the absence of any adsorption this should not favor orientations with phen closest to the electrode over those with bpy closest. In summary, preferential electron transfer to largely independent phen ligands indirectly suggests weak adsorption phenomena may be involved in redox couple I.

Interaction between the platinum surface and phen may be localized in the bond between the 5 and 6 positions of

TABLE IV: E_p for Redox Couples I and II of Tris, Mixed-Ligand Complexes^{a,b}

Ion	Molarity $\times 10^4$	$(E_{pc})_I$	$(E_{pa})_I$	$(E_{pc})_{II}$
$[\text{Rh}(\text{phen})_2(\text{bpy})]^{3+}$	4.53	0.785	0.711	0.932
$[\text{Rh}(\text{bpy})_2(\text{phen})]^{3+}$	5.47	0.795	0.715	0.937
$[\text{Rh}(\text{phen})_3]^{3+}$	4.90	0.793	0.720	0.932

^a Results for complex ions in 0.10 M TEAP-AN solutions at a Pt electrode. ^b $v = 0.10$ V/sec; E_p in -V vs. aqueous SCE.

the 1,10-phenanthroline ring system in accordance with one of the previously described general models for adsorption of doubly bonded systems on platinum.¹¹ Independent studies have suggested the 5-6 position bond may act more like an isolated double bond¹² than would normally be expected for such an aromatic fused-ring system.

Waves for nonadsorbed species seen in the region -1.3 to -2.0 V vs. SCE are, within experimental error, identical for the ions resulting from reduction of all four tris Rh(III) complexes. Differences between the highest unfilled orbitals of $[\text{Rh}(\text{phen})_2]^+$, $[\text{Rh}(\text{bpy})_2]^+$, and probably $[\text{Rh}(\text{phen})(\text{bpy})]^+$, insofar as is reflected in E_p values, would thus appear minimal.

A question not answered in the present study is whether the nature of the bonding is such that electron transfer to a phen in $[\text{Rh}(\text{phen})_2(\text{bpy})]^{3+}$ or $[\text{Rh}(\text{bpy})_2(\text{phen})]^{3+}$ leads to loss of phen preferentially in the following chemical reaction. The other alternative would be that the ratio of free phen to free bpy in solution after prolonged electrolysis was identical with the ratio in the starting complex.

Summary of Reaction Sequence

The reactions undergone by the phen-containing complexes discussed herein appear to parallel those found for rhodium-bipyridine complexes, except that additional waves resulting from the strong adsorption and limited solubility of $[\text{Rh}(\text{phen})_2]^0$ are seen for phen-containing complexes. For clarity and ease of reference a summary of the reactions proposed for phen-containing complexes is found in Figure 10.

Kinetic Information

Nonadsorbed Species. The forward rate constant k_f of the chemical reaction following electron transfer I was calculated for three of the four tris complexes considered in these studies using a method outlined by Nicholson.⁸ The results are shown in Table V. For phen-containing tris species, an anodic peak is exhibited on scan reversal after reduction wave I, at 0.10 V/sec. The transfer of an electron from the cathode to an ion in solution is electrochemically reversible under these conditions. At scan rates above approximately 1 V/sec, the heterogeneous electron transfer to $[\text{Rh}(\text{phen})_3]^{3+}$ becomes irreversible, as evidenced by $|E_{(p/2)c} - E_{pc}|_I > 70-75$ mV. Consequently, the conditions assumed in Nicholson's calculations are not met. Attempts to calculate k_f at increasing scan rates greater than 1 V/sec yield steadily increasing values, e.g., $k_f = 0.12 \text{ sec}^{-1}$ at 0.10 V/sec, while " k_f " = 10 sec^{-1} at approximately 10 V/sec, " k_f " = 20 sec^{-1} at approximately 30 V/sec, and " k_f " = 70 sec^{-1} at approximately 90 V/sec.

Since no anodic peak can be observed for couple I of $[\text{Rh}(\text{bpy})_3]^{3+}$ unless $v > 1$ V/sec, difficulties were anticipated. Although it is qualitatively obvious that the fol-

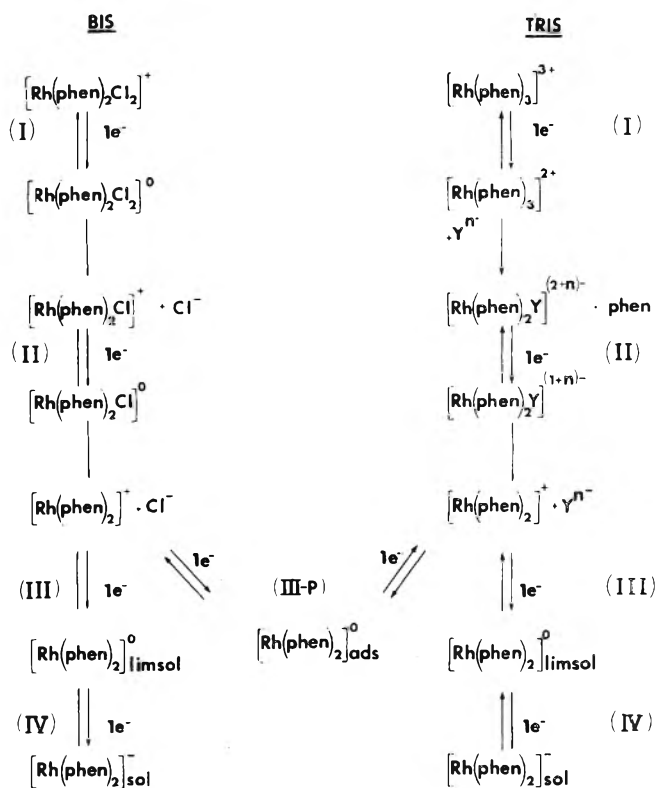


Figure 10. Summary of proposed reactions for phen-containing bis and tris species.

TABLE V: Rate Constants for Tris Rh(III) Starting Materials^{a,b}

Ion	$(k_f)_I, \text{sec}^{-1}$	$k_s, \text{cm/sec}$	
		III	IV
$[\text{Rh}(\text{phen})_3]^{3+}$	0.12 ± 0.04	0.22 ± 0.05	0.15 ± 0.04
$[\text{Rh}(\text{phen})_2(\text{bpy})]^{3+}$	0.14 ± 0.01	c	0.13 ± 0.04
$[\text{Rh}(\text{bpy})_2(\text{phen})]^{3+}$	0.16 ± 0.01	c	0.18 ± 0.04
$[\text{Rh}(\text{bpy})_3]^{3+}$	c	0.14 ± 0.04	0.079 ± 0.04

^a Data derived from solutions of concentration $(5 \pm 1) \times 10^{-4}$ M. ^b Values presented are an average of at least three individual calculations. ^c Oxidation peak poorly defined.

lowing chemical reaction for $[\text{Rh}(\text{bpy})_3]^{3+}$ is much faster than that for the phen analog, the values obtained for k_f of $[\text{Rh}(\text{bpy})_3]^{3+}$ at $v > 9$ V/sec closely parallel those at the same scan rates for $[\text{Rh}(\text{phen})_3]^{3+}$; i.e., neither set of data is valid due to irreversible charge transfer at $v > 1$ V/sec.

Heterogeneous rate constants obtained on the four tris species considered in these studies are also given in Table V. Several gaps are found for the phen-containing complexes due to the lack of a resolvable oxidation peak for various couples, a problem discussed earlier. Those values which are presented for phen-containing complexes should be viewed with caution since the possibility of some contribution from adsorbed species cannot be completely ruled out.

No k_s data are presented for couple III-P since it presumably arises from an adsorbed species and therefore does not fulfill the theoretical criteria on which Nicholson's calculations^{8a} were based. Similarly, data on couple I are excluded because the following chemical reaction can affect

apparent E_p 's in a complex way, particularly in view of the small potential separation from redox couple II.

Adsorbed Species. A number of theoretical relationships have been developed between the potential at which charge transfer occurs for a dissolved species and the potential required for charge transfer to occur when the same species is adsorbed on an electrode.^{9,10} In general, the potential difference may be related to the free energy of adsorption and hence to an equilibrium constant for the adsorption process. The assumptions involved in calculating a potential-dependent parameter, σ , and the potential-independent isotherm constant, K' , are as follows: (a) the adsorption wave and desorption wave under consideration arise from a one-electron charge transfer to strongly adsorbed product of a preceding reduction; (b) the potential scan rate is slow with respect to the potential-independent adsorption rate constant, k_a' , and desorption rate constant, k_d' ($K' = k_d'/k_a'$); (c) the concentration of reduced species at the electrode surface during charge transfer to adsorbed species is adequately described by the Langmuir isotherm.

The phen-containing complexes of this study undergo a series of reactions leading to a species which is adsorbed on a platinum surface and which reduces at potentials sufficiently different from the nonadsorbed species to produce two peaks; however, for satisfaction of assumptions (b) and (c), and "desorption peak" ought to appear at the same potential as the "adsorption peak". In fact the peaks are greatly separated; therefore we have concluded that the models developed by Shain and coworkers^{9,10} are not applicable to the adsorption phenomena of $[\text{Rh}(\text{phen})_2]^0$. The Pt- $[\text{Rh}(\text{phen})_2]^0$ interaction, although very strong, does not inhibit electron transfer as evidenced by the experiments with electrode conditioning B.

Redox Orbitals and Delocalization. Analogous complexes involving two different, though related ligands, such as phen and bpy, are normally expected to show some differences in the energies of lowest unfilled molecular energy levels, and hence in E_p values, which are to some extent a measure of these energies. However, data recently reported for reduction of the ions $[\text{Ru}(\text{bpy})_3]^{2+}$ and $[\text{Ru}(\text{phen})_3]^{2+}$ in acetonitrile⁴ illustrate limits to the generalization. For the bpy complex, $(E_{pc})_{II} = -1.517$ V and $(E_{pc})_{III} = -1.764$ V vs. SCE while for the starting material $[\text{Ru}(\text{phen})_3]^{2+}$, $(E_{pc})_{II} = -1.54$ V and $(E_{pc})_{III} = -1.84$ V. The difference in E_{pc} between successive electron transfers, $\Delta E_{pc} \equiv (E_{pc})_{II} - (E_{pc})_{III}$, is 0.247 V for the bpy species and 0.30 V for the phen. While great significance should not be attributed to a variation of approximately 50 mV, in light of the number of measurements involved in determining these quantities and the possible experimental error in each, the variation between the bpy and phen complexes seems in a reverse direction from normal expectations. Normally, increased delocalization of molecular orbitals into which an electron is transferred leads to a less negative half-wave potential and E_{pc} for the process.¹³ Considering only the relative size of the conjugated ring system, normal expectation is that a tris(phenanthroline) complex ought to be less localized than a tris(bipyridine) complex, implying the corresponding electron transfers ought to be observed at less negative potentials for the phen complex. This is the reverse of the observed trend for the Ru(II) complexes. The reversal is probably due to solvation energy contributions due to identical charges on two different-sized ions.

Vlcek¹³ has generalized that in a metal complex ion the more localized the redox orbital, the more negative the potential required to add an electron. Further, he noted that differences in successive E° values for successive electron transfers depend only slightly upon substitution on the ligand and that this difference becomes smaller with increasing delocalization of the redox orbital.

The Ru complexes do not undergo substantial bidentate ligand loss at potentials positive of approximately -1.9 V implying that the redox orbitals for the first two electron transfers are predominantly ligand localized. Consequently, comparison of the redox orbitals of $[\text{Ru}(\text{bpy})_3]^+$ and $[\text{Ru}(\text{phen})_3]^+$ to those of $[\text{Rh}(\text{bpy})_2]^+$ and $[\text{Rh}(\text{phen})_2]^+$, respectively, seems appropriate. The relative effect on E_{pc} of substituting phen for bpy on the two different metal centers should be similar. For the ions $[\text{Rh}(\text{phen})_2]^{n+}$ size-charge differences, and hence solvation effects, should be reduced by roughly one-third relative to the corresponding differences between Ru tris analogs. Differences in degree of delocalization, based only on size of ring system, should also be reduced by a similar amount. Both effects should lead to more nearly identical half-wave potentials for $[\text{Rh}(\text{bpy})_2]^{n+}$ and $[\text{Rh}(\text{phen})_2]^{n+}$ than was seen for $[\text{Ru}(\text{bpy})_3]^{m+}$ vs. $[\text{Ru}(\text{phen})_3]^{m+}$.

Now if the $E_{1/2}$ for charge transfer leading from +1- to 0-charged species is designated $E_{1/2}^1$ and that for charge transfer leading from 0 to -1 is called $E_{1/2}^2$, then $\Delta E_{1/2}^{1,2}$ represents the difference mentioned above.

Arranged in order of $\Delta E_{1/2}^{1,2}$ corresponding to increasing delocalization, we find $[\text{Ru}(\text{phen})_3]^{n+} < [\text{Ru}(\text{bpy})_3]^{n+} = [\text{Rh}(\text{bpy})_2]^{n+} = [\text{Rh}(\text{phen})_2]^{n+}$. Alternatively there is less difference in energies of redox orbitals accommodating successively transferred electrons in the four-coordinate Rh complexes than in the six-coordinate Ru tris complexes. Only differences between identically charged ions are being considered so solvation energy differences should depend only on size differences.

So far as ligand substitution is concerned, $[\text{Rh}(\text{bpy})_2]^{n+}$ and $[\text{Rh}(\text{phen})_2]^{n+}$ appear so delocalized that "substitution" of $-\text{CH}=\text{CH}-$ between the 6 positions of the rings of 2,2'-bipyridine to "form" phen produces no observable shift in $\Delta E_{1/2}^{1,2}$.

References and Notes

- (1) G. Kew, K. DeArmond, and K. Hanck, *J. Phys. Chem.*, **78**, 727 (1974).
- (2) (a) N. Tanaka and Y. Sato, *Inorg. Nucl. Chem. Lett.*, **2**, 359 (1966); (b) *ibid.*, **4**, 487 (1968); (c) *Electrochim. Acta*, **13**, 335 (1968); (d) *Bull. Chem. Soc. Jpn.*, **41**, 2059 (1968); (e) *ibid.*, **41**, 2064 (1968); (f) *ibid.*, **42**, 1021 (1969).
- (3) (a) D. M. Soignet and L. G. Hargis, *Inorg. Chem.*, **11**, 2349 (1972); (b) *ibid.*, **11**, 2921 (1972); (c) B. V. Tucker, J. M. Fitzgerald, L. G. Hargis, and L. B. Rogers, *J. Electroanal. Chem.*, **13**, 400 (1967); (d) B. R. Baker and B. Dev Mehta, *Inorg. Chem.*, **4**, 848 (1965); (e) R. D. Gillard, J. A. Osborn, and G. Wilkinson, *J. Chem. Soc.*, 4107 (1965); (f) A. A. Vlcek, *Nature (London)*, **189**, 393 (1961).
- (4) N. E. Tokel-Takvoryan, R. E. Hemingway, and A. J. Bard, *J. Am. Chem. Soc.*, **95**, 6582 (1973).
- (5) W. Halper and M. K. DeArmond, *J. Lumin.*, **5**, 225 (1972).
- (6) (a) M. K. DeArmond and J. E. Hillis, *J. Chem. Phys.*, **54**, 2247 (1971); (b) G. C. Kulasingam, W. R. McWhinnie and J. D. Miller, *J. Chem. Soc. A*, 521 (1969).
- (7) B. Martin, W. R. McWhinnie, and G. M. Waind, *J. Inorg. Nucl. Chem.*, **23**, 207 (1961).
- (8) (a) R. S. Nicholson, *Anal. Chem.*, **38**, 1406 (1966); (b) *ibid.*, **37**, 1351 (1965).
- (9) R. H. Wopschall and I. Shain, *Anal. Chem.*, **39**, 1514 (1967).
- (10) M. H. Hulbert and I. Shain, *Anal. Chem.*, **42**, 162 (1970).
- (11) R. F. Lane and A. T. Hubbard, *J. Phys. Chem.*, **77**, 1401 (1973).
- (12) K. DeArmond and W. Halper, *J. Phys. Chem.*, **75**, 3230 (1971).
- (13) A. A. Vlcek, *Proc. Int. Conf. Coord. Chem.*, **14**, 220 (1972).

Oxygen Adducts of Cobalt(II)–Ethylenediamine Complexes in X- and Y-Type Zeolites

R. F. Howe and J. H. Lunsford*

Chemistry Department, Texas A & M University, College Station, Texas 77843 (Received March 14, 1975)

Publication costs assisted by the National Science Foundation

The formation of paramagnetic oxygen adducts in cobalt-exchanged X- and Y-type zeolites containing adsorbed ethylenediamine is described. Infrared and gravimetric adsorption measurements were used to characterize the adsorbed ethylenediamine. In both X and Y zeolites the low-spin $[\text{Co}^{\text{II}}(\text{en})_2\text{O}_2]^{2+}$ adduct is formed in the large cavities and is stable in the presence of O_2 up to 70° . The EPR parameters of this adduct are similar to those of analogous adducts formed in solution. A second O_2^- species, formed only in Y-type zeolites and only in the presence of $\text{Co}(\text{en})_3^{2+}$, shows no ^{59}Co hyperfine structure. The changes in the infrared spectra accompanying formation of this species suggest it is formed by electron transfer from an ethylenediamine ligand.

Transition metal cations exchanged into the faujasite-type zeolites X and Y¹ are capable of forming well-defined complexes with added ligands within the large cavities of the zeolite framework.^{2–5} We have recently studied by electron paramagnetic resonance (EPR) the formation of oxygen adducts of cobalt(II)–amine complexes in zeolite Y, with ammonia, methylamine, and *n*-propylamine as ligands.⁶ The cobalt amine complexes bind oxygen reversibly in the zeolite, but the 1:1 adducts formed are not stable in the presence of oxygen above -78° . Monomeric 1:1 cobalt oxygen adducts have been stabilized in solution by using macrocyclic polydentate ligands.⁷ We describe in this paper an investigation of oxygen adducts formed in cobalt(II)-exchanged X and Y zeolites with ethylenediamine as the ligand. Our objective has been to form 1:1 oxygen adducts which are sufficiently stable for the reactivity of the bound oxygen to be investigated at room temperature or above.

Experimental Section

Two Co^{II} -Y zeolites with differing cobalt contents were prepared from a Linde NaY zeolite (Lot No. 13544-76) by conventional ion exchange; these are designated $\text{Co}_{10.5}\text{NaY}$ and $\text{Co}_{0.75}\text{NaY}$, where the subscripts indicate the number of cobalt ions present per unit cell. A $\text{Co}_{12.5}\text{CaY}$ zeolite was prepared by exhaustive exchange (to greater than 90%) of NaY with calcium, followed by cobalt exchange. A Co_{21}NaX zeolite was prepared from Linde NaX (Lot No. M-1330837). Ethylenediamine (Eastman Kodak) was dried by several distillations over molecular sieve and outgassed by repeated freeze-pumping prior to use. Deuterated ethylenediamine was prepared following the method of Sabatini and Califano.⁸ Ethylenediamine hydrochloride was exchanged with D_2O (99%), dried, and heated with CaO to generate the ethylenediamine. The infrared spectrum of the deuterated material showed that it contained approximately 60% ND_2 , 30% NHD , and 10% NH_2 . Oxygen and oxygen enriched to 44% in ^{17}O and 55% in ^{18}O were used as supplied.

Zeolite samples were dehydrated by heating to 400° in increments of $100^\circ/\text{hr}$ under a vacuum of 10^{-5} Torr. In the EPR experiments, powdered samples were transferred to a quartz side arm prior to recording the spectra. For the infrared experiments, self-supporting wafers ($5\text{--}10\text{ mg cm}^{-2}$) were treated in situ in an infrared cell as described elsewhere.⁹

EPR spectra were recorded at -196 or $+25^\circ$ using Varian E6S and V4502 spectrometers for X-band (9.1 GHz) and Q-band (35 GHz) measurements, respectively. The *g* values were measured using a 2,2-diphenyl-1-picrylhydrazyl (DPPH) standard ($g = 2.0036$). Spin concentrations were calculated by numerical double integration of the recorded derivative spectra and comparison with a phosphorus-doped silicon standard of known spin concentration; the uncertainty in the spin concentration measurements is estimated to be $\pm 30\%$. Simulated EPR spectra were calculated using the computer program SIM 13.⁶ Infrared spectra were recorded on a Beckman IR-9 spectrophotometer operating in the double-beam transmittance mode, with spectral slit widths of $3\text{--}4\text{ cm}^{-1}$ over the range $1200\text{--}2500\text{ cm}^{-1}$ and $6\text{--}8\text{ cm}^{-1}$ above 2500 cm^{-1} . The spectrophotometer was purged with dry air to remove atmospheric water vapor, but absorption by atmospheric CO_2 obscured the region $2300\text{--}2400\text{ cm}^{-1}$.

Gravimetric adsorption experiments were carried out by suspending known weights of zeolite in a quartz bucket from a previously calibrated quartz spring and following changes in the extension of the spring with a cathetometer. Weight changes could be determined to within $\pm 0.2\text{ mg}$.

Results

EPR Spectra. Two paramagnetic oxygen species were observed when oxygen was added to CoNaY zeolites containing adsorbed ethylenediamine. Adsorption of excess ethylenediamine vapor at 25° by adding successive doses until no further uptake was observed, followed immediately by exposure to oxygen (20 Torr), gave the spectrum shown in Figure 1(a). This consists of two overlapping signals: an axially symmetric signal (I) showing no hyperfine structure and two shoulders arising from a second signal (II). Exposure to a high pressure of oxygen (>100 Torr) enhanced signal I relative to signal II. The two signals could be separated by prolonged evacuation at 25° , which removed signal II while leaving signal I reduced in intensity (Figure 1(b)). Signal I was completely destroyed only on outgassing at 100° for 1 hr. Subsequent reexposure to oxygen restored both signals, but with the intensity of signal II considerably enhanced (Figure 1(c)). If the zeolite was outgassed at 200° for 1 hr after adsorption of excess ethylenediamine and then exposed to oxygen at 25° , only signal II was observed (Figure 2). After outgassing at 300° , signal II

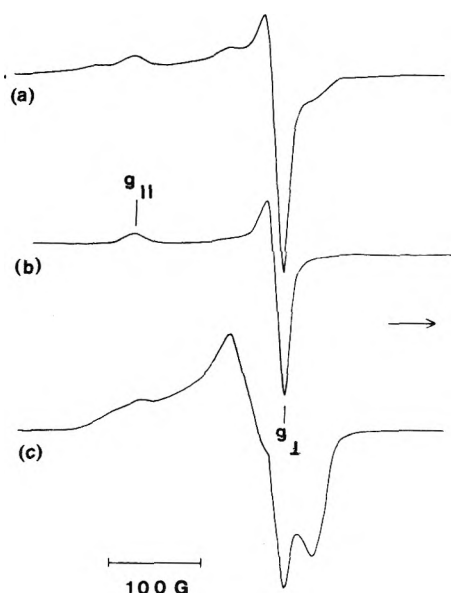


Figure 1. EPR spectra (X band) of CoNaY zeolite containing adsorbed ethylenediamine after addition of oxygen: (a) O_2 added immediately after adsorption of ethylenediamine; (b) evacuated, 25° , 24 hr; (c) outgassed, 100° , 1 hr, and further oxygen added.

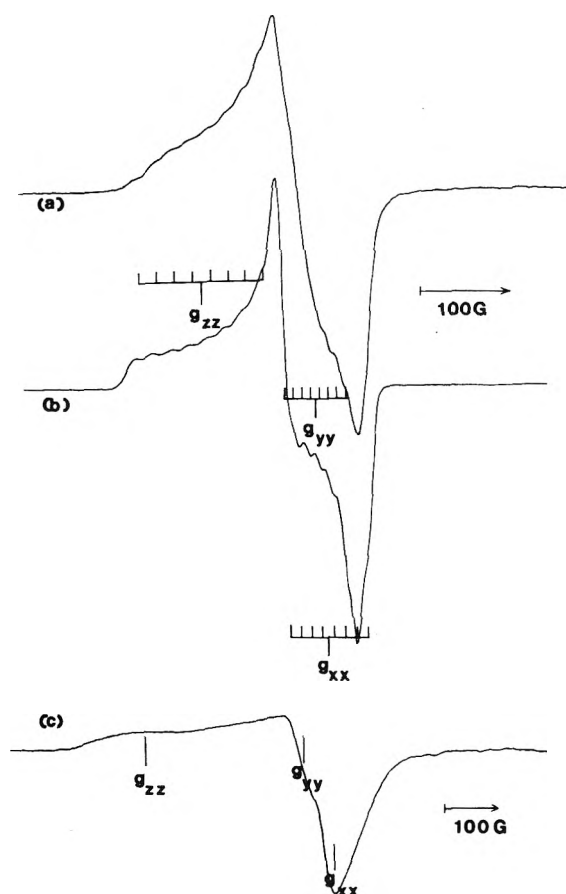


Figure 2. EPR spectra: (a) CoNaY containing adsorbed ethylenediamine outgassed at 200° , then exposed to O_2 (X band); (b) computer simulation of (a); (c) Q-band spectrum of (a).

was again observed on addition of oxygen, but with a much reduced intensity, and no signals at all could be detected on addition of oxygen after outgassing at 400° . Identical behavior was observed if the amount of ethylenediamine

initially added was much less than that required for complete adsorption, except that the signal intensities were correspondingly reduced.

Both signals were stable in the presence of oxygen at 25° and unchanged on recording at -196° . We found that signal II was stable in oxygen up to 75° but was slowly reduced in intensity on heating above that temperature. Maximum intensities of signal I were obtained by exposing the zeolites to 760 Torr of oxygen after adsorption of excess ethylenediamine; these corresponded to spin concentrations of approximately 0.1 and 0.025 per unit cell in $Co_{10.5}NaY$ and $Co_{0.75}NaY$, respectively. Maximum intensities of signal II were obtained by adsorbing ethylenediamine at 25° , outgassing at 200° for 1 hr, and then exposing the sample to about 50 Torr of oxygen at 25° . Higher oxygen pressures gave no intensity increase, and the maximum intensities corresponded to spin concentrations of about 5.0 and 1.0 per unit cell in $Co_{10.5}NaY$ and $Co_{0.75}NaY$.

Figure 3(a) shows signal I formed with oxygen enriched in ^{17}O . This shows one set of six lines centered on g_{\perp} , a second much weaker set of 11 lines also centered on g_{\perp} , and a third set of six lines, only partially resolved, centered on g_{\parallel} . Also shown (Figure 3(b)) is a spectrum calculated with the parameters extracted from the experimental spectrum, assuming axial symmetry. The EPR parameters of signals I and II are summarized in Table I. Figure 3(c) shows signal II formed with the ^{17}O -enriched oxygen. The ^{17}O hyperfine structure in this case overlaps severely with that due to ^{59}Co , and the ^{17}O lines, apart from poorly resolved shoulders at the outer edges of the spectrum, cannot be unambiguously identified. The complexity of the spectrum prevents satisfactory computer simulation.

Signals I and II were also observed from the $Co_{12.5}CaY$ zeolite; substitution of Ca^{2+} for Na^+ caused no change in the EPR parameters of both signals. In the $Co_{21}NaX$ zeolite, only signal II was observed, with the same parameters as in the Y-type zeolites. Exposure to oxygen immediately after adsorption of ethylenediamine gave a very weak signal, and a maximum intensity was observed, as before, by outgassing at 200° for 1 hr before admitting oxygen. Under no conditions have we observed signal I in X-type zeolites.

Blank experiments were carried out with a NaY zeolite containing adsorbed ethylenediamine, but no EPR signals were detected after exposure to oxygen. Likewise, signals I and II were not observed on exposure to oxygen of CoNaY or CoNaX which did not contain adsorbed ethylenediamine.

Infrared Spectra. Zeolite samples dehydrated at 400° were transparent to infrared radiation above about 1200 cm^{-1} . The spectrum of ethylenediamine adsorbed in a NaY zeolite is shown in Figure 4(a). (The frequencies of adsorbed ethylenediamine are summarized in Table II.) Outgassing at 200° drastically reduced the intensity of all the ethylenediamine bands, and after 1 hr at 300° no bands remained in the spectrum. Adsorption of ethylenediamine into $Co_{10.5}NaY$ gave a similar spectrum, but with a number of additional bands between 1200 and 1400 cm^{-1} (Figure 4(b)). As discussed below, these additional bands are attributed to ethylenediamine coordinated to cobalt. Outgassing at 200° for 1 hr caused only a slight reduction in intensity of the coordinated ethylenediamine bands. The band at 1333 cm^{-1} was shifted to 1326 cm^{-1} , and several new bands began to appear as shoulders on the original bands (Figure 5(a)). Outgassing at 300° enhanced these new bands, while further reducing the original bands (Figure 5(b)), and after 1 hr at 400° the coordinated ethylene-

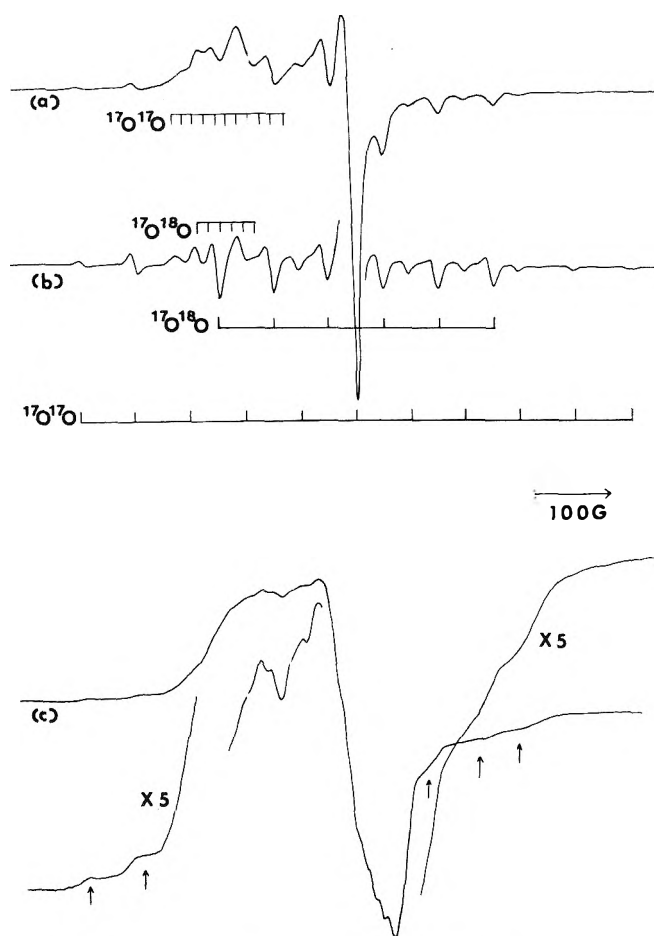


Figure 3. EPR spectra (X band) obtained with O_2 enriched to 44% with ^{17}O : (a) signal I; (b) computer simulation of (a); (c) signal II.

TABLE I: EPR Parameters of O_2^- Species in Zeolites

O_2^- formed in	g_{zz}^a	g_{yy}	g_{xx}	A_{zz}^a	A_{yy}	A_{xx}
$Co(en)_3NaY$ (signal I)	2.102	2.000	2.000	13.5	0 (^{17}O)	72
NaY^b	2.113	2.007	2.002			
NaY^c	2.074	2.007	2.002			
CaY^c	2.046	2.011	2.002			
$Co(en)_2NaY$ (signal II)	2.084	1.998 ^e	1.992	20	10 ^e (^{59}Co)	13
$Co(CH_3-NH_2)_5NaY^d$	2.075	2.010 ^e	1.999	21	12 ^e (^{59}Co)	12

^a Estimated uncertainties: ± 0.002 in g values; ± 1 G in A values.
^b Reference 12. ^c Reference 13. ^d Reference 6. ^e Estimated from computer simulation.

diamine bands were completely removed (Figure 5(c)). Identical spectra were obtained as a function of the outgassing temperature after adsorption of ethylenediamine in the $Co_{21}NaX$ zeolite.

Admission of oxygen (760 Torr) following adsorption of excess ethylenediamine in $Co_{10.5}NaY$ caused immediate changes in the infrared spectrum, as shown in Figure 4(c). The bands due to coordinated ethylenediamine between 1200 and 1400 cm^{-1} were substantially reduced in intensi-

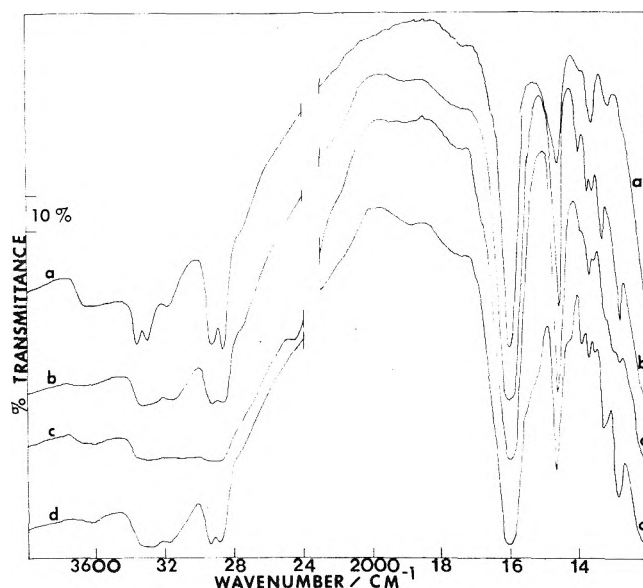


Figure 4. Infrared spectra of adsorbed ethylenediamine: (a) adsorbed in NaY at 25° ; (b) adsorbed in $CoNaY$ at 25° ; (c) exposed to 760 Torr of O_2 ; (d) outgassed, 100° , 1 hr.

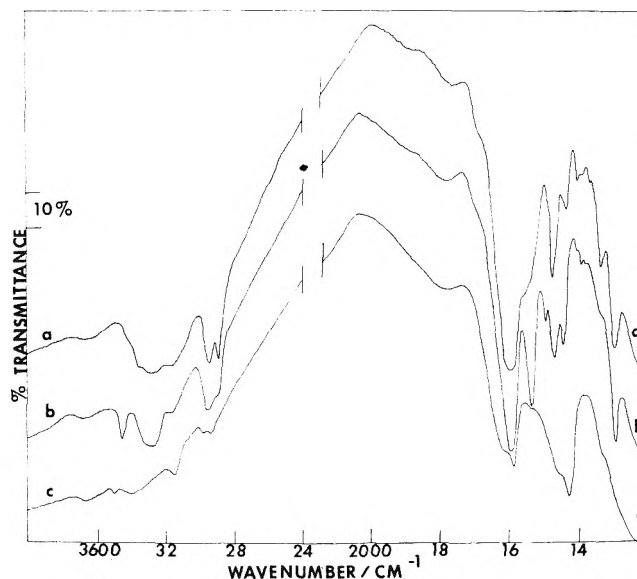


Figure 5. Infrared spectra of ethylenediamine adsorbed in $CoNaY$, outgassed: (a) 200° , 1 hr; (b) 300° , 1 hr; (c) 400° , 1 hr.

ty, and a new band appeared at 1380 cm^{-1} . Above 2000 cm^{-1} , a new band appeared as a shoulder at about 2450 cm^{-1} , while a decrease in transmittance between 3000 and 3200 cm^{-1} suggested the appearance of one or more new bands in this region. Removal of the oxygen by evacuation at 25° caused no change in the spectrum, but after outgassing at 100° for 1 hr the new bands were completely removed and the coordinated ethylenediamine bands restored. Subsequent reexposure to oxygen caused the same changes to occur, but to a lesser extent. Exposure to oxygen after outgassing at 200° for 1 hr caused no change in the spectrum. The spectrum of $Co_{21}NaX$ containing adsorbed ethylenediamine was unchanged on exposure to oxygen.

The same experiments were carried out using partially deuterated ethylenediamine. Figure 6(b) shows the spectrum of $Co_{10.5}NaY$ after adsorption of deuterated ethylenediamine at 25° . Exposure to oxygen gave the spectrum

TABLE II: Observed Frequencies of Adsorbed Ethylenediamine (cm^{-1})^b

Liquid ^a	Adsorbed in NaY	Adsorbed in Co_{21}NaX	Adsorbed in $\text{Co}_{10.5}\text{NaY}$	Adsorbed in $\text{Co}_{10.5}\text{NaY}$ and outgassed, 200°	Assignments ^c
Normal Ethylenediamine					
3351	3370			3345	NH ₂ str
3277	3310	~3300	~3300	3270	
3195	3190		3170	3160	
2926	2930		2935	2940	CH ₂ str
2857	2875	~2900	2880	2890	
1595	1605	1600	1605	1590	NH ₂ def
1456	1467	1468	1467	1467	CH ₂ def
		1400	1400	1397	NH ₂ def
		1375	1375	1375	CH ₂ def
1352	1360		1360	1360	
		1334	1333	1326	NH ₂ def
1310	1315				CH ₂ def
		1280	1283	1285	NH ₂ def
Deuterated Ethylenediamine					
2934 ^d			2938	2942	CH ₂ str
2866			2890	2890	
			2728	2760	NHD str
			2650	2692	
2506			2490	2500	ND ₂ str
2423			2420	2420	
2364					
1451			1467	1468	CH ₂ def
			1440	1440	NHD def
			1383	1384	CH ₂ def
1360			1362	1363	

^a Reference 8. ^b Frequencies accurate to $\pm 3 \text{ cm}^{-1}$ below 2000 cm^{-1} and 8 cm^{-1} above 2000 cm^{-1} . ^c Assignments based on ref 8 and 10. ^d Liquid ethylenediamine- d_4 .

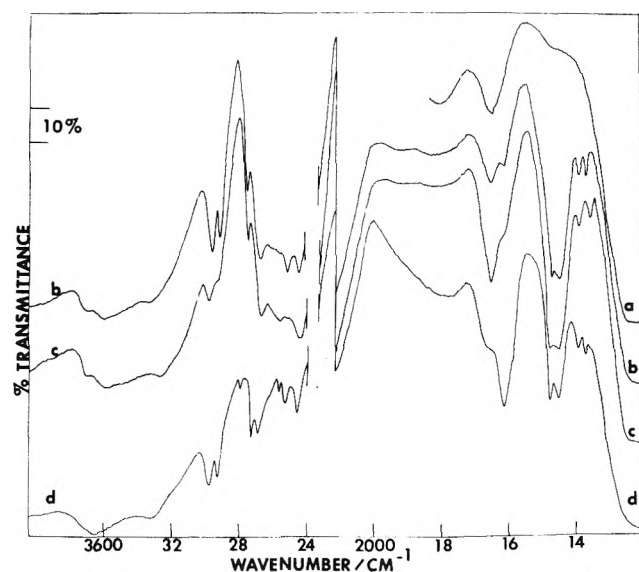


Figure 6. Infrared spectra of adsorbed deuterated ethylenediamine: (a) background spectrum of dehydrated CoNaY ; (b) deuterated ethylenediamine adsorbed at 25° ; (c) exposed to 760 Torr of O_2 ; (d) outgassed, 100° , 1 hr.

shown in Figure 6(c), in which the coordinated ethylenediamine bands are reduced in intensity, and new bands appear at 1354 , 1645 , 2410 , and 2530 cm^{-1} . As before, evacuation of the oxygen at 25° caused no change, but outgassing at 100° for 1 hr gave the spectrum shown in Figure 6(d), in

which the coordinated ethylenediamine bands are restored. After this treatment, however, the bands associated with NH_2 vibrations (see Table II) were increased in intensity, while those associated with ND_2 and CH_2 were decreased. Additional bands appeared at 2692 and 2760 cm^{-1} , but these bands were also observed when the zeolite was outgassed at 100 or 200° without previous exposure to oxygen (Table II). Exposure to oxygen after outgassing at 200° caused no further change in the spectrum.

Adsorption of deuterated ethylenediamine in Co_{21}NaX gave a spectrum identical with that observed from $\text{Co}_{10.5}\text{NaY}$. In this case, exposure to oxygen caused no change in the spectrum, and after subsequent outgassing at 100° only a very slight enhancement of the NH_2 bands was observed.

Gravimetric Adsorption Measurements. Table III summarizes the results of gravimetric adsorption measurements carried out with $\text{Co}_{10.5}\text{NaY}$, $\text{Co}_{0.74}\text{NaY}$, and NaY zeolites. In each case the dehydrated zeolite was exposed to ethylenediamine vapor (10 Torr) at 25° until no further weight increase was observed. The weight changes on subsequent outgassing were then determined. The results are expressed as the number of ethylenediamine molecules remaining adsorbed per unit cell of the zeolite after each outgassing treatment.

Discussion

Adsorption of Ethylenediamine. The gravimetric adsorption data show that the amount of ethylenediamine adsorbed into NaY or CoNaY zeolites on exposure to the

TABLE III: Ethylenediamine Adsorption Data (molecules/unit cell)^a

Treatment	Co _{10.5} NaY	Co _{0.74} NaY	NaY
Adsorbed at 25°	64.5	66.0	63.5
Outgassed at 25°, 12 hr	55.5	58.0	54.0
Outgassed at 100° 1 hr	44.5	46.5	42.0
Outgassed at 200°, 1 hr	23.5	12.5	5.5
Outgassed at 300°, 1 hr	16.5	1.0	<i>b</i>
Outgassed at 400°, 1 hr	7.5	<i>b</i>	<i>b</i>

^a ± 2 molecules/unit cell. ^b Less than 1.0 molecule/unit cell.

vapor at 25° is independent of the cation-exchange level and is approximately equal to the amount of liquid ethylenediamine required to fill completely the zeolite void volume of 0.36 cm³ g⁻¹.¹ The vibrational frequencies of ethylenediamine adsorbed in NaY are close to those reported for liquid ethylenediamine (Table II). In the CoNaY and CoNaX zeolites these same ethylenediamine bands are observed, plus additional bands between 1200 and 1400 cm⁻¹ which are characteristic of CH₂ and NH₂ deformation vibrations of ethylenediamine coordinated to transition metal ions.¹⁰ X-Ray diffraction studies have shown that most of the divalent cations in dehydrated faujasite zeolites reside within the sodalite cages and hexagonal prisms,¹¹ which are inaccessible to ethylenediamine. On adsorption of ethylenediamine, migration of cobalt ions toward or into the large cavities of the zeolite structure evidently occurs.

We can distinguish between the NH₂ and CH₂ bands of coordinated ethylenediamine from the observed frequency shifts when NH₂ is replaced by ND₂ or NHD. The bands at 1283, 1333, and 1400 cm⁻¹, which are shifted below 1200 cm⁻¹, must be due to NH₂ deformation modes, whereas the 1360- and 1375-cm⁻¹ bands are not significantly affected by deuteration and, so, must be due to CH₂ deformation modes. Our assignments of the bands above 1400 cm⁻¹ in the spectra of adsorbed ethylenediamine follow those of Powell and Sheppard¹⁰ and of Sabatini and Califano.⁸ Above 2000 cm⁻¹, the spectrum of deuterated ethylenediamine adsorbed in CoNaY shows, in addition to the expected $\nu(\text{ND}_2)$ and $\nu(\text{CH}_2)$ bands, bands at 2650 and 2728 cm⁻¹ which we tentatively assign to stretching modes of the NHD group coordinated to cobalt, although these occur between 2400 and 2500 cm⁻¹ in the free molecule. The alternative assignment of these bands to OD groups formed by exchange with zeolite OH groups seems unlikely, since such bands would be broadened through interaction with ethylenediamine molecules, as are the bands due to the residual OH groups remaining in the zeolite after dehydration at 400°.

The number of ethylenediamine molecules coordinated to cobalt after adsorption of the vapor at 25° cannot be determined from the infrared spectrum above 1200 cm⁻¹. In the presence of excess ethylenediamine, however, the tris complex, Co(en)₃²⁺, should be the preferred form. The stability constants at 30° in aqueous solution are 5 × 10¹⁰ for Co(en)₂²⁺ and 7 × 10¹³ for Co(en)₃²⁺.¹² After outgassing at 200° for 1 hr, most of the ethylenediamine is removed from NaY. The amount remaining coordinated to cobalt in Co_{10.5}NaY is slightly less than 2 molecules/cobalt ion. (This figure is obtained by subtracting the amount remaining in NaY from the total amount remaining in Co_{10.5}NaY after outgassing at 200°.) The gravimetric data are not suffi-

ciently accurate for the cobalt:ethylenediamine ratio in the low-exchanged Co_{0.74}NaY zeolite to be reliably determined.

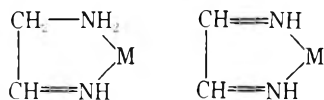
The infrared spectra of ethylenediamine coordinated to cobalt in Co_{10.5}NaY and Co₂₁NaX after outgassing at 200° are not identical with those observed initially. With ethylenediamine, the NH₂ deformation band at 1333 cm⁻¹ is shifted to 1326 cm⁻¹ on outgassing at 200°, and with deuterated ethylenediamine, the NHD stretching bands at 2650 and 2728 cm⁻¹ are shifted to 2692 and 2760 cm⁻¹, respectively. We conclude from the gravimetric and infrared evidence that the bis complex Co(en)₂²⁺ is formed in the cobalt-exchanged zeolites on outgassing at 200°.

All of the adsorbed ethylenediamine is removed from NaY after outgassing above 200°, as shown by both the gravimetric and infrared experiments. In Co_{10.5}NaY, on the other hand, a significant amount of adsorbed material is retained after outgassing at 400°. The infrared spectra show that the bands due to ethylenediamine coordinated to cobalt are almost completely removed after 1 hr at 300°, accompanied by the appearance of a series of new bands between 1200 and 1600 cm⁻¹ and above 3000 cm⁻¹. We attribute these changes to decomposition of ethylenediamine ligands. We have not investigated the nature of the decomposition products in any detail, but the new bands due to these products begin to appear in the spectrum after outgassing at temperatures as low as 200°. The complexity of the spectra recorded after outgassing at high temperatures suggests that the decomposition sequence is not simple. The same decomposition products were apparently formed in the Co₂₁NaX zeolite.

Formation of Oxygen Adducts. The EPR signal I, observed only in the cobalt-exchanged Y-type zeolites, is due to a species containing two equivalent oxygen atoms. This is evident from the spectrum obtained using oxygen-17. A singly labeled superoxide ion with two equivalent oxygens would give six lines of approximately equal intensity for each principal direction. A doubly labeled species with equivalent atoms would be characterized by eleven lines for each principal direction. The observed spectrum shows a set of six lines and a set of eleven lines, with both centered on g_{\perp} , and a set of six lines centered on g_{\parallel} . The set of eleven lines centered on g_{\parallel} due to ¹⁷O¹⁷O cannot be resolved in the experimental spectrum but is included in the computer-simulated spectrum, which agrees well with that observed. Analysis of the ¹⁷O hyperfine splitting constants (Table I) in the usual manner indicates that the unpaired electron is greater than 90% localized on a 2p π^* orbital of O₂. No ⁵⁹Co hyperfine splitting is observed in signal I, so that the oxygen must not be bonded to cobalt. The g values of signal I resemble, but do not exactly equal, those of O₂⁻ formed in NaY zeolites by uv or γ irradiation.^{13,14} The O₂⁻ in NaY is believed to be interacting with Na⁺ cations, since replacement of Na⁺ by Ca²⁺ causes a large change in the value of g_{zz} .¹⁴ The g values of signal I are identical however, in both Co_{10.5}NaY and Co_{12.5}CaY, so that stabilization of the O₂⁻ on Na⁺ or Ca²⁺ seems unlikely.

There seems to be a correlation between the appearance of signal I and the changes in the infrared spectrum of adsorbed ethylenediamine on exposure to oxygen. Signal I and the changes in the infrared spectra are observed only in Y-type zeolites and only in the presence of Co(en)₃²⁺. Signal I is completely destroyed and the original infrared spectrum restored after outgassing at 100°. The changes in the infrared spectra, a reduction in the intensity of the coordinated ethylenediamine bands and the appearance of

new bands, imply that oxidation of ethylenediamine ligands is occurring on exposure to oxygen. Oxidation of ethylenediamine coordinated to Ru(II)¹⁵ or Pt(IV)¹⁶ in solution has been reported to give imine groups



The coordinated imine group is expected to give infrared bands (above 1200 cm^{-1}) around 3300–3400 cm^{-1} ($=\text{N}-\text{H}$ stretch), 3000–3100 cm^{-1} ($=\text{C}-\text{H}$ stretch), 1600 cm^{-1} ($\text{C}=\text{N}$ stretch), 1400 cm^{-1} ($=\text{C}-\text{H}$ deformation), and 1200 cm^{-1} ($=\text{N}-\text{H}$ deformation).¹⁶ The new bands appearing below 2000 cm^{-1} when oxygen is added to ethylenediamine adsorbed in $\text{Co}_{10.5}\text{NaY}$ are consistent with the formation of imine groups. With ethylenediamine, the single new band at 1380 cm^{-1} may be assigned to the $=\text{C}-\text{H}$ deformation mode, while the intense NH_2 deformation band at 1600 cm^{-1} obscures the expected $\text{C}=\text{N}$ stretch band. With deuterated ethylenediamine, the $=\text{C}-\text{H}$ deformation band occurs at 1354 cm^{-1} , and the $\text{C}=\text{N}$ stretch is observed at 1645 cm^{-1} . Above 2000 cm^{-1} , the predicted imine bands cannot be clearly distinguished from those due to ethylenediamine, although obvious changes occur in the spectra in the expected regions, e.g., between 3000 and 3100 cm^{-1} , and in the case of deuterated ethylenediamine, between 2400 and 2500 cm^{-1} . The band appearing as a shoulder at about 2450 cm^{-1} with ethylenediamine (Figure 4(c)) is in the region characteristic of N^+-H stretching vibrations, raising the possibility that the imine group carries a positive charge and should be formulated as $-\text{CH}=\text{NH}_2^+$. However, we have not observed the corresponding N^+-D band with deuterated ethylenediamine. The observed enhancement of the NH_2 bands in the spectrum of deuterated ethylenediamine after exposure to oxygen and subsequent outgassing at 100° supports the proposed imine structure. Loss of protons from both carbon and nitrogen on addition of oxygen provides a mechanism for intramolecular exchange. The protons removed from coordinated ethylenediamine probably protonate surrounding ethylenediamine molecules, but on outgassing at 100° this process is reversed.

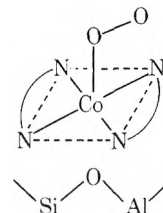
We suggest that formation of the O_2^- species responsible for the EPR signal I occurs through transfer of an electron from a coordinated ethylenediamine ligand to oxygen. This occurs only with the tris complex $\text{Co}(\text{en})_3^{2+}$ and only in the Y-type zeolites. Zeolites X and Y have the same framework structure and differ only in the silicon to aluminum ratio.¹ The higher aluminum content of zeolite X results in a higher density of exchangeable cations within the zeolite structure, but it is not clear why this should inhibit the electron transfer from ethylenediamine to oxygen. No EPR studies have been reported of O_2^- formation in X-type zeolites. Electron transfer from the ligand does not occur with $\text{Co}(\text{en})_2^{2+}$, since in this case direct interaction of oxygen with Co^{2+} can take place giving rise to signal II.

The EPR signal II closely resembles the signals observed previously from other cobalt-amine-oxygen adducts formed in CoNaY zeolites.⁶ Two sets of eight ^{59}Co hyperfine lines can be identified in the observed spectrum, implying axial symmetry. The Q-band spectrum (Figure 2(c)) shows clearly, however, that the g tensor is nonaxial, although the g_{xx} and g_{yy} components are not well enough resolved for their values to be accurately determined. As

with the ammonia-, methylamine-, and *n*-propylamine-oxygen adducts,⁶ the observed X-band spectrum of the ethylenediamine-cobalt-oxygen adduct could not be satisfactorily computer simulated unless nonaxial symmetry was assumed. Figure 2(b) shows a typical computed spectrum, with the parameters given in Table I. The positions of the maxima and minima are correctly predicted; the lack of complete agreement with the experimental spectrum is probably due to the line width associated with g_{yy} being greater than that associated with g_{xx} , which cannot be allowed for by our computer program.

The observed ^{59}Co hyperfine coupling constants for signal II are in the range 10–20 G, comparable to those reported for other cobalt(II)-oxygen adducts.^{6,7} Comparison of the experimental coupling constants with the values of 1350 G¹⁷ and -156 G^{18} calculated for an unpaired electron in a pure *s* or 3*d* orbital, respectively, on $^{59}\text{Co}^{2+}$ indicates that the unpaired electron is only about 3% localized on Co^{2+} orbitals. We may conclude that the electron is mostly localized on the oxygen, since no ^{14}N hyperfine interaction with the ligands is observed; i.e., the oxygen adduct should be formulated as $\text{Co}^{3+}\text{O}_2^-$. Drago¹⁹ has recently suggested that the observation of reduced ^{59}Co hyperfine constants alone is not sufficient evidence for the O_2^- formulation. Definitive evidence for O_2^- should come from ^{17}O hyperfine coupling constants. If the unpaired electron is located in an oxygen $2p\pi^*$ molecular orbital, the ^{17}O hyperfine tensor is expected to have a large anisotropic component. Vansant and Lunsford²⁰ observed ^{17}O hyperfine splitting in a cobalt-ammonia-oxygen adduct in a CoNaY zeolite and concluded that the unpaired electron was about 90% localized in a $2p\pi^*$ molecular orbital. The ^{17}O hyperfine lines in signal II are not sufficiently well resolved for an accurate analysis to be carried out. Nevertheless, the outermost ^{17}O lines are seen to be separated by approximately 80 G (Figure 3(c)) and are up to 400 G removed from the center of the signal. Hyperfine splittings of this magnitude, when compared to the isotropic ^{17}O coupling constant of 21.6 G observed for a cobalt-oxygen adduct in solution,²¹ imply the existence of a large anisotropic component consistent with the O_2^- formulation for the cobalt-ethylenediamine-oxygen adduct.

A maximum intensity of signal II is observed when oxygen is added to a zeolite containing mostly $\text{Co}(\text{en})_2^{2+}$. Accordingly, we suggest the following structure for the cobalt-ethylenediamine-oxygen adduct



where the sixth coordination site is occupied by an oxide ion of the zeolite lattice. The observed nonaxial g tensor is consistent with a nonlinear $\text{Co}-\text{O}-\text{O}$ structure. The suggested structure is similar to those of 1:1 cobalt-oxygen adducts formed in solution, in which the in-plane ligand is a Schiff base²² or porphyrin²³ and the sixth coordination site is occupied by a coordinating base such as pyridine.

The remarkable stability of the $[\text{Co}(\text{en})_2\text{O}_2]^{2+}$ adduct in X and Y zeolites compared with the analogous adducts formed with ammonia, methylamine, and *n*-propylamine, is probably a consequence of the coordination to the zeolite

lattice. In particular, no dimerization to form a 1:2 adduct is observed, although dimeric ethylenediamine-cobalt-oxygen adducts are readily formed in solution,²⁴ and a dimeric ethylenediamine adduct should be no larger than the methylamine-cobalt-oxygen dimer which can form in the large cavities of CoNaY zeolites at room temperature.⁶

Acknowledgments. This research was supported by the National Science Foundation (Grant GP-43041X).

References and Notes

- (1) D. W. Breck, *J. Chem. Educ.*, **41**, 678 (1964).
- (2) E. F. Vansant and J. H. Lunsford, *J. Phys. Chem.*, **76**, 2860 (1972).
- (3) E. F. Vansant and J. H. Lunsford, *J. Chem. Soc., Faraday Trans. 2*, **69**, 1028 (1973).
- (4) I. D. Mikheiken, O. I. Brotikovskii, G. M. Zhidomirov, and V. B. Kazanskii, *Kinet. Catal. (Engl. Transl.)*, **12**, 1279 (1971).
- (5) I. R. Leith and H. F. Leach, *Proc. R. Soc. London, Ser. A*, **330**, 247 (1972).
- (6) R. F. Howe and J. H. Lunsford, *J. Am. Chem. Soc.*, in press.
- (7) R. G. Wilkins, *Adv. Chem. Ser.*, **No. 100**, 111 (1971), and references therein.
- (8) A. Sabatini and S. Califano, *Spectrochim. Acta*, **16**, 677 (1960).
- (9) J. W. Jermyn, T. J. Johnson, E. F. Vansant, and J. H. Lunsford, *J. Phys. Chem.*, **77**, 2964 (1973).
- (10) D. B. Powell and N. Sheppard, *Spectrochim. Acta*, **17**, 68 (1961).
- (11) J. V. Smith, *Adv. Chem. Ser.*, **No. 102**, 401 (1971); P. Gallezot, Y. Ben Taarit, and B. Imelik, *J. Catal.*, **26**, 295 (1972).
- (12) A. E. Martell and M. Calvin, "Chemistry of the Metal Chelate Compounds", Prentice-Hall, New York, N.Y., 1952.
- (13) P. H. Kasai, *J. Chem. Phys.*, **43**, 3322 (1965).
- (14) K. M. Wang and J. H. Lunsford, *J. Phys. Chem.*, **74**, 1512 (1970).
- (15) B. C. Lane, J. E. Lester, and F. Basolo, *Chem. Commun.*, 1618 (1971).
- (16) Y. N. Kukushkin and Y. S. Varshavskii, *Russ. J. Inorg. Chem. (Engl. Transl.)*, **11**, 193 (1966).
- (17) B. R. McGarvey, *J. Phys. Chem.*, **71**, 51 (1967).
- (18) B. A. Goodman and J. B. Raynor, *Adv. Inorg. Chem. Radiochem.*, **13**, 135 (1970).
- (19) B. S. Tovrog and R. S. Drago, *J. Am. Chem. Soc.*, **96**, 6765 (1974).
- (20) E. F. Vansant and J. H. Lunsford, *Adv. Chem. Ser.*, **No. 121**, 441 (1973).
- (21) E. Melamud, B. L. Silver, and Z. Dori, *J. Am. Chem. Soc.*, **96**, 4689 (1974).
- (22) See, for example, B. M. Hoffman, D. L. Diemente, and F. Basolo, *J. Am. Chem. Soc.*, **92**, 61 (1970).
- (23) See, for example, F. A. Walker, *J. Magn. Reson.*, **15**, 201 (1974).
- (24) P. Bijl and G. De Vries, *J. Chem. Soc., Dalton Trans.*, 303 (1972).

Molecular Diffusion and Proton Exchange in Methanol Adsorbed by a Sodium and a Hydrogen Y Zeolite

P. Salvador¹ and J. J. Fripiat*

Laboratoire de Physico-Chimie Minérale, Louvain-la-Neuve, Belgium, and CRSOCI-CNRS, 45045 Orleans-Cedex, France
(Received February 24, 1975)

The pulse magnetic resonance technique and infrared spectroscopy have been used to study the behavior of CH₃OD and CD₃OH occluded at the maximum capacity or at one-third of the full loading in either the sodium Y zeolite or the decationated Y zeolite. In the Na zeolite the diffusion coefficients derived from the diffusional correlation time are in good agreement with similar results reported for other molecules in a similar situation. The behavior of methanol in the zeolitic cage is that of a viscous liquid composed of various "polymeric" units. The broad OH band observed for methanol in this situation is in favor of this model. The spin-lattice proton relaxation rate is mainly contributed by this diffusional motion. In the decationated zeolite the spin-lattice relaxation rate is apparently contributed by a proton-exchange process only. The infrared spectra indicate that methanol interacts with the lattice OH by strong hydrogen bonding. The adsorbed methanol behaves as a vehicle bearing the lattice proton within the zeolitic cage. The proton-exchange process does not appear as being first order. The reason for this special behavior of methanol occluded in the decationated sieve is probably the similarity between the pK_a of the lattice OH (pK_a = -6) and that of CH₃OH₂⁺ (pK_a = -4.5).

Introduction

The adsorption of methanol on cation-exchanged and decationated zeolites has been studied by Geodakyan, Kiselev, and Lygin^{2a} by infrared spectroscopy.

The perturbation of the hydroxyl groups of methanol is determined, at a low filling factor, not only by the effect of exchangeable cations but also by the additional effect of the oxygen framework. Relative to the hydroxyl stretching band in the liquid, the hydrogen bond is weaker. Possibly, hydrogen bonds are formed by the interaction of the meth-

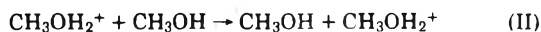
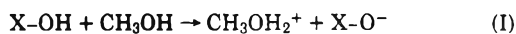
anol hydroxyl with the negatively charged oxygen atoms of the zeolite framework. At a higher filling degree, an additional vibration band similar to that in crystalline methanol is observed. The latter is not subject to the direct influence of the exchangeable cations.

In the spectra of methanol adsorbed by decationated zeolites, it is clear that strong hydrogen bonds are formed with the surface hydroxyl groups. This observation, particularly stressed by Bosacek et al.^{2b} is not surprising in view of the strong proton-donor character of those surface OH groups. Their pK_a values are in the range of -6 (±2) according to recent measurements by Sempels and Rouxhet.³

Cruz et al.^{4,5} have shown that methanol is an interesting

* To whom correspondence should be addressed at CRSOCI-CNRS.

molecule for studying molecular motions and proton exchange by pulse nuclear magnetic resonance in the adsorbed state. By an adequate choice of hydrogenated and deuterated systems, it is indeed possible to make a distinction between different kinds of relaxation mechanisms. Particularly interesting has been, for methanol adsorbed on silica gel, the distinction between molecular diffusion, the tumbling of the adsorbed species, and the proton exchange with surface silanols and between adsorbed species according to the mechanisms



Because of well-marked differences between the adsorption processes of methanol in zeolites and on silica gel it was interesting to repeat a similar study for a Na and a decationated Y zeolite.

In silica gel the pK_a of the surface hydroxyls is between +7 and +8. In presence of a proton acceptor (A) characterized by a pK_a on the order of or higher than that of silica gel, Noller et al.⁶ have explained a continuous absorption by assuming that the protons detached from the SiOH groups and captured by the proton acceptor AH^+ are tunneling in the $\text{AH}^+\cdots\text{A}$ bonds. This interpretation is based on the findings of Zundel et al.,^{7,8} who have shown that hydrogen bonds with symmetrical or almost symmetrical double-minimum potential wells are about 2 orders of magnitude more polarizable than electron systems, causing a continuity of energy level shifts and therefore a continuous absorption.

The pK_a of CH_3OH_2^+ is about -4.5.⁶ This is near the pK_a of the surface OH in decationated zeolite.

From the pK_a of XOH and CH_3OH_2^+ and by combining reactions I and II it may be easily shown that if $[\text{CH}_3\text{OH}]/[\text{XOH}] = 1$ the ratio $[\text{CH}_3\text{OH}_2^+]/[\text{XOH}]$ is 1.2 in the zeolite and about 10^{-6} on the silica gel surface. The activity coefficients are neglected but the orders of magnitude are sufficiently separated to initiate a very different behavior.

In decationated zeolites, the influence of the proton exchange is thus expected to determine the relaxation mechanism. On the contrary, in the sodium sample it should be comparable with that observed for various other occluded liquids. Resing⁹ has made a comparison between the diffusion coefficients computed from the correlation times measured for various adsorbed materials such as H_2O , SF_6 , C_6H_{10} , and C_6H_6 .

The magnetic nuclear resonance study should be completed by some infrared investigation, especially for the decationated sample, in order to check the stability of the hydroxylated lattice in the presence of methanol. It has been indeed pointed out by Bosacek et al.^{2b} that some of the OH groups enter a chemical reaction with methanol, forming firmly bound methoxyl groups. The initial value of isosteric heat of adsorption of methanol by a sodium X sieve obtained by Avgul et al.¹⁰ is rather large, indicating a strong interaction.

Hence, this paper aims to define the behavior of methanol occluded in Na-Y and H-Y near-faujasite molecular sieves, the main tool being the proton pulse NMR spectroscopy.

Procedures

Materials. The Na sieve was prepared in the laboratory by Lerot.¹¹ The chemical composition for the dehydrated

sample¹ was $\text{Na}_{64}\text{Al}_{68}\text{Si}_{122}\text{O}_{384}$. Si:Al = 1.86 is in the domain of a Y near-faujasite. By repeated contacts with a 1 N NH_4Cl solution at room temperature, the sodium sieve was converted into a NH_4 sample at the extent of about 86%. The decationated sample was obtained by the so-called "thin" bed thermal treatment¹² of the NH_4 zeolite under the same conditions as those described for the ir study. The chemical analysis of the decationated sample showed the composition $\text{H}_{55}\text{Na}_9\text{Al}_{68}\text{Si}_{125}\text{O}_{384}$. For this chemical composition, at full loading of the sieve the $[\text{CH}_3\text{OH}]/[\text{XOH}]$ ratio is 15 whereas $[\text{CH}_3\text{OH}_2^+]/[\text{XOH}] \approx 1$.

The sodium and decationated samples will be called Na-Y and H-Y, respectively. The iron content is of the order of 100 ppm.

Adsorption Isotherms. Merck spectroscopy grade CH_3OH was used. Isotherms were obtained with a volumetric adsorption apparatus. The equilibrium pressures were measured within ± 0.05 Torr with a mercury manometer and an accurate cathetometer. Below 10^{-2} Torr, a McLeod gauge was used.

Before any adsorption, the samples were dehydrated or decationated in the adsorption apparatus. The adsorption isotherms, the heats of adsorption, and the diffusion coefficients obtained from isothermal desorption will be discussed elsewhere.¹²

The full loading was derived through the Dubinin equation and it was found equal to 7.5×10^{-3} mol/g for Na-Y and to 10×10^{-3} mol/g for H-Y at 20° .

The reason for this difference is perhaps that methanol has access to the cage inside the cuboctahedron in H-Y but not in Na-Y because the Na cations block the pathway to inside these structure elements.

Infrared Spectroscopy. Na or NH_4 zeolites were pressed into thin wafers of 5–10 mg/cm² average thickness, under a pressure of about 2 kg/cm². These Na zeolite wafers were pretreated in a quartz ir cell at 450° , under a residual pressure of 10^{-6} Torr, for 24 hr. NH_4 zeolite wafers were decationated in the following way. First the system was evacuated at room temperature under a residual pressure of 10^{-6} Torr for 24 hr, and then it was heated under vacuum at $2^\circ/\text{min}$ up to 350° ; this temperature was maintained for 12 hr.

CH_3OH and CH_3OD spectroscopic grade reagents were used. Ir spectra were always recorded at room temperature. The methanol filling degree, expressed relative to the full loading that can be occluded within the zeolite, was the variable parameter for these experiments. When required, surface deuteration was obtained as described in the next section.

The spectra were recorded with a Beckman IR 12 spectrometer. In all cases the spectral line width was negligible with respect to the width of the vibrational bands of the adsorbed material.

NMR Experiments. Samples were pretreated under the conditions used for the ir experiments. Pretreatments were carried out in Pyrex tubes (15-mm i.d.) placed horizontally in a furnace in such a way that the thickness of the powder bed on the wall was less than 3 mm.

After the pretreatment, the sample was cooled and brought into contact with methanol vapor. The quantity of methanol adsorbed was measured volumetrically. The tube was then sealed and placed in the NMR probe. CH_3OH , CH_3OD , and CD_3OH spectroscopic grade reagents were degassed before use by repeated freezing and thawing.

When deuterated samples were required, a few Torr of

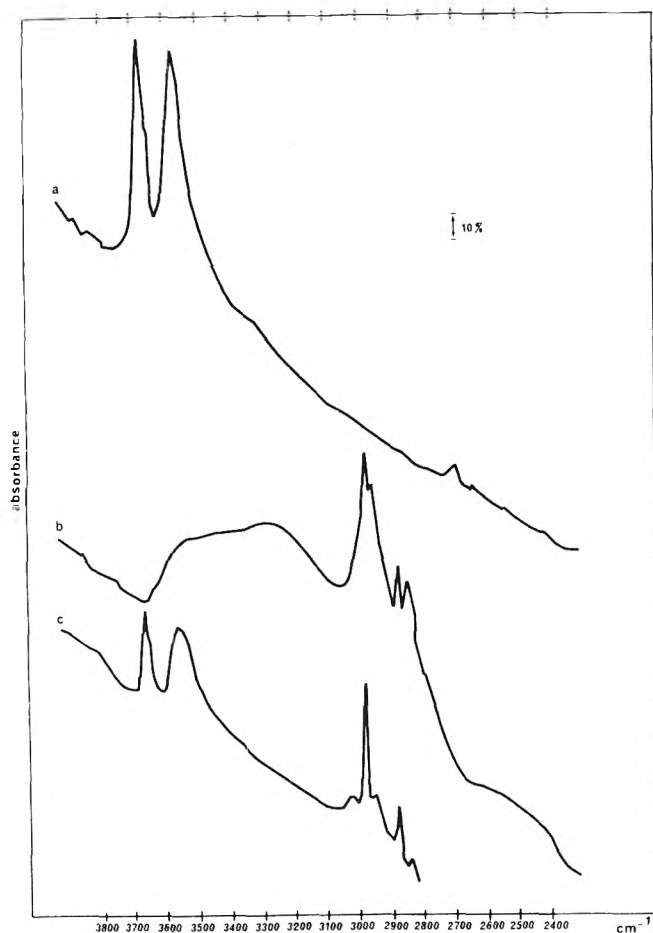


Figure 1. Evolution of the OH stretching region of H-Y upon adsorption of CH_3OH : a, decationated zeolite (see text); b, adsorption at 200° for 5 min under a relative pressure $P/P_0 = 1$ followed by outgassing at 200° till $P < 10^{-5}$ Torr; c, further outgassing for 14 hr at 200° .

C_6D_6 vapor was introduced into the cell containing the decationated sample, while heating at about 150 – 200° .¹⁴ After a few minutes the vapor was pumped off. The procedure was repeated several times. Afterward the sample was again outgassed at 200° for several hours.

The 60-MHz proton pulse NMR measurements were performed with a modified Brüker BKR 302 spectrometer fitted with Tektronic 162 and 163 pulse generators, monitored by an electronic time counter. The 90° pulse duration was of the order of 20×10^{-6} sec and the magnetic field heterogeneity within the sample was between 30 and 40×10^{-3} G. In order to increase the signal to noise ratio, a Nicolet 1072 time averager was used.

The proton longitudinal relaxation time (T_{1p}) was obtained by a 90° – 90° pulse sequence.

The spin-spin relaxation time (T_{2p}) was derived from the free induction signal following a 90° pulse. When the resonance line was sufficiently narrow ($T_{2p} > 2 \times 10^3$ sec), T_2 was also obtained from the decay of the spin-echo signal following a 90° – 180° pulse sequence.

All T_2 values were corrected for the inhomogeneity of the magnetic field. T_2 was obtained either from the characteristic exponential decay for a lorentzian line as generally observed for the decationated samples or from the slope of $\log(M_\perp/M_0)$ vs. t^2 (sec²) in the case of the gaussian line as has been usual for the sodium sieves. In those cases where

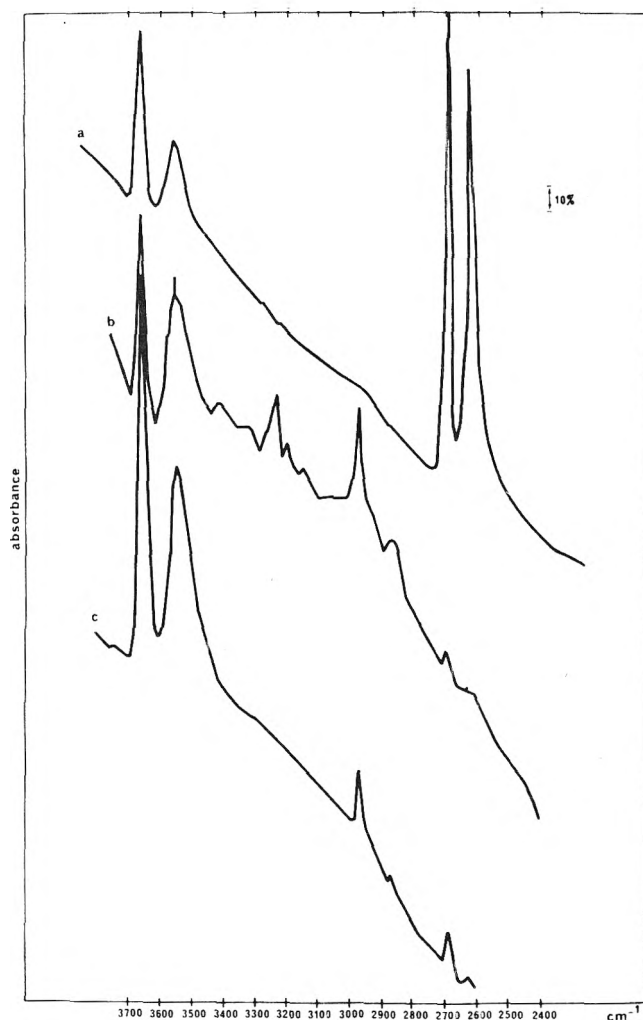


Figure 2. Evolution of the OH and OD stretching regions of H-Y upon adsorption of CH_3OH : a, decationated and partially deuterated zeolite; b, adsorption of CH_3OH at 25° and $P/P_0 = 1$ followed by outgassing at 120° for 30 min till $P < 10^{-5}$ Torr; c, further outgassing at 200° for 30 min.

two clear exponential decays were observed in the signal, the short T_2 was corrected graphically for the long component.

All T_1 values have been measured at two different time intervals on the signal. In the case of two exponential decays, these time intervals were in the same range of values as the two T_2 's. A single T_1 was obtained in all cases. T_1 and T_2 measurements at different temperatures were performed by means of the NMR probe described by Vannice et al.¹⁵

Ir Experimental Results and Discussion

The typical doublet of the lattice OH stretching vibration in H-Y is shown in Figure 1a, the two bands being observed at 3670 and 3565 cm^{-1} , respectively. Spectrum b was obtained after exposing the decationated sample at 200° for 5 min to 30 Torr of methanol vapor followed by outgassing for 5 min under a residual pressure of 10^{-6} Torr.

The high-frequency OH stretching is no more observable but the low-frequency component may be on the left-hand side of a broad band containing also the OH stretching bands of CH_3OH . CH_3 antisymmetrical and symmetrical

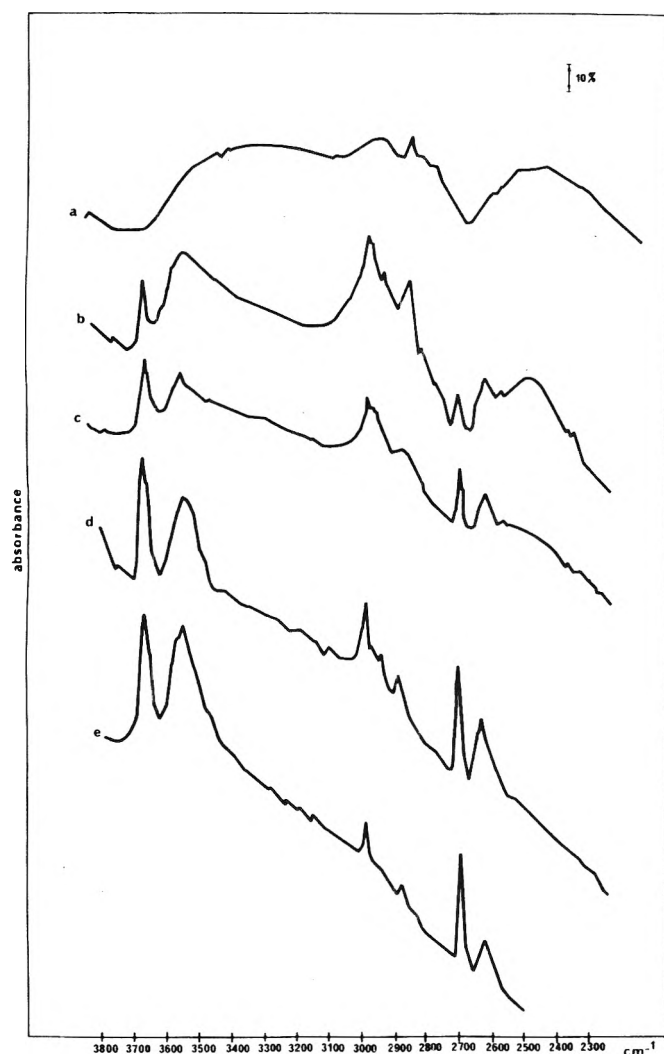


Figure 3. Isotopic exchange between H-Y and CH_3OD : a, two-thirds filling with CH_3OD at room temperature; b, outgassing at room temperature for 12 hr till $P < 10^{-5}$ Torr; c, outgassing at 45° ; d, outgassing at 100° ; e, outgassing at 280° (for 12 hr at each temperature).

stretches contribute to the bands between 3000 and 2800 cm^{-1} . After outgassing at 200° for 14 hr under a residual pressure of 10^{-6} Torr, the initial doublet, though less intense, is clearly visible as well as a weak contribution in the CH region. In the methanol OH stretching region, the base line has the same profile as in the outgassed decationated sample. Therefore it must be concluded that at 200° some methoxylation occurs and that some lattice OH groups are involved in this reaction.

In Figure 2a, the OH and OD stretching regions of a partially deuterated H-Y sample are shown. As the absorption coefficient of an OD stretching is usually about 50% that of the corresponding OH stretch, it may be concluded that deuteration has occurred to a large extent. When exposed to 80 Torr of CH_3OH at room temperature and outgassed at 120° for 30 min under a residual pressure of 10^{-6} Torr, the sample does not contain any more OD groups (Figure 2b). Some methoxylation has occurred as suggested by a residual absorption in the CH stretching region which is not removed by outgassing at 200° for 30 min.

Since the removal of the physically adsorbed CH_3OH cannot be achieved completely below 200° and since at this temperature methanol reacts with the lattice OH, as shown

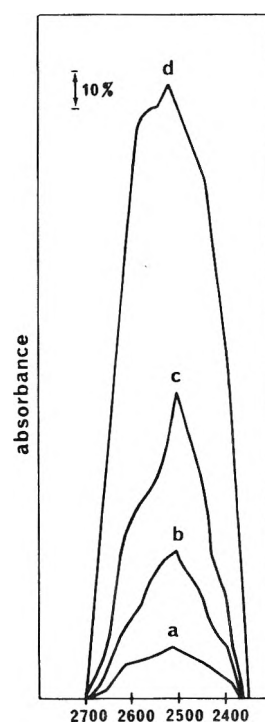


Figure 4. OD stretching band of CH_3OD adsorbed by Na-Y. Degree of filling: a, 0.03; b, 0.06; c, 0.17; d, 0.45.

in Figure 1, the residual CH stretching band shown in Figure 2c may result from the reaction occurring during the outgassing treatment. It must be also concluded that the isotopic $\text{OD} \rightleftharpoons \text{OH}$ exchange occurs very rapidly at room temperature.

This is also clearly visible in Figure 3. Spectrum a is obtained for a filling degree of 70%, the samples being initially hydroxylated and the adsorbate being CH_3OD . So, by contact at room temperature the exchange has been achieved since both the OH and OD stretching regions are very well defined on both sides of the CH stretching region.

After outgassing at room temperature for 12 hr the high-frequency OH stretch at 3670 cm^{-1} and the corresponding OD stretch at 2700 cm^{-1} as well as the CH stretching become clearly observable (spectrum b). After outgassing at 45° and 100° (spectra c and d, respectively), the resolution is still better and the low-frequency OH and OD bands are clearly observed. Finally after outgassing at 280° (spectrum e) the residual CH stretching band is present.

Also, in agreement with the observation made on the change in intensity of the OH stretching bands upon physical adsorption of rare gases,¹⁶ it is clear that the OH groups in the supercage and their corresponding high-frequency stretching band are strongly affected by methanol. Because of the superimposition with the methanol OH bands, the behavior of the OH inside the cuboctahedron and hexagonal prisms giving rise to the low-frequency stretch is ambiguous. According to the methanol content at full loading in H-Y, physically adsorbed methanol should also interact with these OH's. Examination of the absorbance in the region of the low-frequency OH stretch suggests that no interaction occurs. However isotopic exchange involves both kinds of OH.

The strong interaction between the high-frequency OH and methanol suggests of course that a strong hydrogen bond is formed between CH_3OH and the lattice OH in the

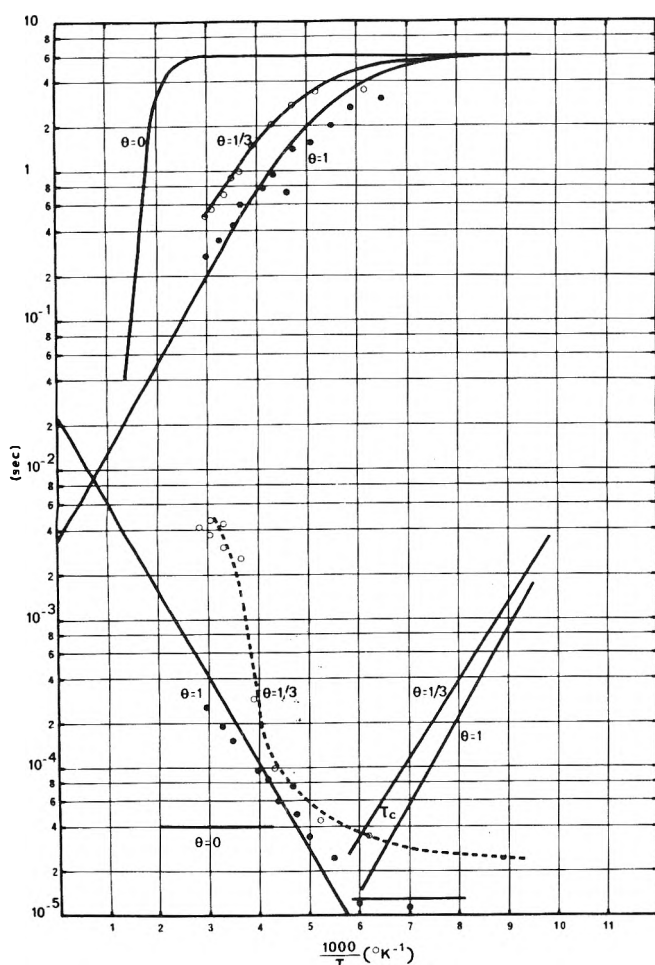


Figure 5. Variation of the spin-lattice (T_1) and spin-spin (T_2) relaxation times with respect to $1000/T$ ($^{\circ}\text{K}^{-1}$) at two filling degrees for CD_3OH in H-Y. The variation observed for T_1 in absence of methanol is from ref 20.

supercage. The isotopic exchange with the low-frequency OH could occur through the OH in the supercage.

As far as the adsorption of methanol by the sodium sieve is concerned, the main feature is the development of a strong absorption in the OH region with increasing filling degree. However, the shape of the band is almost the same at low as at high methanol content. This suggests that the intermolecular interactions are not very sensitive to the methanol content, in agreement with the observations reported by Cruz et al.¹⁷

Pulse NMR Results

The spin-lattice (T_1) and spin-spin (T_2) relaxation times measured between $+80$ and -160° are shown in Figure 5 and Figures 6 and 7 for the H-Y and Na-Y sieves, respectively. Obviously the relaxation mechanism does not depend appreciably on the filling degree of the cage, but an important distinction between the sodium and the decaionated sample appears clear.

Let us consider first Figures 6 and 7 where the proton relaxation times of either CD_3OH or CH_3OD in the Na sieve are compared. In this case no proton exchange with the lattice should occur. However two T_2 values are observed when CD_3OH is used as adsorbate. According to Cruz et al.⁴ the short T_2 should be assigned to proton exchange between CD_3OH molecules and the surface. Actually the so-

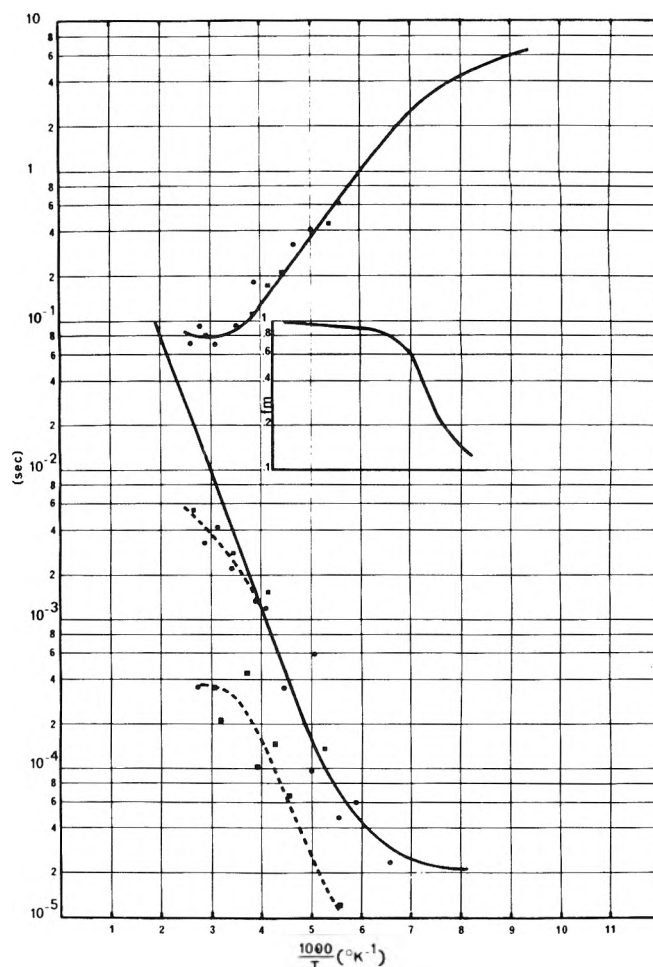


Figure 6. Variation of T_1 and T_2 for CH_3OD (●) and CD_3OH (■) in Na-Y at full loading of the zeolite cage.

dium sieve contains some silanol groups¹⁸ on the broken bonds at the cleavage faces of the microcrystal and also at some hydrolyzed cationic sites. These OH groups can be responsible for the exchange process. However, this contribution to T_1 is small because of the very small number of surface protons available, and the main contribution to the spin-lattice relaxation mechanism could be assigned to a diffusional motion.

The solid lines in Figures 6 and 7 have been computed assuming a distribution of correlation times for the diffusion motion. The fraction of molecules in the "mobile" phase f_m , as defined by Resing,¹⁹ is shown in enclosure in both of these figures. Because of some contribution T_{1p}^{-1} of the paramagnetic impurities^{4,20}

$$T_1^{-1} = T_{1d}^{-1} + T_{1p}^{-1} \quad (1)$$

where T_{1d}^{-1} is the contribution of the diffusional motion to the observed relaxation rate T_1^{-1} .

For a normalized distribution function $P(\tau)$ of the correlation times τ

$$P(\tau)d\tau = \beta^{-1}\pi^{-1/2} \exp[-(Z/\beta^2)]dZ \quad (2)$$

where β is the spreading coefficient of the distribution function and

$$Z = \ln(\tau/\tau_m) \quad (3)$$

τ_m being the average correlation time. Then

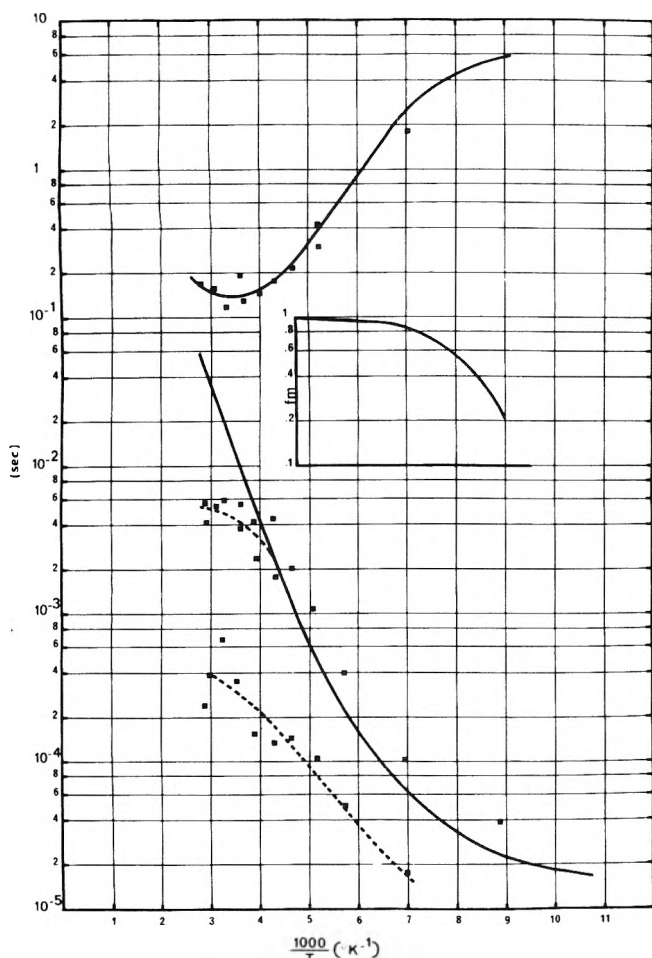


Figure 7. Variation of T_1 and T_2 for CD_3OH in Na-Y at one-third of the maximum content.

$$T_{1d}^{-1} = \frac{2}{3} \frac{S_2}{\omega} \int_0^\infty P(\tau) \left[\frac{\omega\tau}{1 + \omega^2\tau^2} + \frac{4\omega\tau}{1 + 4\omega^2\tau^2} \right] d\tau \quad (4)$$

$$T_{2d}^{-1} = \frac{S_2}{f_m} \int_0^{\tau_c} P(\tau)\tau d\tau \quad (5)$$

$$f_m = \int_0^{\tau_c} P(\tau) d\tau$$

$\tau_c = T_{2,rigid} = (\pi/2S_2)^{1/2}$ (for a gaussian line), S_2 being the second moment.

The details of these calculations for adsorbed methanol have been given previously,⁴ and they will not be repeated here. As may be shown in Figures 6 and 7, a reasonably good fit is obtained between the experimental and theoretical curves using the parameters shown in Table I. \bar{H}_d is the average activation enthalpy for diffusion. A diffusion coefficient (D) can be deduced from τ_m since

$$\tau_m = \tau_0 \exp(\bar{H}_d/RT) \quad (6)$$

$$D = \langle l^2 \rangle / 6\tau \quad (7)$$

If the average quadratic jump distance (l^2) is independent of the filling degree, the diffusion coefficients shown in Figure 8 are obtained. Other diffusion coefficients reported by Resing et al.⁹ for various molecules are indicated for the sake of comparison. The agreement with the present results seems acceptable. In particular, the activation enthalpy and the influence of the filling degree are in line with

TABLE I: Best Fitting Parameters Used in Eq. 4 and 5 for the Diffusion of CH_3OD and CD_3OH in Na-Y

	Filling degree	
	1/3	1
\bar{H}_d , kcal/mol	3.9	4.4
β	3.0	2.5
τ_0 , 10^{-12} sec	1.71	1.94
S_2 , 10^{11} radian ² /sec ²	5.8	9.2
$T_{2,rigid}$, 10^{-5} sec	~1.65	~1.3

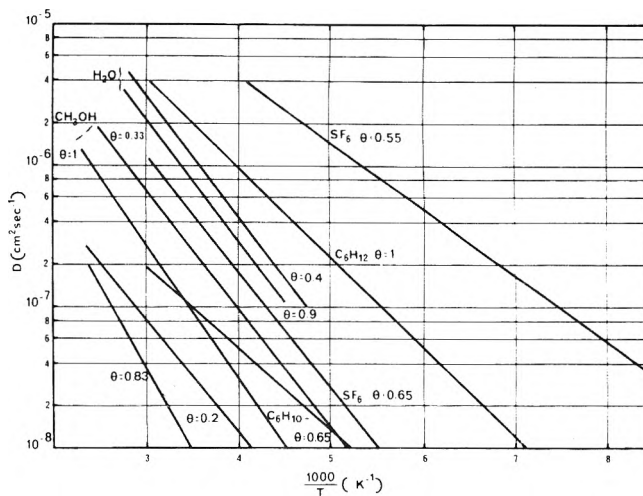


Figure 8. Comparison of the diffusion coefficients obtained for methanol at two degrees of filling with similar data reviewed by Resing.⁹

the observations reported for water and benzene. Again, as shown earlier for silica gel,⁴ methanol appears to behave intermediately between these two molecular species.

In the decationated sieve, because of the rapid exchange between the methanol OH (or OD) and the structural OD or OH, the spin-lattice relaxation rate may be to a large extent contributed by proton jumps if the jump frequency is in the appropriate range with respect to the proton resonance frequency.

This seems to be the case for the spin-spin relaxation time which is near the short T_2 observed for the sodium system. As is shown clearly in Figure 5, T_1 does not evolve with respect to temperature as does the spin-lattice relaxation time found in the sodium sieve.

Because of the absence of an observable minimum in T_1 and the uncertainty on $T_{2,rigid}$ and therefore on the second moment, it is impossible to take into account a distribution of relaxation times; therefore the activation energy (E) obtained from the slope of T_1 might be appreciably lower than the actual value. The parameters in Table II have been used to compute the solid lines in Figure 5.

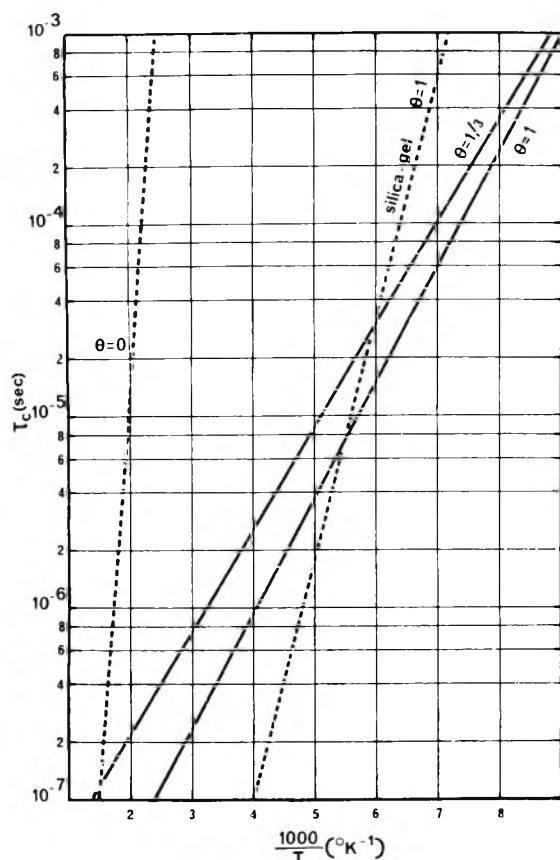
For a filling degree equal to unity, the correlation time intercepts T_2 when it reaches the value of $T_{2,rigid}$. For the lower degree of filling, the variation of T_2 is unusually rapid at about 266°K.

As compared with the parameters shown in Table I, however, E is appreciably smaller than H_d and τ_0 is noticeably longer.

On the basis of a unimolecular reaction or first-order kinetics τ_0 is expected to be in the range 10^{-12} - 10^{-13} sec. This was the case for the proton-exchange process observed

TABLE II: Best Fitting Parameters for the Proton-Exchange Process in the CD₃OH-H-Y System

	Filling degree	
	1/3	1
<i>E</i> , kcal/mol	2.4	2.7
τ_0 , sec	26	4.7
S_2 , 10^9 radian ² /sec ²	~10	~2.7
T_2 , rigid, 10^{-5} sec	~1.0	~2.0


Figure 9. Variation of the correlation time ruling the spin-lattice relaxation time in H-Y unloaded and partially (two-thirds) or totally filled with CD₃OH. For silica gel data see ref 5.

for methanol adsorbed on silica gel. Here, in presence of a more acidic surface, and thus of a higher concentration in protonated species, the 4 orders of magnitude increase observed for τ_0 suggests a different mechanism, perhaps a bi-molecular process.

The correlation time shown in Figure 9 on the left-hand side is that observed by Mestdag et al.²⁰ for a proton jumping from one oxygen to another in a decaionated Y sieve. The activation energy is then 19 kcal/mol. The correlation time for the proton-exchange process observed for CD₃OH at the monolayer coverage for a silica gel is also shown in Figure 9 as an example for a weakly acidic surface.

The H-Y-methanol system should be considered as constituted by a pool of protons belonging either to the lattice OH or to CD₃OH and involved in a fast-exchange process relayed by CD₃OH₂⁺ in high concentration. In other words in the decaionated sieve, the methanol molecule may be considered as a vehicle that transports the lattice acidic

TABLE III: Diffusion Coefficient (cm² sec⁻¹) Obtained from the Desorption Rate¹² at Full Cage for Na-Y and H-Y

Temp. °C	Na-Y	H-Y
55	1.15×10^{-6}	2.2×10^{-6}
115	5×10^{-6}	1.3×10^{-5}
225	4.6×10^{-5}	5.4×10^{-5}

protons within the cage. The relaxation mechanism is therefore entirely different from that observed in the sodium sieve.

Would a diffusional motion contribute appreciably to the relaxation mechanism in the decaionated sieve, then in agreement with similar observations reported for silica gel,⁴ a single T_1 containing the superimposition of the exchange and of the diffusion contributions should be obtained. Hence the experimental results should be comparable with those reported in Figures 6 and 7 with a broader minimum for T_1 .

Because of strong hydrogen bonding between methanol and lattice hydroxyls, some of the occluded species should have a rather low diffusion coefficient. However since at full loading the ratio $[\text{CH}_3\text{OH} + \text{CH}_3\text{OH}_2^+]/[\text{OH}]$ in the supercharge is of the order of 10, the average diffusion coefficient should not differ so much from that obtained for methanol in Na-Y. This is supported by the diffusion coefficients obtained from isothermal desorption processes for both kinds of sieves, as shown in Table III. Obviously they are close to each other and in reasonable agreement with the extrapolated values shown in Figure 8.

The lack of an appreciable diffusional contribution to the observed spin-lattice relaxation rates T_1 for the CD₃OH-H-Y system can be accounted for if the three following conditions are fulfilled.

$$T_1^{-1} = T_1^{-1}{}_{\text{exch}} + T_{1d}^{-1} + T_{1p}^{-1} \quad (8)$$

If the associated correlation times τ_{exch} and τ_d are such that $\tau_{\text{exch}} \gg \tau_d$ and if the $T_{1\text{exch}}$ and T_{1d} minima occur at two very different temperatures, $T_1^{-1}{}_{\text{exch}}$ should dominate T_{1d}^{-1} in the temperature domain where the experimental T_1 and T_2 data are collected.

(b) If the second moment modulated by the proton-exchange process (see reactions I and II) is higher than that modulated by the straight molecular diffusion of CD₃OH, $T_1^{-1}{}_{\text{exch}} > T_{1d}^{-1}$; this is acceptable in view of the large CD₃OH₂⁺ concentration. In CD₃OH₂⁺ the proton-proton distance is of the order of 1.6 Å whereas the H-H distance in CH₃OD is about 1.8 Å.

(c) If the molecular diffusion in H-Y is effected by a peculiarly broad distribution of correlation times, $T_{1d}^{-1}{}_{\text{min}}$ should decrease and the minimum itself should be very shallow. As said before, strong hydrogen bonding with the lattice OH groups and perhaps also the presence of methanol in both the sodalite and the zeolitic cages could be at the origin of this spreading of the distribution function.

Therefore the particular conditions¹⁹ that produce sometimes a T_2 minimum in systems where a proton exchange occurs between two phases are not obeyed and the assumption that the CD₃OH-H-Y system behaves a single pool of protons may well be accounted for by the obvious difference between the relaxation mechanisms observed for methanol occluded in Na-Y and H-Y.

Resing²¹ has analyzed recently the exchange between

chemisorbed and physisorbed molecules and, in particular, the proton exchange between adsorbed water and the OH groups originating from a very limited hydrolysis of the Na-X near-faujasite zeolite. At two-thirds of the maximum water content, the proton lifetime in the OH group is 2×10^{-4} sec at room temperature. Here the correlation time assigned to the proton jumps is 4.6×10^{-7} sec at room temperature and full loading. The jump frequency in the $\text{CD}_3\text{OH-H-Y}$ pool of protons is thus about 1000 times larger than in the system studied in Resing. Since the hydrolysis of Na-X does not generate lattice OH groups with the high acidity²² characterizing those shown by the OH stretching bands in Figures 1-3, this difference is not surprising.

Conclusions

(1) In the Na-Y sieve, the proton relaxation mechanism of adsorbed methanol is ruled by a diffusional motion. The diffusion coefficient at full loading is about half that measured at one-third filling. These coefficients are in the right order of magnitude as compared with those reported for other adsorbed species.

(2) In the decationated sieve, the proton relaxation mechanism of adsorbed CD_3OH is probably ruled by a proton exchange with the acid surface OH groups. The proton-exchange process does not appear to be first order.

Acknowledgments. Many thanks are due to W. E. E. Stone and to P. G. Rouxhet for stimulating discussions.

The help of W. E. E. Stone in the experimental part of this work has been deeply appreciated by P.S.

References and Notes

- (1) On leave of absence from the CSIC on a Juan March fellowship.
- (2) (a) K. T. Geodakya, A. V. Kiselev, and V. I. Lygin, *Russ. J. Phys. Chem. (Engl. Transl.)*, **41**, 227 (1967); (b) V. Bosacek and Z. Tvaruzkova, *Collect. Czech. Chem. Commun.*, **36**, 551 (1971).
- (3) P. G. Rouxhet and R. E. Sempels, *Trans. Faraday Soc.*, **70**, 2021 (1974).
- (4) M. I. Cruz, W. E. E. Stone, and J. J. Fripiat, *J. Phys. Chem.*, **76**, 3078 (1972).
- (5) S. J. Seymour, M. I. Cruz, and J. J. Fripiat, *J. Phys. Chem.*, **77**, 2847 (1973).
- (6) H. Noller, B. Mayerbock, and G. Zundel, *Surf. Sci.*, **33**, 82 (1972).
- (7) E. G. Weidemann and G. Zundel, *Z. Naturforsch., Teil A*, **28**, 236 (1973).
- (8) R. Janoschek, E. G. Weidemann, H. Pfeiffer, and G. Zundel, *J. Am. Chem. Soc.*, **94**, 2387 (1972).
- (9) H. A. Resing and I. S. Murday, *Adv. Chem. Ser.*, **No. 121**, 414 (1973).
- (10) N. N. Avgul, A. G. Bezuz, and O. M. Dzhigit, *Adv. Chem. Ser.*, **No. 102**, 184 (1971).
- (11) L. Lerot, Ph.D. Thesis, University of Louvain, 1974.
- (12) P. Salvador et al., unpublished data.
- (13) G. T. Kern, *Adv. Chem. Ser.*, **No. 121**, 219 (1973).
- (14) P. Jacobs, personal communication.
- (15) M. A. Vannice, M. Boudart, and J. J. Fripiat, *J. Catal.*, **17**, 359 (1970).
- (16) J. L. Wite, A. N. Jelly, J. M. Andre, and J. J. Fripiat, *Trans. Faraday Soc.*, **63**, 461 (1967).
- (17) M. I. Cruz, J. Andre, K. Verdinne, and J. J. Fripiat, *An. Quim.*, **69**, 895 (1973).
- (18) P. A. Jacobs and J. B. Uytterhoeven, *J. Chem. Soc., Faraday Trans. 1*, **69**, 373 (1973).
- (19) H. A. Resing, *Adv. Mol. Relaxation Processes*, **1**, 109 (1967).
- (20) M. M. Mestdag, W. E. E. Stone, and J. J. Fripiat, submitted for publication in *Trans. Faraday Soc.*
- (21) H. A. Resing, *J. Phys. Chem.*, **78**, 1279 (1974).
- (22) H. A. Resing, personal communication.

Infrared Spectra of Matrix Isolated Disulfur Monoxide Isotopes

Alfred G. Hopkins, Francis P. Daly, and Chris W. Brown*

Department of Chemistry, University of Rhode Island, Kingston, Rhode Island 02881 (Received February 10, 1975)

Publication costs assisted by the Petroleum Research Fund

Infrared spectra of natural abundance and isotopically enriched S_2O matrix isolated in Ar have been measured. The vibrational bands of $^{32}\text{S}_2^{16}\text{O}$, $^{32}\text{S}_2^{18}\text{O}$, $^{34}\text{S}_2^{16}\text{O}$, $^{34}\text{S}^{32}\text{S}^{16}\text{O}$, and $^{32}\text{S}^{34}\text{S}^{16}\text{O}$ have been assigned, and the observed frequencies of these isotopes used to calculate the harmonic force constants of S_2O .

Introduction

The species S_2O has been found to be stable for short periods of time in the gas phase at low pressures, and it is thought to be an important species in photochemical, combustion, and electrical discharge reactions of sulfur and oxygen. Schenk and Steudel¹ have shown that S_2O is one of the products formed from the very reactive SO species (reacting with itself), and that S_2O is a good indicator for the prior existence of SO. In early work,^{2,3} S_2O was incorrectly identified SO or $(\text{SO})_2$. Later, Myer and coworkers^{4,5} correctly identified S_2O by mass and infrared spectroscopy.

Several years ago we initiated a program to measure vibrational spectra of all of the sulfur oxides^{6,7} and of small sulfur species.^{6,8,9} Since S_2O is one of the more important sulfur oxides, we have measured the infrared spectra of

most of its isotopic species isolated in inert gas matrices, and determined its harmonic force constants.

Experimental Section

Infrared spectra were measured on a Perkin-Elmer Model 521 infrared spectrometer, which was calibrated with water vapor and polyethylene.¹⁰ S_2O was prepared by passing SO_2 -Ar mixtures through either a radiofrequency (≤ 200 W at 10 MHz) or a microwave (≤ 60 W at 2450 MHz) electrodeless discharge. The "hot" gaseous mixture was condensed onto a CsI substrate in a Cryotip cell at 20°K;¹¹ the discharge region and the substrate were separated by a pinhole (0.8 to 3.5 mm in diameter). The gas was deposited at the rate of 3-6 mmol/hr.

SO_2 (Matheson) was vacuum distilled several times prior

TABLE I: Observed Frequencies and Assignments of Bands in the Spectra of the S₂O Isotopes^a

Frequency, cm ⁻¹	Pure SO ₂	SO ₂ (nat. abund) discharge	SO ₂ (50% ³⁴ S) discharge	SO ₂ (90% ¹⁸ O) discharge	Type of vibration
1156.2		S ₁	S ₁ , S ₂	S ₁	SO stretch
1151.4	P ₁	P ₁	P ₁		SO stretch
1145.7	P ₁ '	P ₁ '	P ₁ '		SO stretch
1144.0			S ₃ , S ₄		SO stretch
1138.6			P ₂ '		SO stretch
1122.3				P ₃	SO stretch
1118.3				P ₃ '	SO stretch
1114.8				S ₅	SO stretch
1100.0				P ₄	SO stretch
1095.8				P ₄ '	SO stretch
672.0		S ₁	S ₁	S ₁	SS stretch
670.9				S ₅	SS stretch
662.8			S ₂ , S ₃		SS stretch
652.9			S ₄		SS stretch
382.0		S ₁	S ₁	S ₁	SSO bending
379.3			S ₂ , S ₃		SSO bending
376.6			S ₄		SSO bending
371.1				S ₅	SSO bending

^a Assignments: P₁ and P₁' = site split components of ³²S¹⁶O₂; P₂' = site split component of ³⁴S¹⁶O₂; P₃ and P₃' = site split components of ³²S¹⁶O¹⁸O; P₄ and P₄' = site split components of ³²S¹⁸O₂; S₁ = ³²S¹⁶O₂, S₂ = ³⁴S³²S¹⁶O, S₃ = ³²S³⁴S¹⁶O, S₄ = ³⁴S²¹⁶O, S₅ = ³²S²¹⁸O.

to being used and it was mixed with Ar (Matheson, 99.998%) by standard manometric procedures. SO₂ enriched in ¹⁸O (~90%) was obtained from Miles Laboratories, whereas SO₂ enriched in ³⁴S (~50%) was generated by heating enriched rhombic sulfur (Oak Ridge National Laboratories) with excess oxygen at 310° for 8 hr in a Pyrex tube fitted with a Teflon stopcock.

Results and Discussion

Infrared Spectra. Infrared spectra in the region of interest of pure SO₂, discharged SO₂ (natural abundance), discharged SO₂ (~50% ³⁴S), and discharged SO₂ (90% ¹⁸O) matrix isolated in Ar (Ar/SO₂ ≈ 400 in all cases) are shown in Figure 1. The observed frequencies and assignments are listed in Table I. Interfering bands due to SO₂ appear only in the SO stretching region. In an Ar matrix the band due to the SO₂ symmetric stretching vibration appears as a strong doublet (P₁ and P₁') due to site splitting;^{12,13} the weaker band observed at ~1139 cm⁻¹ is assigned to the stronger of the site split components of ³⁴SO₂ (in a natural abundance sample the ratio of ³²S to ³⁴S is ~25:1).

In the spectrum of discharged SO₂ (natural abundance) shown in Figure 1b relatively strong new bands appear at 1156.2, 672.0, and 382.0 cm⁻¹. Previously, bands at 1165, 679, and 388 cm⁻¹ were assigned to ³²S₂¹⁶O by Blukis and Myers;⁵ the first band is due to the SO stretching vibration, the second to the SS stretching vibration, and the third to the bending vibration.

In the spectrum of discharged SO₂ (90% ¹⁸O) in Figure 1d, the SO stretching region is rather complex. We might anticipate finding bands for S¹⁸O₂, S¹⁶O¹⁸O, S¹⁶O₂, S₂¹⁸O, and S₂¹⁶O (all with ³²S); however, the predicted ratio of S¹⁸O₂:S¹⁶O¹⁸O:S¹⁶O₂ is ~80:9:1. Thus, we would not expect to see bands due to S¹⁶O₂, whereas we would expect to find two pairs of bands for S¹⁸O₂ and S¹⁶O¹⁸O in the ratio of ~9:1. Two pairs of bands with appropriate intensities are found at 1100.0 and 1095.8 cm⁻¹ for S₁₈O₂ (P₄ and P₄') and

at 1122.3 and 1114.8 cm⁻¹ for S¹⁶O¹⁸O (P₃ and P₃'). Thus, we have two unassigned bands in the expected intensity ratio of ~10:1 at 1144.8 and 1156.2 cm⁻¹, which we assigned to S₂¹⁸O and S₂¹⁶O, respectively. The assignments of the SS stretching and the bending modes are unambiguous; the strongest component in each region is due to S₂¹⁸O and the weaker one (which is a shoulder in the SS stretching region) is due to S₂¹⁶O.

In the spectrum of discharged SO₂ (~50% ³⁴S) shown Figure 1c the SO stretching region is more complex. We expect to find bands due to ³²SO₂, ³⁴SO₂, ³²S₂O, ³⁴S₂O, ³⁴S³²SO, and ³²S³⁴SO (all with ¹⁶O). The bands due to ³²SO₂ (P₁ and P₁') and the stronger site split components of ³⁴SO₂ (P₂') are observed as expected. However, this leaves only two unassigned bands, 1156.2 and 1144.0 cm⁻¹, for the four isotopic species of S₂O. To resolve this problem we calculated the force constants (see the section on force constants) for the two S₂O isotopic species whose frequencies could be clearly assigned, i.e., ³²S₂¹⁶O and ³²S₂¹⁸O, and used these force constants to predict the frequencies of the SO stretching vibrations of the other 34-isotopic species of S₂O. As a result, we found that ³²S₂O (S₁) and ³⁴S³²SO (S₂) had the same SO stretching frequency (1156.2 cm⁻¹), and that ³²S³⁴SO (S₃) and ³⁴S₂O (S₄) had the same frequency (1144.0 cm⁻¹), i.e., the mass of the terminal sulfur atom does not affect the SO stretching frequency. We tried other possible assignments, but the calculated frequencies differed considerably from the observed frequencies.

The assignments in the S-S stretching and in the bending regions for 50% ³⁴S enriched S₂O were straightforward. Three bands were observed in each region; the band at the highest frequency was assigned to ³²S₂O, the one at the next highest to ³²S³⁴SO and ³⁴S³²SO, and the one at the lowest frequency to ³⁴S₂O. The dual assignment of the central band in each region is confirmed by the relative intensities of ~1:2:1 for the three bands.

Force Constants. A normal coordinate analysis was per-

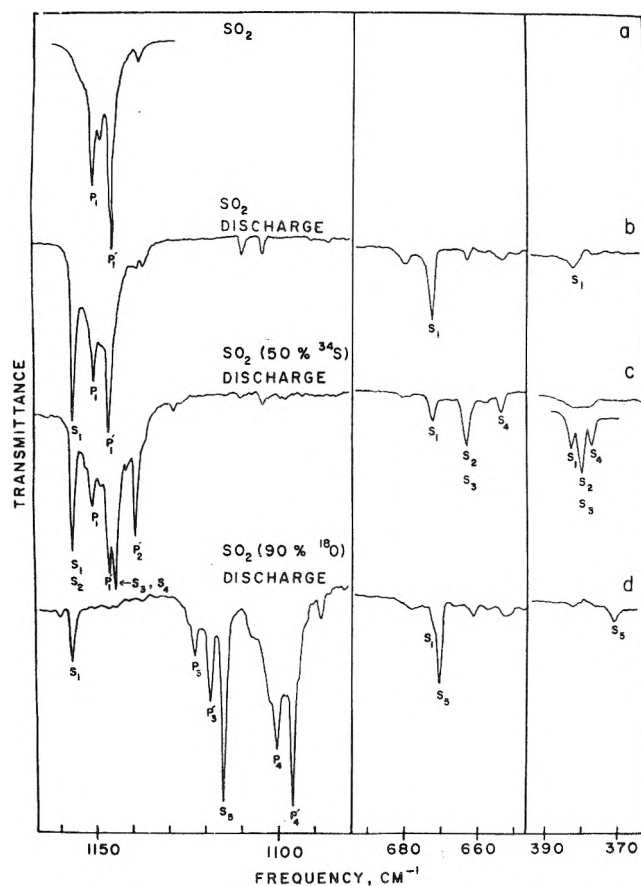


Figure 1. Infrared spectra of pure SO_2 (natural abundance), SO_2 (natural abundance) discharge products, SO_2 (50% ^{34}S) discharge products, and SO_2 (90% ^{18}O) discharge products, isolated in Ar matrices ($\text{Ar}/\text{SO}_2 \approx 400$ in all cases).

formed using the Wilson FG matrix method and the force constant adjustment computer program written by Schachtschneider.¹⁴ The following geometrical parameters were used in the calculations:¹⁵ $r_{\text{SO}} = 1.4594 \text{ \AA}$, $r_{\text{SS}} = 1.8845 \text{ \AA}$, and $\angle_{\text{SSO}} = 118.08^\circ$. The three valence bond force constants for the squared terms in the potential energy expression (K_{SO} , K_{SS} , and K_{α}) and the three for the cross terms ($K_{\text{SO,SS}}$, $K_{\text{SO},\alpha}$, and $K_{\text{SS},\alpha}$) were used in the analysis; the resulting force constants obtained using all five isotopes of S_2O are given in Table II. The observed and calculated frequencies are given in Table III. The average error in frequency for the 15 frequencies is 0.2 cm^{-1} or 0.03%, which strongly supports the reliability of the assignments.

Conclusions

Although assigning the bands of the isotopic species of S_2O was not extraordinarily difficult, the process was much easier after we completed the normal coordinate analysis on the vibrations of $^{32}\text{S}^{16}\text{O}$ and $^{32}\text{S}_2^{18}\text{O}$, i.e., on the vibrations of the isotopes that could be assigned with a degree of certainty. This adds support to the use of normal coordinate analysis in assigning the vibrational bands of simple molecules. Knowledge of the force constants of S_2O should now make it possible to assign the vibrational bands of other lower oxides of sulfur.

TABLE II: Force Constants for S_2O Calculated Using Frequencies from Five Isotopes

	Force constant ^a	σ
K_{SO}	8.249	0.002
$K_{\text{SO,SS}}$	0.151	0.004
$K_{\text{SO},\alpha}$	-0.013	0.005
K_{SS}	4.430	0.002
$K_{\text{SS},\alpha}$	0.242	0.002
K_{α}	1.408	0.001

^a Units: K_{SO} , K_{SS} , and $K_{\text{SO,SS}}$ in mdynes/\AA ; $K_{\text{SO},\alpha}$ and $K_{\text{SS},\alpha}$ in mdynes/radian ; and K_{α} in $\text{mdynes \AA/radian}^2$

TABLE III: Observed and Calculated Frequencies for the Isotopes of S_2O

Isotope	Obsd frequency, cm^{-1}	Calcd frequency, cm^{-1}
$^{32}\text{S}_2^{16}\text{O}$	1156.2	1156.4
	672.2	672.3
	382.0	382.1
$^{32}\text{S}_2^{18}\text{O}$	1114.8	1114.6
	670.9	670.6
	371.1	370.5
$^{34}\text{S}_2^{16}\text{O}$	1144.0	1144.0
	652.9	653.1
	376.6	376.8
$^{32}\text{S}^{34}\text{S}^{16}\text{O}$	1144.0	1144.1
	662.8	662.8
	379.3	379.4
$^{34}\text{S}^{32}\text{S}^{16}\text{O}$	1156.2	1156.2
	662.8	662.8
	379.3	379.4

Acknowledgment. Acknowledgment is made to the donors of the Petroleum Research Fund, administered by the American Chemical Society, for support of this research. Two of us (A.G.H. and F.P.D.) gratefully acknowledge financial aid in the form of NDEA Title IV Fellowships.

References and Notes

- (1) P. W. Schenk and R. Stuedel in "Inorganic Sulfur Chemistry", G. Nickless, Ed., Elsevier, New York, N. Y., 1968, pp 367-418.
- (2) P. W. Schenk, *Z. Anorg. Allg. Chem.*, **211**, 150 (1953); *Chem. Z.*, **67**, 273 (1943).
- (3) A. V. Jones, *J. Chem. Phys.*, **18**, 1268 (1950).
- (4) D. J. Meschi and R. J. Myers, *J. Am. Chem. Soc.*, **78**, 6220 (1956); *J. Mol. Spectrosc.*, **3**, 405 (1959).
- (5) U. Blukis and R. J. Myers, *J. Phys. Chem.*, **69**, 1154 (1965).
- (6) A. G. Hopkins, S.-Y. Tang, and C. W. Brown, *J. Am. Chem. Soc.*, **95**, 3486 (1971).
- (7) A. G. Hopkins and C. W. Brown, *J. Chem. Phys.*, **62**, 25:1 (1975).
- (8) R. E. Barletta and C. W. Brown, *J. Phys. Chem.*, **75**, 4059 (1971).
- (9) A. G. Hopkins and C. W. Brown, *J. Chem. Phys.*, **62**, 1598 (1975).
- (10) E. K. Plyler, A. Danti, L. R. Blaine, and E. D. Tidwell, *J. Res. Natl. Bur. Stand.*, **64**, 1 (1960).
- (11) Cryotip cell, Model AC-2L-110, Air Products and Chemicals, Inc.
- (12) J. W. Hastie, R. Hauge, and J. L. Margrave, *J. Inorg. Nucl. Chem.*, **31**, 281 (1969).
- (13) D. E. Milligan and M. E. Jacox, *J. Chem. Phys.*, **55**, 1003 (1971).
- (14) J. H. Schachtschneider, "Vibrational Analysis of Polyatomic Molecules VI", Shell Development Co., Emeryville, Calif., 1964.
- (15) E. Tiemann, J. Hoeft, F. J. Lovas, and D. R. Johnson, *J. Chem. Phys.*, **60**, 5000 (1974).

Raman Spectroscopic Studies of Binary Systems. II. Effect of Temperature upon Molecular Association in the Ammonia–Hexadeuteriobenzene System

John H. Roberts*

Laboratoire des métaux alcalins dans l'ammoniac liquide, Equipe de recherche associée au C.N.R.S., Faculté libre des Sciences et Hautes Etudes Industrielles, 59 046 Lille, France

and Berlin de Bettignies

Service de Spectrochimie Infrarouge et Raman C.N.R.S. Section de Lille, Université des Sciences et Techniques de Lille B.P. 36, 59 650 Villeneuve d'Ascq, France (Received January 6, 1975)

The Raman spectra of some binary solutions of ammonia and hexadeuteriobenzene have been measured as a function of temperature. It appears that, when the temperature decreases, molecular association increases between ammonia molecules. Further a liquid–liquid phase separation has been observed. In the lower benzene-rich phase, when benzene solidifies as a glassy solid, the spectrum of the N–H stretching region becomes similar to the spectrum of pure liquid ammonia. At temperatures lower than 200°K the observed spectrum is like that of pure solid ammonia.

Spectroscopic studies of molecular association in hydrogen-bonded solvents have shown that similar changes in the degree of association, whether caused by the addition of an electrolyte or simply by a change in temperature, modify the solvent spectra.^{1,2} Near-infrared³ and Raman⁴ studies of association in liquid ammonia have also emphasized the necessity of consistency in the interpretation of temperature and concentration studies. The previous paper in this series examined changes in the state of molecular association of ammonia molecules in the ammonia–hexadeuteriobenzene system as a function of composition.⁵ In this study we have examined the system as a function of temperature, and it will be shown that the results of the two studies support a unified interpretation for the aggregation phenomena exhibited by this system. Aggregation phenomena have been studied in the case of metal–ammonia binary system above and below the critical temperature of liquid–liquid demixion.^{6–10} It would be fruitful to compare the respective interactions of ammonia, which is a polar liquid, with benzene, a nonpolar liquid, or with solvated alkali metals.

Although ammonia and hexadeuteriobenzene (or benzene) are miscible at room temperature, we have found that at some lower temperature, which depends upon the composition of the sample, a liquid–liquid phase separation occurs. At a slightly lower temperature, benzene starts solidifying from the lower benzene-rich phase. It is in equilibrium with an ammonia-rich phase which seems to be partly included in the solid and which remains liquid until considerably lower temperatures. The Raman spectra in the N–H stretching region are drastically modified when the benzene is solidified. These results will be discussed in terms of the state of aggregation of the ammonia molecules in the homogeneous liquid solutions and in the liquid in equilibrium with solid benzene.

Experimental Section

All the spectra reported here were recorded from the

lower part of the samples (benzene-rich phase). The details of sample preparation have been described previously, as have the spectrometer, laser, and data accumulation system.⁵ For this study a cryostat was used for temperatures below ambient and a furnace was used for temperatures above ambient.¹¹ With this system, the temperature can be followed continuously. Minimal variation of temperature occurs during the recording of a spectrum since the rapid scanning monochromator requires about 10 sec, at low speed, to record the spectrum in the N–H stretching region (3100–3450 cm^{-1}). For spectra requiring multiple scans with data accumulation no significant temperature variation was noticed and the reported temperatures are accurate to $\pm 1^\circ$ with variations during the experiments less than 0.5° .

Results

Figure 1 shows the evolution of the spectrum for a sample of mole ratio 1 NH_3 :1.3 C_6D_6 over the temperature range 268–198°K. In Figure 2, a set of spectra is shown for a sample with a mole ratio 1.5 NH_3 :1 C_6D_6 over the temperature range 338–200°K. It must be kept in mind that hexadeuteriobenzene freezes at 278°K and liquid ammonia at 195°K and the various mixtures appear to be solid at different temperatures between these two extremes. Three characteristic types of spectra have been obtained which correspond to the physical state of the sample. At higher temperatures, the spectra are characteristic of liquid mixtures, and at the lowest temperature, of ammonia in the solid state. Spectra in the intermediate temperature region (b, c, and d in Figure 1 and e, f, and g in Figure 2) differ considerably from both the spectra for the liquid solutions and the lowest temperature solids. The temperature range of this intermediate region varies with the composition of the sample, but in all cases studied the lower limit is about 195°K. In this intermediate temperature region, the samples appear to be white glassy solids. In experiments in which the temperature of the samples was lowered gradually, a liquid–liquid phase separation occurred. As the temperature was lowered further, benzene solidified from the benzene-rich phase into a glassy white solid. Other experi-

* Address correspondence to this author at the Department of Chemistry, University of Texas at Austin, Austin, Tex. 78712.

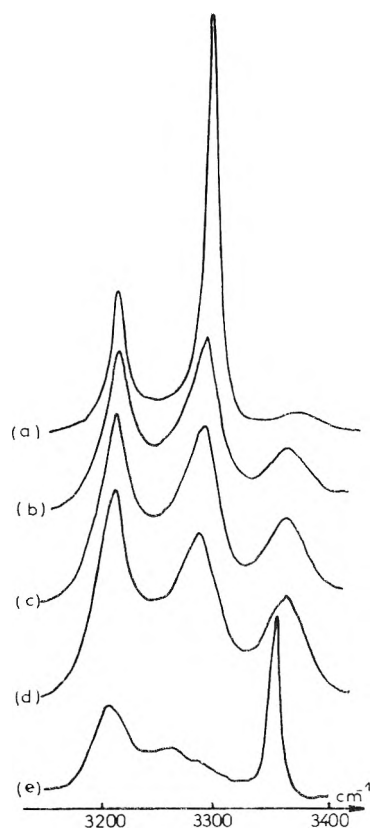


Figure 1. Experimental spectra of the N-H stretching region for a sample of mole ratio 1 NH_3 :1.3 C_6D_6 : (a) liquid 268°K; (b-d) intermediate range (b) 263°K, (c) 225°K, (d) 206°K; (e) solid 198°K. The 3213- and 3301- cm^{-1} lines result from the Fermi resonance between the ν_1 and $2\nu_4$ vibrations. Decomposition of the envelop by RESOL program⁵ yields ν' at 3260 cm^{-1} .

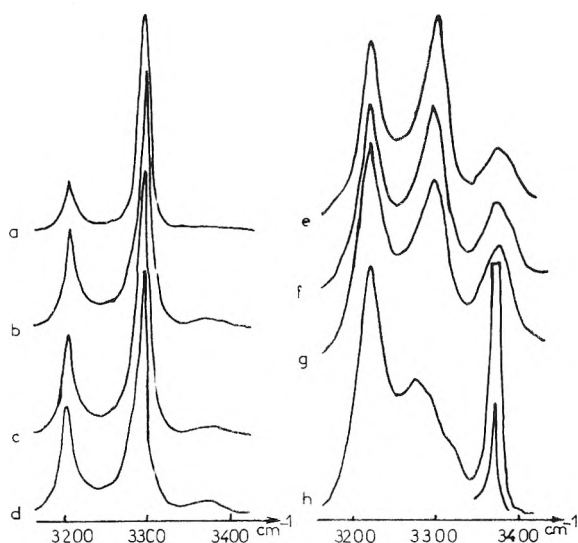


Figure 2. Experimental spectra of the N-H stretching region for a sample of mole ratio 1.5 NH_3 :1 C_6D_6 liquid (a) 338°K, (b) 297°K, (c) 273°K, (d) 251°K; intermediate state (e) 244°K, (f) 228°K, (g) 205°K; solid (h) 200°K. The assignments are the same as in Figure 1.

ments are now being planned to obtain Raman spectra of both phases in the liquid-liquid and liquid-solid equilibrium in an effort to gain more insight into the aggregation processes involved in the phase separation. Figure 3 shows the experimental frequency shifts of ν_1 of ammonia for sev-

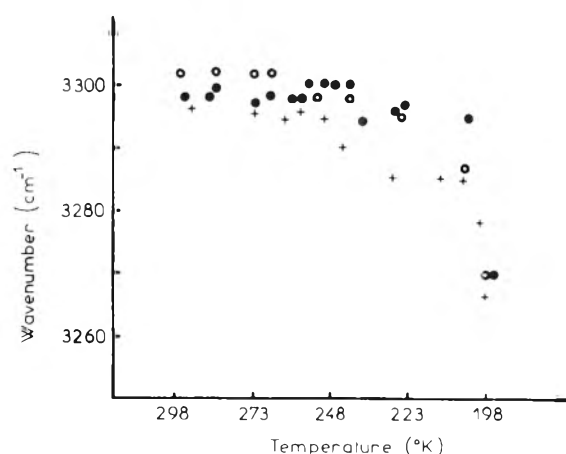


Figure 3. Experimental frequency shifts of 3301- cm^{-1} band of ammonia as a function of temperature: (O) 1 NH_3 :1.3 C_6D_6 ; (●) 1.5 NH_3 :1 C_6D_6 ; (+) 3 NH_3 :1 C_6D_6 .

eral samples as a function of temperature. The assignments used here are in agreement with the majority of other workers in this field, as previously discussed.⁵ The question of assignment for ν_1 and $2\nu_4$, the bands in Fermi resonance, as a function of temperature will be considered in detail in the Discussion section.

For the sample with mole ratio 1.5 NH_3 :1 C_6D_6 the half-widths increase from 18 to 48 cm^{-1} for the 3213- cm^{-1} band and from 24 to 42 cm^{-1} for the 3301- cm^{-1} band, as the temperature decrease in relative intensity of both ν' , the symmetric stretch of associated ammonia molecules with C_s symmetry, and ν_3 the asymmetric stretch of ammonia as the temperature of the liquid solutions is lowered. Spectra in the N-H stretching region of all the low temperature solid samples below 195°K were identical with that of solid ammonia.

Discussion

In spectroscopic studies of hydrogen-bonded liquid systems it has often been shown that the changes in the X-H stretching region of the spectrum can be attributed to changes in the degree of hydrogen bonding.^{12,13} If a mixture model for a liquid system is valid the changes in the spectrum should be consistent whether the perturbation to the hydrogen-bonded structure is caused by the addition of an electrolyte, dilution with a strongly interacting liquid, dilution with a noninteracting liquid, or with changes in temperature. The expectation that the extent of hydrogen bonding in liquid ammonia should increase as the temperature is lowered is borne out by the results of this study. In Figures 1 and 2 it is clear that ν increases in relative intensity as the temperature decreases, and, thus, it is evident that unassociated ammonia molecules with C_{3v} symmetry are being converted into associated ammonia molecules with C_s symmetry. The increase in the relative intensity of ν_3 , Figures 1 and 2, as the temperature decreases is in agreement with this interpretation as are the frequency shifts of the N-H stretching modes to lower frequency and the increase in the half-widths of ν_1 and $2\nu_4$ Figure 3.

The previous paper in this series examined the behavior of the ammonia-hexadeuteriobenzene system as a function of concentration.⁵ The results of this temperature study are in agreement with the concentration study, i.e., similar changes in the Raman spectrum are observed when the ammonia structure is subjected to stresses, arising from differ-

ent sources, which are relieved by similar changes in the extent of hydrogen bonding.

Another phenomenon which affects the Raman spectrum in the N-H stretching region is the Fermi resonance interaction between ν_1 and $2\nu_4$ of ammonia molecules with C_{3v} symmetry. Fermi resonance can occur in a molecule when an overtone or a combination and a fundamental have nearly the same frequency and are both of the same symmetry species.¹⁴ There is then a mixing of the two states and the overtone, which would normally have negligible intensity in the Raman spectrum, is said to borrow intensity from the fundamental so that the intensities of the two bands in the spectrum are more nearly equal. Also, the observed bands are shifted, one to higher frequency and one to lower frequency, from the frequency where the accidental degeneracy occurs.¹⁴ The separation between the two bands, and thus their positions, varies as the separation of the unperturbed levels varies. Since there is a mixing of the two states the experimentally observed bands cannot rigorously be labeled ν_1 and $2\nu_4$ since both of the observed bands are a mixture of the two vibrations. In a first approximation, it can be said that the more intense of the two bands in Fermi resonance is composed to a greater extent of ν_1 , since the fundamental supplies the intensity observed in both bands. In the case of liquid ammonia there is a reversal in position of the more intense band as the temperature is lowered, and so assignments of the two bands based upon their preponderant character should be reversed for high and low temperature.¹⁵

When the symmetry of the ammonia molecule is lowered from C_{3v} to C_s , as is the case for ammonia molecules with an N-H group involved in a hydrogen bond, the degeneracy of ν_4 is lifted and the energy levels of the two bands are separated considerably. Although these bands have not yet been observed in the Raman spectra of liquid ammonia, probably due to a much reduced intensity in comparison to the already weak ν_4 of ammonia with C_{3v} symmetry, their separation may be such that Fermi resonance is no longer possible. A calculation of the frequency expected for ν_1 in the absence of any perturbation yields 3260 cm^{-1} .¹⁵ This result and the observation of the polarized band at 3260 cm^{-1} , which is due to associated ammonia molecules, suggest that in ammonia molecules with C_s symmetry Fermi resonance may not occur.

Raman spectra for ammonia molecules, such as those reported here, Figure 1 and 2, for the intermediate temperature range are characterized by two features. The half-widths of the bands are much greater than for the homogeneous solutions at higher temperature and when the tem-

perature is lowered they tend to the characteristic values of pure liquid ammonia. The relative intensity of ν_3 is much greater than in the homogeneous solution and also greater than in pure liquid ammonia at the same temperature. The later difference seems to decrease with decreasing temperature. All these properties are well interpreted if, in the intermediate range of temperature, a very dilute solution of benzene in ammonia is in equilibrium with solid benzene. The fact that spectra for all samples below 195°K are identical with pure solid ammonia strongly suggests that these solid mixtures must be viewed as being dispersions of aggregates of solid ammonia in a benzene matrix.

It may be asked if the intermediate range spectra might be indicative of the formation of weak hydrogen-bonded complexes. The phase separation and the close resemblance of the spectra below 195°K to that of pure solid ammonia would seem to rule out complex formation, and preliminary studies on the ammonia-carbon tetrachloride system have shown that similar phenomena occur in this system.¹⁶ Further work now in progress on these systems may yield a better understanding of the aggregation process that occurs immediately before the liquid-liquid phase separation and of the phase diagram of the system.

Acknowledgments. We wish to thank Professor G. Lepoutre for his helpful discussion, and the National Science Foundation and The Centre National de la Recherche Scientifique for the Exchange of Scientists grant to J.H.R.

References and Notes

- (1) J. D. Worley and I. M. Klotz, *J. Chem. Phys.*, **45**, 2868 (1966).
- (2) G. E. Walrafen, *J. Chem. Phys.*, **52**, 4176 (1970).
- (3) J. H. Roberts and J. J. Lagowski in "Electrons in Fluids, the Nature of Metal-Ammonia Solutions", J. Jortner and N. R. Kestner Ed., Springer-Verlag, Berlin, 1973.
- (4) A. T. Lemley, J. H. Roberts, K. R. Plowman, and J. J. Lagowski, *J. Phys. Chem.*, **77**, 2185 (1973).
- (5) J. H. Roberts and B. de Bettignies, *J. Phys. Chem.*, **78**, 2106 (1974).
- (6) G. Lepoutre and J. P. Lelieur in "Metal-Ammonia Solutions, Colloque Weyl II", J. J. Lagowski and M. J. Sienko, Ed., Butterworths, London, 1970.
- (7) G. Lepoutre in ref 3, p 181.
- (8) M. J. Sienko and P. Chieux in ref 6, p 339.
- (9) P. Chieux, *Phys. Lett. A*, **48**, 493 (1974).
- (10) B. L. Smith and W. H. Koehler in ref 3, p 145; M. G. De Backer, P. F. Rusch, B. De Bettignies, and G. Lepoutre, ref 3, p 161; P. F. Rusch and J. J. Lagowski, ref 3, p 169.
- (11) B. De Bettignies, Thèse 3ème Cycle, Lille, 1971.
- (12) G. C. Pimentel and A. L. Mc. Clellan, "The Hydrogen Bond", W. H. Freeman, San Francisco, Calif., 1960.
- (13) "Hydrogen-Bonded Solvent Systems", A. K. Covington and P. Jones, Ed., Taylor and Francis, London, 1968.
- (14) G. Herzberg, "Molecular Spectra and Molecular Structure", Vol. II, Van Nostrand, Princeton, N.J., 1962.
- (15) B. de Bettignies and F. Wallart, *C. R. Acad. Sci., Paris*, **271**, 640 (1970).
- (16) J. H. Roberts and B. de Bettignies, unpublished results.

Electron Spin Resonance Spectra of Certain Fluorohydride Radicals of Phosphorus, Arsenic, and Antimony^{1a}

A. J. Colussi,^{1b} J. R. Morton,* and K. F. Preston

Division of Chemistry, National Research Council of Canada, Ottawa K1A 0R9, Canada (Received December 16, 1974)

Publication costs assisted by the National Research Council of Canada

Isotropic ESR spectra of a series of phosphorus fluorohydride radicals $\text{PH}_n\text{F}_{4-n}$, where $n = 0-4$, have been observed in γ -irradiated solid solutions of PF_3 , PF_2H , and PH_3 in neopentane or SF_6 . The spectra of AsH_3F and SbH_3F are also reported. The hyperfine interactions of these radicals are consistent with a totally symmetric semioccupied orbital in a framework possessing either C_{2v} or C_s symmetry. The relative merits of Hückel and INDO molecular orbital calculations in predicting the various observed trends are discussed.

Introduction

The existence of free radicals derived from tetravalent phosphorus (phosphoranyl radicals) is now well established.²⁻⁷ These radicals have attracted considerable interest among both ESR spectroscopists and theoreticians because of their unusual structure. Thus, the spectra of both PF_4 ⁴ and PH_4 ⁵ show, in addition to a large ³¹P hyperfine interaction, interactions with two pairs of equivalent ligand nuclei, indicating trigonal bipyramidal geometries for both species. Since all phosphoranyl radicals (and a number of isoelectronic radicals) may be regarded as derivatives of one or other of these species, there is good reason to believe that all radicals of tetracoordinated phosphorus have trigonal bipyramidal structures. This is borne out by ESR hyperfine interaction measurements for radicals such as ROPH_3 ,^{2a} PCl_4 ,⁶ POCl_3 ,⁷ and SOF_3 .⁸

While there remains little doubt concerning the molecular geometry of these radicals, their electronic structure is still a subject of debate. Higuchi, in his theoretical study⁹ of PF_4 , was able to account for the experimental data with either the valence-bond or molecular orbital approach by assuming phosphorus 3d orbital participation. Hückel and INDO MO calculations for PF_4 and PH_4 , on the other hand, reproduce the experimental hyperfine measurements with a minimal basis set of s and p orbitals only.³ Furthermore, a number of additional features brought out by recent studies of derivatives of PH_4 ^{2a} and PF_4 ^{3,7} are more readily explained in terms of MO theory. For example, the greater stability of apically substituted derivatives of PH_4 and PF_4 is consistent with the charge-density distributions predicted by INDO MO calculations. Moreover, the effect of increasing electronegativity of RO in ROPF_3 radicals³ upon the various hyperfine interactions is readily accounted for in terms of a semioccupied orbital which is an antibonding, three-center (Rundle¹⁰) MO involving the phosphorus atom and the two apical ligands.

In this paper we present hyperfine interaction measurements for some simple phosphoranyl radicals $\text{PH}_n\text{F}_{4-n}$ (where $n = 0-4$) and for the related species AsH_3F and SbH_3F . The data show trends consistent with a simple MO description of the semioccupied orbital, in which d orbital participation is ignored.

Experimental Section

Samples of SF_6 , neopentane, or neopentane-*d*₁₂ were

doped with approximately 5% PF_3 , PH_3 , or PF_2H by mixing appropriate proportions of the two gases, followed by condensation of the mixture into an ESR sample tube. The samples were irradiated at -196° with γ rays from a 9000-Ci ⁶⁰Co source, and their ESR spectra examined at -170° with a Varian E-12 spectrometer.³

PF_3 and SF_6 were obtained from Ozark-Mahoning Inc., Tulsa, Okla., the PH_3 was a gift from the Defence Research Board Laboratories, Ottawa; AsH_3 was obtained from Matheson Gas Products Inc., East Rutherford, N.J.; PF_2H was prepared by the method of Rudolph and Schiller;¹¹ a sample of antimony metal enriched to 99% in the isotope ¹²³Sb was obtained from Oak Ridge National Laboratory, Oak Ridge, Tenn., and was used to prepare ¹²³SbH₃.¹²

Results

A. Phosphorus-Centered Radicals. An irradiated sample of SF_6 containing a few percent PF_3 exhibits the powerful ESR spectrum attributed by Fessenden and Schuler⁴ to the radical PF_4 . The *g* factor and hyperfine data (Table I) were obtained by exact diagonalization of the appropriate spin matrix under the assumption that all hyperfine interactions had the same (positive) sign. As Fessenden has shown,¹³ this combination leads to a much smaller standard deviation in the spectral parameters than any other. Our data for PF_4 - SF_6 are in virtually exact agreement with those of Fessenden,¹³ but differ substantially from those of Nelson, Jackel, and Gordy.¹⁴ These authors generated an anisotropic spectrum of PF_4 in a PF_3 matrix at 4°K . The discrepancy between their data and ours could be a matrix or a temperature effect, but is probably an artifact resulting from the inherent difficulties of interpreting anisotropic spectra.

Irradiation of a matrix consisting of 5% PH_3 in neopentane enabled us to detect the spectrum of PH_4 at -170° .⁵ Its four protons are equivalent in pairs—apical and equatorial. Exact analyses of the data show unequivocally that the signs of the ³¹P hyperfine interaction and that of the two apical protons are the same (positive). The results of these calculations appear in Table I.

In addition to the two prototype radicals PF_4 and PH_4 we were also able to generate and detect (Table I) certain other radicals in the series $\text{PH}_n\text{F}_{4-n}$. For example, after irradiation of a matrix of PH_3 in SF_6 we detected a spectrum attributable to PH_3F . A very interesting result was the de-

TABLE I: ESR Data^a for Certain $\text{PH}_n\text{F}_{4-n}$ Radicals

Radical	g value	³¹ P hfs, ^b G	Apical hfs, ^b G	Equatorial hfs, G
PF_4	2.0009	1322.0	293.5	59.5
$\text{PF}_3\text{H}_{\text{eq}}^c$	2.0016	1030.8	225.2(F)	38.5 (F) 38.5 (H) 5.9 (D)
$\text{PF}_3\text{H}_{\text{eq}}$	2.0020	1027.3	226.8 (F)	35.0 (F) 35.0 (H) 5.1 (D)
$\text{PH}_3\text{F}_{\text{ap}}$	2.0032	721.3	347.2 (F) 130.1 (H)	12.6 (H)
PH_3^c	2.0030	519.3	198.7 (H) 30.2 (D)	6.0 (H) Not res (D)

^a Errors are ± 2 in last significant figure given. ^b Shown to have the same sign by best-fit procedures.¹³ ^c In neopentane; others in SF_6 .

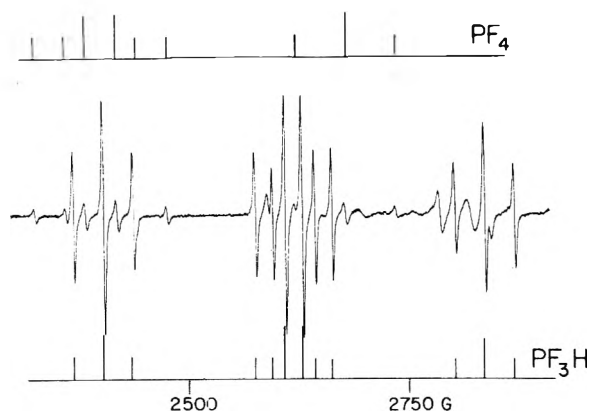


Figure 1. The $M(I_{31}) = 0.5$ transition of $\text{PF}_3\text{H}_{\text{eq}}$ observed in 5% PF_2H in SF_6 at approximately 9.1 GHz. The hyperfine interactions of the ^1H and ^{19}F equatorial ligands are accidentally equal in this radical.

tection in both PF_3 -neopentane and PF_2H - SF_6 of a spectrum which appeared to be that of PF_2H_2 (i.e., the hyperfine pattern indicated two pairs of apparently equivalent ligands (Figure 1)). However, deuteration studies with both PF_3 -neopentane- d_{12} and PF_2D - SF_6 revealed that the radical possessed only one equatorial proton, whose hyperfine interaction happened to be the same as that of the equatorial fluorine nucleus. The species was thus identified as $\text{PF}_3\text{H}_{\text{eq}}$; its parameters in both neopentane and SF_6 are given in Table I. Unfortunately, we have not been able as yet to obtain an ESR spectrum of the radical PF_2H_2 .

B. Radicals AsH_3F and SbH_3F . Irradiation of a matrix consisting of $\sim 5\%$ AsH_3 in SF_6 at -196° resulted in the formation of the radical AsH_3F . Its ESR spectrum at -170° consisted of 16 7.7-G, 1:2:1 triplets, of which four (the $M(I_{\text{As}}) = -0.5$ transition) were obscured by the radicals SF_5 and SF_6^- . The spectral parameters (g , hyperfine interactions) were determined by computerized diagonalization of the appropriate spin matrix, a process which clearly demonstrated that the signs of the ^{75}As , ^{19}F , and apical proton hyperfine interactions were all positive. Table II shows the average values of several independent determinations of these parameters.

Irradiation of an SF_6 matrix containing dissolved SbH_3 enabled us to detect the ESR spectrum of SbH_3F at -170° . In this case, however, analysis of the spectrum was complicated by the following factors: (a) the existence of two mag-

TABLE II: ESR Parameters of PH_3F , AsH_3F , and SbH_3F Radicals^a

Radical	g value	Central atom hfs, G	Apical hfs, G	Equatorial hfs, G
$^{31}\text{PH}_3\text{F}$	2.0032	721.3	347.2 (F) 130.1 (H)	12.6 (H)
$^{75}\text{AsH}_3\text{F}$	2.0093	860.7	300.7 (F) 167.5 (H)	7.7 (H)
$^{123}\text{SbH}_3\text{F}$	2.0158	1048.9	233.8 (F) 178.7 (H)	Not res (H)

^a Errors are ± 2 in last significant figure given.

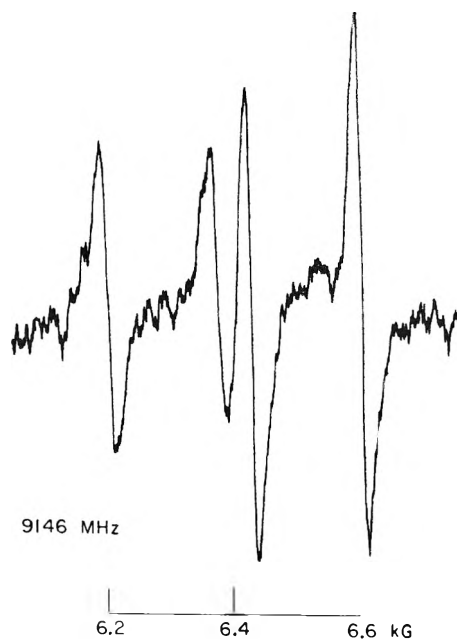


Figure 2. The $M(I_{123}) = -3.5$ transition of SbH_3F enriched to 99% in the isotope ^{123}Sb ($I = 3.5$).

netic isotopes of antimony (^{121}Sb , 57.25%, $I = 2.5$ and ^{123}Sb , 42.75%, $I = 3.5$) and (b) the anticipation of exceedingly large hyperfine interactions for both isotopes. The combined effect of these two factors led us to anticipate that for $^{121}\text{SbH}_3\text{F}$, only the $M(I_{121}) = -2.5$ transition would be accessible but that for $^{123}\text{SbH}_3\text{F}$ both the $M(I_{123}) = -3.5$ and -2.5 transitions would be accessible. We therefore prepared SbH_3 from a sample of antimony enriched to 99% in the isotope ^{123}Sb . The $M(I_{123}) = -3.5$ (Figure 2) transition was analyzed to yield for the apical ^{19}F and ^1H hyperfine interactions the values 234 and 178 G, respectively. The equation

$$a = (2H - 2)/(2I + 1 - H) \quad (1)$$

enables one to calculate the hyperfine interaction (a) of a nucleus (spin I) from the transition at highest field (H), if both a and H are expressed in units of $\nu/g\beta$, where ν is the microwave frequency and $\beta = 1.399611$ MHz/G. At 9146 MHz, this transition occurred at 6402 G, yielding (assuming $g = 2.0000$ in eq 1) a provisional value for a_{123} of 1038 G. Unfortunately, the $M(I_{123}) = -2.5$ transition was obscured by the powerful spectra of SF_5 and SF_6^- in the $g = 2$ region, and so accurate values of the g factor and hence the antimony hyperfine interactions could only be obtained

with the aid of the "forbidden" transition $|4, -4\rangle \leftarrow |3, -3\rangle$ (low-field, $|F, M(F)\rangle$ quantum numbers) of $^{123}\text{SbH}_3\text{F}$. This transition, for which $a = (2H + 2)/(8 + H)$ in units of $\nu/g\beta$, occurred at 1138 G and, combined with the $M(I) = -3.5$ transition, yielded $g = 2.0158$, $a_{123} = 1049$ G. Using this g value we calculated a value for a_{121} of 1929 G from the $M(I_{121}) = -2.5$ transition observed at 6961 G in natural SbH_3 . The ratio of the observed hyperfine interactions, $a_{121}/a_{123} = 1.839$, was in close agreement with the ratio of the magnetogyric ratios (1.847).

The proton and fluoron hyperfine interactions in SbH_3F were assigned (Table II) on the basis of the line-width variation apparent (Figure 2) in the spectrum. The larger hyperfine interaction is clearly associated with considerable anisotropy, and was therefore assigned to the fluorine nucleus. Assuming this interaction to be positive (as in AsH_3F), a greater (or lesser) width is expected for the low-field ($M_I(F_{ap}) = 0.5$) pair of lines if the inner product of the anisotropic g and ^{19}F hyperfine tensors is positive (or negative).¹⁵ This product is likely to be larger for the apical fluorine atom than for the apical proton, because of the expected large contribution of F(2p) orbitals to the semioccupied orbital.

Discussion

It has been well established by ESR spectroscopy that all of the radicals whose spectra we shall be discussing possess ground states which are totally symmetric in either C_{2v} or C_s symmetry. In the former case the four ligands are equivalent in pairs, the pair subtending the smaller angle at the central atom being called the equatorial ligands, the other pair being called apical. It follows from the totally symmetric ground-state of these radicals that the orbital occupied by the unpaired electron can possess considerable central-atom ns character, a fact which accounts for the dominant feature of all the spectra: the exceedingly large central-atom hyperfine interaction. In addition, of course, the semioccupied orbital contains contributions from various ligand atomic orbitals (ns , or appropriate combinations of np). The data in Table I demonstrate that successive replacement of F atoms by H atoms in PF_4 results in a monotonic decrease in the ^{31}P hyperfine interaction, a trend consistent with the antibonding nature of the half-filled orbital in these radicals. The pronounced effect of equatorial substitution, however, is somewhat surprising since it presumably implies that the description of the semioccupied orbital as a Rundle orbital^{3,7} is not entirely adequate.

We have suggested elsewhere³ that in the radicals ROSF_4 and ROPF_3 the contribution to the semioccupied orbital by the fluorine atom trans to RO consisted primarily of F(2p) atomic orbitals. The total contribution of F(2s) including polarization effects was demonstrably small. Increasing the electronegativity in R caused the trans ^{19}F hyperfine interaction to decrease, an effect which we tentatively ascribed to a decrease in the polarizability factor Q_{FM}^{F} (i.e., operating on the F(2p) contribution) rather than due to a decrease in any direct F(2s) participation. In the present case, however, very different conditions obtain: the apical H(1s) contribution to the semioccupied orbital in PH_4 is approximately 40%, and there can be no contribution from p orbitals on hydrogen. Therefore, the decrease in the trans proton hyperfine interaction on substitution of a more electronegative fluorine atom or *tert*-butoxy^{2a} ligand for an apical proton can only be due to a decrease in the contribution of the apical proton 1s orbital to the

semioccupied orbital. Such a direct effect may also be operative in ROSF_4 and ROPF_3 , although it is impossible to determine the relative importance of the two mechanisms.

The ^{75}As hyperfine interaction in AsH_3F can be compared with those of certain other arsenic-centered radicals. The general trends discussed above for phosphoranyl radicals are apparent. The largest ^{75}As hyperfine interaction occurs for the radical AsF_4 (1576 G¹⁶), and the smallest for $\text{As}(\text{C}_6\text{H}_5)_4$ (541 G¹⁷). The effect of an electronegative ligand in the apical position is apparent from the value for $\text{As}(\text{C}_6\text{H}_5)_3\text{OC}(\text{CH}_3)_3$ (666 G¹⁸); two apical *tert*-butoxy ligands increase the ^{75}As interaction still further, to 792 G.¹⁸

We turn now to a brief discussion of the effects on the spin-density distribution of a change in the central-atom electronegativity along a series such as PH_3F , AsH_3F , and SbH_3F (the radicals PF_4 and AsF_4 have been discussed elsewhere¹⁶). For this purpose we need a reliable factor to relate the central-atom hyperfine interaction to its valence s spin density. For want of a better method, and with certain reservations,¹⁹ we identify unit valence s spin density on the central atom (M) with the factor $(8\pi/3)\gamma_e\gamma_M\psi^2(0)$ as calculated from Froese's wave function.²⁰ For the nuclei $^{31}\text{P}(3s)$, $^{75}\text{As}(4s)$, and $^{123}\text{Sb}(5s)$ the values 3638, 3393, and 3266 G, respectively, were obtained. From these figures and the corresponding hyperfine interactions (Table II) the contribution of central-atom ns character to the semioccupied orbital may be calculated to be approximately 0.32 in the case of SbH_3F , 0.25 for AsH_3F , and 0.20 for PH_3F . This decrease in central-atom s character with increasing electronegativity at that atom is due to the antibonding nature of the semioccupied orbital. As is also evident from Table II, the spin released from the central atom upon increasing its electronegativity reappears as increasing F($2p_z$) or F(2s) contributions to the semioccupied orbital. This effect (and the concomitant reduction in the H_{ap} hyperfine interaction) is probably due to the weakly $\text{H}_{ap}\cdots\text{F}$ bonding nature of the semioccupied orbital.

Molecular Orbital Calculations

We have carried out molecular orbital calculations on the phosphorus-centered radicals listed in Table I. The INDO I ($K = 1$) parameterization,²¹ with a minimal basis set of valence s and p atomic orbitals, was used. As has been mentioned elsewhere,³ the minimum energy configuration of both PH_4 and PF_4 is predicted by the INDO I method to have neither D_{4h} (square planar) nor T_d (tetrahedral), but C_{2v} symmetry. This, in itself, is gratifying agreement with the experimental observations. The INDO method furthermore predicts that the observed radicals PF_3H_{eq} and PH_3F_{ap} are more stable by several kilocalories per mole than their conformers PF_3H_{ap} and PH_3F_{eq} , respectively. On the other hand, however, the INDO approximation reproduces only the grossest features of the spin-density distributions. For the purposes of comparing atomic spin densities with experimental hyperfine interactions we use as conversion factors the parameter $(8\pi/3)\gamma_e\gamma_M\psi_{ns}^2(0)$, which may be calculated from Froese's wave function²⁰ to be 3638 G for ^{31}P and 17,100 G for ^{19}F . For protons we use the factor 507 G. In Table III the calculated ^{31}P , ^{19}F , and ^1H hyperfine interactions are given for the radicals PF_4 , PF_3H_{eq} , PH_3F_{ap} , and PH_4 .

It will be seen that the experimental trend in the ^{31}P hyperfine interactions down the series of radicals is not adequately reproduced by the INDO method. However, much better overall agreement with experiment was obtained not

TABLE III: Calculated Values of ^{31}P , ^{19}F , and ^1H Hyperfine Interactions^a in Certain Phosphorus Fluorohydrides

Radical	^{31}P		Apical ligands		Equatorial ligands	
	Hückel	INDO	Hückel	INDO	Hückel	INDO
PF_3	1464	569	243	71	41	4
$\text{PF}_3\text{H}_{\text{eq}}$	1300	609	232	79	33 (F) 30 (H)	5 11
$\text{PH}_3\text{F}_{\text{ap}}$	1045	506	438 (F) 32 (H)	201 31	26	24
PH_3	930	674	155	245	2	2

^a Values (gauss) obtained by multiplying atomic spin densities by 507 G (^1H), 17,100 G (^{19}F), or 3638 G (^{31}P).

only for ^{31}P , but also for ^1H and ^{19}F interactions by using the Hückel-level spin densities corresponding to the INDO-optimized geometries.

NOTE ADDED IN PROOF: Very recently K. Sogabe (*J. Sci. Hiroshima Univ., Ser. A*, **39**, 225 (1975)) reported an intense spectrum of $\text{PF}_3\text{H}_{\text{ap}}$, detected in γ -irradiated $\text{PF}_2\text{H}\text{-SF}_6$ mixtures. In spite of many attempts to generate this spectrum under a variety of experimental conditions, we have been unable to do so. We wish to emphasize, however, that NMR analyses obtained both before and after γ

irradiation clearly indicated that our samples of PF_2H in SF_6 contained PF_2H and no detectable amounts of other phosphorus fluorides.

Acknowledgments. We thank Dr. K. Sogabe for a preprint of the above-mentioned article and Dr. S. K. Brownstein for NMR spectra.

References and Notes

- (1) (a) NRCC No. 14768. (b) NRCC Postdoctorate Fellow 1974.
- (2) (a) P. J. Krusic, W. Mahler, and J. K. Kochi, *J. Am. Chem. Soc.*, **94**, 6033 (1972); (b) D. Griller and B. P. Roberts, *J. Chem. Soc., Perkin Trans. 2*, 1339 (1973).
- (3) A. J. Colussi, J. R. Morton, and K. F. Preston, *J. Phys. Chem.*, **79**, 651 (1975).
- (4) R. W. Fessenden and R. H. Schuler, *J. Chem. Phys.*, **45**, 1845 (1966).
- (5) A. J. Colussi, J. R. Morton, and K. F. Preston, *J. Chem. Phys.*, **62**, 2004 (1975).
- (6) G. F. Kokoszka and F. E. Brinkman, *J. Am. Chem. Soc.*, **92**, 1199 (1970).
- (7) T. Gillbro and F. Williams, *J. Am. Chem. Soc.*, **96**, 5032 (1974).
- (8) J. R. Morton and K. F. Preston, *J. Chem. Phys.*, **58**, 2657 (1973).
- (9) J. Higuchi, *J. Chem. Phys.*, **50**, 1001 (1969).
- (10) R. E. Rundle, *Surv. Prog. Chem.*, **1**, 81 (1963).
- (11) R. W. Rudolph and H. W. Schiller, *J. Am. Chem. Soc.*, **90**, 3581 (1968).
- (12) W. L. Jolly and J. E. Drake, *Inorg. Synth.*, **7**, 34 (1963).
- (13) R. W. Fessenden, *J. Magn. Resonance*, **1**, 277 (1969).
- (14) W. Nelson, G. Jackel, and W. Gordy, *J. Chem. Phys.*, **52**, 4572 (1970).
- (15) A. Hudson and G. R. Luckhurst, *Chem. Rev.*, **69**, 191 (1969).
- (16) A. J. Colussi, J. R. Morton, and K. F. Preston, *Chem. Phys. Lett.*, **30**, 317 (1975).
- (17) S. A. Fieldhouse, H. C. Starkie, and M. C. R. Symons, *Chem. Phys. Lett.*, **23**, 508 (1973).
- (18) E. Furimsky, J. A. Howard, and J. R. Morton, *J. Am. Chem. Soc.*, **95**, 6574 (1973).
- (19) J. H. Mackey and D. E. Wood, *J. Chem. Phys.*, **52**, 4914 (1970).
- (20) C. Froese, *J. Chem. Phys.*, **45**, 1417 (1966).
- (21) A. R. Gregory, *J. Chem. Phys.*, **60**, 3713 (1974).

Electron Spin Resonance Study on the Structure of Radical Pairs in Irradiated Oriented Polyethylene

Takashi Fujimura* and Naoyuki Tamura

Takasaki Radiation Chemistry Research Establishment, Japan Atomic Energy Research Institute, Takasaki, Gunma-ken, Japan
(Received January 10, 1975)

Publication costs assisted by the Japan Atomic Energy Research Institute

A well-resolved $\Delta M_s = 1$ ESR spectrum due to radical pairs was observed in oriented polyethylene irradiated at 77°K; this spectrum is ascribed to the pair of alkyl radicals. The change of the fine splitting with the angle between the magnetic field and the draw direction reveals that the radical pairs produced are intrachain type rather than interchain type. When the magnetic field is parallel to the chain axis, the maximum fine splitting, 371 G, is obtained. This splitting is due to interactions between members of the radical pair; interspin distance is calculated to be 5.31 Å. The concentration of the paired radicals giving the observed $\Delta M_s = 1$ spectrum is about 0.3% of that of the total radicals. On warming the sample above 77°K, the intensity of the $\Delta M_s = 1$ spectrum due to the radical pair decreases faster than that of the $\Delta M_s = 2$ spectrum. Some evidence was also found for the existence of other types of radical pairs in irradiated polyethylene.

Introduction

The pairwise trapping of radicals has been reported in many organic substances irradiated at low temperatures by detecting the electron spin resonance (ESR) signals due to the $\Delta M_s = 1$ transition,^{1,2} and interest has greatly increased in the study of their structure and correlation with radiation chemical reactions.²

The pairwise trapping of radicals in irradiated polymers has been found by detecting the ESR signals of $\Delta M_s = 2$.^{3,4} Iwasaki, Ichikawa, and Ohmori⁴ obtained the $\Delta M_s = 2$ spectra due to radical pairs in irradiated polyethylene and other polymers and found the existence of radical pairs in the polymers irradiated at 77°K. The $\Delta M_s = 1$ spectrum of radical pairs in polymers has not been clearly obtained. The failure to observe the $\Delta M_s = 1$ spectrum has been attributed to the presumption that the paired radicals have not a specific distance in the case of polymers because of the complicated structure of polymers.⁴ It is difficult, however, to obtain reliable information about the structure and behavior of radical pairs from the $\Delta M_s = 2$ spectrum only.

We considered that the $\Delta M_s = 1$ spectrum of radical pairs should be clearly observed in the polymeric system, if some regularity is given in the system. On the basis of this idea, we have previously obtained the $\Delta M_s = 1$ spectrum with hyperfine structure due to radical pairs trapped in a single-crystal mat of polyethylene irradiated at 77°K.⁵ Furthermore, using an oriented polyethylene, we have succeeded in obtaining the well-resolved $\Delta M_s = 1$ spectrum due to radical pairs.⁶ Here, details of the structure and of the thermal decay of radical pairs in irradiated oriented polyethylene will be reported.

Experimental Section

Samples used are high-density polyethylene, Sholex 6050, purified with boiling xylene. A sheet of thickness 0.5 mm was formed by compression molding at 180°, quenched in ice water, and then cut into strips 3 cm wide. The strips were drawn at 60°, until an elongation of about 1000% was obtained. Good orientation of the c axis in this sample was

obtained; the width at half-maximum of the angular distribution as measured from the [002] X-ray reflection is within 7°.

Irradiations were performed in vacuo at 77°K with a Cockcroft-Walton type of electron beam which provides a dosage of 15 Mrads. The energy of the electrons was 2 MeV and the current 500 μ A; the dose rate was about 0.16 Mrads/sec. Some experiments were carried out with ⁶⁰Co γ rays to a dosage of 15 Mrads; the dose rate was 0.7 Mrads/hr. The spurious ESR signal from the irradiated quartz ampoule was eliminated by heating the ampoule while the sample was cooled in liquid nitrogen at the opposite end of the ampoule. ESR measurements were made at 77°K with Varian V-4502 X-band spectrometer. Some measurements were made with Varian E-4 spectrometer.

Results

The $\Delta M_s = 1$ spectrum obtained with drawn polyethylene irradiated in vacuo at 77°K with electrons is shown in Figure 1, when the magnetic field is parallel to the draw direction or the chain axis of polyethylene. Well-resolved multiplets are obviously observed on both sides of the main sextet spectrum; the sextet comes from the isolated alkyl radicals $-\text{CH}_2-\dot{\text{C}}\text{H}-\text{CH}_2-$. The outer multiplets consist of eleven lines as estimated later. The separation between the two eleven lines is 371 G and the hyperfine splitting of the eleven lines is 17 G, which is half of the value, 33.5 G, of the main sextet. When the sample was irradiated with γ rays, the spectrum of the same shape and intensity was observed.

The spectrum changes with the angle γ between the magnetic field and the draw direction as shown in Figure 2. A remarkable change of the outer spectrum is observed even at the small change of angle γ . When the magnetic field is perpendicular to the draw direction, the outer spectrum is hardly observed (see Figure 2d). The change of the main sextet spectrum is well explained by the change of α -H coupling of the alkyl radicals as already reported.⁷

The observed angular dependence of the fine splitting is

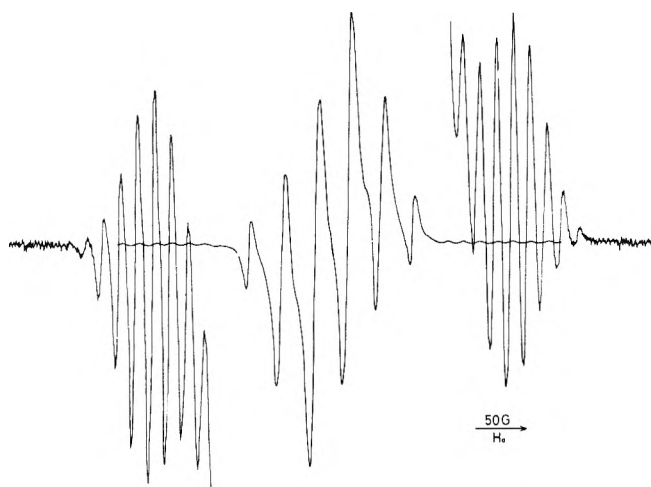


Figure 1. The $\Delta M_s = 1$ spectrum in drawn polyethylene irradiated at 77°K. Magnetic field is parallel to the draw direction or chain axis of polyethylene. Outer parts of the spectrum are recorded at increased gain (200X).

indicated by open circles in Figure 3. When the angle γ is changed from zero, the fine splitting decreases. At about 20° it becomes difficult to determine the spectral position, since the spectrum is smeared out and its height decreases rapidly.

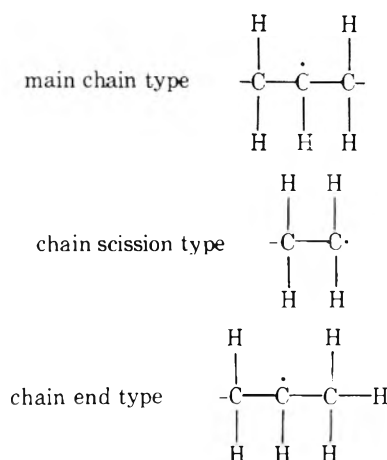
The $\Delta M_s = 2$ spectra are also obtained at $g \approx 4$ with the same sample as shown in Figure 4. When the magnetic field is parallel to the draw direction, the spectrum was estimated to consist of eleven lines with hyperfine splitting of 17 G which is the same as that of the $\Delta M_s = 1$ outer spectrum. When the magnetic field is perpendicular to the draw direction, a well-resolved spectrum was not obtained. These results reveal that the outer parts of the $\Delta M_s = 1$ spectra undoubtedly come from radical pairs. The intensity ratio of the outer spectrum due to radical pairs to the main sextet due to isolated radicals is 3×10^{-3} . The anisotropy of the $\Delta M_s = 2$ spectrum can be explained by the anisotropy of hyperfine splitting in the isolated alkyl radical.

The radical pairs are less stable than the isolated radicals at 77°K. On warming of the sample, the radical pairs decay rapidly as shown in Figure 5, where the intensities of the $\Delta M_s = 2$ and $\Delta M_s = 1$ spectra due to the paired radicals are plotted against the temperature of heat treatment. Heat treatment of the sample was carried out by warming the sample irradiated at 77°K to the given temperature for 5 min and then cooling it back to 77°K for the measurement. It can be seen that both $\Delta M_s = 1$ and $\Delta M_s = 2$ spectra begin to decay at about 130°K. However, the decay amount of the $\Delta M_s = 2$ spectrum is smaller than that of the $\Delta M_s = 1$ spectrum. Around 200°K the $\Delta M_s = 1$ spectrum decays faster than the $\Delta M_s = 2$ spectrum. It is observed that the $\Delta M_s = 2$ spectrum still remains at the temperature where the $\Delta M_s = 1$ spectrum has almost decayed. The $\Delta M_s = 1$ spectrum due to the isolated radical does not decay even at 150°K. The decay curve of the $\Delta M_s = 1$ spectrum due to isolated radicals as well as that of the $\Delta M_s = 2$ spectrum due to radical pairs in powder sample will be shown elsewhere.

Discussion

Type of Radicals Composing a Radical Pair. The fol-

lowing three types of radicals can be presumed for radical pairs in the irradiated polyethylene.



In the $\Delta M_s = 2$ spectrum, when the magnetic field is parallel to the draw axis, the observed intensity ratio of the central seven lines is 1:2.3:4.3:5.3:4.4:2.4:1. In the $\Delta M_s = 1$ spectrum (Figure 1) due to radical pairs, the intensity ratio of the central seven lines of the lower field spectrum is 1:2.5:4.4:5.2:4.4:2.8:1.8 and that of the higher field spectrum is 1.4:2.6:4.3:5.1:4.4:2.5:1. These results are in good agreement with 1:2.67:4.67:5.60:4.67:2.67:1, which is the theoretical intensity ratio of the central seven lines in eleven lines. Since an eleven-line spectrum comes from ten equally coupled protons, the radical pairs giving the $\Delta M_s = 1$ and $\Delta M_s = 2$ spectra are presumed to consist of the main chain type. The spectral intensity ratios calculated for the radical pairs of chain-scission and chain-end types do not agree with that of the observed spectra.

Structure of Radical Pairs for the Observed Spectrum. In the $\Delta M_s = 1$ spectrum a fine splitting, d , due to radical pair can be expressed as follows, if the point dipole approximation is valid¹

$$d = 3g\beta(1 - 3\cos^2\theta)/2r^3 \quad (1)$$

where g is the g tensor, β is the Bohr magneton, and θ is the angle between the magnetic field H_0 and the vector r connecting two radicals of a radical pair.

In order to calculate the theoretical angular dependence of the fine splitting in the oriented sample, a coordinate system is fixed in the sample as shown in Figure 6. The z axis of this coordinate frame is taken to be along the draw axis, and the magnetic field defines the yz plane. The vector r is defined by angles θ and ϕ in this frame, and γ is the angle between H_0 and the draw axis. In this frame, angle θ is expressed by

$$\cos\theta = \sin\theta\sin\phi\sin\gamma - \cos\theta\cos\gamma \quad (2)$$

Various types of radical pairs can be postulated for the main-chain alkyl radicals by use of the crystallographic data of polyethylene. Since the crystal lattice constants of drawn polyethylene at 77°K are not known, they were estimated by multiplying the lattice constants of powdered polyethylene at 77°K⁸ by the ratio of the lattice constants of the 10 times drawn polyethylene to those of an undrawn one at room temperature.⁹ The estimated constants are $a = 7.184$ Å, $b = 4.909$ Å, and $c = 2.547$ Å. Figure 7 shows the crystal structure of drawn polyethylene with the estimated lattice constants at 77°K. The values of r and θ can be cal-

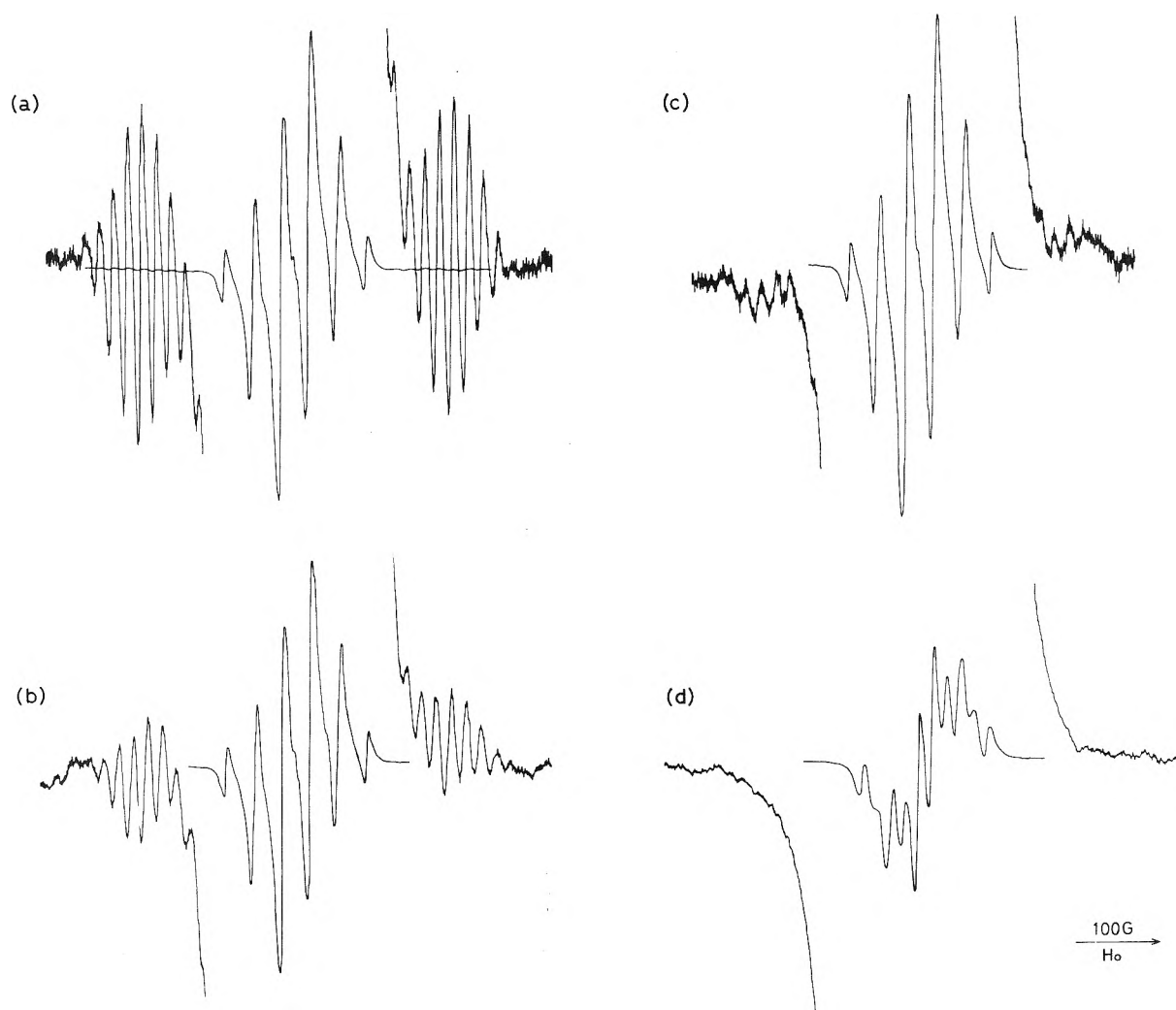


Figure 2. Angular dependence of the $\Delta M_s = 1$ spectra in drawn polyethylene irradiated at 77°K. The angle γ between magnetic field H and draw direction is (a) 0° , (b) 10° , (c) 15° , and (d) 90° .

culated for various sets of radical pairs by using this constant. When the values of r and θ are substituted in eq 1 and 2, the corresponding d values are calculated. Four d values near the observed value, 371 G, are selected as shown in Table I. It is found that the radical pairs of the interchain type $C_0-C_{7,0}$, which is the radical pair produced between C_0 and $C_{7,0}$ carbon atoms (see Figure 7), and $C_0-C_{8,-1}$ and the intrachain type C_0-C_4 have values relatively close to those observed. However, these intercarbon distances are not so different that the structure of the radical pair cannot be decided only from this comparison.

In order to decide the structure of radical pairs, the angular dependence of the fine splitting should be considered. By using eq 1 and 2, the calculated angular dependences of fine splittings are obtained as shown in Figure 3 for three types of radical pairs selected above. The calculated curve obtained with the radical pairs C_0-C_4 of the intrachain-type agrees relatively well with the observed result. However, the curves with interchain radical pairs $C_0-C_{7,0}$ and $C_0-C_{8,-1}$ differ with the observed result. The calculated curves of other radical pairs were also examined; they are far from agreement with the observed result.

These results suggest that the observed spectrum of the radical pairs is attributed to the intrachain radical pair C_0-C_4 (0° intrachain type) where the vector connecting two

radicals is parallel to the chain axis. The difference between the observed d value, 371 G, and the calculated d value, 419 G, may be explained by the following consideration. Since the spin densities at the α carbons of two alkyl radicals which compose a radical pair are smaller than 1, the interaction between two radicals is expected to be reduced¹⁰ and the observed d value may be smaller than the calculated value.

Other Types of Radical Pairs. It was presumed that the observed spectrum of radical pairs in irradiated drawn polyethylene is attributed to the 0° intrachain type. However, there are some evidences suggesting the existence of other types of radical pairs. When the sample irradiated at 77°K is heated, the $\Delta M_s = 1$ spectrum due to radical pairs decays faster than the $\Delta M_s = 2$ spectrum as shown in Figure 5. The intensity of the $\Delta M_s = 2$ spectrum reflects all radical pairs present in the sample, while the intensity of the $\Delta M_s = 1$ spectrum reflects the radical pair which is presumed to be the 0° intrachain type. This fact suggests the existence of different types of radical pairs from the observed type.

The presence of other types of radical pairs is also suggested by the following results. Figure 8 shows the intensity of $\Delta M_s = 2$ spectrum vs. the angle between H_0 and the chain axis. It is noticed that the intensity is almost inde-

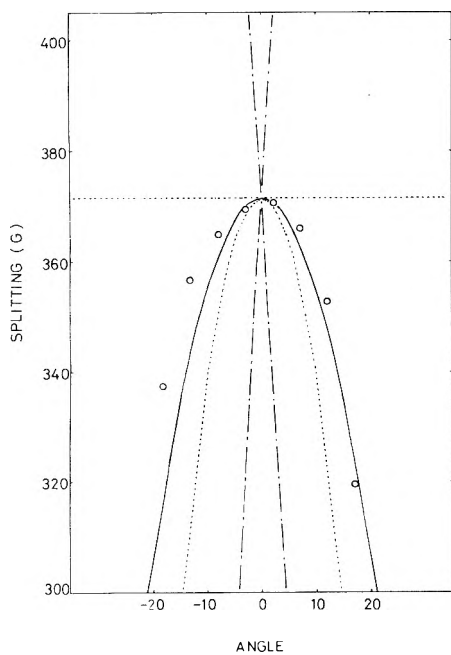


Figure 3. Angular dependence of the observed and calculated d values of $\Delta M_s = 1$ spectra due to radical pairs in drawn polyethylene irradiated at 77°K. Circles indicate observed values. Calculated values: —, C_0-C_4 ; - - -, $C_0-C_{7,0}$; - · - ·, $C_0-C_{8,-1}$. (see Figure 7) The calculated d values at $\gamma = 0^\circ$ are fitted to the observed values.

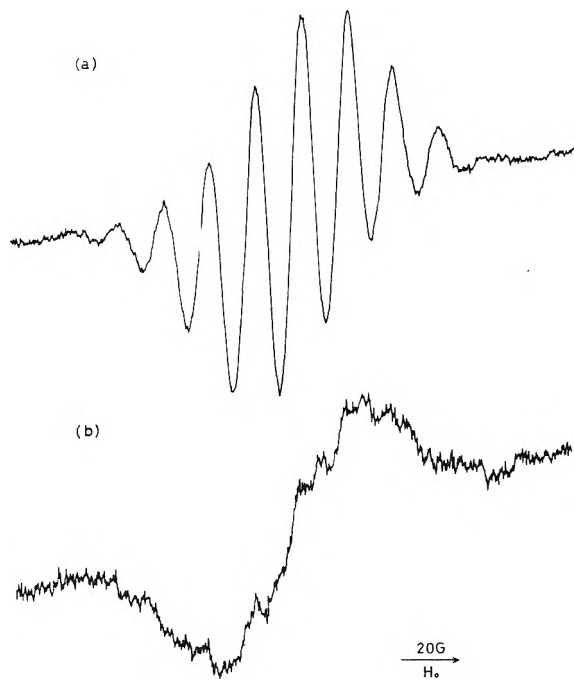


Figure 4. The $\Delta M_s = 2$ spectra in drawn polyethylene irradiated at 77°K. The angle γ between magnetic field H and draw direction is (a) 0° and (b) 90° .

pendent of the angle. The ratio of transition probability for $\Delta M_s = 2$ to that for $\Delta M_s = 1$ is given by¹¹

$$I_2/I_1 = \frac{1}{8}(d_{\parallel} \sin 2\theta/H_0)^2 \quad (3)$$

Here, d_{\parallel} is the value of d when θ is zero in eq 1. If the radical pairs produced in the drawn polyethylene are composed of 0° intrachain type only, the $\Delta M_s = 2$ spectrum should

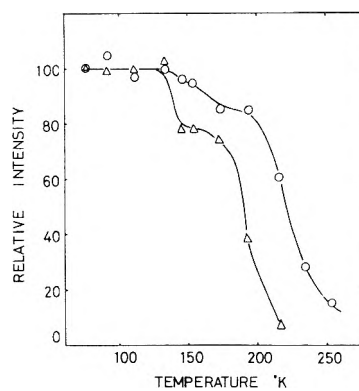


Figure 5. Decay curves of the spectra due to radical pairs: O, $\Delta M_s = 2$; Δ , $\Delta M_s = 1$.

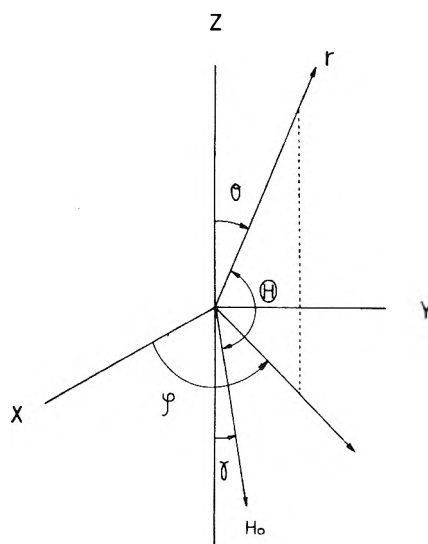


Figure 6. Coordinates relating draw and field axes. The magnetic field defines the yz plane.

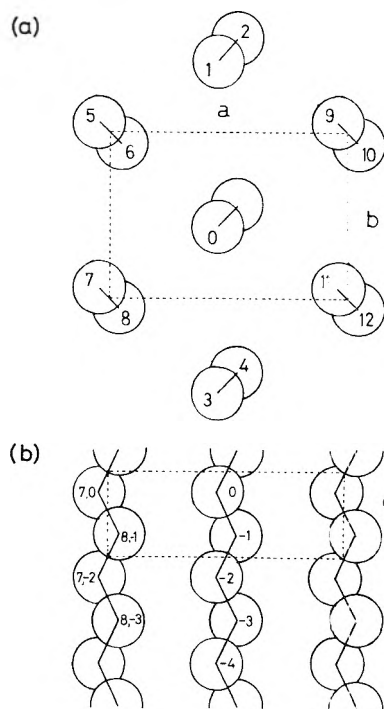


Figure 7. Crystal structure of polyethylene at 77°K: (a) projection on (001); (b) projection on (010).

TABLE I: Intercarbon and Interspin Distances and d Values for the Radical Pairs Selected

Type of selected radical pairs	Intercarbon distance, Å	$\cos \theta$	d_{calcd} , G	$d_{\text{obsd}}^a - d_{\text{calcd}}$, G	Inter-spin distance, Å
$C_0-C_{5,0}$	4.70	0	265	106	4.21
$C_0-C_{7,0}$	4.03	0	421	-50	4.21
$C_0-C_{8,-1}$	4.06	0.313	290	81	3.75
C_0-C_4	5.10	1	419	-48	5.31

^a Observed d value is 371 G.

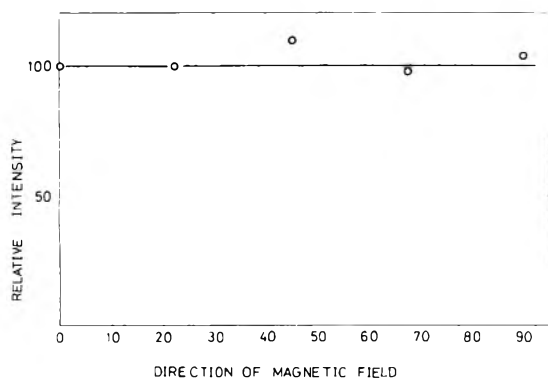


Figure 8. Intensity of the $\Delta M_s = 2$ spectrum vs. the angle γ between magnetic field and z axis.

not be observed when γ is zero, since in this case θ becomes 0° and I_2/I_1 equals zero. Actually, however, the spectrum is observed. This result suggests the existence of the other types of radical pairs, where the vector connecting two radicals is neither 0° nor 90° to the chain axis.

Although the existence of interchain radical pairs is suggested, the problem is that they do not give distinct $\Delta M_s = 1$ spectra. In the drawn polyethylene used here, the chain axes are well oriented, but there is disorder in the interchain directions because of the presence of the amorphous or the defective crystalline regions. This situation presumably causes a rather broad distribution of the d values, which smears out the $\Delta M_s = 1$ spectra of interchain paired radicals. In the case of intrachain radical pairs, however, the distance between paired radicals is fixed through the covalent bond, and thus a distinct spectrum is obtained if the sample has a good orientation of chains.

In our recent investigation with the single crystal of *n*-eicosane, several interchain radical pairs have been observed, while the radical pairs of the intrachain type such as C_0-C_4 in the drawn polyethylene have not been clearly observed.¹² This observation may support the existence of the interchain radical pairs presumed in polyethylene.

Acknowledgment. We wish to thank Mr. N. Hayakawa, Mr. T. Seguchi, and Dr. I. Kuriyama for valuable discussions and Mr. O. Yoda for X-ray diffraction measurements.

References and Notes

- (1) Y. Kurita, *J. Chem. Phys.*, **41**, 3926 (1964).
- (2) Ya. S. Lebedev, *Radiat. Eff.*, **1**, 213 (1969).
- (3) M. Iwasaki and T. Ichikawa, *J. Chem. Phys.*, **46**, 2851 (1967).
- (4) M. Iwasaki, T. Ichikawa, and T. Ohmori, *J. Chem. Phys.*, **50**, 1984 (1969).
- (5) T. Fujimura, N. Hayakawa, and N. Tamura, *Rep. Prog. Polym. Phys. Jpn.*, **14**, 557 (1971).
- (6) T. Fujimura and N. Tamura, *J. Polym. Sci., Polym. Lett. Ed.*, **10**, 469 (1972).
- (7) A. G. Kiselev, M. A. Mokulskii, and Yu. S. Lazurkin, *Vysokomol. Soedin.*, **2**, 1678 (1960).
- (8) P. R. Swan, *J. Polym. Sci.*, **56**, 403 (1962).
- (9) W. Glenz, N. Morosoff, and A. Peterlin, *J. Polym. Sci., Polym. Lett. Ed.*, **9**, 211 (1971).
- (10) A. Dulčić and J. N. Herak, *Mol. Phys.*, **26**, 605 (1973).
- (11) Y. Kurita, *Nippon Kagaku Zasshi*, **85**, 833 (1964).
- (12) T. Fujimura and N. Tamura, unpublished results.

Molecular Orbital Calculations on the Nitrogen Nuclear Spin-Spin Coupling Constants

Shinichi Nagata,* Tokio Yamabe, Kimihiko Hirao, and Kenichi Fukui

Department of Hydrocarbon Chemistry, Faculty of Engineering, Kyoto University, Sakyo-ku, Kyoto, Japan

(Received November 11, 1974; Revised Manuscript Received June 2, 1975)

Nuclear spin-spin coupling constants between ^{15}N and ^{13}C or ^1H were calculated by means of the "sum-over-states" perturbation and the "finite perturbation" methods using the INDO MO's. For $J(^{13}\text{C}, ^{15}\text{N})$ coupling constants, we discuss the difference of the contributions from three kinds of mechanisms, FC, SD, and OB terms. The significant effect of lone-pair orientation is demonstrated not only for $^2J(^{15}\text{N}-\text{C}-^1\text{H})$ couplings in imines and oximes but also for $^2J(^{17}\text{O}-\text{C}-^1\text{H})$ in protonated formaldehyde.

Introduction

Experimental data of indirect spin-spin coupling constants have recently been reported on many kinds of molecules containing ^1H , ^{13}C , ^{15}N , ^{19}F , ^{31}P , etc. The coupling constant reflects the magnitude of spin-spin interaction between two coupled nuclei in a molecule and then provides valuable structural and stereochemical information

as well as insights into the nature and distribution of bonding electrons. Especially, it is very interesting and noticeable from the point of view of molecular structure determination that the coupling constants are markedly affected by the orientation of the lone-pair electrons of the nitrogen atom in the coupling between the ^{15}N nucleus and other ones.¹ Lehn and coworkers² showed experimentally that

the ${}^2J({}^{15}\text{N}, {}^1\text{H})$ couplings of protons *cis* and *trans* to the nitrogen lone pair in formaldoxime were considerably different not only in magnitude but also in their signs. Since the advent of this finding, similar observations have been made with respect to a large number of compounds containing nitrogen atom, e.g., *cis*- and *trans*-acetaldoxime,² aziridine,³ *N*-nitrosodimethylamine,⁴ quinoline,⁵ oxaziridine,⁶ *N*-alldimine,⁷ etc. In addition, in order to make clear the effect of lone-pair orientation, there have appeared a large number of experimental investigations concerning the change of N-H coupling constants in both the sign and the magnitude brought about by the protonation to the nitrogen lone pair.² Furthermore, from several experimental results of the coupling constants between ${}^{15}\text{N}$ and ${}^{13}\text{C}$ nuclei, Binsch and coworkers⁸ proposed the following empirical equation for the relation between the ${}^{15}\text{N}$ - ${}^{13}\text{C}$ coupling constant and the product of the *s* characters of the nitrogen and the carbon orbitals forming the σ bond, assuming a predominance of the Fermi contact term: $S_{\text{N}}S_{\text{C}} = 80[{}^1J({}^{15}\text{N}-{}^{13}\text{C})]$. Large deviations, however, were noted particularly for those compounds with a multiple bond between nitrogen and carbon atoms. Such a phenomenon was attributed to the low-lying excited states or the effects of contributions to the total coupling mechanism from the orbital term.

On the other hand, the theory of the indirect spin-spin coupling of nuclei is based on the consideration of three types of interactions which was formulated by Ramsey,⁹ i.e., Fermi contact (FC), spin-dipolar (SD), and orbital (OB) interactions. Applications of the formula, using a wave function obtained in LCAO form from MO theory, were made by McConnell¹⁰ and later by Pople and Santry.¹¹ Furthermore, a new approach to the problem of evaluating nuclear spin coupling constants has recently been made by Pople et al., i.e., the "finite perturbation theory".¹² Until now, among the three sorts of interactions mentioned above, the FC term was found to be predominant in the case of the proton couplings by Ramsey and Purcell⁹ and in most of later theoretical studies.¹⁰ This term, however, was found not always dominant for the couplings between nuclear pairs other than protons.¹³ There have been far fewer theoretical studies concerning the coupling constants between the ${}^{15}\text{N}$ nucleus and other ones in comparison with those of the ${}^1\text{H}$ or ${}^{13}\text{C}$ coupling constants. For example, Maciel et al.¹⁴ calculated the $J({}^{13}\text{C}, {}^{15}\text{N})$ coupling constants (only the FC term considered) using a finite perturbation method within INDO approximation and concluded that the calculation did not satisfactorily reproduce the C-N coupling constant, whereas the C-C and the C-H couplings were well explained. Further, Lichter et al.¹⁵ have recently studied the geometrical dependences of ${}^{13}\text{C}$ - ${}^{15}\text{N}$ coupling constants of various oximes by the same manner. On the other hand, there have appeared a few theoretical investigations¹⁶ of the coupling constants between ${}^{15}\text{N}$ and ${}^1\text{H}$ nuclei by the finite perturbation method employing both CNDO/2 and INDO wave functions and they pointed out the difference of two N-H coupling constants, probably induced by the effect of lone-pair orientation, without further detailed theoretical interpretations.

In this paper, we have used the "sum-over-states" perturbation approach within the INDO framework to estimate the order of magnitude of the above-mentioned three components of the nuclear spin coupling constants between ${}^{15}\text{N}$ and ${}^{13}\text{C}$ in several molecules. Furthermore, we discuss the ${}^{15}\text{N}$ -C- ${}^1\text{H}$ coupling constants of a molecule, $\text{CH}_2=\text{NH}$, in comparison with those of $\text{CH}_2=^+\text{OH}$ in

order to evaluate clearly the nitrogen or oxygen lone-pair effect upon the magnitude of these coupling constants by the finite perturbation method.

Results and Discussion

At first, we tried to carry out the calculation of the coupling constants between ${}^{15}\text{N}$ and ${}^{13}\text{C}$ or ${}^1\text{H}$ by using both the "sum-over-states" perturbation and the "finite perturbation" methods within the INDO approximation,¹⁷ respectively. Computational details were described earlier.^{12,13e} The values of $s_{\text{A}}^2(0)$ and $s_{\text{B}}^2(0)$, the valence *s*-orbital electron densities of atom A and atom B, used for present calculation are the same as the previous ones of Pople et al.¹² Further, the following values of $\langle r^{-3} \rangle_i$ for the calculation by the "sum-over-states" perturbation were used: 1.430 for carbon and 2.472 for nitrogen atoms. The equilibrium geometries of $\text{CH}_2=\text{NH}$ and $\text{CH}_2=^+\text{OH}$ were taken from *ab initio* calculations¹⁸ and others were cited from Sutton's table.¹⁹

(1) *C-N Coupling.* The calculated C-N coupling constants are summarized in Table I together with the values of C-C coupling constants for the sake of comparison. The calculated values of both $J({}^{13}\text{C}, {}^{13}\text{C})$ and $J({}^{13}\text{C}, {}^{15}\text{N})$ are somewhat lower than experimental ones. It may be attributed to the larger values of transition energy ${}^{1,3}\Delta E_{i \rightarrow j}$ overestimated by the INDO approximation. But the relative magnitude of calculated values of both $J({}^{13}\text{C}, {}^{13}\text{C})$ and $J({}^{13}\text{C}, {}^{15}\text{N})$ is parallel with observed ones. Moreover, by a careful examination of this table, some characteristic features are revealed. First, in the C-C, C=C, and C \equiv C coupling constants, the FC term is dominant, consistent with results of Pople et al.,¹⁴ which took only the FC term into account and pointed out a monotonic relationship between P_{scsc}^2 and $J({}^{13}\text{C}, {}^{13}\text{C})$ (P_{scsc} is the carbon 2*s*-carbon 2*s* element of the first-order density matrix). Second, the investigation of the C-N coupling constant in terms of the three kinds of contributions is of interest. The observed values of C-N coupling constants including the sign have been reported for methylamine, acetonitrile, and methyl isocyanide only as shown in Table II. The calculated values of negative ${}^1J({}^{13}\text{C}-{}^{15}\text{N})$ of methylamine and methyl isocyanide, negative ${}^1J({}^{13}\text{C}\equiv{}^{15}\text{N})$ of acetonitrile, and positive ${}^2J({}^{13}\text{C}-\text{C}\equiv{}^{15}\text{N})$ of acetonitrile are in agreement with the experimental evidences. Speaking from the result of the present calculation, the coupling constants for ${}^1J({}^{13}\text{C}=\text{N})$ are predicted to be positive, inconsistent with results of Pople et al.,¹⁴ who took into account only the FC term. As will be seen in the later discussion, the OB term plays a more important role than the FC term in this case. Thus, these may be reasonable and reliable enough to permit discussion of the difference of the contributions of C-N, C=N, and C \equiv N coupling constants.

On the one-bond coupling constant, ${}^1J({}^{13}\text{C}-{}^{15}\text{N})$, it is easily seen from Table I that the FC term is dominant and that the less important SD term cancels out the OB term. For ${}^1J({}^{13}\text{C}=\text{N})$ and ${}^1J({}^{13}\text{C}\equiv{}^{15}\text{N})$, however, the OB and SD terms appear to make significant contributions as well as the FC term. This result explains well the previous experimental and theoretical results^{7,19} that the coupling constants of $J({}^{13}\text{C}=\text{N})$ and $J({}^{13}\text{C}\equiv{}^{15}\text{N})$ clearly fall far off the straight line when, as usual, only the contribution from the FC term is taken into account. Thus, it is worthwhile to note that the main difference between C-C and C-N coupling mechanisms is the nonnegligible contributions of the OB and SD terms in C=N and C \equiv N coupling

TABLE I: Calculated Coupling Constants ${}^1J({}^{13}\text{C}, {}^{15}\text{N})$ and ${}^1J({}^{13}\text{C}, {}^{15}\text{N})^e$

	FC	SD	OB	Total	Exptl
$\text{H}_3\text{C}^*-\text{NH}_2$	-5.27	-0.55	+0.89	-4.93	-4.5 ^a
$\text{H}_3\text{C}^*-\text{CH}_3^d$	+14.01	+1.19	-1.87	+13.33	+34.6 ^b
$\text{H}_2\text{C}^*=\text{NH}$	+6.58	-1.90	+12.04	+16.72	
$\text{H}_2\text{C}^*=\text{CH}_2^d$	+45.16	+2.95	-11.34	+36.77	+67.2 ^b
$\text{H}_3\text{C}-\text{C}^*\equiv\text{N}^*$	+5.01	-5.04	-1.02	-1.05	-17.5 ^c
$\text{HC}^*\equiv\text{CH}^d$	+119.05	+9.19	+12.53	+140.77	+170.6 ^b

^a L. Paolillo and E. D. Becker, *J. Magn. Reson.*, 3, 200 (1970).
^b D. M. Graham and C. E. Molloway, *Can. J. Chem.*, 41, 2114 (1963). ^c W. McFarlane, *Mol. Phys.*, 10, 603 (1966). ^d C-C coupling constants were already obtained from the same method as ours by H. Nakatsuji, I. Morishima, H. Kato, and T. Yonezawa, *Bull. Chem. Soc. Jpn.*, 44, 2010 (1971). ^e Calculations carried out by means of the "sum-over-states" perturbation method.

TABLE II: Calculated Coupling Constants, $J({}^{13}\text{C}, {}^{15}\text{N})$, for Single, Double, and Triple Bonds^a

	Calcd	Exptl
$\text{H}-\text{C}^*-\text{NH}_2$	-4.93	-4.5
$\text{H}_2\text{C}^*-\text{NH}_2$	-7.25	< 8
$\text{Ph}-\text{C}^*=\text{N}-\text{CH}_3$		7.1 ^a
$\text{H}-\text{C}^*=\text{N}-\text{OH}$	+16.18	2.96 ^a
$\text{H}-\text{C}^*=\text{N}-\text{H}$	+16.72	
$\text{H}_2\text{C}^*=\text{N}-\text{OH}$	+30.16	
$\text{H}-\text{C}^*=\text{N}-\text{H}$	-7.11	
$\text{HC}\equiv\text{N}$	-1.05	-17.5 ^b (${}^1J({}^{13}\text{C}=\text{N})$)
	+2.26	+3.0 ^b (${}^2J({}^{13}\text{C}-\text{C}=\text{N})$)
$\text{CH}_2\equiv\text{N}$	+17.98	9.1 ^c (${}^1J({}^{15}\text{N}=\text{C})$)
	-4.72	-10.7 ^c (${}^1J({}^{13}\text{C}-\text{N})$)

^a See ref 7. ^b W. McFarlane, *Mol. Phys.*, 10, 603 (1966). ^c W. McFarlane, *J. Chem. Soc. A*, 1660 (1967). ^d Calculations carried out by means of the "sum-over-states" perturbation method.

constants. Moreover, the examination of the electronic parts demonstrates that the FC term of ${}^1J({}^{13}\text{C}-{}^{15}\text{N})$ and ${}^1J({}^{13}\text{C}=\text{N})$ and the OB term of ${}^1J({}^{13}\text{C}=\text{N})$ come mainly from $n \rightarrow \pi^*$ or $n \rightarrow \sigma^*$ term. This result also indicates the significance of the nitrogen lone pair to the coupling mechanism.

So we carried out calculations for pyridine and pyridinium ion in order to clarify the change of C-N coupling constants according to the protonation to the nitrogen lone pair. The calculated results are shown in Table III and Figure 1. For these compounds, we have only the experimental C-N coupling constants without the sign information. The calculated result, however, seems to reflect correctly the following trend which is found in the experimental absolute value; for one-bond coupling a large negative contribution is induced, accompanied by the change of sign by protonation, and two-bond and three-bond couplings have small negative values. It is easily seen from Table III that, experimentally as well as theoretically, one-bond coupling

TABLE III: Calculated Coupling Constants, $J({}^{13}\text{C}, {}^{15}\text{N})$, for Pyridine and Pyridinium Ion^b

	Pyridine		Pyridinium ion	
	Calcd	Exptl ^a	Calcd	Exptl ^a
${}^1J({}^{13}\text{C}, {}^{15}\text{N})$	+13.55	0.45	-11.59	12.0
${}^2J({}^{13}\text{C}, {}^{15}\text{N})$	-1.57	2.4	-0.23	2.1
${}^3J({}^{13}\text{C}, {}^{15}\text{N})$	-7.40	3.6	-9.64	5.3

^a R. L. Lichter and J. D. Roberts, *J. Am. Chem. Soc.*, 93, 5218 (1971). ^b Calculations carried out by means of the "sum-over-states" perturbation method.

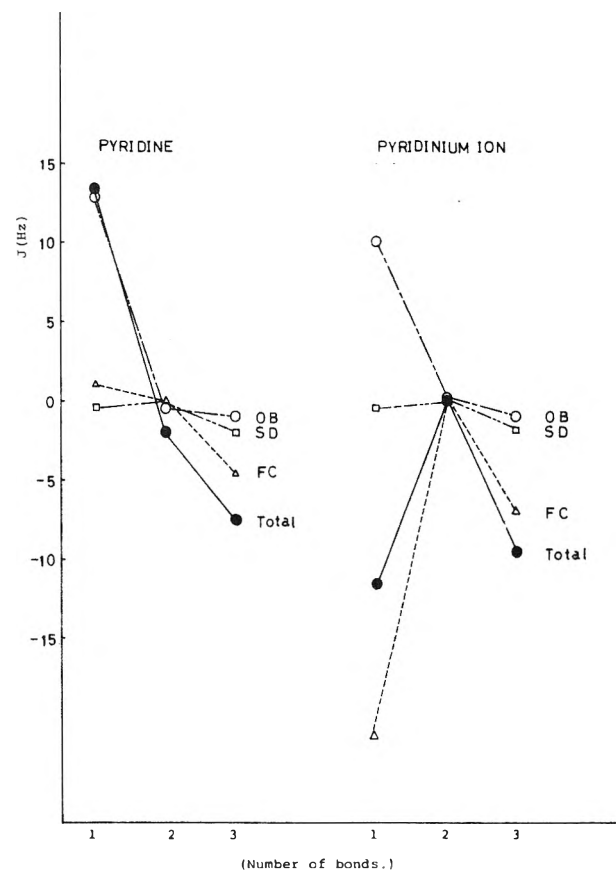


Figure 1. The change of the contributions from three mechanisms due to the difference of number of bonds for pyridine and pyridinium ion.

is most strongly affected by protonation. This may indicate that the protonation to the nitrogen lone pair in pyridine induces a partial single-bond character in the C=N bond, which is a small effect in two- or three-bond coupling cases. Moreover, it is easily seen from Figure 1 that there exists a large difference in the relative importance of the three contributions, FC, SD, and OB terms, between pyridine and pyridinium ion. This may be attributed to the difference of one-, two-, and three-bond couplings discussed above; for two- and three-bond couplings there seems to be little change of each contribution caused by protonation, while for the one-bond coupling the OB term makes a significant contribution for pyridine and the FC term has a strongly negative value for pyridinium ion. This result may also correspond to the partial single-bond character of the directly connected double bond introduced by protonation.

TABLE IV: Net Charge Densities of H_A and H_B Atoms of Methyleneimine

	H_A	H_B		H_A	H_B
$\theta = 0^\circ$	0.9453	1.0724	$\theta = 70^\circ$	1.0336	1.0014
$\theta = 30^\circ$	1.0295	1.0543	$\theta = 90^\circ$	0.9966	0.9770
$\theta = 55^\circ$	1.0411	1.0216			

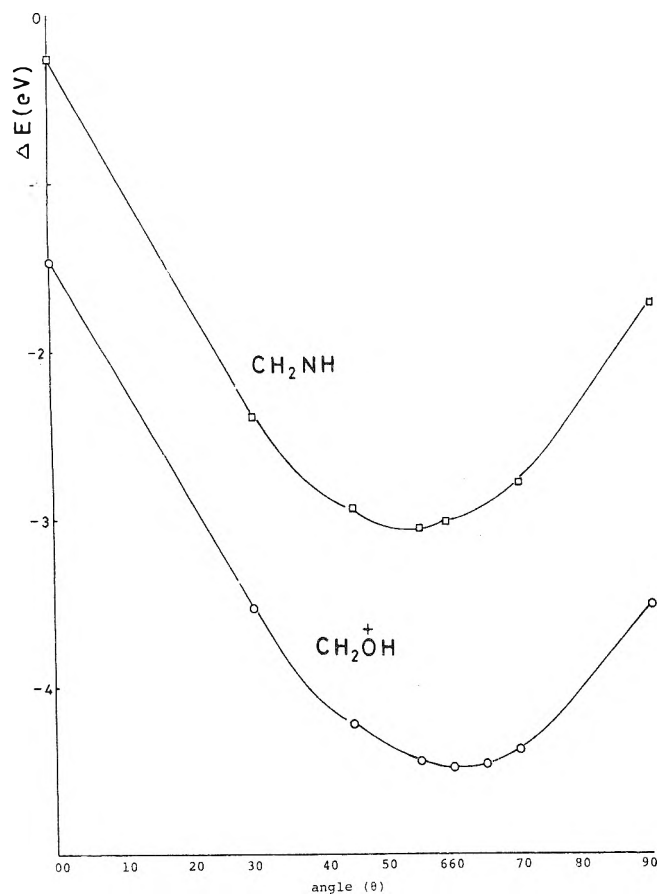
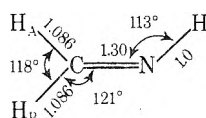


Figure 2. Total energy of methylenimine and protonated formaldehyde for angle variation of θ .

(2) *N—H Coupling.* The information for $J(^{15}\text{N}, ^1\text{H})$ coupling constants including their sign has recently been obtained in regard to several kinds of molecules by means of double-resonance experiments in comparison with those of $J(^{13}\text{C}, ^{15}\text{N})$. We are interested in the experimental result that the lone-pair orientation has a significant effect on the sign and magnitude of coupling constants for oxime compounds. Then, we investigated the geometrical dependence of the two $^2J(^{15}\text{N}-\text{C}-^1\text{H})$ coupling constants, syn and anti with respect to the $\text{N}-\text{H}$ bond, to make clear the lone-pair effect. As a typical and simple model of oximes, we took up the virtual molecule methylenimine. According to the previous study of the ab initio calculation^{18a} for this compound, the geometry minimizing the total energy was predicted as



First, we calculated the $^2J(^{15}\text{N}-\text{C}-^1\text{H})$ coupling constants by the use of this geometry, which gave 1.17 Hz for

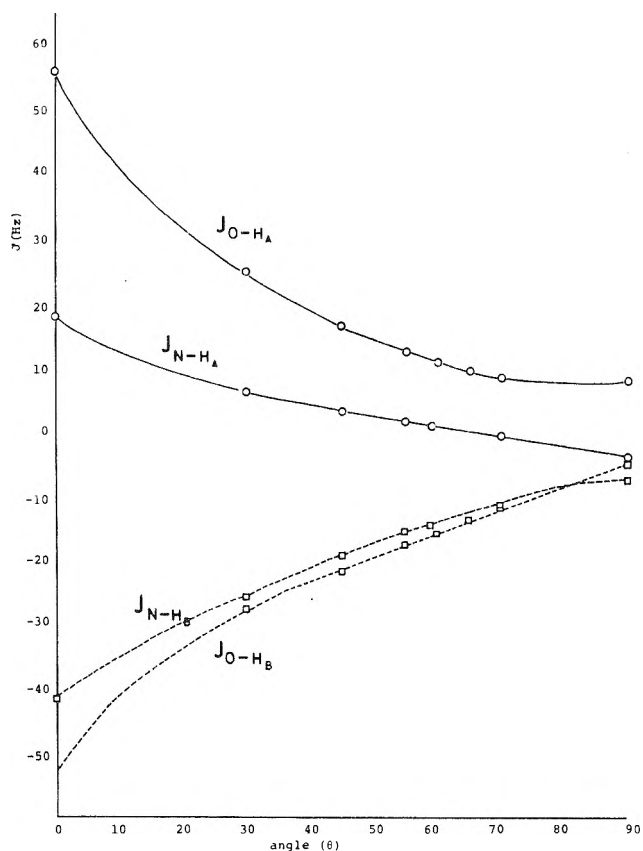


Figure 3. Calculated coupling constants, $^2J(^{15}\text{N}-\text{C}-^1\text{H})$ and $^2J(^{17}\text{O}-\text{C}-^1\text{H})$, for angle variations of θ .

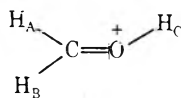
$^2J(^{15}\text{N}-\text{C}-^1\text{H}_A)$ and -14.35 Hz for $^2J(^{15}\text{N}-\text{C}-^1\text{H}_B)$. This result is consistent with the observed values for formaldoxime (2.68 and -13.88 Hz). Then, we tried to calculate them by varying the angle $\theta = \text{H}_A\text{CX}$ only (CX is the line in the $\text{C}=\text{N}$ direction). It may be reasonable from the following point of view that the nitrogen lone pair and hydrogen atom of the $\text{N}-\text{H}$ bond may affect the two $\text{C}-\text{H}$ bonds. The result of total energy as shown in Figure 2 demonstrates that it is most stable at $\theta = 55^\circ$, which seems in accord with the microwave data²⁰ for formaldoxime; $\text{H}_A\text{CX} = 58^\circ 14'$ and $\text{H}_B\text{CX} = 64^\circ 27'$.

Recently, a calculated result was reported on methylenimine, using a 4-31G Gaussian basis set.²¹ The optimized equilibrium geometry is not only completely opposite to the relative magnitude of the two H_ACX angles experimentally obtained for formaldoxime, but also it is inconsistent with the values of $\text{N}-\text{H}$ coupling constants (-13.13 and -8.85 Hz), if we employed these geometrical values.

Now, we calculated the coupling constants $^2J(^{15}\text{N}-\text{C}-^1\text{H})$ for geometries with various H_ACX angles. The calculated results are shown in Figure 3, which demonstrates that the coupling constants $^2J(^{15}\text{N}-\text{C}-^1\text{H})$ are very sensitive for a variation of angle θ . For the conformer ($\theta = 55^\circ$) predicted by minimization of the INDO total energy, the difference between two coupling constants becomes considerably larger than that of $\theta = 59^\circ$ and is much more consistent with the experimental result of formaldoxime.

Next, we calculated the $^2J(^{17}\text{O}-\text{C}-^1\text{H})$ coupling constant of protonated formaldehyde by the same manner, because this molecule is identical with methylenimine from the point of view in making clearer the lone-pair effect although the coupling constant $^2J(^{17}\text{O}, ^1\text{H})$ has not been

TABLE V: Calculated Coupling Constants (Hz) $J(^{13}\text{C}, ^1\text{H})$ and $J(^1\text{H}, ^1\text{H})$ of Protonated Formaldehyde^b



	Calcd	Exptl ^a		Calcd	Exptl ^a
$J(\text{C}-\text{H}_\text{A})$	+179.03	+198.4	$J(\text{H}_\text{A}-\text{H}_\text{B})$	+12.83	+21.7
$J(\text{C}-\text{H}_\text{B})$	+188.56	+209.8	$J(\text{H}_\text{A}-\text{H}_\text{C})$	+4.04	+9.0
$J(\text{C}-\text{H}_\text{C})$	-11.03	-8.7	$J(\text{H}_\text{B}-\text{H}_\text{C})$	+17.47	+19.0

^a A. M. White and G. A. Olah, *J. Am. Chem. Soc.*, **91**, 2943 (1969). ^b Calculations carried out by means of the "finite" perturbation method.

found out experimentally. The result obtained by changing the angle θ is shown in Figure 3, which suggests that $^2J(^{17}\text{O}-\text{C}-^1\text{H})$ coupling constant has a quite similar trend compared to $^2J(^{15}\text{N}-\text{C}-^1\text{H})$. This may be the proof that there exists the same effect of lone-pair orientation for two-bond coupling constants in these molecules. The total energy of this molecule for the angle variation, however, was minimized at $\theta = 60^\circ$, which implies the symmetrical geometry concerning to the $\text{C}=\text{O}$ line. This result obtained from INDO approximation is in good agreement with the ab initio calculation^{18b} and may be reasonable from the following trend that the electron cloud of the cationic lone pair of the oxygen atom in protonated formaldehyde is not so extended as the neutral one, i.e., nitrogen atom in methylenimine. The reliability of the present calculation seems to be indicated in Table V, where calculated coupling constants, $J(^{13}\text{C}, ^1\text{H})$ and $J(^1\text{H}, ^1\text{H})$, of protonated formaldehyde are in good agreement with experimental ones including both the sign and magnitude.

Conclusion

In the case of coupling constants between ^{15}N and ^{13}C , the SD and OB terms are found theoretically to make a significant contribution in addition to the FC term, especially in multiple bonds. Moreover, in the protonation to the nitrogen lone pair it was demonstrated that one-bond coupling is most strongly affected and that two- and three-bond couplings do not make so remarkable a change.

On the other hand, the large difference between $^2J(^{15}\text{N}-\text{C}-^1\text{H}_\text{A})$ and $^2J(^{15}\text{N}-\text{C}-^1\text{H}_\text{B})$ was attributed to the indirect effect of the nitrogen lone-pair orientation. A similar trend was also found in the case of protonated formal-

dehyde. Furthermore, these couplings are very sensitive to a variation of angle θ ; that is, $^2J(^{15}\text{N}-\text{C}-^1\text{H}_\text{A})$ and $^2J(^{17}\text{O}-\text{C}-^1\text{H}_\text{A})$ increase, and $^2J(^{15}\text{N}-\text{C}-^1\text{H}_\text{B})$ and $^2J(^{17}\text{O}-\text{C}-^1\text{H}_\text{B})$ decrease as the angle θ becomes small.

Acknowledgments. The authors wish to thank Professor H. Kato and Dr. S. Inagaki for their helpful discussions and suggestions. We express our appreciation to the Computer Center of Kyoto University for the use of the FACOM 230-75 computer.

References and Notes

- (1) T. Axenrod, "Nitrogen NMR", G. Webb and M. Witanowski, Ed., Plenum Press, New York, N.Y., 1972, p 261; E. W. Randall and D. G. Gillies, *Prog. Nucl. Magn. Reson. Spectrosc.*, **119** (1971).
- (2) J. P. Kintzinger and J. M. Lehn, *Chem. Commun.*, 660 (1967); D. Crépau and J. M. Lehn, *Mol. Phys.*, **14**, 547 (1968); D. Crépau, J. M. Lehn, and R. R. Dean, *ibid.*, **16**, 225 (1969).
- (3) M. Ohtsuru and K. Tori, *Tetrahedron Lett.*, 4043 (1970); M. Ohtsuru, K. Tori, J. M. Lehn, and R. Seher, *J. Am. Chem. Soc.*, **91**, 1187 (1969).
- (4) T. Axenrod and P. S. Pregosin, *Chem. Commun.*, 702 (1968).
- (5) R. L. Lichter and J. D. Roberts, *Spectrochim. Acta, Part A*, **26**, 1813 (1970); K. Tori, M. Ohtsuru, K. Aono, Y. Kawazoe, and M. Ohnishi, *J. Am. Chem. Soc.*, **89**, 2765 (1967).
- (6) W. B. Jennings, D. R. Boyd, C. G. Watson, E. D. Becker, R. B. Bradley, and D. M. Jerina, *J. Am. Chem. Soc.*, **94**, 8501 (1972).
- (7) H. J. C. Yeh, H. Ziffer, D. M. Jerina, and D. R. Boyd, *J. Am. Chem. Soc.*, **95**, 2741 (1973).
- (8) G. Binsch, J. B. Lambert, B. W. Roberts, and J. D. Roberts, *J. Am. Chem. Soc.*, **86**, 5564 (1964).
- (9) N. F. Ramsey and E. M. Purcell, *Phys. Rev.*, **85**, 143 (1952); N. F. Ramsey, *ibid.*, **91**, 903 (1953).
- (10) H. M. McConnell, *J. Chem. Phys.*, **24**, 460 (1956); M. Karplus, *ibid.*, **30**, 11 (1956); H. S. Gutowsky, M. Karplus, and D. M. Grant, *ibid.*, **31**, 1278 (1959); M. J. Stephens, *Proc. R. Soc. London, Ser. A*, **243**, 274 (1957).
- (11) J. A. Pople and D. P. Santry, *Mol. Phys.*, **8**, 1 (1964).
- (12) J. A. Pople, J. W. McIver, Jr., and N. S. Ostlund, *J. Chem. Phys.*, **49**, 2960, 2965 (1968).
- (13) (a) J. A. Pople, *Mol. Phys.*, **1**, 216 (1958); (b) J. N. Murrell, P. E. Stephenson, and G. T. Jones, *ibid.*, **12**, 265 (1967); (c) H. Nakatsuji, H. Kato, I. Morishima, and T. Yonezawa, *Chem. Phys. Lett.*, **4**, 607 (1970); (d) A. C. Blizard and D. P. Santry, *J. Chem. Phys.*, **55**, 950 (1971); (e) K. Hirao, H. Nakatsuji, H. Kato, and T. Yonezawa, *J. Am. Chem. Soc.*, **94**, 4078 (1972); (f) K. Hirao, H. Nakatsuji, and H. Kato *ibid.*, **95**, 31 (1973).
- (14) G. E. Maciel, J. W. McIver, Jr., N. S. Ostlund, and J. A. Pople, *J. Am. Chem. Soc.*, **92**, 4151, 4497, 4506 (1970).
- (15) R. L. Lichter, D. E. Dorman, and R. Wasylshen, *J. Am. Chem. Soc.*, **96**, 930 (1974).
- (16) (a) M. S. Gopinathan and P. T. Narashimhan, *Mol. Phys.*, **22**, 473 (1970); (b) R. Wasylshen and T. Schaefer, *Can. J. Chem.*, **50**, 2989 (1972).
- (17) J. A. Pople, D. L. Beveridge, and D. A. Dobosh, *J. Chem. Phys.*, **47**, 2026 (1967).
- (18) (a) For $\text{CH}_2=\text{NH}$, J. M. Lehn, B. Munsch, and P. Millie, *Theor. Chim. Acta*, **16**, 351 (1970); (b) for $\text{CH}_2=\text{OH}^+$, P. Ros, *J. Chem. Phys.*, **49**, 4903 (1968).
- (19) *Chem. Soc., Spec. Publ.*, No. 11 (1958); *Suppl.*, No. 18 (1965).
- (20) I. N. Levin, *J. Chem. Phys.*, **38**, 2326 (1963).
- (21) R. Macaulay, L. A. Burnelle, and C. Sandorfy, *Theor. Chim. Acta*, **29**, 1 (1973).

Nuclear Magnetic Resonance Investigation of Cobalt(III) Outer-Sphere Complexes in Aqueous Solutions

K. L. Craighead, P. Jones, and R. G. Bryant*

Department of Chemistry, University of Minnesota, Minneapolis, Minnesota 55455 (Received October 31, 1974; Revised Manuscript Received May 15, 1975)

Publication costs assisted by the National Institutes of Health

Nuclear magnetic resonance relaxation time measurements are reported for nuclei participating in weak outer-sphere complexes of cobalt(III) complex ions. The data are analyzed in terms of outer-sphere association constants and line broadening parameters. Analysis of the relaxation times in the outer-sphere complexes is made with the aid of measurements on model systems to evaluate some of the several contributions to the relaxation rates. It is concluded that the solvent-solute interaction of halide ions in outer-sphere association with tris(diamine) chelates of cobalt(III) is significantly perturbed. Within experimental errors, both optical and NMR methods gave the same values for equilibrium constants.

Introduction

The existence of ion pairs or outer-sphere metal complexes is often postulated to explain data from a variety of experiments ranging from thermodynamic measurements¹ on electrolyte solutions to kinetic measurements on inorganic² reactions. Nevertheless relatively little detailed information has been presented concerning ion pair structure or other physical properties in aqueous solutions. Experimental difficulties in the study of outer-sphere complexes are acute in aqueous solutions. Reports of outer-sphere association constants between simple inorganic anions and complex cations have differed significantly if different measuring techniques are used in the same or different laboratories.³ For example, the suggestion based on NMR experiments that hydrophobic substituents such as alkyl groups on one ion will promote ion association⁴ is not supported by conductance or spectrophotometric results.³ It might be suggested that these discrepancies are associated with the selective detection of different ion pair structures by different physical techniques. However, assuming that equilibrium thermodynamics may be applied, Orgel and Mulliken⁵ have shown that even if a large number of structurally different 1:1 ion pairs are formed, analysis of the data from any experiment should yield the same value for the apparent 1:1 association constant. The observed equilibrium constant will be the sum of equilibrium constants for the formation of each structural type. According to this analysis each physical technique should yield the same equilibrium constant even if some structural types of 1:1 complex have a negligible extinction coefficient or its equivalent for a particular measurement. On the other hand, if the equilibrium under study is complicated by additional weak associations due to presumably passive electrolyte ions, such as perchlorate ion, Johansson⁶ has pointed out that different types of measurement may lead to different results depending on the experimental details.

The present investigation was undertaken to examine the equilibrium constants and structural properties of the outer-sphere complexes of various cobalt(III) amine complexes in water using both broad line NMR and optical methods.

Experimental Section

Spectrophotometric equilibrium measurements were made on a Cary 14 spectrophotometer using a short path-length cell so that the same metal complex concentrations could be used in NMR measurements. The cell was calibrated at 545 nm using potassium permanganate in 1 *M* sulfuric acid by comparison with a standard 1.00-cm cell and by comparison with Lingane and Collat's⁷ value for the extinction coefficient of 2.31 *M*⁻¹ cm⁻¹. Temperature was controlled at 25.0 or 30.0°.

NMR spectra were recorded on a Varian DP-60 NMR spectrometer employing methods described previously.⁸ Samples were contained in 15-mm o.d. test tubes. For bromine measurements temperature was controlled with a Varian variable temperature controller because ⁸¹Br line widths are very sensitive to small changes in temperature. In all experiments the radiofrequency power was adjusted to be below saturation. For the broadest bromine lines where derivative spectra were obtained, the modulation amplitude was adjusted to obtain negligible modulation broadening. Line widths were measured as the full-width at half-height of the absorption mode signal. For the derivative signals line widths were measured between extrema and corrected to the absorption mode width by multiplying by 1.732. In all cases the magnetic field was calibrated from side band separations.

⁵⁹Co chemical shift measurements were made using 16-mm sample tubes with standard 5-mm thin walled NMR tubes containing the reference solution placed coaxially inside.

³⁵Cl measurements of *T*_{1ρ} were made using the adiabatic half passage experiments.⁹ The field was swept off resonance with a 100 to 200 mA current placed on the probe helmholtz coils on top of the audiomodulation. The transient signal taken from the PAR Model 121 lock-in detector was accumulated on a Varian C-1024 CAT or recorded directly on a Midwestern Instruments LCRII oscillographic recorder. *T*_{1ρ} values were extrapolated to zero *H*₁. The response of this configuration was measured to be 0.05 sec for a modulation frequency of 500 Hz and was not determined by the lock-in amplifier time constant.

Data were fit to assumed equilibrium models both manually and using a least-squares fitting program described by Bevington.¹⁰ In some cases the data were not of sufficient precision to permit establishment of a unique minimum on the least-squares surface so that equilibrium data are reported to only one figure.

[Co(NH₃)₆]Cl₃,¹¹ [Co(NH₃)₅Cl]Cl₂,¹² [Co(NH₃)₅Br]Br₂,¹³ [Co(NH₃)₅(OH₂)](ClO₄)₃,¹⁴ [Co(NH₃)₄(OH₂)₂](ClO₄)₃,¹⁵ [Co(en)₃]Cl₃,¹⁶ and [Co(pn)₃]Cl₃¹⁷ were synthesized according to standard procedures. Butylenediamine (bn) was prepared as described by Cooley, Liu, and Bailar.¹⁸ [Co(bn)₃]Cl₃ was prepared by diluting 14 ml of the bn prepared above (~0.1 mol) with 15 ml water and partly neutralizing with 4 ml of concentrated HCl (0.047 mol) in 15 ml of water. This mixture was poured into a solution of 3.6 g of CoCl₂·6H₂O (0.015 mol) in 11 ml of water and air was rapidly bubbled through the solution for 3 hr. The dark, red-brown colored solution was evaporated on a steam bath until a crust formed over the surface and was then cooled in an ice bath. Concentrated HCl (3 ml) and 70 ml of absolute ethanol were added to precipitate the salt, which was filtered and washed with absolute ethanol. The product was recrystallized three times from a small amount of warm water with cold absolute ethanol and dried under vacuum at room temperature.

Perchlorate and bromide salts of the complexes were prepared by dissolving the chloride salts in a minimum amount of warm water, adding concentrated HClO₄ or HBr while cooling in an ice bath, filtering, and washing with absolute ethanol. Three recrystallizations were performed using the same procedure.

Results and Discussion

Table I summarizes the effects of a series of cobalt(III) complexes on ³⁵Cl and ⁸¹Br line widths in aqueous chloride and bromide solutions. Table II shows changes in the ⁵⁹Co resonance line width and chemical shift for Co(en)₃³⁺ in the presence of various anions.

There may be a number of reasons for the decrease in ³⁵Cl and ⁸¹Br relaxation times caused by Co(III) complexes. These include quadrupole relaxation due to viscosity changes affecting the correlation times characterizing the solution, relaxation mechanisms other than quadrupole relaxation, and quadrupole relaxation caused by inner-sphere substitution and outer-sphere complex formation. Direct measurements made on the solutions used in obtaining the data for Table III indicate that over the range of concentrations used, the viscosity changes are approximately 5–10% and therefore cannot account for the effects shown in Table I. Viscosity corrections were applied before calculating association constants.

For ³⁵Cl and ⁸¹Br, the nuclear electric quadrupole moment dominates the nuclear spin relaxation. Often a most efficient relaxation mechanism is the interaction of the nuclear magnetic moment with electron magnetic moments. However, the cobalt(III) complexes studied are diamagnetic and therefore this relaxation mechanism is not important. The absence of paramagnetic effects is supported by measurements of the water proton relaxation rate in these solutions.

Some of the cobalt(III) complexes studied undergo substitution reactions with chloride and bromide ions. Half-lives for these reactions are on the order of several hours to days.¹⁹ Since these reactions are so slow, separate NMR signals should be observed for each substituted product

TABLE I: ³⁵Cl and ⁸¹Br NMR Line Broadening in Aqueous Bromide and Chloride Solutions of Co(III) Complexes

Complex	⁸¹ Br broadening, ^a Hz	³⁵ Cl broadening, ^b Hz	Ligand concn, <i>M</i>
Co(NH ₃) ₆ ³⁺		1.5	0.50
Co(NH ₃) ₅ Br ²⁺	50		<i>c</i>
Co(NH ₃) ₅ (H ₂ O) ³⁺	30		<i>c</i>
Co(NH ₃) ₄ (H ₂ O) ₂ ³⁺		3	0.50
Co(en) ₃ ³⁺	90		0.60
Co(en) ₃ ³⁺		5	0.6
Co(en) ₃ ³⁺		18	0.5
Co(pn) ₃ ³⁺	500		0.45
Co(pn) ₃ ³⁺		38	0.6
Co(bn) ₃ ³⁺	1230		0.45
Co(bn) ₃ ³⁺		72	0.6

^a Line width increase over 450 Hz of 0.6 *M* Na⁸¹Br at 25°. ^b Line width increase over 12 Hz of 0.5 *M* Na³⁵Cl at ambient temperature of 27 ± 2°. ^c Saturated solution of the complex bromide salt, no other salts present.

TABLE II: ⁵⁹Co NMR Line Widths and Chemical Shifts of Aqueous [Co(en)₃]L₃ Solutions

Complex	Total metal concn, <i>M</i>	⁵⁹ Co line width, Hz	⁵⁹ Co shift, ppm
[Co(en) ₃](ClO ₄) ₃	0.20	120	0 = reference
[Co(en) ₃]Cl ₃	0.20	120	+5
[Co(en) ₃]Br ₃	0.20	110	-27
[Co(en) ₃]I ₃	Saturated	130	-8
[Co(en) ₃]Cl ₃	0.20 + 0.1 <i>M</i> phosphate at pH 6	120	+12
[Co(en) ₃]Cl ₃	0.20 + 0.1 <i>M</i> phosphate at pH 10.5	180	+43

TABLE III: Outer-Sphere Association Constants for Co(III) Complexes with Chloride and Phosphate Ions from ³⁵Cl and ⁵⁹Co Line Width and Chemical Shift Measurements

Complex	<i>K</i> _{os}	Δ <i>ν</i> _{os} , Hz	Δ <i>ω</i> _{os} , ppm	Nucleus obsd
[Co(en) ₃] ³⁺ , Cl ⁻	1	200		³⁵ Cl
[Co(pn) ₃] ³⁺ , Cl ⁻	1	400		³⁵ Cl
[Co(bn) ₃] ³⁺ , Cl ⁻	1	1000		³⁵ Cl
[Co(en) ₃] ³⁺ , PO ₄ ³⁻	30	260	122	⁵⁹ Co
[Co(pn) ₃] ³⁺ , PO ₄ ³⁻	20 ^a		89	⁵⁹ Co

^a Derived for [*trans*-Δ-Co(-)pn]₃³⁺ and [*trans*-Λ-Co(+)-pn]₃³⁺.

species. However, the line width for a halogen in the first coordination sphere of a cobalt complex will be several orders of magnitude larger than that observed for the uncoordinated species, and would not be observed employing the conditions used here to observe the free ion.

⁵⁹Co chemical shifts have been previously related to outer-sphere complex formation.²⁹ The present study supports this conclusion and will indicate that the ⁵⁹Co line width monitors the same chemical interactions.

Assuming then that these relaxation time and chemical shift changes can be attributed to outer-sphere complex formation, it is possible to determine outer-sphere association constants from these effects. The equilibrium constant, K_{os} , for the association of a cation M and an anion L to form an outer-sphere complex (or ion pair), X, can be measured from the concentration dependence of a physical property of either the cation or the anion. Exchange of either partner between free sites and ion pair sites is expected to be diffusion controlled²⁰ and therefore very fast compared with NMR shifts or line widths. In this case the observed NMR line width and chemical shift for a nucleus exchanging rapidly between free and ion pair sites will be a weighted average of the values for each site in solution.²¹ If a property of the metal complex is measured, the line width, chemical shift, or optical density, represented by ω_{obsd} , is given by

$$\omega_{obsd} = \frac{(M) - [X]}{(M)} \omega_f + \frac{[X]}{(M)} \omega_b \quad (1)$$

where ω_f and ω_b are the observables for the free and bound sites, respectively, [X] is the ion pair concentration, and (M) is the total metal concentration. By combining eq 1 with the expression for K_{os}

$$K_{os} = [X]/[M][L] \quad (2)$$

the following equation is obtained:

$$K_{os}(M)\omega_{obsd}^2 - \{K_{os}(M)(\omega_b + \omega_f) + K_{os}(\omega_b - \omega_f) + \omega_b - \omega_f\}\omega_{obsd} + \{K_{os}[L](\omega_b(\omega_b - \omega_f) + K_{os}(M)\omega_b\omega_f + \omega_b\omega_f - \omega_f^2)\} = 0 \quad (3)$$

If changes in [L] are negligible during the experiment, the concentration dependence of the observable becomes

$$\omega_{obsd} = \frac{\omega_f + K_{os}[L]\omega_b}{1 + K_{os}[L]} \quad (4)$$

Similarly, if a property of the anion is measured, eq 3 is replaced by

$$K_{os}[L]\nu_{obsd}^2 - \{K_{os}[L](\nu_b + \nu_f) + K_{os}(M)(\nu_b - \nu_f) + \nu_b - \nu_f\}\nu_{obsd} + \{K_{os}(M)\nu_b(\nu_b - \nu_f) + K_{os}[L]\nu_b\nu_f + \nu_b\nu_f - \nu_f^2\} = 0, \quad (5)$$

where ν_b and ν_f are the values of the observable for the anion in the outer-sphere complex and free in solution, respectively. This may be reduced to

$$\nu_{obsd} = \nu_f + \frac{K_{os}(M)\nu_b}{1 + K_{os}[L]} \quad (6)$$

if outer-sphere complex concentration is small compared with total ligand concentration. For many of the cases shown in Tables I and II it was not possible to determine ion pair association constants, either because the complex solubility is too low or because the effects are too small to observe changes outside experimental error as a function of ligand concentration. Formation constants that were determined by fitting the concentration dependence of NMR and optical data to one of the eq 1-6 are shown in Table III. Examples of the data and calculated curves are shown in Figures 1-3. For the chloride ion pairs the approximate expression yields the same results as the more exact equations; however, for the phosphate experiments eq 3 is necessary.

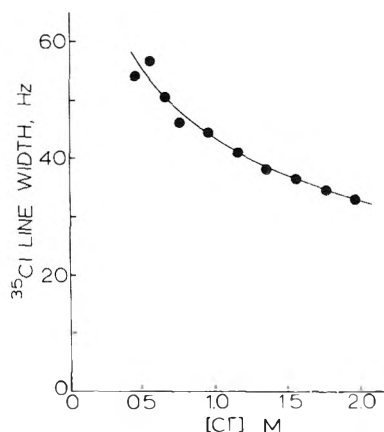


Figure 1. ^{35}Cl NMR line width vs. chloride ion concentration for 0.15 M $[\text{Co}(\text{pn})_3]\text{Cl}_3$ at ambient temperature.

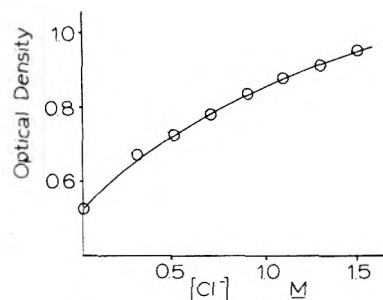


Figure 2. Absorbance at 261 nm and 25.0° for 0.10 M $[\text{Co}(\text{pn})_3](\text{ClO}_4)_3$ vs. $[\text{Cl}^-]$.

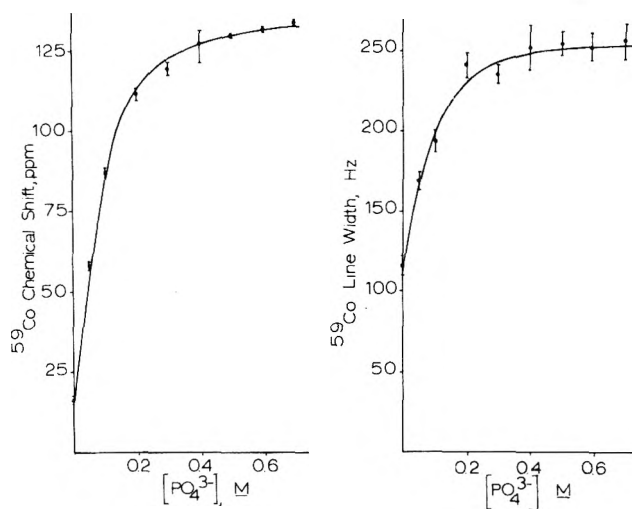


Figure 3. ^{59}Co chemical shift and line width for 0.10 M $[\text{Co}(\text{en})_3]\text{Cl}_3$ vs. phosphate concentration at pH 13.5 and ambient temperature. Shift reference is saturated $[\text{Co}(\text{en})_3](\text{ClO}_4)_3$.

Although the error in measuring NMR line widths in these experiments is 5% or less, the concentration range available for the study of the equilibria involved is small. The precision and accuracy of the derived equilibrium constants is therefore limited. The optical methods did in general give slightly different values for the equilibrium constants. However, large values of the reduced χ^2 statistic for the NMR data make it impossible to conclude that the NMR results for outer-sphere complex association constants disagree with the somewhat more precise optical experiments.

Outer-sphere complex formation constants are known to be a function of ionic strength. They become quite large in dilute solutions, but the dependence on ionic strength is weaker in concentrated electrolytes.² In many cases ionic activity is controlled by maintaining a supporting electrolyte concentration an order of magnitude higher than the concentration of the species studied. In the present study it is difficult to use this method because extremely high salt concentrations are required which cause additional difficulties such as precipitation of the metal complexes being studied. Some authors choose to maintain total electrolyte concentration constant. The solution composition changes using this procedure, however, and activities of individual ions may vary significantly even though the total ionic strength remains constant.

An attempt was made to assess the effects of ionic strength on the association constants measured here. Ionic strength was controlled for the chloride system by adding sodium perchlorate to maintain the total ionic strength at 2.8 *M*. Differences in the ³⁵Cl NMR data between experiments in which ionic strength is controlled and when it is not are within the experimental uncertainties. On the other hand, in analyzing the data from the optical experiments performed in the presence of perchlorate ion a weak interaction between the perchlorate ion and the metal complex was required to fit the data. In this case the equation for the observed extinction coefficient becomes

$$\epsilon_{\text{obsd}} = \frac{\epsilon_1 + K_1[\text{Cl}^-]\epsilon_1 + K_2[\text{ClO}_4^-]\epsilon_2}{1 + K_1[\text{Cl}^-] + K_2[\text{ClO}_4^-]} \quad (7)$$

where ϵ_1 , K_1 and ϵ_2 , K_2 represent the extinction coefficients and association constants for chloride and perchlorate ion outer-sphere complexes, respectively. The constants used are summarized in Table IV. Evidence from ¹⁷O, ³⁵Cl, and ²³Na NMR investigations suggests that perchlorate does interact with cations such as $[\text{Cr}(\text{H}_2\text{O})_6]^{3+}$, Mn^{2+} , and Na^+ in aqueous solutions.²²⁻²⁵ Conductance data may also be explained by assuming formation of ion pairs between complex cations and perchlorate ion where formation constants are similar to those with other univalent anions.²⁶⁻²⁸ An assumption that perchlorate ion will be ineffective in forming outer-sphere complexes because it is a poor first coordination sphere ligand appears unwarranted.

Martin and Fung²⁹ have measured a K_{os} value of 12 ± 2 for the outer-sphere complex $[\text{Co}(\text{en})_3]^{3+}$, PO_4^{3-} from ⁵⁹Co chemical shift data. In the present work the value obtained from both line width and shift measurements is 30 M^{-1} . This difference may result from using the potassium rather than the tetramethylammonium phosphate. However, this difference could also arise from slight differences in pH or experimental errors in one or both experiments.

There may be some error in the calculation of K_{os} from these data if 1:2 complexes exist to any significant extent. By including such species, eq 4 becomes

$$\omega_{\text{obsd}} = \frac{\omega_1 + [\text{L}](K_1\omega_1 + [\text{L}]K_1K_2\omega_2)}{1 + [\text{L}](K_1 + [\text{L}]K_1K_2)} \quad (8)$$

where ω_1 , ω_2 , K_1 , and K_2 are values for the physical observable and the outer-sphere association constant for 1:1 and 1:2 complexes, respectively. This expression differs from that for 1:1 complexes alone by the addition of the K_2 term. Since ω_1 and ω_2 are expected to be about the same size, and L is of the order of 1, the second term will be negligible if $K_2 \ll K_1$. It is expected that 2:1 halide:complex ion pairs will be extremely weak and at the concentrations

TABLE IV: Optical Parameters for Outer-Sphere Complexes of $[\text{Co}(\text{en})_3]^{3+}$ and $[\text{Co}(\text{pn})_3]^{3+}$

	ϵ_1 , $M^{-1} \text{ cm}^{-1}$	ϵ_2 , $M^{-1} \text{ cm}^{-1}$	K_1 , M^{-1}	K_2 , M^{-1}
$[\text{Co}(\text{en})_3]^{3+}$	1.35	0.55	0.65	0.22
$[\text{Co}(\text{pn})_3]^{3+}$	1.38	0.70	0.68	0.12

used in these experiments will not be important. Because of charge neutralization, 2:1 species are not expected to form in the phosphate systems. Therefore, no significant error should be introduced by neglecting second-order terms. This appears to be justified since within the precision of our data, no second-order ligand dependence could be observed.

The results in Table III demonstrate that there is no dramatic dependence of K_{os} on the degree of ligand alkylation for the outer-sphere complexes with chloride ion. For these ion pairs, therefore, hydrophobic substituents do not enhance ionic association. On the other hand, K_{os} for the phosphate ion pair with $[\text{Co}(\text{en})_3]^{3+}$ is almost twice that for $[\text{Co}(\text{pn})_3]^{3+}$. It is dangerous to ascribe the difference in the interaction of phosphate ion with these complexes entirely to ligand hydrophobicity, however, because the degree of association may also be affected by other factors such as the conformational equilibria of the chelate rings. There is evidence to suggest that phosphate association occurs preferentially with isomers having three N-H bonds directed along the C_3 axis of the complex.³⁰ Since the distribution of conformational isomers may be different for the ethylenediamine and the propylenediamine complexes, ligand hydrophobicity may make only a minor contribution to the observed differences.⁴

In the limit of extreme narrowing, the line width at half-height, $\Delta\nu$, of a quadrupole relaxed nucleus may be described by an equation of the form

$$\pi\Delta\nu = \frac{1}{T_2} = \frac{1}{8} \frac{2I + 3}{I^2(2I - 1)} \left(\frac{eQ}{h} \right)^2 J \quad (9a)$$

where T_2 is the transverse relaxation time of the nucleus with spin angular momentum I , Q the nuclear electric quadrupole moment, and J the Fourier transform of the correlation function characterizing the electric field gradient components at the nucleus.³⁸ Calculation of relaxation rates requires knowledge of or a model for the motions contributing to the correlation function. Several approaches have been taken that include detailed consideration of ion-ion, ion-solvent, and solvent-solvent interactions. A discomforting feature of the detailed approach presented is that they have been based on quite different assumptions, yet achieve reasonable agreement with experiment. When an observed ion associates directly with another ion in solution, as in the cases reported here, there may be merit in considering the limiting case appropriate to covalent bond formation when eq 9a reduces to

$$\frac{1}{T_2} = \frac{3}{40} \frac{2I + 3}{I^2(2I - 1)} \left(1 + \frac{\eta^2}{3} \right) \left(\frac{e^2qQ}{h} \right)^2 \tau_c \quad (9b)$$

where q is the electric field gradient at the observed nucleus, η the asymmetry parameter describing the deviation of the electric field gradient tensor from cylindrical symmetry, and τ_c is the correlation time for the reorientation of q . When q arises from a covalent bond, τ_c becomes the rotational correlation time.³¹ While this equation may be an in-

complete description in the case at hand, it displays explicitly two major variables, namely, the magnitude of the electric perturbation and its time dependence.

Association constants for the series of outer-sphere complexes $[\text{Co}(\text{en})_3]^{3+}$, Cl^- to $[\text{Co}(\text{bn})_3]^{3+}$, Cl^- are essentially the same. However, the line width of chloride ion in the outer-sphere complex changes by about a factor of 10 over the series. For example, the line width of the chlorine resonance for chloride ion associated with $[\text{Co}(\text{bn})_3]^{3+}$ is almost two orders of magnitude larger than that of the free chloride ion line width of the control solutions. This dramatic alteration in relaxation time may reflect changes in either the average electric environment of the chlorine nucleus or its time dependence.

Rotational correlation times of transition metal complexes such as $[\text{Cr}(\text{H}_2\text{O})_6]^{3+}$ are about 4×10^{-11} sec.³² Correlation times for ions such as chloride are difficult to define. These must be associated with molecular events such as rotation or solute collisions with solvent which are not likely to differ from 40 psec by more than a factor of 10.³³ If chloride ion association with the transition metal complexes were sufficiently strong so that the two species rotated as a unit, the chloride ion could experience a change in correlation time for the quadrupole interaction on the order of a factor of 10 or less. The maximum ^{35}Cl line width expected for the outer-sphere complex site assuming only the extreme correlation time changes would be approximately 150 Hz or less. These crude estimates suggest that the observed changes in $\Delta\nu_{\text{os}}$ have major contributions from changes in the field gradient factors of eq 9. This conclusion is consistent with earlier deductions drawn from similar studies of the alkyl ammonium ion-halide interactions in water.³⁴⁻³⁷

Factors which may account for electric field gradient changes have been discussed by several authors and several approaches to the question based on very different assumptions have been shown to be capable of accounting for the magnitudes of the effects encountered in aqueous solutions.³⁸⁻⁴⁰ For example, electric gradients may be generated by fluctuations in the electric field caused by the rotational or vibrational motion of water dipoles adjacent to the ion or by the large pulse of electric asymmetry generated when a colliding molecule or ion recoils from the repulsive part of the pair potential. It also seems possible that temporary defects in the solvation of an anion or cation could contribute significantly to the relaxation.

In the present case of halide ion relaxation, electric fields at the anion nucleus in the outer-sphere complex generated by the presence of the adjacent tripositive cation could be significant. However, calculation of the field gradient from the adjacent ion shows that this contribution to the relaxation rate is small.⁴² The magnitude of such a gradient should be inversely proportional to the size of the cation, but the data show the opposite trend. In some cases where outer-sphere complexes have been reported by other methods³ for the ions listed in Table I, very small effects are observed in the halide NMR spectrum. These observations suggest that the electrostatic contribution to the field gradient expected from the cation is not a dominant factor in determining the total relaxation rate of the anion in the outer-sphere complex.

Concentrations of the solutions studied were high by the standards of electrolyte theory.²⁷ However, in a solution 0.1 M in $[\text{Co}(\text{en})_3]\text{Cl}_3$ and 1.5 M in NaCl, there are on the average slightly more than 16 water molecules available to sol-

vent each ion. This is certainly sufficient to provide complete solvation in the sense of a first hydration level with water remaining for higher order interactions. Therefore insufficient primary solvation of the separate ions does not explain the observations.

In light of these considerations solvation sphere perturbations by associated cations remain as the most probable source of electric field gradient changes around halide ions in outer-sphere complexes. This idea has been advanced previously in discussions of halide relaxation in the presence of alkyl ammonium ions³⁴⁻³⁶ and recently criticized.³⁷ In order to obtain information about structural details of the outer-sphere complex from halide NMR line broadening parameters, it is necessary to determine the contributions of various structural types of outer-sphere complexes to the observed line width parameters. The values of $\Delta\nu_{\text{b}}$ shown in Table III are expected to be weighted averages taken over a number of cation associated sites in solution. Thus

$$\Delta\nu_{\text{b}} = \sum_{i=1}^n P_i \Delta\nu_i \quad (10)$$

where n is the number of outer-sphere structures, and P_i the probability that the nucleus will be found at a site with line width $\Delta\nu_i$.

Ion pairs are often divided into classes based on the presumed degree of solvent interaction with the associated ions. A direct interaction between cation and anion with no intervening solvent molecules is classified as a contact ion pair.⁴¹ Solvent-shared ion pairs have one solvent molecule between the ions that is common to both solvation spheres. In solvent-separated ion pairs, the primary solvation of the cation and anion remains essentially complete in the associated product.

To assess the relative contributions of different structures to an observed line width, model systems were chosen to approximate the various types of ion pairs. The effects of first solvation sphere changes on the ^{35}Cl relaxation of chloride ion such as would be provided by contact ion pair formation can be approximated from the relaxation time changes upon introducing other solvent molecules. For lithium chloride in methanol-water mixtures, the ^{35}Cl line width is directly proportional to methanol mole fraction and increases from 12 Hz in pure water to 180 Hz in pure methanol as shown in Figure 4. This change is small compared with a 1000-Hz line width calculated for the $[\text{Co}(\text{bn})_3]^{3+}$, Cl^- ion pair. However, a relatively small effect from methanol is not surprising if methanol is considered as methyl-water. This result shows that even this subtle change in the first solvation sphere of chloride ion will produce large changes in the ^{35}Cl relaxation time.

A quadrupole-relaxed nucleus with an intact first coordination sphere provides a model for a solvent-shared or solvent-separated ion pair. Two such ions were selected to assess these effects: $[\text{Cl}(\text{en})_3]^{3+}$ and ClO_4^- . In the first case, relaxation time changes due to the presence of various outer-sphere ligands were measured for the ^{59}Co resonance of $[\text{Co}(\text{en})_3]^{3+}$ and the results are listed in Table II. Except for the phosphate outer-sphere complex, no appreciable effect on the ^{59}Co line width is observed in the presence of these anions. Chloride, bromide, and iodide ions produce no more effect than the more weakly associated perchlorate ion. $\Delta\nu_{\text{b}}$ calculated for the phosphate ion pair is 260 Hz, which is only a factor of two larger than the line width of the uncomplexed ion. Separate measurements of the cobalt

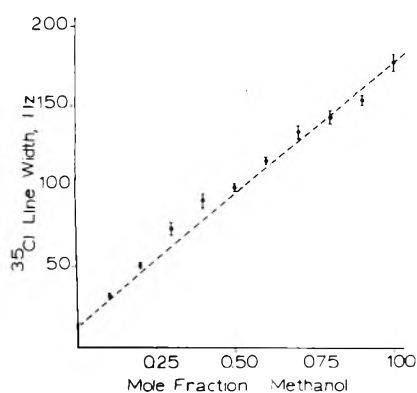


Figure 4. ^{35}Cl NMR line width vs. mole fraction of methanol in 1.0 M lithium chloride solutions in water-methanol.

complex rotational correlation time demonstrate that the correlation time changes by at least a factor of two when the phosphate ion is associated. Therefore, no change in the field gradient term is required to explain the change in the ^{59}Co line width.⁴² It is critical to note that placement of a highly charged ion in the second coordination sphere of the cobalt complex appears to make a negligible contribution to the ^{59}Co relaxation rate. This suggests that electrostatic effects are very efficiently attenuated by the symmetric and covalent first coordination sphere.

To the extent that the rigid tetrahedral arrangement of oxygen atoms in perchlorate ion resembles the nearest neighbor structure of chloride ion, measurements of ^{35}Cl in perchlorate ion should reflect the importance of second coordination sphere effects in chloride ion relaxation. The ^{35}Cl relaxation time of perchlorate ion is expected to be long because in perfect tetrahedral symmetry the quadrupole contribution to relaxation would vanish. The ^{35}Cl relaxation time may be determined by measuring $T_{1\rho}$,⁹ which is equal to T_2 in the limit of very small H_1 and in the absence of any slow processes in solution. $T_{1\rho}$ measurements summarized in Table V show that T_2 for ^{35}Cl in 2.2 M NaClO_4 is 0.25 sec, giving a line width of about 1 Hz in aqueous solution. Increasing NaClO_4 concentration and the addition of $[\text{Co}(\text{en})_3]^{3+}$ and $[\text{Co}(\text{pn})_3]^{3+}$ do not produce any measurable effect on the ^{35}Cl $T_{1\rho}$ when viscosity corrections are made. This result is in agreement with the expectation that second coordination sphere perturbations should have small effects on the perchlorate ^{35}Cl relaxation time, however, it is inconclusive since the outer-sphere complexes are weak.

A more drastic change in the presumed second coordination sphere of perchlorate ion occurs if it is placed in a non-aqueous solvent such as acetone. For 3 M NaClO_4 in acetone, the ^{35}Cl line width of the absorption mode signal is 28 Hz. After viscosity corrections, this corresponds to a relaxation time of 0.025 sec, which is ten times shorter than the T_2 value measured in aqueous solution. To the extent that perchlorate is a useful model, these results conflict with those from the ^{59}Co measurements. A possibly critical difference between these two systems is that perchlorate ion is four coordinate and cobalt six coordinate. It may be that neither model is an accurate representation of aqueous chloride ion. Even with the large change in the perchlorate ion relaxation time attending the introduction of acetone, the relaxation rates are small compared with those observed for chloride ion in association with complex cations where perturbations of the primary hydration is possible.

TABLE V: ^{35}Cl $T_{1\rho}$ in Sodium Perchlorate Solutions

$[\text{NaClO}_4]$, M	Solvent	Other ions present	$T_{1\rho}$, ^a sec
2.2	H_2O		0.25
3.7	H_2O		0.25
7.5	H_2O		0.14
15	H_2O		0.09
3.5	Acetone		0.011 (0.025) ^b
2.2	H_2O	0.1 M $[\text{Co}(\text{en})_3]^{3+}$ - $(\text{ClO}_4)_3$	0.26 (0.25) ^b
2.2	H_2O	0.1 M $[\text{Co}(\text{pn})_3]^{3+}$ - $(\text{ClO}_4)_3$	0.20 (0.25) ^b

^a Estimated error is 10%. ^b Corrected for viscosity.

Therefore we suggest that the changes observed in the chloride ion relaxation times are due primarily to perturbations of the first hydration sphere.

Assuming that association constants are similar for all outer-sphere complexes of the trivalent cations with a given anion, which is supported by the K_{os} values determined here, the differences in halide line widths can be attributed to different effects on the primary solvation spheres of the associated anions. The effects increase in the order $[\text{Co}(\text{NH}_3)_6]^{3+} < [\text{Co}(\text{NH}_3)_5\text{OH}_2]^{3+} < [\text{Co}(\text{NH}_3)_4(\text{OH}_2)_2]^{3+} < [\text{Co}(\text{en})_3]^{3+} < [\text{Co}(\text{pn})_3]^{3+} < [\text{Co}(\text{bn})_3]^{3+}$. It is tempting to suggest detailed models based on these results; however, these experiments by themselves do not provide compelling evidence to support them. The ligands in $[\text{Co}(\text{en})_3]^{3+}$, $[\text{Co}(\text{pn})_3]^{3+}$, and $[\text{Co}(\text{bn})_3]^{3+}$ are increasingly hydrophobic and $\Delta\nu_{os}$ values for chloride ions associated with these complexes increase in the same order. The effects of alkyl groups on the structure of water have been investigated extensively, particularly in the case of tetraalkylammonium salts. Collectively this work indicates that the alkyl groups do affect the nature of water in their vicinity including that in hydration domains of other ions. The extension of this conclusion to suggest that alkyl groups coordinated to metals such as in the diamine series should alter the water structure in the solvation domain of an associated outer-sphere ligand such as chloride ion is supported by the present work.

Acknowledgment. This work was supported by The Merck Company, The Research Corporation, The Graduate School, and The Chemistry Department, University of Minnesota, and the National Institutes of Health, GM 19719.

Helpful discussions with Professors Harold Friedman and H. G. Hertz are gratefully acknowledged.

References and Notes

- (1) R. A. Robinson and R. H. Stokes, "Electrolyte Solutions", Butterworths, London, 1959.
- (2) F. A. Posey and H. Taube, *J. Am. Chem. Soc.*, **75**, 1463 (1953).
- (3) M. T. Beck, *Coord. Chem. Rev.*, **3**, 91 (1968).
- (4) T. R. Stengle and C. H. Langford, *J. Phys. Chem.*, **69**, 3299 (1965).
- (5) L. E. Orgel and R. S. Mulliken, *J. Am. Chem. Soc.*, **79**, 4839 (1957).
- (6) L. Johansson, *Coord. Chem. Rev.*, **12**, 241 (1974).
- (7) J. J. Lingane and J. W. Collat, *Anal. Chem.*, **22**, 166 (1950).
- (8) R. G. Bryant, Y. Legler, and M. Han, *Biochemistry*, **11**, 3846 (1972).
- (9) I. Solomon, *C. R. Acad. Sci.*, **92**, 248 (1959).
- (10) P. R. Bevington, "Data Reduction and Error Analysis for the Physical Sciences", McGraw-Hill, New York, N.Y., 1969.
- (11) L. E. Conroy and R. S. Tobias, "General Chemistry Laboratory Operations", Macmillan, New York, N.Y., 1965, p 150.
- (12) G. G. Schlessinger, *Inorg. Syn.*, **9**, 160 (1967).

- (13) H. Diehl, H. Clark, and H. H. Willard, *Inorg. Syn.*, **1**, 186 (1939).
- (14) A. C. Rutenberg and H. Taube, *J. Chem. Phys.*, **20**, 825 (1952). Prepared from $\text{Co}(\text{NH}_3)_4\text{CO}_3\text{NO}_3 \cdot \frac{1}{2}\text{H}_2\text{O}$ which was synthesized as described by F. Basolo and R. K. Murmann, *Inorg. Syn.*, **4**, 171 (1953).
- (15) S. M. Jorgenson, *Z. Anorg. Chem.*, **2**, 294 (1892). Prepared from $\text{Co}(\text{NH}_3)_4\text{CO}_3\text{NO}_3 \cdot \frac{1}{2}\text{H}_2\text{O}$ which was synthesized as described by G. Schlessinger, *Inorg. Syn.*, **6**, 173 (1960).
- (16) J. B. Work, *Inorg. Syn.*, **2**, 221 (1946).
- (17) I. L. Jenkins and C. B. Monk, *J. Chem. Soc.*, 68 (1951).
- (18) W. E. Cooley, C. Fan Liu, and J. C. Bailar, Jr., *J. Am. Chem. Soc.*, **81**, 4189 (1959).
- (19) F. Basolo and R. G. Fearson, "Mechanisms of Inorganic Reactions", Wiley, New York, N.Y., 1967.
- (20) A. Elder and S. Petrucchi, *Inorg. Chem.*, **9**, 19 (1970).
- (21) T. J. Swift and R. E. Connick, *J. Chem. Phys.*, **31**, 307 (1962).
- (22) M. Alei, Jr., *Inorg. Chem.*, **3**, 44 (1964).
- (23) F. Klanberg, J. P. Hunt, and H. W. Dodgen, *Inorg. Chem.*, **2**, 139 (1963).
- (24) G. J. Templeman and A. L. Van Geet, *J. Am. Chem. Soc.*, **94**, 5578 (1972).
- (25) K. L. Craighead and R. G. Bryant, submitted for publication.
- (26) M. G. Burnett, *J. Chem. Soc. A*, 2480 (1970).
- (27) R. A. Robinson and R. H. Stokes, "Electrolyte Solutions", 2nd ed, Butterworths, London, 1959, p 243.
- (28) G. H. Nancollas, "Interactions in Electrolyte Solutions", Elsevier, Amsterdam, 1966, pp 25, 74.
- (29) T. H. Martin and B. M. Fung, *J. Phys. Chem.*, **77**, 637 (1973).
- (30) S. F. Mason and B. J. Norman, *J. Chem. Soc. A*, 307 (1966).
- (31) A. Abragam, "The Principles of Nuclear Magnetism", Oxford University Press, London, 1961, Chapter 8.
- (32) H. G. Hertz, in "Water, a Comprehensive Treatise", Vol. 3, Felix Franks, Ed., Plenum Press, New York, N.Y., 1973, Chapter 7.
- (33) H. G. Hertz, G. Keller, and H. Versmold, *Ber. Bunsenges. Phys. Chem.*, **73**, 549 (1969).
- (34) B. Lindman, S. Forsen, and E. Forslind, *J. Phys. Chem.*, **72**, 2805 (1968).
- (35) B. Lindman, H. Wennerstrom, and S. Forsen, *J. Phys. Chem.*, **74**, 754 (1970).
- (36) W. Wennerstrom, B. Lindman, and S. Forsen, *J. Phys. Chem.*, **75**, 2936 (1971).
- (37) H. G. Hertz and M. Holz, *J. Phys. Chem.*, **78**, 1002 (1974).
- (38) H. G. Hertz, *Ber. Bunsenges. Phys. Chem.*, **77**, 531 (1973).
- (39) C. Devereil, *Prog. Nucl. Magn. Resonance Spectrosc.*, **4**, 235 (1969).
- (40) K. A. Valiev, *Z. Strukt. Chim.*, **3**, 653 (1962).
- (41) E. S. Gould, "Mechanism and Structure in Organic Chemistry", Holt, Rinehart and Winston, New York, N.Y., 1959, p 580.
- (42) K. L. Craighead and R. G. Bryant, submitted for publication.

Crystal Structures of Hydrated and Dehydrated Divalent-Copper-Exchanged Faujasite

I. E. Maxwell* and J. J. de Boer

Koninklijke/Shell-Laboratorium, Amsterdam (Shell Research B.V.), Holland (Received October 29, 1974)

Publication costs assisted by Koninklijke/Shell-Laboratorium, Amsterdam

The crystal structures of hydrated and dehydrated Cu^{2+} -exchanged faujasite have been determined by single-crystal X-ray diffraction techniques. The space group is $Fd3m$ ($a = 24.713(5)$ Å, hydrated; $a = 24.643(5)$ Å, dehydrated). Reflection data were collected with $\text{Cu K}\alpha$ ($\lambda 1.54182$ Å) radiation using two natural single crystals each with a maximum dimension of approximately 0.2 mm. A total of 218 and 212 unique observed reflections were obtained by counter methods, and the structures were refined by least-squares techniques to final conventional R factors of 0.046 and 0.050, for hydrated and dehydrated forms, respectively. In the hydrated form only the copper ions in site I' have been located with certainty. By contrast, in the dehydrated form copper ions are located at sites I, I', II', II, and III. The site III cations are very favorably sited for interaction with adsorbate molecules. In the dehydrated form, the relatively strong binding of the Cu^{2+} ions to the zeolite framework is shown to significantly lengthen the Si(Al)-O bonds.

Introduction

Over the past few years numerous studies have been made of transition-metal ion-exchanged zeolites. In particular, divalent copper-exchanged zeolite Y has been shown to exhibit catalytic activity in oxidation,¹⁻⁸ cracking,⁹ and isomerization reactions.¹⁰ A prerequisite for characterizing the nature of the active species would be a detailed knowledge of the catalyst structure. This requires the determination not only of the siting of the copper cations in the zeolite but also of any modification of the zeolite framework resulting from the Cu^{2+} exchange.

Divalent copper-exchanged zeolite Y has been extensively studied by electron spin resonance spectroscopy.¹¹⁻¹⁸ These studies have shown that the Cu^{2+} cations are distributed over different sites within the zeolite framework and that the populations of these sites are markedly dependent on the presence of adsorbed molecules, e.g., water, ammonia, and butene. However, they have not revealed the exact siting of the copper cations or any modifications of the

framework structure. Such structural details can, in principle, be determined by X-ray diffraction analysis. Gallezot et al.¹⁹ performed powder X-ray diffraction studies of dehydrated partially Cu^{2+} -exchanged zeolite Y, before and after adsorption of various molecules. However, powder diffraction techniques, inherently, yield less precise structural data than single-crystal techniques.

In an attempt to obtain detailed structural information we have carried out single-crystal X-ray studies of Cu^{2+} -exchanged hydrated and dehydrated forms of natural faujasite.

Experimental Section

Crystals of natural faujasite which have initially been exchanged with K^+ were further exchanged with Cu^{2+} cations, by contacting them for 3 weeks with 1 *M* solutions of copper sulfate or acetate. With both anions there was no detectable loss in crystallinity. The amount of material was insufficient to determine the Si/Al ratio or the degree of

Cu^{2+} exchange by chemical analysis. However, the Si/Al ratio could be estimated from the unit cell constant of the original, hydrated K^+ -exchanged form.

To our knowledge ion-exchange isotherms have only been published for the $\text{Cu}^{2+}/\text{Na}^+-X$ system.²⁰ Nevertheless, these show that the selectivity is very much in favor of Cu^{2+} ions in the zeolite surface and that 100% exchange can be readily achieved. The $\text{Cu}^{2+}/\text{Na}^+-Y$ ion-exchange system would not be expected to be markedly different, thus we would expect to have achieved close to 100% Cu^{2+} exchange of the faujasite crystals.

Mortier and Bosmans²¹ carried out powder X-ray analyses of four hydrated K^+ -exchanged synthetic zeolites, types X and Y, with different Si/Al ratios. As shown in Figure 1, the relationship between the unit cell constants and the number of cations per unit cell is approximately linear. Using this graph and the measured cell constant for our sample of K^+ -exchanged natural faujasite ($a = 24.761(5)$ Å), we find a unit cell formula of $\text{K}_{56}(\text{AlO}_2)_{56}(\text{SiO}_2)_{136} \cdot x\text{H}_2\text{O}$ and thus a Si/Al ratio of 2.42. This is in good agreement with the Si/Al ratio for natural faujasite reported by Baur²² (Si/Al = 2.31). Data collection of the hydrated form was carried out by simply mounting a suitable single crystal on a glass fibre. For the dehydrated form a crystal was firmly wedged inside a thin-walled Lindeman glass capillary. The crystal was then heated at 150° for 20 hr while the capillary was evacuated to 10^{-3} Pa ($= 10^{-5}$ Torr). Both crystals (each with maximum dimensions of approximately $0.2 \times 0.1 \times 0.1$ mm) were aligned about [110] and then placed on a Nonius three-circle automatic diffractometer equipped with scintillation counter and pulse-height discriminator. Least-squares cell refinement based on θ , $-\theta$ ($\theta \leq 15^\circ$) values measured for several reflections with Cu $K\alpha$ radiation ($\lambda 1.54182$ Å) gave the following lattice parameters: hydrated, $a = 24.713(5)$ Å; dehydrated $a = 24.643(5)$ Å.

For both forms six equivalent data sets were collected, using Ni-filtered Cu $K\alpha$ radiation ($\theta \leq 50^\circ$). The $\theta - 2\theta$ scan method was used with a scanning speed of $0.6^\circ/\text{min}$ (in θ) and a scan range of 0.7° . Backgrounds were measured for half of the scan time on each side of the reflection. Control reflections monitored at regular intervals showed no significant variations in intensity, for both crystals, during data collection. Initial standard deviations in observed structure factors were calculated from counting statistics, but these were later found to be inadequate. Lorentz, polarization, and ϕ -dependent absorption corrections ($\mu_{\text{CuK}\alpha} = 5.2 \text{ mm}^{-1}$) were applied, that latter by means of a semiempirical method as described by Furnas.²³ The ϕ -dependent absorption corrections were obtained by averaging the measurements from several reflections of the type hh0. The variation with θ was found to be negligible and the θ -dependent absorption correction was neglected. The data were then scaled and averaged to yield 218 and 212 unique reflections with estimated conventional R factors of 0.03 and 0.04 for hydrated and dehydrated crystals, respectively.

Structure Determination

Full matrix least-squares refinements were initially carried out on the basis of the framework parameters for natural faujasite.²⁴ Copper cations and water molecules were located from a series of difference Fourier syntheses and included in subsequent cycles of refinement. Parameters with high correlation coefficients, such as occupancy and temperature factors, were varied separately in alternating cy-

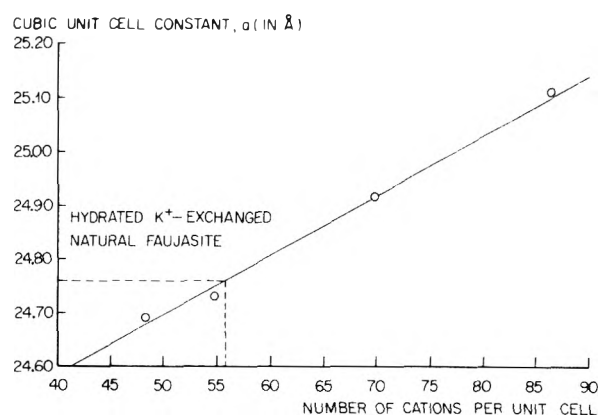


Figure 1. Plot of cubic unit cell constant against number of cations per unit cell for hydrated K^+ -exchanged X and Y zeolites.

cles. Scattering factors for the ions Cu^{2+} , O^- , Si^{2+} , and Al^{3+} were used throughout the refinements.²⁵ In both structures, the agreement between observed and calculated structure factors was poor for the 111 reflection. This was also true for the 220 reflection of the hydrated form (vide infra). These reflections were therefore removed in the final stages of the refinements. The maximum peaks on final difference Fourier syntheses were approximately $0.1 \text{ e}/\text{Å}^3$ in both structures. Most of these were either diffuse or at chemically unacceptable locations. There was no evidence of significant anisotropic thermal motion of framework atoms from difference syntheses. In view of this and of the rather limited amount of reflection data, anisotropic refinement was not attempted.

Plots of $\langle (F_o - F_c)^2 \rangle$, in ranges of $\sin \theta/\lambda$, at early stages in the refinement of both structures, revealed that the initial weighting scheme based on counting statistics was unsatisfactory. The estimated standard deviations were accordingly modified such that for $0 < \sin \theta/\lambda \leq 0.2062 \text{ Å}^{-1}$, $\sigma(F_o) = 9.10$, hydrated; and 5.63, dehydrated; for $0.2062 < \sin \theta/\lambda \leq 0.2598 \text{ Å}^{-1}$, $\sigma(F_o) = 5.46$, hydrated; 4.10 dehydrated; and for $\sin \theta/\lambda > 0.2598 \text{ Å}^{-1}$, $\sigma(F_o) = 3.51$ hydrated; and 4.10 dehydrated.

The final residuals were R_1 , 0.046 and 0.050, and R_2 , 0.042 and 0.049, for hydrated and dehydrated structures, respectively (where $R_1 = \sum \|F_o - F_c\| / \sum \|F_o\|$, $R_2 = [\sum \omega (F_o - F_c)^2 / \sum \omega F_o^2]^{1/2}$ and $\omega = \sigma^{-2}(F_o)$). Final values for the error in an observation of unit weight were 0.96 (hydrated) and 1.00 (dehydrated). The refined positional, occupancy, and temperature factors are given in Table I. Listings of observed and calculated structure factors (Tables II and III) are available elsewhere.²⁶

Discussion

The sitings of cations and water molecules in hydrated and dehydrated divalent-copper-exchanged faujasite, as determined from the X-ray analyses, are compared in Table IV. Assignments have been made on the basis of the cation- H_2O framework distances (see Table V). In some instances it was difficult to make a clear distinction between water molecules and cations (e.g., OW(2), OW(6), OW(7) hydrated form and OW dehydrated form). In these cases the observed electron density could be due either to copper ions that are very weakly bound to the framework (and therefore presumably strongly bound to water) or to strongly bound water molecules.

Copper cations are evidently rather mobile and mainly bound to water molecules in the hydrated form. Only 6.3(2)

TABLE I: Positional, Thermal, and Occupancy Parameters for Hydrated and Dehydrated Divalent-Copper-Exchanged Faujasite

Atom	Position ^a	Occupancy factor ^b	X	Y	Z	B, Å ²
(a) Hydrated						
(Si,Al)	192(i)	1.0	0.0362(1)	0.3037(1)	0.1247(1)	1.42(8)
O(1)	96(h)	1.0	0	-0.1062(4)	0.1062(4)	2.9(2)
O(2)	96(g)	1.0	0.0033(5)	-0.1431(3)	0.0033(5)	2.7(2)
O(3)	96(g)	1.0	0.0761(5)	-0.0329(3)	0.0761(5)	2.6(2)
O(4)	96(g)	1.0	0.0717(4)	0.3224(3)	0.0717(4)	2.2(2)
Cu(I')	32(e)	0.196(7)	0.071(1)	0.071(1)	0.071(1)	3.6(3)
OW(1)	32(e)	0.84(4)	0.082(1)	0.168(1)	0.082(1)	3.5(4)
OW(2)	32(e)	0.70(4)	0.016(2)	-0.266(2)	0.016(2)	5.9(7)
OW(3)	8(a)	0.10(1)	1/8	1/8	1/8	0.1(9)
OW(4)	192(i)	0.16(2)	0.173(3)	-0.197(3)	0.048(3)	11.4(1.9)
OW(5)	192(i)	0.16(2)	0.075(3)	-0.201(3)	0.109(3)	10.1(2.0)
OW(6)	96(g)	0.18(3)	0.031(6)	0.427(4)	0.031(6)	10.8(2.3)
OW(7)	96(g)	0.12(2)	0.006(6)	0.386(4)	0.006(6)	5.7(2.1)
(b) Dehydrated						
(Si,Al)	192(i)	1.0	0.0359(1)	0.3038(1)	0.125(1)	1.67(8)
O(1)	96(h)	1.0	0	-0.1062(5)	0.1062(5)	3.6(2)
O(2)	96(g)	1.0	0.0030(6)	-0.1432(4)	0.0030(6)	4.3(2)
O(3)	96(g)	1.0	0.0737(5)	-0.0317(4)	0.0737(5)	3.9(2)
O(4)	96(g)	1.0	0.0733(5)	0.3209(4)	0.0733(5)	3.0(2)
Cu(I)	16(c)	0.095(13)	0	0	0	8.2(2.0)
Cu(I'A)	32(e)	0.355(7)	0.0401(7)	0.0401(7)	0.0401(7)	3.3(2)
Cu(I'B)	32(e)	0.086(9)	0.073(5)	0.073(5)	0.073(5)	8.9(1.6)
Cu(II')	32(e)	0.025(5)	0.047(7)	0.203(7)	0.047(7)	0.0(1.8)
Cu(IIA)	32(e)	0.118(6)	0.031(2)	0.219(2)	0.031(2)	1.1(4)
Cu(IIB)	32(e)	0.048(5)	0.006(4)	0.244(4)	0.006(4)	0.6(1.0)
Cu(III)	192(i)	0.017(3)	0.017(3)	0.418(3)	0.084(3)	3.2(1.7)
OW	32(e)	0.166(26)	0.013(6)	-0.263(6)	0.013(6)	2.5(1.9)

^a Origin at center (3m). ^b Standard deviations in units of the least significant digits of the corresponding parameter are given in parentheses in all tables.

cations per unit cell could be located at site I' inside the sodalite cage. (The site nomenclature is as follows: site I, center of hexagonal prism; site II, six-membered ring face of sodalite cage on the supercage side; site I' and II' lie on the other sides of the six-membered rings, opposite sites I and II, respectively, inside the sodalite cage.) Moreover, these cations are only relatively weakly bonded to the zeolite framework: Cu(I')-O(3) = 2.58(3) Å (cf., $r_{Cu^{2+}} + r_{O^{2-}} = 2.09$ Å). Water molecules are located at site II' [OW(1)], the center of the sodalite cage [OW(3)], and inside the supercage [OW(4)-OW(7)].

In marked contrast to the hydrated form, in the dehydrated form almost all the copper ions (25.1 per unit cell (puc) vs. 28 puc for complete exchange) have been located. The cations are distributed over several different sites, although site I', as in the hydrated form, is clearly favored with a total of 14.2 cations puc. Most of the cations at this site are strongly bound to the zeolite framework [Cu(I'A)-O(3) = 2.12(1) Å] and a smaller number of cations are less firmly bound [Cu(I'B)-O(3) = 2.56(1) Å] and are therefore presumably interacting with residual water (see Figure 2). A similar cation-framework coordination geometry exists at the single six-membered ring which faces onto the supercage (site II). Copper ions, Cu(II') and Cu(IIA), are strongly bound to the zeolite framework [Cu(II')-O(2) = 2.29(9) Å; Cu(IIA)-O(2) = 2.22(1) Å] and a smaller number of cations that are less strongly bound to the framework appear

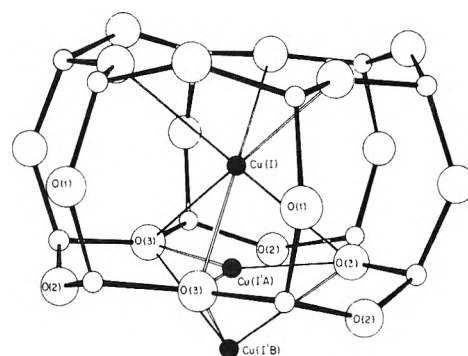


Figure 2. Perspective view showing the coordination of Cu(I), Cu(I'A), and Cu(I'B) cations to the hexagonal prism in dehydrated divalent-copper-exchanged faujasite (see ref 30).

to be interacting with residual water in the supercage [Cu(IIB)-O(2) = 2.51(10) Å, see Figure 3].

More interestingly, copper cations, Cu(III), have been unequivocally located inside the supercage (sites other than site II). The site has no crystallographic symmetry and the cation coordination to the framework oxygen atoms is most unusual (see Figure 4). These cations are located at the edges of the four-membered rings formed by the O(1) and O(4) oxygen atoms. The bonding of the copper ions to these oxygen atoms is very unsymmetrical, the

TABLE IV: Comparison of Sitings of Cations and Water Molecules in Hydrated and Dehydrated Divalent-Copper-Exchanged Faujasite

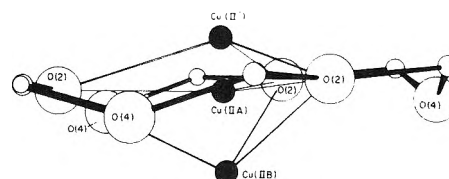
		Hydrated		Dehydrated				
	Atom	Coordinates ^a	No. per unit cell	Atom	Coordinates	No. per unit cell		
Inside dense cage structure	{	Cu(I')	0.071(1) ^a	6.3(2)	Cu(I)	0 ^a	1.5(2)	
		OW(3)	0.125 ^a	3.2(3)	Cu(I'A)	0.0401(7) ^a	11.4(2)	
		OW(1)	0.168(1) ^a	26.9(1.3)	Cu(I'B)	0.073(5) ^a	2.8(3)	
Inside or on the periphery of supercage structure	OW(2)	0.266(2) ^a	22.4(1.3)	Cu(II')	0.203(7) ^a	0.8(2)		
	{	0.173(3)	31(4)	Cu(IIA)	0.219(2) ^a	3.8(2)		
		-0.197(3)		Cu(II B)	0.244(4) ^a	1.5(2)		
		0.048(3)		OW	0.263(6) ^a	5.3(8)		
	{	0.075(3)	31(4)	Cu(III)	{	0.017(3)		
		-0.201(3)					0.418(3)	
		0.109(3)						0.084(3)
	{	0.031(6)	17(3)					
		0.427(4)						
	{	0.031(6)	12(2)					
0.006(6)								
{	0.386(4)	12(2)						
	0.006(6)							
Total Cu ²⁺ located			6.3					
Total H ₂ O located			143.5			5.3		

^a Coordinates belong to set 32(e), $x = y = z$.

TABLE V: Cation-Water Framework Distances (Å) for Hydrated and Dehydrated Divalent-Copper-Exchanged Faujasite

Atoms	Distance	Atoms	Distance
(a) Hydrated			
Cu(I')-O(3)	2.58(3)	OW(4)-O(1)	3.03(6)
Cu(I')-O(2)	3.15(2)	OW(4)-O(4)	3.14(7)
Cu(I')-OW(3)	2.31(5)	OW(5)-O(1)	3.00(7)
Cu(I')-OW(1)	2.42(4)	OW(5)-O(2)	3.47(7)
OW(1)-O(2)	3.06(4)	OW(6)-O(4)	2.94(13)
OW(1)-O(3)	3.64(5)	OW(6)-O(1)	3.38(10)
OW(2)-O(2)	3.08(6)	OW(7)-O(4)	2.79(18)
OW(2)-O(4)	3.37(6)	OW(7)-O(1)	3.50(14)
(b) Dehydrated			
Cu(I)-O(3)	2.68(2)	Cu(IIA)-O(2)	2.22(1)
Cu(I)-O(2)	3.53(2)	Cu(IIA)-O(4)	2.92(1)
Cu(I'A)-O(3)	2.12(1)	Cu(II B)-O(2)	2.51(10)
Cu(I'A)-O(2)	2.95(1)	Cu(II B)-O(4)	3.03(6)
Cu(I'B)-O(3)	2.56(1)	Cu(III)-O(1)	2.16(7)
Cu(I'B)-O(2)	3.15(2)	Cu(III)-O(4)	2.77(7)
Cu(II')-O(2)	2.29(9)	OW-O(2)	2.99(9)
Cu(II')-O(4)	3.05(10)	OW-O(4)	3.35(9)

interaction with O(1), Cu(III)-O(1) = 2.16(7) Å, being much stronger than with O(4), Cu(III)-O(4) = 2.77(7) Å. The short Cu(III)-O(1) distance means that the assignment of this electron density to a copper cation is unequivocal since

**Figure 3.** Perspective view showing the coordination of Cu(II'), Cu(IIA), and Cu(II B) cations to the single six-membered ring in dehydrated divalent-copper-exchanged faujasite (see ref 30).

such a close approach to framework oxygen ions is not possible for residual water molecules on unexchanged K⁺ ions. Noteworthy is the water molecule, OW(6), which in the hydrated form is also located in the vicinity of the Cu(III) cation but more distant from the framework as expected (i.e., OW(6)-O(4), 2.94(13) Å, OW(6)-O(1), 3.38(10) Å).

To our knowledge there are no other published X-ray data on cations (other than site II type) that have been located inside the supercage and are bound to the framework. However, there has been considerable speculation as to the most probable siting of these so-called site III type cations.

Conventionally most authors²⁷ have supposed that site III type cations are located at the center of the square faces of the sodalite unit, which is in contrast to the present results. Further studies will be necessary to determine whether this observed site is specific to Cu²⁺ cations or whether it is also occupied by other divalent and monovalent cations. Olson²⁴ has referred to unpublished X-ray

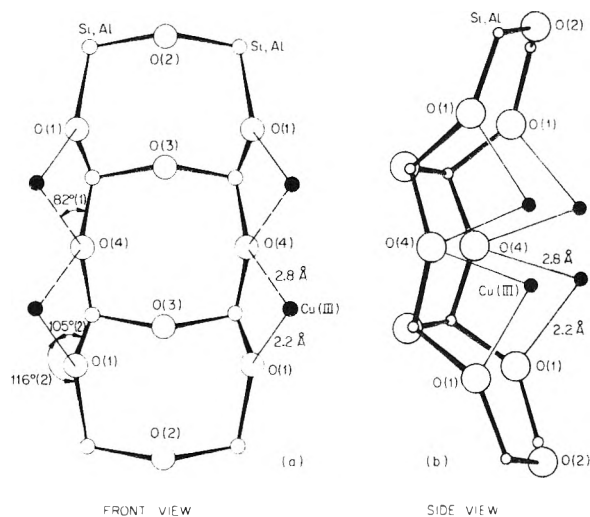


Figure 4. Perspective views of Cu^{2+} cations coordinated to the oxygen atoms at the edges of the four-membered rings in the supercages of dehydrated divalent-copper-exchanged faujasite (see ref 30).

data on dehydrated NaX , where Na^+ ions were also located at the edges of the square faces. This suggests that this site may be generally occupied irrespective of the type of cation (cf., sites I, I', II, and II'). The lack of symmetry together with the low occupancy factors have clearly been responsible for the previous difficulties in locating site III type cations by X-ray analysis.

As previously mentioned, the Cu(III) cations are almost exclusively bonded to the bridging hexagonal prism oxygen atoms, O(1). These cations are therefore located at a position in the supercage which is highly accessible to adsorbed molecules, namely, at the entrances to the large cavities (see Figure 5). Cations at site II, however, which are also accessible to adsorbed molecules, are partially shielded from adsorbent molecules by the six-membered ring oxygen atoms. Thus site III Cu^{2+} cations would appear to be the most favorably sited to interact with adsorbent molecules and are therefore likely to be the catalytically most active sites. Interestingly, this site is remarkably similar to the proposed siting or protons in hydrogen faujasite. From X-ray studies, Olson and Dempsey²⁸ concluded on the basis of $\text{Si(Al)}-\text{O}$ bond distances that the most reactive protons in hydrogen faujasite were also attached to the bridging oxygens, O(1), of the hexagonal prism.

As indicated in Table VI the $\text{Si(Al)}-\text{O}$ distances in the dehydrated form show a marked variation whereas those in the hydrated form remain equal (within 1 estimated standard deviation). This difference can be related to the interaction between framework oxygen atoms and the copper cations. In the hydrated form there are no strong cation-framework interactions, the closest approach being that of $\text{Cu(I)}-\text{O(3)} = 2.58(3)$ Å. However, for the dehydrated form there are several rather strong interactions between various copper cations and oxygen atoms. In Figure 6 the $\text{Si(Al)}-\text{O}$ distances for the dehydrated form are plotted against the percentage of each type of oxygen atom in close contact with a copper cation (these values are less than 100% due to partial occupancy of sites by cations). Clearly, there is an approximately linear relationship between these two quantities. By extrapolation it can be seen that for 100% involvement of oxygen atoms in bonding with copper cations the $\text{Si(Al)}-\text{O}$ bond distance is lengthened to 1.69 Å (cf., 1.63 Å for 0% divalent copper-oxygen bonding), indicating

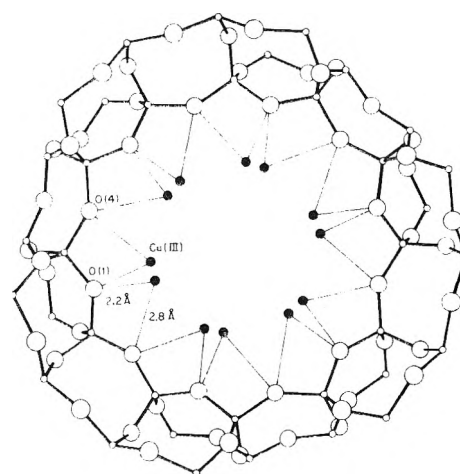


Figure 5. Perspective view showing the siting of Cu^{2+} cations at the pore entrance to the supercage in dehydrated divalent-copper-exchanged faujasite (see ref 30).

TABLE VI: Framework Distances (Å) and Bond Angles (degrees) for Hydrated and Dehydrated Divalent-Copper-Exchanged Faujasite

Atoms	Hydrated	Dehydrated
$\text{(Si,Al)}-\text{O(1)}$	1.644(6)	1.628(7)
$\text{(Si,Al)}-\text{O(2)}$	1.643(5)	1.640(5)
$\text{(Si,Al)}-\text{O(3)}$	1.647(4)	1.661(5)
$\text{(Si,Al)}-\text{O(4)}$	1.644(5)	1.629(5)
Mean value	1.645	1.640
$\text{(Si,Al)}-\text{O(1)}-\text{(Si,Al)}$	138.5(1.0)	138.3(1.2)
$\text{(Si,Al)}-\text{O(2)}-\text{(Si,Al)}$	146.0(7)	144.8(8)
$\text{(Si,Al)}-\text{O(3)}-\text{(Si,Al)}$	141.8(6)	137.9(7)
$\text{(Si,Al)}-\text{O(4)}-\text{(Si,Al)}$	140.5(7)	145.3(8)
Mean value	141.7	141.6
$\text{O(1)}-\text{O(2)}$	2.702(14)	2.696(16)
$\text{O(1)}-\text{O(3)}$	2.714(13)	2.696(17)
$\text{O(1)}-\text{O(4)}$	2.648(5)	2.655(5)
$\text{O(2)}-\text{O(3)}$	2.669(8)	2.649(9)
$\text{O(2)}-\text{O(4)}$	2.667(6)	2.650(8)
$\text{O(3)}-\text{O(4)}$	2.710(16)	2.717(18)
Mean value	2.685	2.677
$\text{O(1)}-\text{(Si,Al)}-\text{O(2)}$	110.6(7)	111.2(8)
$\text{O(1)}-\text{(Si,Al)}-\text{O(3)}$	111.1(6)	110.1(8)
$\text{O(1)}-\text{(Si,Al)}-\text{O(4)}$	107.3(6)	109.2(7)
$\text{O(2)}-\text{(Si,Al)}-\text{O(3)}$	108.4(6)	106.7(7)
$\text{O(2)}-\text{(Si,Al)}-\text{O(4)}$	108.4(6)	108.3(6)
$\text{O(3)}-\text{(Si,Al)}-\text{O(4)}$	110.9(8)	111.3(9)
Mean value	109.5	109.5

a decrease in bond order. Similar effects were reported by Olson²⁴ for dehydrated Ni^{2+} faujasite and dehydrated CaX and SrX zeolites.²⁸

This decrease in $\text{Si(Al)}-\text{O}$ bond order in dehydrated divalent copper-exchanged faujasite might explain some of the results obtained in oxygen mobility studies of zeolite Y.²⁹ These studies showed that the activation energy for oxygen exchange with the lattice decreased markedly on exchanging Na^+ for Cu^{2+} cations (NaY , $E_{\text{exch}} = 45$ kcal/mol; Cu^{2+}Y , $E_{\text{exch}} = 23$ kcal/mol). Evidently, the oxygen bonding to the lattice is weakened in the presence of Cu^{2+} cations, as is seen from the X-ray results. Unfortunately, X-ray structural data on dehydrated NaY are not available

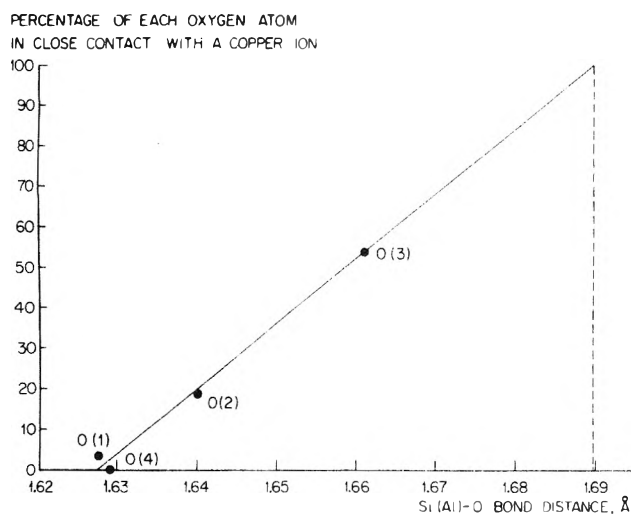


Figure 6. Plot of Si(Al)-O bond distance against the percentage of each oxygen atom in close contact with a copper ion in dehydrated divalent-copper-exchanged faujasite.

for comparison. However, it would seem that exchangeable cations, particularly those with a high polarizing power, can have a pronounced influence on the chemical bonding within the zeolite framework itself.

The present X-ray study cannot be directly compared with the powder diffraction studies of Gallezot et al.²⁰ since the copper-exchange levels and dehydration temperatures (150° present study, 500° Gallezot et al.²⁰) are different. Nevertheless, the distributions of Cu²⁺ cations over sites I and I' are surprisingly similar (site I, 1.5(2) puc, 3.2; site I', 11.4(2), 11.1(2)); for the present study and that by Gallezot et al.²⁰ respectively). This would seem to emphasize the strong preference of Cu²⁺ cations for site I'. By contrast, in dehydrated nickel(II)-exchanged faujasite (and zeolite Y) Ni²⁺ cations are preferentially located inside the hexagonal prisms at site I. This difference in site preference between two cations of such similar ionic radii ($r_{\text{Ni}^{2+}} = 0.72$, $r_{\text{Cu}^{2+}} = 0.69$ Å) would appear to be related to preferred coordination geometries (octahedral coordination for site I and trigonal coordination for site I') as determined by the different electronic properties of the cations.

Supplementary Material Available. Listings of observed

and calculated structure factor amplitudes (Tables II and III) will appear following these pages in the microfilm edition of this volume of the journal. Photocopies of the supplementary material from this paper only or microfiche (105 × 148 mm, 24× reduction, negatives) containing all of the supplementary material for the papers in this issue may be obtained from the Journals Department, American Chemical Society, 1155 16th St., N.W., Washington, D.C. 20036. Remit check or money order for \$4.00 for photocopy or \$2.50 for microfiche, referring to code number JPC-75-1874.

References and Notes

- (1) I. Mochida, S. Hayata, A. Kato, and T. Seiyama, *J. Catal.*, **15**, 314 (1969).
- (2) I. Mochida, S. Hayata, A. Kato, and T. Seiyama, *J. Catal.*, **23**, 31 (1971).
- (3) I. Mochida, T. Jitsumatsu, A. Kato, and T. Seiyama, *Bull. Chem. Soc. Jpn.*, **44**, 2595 (1971).
- (4) C. Naccache and Y. Ben Taarit, *J. Catal.*, **22**, 171 (1971).
- (5) S. Roginskii, O. V. Altshuler, O. M. Vinogradova, V. A. Seleznev, and I. L. Tsitovskaya, *Dokl. Akad. Nauk. SSSR*, **196**, 872 (1970).
- (6) G. K. Borekov, N. N. Bobrov, N. G. Maksimov, V. F. Anufrienko, K. G. Ione, and N. A. Shestakova, *Dokl. Akad. Nauk. SSSR*, **201**, 887 (1971).
- (7) I. Mochida, S. Hayata, A. Kato, and T. Seiyama, *Bull. Chem. Soc. Jpn.*, **44**, 2282 (1971).
- (8) O. V. Altshuler, I. L. Tsitovskaya, O. M. Vinogradova, and V. A. Seleznev, *Izv. Akad. Nauk. SSSR*, 2145 (1972).
- (9) K. Tsutsumi, S. Fujii, and H. Takahashi, *J. Catal.*, **24**, 146 (1972).
- (10) C. Dimitrov and H. F. Leach, *J. Catal.*, **14**, 336 (1969).
- (11) A. Nicula, D. Stamires, and J. Turkevich, *J. Chem. Phys.*, **42**, 3684 (1965).
- (12) J. T. Richardson, *J. Catal.*, **9**, 178 (1967).
- (13) H. B. Slot and J. L. Verbeek, *J. Catal.*, **12**, 216 (1968).
- (14) C. Naccache and Y. Ben Taarit, *Chem. Phys. Lett.*, **11**, 11 (1971).
- (15) J. Turkevich, Y. Ono, and J. Soria, *J. Catal.*, **25**, 44 (1972).
- (16) I. R. Leith and H. F. Leach, *Proc. R. Soc., Ser. A*, **330**, 247 (1972).
- (17) E. F. Vansant and J. H. Lunsford, *J. Phys. Chem.*, **76**, 2860 (1972).
- (18) C. Naccache, M. Che, and Y. Ben Taarit, *Chem. Phys. Lett.*, **13**, 109 (1972).
- (19) P. Gallezot, Y. Ben Taarit, and B. Imelik, *J. Catal.*, **26**, 255 (1972).
- (20) F. Wolf, D. Ceacareanu, and K. Pilchowski, *Z. Phys. Chem. (Leipzig)*, **252**, 50 (1973).
- (21) W. J. Mortier and H. J. Bosmans, *J. Phys. Chem.*, **75**, 3327 (1971).
- (22) W. H. Baur, *Am. Mineral.*, **49**, 697 (1964).
- (23) T. C. Furnas, "Single Crystal Orienter Instruction Manual", General Electric Company, Milwaukee, Wisc., 1957.
- (24) D. H. Olson, *J. Phys. Chem.*, **72**, 4366 (1968).
- (25) "International Tables for X-ray Crystallography", Vol. II, Kynoch Press, Birmingham, England, 1969.
- (26) See paragraph at end of text regarding supplementary material.
- (27) J. V. Smith, *Adv. Chem. Ser.*, No. 101, 171 (1971).
- (28) D. H. Olson and E. Dempsey, *J. Catal.*, **13**, 221 (1969).
- (29) G. V. Antoshin, Kh. M. Minachev, E. N. Sevastianov, D. A. Kondratjev, and C. Z. Newy, *Adv. Chem. Ser.*, No. 101, 514 (1971).
- (30) Because of partial occupancy of sites by Cu²⁺ ions and repulsive forces, simultaneous occupancy of Cu²⁺ ion sites shown in Figures 2-5 is not expected.

Polar Tensors and Effective Charges of Br₂CO

A. B. M. S. Bassi and Roy E. Bruns*

Instituto de Química, Universidade Estadual de Campinas, Campinas, SP, Brazil (Received February 24, 1975)

Publication costs assisted by Fundação de Amparo à Pesquisa do Estado de São Paulo

Polar tensors and effective charges of Br₂CO have been calculated and the recently reported sign ambiguity for the B₁ symmetry dipole moment derivatives has been confirmed. Small changes in the values of the dipole moment derivatives of Cl₂CS, due to a sign ambiguity in earlier treatments, are also reported. The effective charges of Br₂CO are compared with those calculated for other X₂CY (X = F, Cl; Y = O, S) molecules.

Recently, Prasad and Singh¹ have pointed out a sign ambiguity in the dipole moment derivatives of the B₁ symmetry species of Br₂CO.² Using the polar tensor formalism^{3,4} and the effective charges^{4,5} of the X₂CY molecules (X = F, Cl, Br; Y = O, S) we have been able to affirm the conclusions of Prasad and Singh for Br₂CO and to ascertain that a sign ambiguity also exists in the B₁ symmetry species of Cl₂CS.⁶ As the polar tensor and effective charge values of the X₂CY molecules⁷ are of interest in their own right the previously unreported values for Br₂CO are presented in this report.

The atomic polar tensor (for atom α) is composed of the derivatives of the molecular dipole moment with respect to the atomic cartesian coordinates

$$\mathbf{P}_x^{(\alpha)} = \begin{pmatrix} \partial p_x / \partial x_\alpha & \partial p_x / \partial y_\alpha & \partial p_x / \partial z_\alpha \\ \partial p_y / \partial x_\alpha & \partial p_y / \partial y_\alpha & \partial p_y / \partial z_\alpha \\ \partial p_z / \partial x_\alpha & \partial p_z / \partial y_\alpha & \partial p_z / \partial z_\alpha \end{pmatrix} \quad (1)$$

The polar tensor for the X₂CY molecules is defined as a juxtaposition of its atomic polar tensors

$$\mathbf{P}_x = (\mathbf{P}_x^{(C)} | \mathbf{P}_x^{(Y)} | \mathbf{P}_x^{(X_1)} | \mathbf{P}_x^{(X_2)}) \quad (2)$$

The values of \mathbf{P}_x are calculated directly using the matrix equation

$$\mathbf{P}_x = \mathbf{P}_Q \mathbf{L}^{-1} \mathbf{U} \mathbf{D} \mathbf{M}^{1/2} + \mathbf{P}_\rho \delta \mathbf{M}^{1/2} \quad (3)$$

The first term in eq 3 represents purely vibrational contributions to \mathbf{P}_x . The \mathbf{P}_Q matrix is of dimension $3(3N - 6)$ and contains values $\alpha_i^2 \partial p_m / \partial Q_i$ ($m = x, y, \text{ or } z; i = 1, 2, \dots, 3N - 6$) which are evaluated directly from the infrared intensities.⁴ The signs of the elements of the \mathbf{P}_Q matrix are those suggested on the basis of semiempirical CNDO molecular orbital investigations.⁸ The matrices \mathbf{L}^{-1} , \mathbf{U} , and $\mathbf{D} \mathbf{M}^{1/2} = \mathbf{B}$ are the standard coordinate transformation matrices involved in the evaluation of the force fields of molecules. The second term in eq 3 expresses the rotational contribution to \mathbf{P}_x and has been described previously.⁴ The values of \mathbf{P}_x are determined in part by the signs of the elements in \mathbf{P}_Q and \mathbf{P}_ρ (those of the latter matrix being specified by the sign of the equilibrium dipole moment). Previous analysis of infrared intensity data was hampered by the lack of an analytical expression which clearly indicates the effect of the different sign choices for the equilibrium moment and the $\partial p / \partial Q_i$ on the values of the dipole moment derivatives with respect to the symmetry coordinates, $\partial p / \partial S_j$.

A knowledge of the polar tensor values leads to a

straightforward determination of the effective charge values,⁴ ξ_α , of atom α

$$\xi_\alpha^2 = \text{TR}[\mathbf{P}_x^{(\alpha)} (\mathbf{P}_x^{(\alpha)})'] = (\partial p / \partial x_\alpha)^2 + (\partial p / \partial y_\alpha)^2 + (\partial p / \partial z_\alpha)^2 \quad (4)$$

Here, $\text{TR}[\mathbf{P}_x^{(\alpha)} (\mathbf{P}_x^{(\alpha)})']$ represents the trace of the matrix product of the atomic polar tensor with its transpose. The effective charges are of special interest as they can, in principle, be determined from the intensity sum of all the fundamental bands of a molecule

$$\sum_k A_k = N\pi/3c^2 \left\{ \sum_{\alpha=1}^N \xi_\alpha^2 / m_\alpha - \Omega \right\} \quad (5)$$

In this equation m_α represents the mass of atom α , Ω corresponds to a rotational correction which depends on the equilibrium dipole moment and the principal moments of inertia of the molecule, and A_k is the experimental infrared intensity of the k th fundamental band.

The polar tensor and effective charge values of the X₂CY molecules (X = F, Cl; Y = O, S) have been shown⁷ to be related by the empirical equations

$$\mathbf{P}_x^{(\alpha_1)}(\text{Cl}_2\text{CO}) - \mathbf{P}_x^{(\alpha_2)}(\text{F}_2\text{CO}) = \mathbf{P}_x^{(\alpha_3)}(\text{Cl}_2\text{CS}) - \mathbf{P}_x^{(\alpha_4)}(\text{F}_2\text{CS}) \quad (6)$$

and

$$\xi_{\alpha_1}(\text{Cl}_2\text{CO}) - \xi_{\alpha_2}(\text{F}_2\text{CO}) = \xi_{\alpha_3}(\text{Cl}_2\text{CS}) - \xi_{\alpha_4}(\text{F}_2\text{CS}) \quad (7)$$

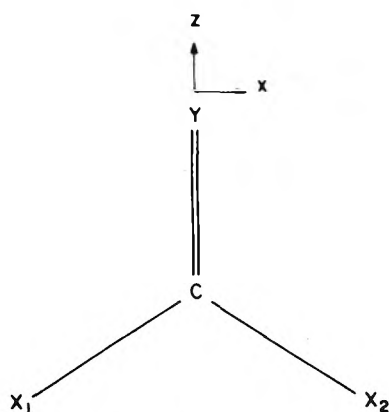
where $\alpha_1 = \alpha_3 = \text{Cl}$ and $\alpha_2 = \alpha_4 = \text{F}$, $\alpha_1 = \alpha_2 = \text{O}$ and $\alpha_3 = \alpha_4 = \text{S}$, or $\alpha_1 = \alpha_2 = \alpha_3 = \alpha_4 = \text{C}$. A knowledge of the atomic polar tensors and effective charges of Br₂CO leads to a prediction of the vibrational intensity parameters of Br₂CS through equations similar to (6) and (7) if they can be extended to the bromine substituents.

The polar tensor values for Br₂CO, corresponding to the preferred sign choice of Prasad and Singh¹ are presented in Table I. The atomic cartesian coordinates are defined in Figure 1. The sign ambiguity can be described as follows. As the two normal coordinates of B₁ symmetry, Q_4 and Q_5 , produce dipole moment changes in the x direction a reversal of the signs of $\partial p_x / \partial Q_4$ and $\partial p_x / \partial Q_5$ as well as a sign change for the equilibrium moment results in a change of all the signs for the first row elements of the atomic polar tensors. Elements contained in the other rows are not affected. This corresponds to a change in the $\partial p / \partial S_j$ values of the B₁ symmetry species. As the rotational contributions to \mathbf{P}_x in eq 3 are large for Br₂CO (up to 0.10 e) the values of

TABLE I: Polar Tensor of Br₂CO (e)^{a,b}

$P_Y^{(C)}$			$P_Y^{(O)}$			$P_Y^{(Br_1)^c}$		
1.58 ± 0.04	0.0	0.0	-0.83 ± 0.02	0.0	0.0	-0.37 ± 0.01	0.0	-0.36 ± 0.02
0.0	0.19 ± 0.01	0.0	0.0	-0.17 ± 0.02	0.0	0.0	0.04 ± 0.02	0.0
0.0	0.0	1.40 ± 0.10	0.0	0.0	-1.10 ± 0.03	-0.19 ± 0.04	0.0	-0.15 ± 0.03

^a The values of the polar tensor elements are multiples of the electronic charge, e . $1 \text{ D \AA}^{-1} = 0.2082 e = 3.335 \times 10^{-20} \text{ C}$. ^b The L^{-1} matrix used in the calculation of these polar tensors is from ref 2. The U matrix and cartesian coordinate system correspond to those of ref 8. The above polar tensors correspond to a sign choice of $\partial p/\partial Q_i > 0$ for $i = 3, 5$ and $\partial p/\partial Q_i < 0$ for $i = 1, 2, 4, 6$. In ref 8 $\partial p/\partial Q_4$ was chosen to be positive and $\partial p/\partial Q_5$ was given a negative sign. ^c The diagonal polar tensor elements for Br₂ (see Figure 1) are equal to those of Br₁. The off-diagonal elements of Br₂ have the same magnitudes but opposite signs to those of Br₁.

Figure 1. The cartesian coordinate system for the X₂CY molecules.

$\partial p/\partial S_j$ which are now preferred (corresponding to the $-+$ sign combination for $\partial p_x/\partial Q_4$ and $\partial p_x/\partial Q_5$, respectively) are markedly different from those chosen previously.⁸ As Prasad and Singh¹ have pointed out, the electronic distortions for the various vibrational displacements deduced from the recalculated values of the $\partial p/\partial S_j$ are more consistent with those found for F₂CO and Cl₂CO. All of the polar tensor elements in Table I with the exception of $\partial p_y/\partial y_{Br}$ have the same signs as their corresponding elements in the tensors for the latter molecules. This element has values of $-0.11, 0.00$ and $0.04 e$ for F, Cl, and Br, respectively. These values are expected to become more positive for the heavier atoms.

For Cl₂CS there is only a sign change in the rotational term of eq 3. As the experimental dipole moment (0.28 D) of Cl₂CS is larger than the recently measured value of 0.08 D⁹ for F₂CS the chlorine atoms appear to be situated at the positive end of the dipole ($^{+}Cl_2CS^{-}$). This sense of the moment has been predicted by CNDO calculations¹⁰ and was used in our calculation of the polar tensor of Cl₂CS.⁷ Table II gives the values of the $\partial p/\partial S_j$ of the B₁ symmetry species corresponding to this polar tensor along with the original values.⁶ Because the rotational contributions are small the differences in magnitudes are less than 0.04 e. The sense of the dipole moment of F₂CS is not of importance in the calculation of dipole moment derivatives, as the rotational contributions are smaller than the experimental errors arising in the vibrational analysis.

The effective charges of Br₂CO evaluated from eq 4 are compared with those for the other X₂CY molecules in Table III. The decrease in the carbon effective charge with substitution of Br for Cl is 0.42 e strikingly similar to the decreases in ξ_C on substitution of Cl for F (0.35, X₂CO; 0.41, X₂CS). The corresponding increases in ξ_O are 0.23 and 0.12 e. The value of ξ_{Br} (0.45 e) is about one-half of the

TABLE II: Recalculated Values of the $\partial p/\partial S_j$ for Cl₂CS (B₁ Symmetry) from the Experimental Intensities of Ref 6^a

Signs of $\partial p/\partial Q_4$ and $\partial p/\partial Q_5$	Ref 6 values		Recalculated values	
	$\partial p_x/\partial S_4$	$\partial p_x/\partial S_5$	$\partial p_x/\partial S_4$	$\partial p_x/\partial S_5$
++	-0.95	+0.08	-0.95	+0.15
-- ^b	+0.97	-0.14	+0.95	-0.10
+-	-1.05	-0.03	-1.07	+0.02
-+	+1.07	-0.03	+1.08	+0.04

^a Units of e. ^b Preferred set of signs for the $\partial p/\partial Q_i$. The (--) sign choice, $\partial p/\partial Q_4$ and $\partial p/\partial Q_5$ both negative, was also chosen previously in ref 10.

TABLE III: Experimental Effective Charges of F₂CO, F₂CS, Cl₂CO, Cl₂CS, and Br₂CO

X ₂ CY	ξ_C	ξ_Y	ξ_X
F ₂ CO	2.88 ± 0.06	1.04 ± 0.03	1.05 ± 0.02
Cl ₂ CO	2.53 ± 0.09	1.16 ± 0.04	0.86 ± 0.03
Br ₂ CO	2.11 ± 0.10	1.39 ± 0.04	0.45 ± 0.04
F ₂ CS	2.43 ± 0.06	0.65 ± 0.03	1.06 ± 0.03
Cl ₂ CS	2.02 ± 0.09	0.78 ± 0.04	0.87 ± 0.04
Br ₂ CS ^a	(1.66 ± 0.22)	(1.00 ± 0.10)	(0.46 ± 0.10)

^a Values of Br₂CS evaluated using an equation analogous to (7), and the effective charges of F₂CS and F₂CO. Effective charge values of Br₂CS using the values of Cl₂CS and Cl₂CO are very similar (1.60, 1.01, and 0.47 e).

value of ξ_{Cl} (0.86 e) in Cl₂CO. As the effective charges of F and Cl are both invariant to substitution of oxygen for sulfur we might tentatively predict a bromine effective charge for Br₂CS extremely close to the one found for Br₂CO. This is borne out by the estimation of the effective charges of Br₂CS, also listed in Table III, when Br₂CO and Br₂CS are substituted in eq 7 for Cl₂CO and Cl₂CS. The effective charge of carbon which is seen to decrease by 0.41 e upon substitution of Cl for F in the thionyl halides is calculated to decrease by a similar amount, 0.36 e, when Cl is replaced by Br.

These effective charge values of Br₂CO emphasize the previous observation⁷ that this parameter reflects the electronegativities of atoms in molecules. The effective charges of the halogens decrease as does their electronegativities for the heavier atoms. The oxygen effective charges increase and those of carbon decrease with substitution of the less electronegative halogens. It is worth noting that ξ_C in Cl₂CO and F₂CS have similar magnitudes as does this parameter in Br₂CO and Cl₂CS. A knowledge of the rela-

tionship between the effective charges and the electronegativities (or other atomic or bond properties) awaits the evaluation of more effective charge values for other molecules. Presently we are extending these calculations to aid our understanding of the effective charge parameter.

Acknowledgments. Financial support from the Fundação de Amparo à Pesquisa do Estado de São Paulo (FAPESP) and the Financiadora de Estudos e Projetos (FINEP) is gratefully appreciated.

References and Notes

- (1) P. L. Prasad and S. Singh, *Chem. Phys. Lett.*, **24**, 543 (1974).
- (2) M. J. Hopper, J. W. Russell, and J. Overend, *J. Chem. Phys.*, **48**, 3765 (1968).
- (3) J. F. Biarge, J. Herranz, and J. Morcillo, *An. R. Soc. Esp. Fis. Quim., Ser. A*, **57**, 81 (1961).
- (4) W. B. Person and J. H. Newton, *J. Chem. Phys.*, **61**, 1040 (1974).
- (5) W. T. King, G. B. Mast, and P. P. Blanchette, *J. Chem. Phys.*, **56**, 4440 (1972).
- (6) M. J. Hopper, J. W. Russell, and J. Overend, *Spectrochim. Acta, Part A*, **28**, 1215 (1972).
- (7) A. B. M. S. Bassi and R. E. Bruns, *J. Chem. Phys.*, **62**, 3235 (1975).
- (8) R. E. Bruns and R. K. Nair, *J. Chem. Phys.*, **58**, 1849 (1973).
- (9) A. J. Careless, H. W. Kroto, and B. M. Landsorg, *Chem. Phys.*, **1**, 371 (1973).
- (10) R. E. Bruns, *J. Chem. Phys.*, **58**, 1855 (1973).

Soret Coefficient of 1 N Lithium Iodide

Douglas R. Caldwell

School of Oceanography, Oregon State University, Corvallis, Oregon 97331 (Received January 6, 1975)

Publication costs assisted by the National Science Foundation

The thermal diffusion (Soret) coefficient of aqueous 1 N LiI solutions, measured by the thermohaline instability method at atmospheric pressure, is found to be negative at temperatures below 44° and appears likely to remain negative to the boiling point. A temperature gradient imposed on this solution creates large concentration gradients which are useful for studying convective effects in solutions. By observing the frequency of oscillation at the onset of convection, as well as the temperature gradient, a second estimate of the Soret coefficient is obtained. Excellent agreement between the two estimates is found.

Introduction

The thermal diffusion (Soret) coefficient, S_T , of a solution can be positive or negative. In a given solution, it may even change sign with temperature or pressure.¹ Concentration gradients caused by Soret fluxes can cause convective motions which affect various processes and measurements. Recently much work, both experimental²⁻¹¹ and theoretical,¹²⁻¹⁹ has been done on Soret-caused convection, but more interesting results could be obtained if solutions with larger induced density gradients were available, gradients which oppose those directly induced by the temperature field. Such mixtures as water-methanol,¹⁴ CCl₄-C₆H₁₂, and H₂O-C₂H₅OH⁷ have been used, but large density gradients in this sense cannot be obtained. An index of the separation is a "stability ratio", $\gamma \equiv S_T c(1-c)\beta'/\beta$, c being the mass fraction of solute, β the thermal expansion, and β' the solute expansion coefficient $\rho^{-1}(\partial\rho/\partial c)$. Here ρ is the density of the solution. Large negative values of γ are required so a large negative value of S_T in a solution with high concentration and low thermal expansion is desired.

In their investigation of a number of electrolytes in 0.01 M concentration, Snowden and Turner²⁰ found the largest negative value for S_T in LiI, $-1.44 \times 10^{-3} \text{ deg}^{-1}$, at 25.3°. Except for earlier, less accurate measurements,²¹ this is the only determination of S_T for LiI. Longworth²² showed that for concentrated KCl solutions, S_T increased (became more positive) with molality and temperature. For dilute

solutions of KCl, however, S_T decreases with concentration, while still increasing with temperature. Apparently then, if the behaviour of KCl is typical of electrolytes, S_T can be expected to become more positive as the temperature increases but in varying with concentration seems to have a minimum in the 0.1-1 M range.

Putting the above considerations together, S_T for 1 N solutions of LiI might well be negative, at least at low temperatures, even for large concentrations. Measurement of S_T could not proceed with the methods used in the studies mentioned above because of convective effects. Therefore the "thermohaline instability" method²³ was used, with an improvement in that two independent predictions of the theory were used to derive values of S_T , thus giving an estimate of systematic errors. The reader is referred to that previous paper²³ for an explanation of the method, a drawing of the apparatus, and definitions of some terms.

The only change in the apparatus was that a 0.15-cm diameter thermistor probe was positioned in the lower part of the fluid layer for observation of temperature oscillations. It projected into the layer from the side wall, the temperature-sensing bead being located about 3 cm from the wall and about 0.3 cm from the bottom boundary.

Procedure

As before,²³ the critical Rayleigh number, R_c , for onset of convection in a horizontal layer of the solution (now 1.12

TABLE I: Results

T , °C	ΔT_c , °C	R_c	$10^3 S_T(R_c)$, deg $^{-1}$	$\gamma(R_c)$	$Q^*(R_c)$, cal/mol	$1/\sigma_c$, sec	$10^3 S_T(\sigma_c)$, deg $^{-1}$	$\gamma(\sigma_c)$	$Q^*(\sigma_c)$, cal/mol
13.70	16.87	340,000	-0.310	1.10	-101				
17.52	1.04	27,000	-0.320	1.00	-108				
21.74	0.248	7,810	-0.306	0.84	-108	153	-0.291	0.80	-100
29.20	0.099	4,050	-0.269	0.62	-91	270	-0.248	0.57	-98
33.97	0.059	3,000	-0.218	0.47	-98				
43.65	0.040	2,800	-0.222	0.43	-88				

cm deep) heated from below was determined, by plotting the nondimensionalized temperature gradient, R , vs. the nondimensionalized heat flux, $R \times Nu$, R being the Rayleigh number and Nu the Nusselt number. Using the theory of Hurle and Jakeman,¹⁴ S_T was calculated from R_c . Their theory also predicts the frequency of oscillation of temperature in the fluid at the onset of convection, σ_c , and for several of the experiments this frequency was determined and used to calculate S_T as well. One advantage of using both σ_c and R_c is that the physical properties of the fluid enter in different ways, so errors in their assumed values will appear as deviations in calculated values of S_T . Also agreement between values of S_T calculated in the different ways increases our confidence in the applicability of the method.

Sources for values of physical constants used in the calculations were as follows: (1) ρ , β : ref 24; (2) viscosity: tests with a viscometer showed little difference between the LiI solution and distilled water, so pure water values were used; (3) thermal conductivity: in the absence of information, pure water values were used.

Results

At lower temperatures the concentration gradient due to Soret flux is so large that extremely large (thermal) Rayleigh numbers are attained without evidence of convection (Figure 1). A Rayleigh number of 335,000 was required in this case for convection to occur, 196 times the value required for convection in a pure fluid in the same apparatus. (For γ greater than about 1, convection cannot begin by this process at all.) R_c is taken as the highest Rayleigh number attained.

The initial convective motions are oscillatory, but the observation of these initial oscillations is difficult, because when the motions have grown sufficiently large, a finite-amplitude mode is triggered, which has a longer period not calculable from the linear theory. If oscillations can be recorded (Figure 2) before this triggering occurs, then the measured period does not vary with time and is the one predicted by the theory. Negative values of S_T and the corresponding heat of transport, Q , are indeed found in all experiments (Table I). The variation with temperature (Figure 3) is as expected, S_T becoming less negative as the temperature is increased. Extrapolating the points shown, risky because of the scatter and small range of observations, it seems that S_T might remain negative to the boiling point.

The parameter γ used by Hurle and Jakeman as defined above to indicate the relative contributions of solute and temperature variation to the density gradient in the steady state (Table I, Figure 3) varies much more than S_T with temperature because the thermal expansion varies so much in this range. At temperatures below 10° it is so large that

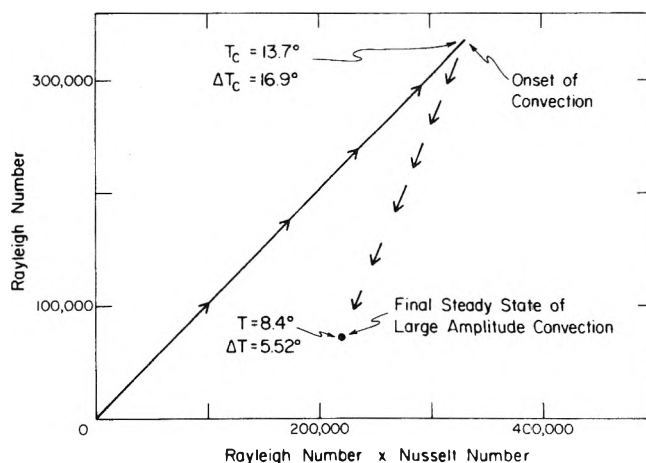


Figure 1. Nondimensional temperature difference, the Rayleigh number, vs. nondimensional heat flux, the Rayleigh number times the Nusselt number, for a 1.12 cm deep layer of 1 N LiI heated from below. The mean temperature, T_c , and the temperature difference at onset of convection, ΔT_c , are given. When the small oscillations in the fluid trigger a large-amplitude motion, the temperature difference drops to a much lower value. The mean temperature, T_m , also drops because the cooler upper plate is maintained at a constant temperature by the bath and the heat flux is held constant throughout. The Rayleigh number is defined as $g\beta\Delta Td^3/\nu\kappa$, where g is the acceleration of gravity, β the thermal expansion, ΔT the temperature difference across the layer of depth d , ν the kinematic viscosity, and κ the thermal diffusivity. The Nusselt number is the ratio of heat transported through the layer to that which would be transported by molecular effect alone in the absence of convection. The values at 13.7° are doubtful because γ varied so much within the fluid layer that the density gradient was stable in some parts of the layer and unstable in others.

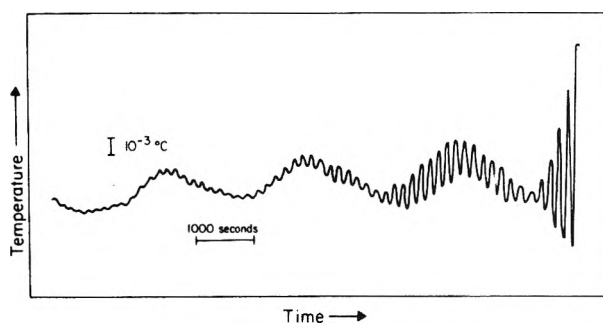


Figure 2. Temperature of the thermistor inserted in the fluid layer vs. time, after sudden change in heat flux from just below to just above critical. The mean temperature of the fluid was 21.74°; the temperature difference across the layer, 0.248°. The oscillations used in the calculation are the shorter ones. The cause of the longer oscillations is unknown.

the solution is stable against convective disturbances for any value of the Rayleigh number. The molar heat of transport was calculated following Agar and Turner.²¹ The

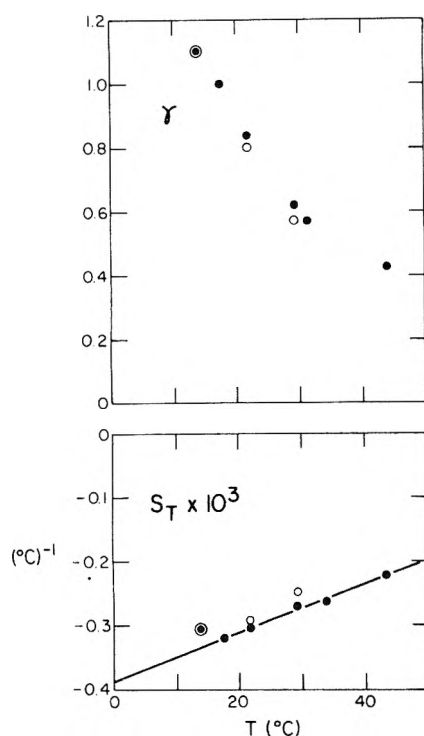


Figure 3. Soret coefficient, S_T , and stability parameter, γ , vs. mean temperature T . Symbols: ●, value calculated from the critical Rayleigh number; ○, value calculated from period of thermal oscillation at onset of convection.

values are much lower than those observed in dilute solutions.²⁰

The values of S_T calculated from σ_c (Figure 3) are just a bit less negative than the ones derived from R_c . The average discrepancy is less than 6%.

If the point at 13.7° is ignored, as it might well be because the temperature difference in this case is so great that the density gradient varies from stable to unstable

with vertical position in the fluid, then the values calculated from R_c can be fit by the formula

$$S_T = 10^{-3}(-0.391 (\pm 0.029) + 0.0042 (\pm 0.0004)T) \text{ deg}^{-1}$$

with a least-squares error of 0.020, T being the temperature in degrees Celsius. The numbers in parentheses are the estimated errors of the fit. Extrapolating to higher temperatures, S_T does not become positive until $T = 104^\circ$.

Acknowledgments. Financial support was provided by the Physical Oceanography Section of the National Science Foundation under Grants GA23336 and DES74-17968.

References and Notes

- (1) D. R. Caldwell, *Deep-Sea Res. Oceanogr. Abstr.*, **21**, 369-376 (1974).
- (2) D. T. J. Hurle, *Philos. Mag.*, **13**, 305-310 (1966).
- (3) J. C. Legros, W. A. Van Hook, and G. Thomaes, *Chem. Phys. Lett.*, **1**, 696-701 (1968).
- (4) J. C. Legros, W. A. Van Hook, and G. Thomaes, *Chem. Phys. Lett.*, **2**, 249-251 (1968).
- (5) J. C. Legros, W. A. Van Hook, and G. Thomaes, *Chem. Phys. Lett.*, **2**, 251-252 (1968).
- (6) E. J. Harp and D. T. J. Hurle, *Philos. Mag.*, **17**, 1033-1038 (1968).
- (7) J. C. Legros, D. Rasse, and G. Thomaes, *Chem. Phys. Lett.*, **4**, 632-634 (1970).
- (8) D. R. Caldwell, *J. Fluid Mech.*, **42**, 161-175 (1970).
- (9) J. K. Platten and G. Chavepayer, *Phys. Lett. A*, **40**, 287-288 (1972).
- (10) D. T. J. Hurle and E. Jakeman, *Phys. Lett. A*, **43**, 127-129 (1973).
- (11) D. R. Caldwell, *J. Fluid Mech.*, **64**, 347-367 (1974).
- (12) D. T. J. Hurle and E. Jakeman, *Phys. Fluids*, **12**, 2704-2705 (1969).
- (13) M. G. Velarde and R. S. Schecter, *Chem. Phys. Lett.*, **12**, 312-315 (1971).
- (14) D. T. J. Hurle and E. Jakeman, *J. Fluid Mech.*, **47**, 667-687 (1971).
- (15) R. S. Schecter, I. Prigogine, and J. R. Hamm, *Phys. Fluids*, **15**, 379-386 (1972).
- (16) J. C. Legros, J. K. Platten, and P. G. Poty, *Phys. Fluids*, **15**, 1383-1390 (1972).
- (17) J. K. Platten and G. Chavepayer, *Phys. Fluids*, **15**, 1555-1557 (1972).
- (18) M. G. Velarde and R. S. Schecter, *Phys. Fluids*, **15**, 1707-1714 (1972).
- (19) J. C. Legros, P. Poty, and G. Thomaes, *Physica (Utrecht)*, **64**, 481-496 (1973).
- (20) P. N. Snowden and J. C. R. Turner, *Trans. Faraday Soc.*, **56**, 1409-1418 (1960).
- (21) J. N. Agar and J. C. R. Turner, *Proc. R. Soc. London, Ser. A*, **255**, 307-330 (1960).
- (22) L. G. Longworth, *J. Phys. Chem.*, **61**, 1557-1562 (1957).
- (23) D. R. Caldwell, *J. Phys. Chem.*, **77**, 2004-2008 (1973).
- (24) "International Critical Tables", McGraw-Hill, New York, N.Y.

Pressure Dependence of Thermal and Fickian Diffusion in 0.1 N Sodium Chloride

Douglas R. Caldwell

School of Oceanography, Oregon State University, Corvallis, Oregon 97331 (Received January 23, 1975)

Publication costs assisted by the National Science Foundation

A nonlinear dependence of the Soret coefficient on pressure in a 0.1 N NaCl solution at 17.65° is found in conductance cell experiments. The pressure dependence of the isothermal solute diffusivity at 11.24° in the same solution is not large enough to be measurable within the limits of the procedures used. It is 50% probable that the pressure coefficient of the solute diffusivity lies between +1.0 and -1.8%/kbar.

Introduction

In the past few years, sharp thermal gradients have been found in the oceans at various depths which indicate the presence of layers of sea water in which heat and salt may be transported by molecular diffusion, rather than turbulent diffusion.¹ Laboratory experiments in solutions have shown that layering is inherent in the process of thermal convection, and again diffusive interfaces are found.² For the first time, the molecular transport properties of salt solutions were seen to be significant to the study of the ocean, and work was undertaken to measure them. Thermal and Fickian diffusion coefficients were measured in NaCl solutions as the beginning of a program of defining these quantities in the complicated solution that is sea water.^{3,4} In these studies, the pressure dependence is quite important because of the high pressures found in the ocean depths.

To the resolution of these first experiments the pressure dependence of the thermal diffusion (Soret) coefficient was taken to be linear and the Fickian diffusivity was taken to be independent of pressure. To see if nonlinearity in the pressure dependence of S_T and a nonzero pressure dependence of D were masked by the restricted pressure range and the scatter in the above-mentioned measurements, further, more careful experiments were undertaken, with the pressure range extended to 0.96 kbar.

Sodium chloride was chosen as the solution to study because of the fact that its properties, especially electrical conductivity, are fairly well-known and because of its importance in ocean waters. A somewhat lower concentration was used than before in order to decrease the effect of polarization impedances at the electrodes. The chosen value of the mean temperature, T_m , of 17.65°, with a temperature difference, ΔT , across the cell of 8.9°, gives the highest pressure derivative of S_T for which S_T remains negative throughout the cell at all pressures. At lower temperatures positive Soret diffusion would cause convection in the sample. A smaller value of ΔT could not be used because of the limitation in precision of the conductivity measurement,¹⁰⁻⁶

A total of 114 measurements of S_T and D were made, over 1 year, each measurement consuming 2 days. Long waits of weeks were required for the polarization layers to reach equilibrium after pressure changes. Several experimental difficulties were encountered, including the leveling of the cell in its position inside the pressure bomb, the time required for thermal gradients to come to equilibrium, and the changes in the polarization layers at the electrodes with pressure.

Apparatus and Procedures

No significant changes were made in the cell, pressure system, bath, or electrical system since their previous descriptions in the literature,^{3,4} so only a brief description is given here. The cell itself, operating on the conductivity ratio principle, is patterned after that used by Snowdon and Turner,⁵ with some improvements and a modernized electronic system which allows more precise measurement of the ratio with less heat dissipated in the sample, even with samples of relatively high conductivity.

The sample is contained in a cylindrical cavity 1.27 cm high and 1.27 cm in diameter and is confined between horizontal-plate platinized-platinum electrodes (Figure 1). A part of the sample in horizontal hole drilled in the confining acrylic material constitutes an electrical tap located approximately at the vertical halfway point. The turns ratio of a variable autotransformer completing an ac bridge with the cell, when adjusted for null with a phase-sensitive detector, gives a measure of the ratio of electrical conductance across the bottom half of the sample to that across the whole.

When a vertical temperature gradient is imposed, from above, the movement of solute downward can be tracked with the turns ratio, X . When the heat is first applied, the conductance ratio change is caused mainly by the change of conductivity with temperature. After thermal equilibrium is reached, further changes in X are caused by solute movement. From this latter change S_T can be calculated, with correction for the initial period of temperature change. The time required for the salt to complete its migration can be used to calculate D .^{4,5}

In practice, more consistent results are obtained by making the measurements after the heat is turned off and extrapolating backward to obtain the concentration variation accompanying a temperature gradient, this gradient having been applied long enough for diffusive equilibrium to be reached. The mean temperature is taken to be the average of the temperatures at the end plates, 17.65°, for the S_T measurement. (The value of D obtained by this procedure is the *isothermal* diffusion coefficient, at the bath temperature, 11.24°.) The temperature gradient in these experiments decayed with an e-folding time of about 8 min. The total change in X caused by temperature change was 0.027, so it takes 82 min for the temperature effect on X to be reduced to the 10^{-6} level, the degree of precision in X . Therefore, the first measurement of X used in calculations was taken 100 min after the heat was turned off. The e-folding time for solute motion was about 300 min, so plenty of time

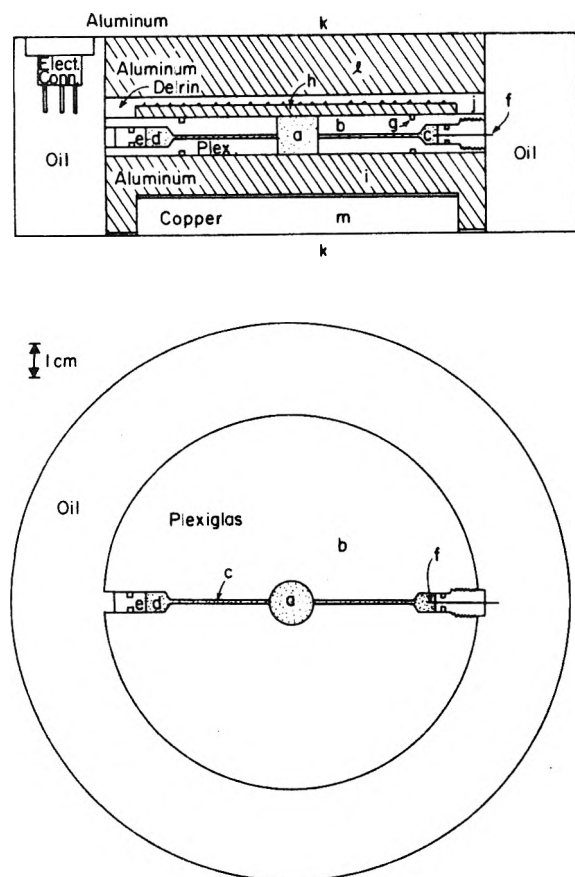


Figure 1. The diffusion cell. Top: The measured diffusion takes place in the solution contained in the cylindrical space (a) in the Plexiglas plate (b). The filling hole (c), 0.08-cm diameter, leads from the diffusion area to a cylinder (d) and piston (e) which allow for compression and expansion. Diametrically opposite is a smaller hole leading to a platinum wire (f). Platinum sheets (0.012 cm thick) extend past the O rings (g) at the top and bottom of plate (b). The platinum sheets are insulated by thin (0.012-in.) Mylar sheets from the top aluminum plate (h) and the bottom aluminum plate (i). Plate (h) is heated by Evanohm wire pressed into spiral grooves in the Delrin insulator (j). Thermal contact with the inside surfaces of the pressure bomb (k) is provided by aluminum plates (i) and (l). The device is hung from the bomb lid by screws, so thermal contact with the bottom of the bomb is made certain by a copper plate (m) which is free to slide relative to plate (i). The space at the sides of the device is used for electrical connectors (not shown) mounted on the bomb lid. Transformer oil is used as the hydraulic fluid. Bottom: Plan view of plate (b).

remained to follow the changes in X caused by solute migration.

The heat was turned off first thing in the morning and periodic readings were made all day with a final one the following morning. Then the heat was turned on again; since 99% of the solute motion took place in 24 hr, another run could be made the next day.

Snowdon and Turner⁵ avoided the initial period of thermal change by turning the heat on with their cell upside-down, letting convection mix the solution while thermal equilibrium was being reached, and then inverting it suddenly and monitoring the establishment of the solute gradient after convection had died out, only a few minutes. The wait was then only for the thermal profile within the sample, rather than throughout the apparatus, to come to equilibrium. Our apparatus weighs over 100 kg and works well only in a water bath, so inverting it was not seriously considered.

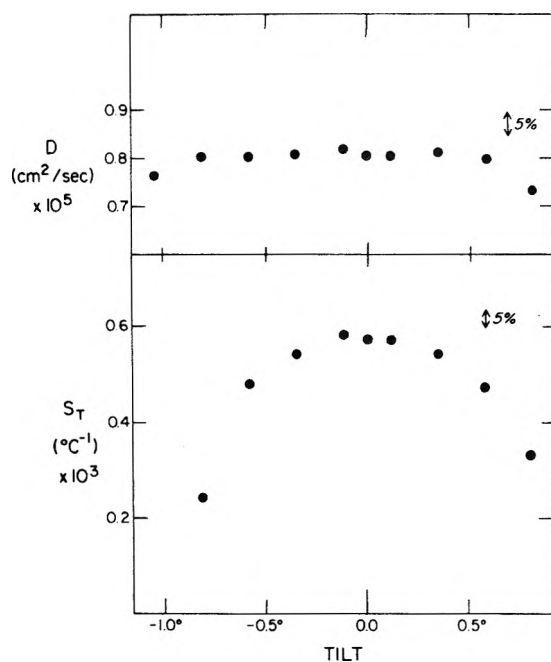


Figure 2. Soret coefficient, S_T , and solute diffusivity, D , vs. tilt of cell in a 0.1 N NaCl solution at 5.2° mean temperature and 0.538-kbar pressure. The cell had already been "leveled" in the orthogonal direction. The zero for the tilt axis on this plot represents the initial guess.

Characteristic of this type of cell is its sensitivity to leveling.⁶ This presented a particular difficulty with the pressure system because of the difficulty in "carrying" a level from the cell surfaces to some surface external to the bomb where a level could be placed. The best procedure was found to be "letting the apparatus level itself", that is, making experimental runs with various settings of the leveling screws on the base of the bath to find the setting for which the highest value of S_T was obtained (Figure 2). This is assumed to be the level setting; deviations are assumed to cause convection which reduces the apparent value of S_T . Great deviations from the optimum position are required to affect the measurement of D . This procedure was carried out at several pressures, but no significant difference was found in the "level" position; apparently pressurization does not affect the leveling of the cell.

The only experimental parameter of concern is X . It is limited in precision to 10^{-6} because of the electrical noise level in our laboratory even though a lock-in system is used for signal detection. A change in conductance of this amount corresponds to a temperature variation across the cell of less than 10^{-4} °, the reason a great deal of work went into building a temperature bath which regulates to this precision. The thermal shielding of the pressure bomb also helps keep out stray gradients.

Three readings were used in the calculations, taken at 100 min, at approximately 600 min, and at about 1400 min. The ratio of these times to the e-folding time is 0.33, 2.0, and 4.67. Relative values of the change in X due to concentration, in terms of the initial concentration are 0.720, 0.135, and 0.009. An error of 10^{-6} in the 600-min time causes an error of approximately 1.2% in D , errors in the other readings being less significant. An error of 10^{-6} in the 1400-min reading caused the major error in S_T , about 2%. Other readings confirmed the exponential character of the decay of the concentration gradient.

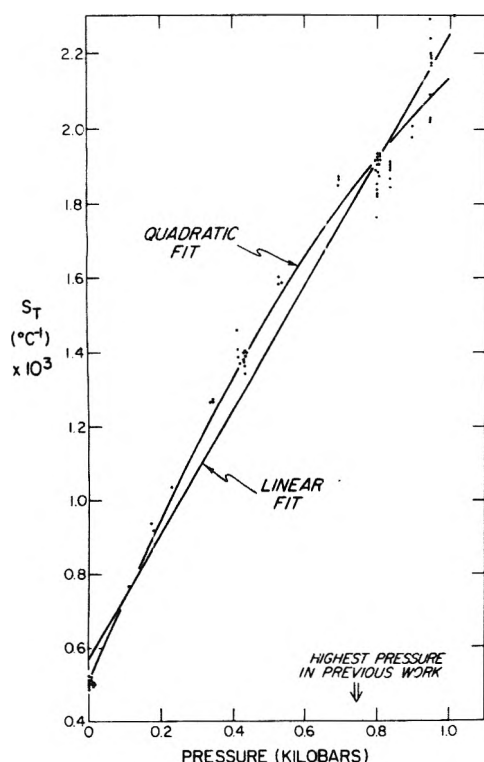


Figure 3. Measured values of S_T vs. pressure in 0.1 N NaCl at 17.65° mean temperature.

Pressure Dependence of the Soret Coefficient

For an assessment of the linearity of the pressure dependence of S_T at 17.65° 81 data points were used (Figure 3). All runs in which the cell was tilted more than 20 min of arc relative to the "level" position were rejected. Linear and quadratic least-squares fits were made, with the results (S_T in deg^{-1} , P in kilobars)

$$S_T(P) = 10^{-3}(0.568 + 1.682P) \quad \sigma = 0.0857$$

$$S_T(P) = 10^{-3}(0.512 + 2.313P - 0.686P^2) \quad \sigma = 0.0645$$

The F value calculated from the values of σ , the standard deviations of the errors, is 64, significant beyond doubt; the probability of exceeding $F = 12$ for this many degrees of freedom is 0.001 for purely statistical variations. It is quite possible that there is some physical reason for a change in behavior at about 0.75 kbar and that one continuous curve is not appropriate. More data, particularly at higher pressures, would be required to make a meaningful assessment of this possibility. Thus, the dependence of S_T on pressure is not linear. This nonlinearity did not show up in the previously reported experiments because of their lesser pressure range.

Pressure Dependence of Diffusivity

In previous experiments³ we were unable to define the pressure dependence of D , more than to say that $\partial D/\partial P$ lies between $+4 \times 10^{-7}$ and $+38 \times 10^{-7} \text{ cm}^2 \text{ sec}^{-1} \text{ kbar}^{-1}$, in 0.5 N NaCl. This conclusion resulted from an analysis of 51 measurements at a wide range of temperatures. In the experiments presently described, 104 measurements taken over a larger pressure range (Figure 4) at 11.24°, do not show any obvious positive pressure coefficient. (The temperature appropriate to the diffusivity measurement is 11.24°, the temperature of the isothermal cell with no heat flux imposed.)

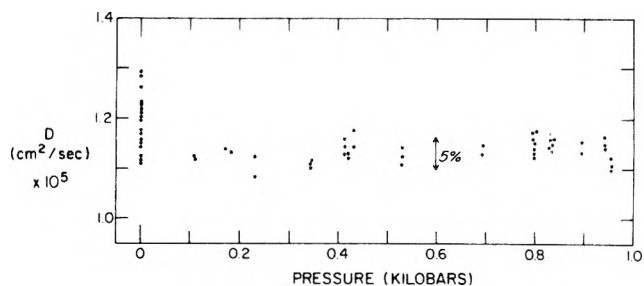


Figure 4. Measured values of D vs. pressure in 0.1 N NaCl at 11.24°.

TABLE I: Statistics of Salt Diffusivity Data

Pressure range	Sample size	Std dev	Skewness	Kurtosis	Mean	Std error in mean
Atm only	17	0.057	0.15	2.00	1.1949	0.0138
>Atm and <0.6 kbar	31	0.024	0.43	2.59	1.1435	0.0044
>0.6 kbar	55	0.018	-0.14	2.75	1.1415	0.0024

For analysis the data were divided into three classes by pressure (Table I). At atmospheric pressure the data show a different character than at higher pressures. The mean is larger by more than 3 times its standard error and the standard deviation is 2.4 times larger than that of either of the other two classes. These discrepancies might be caused by air bubbles in the cell, which are very difficult to eliminate even though the sample is loaded into the cell under vacuum. The error in X caused by a bubble moving vertically from one half of the cell to the other is approximately given by 4 times the ratio of the bubble volume to the cell volume. Thus an error greater than 10^{-5} in X is caused by such a movement of a 0.02-cm diameter bubble. This change in X could cause a 10% error in D , larger than the scatter observed at atmospheric pressure. At the lowest pressure above atmospheric, 0.11 kbar, the volume of a bubble would be reduced by a factor of 100, so its effect would be lessened by that factor and would be insignificant.

If the atmospheric pressure data are ignored and the remaining two classes, above and below 0.6 kbar, considered, no significant difference is seen (Table I). These two sets are quite similar, their means differing by less than the standard error in either mean. So no significant trend with pressure has been found.

If the assumption is made that the pressure dependence is linear, further analysis of these data reveals that there is a 50% probability that $D^{-1}(\partial D/\partial P)$ lies between $-1.8\%/kbar$ and $+1.0\%/kbar$. The viscosity of electrolytic solutions displays a complicated behavior with pressure, first decreasing as pressure is raised and then increasing again. To see if any such behavior could be present in D , a quadratic function was fitted by the method of least squares to all data for pressure above atmospheric. The standard deviation of deviations of the data relative to this function was 0.02016, which must be compared to a standard deviation of the data itself, relative to its mean, of 0.02018. The F test shows the difference to be insignificant.

Thus it must be concluded that no variation with pressure is shown by these data. To search for the variation, either the experimental precision must be improved, to be substantially better than 1%, or a much greater range in pressure must be available, several kilobars at least.

Acknowledgments. Financial support was provided by the Physical Oceanography Section of the National Science Foundation under Grants GA23336 and DES74-17968.

References and Notes

- (1) C. S. Cox, *EOS, Trans. Am. Geophys. Union*, **52**, 236-238 (1971).
- (2) J. S. Turner, "Buoyancy Effects in Fluids", Cambridge University Press, New York, N.Y., 1973.
- (3) D. R. Caldwell, *Deep-Sea Res. Oceanogr. Abstr.*, **21**, 369 (1974).
- (4) D. R. Caldwell, *Deep-Sea Res. Oceanogr. Abstr.*, **20**, 1029 (1973).
- (5) P. N. Snowdon and J. C. R. Turner, *Trans. Faraday Soc.*, **56**, 1409 (1960).
- (6) J. N. Agar and J. C. R. Turner, *Proc. R. Soc. London, Ser. A*, **255**, 307 (1960).

A Relationship between Hydroxyl Proton Chemical Shifts and Torsional Frequencies in Some Ortho-Substituted Phenol Derivatives

Ted Schaefer

Department of Chemistry, University of Manitoba, Winnipeg, Canada R3T 2N2 (Received March 11, 1975)

Publication costs assisted by the National Research Council of Canada

A linear correlation between the chemical shift of the hydroxyl proton and the torsional frequency of the hydroxyl group for some ortho-substituted phenol derivatives in solution implies that a shift of 1 ppm is correlated with a change of 60 cm^{-1} in the torsion frequency. The correlation is discussed in terms of the factors thought to influence the chemical shift and doubts are raised concerning some of the current interpretations. The main factor determining the chemical shift and the torsional frequency changes in these molecules appears to be the strength of the intramolecular hydrogen bond. Tentative equations relating these changes to the hydrogen bond energy are suggested.

Introduction

The chemical shift of the proton magnetic resonance of the hydroxyl proton in phenol has not been calculated from first principles. However, if the shift in an inert solvent is taken as a reference value, the changes caused by substituents on the benzene ring or by intermolecular perturbations can be at least qualitatively predicted in terms of the following concepts. The reaction field of the solvent^{1,2} induces upfield or downfield shifts, depending on the orientation of the molecular dipole with respect to the O-H bond axis. Inter- and intramolecular hydrogen bond formation causes a deshielding of as much as 5 ppm, depending on the distance between the proton and the lone pairs of the acceptor³⁻⁶ and on the magnetic anisotropy^{7,8} of the acceptor moiety. Electron density changes in the 1s orbital of the hydrogen atom in the O-H bond, induced by a polarization of the O-H bond by the electric dipoles of the substituents¹ or by alterations in the π electron densities at the contiguous carbon atom or oxygen atom,⁹⁻¹¹ cause a proportional change in the chemical shift. Severe steric crowding can lead to a deshielding via a distortion of the electron distribution near the proton by the strong, time-dependent electric fields of the proximate bonds;^{12,13} or lead to an increase in shielding as the hydroxyl group is forced out of the ring plane,¹⁴ thereby removing the proton from the deshielding region of the magnetically anisotropic benzene ring. Furthermore, the magnetic anisotropy of the substitu-

ents can in principle alter the proton chemical shift according to the size of certain geometric factors.

Clearly, in a given phenol derivative it may be difficult or impossible to disentangle the various shielding parameters, particularly for polysubstitution and for measurement in solution. A correlation of the chemical shift with another molecular parameter can be of use in predicting either of these parameters in a new compound and, in favorable cases, may eliminate some of the possible contributions to the observed shift parameter. A very rough correlation between the phenolic proton chemical shift, δ_{OH} , and the O-H stretching frequency has been noted for some phenol derivatives.^{15,16} Similar rough correlations between gas-to-solution chemical shifts and stretching frequencies are known³ for other molecules, presumably reflecting the strength of the intermolecular interactions.

The torsional frequency, ω_t , of the hydroxyl group rotor in phenol is directly related to the barrier to rotation about the C₁-O bond,^{17,18} depending on the reduced moment of inertia about the bond. Para substituents which decrease the conjugation of the oxygen atom with the π system of the ring i.e., increase the π electron density at C₁, lower the barrier and hence ω_t . It is suggested¹⁹ that in polysubstituted phenols ω_t is a direct measure of the π electron density at the carbon atom.

It is the purpose of this article to point out a linear relationship between ω_t and δ_{OH} for some classes of phenol derivatives and to indicate the possible uses of it. Only those

TABLE I: Hydroxyl Proton Chemical Shifts and Torsional Frequencies in Phenol Derivatives

Phenol	ω_t , cm^{-1}	δ_{OH} , ppm ^a	Ref	Phenol	ω_t , cm^{-1}	δ_{OH} , ppm ^a
1. phenol	310	4.29	24, 25	13. 2,4,6-tri-Br	393	5.69
2. 2-CHO	713 ^b	10.98	26	14. 2-F-4,6-di-Br		5.28
3. 2-NO ₂	675	10.54 ^c	4	15. 2-F-4,6-di-Cl		5.24
4. 2-F-6-NO ₂	676	10.45		16. 2-F-4,6-di-I		5.30
5. 2-NO ₂ -5-F		9.81		17. 2-Br-4,6-di-Cl	393	5.65
6. 2-NO ₂ -3-F		10.44		18. 2-I-4,6-di-Cl		5.82
7. 2-CHO-6-OCH ₃		10.78 ^c	27	19. 2-I-4,6-di-Br		5.72
8. 2- <i>i</i> -Pr	301	4.32	28	20. 4-Br-2,6-di-Cl	396	5.65
9. 2- <i>t</i> -Bu	307	4.48	28	21. 2,3,5,6-tetra-F	348	5.16
10. 2-CH ₃ -6- <i>t</i> -Bu	297	4.50	28	22. 2-CHO-4,6-di-Cl		11.25
11. 2,6-di- <i>t</i> -Bu	286 ^d	4.97	28	23. 2-CF ₃ -4,6-di-Br		5.83
	245					
12. 2,4,6-tri-Cl	393	5.60 ^c	4			

^a Relative to internal tetramethylsilane in CCl₄ solutions at concentrations less than 5 mol %. ^b In CS₂ solution, values from ref 19. ^c Converted to TMS reference from C₆H₁₂ by adding 1.40 ppm. ^d Fermi resonance pairs.

phenols are considered for which intermolecular hydrogen bonding or exchange with impurities are unlikely or for which the shift has been extrapolated to infinite solution in CCl₄.

Experimental Section

Phenol derivatives were obtained commercially or were synthesized by standard methods. Measurements of the chemical shift of the hydroxyl proton relative to internal tetramethylsilane were made at 100 MHz on 0.5–4 mol % solutions in CCl₄ at 32°, most of the available shifts in the literature having been measured in this solvent. The ω_t values from ref 19 were made in C₆H₁₂ solutions at concentrations lower than 0.06 M but our NMR instrumentation made the measurements at such concentrations very difficult because many of the hydroxyl proton peaks were multiplets arising from long-range spin-spin coupling to ring protons or ¹⁹F nuclei, thereby reducing the signal-to-noise ratios. On the other hand, the presence of the couplings proved the absence of intermolecular proton exchange with water or other impurities in solution and, in the presence of two ortho substituents, implies the absence of intermolecular contributions to the chemical shift other than the general reaction field effects. That these effects are present is indicated by the low-field shifts of about 0.1 ppm in CCl₄ relative to C₆H₁₂ solutions observed for some of the phenols and expected on the basis of the higher dielectric constant of CCl₄.

Results and Discussion

In Table I the proton chemical shifts, δ_{OH} , are entered together with torsional frequencies,¹⁹ ω_t . In Figure 1, δ_{OH} values are plotted vs. ω_t . In Figure 1 the slope of the line is such that 1 ppm is equivalent to 60 cm⁻¹. The linearity indicates that, if ω_t is a measure of the substituent effect on the π electron density, ρ , in the ring¹⁹ in the polysubstituted benzenes, the δ_{OH} is also a measure of ρ . Yet, of the factors discussed above as determinants of δ_{OH} , only some are expected to display a linear dependence on ρ .

The relatively large downfield shifts of about 5 ppm caused by NO₂ and CHO groups can arise from their large magnetic anisotropies⁷ and/or the intense electric fields¹⁶ arising from these substituents. The latter two quantities are usually accepted as at least partial causes of the down-

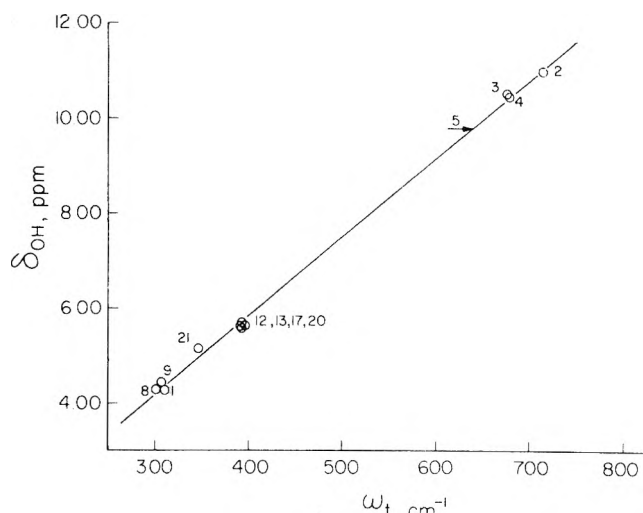


Figure 1. The hydroxyl proton chemical shifts of some phenol derivatives, numbered as in Table I, are plotted vs. the torsional frequencies, ω_t . The arrow indicates a predicted value of ω_t .

field shifts because otherwise an approximate application²⁰ of the Lamb shielding formula indicates a loss of as much as 0.3 electrons from the hydrogen 1s orbital.

The magnetic anisotropy of the CHO or NO₂ groups cannot change ω_t . The correlation in Figure 1 indicates that the magnetic anisotropy of the two groups is perhaps a minor contributor to the chemical shift. A similar argument is then indicated for other phenol derivatives in Table I. Now, the magnetic anisotropy of the carbonyl group, as derived from chemical shift data,²¹ is not small; again emphasizing the vexed question²² of how to calculate the magnetic anisotropy contributions to proton chemical shifts.

However, another possible contribution³ to the chemical shift produced by the hydrogen bonding is the quenching of the neighboring-atom magnetic anisotropy. The present correlation may constitute evidence for such quenching.

Energy of the Intramolecular Hydrogen Bond

In that event the major contributors to the chemical shifts in Table I are the strong electric fields produced by the ortho substituents at the site of the OH bond. These

fields deform the electron distribution about the proton and decrease the proton shielding. Rather involved but approximate calculations¹⁶ of electric field effects on the chemical shift of the hydroxyl proton in intermolecularly hydrogen bonded phenol predict a very nearly linear relationship between the chemical shift and the energy of the hydrogen bond. It can be written as

$$\Delta\delta = -0.4 \pm 0.2 + E \quad (1)$$

where $\Delta\delta$ is given in parts per million relative to phenol and E in kilocalories/mole. It is uncertain whether this equation is correct for intramolecular bonds, but it may allow an estimate of their energy. If so, the correlation in Figure 1 implies (1 ppm being equivalent to 60 cm^{-1})

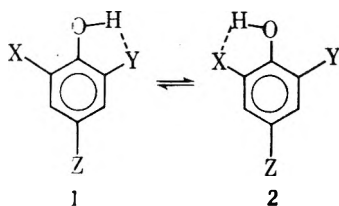
$$0.017\Delta\omega_t = -0.4 \pm 0.2 + E \quad (2)$$

where $\Delta\omega_t$ is in $(\text{centimeter})^{-1}$ relative to phenol.

As a check on eq 2 the value of ω_t in the hydrogen bonded form of *o*-fluorophenol,¹⁹ 366 cm^{-1} , yields 1.35 ± 0.2 kcal/mol for the energy of the hydrogen bond, compared to -1.44 ± 0.12 kcal/mol found for the enthalpy of formation from a full analysis of the far-infrared spectrum.¹⁹ The agreement is encouraging.

The energy of the intramolecular bonds in chelated phenols such as compounds 2, 3, and 4 in Table I have never been directly determined.²³ Equations 1 and 2 predict the hydrogen bond energy of compound 2 as 7.2 ± 0.2 kcal/mol.

The ortho-disubstituted halophenols in Table I are predicted to have hydrogen bond energies of less than 2 kcal/mol. Only one chemical shift is measured for each compound because rapid conversion from 1 to 2 occurs. Appar-



ently only one ω_t value is available for compounds 13, 17, 20, and 21 and the predicted energies must therefore be considered as mean values for 1 and 2. Nevertheless, the predicted energies are reasonable in view of the enthalpies found for the ortho halophenols,¹⁹ all less than 2 kcal/mol.

It is very probable, therefore, that for ortho-substituted phenols both δ_{OH} and ω_t are mainly a measure of the strength of the intramolecular hydrogen bond. However, when the ortho substituents are not hydrogen bond acceptors, eq 1 and 2 will not apply. For example, strong intramolecular repulsive interactions¹² will deshield the hydroxyl proton and are probably the cause of the deviation of δ_{OH} by about 1.5 ppm to low field of the correlation line in

Figure 1 for 2,6-di-*tert*-butylphenol (compound 11). These deviations become smaller as the size of the ortho alkyl substituents decreases (compounds 8, 9, and 10 in Table I).

Practical Considerations

δ_{OH} can be severely altered by intermolecular proton exchange with impurities in solute or solvent or by intermolecular association and, in studies of intramolecular hydrogen bond formation in mono-ortho-substituted phenols, e.g., the correlation may serve as a check that the observed shift does not contain unwanted contributions. Alternatively, the observed shift may allow an assignment of the torsional band in the sometimes very complex far-infrared spectrum.

Acknowledgments. I am grateful to Dr. J. B. Rowbotham for help with the measurements and to a referee for most helpful comments. This work was supported by the National Research Council of Canada.

References and Notes

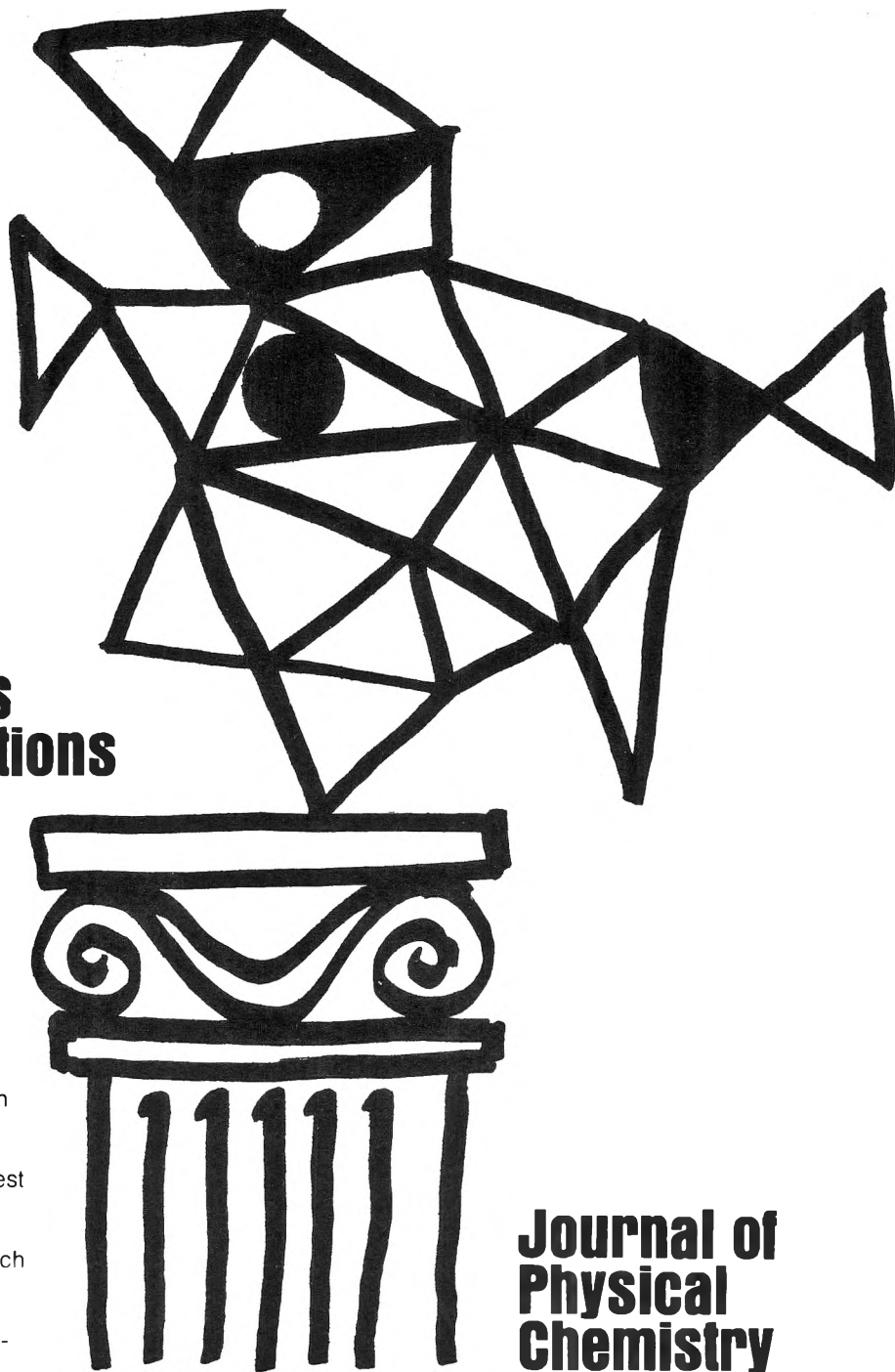
- (1) A. D. Buckingham, *Can. J. Chem.*, **38**, 300 (1960).
- (2) A. D. Buckingham, T. Schaefer, and W. G. Schneider, *J. Chem. Phys.*, **32**, 1227 (1960).
- (3) W. G. Schneider, H. J. Bernstein, and J. A. Pople, *J. Chem. Phys.*, **28**, 601 (1958).
- (4) L. W. Reeves, E. A. Allen, and K. O. Stromme, *Can. J. Chem.*, **38**, 1249 (1960).
- (5) A. L. Porte, H. S. Gutowsky, and I. M. Hunsberger, *J. Am. Chem. Soc.*, **82**, 5057 (1960).
- (6) J. C. Davis, Jr., and K. K. Deb, *Adv. Magn. Resonance*, **4**, 201 (1970).
- (7) H. M. McConnell, *J. Chem. Phys.*, **27**, 226 (1957).
- (8) J. A. Pople, *Proc. Roy. Soc. (London), Ser. A*, **239**, 550 (1957).
- (9) G. Fraenkel, R. E. Carter, A. MacLachlan, and J. H. Richards, *J. Am. Chem. Soc.*, **82**, 5846 (1960).
- (10) T. Schaefer and W. G. Schneider, *Can. J. Chem.*, **41**, 966 (1963).
- (11) G. K. Hamer, I. R. Peat, and W. F. Reynolds, *Can. J. Chem.*, **51**, 897 (1973).
- (12) T. Schaefer, W. F. Reynolds, and T. Yonemoto, *Can. J. Chem.*, **41**, 2969 (1963).
- (13) N. Boden, J. W. Emsley, J. Feeney, and L. H. Sutcliffe, *Mol. Phys.*, **8**, 133 (1964).
- (14) J. A. Pople, *J. Chem. Phys.*, **24**, 1111 (1956).
- (15) E. A. Allan and L. W. Reeves, *J. Phys. Chem.*, **66**, 613 (1962).
- (16) I. Granacher, *Helv. Phys. Acta*, **34**, 272 (1961).
- (17) L. Radom, W. J. Hehre, J. A. Pople, G. L. Carlson, and W. G. Fateley, *J. Chem. Soc., Chem. Commun.*, 308 (1972).
- (18) A. S. Manocha, G. L. Carlson, and W. G. Fateley, *J. Phys. Chem.*, **77**, 2094 (1973).
- (19) W. G. Fateley, G. L. Carlson, and F. F. Bentley, *J. Phys. Chem.*, **79**, 199 (1975).
- (20) J. A. Pople, W. G. Schneider, and H. J. Bernstein, "High-Resolution Nuclear Magnetic Resonance", McGraw-Hill, New York, N.Y., 1959.
- (21) J. W. ApSimon and H. Bierbeck, *Can. J. Chem.*, **49**, 1328 (1971).
- (22) W. T. Raynes, *Chem. Soc. Spec. Publ.*, **1**, 1 (1972); **2**, 1 (1973); **3**, 3 (1974).
- (23) U. Koelle and S. Forsén, *Acta Chem. Scand. Sect. A*, **28**, 531 (1974).
- (24) T. Gramstad and E. D. Becker, *J. Mol. Struct.*, **5**, 253 (1970).
- (25) M. Nakano, N. I. Nakano, and T. Higuchi, *J. Phys. Chem.*, **71**, 3954 (1967).
- (26) G. Pala, *Nature (London)*, **204**, 1190 (1964).
- (27) S. Forsén and R. A. Hoffman, *J. Mol. Spectrosc.*, **20**, 168 (1966).
- (28) B. G. Somers and H. S. Gutowsky, *J. Am. Chem. Soc.*, **85**, 3065 (1963).

**New concepts
new techniques
new interpretations**

**... together
with valuable reports
on classical areas**

They are all waiting for you between the covers of our well-balanced JOURNAL OF PHYSICAL CHEMISTRY. Whatever your particular interest in physical chemistry, you'll find the JOURNAL's broad range of experimental and theoretical research reports are relevant and beneficial to your work. Each biweekly issue brings you an average of 30 authoritative, comprehensive reports on fundamental aspects of atomic and molecular phenomena, as well as timely notes, communications and reports plus the proceedings of selected symposia.

Join your fellow physical chemists who rely on JPC as an excellent biweekly source of data in both new and classical areas. Just complete and return the form to start your own subscription.



Journal of Physical Chemistry

**The Journal of Physical Chemistry
American Chemical Society**

1155 Sixteenth Street, N.W.
Washington, D.C. 20036

1975

Yes, I would like to receive the JOURNAL OF PHYSICAL CHEMISTRY at the one-year rate checked below:

	U.S.	Canada**	Latin America**	Other Nations**
ACS Member One-Year Rate*	<input type="checkbox"/> \$20.00	<input type="checkbox"/> \$24.50	<input type="checkbox"/> \$24.50	<input type="checkbox"/> \$25.00
Nonmember	<input type="checkbox"/> \$80.00	<input type="checkbox"/> \$84.50	<input type="checkbox"/> \$84.50	<input type="checkbox"/> \$85.00
Bill me <input type="checkbox"/>	Bill company <input type="checkbox"/>	Payment enclosed <input type="checkbox"/>		

Air freight rates available on request

Name _____

Street _____

Home
Business

City _____

State _____

Zip _____

Journal subscriptions start on January '75

*NOTE: Subscriptions at ACS member rates are for personal use only. **Payment must be made in U.S. currency, by international money order, UNESCO coupons, U.S. bank draft, or order through your book dealer.

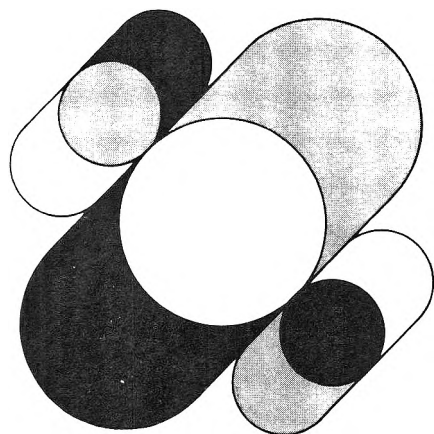


... another ACS service

Nonequilibrium Systems In Natural Water Chemistry

ADVANCES IN CHEMISTRY
SERIES No. 106

Thirteen papers from a symposium by the Division of Water, Air, and Waste Chemistry of the American Chemical Society, chaired by J. D. Hem.



Which is more important: efficient exploitation of our natural resources or a stable ecosystem? What is the relationship between a wide variety of life forms and a healthy environment? What do geology and groundwater flow patterns have to do with the chemical composition of water? How may one predict when a lake will reach equilibrium or tell how long it has supported life?

This volume features:

- principles of water pollution control
- methods of analysis for dissolved chemicals
- mathematical models
- discussion of stratified lakes
- chemical processes in a carbonate aquifer
- decomposition and racemization of amino acids

342 pages with index Cloth (1971) \$11.00
Postpaid in U.S. and Canada; plus 40 cents elsewhere.
Set of L.C. cards with library orders upon request.

Other books in the ADVANCES IN CHEMISTRY SERIES on water chemistry include:

No. 105 Anaerobic Biological Treatment Processes

Nine papers survey the state of the art of this natural process for waste treatment, with three papers on methane fermentation, others on process control and design. Considers volatile acid formation, toxicity, synergism, antagonism, pH control, heavy metals, light metal cations.
196 pages with index Cloth (1971) \$9.00

No. 79 Adsorption from Aqueous Solution

Fifteen papers discuss thermodynamic and kinetic aspects of adsorption phenomena and the results of studies on a variety of adsorbate-adsorbent systems.
212 pages with index Cloth (1968) \$10.00

No. 73 Trace Inorganics in Water

Research reports; analytical developments including atomic absorption, flame emission, and neutron activation; and broad reviews, such as effects of trace inorganics on the ice-water system and the role of hydrous manganese and iron oxides on fixing metals in soils and sediments.
396 pages with index Cloth (1968) \$12.50

No. 67 Equilibrium Concepts in Natural Water Systems

Sixteen papers represent the collaboration of aquatic chemists, analytical chemists, geologists, oceanographers, limnologists, and sanitary engineers, working with simplified models to produce fruitful generalizations and valuable insights into the factors that control the chemistry of natural systems.

344 pages with index Cloth (1967) \$11.00

No. 38 Saline Water Conversion—II

Fourteen papers from two symposia; includes recovery of minerals from sea water, minimizing scale formation, wiped thinfilm distillation, diffusion still, solar flash evaporation, osmosis, electrodialysis (3 paper), research in Israel, hydrate process.

199 pages Paper (1963) \$8.00

No. 27 Saline Water Conversion

Thermodynamics of desalting, solvent extraction, freezing, centrifugal phase barrier recompression distillation, multi-stage flash evaporation, ion exchange, osmosis, and electrochemical demineralization.

246 pages Paper (1960) \$9.00

Order from: **Special Issues Sales, American Chemical Society**
1155 Sixteenth St., N.W., Washington, D.C. 20036